Metallization of Polymers

Melallization of Polymers

Edward Sacher, EDITOR
École Polytechnique

Jean-Jacques Pireaux, EDITOR
Facultés Universitaires Notre-Dame de la Paix

Steven P. Kowalczyk, EDITOR
IBM Corporation

The paper used in this publication meets the minimum requirements of American National Standard for Information Sciences—Permanence of Paper for Printed Library Materials, ANSI Z39.48–1984. ∞

ACS Symposium Series

M. Joan Comstock, *Series Editor*

1990 ACS Books Advisory Board

Foreword

THE ACS SYMPOSIUM SERIES was founded in 1974 to provide a medium for publishing symposia quickly in book form. The format of the Series parallels that of the continuing ADVANCES IN CHEMISTRY SERIES except that, in order to save time, the papers are not typeset, but are reproduced as they are submitted by the authors in camera-ready form. Papers are reviewed under the supervision of the editors with the assistance of the Advisory Board and are selected to maintain the integrity of the symposia. Both reviews and reports of research are acceptable, because symposia may embrace both types of presentation. However, verbatim reproductions of previously published papers are not accepted.

Preface

THE IDEA FOR A MEETING ON THE METALLIZATION of polymers originated at the American Chemical Society National Meeting held in New Orleans in the summer of 1987. Several attendees recognized the need for a forum to discuss ancillary topics important to polymer chemists but not normally considered at national meetings. One such topic was the adhesion of metallization to polymers, particularly as used in thin film multilayer microelectronic devices. It was known to be relatively easy to get a polymer coating to adhere to a metal substrate, but far more difficult to get a metal coating to adhere to a polymer substrate. Because of the industrial importance of this topic, Dick Ikeda, then chairman of the Division of Polymer Chemistry, Inc., proposed that the division sponsor such a meeting, with Ed Sacher involved in its organization.

To gauge interest in a meeting on the metallization of polymers, some hundred questionnaires were sent worldwide to people involved in this area. The questionnaire gave the scope of the meeting, suggested session topics, and asked for preferred times and locations. Response was surprisingly positive; many respondents offered their help. The meeting was finally set for September 24–28, 1989, in Montreal.

Coeditors Jean-Jacques Pireaux and Steven P. Kowalczyk helped to organize the meeting. From the outset we worked together, sharing ideas and labor alike. Our discussions confirmed in our minds the need for major session topics on:

- analytical techniques—What do we wish to know about the unmetallized surface, the metallization process, and the interface? Which techniques are available? What can they tell us? We felt it important to include discussion of trace element detection techniques because some elements in trace amounts can severely limit the life of some multilayer microelectronic devices.

- surface morphology—What does the polymer surface look like? Is it different from the bulk? If so, why? How is the surface affected by the deposition process? Can the surface be modified to advantage?

- interfacial interactions—Under which circumstances does the metal adhere? Is there any chemical reaction? Can something be learned from model systems?

- adhesion—How does the metallization adhere? How can such adhesion be improved? Can it be quantified?

These contributions and the conference attendees attest to the academic and industrial importance of this subject. Although there were as many attendees from academe as from industry, the contributions even from industry were largely fundamental. This attention to fundamentals is interpreted as both an effort to understand the intricate question of adhesion and an effort to protect proprietary processes.

The chapters in this volume present a concise overview of surface analytical techniques from the specific viewpoint of surface morphology and its modification at the polymer–metal interface. A consistent picture begins to emerge of the chemical reactions occurring on metal deposition and why this leads to metal adhesion. The coeditors hope this information will be timely and useful.

The organizers of the International Symposium on the Metallization of Polymers wish to thank the following industrial sponsors: AKZO, BASF, Exxon, Rhône Poulenc, and Sabena.

EDWARD SACHER
École Polytechnique
Montreal, Quebec H3C 3A7, Canada

JEAN-JACQUES PIREAUX
Facultés Universitaires Notre-Dame de la Paix
B–5000 Namur, Belgium

STEVEN P. KOWALCZYK
IBM Corporation
Yorktown Heights, NY 10598

July 27, 1990

Chapter 1

The Present State of Metallized Polyimide

Edward Sacher

Groupe des Couches Minces and Département de Génie Physique, École Polytechnique, C.P. 6079, Succursale A, Montreal, Quebec H3C 3A7, Canada

Due to the incorporation of mechanical stresses during polymer/metal multilayer device fabrication, strong interfacial adhesion must be maintained in order to sustain mechanical integrity. Here we consider the adhesion of metal deposited onto polymer. In order to assure chemical bonding of the sort leading to strong adhesion, one must consider the structure (and modification) of the polymer surface, the energy released by the depositing metal and how it is taken up in reaction, and the aging effect of contaminant ions on the fabricated device.

Polymer/metal multilayer devices are used in the microelectronics industry. These devices are composed of alternating layers of polymer and metal, the metal is etched into lines and, except where via holes permit the contact of different metal layers, the polymer serves as an insulator. Because the polymer must withstand rather hostile environments during fabrication, the choice is narrowed to those which are stable to chemical treatment, high temperature (for short periods of time) and humidity. The polymers of choice here are the polyimides, although others are certainly used.

Each of the components, polymer and metal, has both thermal and hygroscopic expansion coefficients which may differ between components by orders of magnitude. Thus, the very act of fabrication introduces internal stresses into the device. If permitted to act, these stresses are capable of ripping apart the device, destroying it Such destruction is prevented by strong interfacial adhesion, maintained at every step during manufacture, as well as throughout the use life of the device.

POLYMER ADHESION TO METAL

Now, the adhesion of polymer to metal presents no difficulty: poor adhesion of the polymer to the bare metal substrate is improved through the use of silane adhesion promotors(1-7). These are

orthoesters of silane, having the general formula $Z-R-Si(OR')_3$, where Z is a functional group specifically chosen to react with the polymer, and R and R' are alkyl groups. When added to water, the orthoester hydrolyzes (sometimes slowly) to the silanetriol, $-Si(OH)_3$, whose hydroxyl groups are extremely reactive. These groups react with each other as well as with hydroxyl groups on clean metal surfaces, to deposit a thin polysiloxane layer strongly bound to the metal. Among the groups lying at the new surface are the Z groups capable of reacting with the polymer to chemically bond it to the polysiloxane. This chemical bonding is accomplished with a minimal increase in thickness (~100Å), through the introduction of a surface-reactive polysiloxane rubber layer capable of dissipating some of the internal stresses.

Sadly, such adhesion promotors are not available for the adhesion of metal being deposited onto a polymer surface. Here, one must rely entirely on reactions provoked by the deposition process to provide the adhesion. This requires a thorough understanding of both the polymer surface and the deposition process.

POLYMER SURFACE STRUCTURE

There is an excess energy at a surface, measurable as a surface tension(8). This causes the surface layer of a curing polymer to react farther and faster than the bulk. In the case of polyimide, it also promotes some surface layer structural rearrangement (~8%) to isoimide(9), causing changes in both mechanical(10) and electrical(11) properties. Further, a recent IR study(12) demonstrated that the polyimide structure obtained on curing depended on the cure schedule.

Indeed, the whole question of polyimide structure has yet to be properly addressed. As normally written, the precursor polyamic acid cyclizes to a 5-member polyimide ring, splitting out water; however, objections(13) have been raised to this cyclization. In particular, reactions carried out on monomers show(14-16) that imide formation requires prolonged heating in the presence of dehydrating agents and that such imides revert quickly to the amic acid reactant in the presence of atmospheric moisture. This makes it highly unlikely that a polyimide film formed through the cyclization of the polyamic acid would be as stable as such films are found to be. Yet, IR evidence(17) leaves no doubt that the polyamic acid has imidized.

Several lines of investigation have been brought together (13) to suggest that what in fact happens to the polyamic acid is that it transimidizes. That is, imidization takes place between adjacent chains. This explains many facts, such as the loss of solubility on imidization, the compatibility of the data with second order kinetics and the lack of XPS data indicating increased electron delocalization on imide formation. It would appear that the polymer structure is largely a crosslinked transimide and that, at its surface, it contains ~8% isoimide. This is the structure upon which the metal deposits.

Burkstrand has shown(18-25) that evaporated metals react only with oxidizing polymers. In the case of polystyrene, for example, reaction takes place only at surface sites oxidized during polymer

fabrication (e.g., the melt extrusion of polymer films). Thus, to assure good adhesion to hydrocarbon polymers, the surface must be treated in such a way as to introduce oxidizing groups. While several types of surface oxidation treatment are available, the use of plasmas seems to be the treatment of choice(26-34).

METAL DEPOSITION

Because the adhesion of a deposited metal depends on the formation of chemical bonds across the interface, one must determine if the metal deposition process is capable of releasing the energy necessary to cause reaction between the depositing metal atoms and the polymer surface. For metal deposition by sputtering, the answer is an unqualified yes: for both Cu (35,36) and Ni(35), for example, there is an impact energy maximum near 950 kJ/mole and an average energy near 3500 kJ/mole. These values should be compared with covalent bond energies, which are in the 340-400 kJ/mole range.

The situation for metal deposition by evaporation is somewhat different: the average impact energies of such atoms are of the order of 10 kJ/mole(37). However, at least for the metals one would normally use, their condensation energies, the negative of the heat of sublimation(38), are of the same order of magnitude as covalent bond energies. One should note that this heat of condensation is for metal condensing on metal. That is, after several monolayers are deposited, assuming no reaction of the initial monolayers, enough heat may be released to break covalent bonds.

One should more properly consider the condensation energy of the first monolayer of metal on polymer. No experimental values exist, making it necessary to infer reaction from other data. Here, there is a great divergence of opinion, not only as to whether reaction occurs but, if so, where the structure is attacked. A particular example of this is found in the deposition of Cr onto polyimide, where all agree that reaction occurs: one group maintains that the Cr forms a π-complex with the aromatic ring of the dianhydride moiety(39,40) while another insists that reaction occurs with the carbonyl oxygens(41,42).

Let us, for a moment, consider the reaction of evaporated metal atoms with monomers. While here, too, there appear to be no data on condensation energies, there is a large body of experimental data(43-47) which demonstrate compound formation under conditions less apt to sustain chemical reactions than those during polymer metallization. This strongly suggests that, with the exception of purely aliphatic, non-oxidizing substrates, reaction probably does take place. To demonstrate this, let us consider several recent XPS studies of metallized polyimide; these metals include Al(48-50), Au(51), Ce(52), Co(53), Cr(42), Ge(54) and Ti(55). Whether the authors posit reaction between metal and polymer or not, the metal XPS spectra at very low coverages all show either a chemical shift to higher binding energy or a shoulder at the higher binding energy side of the peak, neither of which is seen at greater depositions. Such behavior indicates the formation of ionic species. Clearly, then, the question is not whether reaction occurs but where it occurs and how this conveys adhesion.

IONIC CONTAMINATION

The question of trace ionic contaminants is often overlooked. There is no doubt, however, that trace ions initially present in the polymer or subsequently introduced during the manufacturing process can wreak havoc with the device as well as with device-mounted components as the device ages and the ions migrate. Thus, not only can Na ions migrate to and destroy an FET by lowering the threshold resistance in the gate, halide ions can attack some metals, which may lead to a loss of interfacial adhesion and will certainly lead to a loss of conduction.

While it is true that, with the exception of the proton, the trace ions found in polymers do not migrate in the absence of water(11,56-58), it is also true that microelectronic devices and components are not hermetically sealed: they are always exposed to atmospheric humidity. It is, therefore, necessary to know, both qualitatively and quantitatively, which trace ions are present. This writer has had experience(59) with four techniques which are capable of identifying contaminants in the ppm-ppb (i.e. ug/ml-ng/ml) concentration region. Each has its own advantages and disadvantages, necessitating the simultaneous use of several of the techniques found in Table I. A particular advantage of ion

Table I. Techniques Capable of Detecting Trace Contaminants in the ppm-ppb Concentration Range

	Ion Chromatography	Plasma Spectroscopy	Neutron Acti- vation Analysis	Proton-Induced Xray Emission
Agueous solutions	Yes	Yes	Yes	Yes
Solid	No	Yes (slurry)	Yes	Yes
Species detected	Ions	Ions, atoms (no distinction)	Ions, atoms (no distinction)	Ions, atoms (no distinction)
Advantages	Fast; Sensitive to some organic species	Fast	Large range of elements	Fast; Large range of elements
Disadvantages	Limited number of ions	Cost per ele- ment detector	Slow; Poor deconvolution	Not sensitive to high atomic

chromatography, for example, is its sensitivity to some organic ions. It was in this fashion that polyimide was shown to undergo a slow surface hydrolysis(59): ion chromatography showed the presence of both carboxylate and substituted ammonium ions, the hydrolysis products of polyimide, whose concentrations increased with water immersion time. It should be noted that these carboxylate ions, like halide ions, attack some metals, and could ultimately lead to a loss of adhesion between metal and polymer or to the formation of a brittle insulating layer. Internal stresses could then destroy the device.

ADHESION MECHANISM(S)

Here, the question of how the metal adheres to the substrate remains largely unanswered. A review on this subject(60), now more than a decade old, could do no more than list the then extant proposed

mechanisms (mechanical/interlocking, weak boundary layer, chemical, electrostatic) and offer experimental evidence which tended to support each of them. The general conclusion was that one or more of these mechanisms gave rise to the observed adhesion.

Little has changed during the intervening years, with the exception that the chemical mechanism is presently favored (25,48-55,61-74), the reason being that adhesion is clearly observed in association with the occurrence of chemical reaction. This does not answer the question of how chemical reaction leads to adhesion or why exposure to atmospheric humidity is so detrimental(73).

CONCLUSIONS

The interface of metallized polymers has been considered from the points of view of the polymer surface, reaction during metal deposition and the effect of contaminant ions. Each is discussed in terms of the critical factors which maintain the mechanical integrity of polymer/metal multilayer devices, in light of the present view that interfacial chemical reactions are involved. Thus, the true structure of the polyimide surface is described, followed by a discussion of why metal deposition provokes a chemical reaction with the substrate polymer. Trace ions are then considered, from the point of view that subsequent reaction with polymer and/or metal can lead to the failure of interfacial adhesion.

ACKNOWLEDGMENTS

LITERATURE CITED

1. Kinloch, A.J., Dukes, W.A.. Gledhill, R.A., in Adhesion Science and Technology, L.-H. Lee, Ed., Plenum: New York, 1975; p. 597.
2. Getting, M., Baker, F.S., Kinloch A.J., J. Appl. Polym. Sci., 1977, 21, 2375.
3. Paik Sung, C.S., Lee, S.H., Sung, N.H., in Adhesion and Adsorption of Polymers, L.-H. Lee, Ed., Plenum: New York, 1980; p. 757.
4. Boerio, F.J., Williams, J.W., Appl. Surf. Sci., 1981, 7, 19.
    5. Boerio, F.J., Williams, J.W., Burkstrand, J.M., J. Colloid Interface Sci., 1983, 91, 485.
6. Boerio, F.J., Polym. Preprints, 1983, 24(1), 204.
7. Much practical information is available from vendors, including Dow Corning Corporation, Petrarch Systems and Union Carbide Corporation.
8. Cherry, B.W., Polymer Surfaces, Cambridge University Press: New York, 1981; Chapter 1.
9. Chauvin, C., Sacher, E., Yelon, A., J. Appl. Polym. Sci., 1986, 31, 583 and references therein.
10. Sacher, E., Susko, J.R., J. Appl. Polym. Sci., 1979, 23, 2355.
11. Sacher, E., IEEE Trans. Electr. Insul., 1979, EI-14, 85.
12. Baise, A.I., J. Appl. Polym. Sci., 1986, 32, 4043.

13. Sacher, E., J. Macromol. Sci., 1986, B25, 405 and references therein.
14. Mehta, N.B., Phillips, A.P., Liu, F.F., Brooks, R.E., J. Org. Chem., 1960, 25, 1012.
15. Matsuo, T., Bull. Chem. Soc. Japan, 1964, 37, 1844.
16. Verbicky, J.W., Jr., Williams, L., J. Org. Chem., 1981, 46, 175.
17. Ishida, H., Wellinghoff, S.T., Baer, E., Koenig, J.L., Macromolecules, 1980, 13, 826.
18. Burkstrand, J.M., Surf. Sci., 1978, 78, 513.
19. Burkstrand, J.M., J. Vac. Sci. Technol., 1978, 15, 223.
20. Burkstrand, J.M., Appl. Phys. Lett., 1978, 33, 387.
21. Burkstrand, J.M., J. Appl. Phys., 1979, 50, 1152.
22. Burkstrand, J.M., J. Vac. Sci. Technol., 1979, 16, 363.
23. Burkstrand, J.M., Phys. Rev. B, 1979, 20, 4853.
24. Burkstrand, J.M., ACS Symp. Ser., 1981, 162, 339.
25. Burkstrand, J.M., J. Appl. Phys., 1981, 52, 4795.
26. Hall, J.R., Westerdahl C.A.L., Devine A.T., Bodnar, M.J., J. Appl. Polym. Sci., 1969, 13, 2085.
27. Carlsson, D.J., Wiles, D.M., Can. J. Chem., 1970, 48, 2397.
28. Blais, P., Carlsson, D.J., Suprunchuk, T., Wiles, D.M., Textile Res. J., 1971, 41, 485.
29. Blais, P., Carlsson, D.J., Wiles, D.M., J. Appl. Polym. Sci., 1971, 15, 129.
30. Hall, J.R., Westerdahl, C.A.L., Bodnar, M.J., Levi, D.W., J. Appl. Polym. Sci., 1972, 16, 1465.
31. Clark, D.T., Dilks, A., in Characterization of Metal and Polymer Surfaces, L.-H. Lee, Ed., Academic Press: New York, 1977; p. 101.
32. Blythe, A.R., Briggs, D., Kendall, C.R., Rance, D.G., Zichy, V.J.I., Polymer, 1978, 19, 1273.
33. Peeling, J., Jazzar, M.S., Clark, D.T., J. Polym. Sci. Polym. Chem. Ed., 1982, 20, 1797.
34. Amouroux, J., Gicquel, A., Cavvadias, S., Morvan, D., Arefi, F., Pure Appl. Chem., 1985, 57, 1207.
35. Oechsner, H., Z. Physik, 1970, 238, 433.
36. Hart, R.G., Cooper, C.B., Surf. Sci., 1980, 94, 105.
37. Meyer, K., Schuller, I.K., Falko, C.M., J. Appl. Phys., 1981, 52, 5803.
38. Honig, R.E., RCA Reviews, 1957, 18, 195.
39. Rossi, A.R., Sanda, P.N., Silverman, B.D., Ho, P.S., Organometallics, 1987, 6, 580.
40. Haight, R., White, R.C., Silverman, B.D., Ho, P.S., J. Vac. Sci. Technol., 1988, A6, 3188.
41. Jordan, J.L., Kovac, C.A., Morar, J.F., Pollak, R.A., Phys. Rev. B, 1987, 36, 1369.
42. Kovak, C.A., Jordan-Sweet, J.L., Goldberg, M.J., Clabes, J.G., Viehbeck, A., Pollak, R.A., IBM J. Res. Develop., 1988, 32, 603.
43. Moskovits, M., Ozin, G.A., Cryochemistry, Wiley-Interscience: New York, 1976.
44. Blackborrow, J.R., Young, D., Metal Vapor Synthesis in Organometallic Chemistry, Springer-Verlag: New York, 1979.
45. Klabunde, K.J., Chemistry of Free Atoms and Particles, Academic Press: New York, 1980.

46. Ozin, G.A., Chemtech, 1985, 15, 488.
47. Ozin, G.A., Chem. Modif. Surf., 1988, 2, 161.
48. Ho, P.S., Hahn, P.O., Bartha, J.W., Rubloff, G.W., Le Goues, F.K., Silverman, B.D., J. Vac. Sci. Technol., 1985, A3, 739.
49. Bartha, J.W., Hahn, P.O, Le Goues, F., Ho, P.S., J. Vac. Sci. Technol., 1985, A3, 1390.
50. Atanasoska, Lj., Anderson, S.G., Meyer, H.M., III, Lin, Z., Weaver, J.H., J. Vac. Sci. Technol., 1987, A5, 3325.
51. Meyer, H.M., III, Anderson, S.G., Atanasoska, Lj., Weaver, J.H., J. Vac. Sci. Technol., 1988, A6, 30.
52. Clabes, J.G., J. Vac. Sci. Technol., 1988, A6, 2887.
53. Anderson, S.G., Meyer, H.M., III, Weaver, J.H., J. Vac. Sci. Technol., 1988, A6, 2205.
54. Atanososka, Lj., Meyer, H.M., III, Anderson, S.G., Weaver, J.H., J. Vac. Sci. Technol., 1988, A6, 2175.
55. Ouhuchi, F.S., Freilich, S.C., J. Vac. Sci. Technol., 1986, A4, 1039.
56. Barker, R.E., Jr, Thomas, C.R., J. Appl. Phys., 1964, 35, 3205.
57. Barker, R.E., Jr., Sharbaugh, A.H., J. Polym. Sci.: Part C, 1965, 10, 139.
58. Barker, R.E., Jr., Pure Appl. Chem., 1976, 46, 157.
59. Sacher, E., IEEE Trans. Electr. Insul., 1983, EI-18, 369.
60. Mittal, K.L., J. Vac. Sci. Technol., 1976, 13, 19.
61. Buckley, D.H., Brainard, W.A., in Advances in Polymer Friction and Wear, L.-H. Lee, Ed., Plenum: New York, 1974; p. 315.
62. Roberts, R.F., Schonhorn, H., Polym. Preprints, 1975, 16(2), 146.
63. Roberts, R.F., Ryan, F.W., Schonhorn, H., Sessler, G.M., West, J.E., J. Appl. Polym. Sci., 1976, 20, 255.
64. Evans, J.R.G., Packham, D.E., J. Adhesion, 1978, 9, 267.
65. Tsukada, T., Hosokawa, N., J. Vac. Sci. Technol., 1974, 16, 348.
66. Vogel, S.L., Schonhorn, H., J. Appl. Polym. Sci., 1979, 23, 495.
67. Soeda, F., Hayashi, K., Ishitani, A., J. Electron Spectrosc. Relat. Phenom., 1982, 27, 205.
68. Burkstrand, J., J. Vac. Sci. Technol., 1982, 20, 440.
69. Ellul, M.D., Gent, A.D., J. Polym. Sci.: Polym. Chem. Ed., 1984, 22, 1953.
70. Bodö, P., Sundgren, J.-E., Surf. Interface Anal., 1986, 9, 437.
71. de Puydt, Y., Bertrand, P., Lutgen, P., Surf. Interface Anal, 1988, 12, 486.
72. Gerenser, L.J., J. Vac. Sci. Technol., 1988, A6, 2897.
73. Chauvin, C., Sacher, E., Yelon, A., Groleau, R., Gujrathi, S., in Surface and Colloid Science in Computer Technology, K.L. Mittal, Ed., Plenum: New York, 1987; p. 267.
74. Brown, H.R., Yang, A.C.M., Russell, T.P., Volksen, W., Kramer, E.J., Polymer, 1988, 29, 2807.

Chapter 2

Photoelectron Spectroscopies Applied to Polymer–Metal Interactions

Steven P. Kowalczyk

T. J. Watson Research Center, IBM Corporation, Box 218, Yorktown Heights, NY 10598

The application of photoelectron spectroscopy (PES) for the investigation of polymer-metal interfaces is discussed in this chapter. The information obtainable from both core-level spectra and valence-band spectra is briefly described. The approach of model compounds to study specific interactions is shown to be a useful aid to the understanding of polymer-metal reactivity. Emphasis is given to a number of experimental aspects relevant to polymer-metal interface studies, such as sample preparation and problems such as beam induced damage. Some of the advantages of synchrotron radiation and small spot x-ray sources are demonstrated. Most of the illustrative examples will come from polyimide-metal interface studies directed at investigating the role of interfacial chemistry in adhesion at these interfaces and the non-equivalence of polymer-on-metal and metal-on-polymer interfaces.

Photoelectron spectroscopy (PES) has become an important and widely used tool in material science (1-3). It has been a particularly fruitful technique for the investigation of polymers (4-9). In this review, we will focus on the application of photoelectron spectroscopy to the investigation of the interfaces between metals and polymers. These studies are directed primarily to understand the role of interfacial chemistry in the adhesion between metals and polymers. Two aspects, which will be emphasized here, are the experimental approaches in PES studies of polymer/metal interfaces and the types of information accessible from the PES experiments. The experimental emphasis will be on preparation of appropriate samples for polymer/metal interface studies, practical problems

such as charging and beam induced damage, and the useful-
ness of synchrotron radiation and small area x-ray
sources. The information available from core-level spec-
tra including satellites and valence-band spectra will be
discussed. The examples used to illustrate the above
will primarily come from studies of interfacial chemistry
and its contribution to adhesion at polyimide/metal inter-
faces. Polyimide is a polymer of intense current inter-
est in the microelectronic industry as a thin firm di-
electric constant and a number of other attractive prop-
erties (10-14).
     Photoelectron spectroscopy consists of irradiating
the sample being investigated with a monoenergetic source
of photons and energy analyzing the emitted photoelec-
trons (15). The two key features of the PES experiment
are that the measured energies are very sensitive to the
chemical environment (chemical-shift phenomenon) (15) and
the analyzed photoelectrons have mean free paths on the
order of 20A (surface sensitivity) (16,17). The first
feature makes core-level spectra such a powerful and
widely used tool to obtain chemical information, while
the second feature makes the PES technique a potent sur-
face sensitive spectroscopy and necessitates ultra high
vacuum (UHV) techniques and care in sample preparation
but allows the study of interfaces and surfaces in a
straightforward and well-characterized manner. We will
start by discussing several important experimental as-
pects relevant to the application of PES in polymer-metal
interface studies.

EXPERIMENTAL

Charging. Most polymers are insulating and thus present
the problem of charging (18). While this presents prob-
lems in obtaining absolute binding energies, in many
cases this is not a serious hindrance as the spectra
often can be used as fingerprints or can be referenced
to a fiducial such as the valence-band maximum or a prom-
inent well known core-level feature. Homogeneous charg-
ing besides leading to binding energy shifts can signifi-
cantly broaden spectra thus seriously degrading resolu-
tion and inhibiting interpretation. A sample with non-
uniform morphology often results in inhomogeneous charg-
ing which can further degrade spectra by severe distor-
tion of lineshapes to the extent that any interpretation
is problematic. These effects are often alleviated or
minimized by charge neutralization to compensate for the
surface charge by flooding the surface with low energy
electrons (18). While this approach is often useful,
possible damage induced by the electron beam must be
carefully monitored for inorganic materials. It is also
possible to over compensate for the charging induced
binding energy shift. The use of thin films approximate-
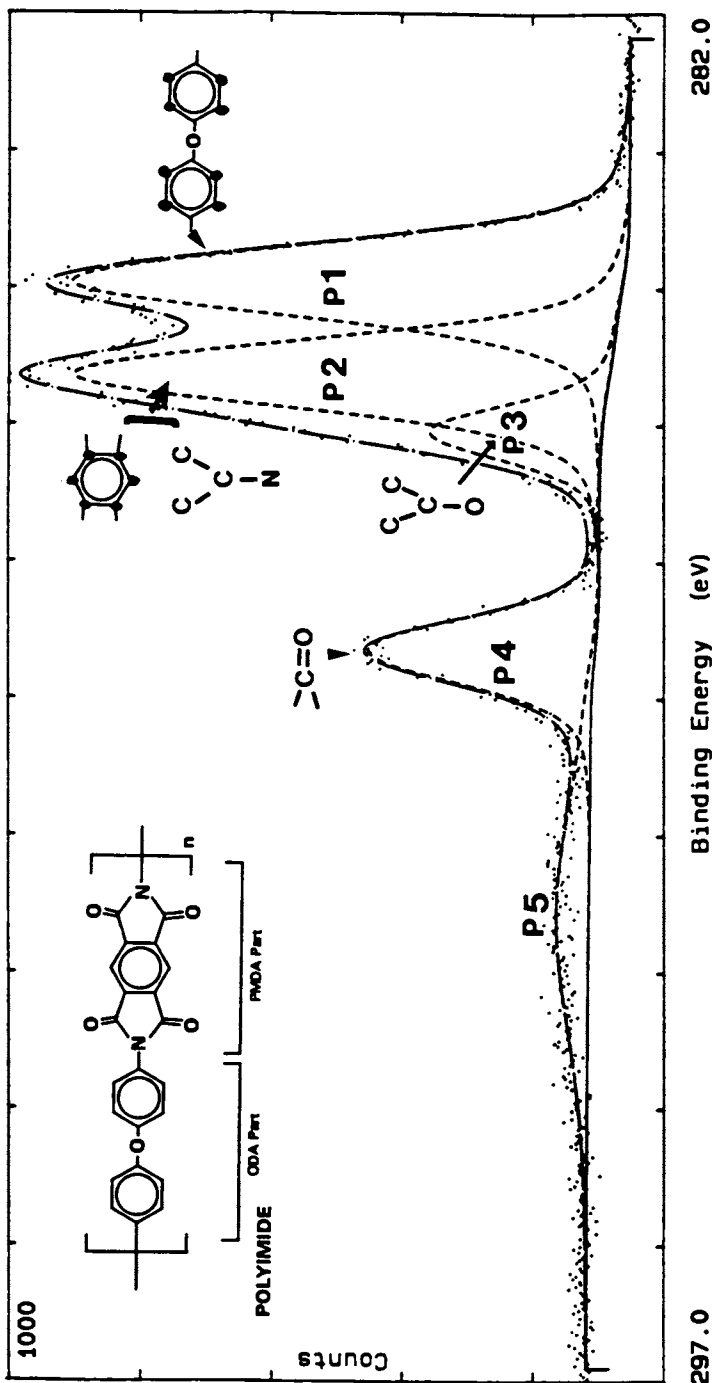ly 1000A thick can minimize charging effects. Figure 1

Figure 1. C 1s spectrum of a polyimide (PMDA-ODA) film.

shows a carbon 1s spectrum from a 1900A thick polyimide
(PMDA-ODA) film obtained without the use of charge neutra-
lization but nonetheless with very good resolution.

Beam Induced Effects. One problem in the study of organic
films is beam induced damage. The photograph of Figure 2
shows an insitu grown pryomellitic dianhydride (PMDA) film
and an oxydianiline (ODA) film after long exposure (~15
hours) to the monochromatized Al Kα x-ray source of a
Hewlett Packard 5950A electron spectrometer. The films
were~10,000A thick. The ODA film clearly shows the pat-
tern of the 1mm by 5mm x-ray beam, while the pattern in
the PMDA film is more complex. After exposure to air dur-
ing storage and for transfer, these films were studied
with a Surface Science Instruments small-spot x-ray photo-
electron (XPS) spectrometer. Figure 3 shows the C 1s
spectra obtained with a small spot x-ray beam (150µ) from
two spots on the surface of the PMDA film, one near the
center of the discolored area and the other near one edge.
No change in lineshape is observed across the sample but
there is a smooth shift of observed binding energy with
the minimum binding energy obtained at the center of the
damage area and increasing binding energy towards either
side. O 1s spectra rigidly shifts in binding energy with
the C 1s spectra and also does not undergo any lineshape
change. Finally there is no variation of the C to O ratio
across the sample. Thus the explanation for the beam ef-
fects in the PMDA film is that the x-ray beam induces
heating with a thermal gradient across the sample with the
temperature highest at the center where the x-ray beam im-
pinges the sample, and lower towards the edges which are
not directly illuminated by the x-rays. This heating is
sufficient to evaporate PMDA from the surface under ir-
radiation. Because of the thermal gradient, there is the
interference fringe pattern on the film reflecting varia-
tion in film thickness due to different evaporation rates
across the film. The film thickness variation produces
the variation in charging across the sample and the re-
sulting U-shape curve in binding energy as a function of
position across the sample with the greatest charging at
the edges where the film is thickest due to the least a-
mount of evaporation arising from its lower temperature.
Time dependent charging as well as lineshape distortion
could be observed during some experiments on the in situ
grown PMDA films as the film thickness was changing dur-
ing the measurement. A rise in system pressure (~one
order of magnitude) also could be observed upon x-ray ir-
radiation of the sample. While this continuously produces
a fresh clean surface, it makes the experiments diffi-
cult! Thus experiments on a sample like PMDA and other
similar monomers would be best performed at low tempera-
tures.
     ODA presents a different beam induced effect. Small
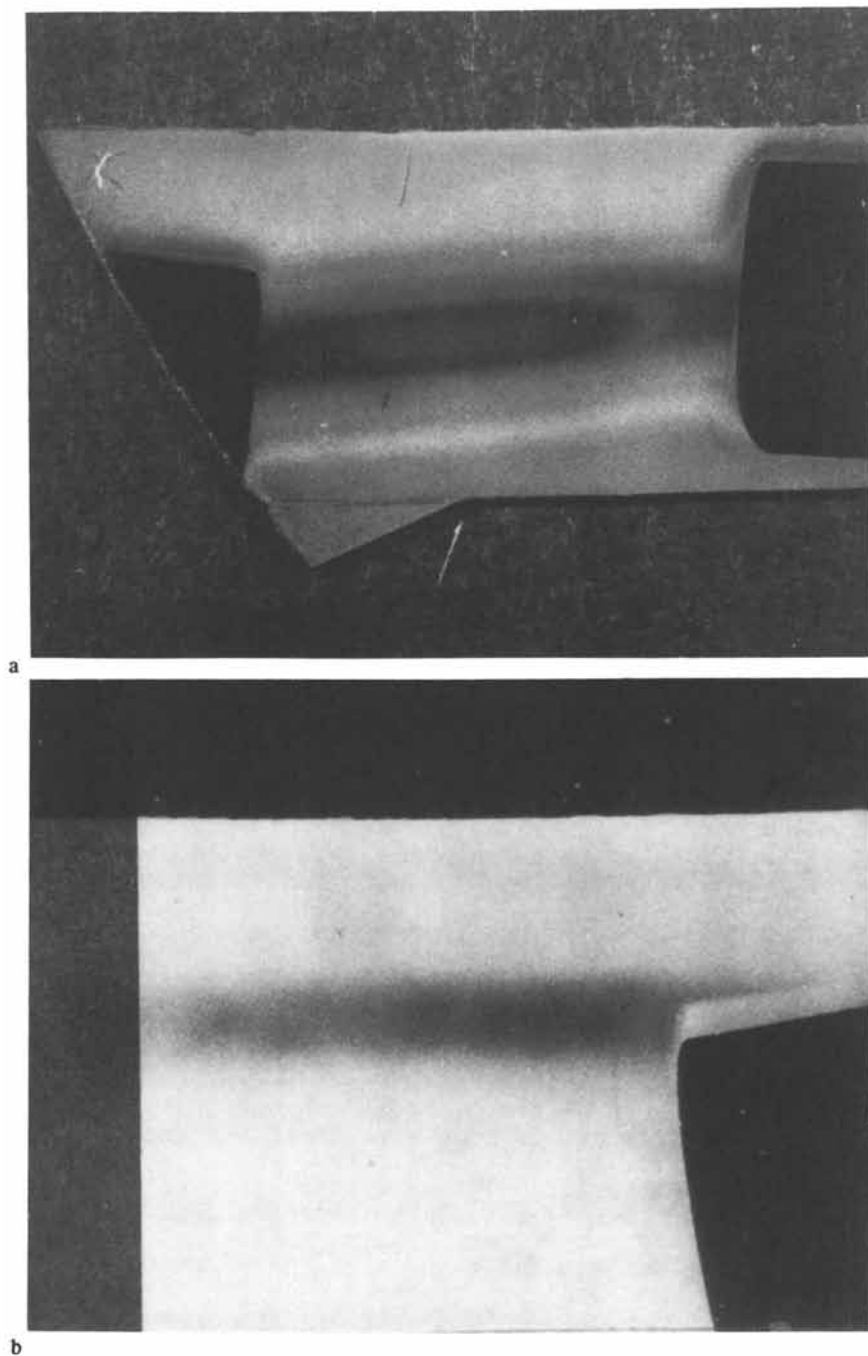spot XPS analysis across the sample does not show any

Figure 2. Photograph of x-ray beam induced damage in
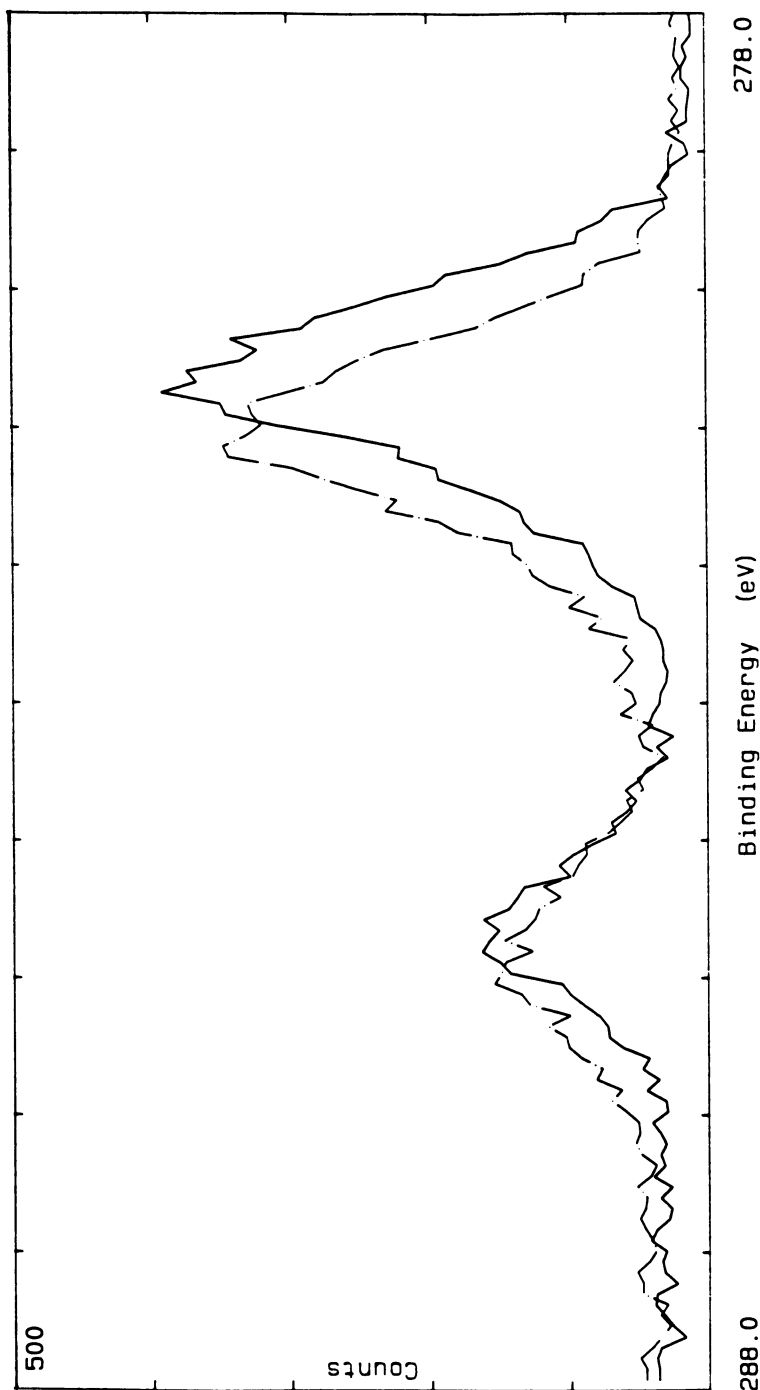(a) PMDA and (b) ODA films.

Figure 3. Carbon 1s spectra obtain by small spot analysis (15Cµ) from two positions on a previously beam damaged PMDA film.

variation in core-level binding energy for any particular
feature. However, there is a change in the O 1s lineshape
and a variation in the C/O and N/O ratios with both ratios
increasing. This behavior suggests photo-induced bond
cleavage, probably at the ether linkage though detailin-
terpretation would require further controlled experiments
without ambient exposure. Both uncured PMDA-ODA polyimide
precursor (polyamic acid) and fully cured PMDA-ODA (poly-
imide) did not exhibit either of the above effects upon
similar exposures. The above illustrates the utility of
small area x-ray beams and why techniques with intense
beams such as Auger electron spectroscopy have limited
utility in studies on these materials.

Ion beams are often utilized to prepare clean sur-
faces for PES studies or for depth profiling through a
sample. This causes problems in polymer studies as the
surface can be chemically degraded as has been demonstra-
ted in the case of polyimide (19,20). This effect, how-
ever, has been used to increase metal/polymer adhesion,
while the exact mechanism (chemical, mechanical) for the
improved adhesion for the metals to polyimide is not yet
completely understood (21,22).

Angle Dependence. The effective escape depth in a PES ex-
periment can be substantially decreased by using a low
electron exit angle geometry, if one has a sufficient
angle resolved electron analyzer (23). The effective es-
cape depth varies as the $\sin \theta$ of electron exit angle, θ,
the angle between the exiting electron and the sample sur-
face. The surface sensitivity can easily be increased by
an order of magnitude. This can be very useful for deter-
mining the orientation of an organic monolayer on a metal.
As an example using a modestly angle-resolved analyzer
(30° acceptance angle) a monolayer of dodecanethiol, an
alkane chain with S at one end, was applied to a gold
surface using the method of Whitesides et al (24). The
C/Au and S/Au ratios were investigated as a function of
exit angle. We observe that the Au/S ratio is nearly con-
stant upon varying the exit angle, while the C/Au ratio
varies by more than a factor of 3 upon variation of the
exit angle with the ratio increasing to lower (more sur-
face sensitive) exit angles. This is consistent with the
structureof a monolayer of the molecules being oriented
nearly perpendicular and attached to the Au surface via
the S end of the molecule. Much work on this interesting
class of compounds has been carried out recently by G. M.
Whitesides and collaborators (see reference 24 and refer-
ences therin). This type of measurement would greatly
benefit from the use of higher angular resolution. Ex-
periments with angular resolution of 2° to 6° are quite
feasible (23).

Photon Source. There are three main types of photon
sources used in PES. The most common laboratory source

is an x-ray tube with either Al (1486.6 eV) or Mg
(1256.6 eV) Kα radiation. Al sources have an advantage as
they can be monochromatized to achieve superior resolution
and eliminate bremstalung and satellite lines from PES
spectra. Also, al Kα x-rays have been focussed to small
spot size, ~100μ (25). The other common laboratory
source is the rare gas (ultra violet) discharge lamp,
utilizing primarily the He I (21.1 eV) or He II (40.8 eV)
resonance lines. These have the disadvantage that rela-
tively few core levels of interest (e.g. C 1s, O 1s, N 1s,
or F 1s) can be accessed nor can the entire valence band
be measured. Synchrotron radiation provides a variable
range of photon energies (most commonly in the range of
~20-1000 eV with the current generation of synchrotrons
and available monochromators). This allows advantage to
be taken of the energy dependence of the electron ineleas-
tic mean path for increased surface sensitivity. Figure
4 shows a Si (111) surface covered with a thin layer of
the polyimide precursor,polyamic acid taken at two differ-
ent photon energies. The enhancement of the reacted
chemically shifted Si intensity at higher binding energy
to the unreacted Si can be seen in the spectrum obtained
at the lower more surface sensitive photon energy. A-
nother aspect of synchrotron radiation is the energy de-
pendence of the photoionization cross section. This is
particularly useful in valence-band studies where various
levels can be modulated by variation of the photon energy
and will be discussed in a latter section.

Sample Preparation. The best method to study interfaces
involves preparing the interface in situ with a thin over-
layer such that core levels from both sides of the inter-
face can be observed (see Figure 5). The interface can
be built up from a submonolayer coverage upto several
layers to form a fully developed ("burried") interface.
The metal-on-polymer interface has been the most studied
interface as metals can conveniently be deposited by evap-
oration in situ in a controllable fashion in a UHV system
(26-33). In the case of polyimide, Cu and Cr have been
the most studied metals but other metals including Ni, Co,
Al, Au, Ag, Ge, Ce, Cs, and Si have been studied. The
best experimental arrangement includes a UHV system with
a load lock introduction chamber, a preparation chamber
with evaporators, heating capabilities, etc., and a sepa-
rate analysis chamber. All the chambers are separated by
gate valves and the samples are transferred between cham-
bers under vacuum. Alternative metal deposition sources
such as organometallic chemical vapor deposition are prom-
ising and such techniques possibly can lead to different
interface formation than obtained by metal evaporation(34).
    For polymer film preparation, especially for the in-
vestigation of polymer-on-metal interactions, a molecular
beam deposition (MBD) technique is necessary. This tech-
nique was first demonstrated for polyimide by Salem and co-
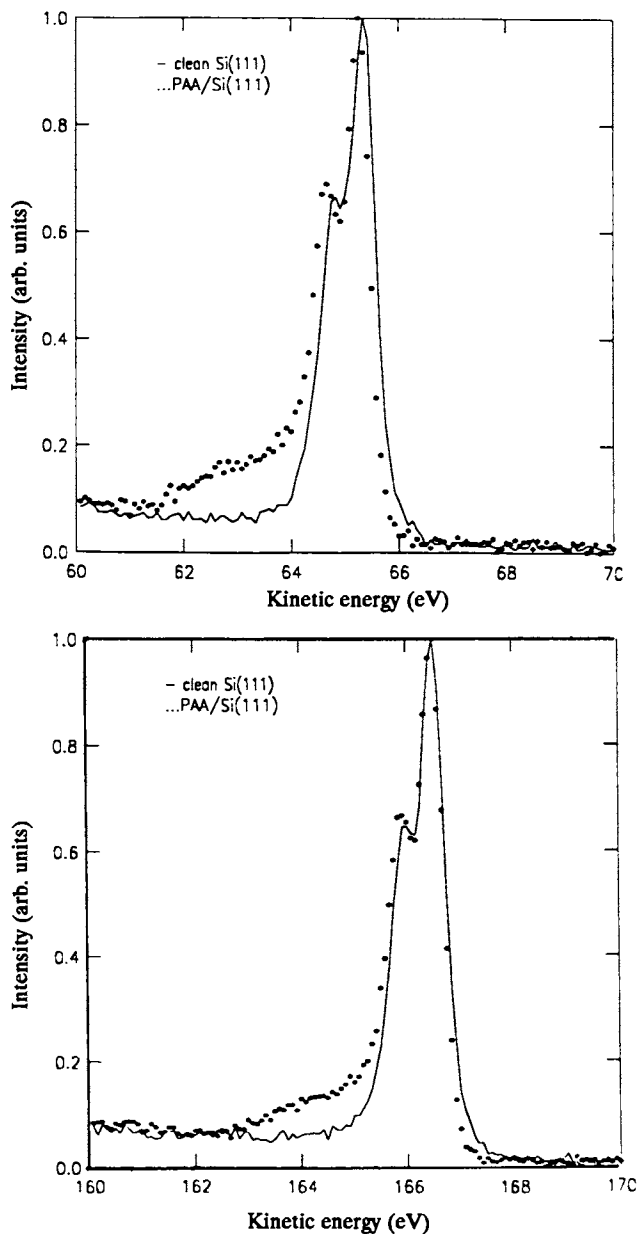
Figure 4. Si 2p after deposition of ~4A of polyamic acid on Si(111). The upper spectrum was obtained with hv = 167 eV and the lower spectrum with hv = 267 eV. The Si 2p½ spin-orbit component has been subtracted for clarity.
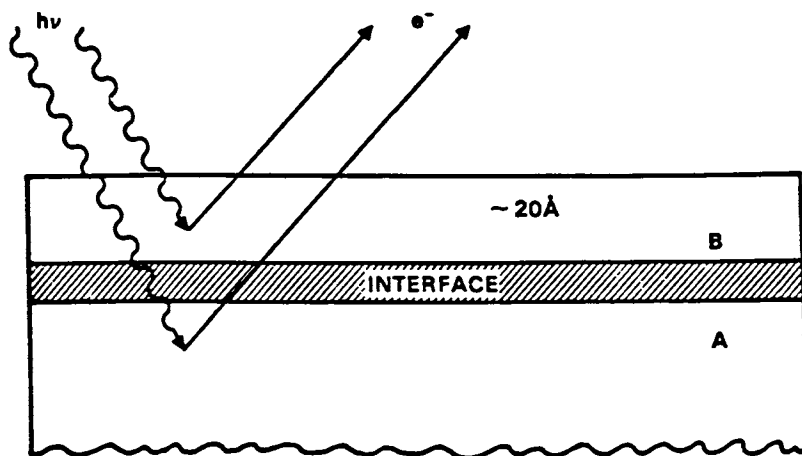
Figure 5. Schematic of an interface sample suitable for
PES interface analysis, where A and B are either a
polymer or metal of interest.

workers (35) and applied to UHV interface studies by
Grunze and co workers (36-39). This technique involves
the use of molecular beams of PMDA and ODA, which form
polyamic acid on the surface, which upon curing (heating
to 400°) cycloimidizes the polyamic acid to form polyi-
mide. The table shows a comparison of energy splittings
and intensity of the five main features in the C 1s spec-
trum between a MBD polyimide (PMDA-ODA) film and a spun
film. This technique allows the study of the polymer-on-
metal interface formation. It allows the metal surface to
be controllably prepared in UHV prior to coating with the
polymer. Thus an atomically clean surface can be prepared
or a particular oxide surface grown prior to polymer over-
growth. This technique elimiated the use of solvents,
which can introduce other complicating effects.

Table I. Comparison between spun and MBE PI

sample	spun		MBE	
Peak	E(eV)	I	E(eV)	I
P1	0.00	36.1	0.00	36.1
P2	1.03	34.2	1.03	36.1
P3	1.66	8.2	1.66	6.4
P4	4.04	13.8	4.04	12.4
P5	6.4,8.1	7.6	6.5,8.3	8.9

Spun-on polymer films can be used as substrates for
investigation of metal-on-polymer interfaces. Good poly-
imide surfaces can be prepared from as received, freshly
spun films. However, polyimide is known to be very suscep-
tible to water uptake. Heating to 350°in UHV appears to
regenerate the polyimide if it has been exposed to ambient
for any length of time. For polymer-on-metal studies when
using spun-on polyimide, the metal surface is mostly lim-
ited to a native oxide covered surface rather than atomic-
ally clean metal surfaces as these interfaces are not usu-
ally prepared under vacuum. This is nonetheless of great
interest as such metal surfaces are technologically im-
portant surfaces. One must be cautious about spun thin
films of 50A or less necessary for interface studies as
they may not be pinhole free. Solvent used in spun-on
films themselves may cause important effects (40-42). A-
gain this itself is of interest. Comparison of spun films
with MBD films can help to isolate the role of solvents in
reactions during the cure of the polymer (40).
        Peel tests, where the force to peel a strip of one
material (metal) from another (polymer) is measured, is a
common technique to obtain a measure of adhesion strength.

Both peeled surfaces subsequently can be analyzed by PES
to determine the point of failure (43). This can be use-
ful to distinguish between adhesisve and cohesive failure
as well as the presence of contamination at the point of
failure. It is limited in obtaining detailed information
about the initial interfacial chemistry as the peel is
normally performed ex-situ.
     Surface modification prior to metallization is ano-
ther important area of research. For example, presputter-
ing can be an important treatment for adhesion enhancement
(21,22) but contamination effects due to redeposition ef-
fects are common. Wet chemical treatments and dry (gas
phase) etchings are other areas of pretreatments under
active current investigation (44,45).

INFORMATION FROM PES

Core-level Spectra: One-hole States, Satellites, Relaxa-
tion. Core-level spectra have been the most utilized fea-
ture of PES investigations of polymers. The first stage
of polymer/metal interface studies is to obtain and under-
stand the spectra of the materials prior to interface for-
mation. Figure 6 shows C 1s spectra from two different
polyimides, PMDA-ODA and BPDA-PDA (bisphenyldianhydride-
phenyldiamine). These two polyimides have different chem-
ical structures which produce very different characteris-
tic core-level spectra. PMDA-ODA polyimide has been well
characterized and the main features of the core-level
spectra are well understood (46,47). The different ring
structure (different number of carbonyl groups on the
anhydride rings) between PMDA-ODA and BPDA-PDA leads to
different electron charge distribution thus the shifts
between the anhydride and amine rings is different in the
two polyimides. Figure 6 also shows the C 1s spectrum of
the polyamic ester of PMDA-ODA, an alternative precursor
to polyamic acid for the preparation of PMDA-ODA polyi-
mide. The polyamic ester spectra is of course quite dif-
ferent than the polyimides especially in the carbonyl re-
gion. However, upon curing, the polyimide formed is simi-
lar to the one form from the PMDA-ODA polyamic acid (com-
pare Figures 6a and 6d).
     Figure 7 follows the interface formation between Cr
and polyimide, both in the case of Cr on polyimide and
polyimide (initially polyamic acid) on Cr. The C 1s spec-
tra show significant changes as the interface developes.
There is actually a remarkable correspondence between the
two types of interfaces (48). N 1s and O1s spectra also
exhibit similar striking correspondence. These results
tend to support the reaction via the carbonyl moiety (32)
than the delocalized Cr arene complex formation interpre-
tation (30).
     Core-level spectra of the metal generally have been
little utilized in polymer/metal interface studies. Metal
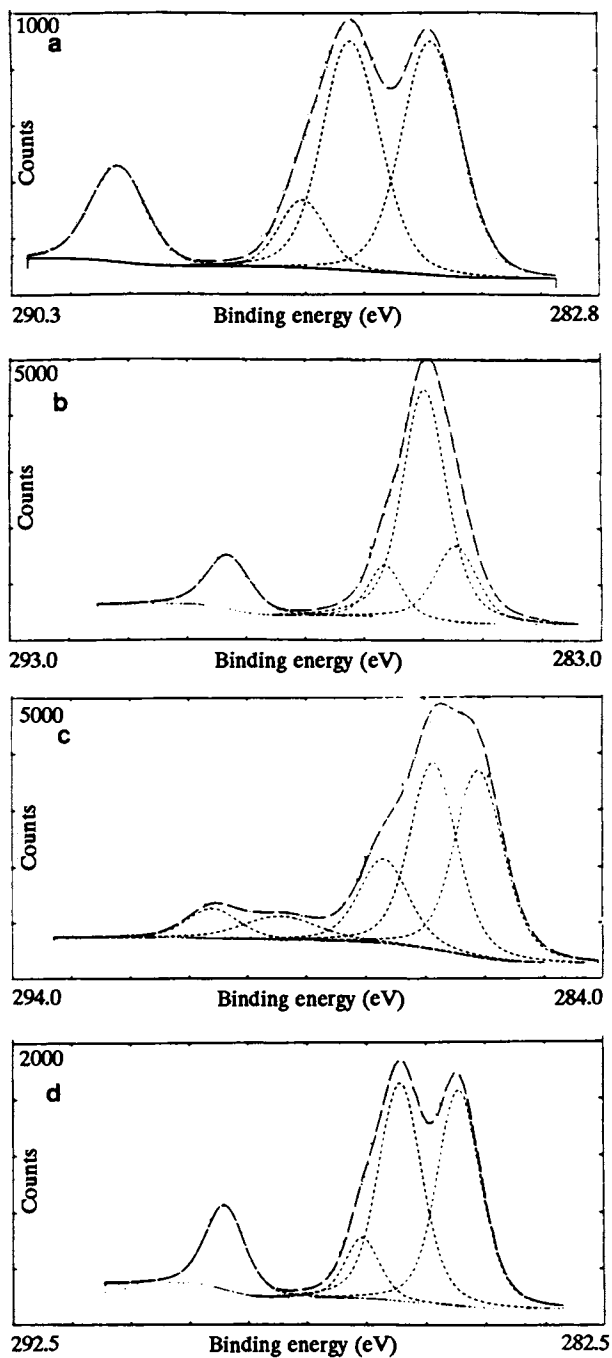core levels are often much broader than the C 1s, O 1s, or

Figure 6. Carbon 1s spectra from two different polyimides: (a) PMDA-ODA, (b) BPDA-PDA, (c) Polyamic ester, and (d) Cured polyamic ester.
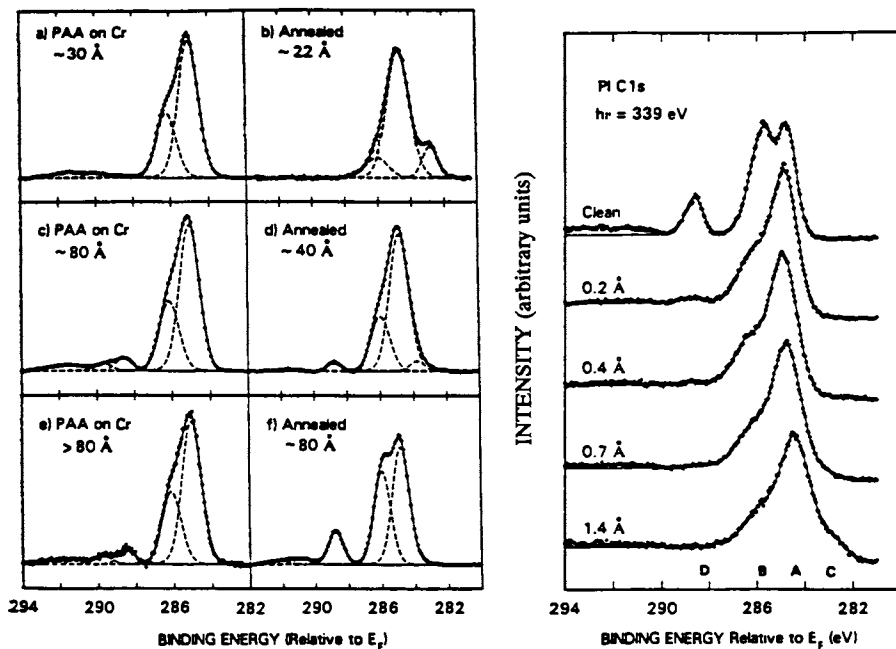
Figure 7. C 1s spectra from polyamic acid on Cr, cured polyamic acid on Cr (Reproduced from Ref. 48. Copyright 1989 American Chemical Society.) and Cr on polyimide interfaces. (Reproduced with permission from Ref. 32. Copyright 1987 American Physical Society.)

N 1s levels and the chemical shifts also tend to be small-
er(48,49). Figure 8 shows Cr 2p spectra where little
change is observed upon polyamic acid absorption although
corresponding C 1s and O 1s spectra (see Figure 7) show
disappearance of the carbonyl functional group. Upon cur-
ing there is evidence of considerable broadening on the
high binding energy side of the Cr 2p peak, evidence for
oxidation but not very much detailed information can be
deduced from this spectrum, while again the corresponding
C 1s, O 1s, and N 1s show the fragmentation of polyimide
the formation of carbides, oxides, and nitrides (48).
Figure 4, which shows the Si 2p spectra, is one case where
detailed structure about chemical information is observed
from the non-polymer core-level spectrum. Si +1, +2, and
+3 states can be clearly seen after spin-orbit deconvolu-
tion (48). It should also be noted that the interpreta-
tion of core-level shifts for small coverages of metal is
further complicated by size effects.

In any detailed interpretation of core-level spectra,
the entire spectral distribution must be taken into ac-
count to obtain a complete characterization. The C 1s
spectrum from an ODA film is shown in Figure 9. This
spectrum besides exhibiting the two main features corres-
ponding to the two types of inequivalent carbons in ODA,
exhibits weaker structure at about 6 eV higher binding
energy. These features are shake-up structures due to
multielectron transitions during the photoemission pro-
cess from a deep core level, e.g. π to π^* transitions.
These transitions which involve the highest occupied and
lowest unoccupied molecular orbitals give further infor-
mation concerning the electronic structure of these mater-
ials. Shakeups can have important effects on the observed
intensity distribution. In the case of PMDA the intensity
ratio of the two C 1s peaks is not the 1.50 expected by
stoichiometry (6 aromatic carbons/4 carbonyl carbons) but
1.42. Likewise for the ratio between the bridging O and
the carbonyl oxygen is 1.7 and not the stoichiometric 2.0.
Recent self-consistent extended basis set calculations
which have considered multielectron effects, relaxation,
etc., have given these ratios as 1.41 and 1.8, quite com-
patible with the experimental values (50). The missing
intensity is accounted for by considering the complete
photoemission process (50). Another consideration in
interpretation and data treatment is the inelastic back-
ground (51,52), which we will only mention here.

Valence-band Spectra: Electron Density of States. Valence
band spectra, which in the case of polymers are very molec-
ular-like as there is little dispersion in the bands, have
been less used, especially in polymer-metal interface
studies. They offer potentially much deeper understanding
of interactions but are harder to obtain and need to be
closely coupled to theoretical work for interpretation
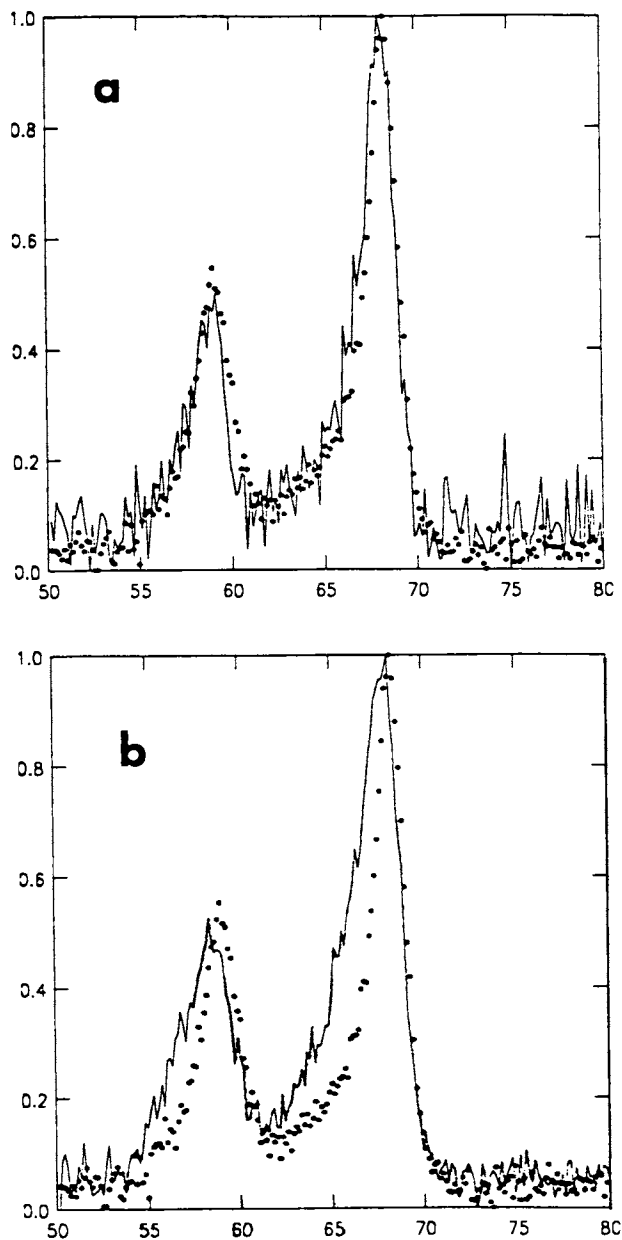(53). Recent theoretical studies of polyimide has shown

Figure 8. (a) Comparison of Cr 2p spectra of Cr metal with ~30A of polyamic acid coverage and (b) the same after cure of polyamic acid. The dotted spectrum in each case is from the initial Cr metal surface.

good agreement with photoelectron spectra (53). The next
step is to apply this information to the polyimide/metal
systems: (a) firstly, to observe which valence (molecular)
levels of the polymer are altered upon interface formation
and (b) to perform more sophisticated calculations direct-
ly on the polymer-metal system to see the molecular orbit-
al-metal valence-level interaction and the new valence-
level structure. Here synchrotron radiation may provide
an important advantage. The technique used in adsorbate
studies on metals to enhance adsorbate emission relative
to metal emission is quite applicable. This involves us-
ing cross-section modulation (54-57). For example at cer-
tain energies, the C 2p derived levels from the polymer
may be more intense than the metal d band, while at ano-
ther energy, these intensity ratios maybe reverse. The
variation of the C/metal ration as f(hv) can be quite sig-
nificant (56,57). The cross-section variation for polyi-
mide can be seen in Figure 10 which shows the polyimide
valence-band spectra in the range of $80 \leq hv \leq 1486.6$ eV.
With ultra violet sources (He I) the entire valence band
could not be obtained (29,58). Interestingly, the two
polyimides, PMDA-ODA and BPDA-PDA which showed such dis-
tinctly different core-level spectra (Figure 6) show quite
similar valence-band spectra (Figure 11) with only subtle
differences. Figure 12 and Figure 13 show the cross-sec-
tion modulation for polyamic acid on Cu and Cr. Detailed
analysis of these spectra will lead to further understand-
ing of the polymer-metal interaction.

Model Compounds. To simplify and refine interpretations
of polymer-metal interactions, model compounds have been
used to study specific interactions. In the case of metal-
on-polymer for example, Jordan-Sweet and co-workers have
used poly (methyl phenylene oxide) and poly (vinyl methyl
ketone) to study the Cu and Cr interactions with various
sites on polyimide (32). There have been fewer studies
using model compounds to study the inverse interface, poly-
mer-on-metal. Pthalimide has been used for model studies
of polyimide on Cu (59,60). There have been studies of
PMDA on Ag by Grunze et. al. (37,38). Figure 14 shows the
C 1s spectrum for a thick and a thin PMDA film on copper.
These spectra are similar to the results on silver by
Grunze and co-workers (37). Note the change of the car-
bonyl carbon relative to the aromatic carbon for the thin
film versus that for the thick film. This implies the
loss of approximately one of the four carbonyls upon inter-
action with the copper surface and that one of the remain-
ing carbonyls is in a different bonding configuration than
the other two carbonyls. Carboxylate complex formation is
likely. This explanation is consistent with the Grunze et
al interpretation for PMDA on Ag based on XPS and infra-
red reflectance absorption measurements (37). One must be
cautious because of beam effects mentioned above for PMDA,
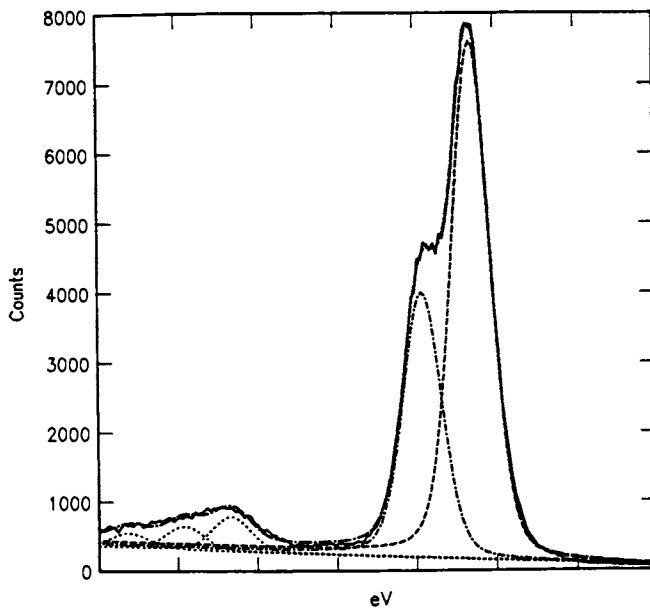but the first absorbed layer is probably more tightly
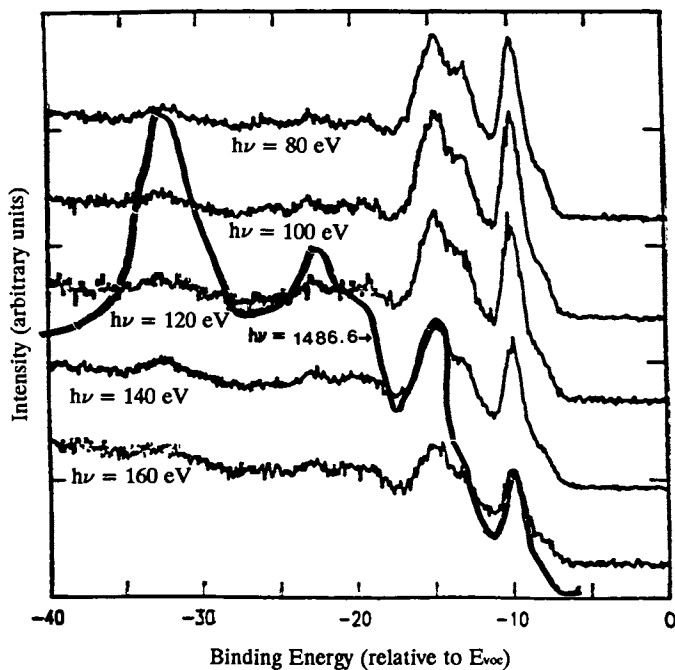
Figure 9.   C 1s spectrum from ODA.

Figure 10. Polyimide (PMDA-ODA) valence-band spectra as a function of photon energy.
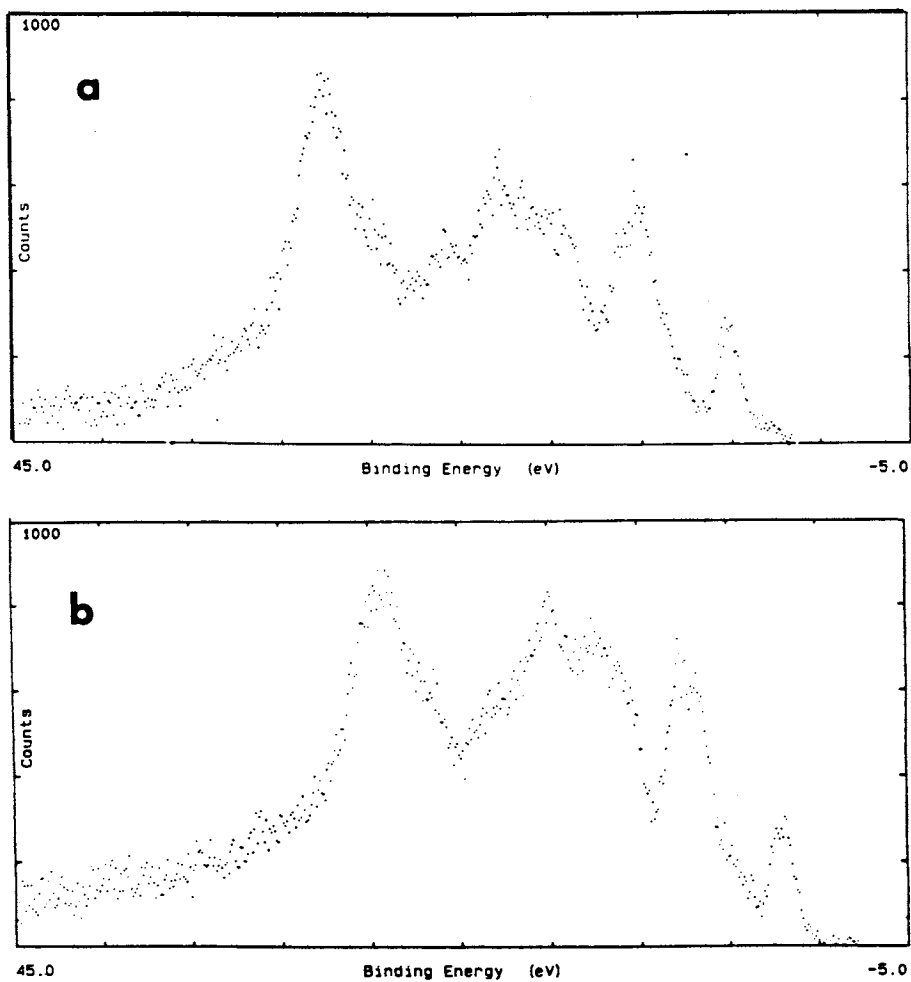
Figure 11. Valence-band spectra (hv = 1486.6 eV) of
(a) PMDA-ODA and (b) BPDA-PDA.

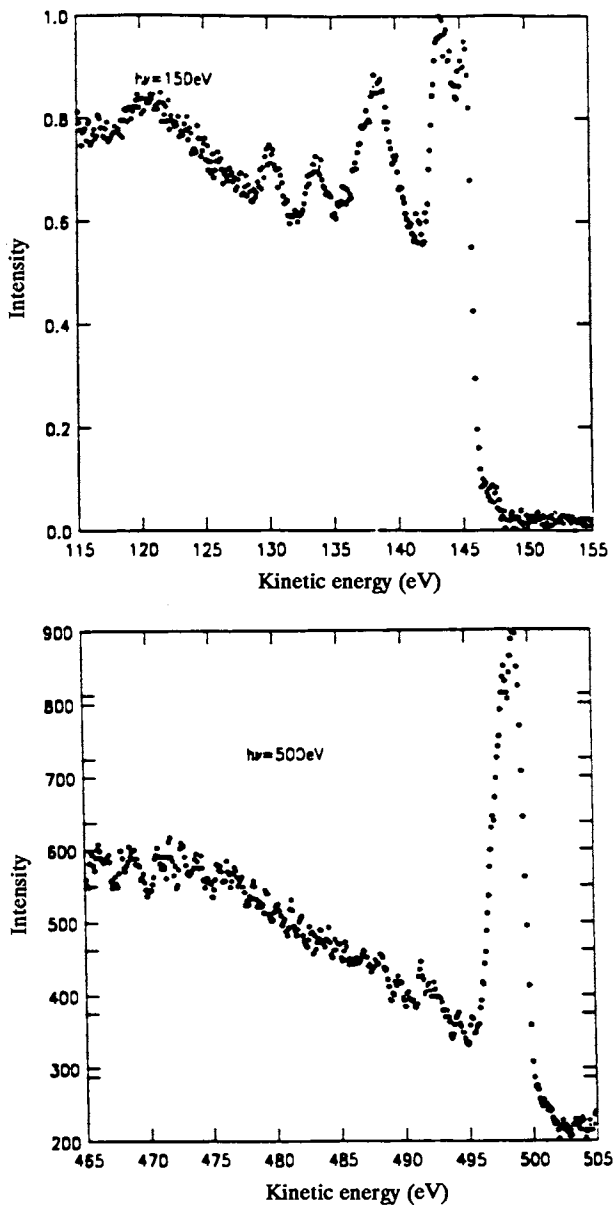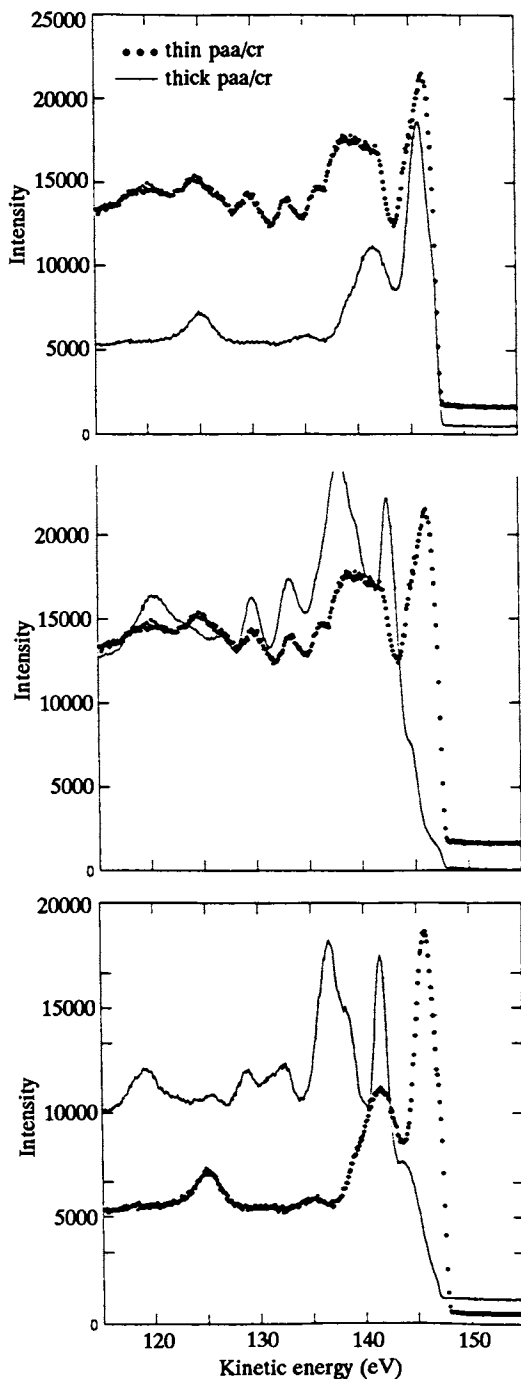Figure 12. Valence-band spectra from PMDA-ODA polyamic acid on Cu taken at hv = 150 eV and hv = 500 eV.

Figure 13. Valence-band spectra taken at hv = 150 eV
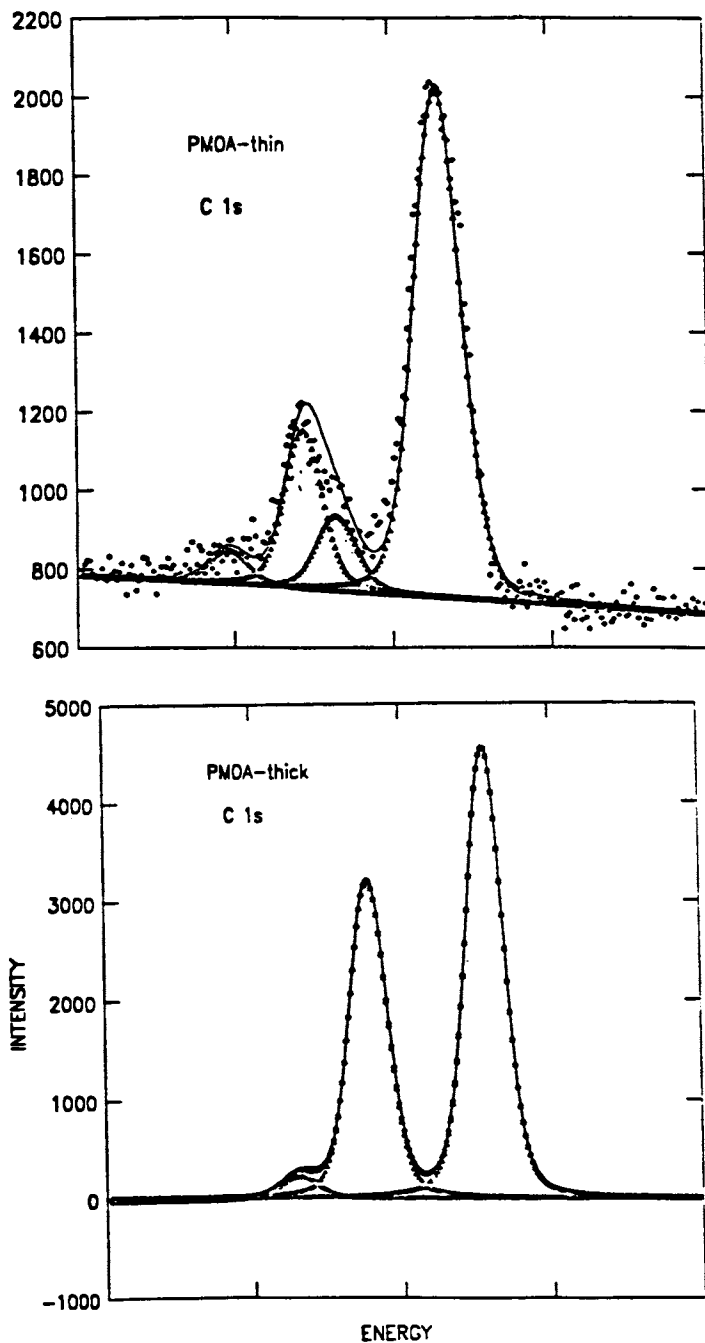for varying thickness of polyamic acid and polyimide
on Cr.

Figure 14. C 1s spectra from a thick and a thin PMDA film.

bound and stable than subsequent layers. One caveat to be
concerned about in directly applying results from model
compound studies to polymer systems is possible steric
and/or orientation effects in the larger polymer which may
hinder reactivity at nominally equivalent reaction sites.

SUMMARY

PES is an invaluable tool for the investigation of polymer
metal interfaces as long as certain experimental precau-
tions are observed. Interfacial interactions can be fol-
lowed from the initial submonolayer regime to the comple-
tion of the interface. Changes as a function of thermal
treatments can be followed. Both metal-on-polymer and
polymer-on-metal interfaces can be studied. Core-level
spectra are very good chemical fingerprint for which func-
tional sites are reactive. Information about bond break-
ing and molecular reorganization can be obtained. Model
compound studies are a useful complement to isolate the
role of specific interactions and to give insight to the
more complicated macromolecular systems. Valence-band
spectra coupled with sophisticated theoretical calcula-
tions will allow more detailed interpretation than avail-
able solely from core-level spectra. However, in compli-
cated systems such as these, it is important to couple
PES studies with results from other experimental probes
such as peel strength, transmission electron spectroscopy,
infrared spectroscopy, reflection electron energy loss
spectroscopy, etc. PES studies of the polyimide-metal
interfaces have already helped advance the understanding
of the role of interfacial chemistry in adhesion and
demonstrate the inequivalence of metal-on-polymer to
polymer-on-metal for polyimide/metal interfaces.

ACKNOWLEDGMENTS

LITERATURE CITED

1. Briggs, D. Ed.; <u>Handbook of X-ray and Ultraviolet Photoelectron Spectroscopy</u>; Heyden & Sons Ltd.: London, 1977.
2. Windawi, H.; Ho, F.F.L. Eds.; <u>Applied Electron Spectroscopy for Chemical Analysis</u>; John Wiley & Sons: New York, 1982.
3. Briggs, D.; Seah, M. P. Eds.; <u>Practical Surface Analysis by Auger and X-Ray Photoelectron Spectroscopy</u>; John Wiley & Sons Ltd.: Chichester, 1983.
4. Clark, D. T.; <u>Pure & Appl. Chem.</u>, 1982, <u>54</u>, 415/
5. Briggs, D.; <u>Polymer</u>;1984, <u>25</u>, 1379.
6. Dilks, A.; <u>Analytical Chem.</u>, 1981, <u>53</u>, 802A.
7. Pireaux, J. J.; Riga, J.; Caudano, R.; Verbist, J.; <u>Am. Chem.Soc. Symp.</u>; 1981, <u>162</u>, 169.
8. Salaneck, W. R; <u>CRC Crit. Rev. Sol. St. Mat. Sci.</u>; 1985, <u>12</u>, 267.
9. Leary H. J.,Jr.; Campbell, D. S.; <u>Surf. Interface Anal.</u>; 1979, <u>1</u>, 75.
10. Rothman, L. B.; <u>J. Electrochem. Soc.</u>; 1980, <u>127</u>,2216.
11. Wilson, A.M.; <u>Thin Solid Films</u>; 1981, <u>83</u>,145.
12. Lee, Y.K.; Fryd, M.; <u>In the Chemistry of the Semiconductor Industry</u>; Moss, S.J.; Ledwith, A. Eds.; Blackie; Glasgow, 1987; p. 282.
13. Schmitt, G.P.; Appelt, B.K.; Gotro, J.T.; <u>In Principles of Electronic Packaging</u>; Seraphim, D.P.; Lasky, R.C.; Li, C.Y. Eds.; McGraw Hill Book Company: New York, 1989; p. 334.
14. Tummala, R.R.; Keyes, R.W.; Grobman, W.D.; Kapur, S. <u>In Microelectronic Packaging Handbook</u>; Tummala, R.R.; Rymaszewski, E.J. Eds; Van Nostrand Reinhold: New York 1989; p. 673.
15. Siegbahn, K.; Nordling, C.N.; Fahlman, A.; Nordberg, R Hamrin, K.; Hedman, J.; Johansson, G.; Bermark, T.; Karlsson, S.E.; Lindgren, I.: Lindberg, B.; <u>ESCA: Atomic, Molecular, and Solid State Structure Studied by Means of Electron Spectroscopy</u>; Almqvist and Wiksell; Uppsala, 1967.
16. Seah, M.P.; Dench, W.A.; <u>Surf. Interface Anal.</u>; 1979, <u>1</u>, 2.
17. Powell, C.J.; <u>J.Electron Spectrosc.</u>; 1988, <u>47</u>, 197.
18. Barr, T.L.; <u>J.Vac.Sci. Technol.</u>; 1989, <u>17</u>, 1677.
19. Bachman, B.J.; Vasile, M.J.; <u>J.Vac. Sci. Technol.</u>; 1989, <u>A7</u>, 2709.
20. Bodo, P.; Sundgren, J.E.;<u>J.Vac. Sci. Technol.</u>; 1988, <u>A6</u>, 2396.
21. Vasile, M.J.; Bachman, B.J.;<u>J. Vac. Sci. Technol.</u>; 1989, <u>A7</u>, 2992.
22. Oh, T.S.; Kowalczyk, S.P.; Hunt, D.J.; Kim, J.; <u>J. Adhesion Sci. Technol.</u>; 1990, <u>4</u>.
23. Fadley, C.S.; <u>Prog. Sol. St. Chem.</u>; 1976,<u>11</u>, 265.
24. Bain, C.S.; Troughton, E.B.; Tao, Y,T.; Evall, J.; Whitesides, G.M.; Nuzzo, R.G.; <u>J. Am. Chem. Soc.</u>; 1989,<u>111</u>,321.

25. Chaney, R.L.; Surf. Interface Anal.; 1987, 10,36.
26. Burkstrand, J.M.; Am. Chem. Soc. Symp.; 1981, 162, 339.
27. Waldrop, J.R.; Cohen, M.J.; Heeger, A.J.; MacDiarmid, A.G.; Appl. Phys. Letters; 1981, 38,53.
28. Chou, N.J.; Dong, D.W.; Kim, J.; Liu, A.C.; J. Electrochem. Soc.; 1984,131, 2335.
29. White, R.C.; Haight, R.; Silverman, B.D.; Ho, P.S.; Appl. Phys. Letters; 1987, 51,481.
30. Haight, R.; White, R.C.; Silverman, B.D.; Ho, P.S.; J. Vac. Sci. Technol.; 1988,A6, 2188.
31. Ohuchi F.S.; Freilich, S.C.; J. Vac. Sci. Technol.; 1986, A4, 1039.
32. Jordan, J.L.: Kovac, C.A.; Morar, J.F.; Pollak, R.A.; Phys. Rev.; 1987, B36, 1369.
33. Clabes, J.G.; Goldberg, M.J.; Viehbeck, A.; Kovac, C.A.; J. Vac. Sci. Technol.; 1988, A6, 985.
34. McFeely, F.R.; Terminello, L.J.; Kowalczyk, S.P.; Appl. Phys. Letters; 1990,22.
35. Salem, J.R.; Sequeda, F.O.; Duran, J.; Lee, W.Y.; Yang, R.M.; J. Vac. Sci. Technol.; 1986, A4, 369.
36. Grunze M.; Lamb, R.N.; J. Vac. Sci. Technol.; 1987, A5, 1685.
37. Grunze M.; Lamb, R.N.; Chem. Phys. Letters; 1987, 133 283.
38. Lamb, R.N.; Baxter, J.; Grunze, M.; Kong, C.W.; Unertl, W.N.; Lamgmuir; 1988, 4, 249.
39. Grunze, M.; Baxter, J.P.; Kong, C.W.; Lamb, R.N.; Unertl, W.N.; Brundle, C.R.; In Deposition and Growth: Limits for Microelectronics; Rubloff, G.W., Ed.; American Institute of Physics; New York, 1988; p. 355.
40. Kowalczyk, S.P.; Kim, Y.H.; Walker, G.F.; Kim, J.; Appl. Phys. Letters; 1988, 52, 375.
41. Kowalczyk, S.P.; Kim, Y.H.; Walker, G.F.; Kim, J.; J. Vac. Sci. Technol.; 1988, A6, 1377.
42. Kim, Y.H.; Kim, J.; Walker, G.F.; Feger, C.; Kowalczyk S.P.; J. Adhesion Sci. Technol.; 1988, 2, 95.
43. Buchwalter, L.P.; Lacombe, R.H.; J. Adhesion Sci. Technol.; 1988, 2, 463.
44. Lee, K.W.; Kowalczyk, S.P.; In Metallization of Polymers; Sacher, E.; Pireaux, J.J.; Kowalczyk, S.P., Eds.; American Chemical Society: Washington,D.C.1990.
45. Matienzo, L.J.; Emmi, F.; Egitto, F.D.; Van Hart, D.C. Vukanovic, V.; Takacs, G.A.; J. Vac. Sci. Technol.; 1986, A6, 950.
46. Buchwalter, P.L.;Baise, A.I.; In Polyimides; Mittal, K.L., Ed.; Plenum: New York, 1984; 537.
47. Silverman, B.D.; Bartha, J.W.; Clabes, J.G.; Ho, P.S. J. Polymer Sci.; 1986, A24, 2325.
48. Kowalczyk, S.P.; Jordan-Sweet, J.L.; Chem. Mat.; 1989 1, 592.
49. Clabes, J.G.; J. Vac. Sci. Technol.; 1988, A6, 2887.

50. Bagus, P.S.; Coolbaugh, D.; Kowalczyk, S.P.; Pacchioni, G.; Parmigiani, F. Proc.; <u>4th Int. Conf. on Electron Spectroscopy</u>; 1989, px.
51. Tougaard, S.; <u>Surf. Interface Anal.</u>; 1988,11,453.
52. Bernasconi, J.; Cartier, E.; Pfluger, P.; <u>Phys. Rev.</u>; 1988, <u>B38</u>, 12567.
53. Kowalczyk, S.P.; Stafstrom, S.; Brédas, J.L.; Salaneck W.R.; Jordan-Sweet, J.L.; <u>Phys. Rev.</u>; 1990, <u>B41</u>,1645.
54. Gelius, U.; <u>In Electron Spectroscopy</u>; Shirley, D.A., Ed.; North Holland: Amsterdam, 1972; p.311.
55. Cavell, R.G.; Kowalczyk, S.P.; Ley, L.; Pollak, R.A.; Mills, B.; Shirley, D.A.; Perry, W.; <u>Phys. Rev.</u>; 1973 B7, 5313.
56. Wehner, P.S.; Kevan, S.D.; Williams, R.S.; Davis, R.F. Shirley, D.A.; <u>Chem. Phys. Letters</u>; 1978, <u>57</u>, 334.
57. Yeh, J.J.; Lindau, I.; <u>At. Data Nucl. Data Tables</u>; 1985,32,1.
58. Hahn, P.O.; Rubloff, G.W.; Ho, P.S.; <u>J. Vac. Sci. Technol.</u>; 1984, <u>A2</u>, 756.
59. Salaneck, W.R.; Stafström, S.; Bredas, J.L.; Andersson S.; Bodö, P.; Kowalczyk, S.P.; Ritsko, J.J.; <u>J. Vac. Sci. Technol.</u>; 1988, <u>A6</u>, 3134.
60. Stafström, S.; Bodö, P.; Salaneck, W.R.; Bredas, J.L.; <u>In Metallization of Polymers</u>; Sacher, E.; Pireaux, J.J.; Kowalczyk, S.P., Eds.; American Chemical Society Washington, D.C., 1990.

Chapter 3

Using Near-Edge Soft X-ray Absorption Spectroscopy To Study Organic Polymers and Metal–Polymer Interactions

Jean L. Jordan-Sweet

T. J. Watson Research Center, IBM Corporation, Box 218, Yorktown Heights, NY 10598

The near-edge structures of C1s, O1s and N1s absorption spectra reveal a significant amount of information about the excited electronic states of organic materials. Near-Edge (NEXAFS) spectra typically show two types of features. Sharp peaks just below or above the K-edge represent transitions from core levels to unoccupied π^* molecular orbitals. Broader peaks at higher photon energies represent transitions from core levels to the higher- lying σ^* molecular orbitals. Systematic studies by others of simple organic molecules and polymers have laid a groundwork for what types of information can be obtained with NEXAFS spectroscopy.

These principles were used to assign C1s, O1s and N1s NEXAFS spectra of polymers important to the microelectronics industry. Interpretation of polyamic acid and polyimide spectra were aided by assigning the spectra of simpler polymers and monomers. The compounds studied in the form of spun films were poly(vinyl methyl ketone) (PVMK), poly(dimethyl phenylene oxide) (PMPO), poly(pyromellitimido 4,4-methylene bis-cyclohexyl amine) (PMDA-MBCA PI), and poly(pyromellitimido oxydianiline) (PMDA-ODA PI); and in the form of MBE-deposited films were poly(amic acid) (PAA), and PMDA-ODA PI. Changes in the NEXAFS spectra as a function of evaporated Cr overlayer thickness were measured for PVMK, PMPO and PMDA-ODA PI. Evolution of the NEXAFS spectra as a function of deposited organic film thickness and thermal treatment were measured for PAA on Cu and Cr substrates.

This paper will discuss the use of Near-Edge X-ray Absorption Fine Structure (NEXAFS) Spectroscopy to study the unoccupied π^* molecular orbital (MO) structures of polymers and polymer-metal interfaces. A collection of systematic NEXAFS and EELS studies of simple organic compounds by J. Stöhr and others (1-10) has led to recent advances in the understanding and interpretation of this technique. It's application to complicated polymers and polymer-metal interactions has only begun, but NEXAFS spectroscopy promises to be an important complement to other photoelectron spectroscopies.

Knowledge of the low-lying unoccupied state electronic structure of a system provides information about the physical extent and location of antibonding orbitals and their interactions (overlap) with nearby antibonding orbitals. Changes in the energies of, transition probabilities to, and occupation lifetimes of these electronic states imply changes specific chemical bonds. For example, involvement of the π^* or σ^* MO's of a molecule in chemisorption onto a substrate or in reaction with a deposited metal atom can be seen as energy shifts, intensity changes and/or broadening in the near-edge absorption peaks pertaining to those MO's. Thus, the monitoring of NEXAFS spectral changes as a function of metal deposition onto a polymer or of polymer formation and thermal treatment yields information about chemical bond changes which are of great interest to industries concerned with metallization of polymers.

Section II of this paper contains a description of the mechanism of NEXAFS spectroscopy, experimental setup and the types of information that can be obtained. Section III presents examples of work by others which serve as an important basis for the interpretation of our studies, and also several experiments on oriented polymer films and Langmuir-Blodgett films. Section IV describes a study of the chemical interaction that takes place when chromium metal is evaporated onto spun polymers, including polyimide. Section V describes the results of a study of poly(amic acid) films grown by epitaxy on clean surfaces of copper and chromium, and the effect of annealing to induce imidization.

Background

NEXAFS spectroscopy complements Ultraviolet Photoelectron Spectroscopy (UPS) and X-ray Photoelectron Spectroscopy (XPS) (Figure 1). In XPS, electrons are excited from a core electronic level out into the vacuum and detected by an electron energy analyzer. The difference between the excitation energy and the kinetic energy of the detected photoelectron yields the binding energy of an electron in that core level orbital. Because these core electrons are relatively tightly bound, XPS binding energies undergo only small shifts of one or two eV as a result of changes in the electronic environment around the nucleus (due to oxidation, reduction, covalent bonding changes, etc.). UPS probes the valence bond structure of materials. Changes in bonding result in drastic changes in the UPS spectrum which requires calculations for detailed interpretation. NEXAFS, on the other hand, is a probe of the unoccupied electronic states and is element-specific like XPS. A core level (usually K-shell) electron is excited into an antibonding molecular orbital by an incident photon of the correct energy. Once the system is in an excited state, there is Coulombic attraction between the core hole and the excited electron (exciton) which decreases the energy of that excited state (11,3). If the antibonding orbital was just above the vacuum level before being occupied, this Coulombic attraction can can pull it below the ionization potential for the core level when it becomes occupied. In this case, commonly for π^* LUMO's, the transition results in a bound state which is localized at the atom. When the exciton returns to its ground state, its energy is dissipated by either Auger processes or by fluorescence.

Transitions to higher-lying σ^* orbitals result in broader, higher energy "shape" resonances, which are trapped between the excited atom and its neighbor along the σ bond (11,3). It has been shown (1-3) that the energy (above the ionization potential) of a σ^* shape resonance is inversely proportional to the bond length between the atoms, provided that the resonance is localized between them. NEXAFS transitions follow dipole selection rules, so that the transition probability is maximized when the electric vector of the exciting electromagnetic wave is parallel to the p atomic orbital component of the final state molecular orbital (11,4).

The experimental setup requires a source of photons which can be tuned through the K-edge of the element of interest. For all of the studies presented in this paper, this is the carbon K-edge at ~285 eV. If the orientation of the σ^* or π^* or-
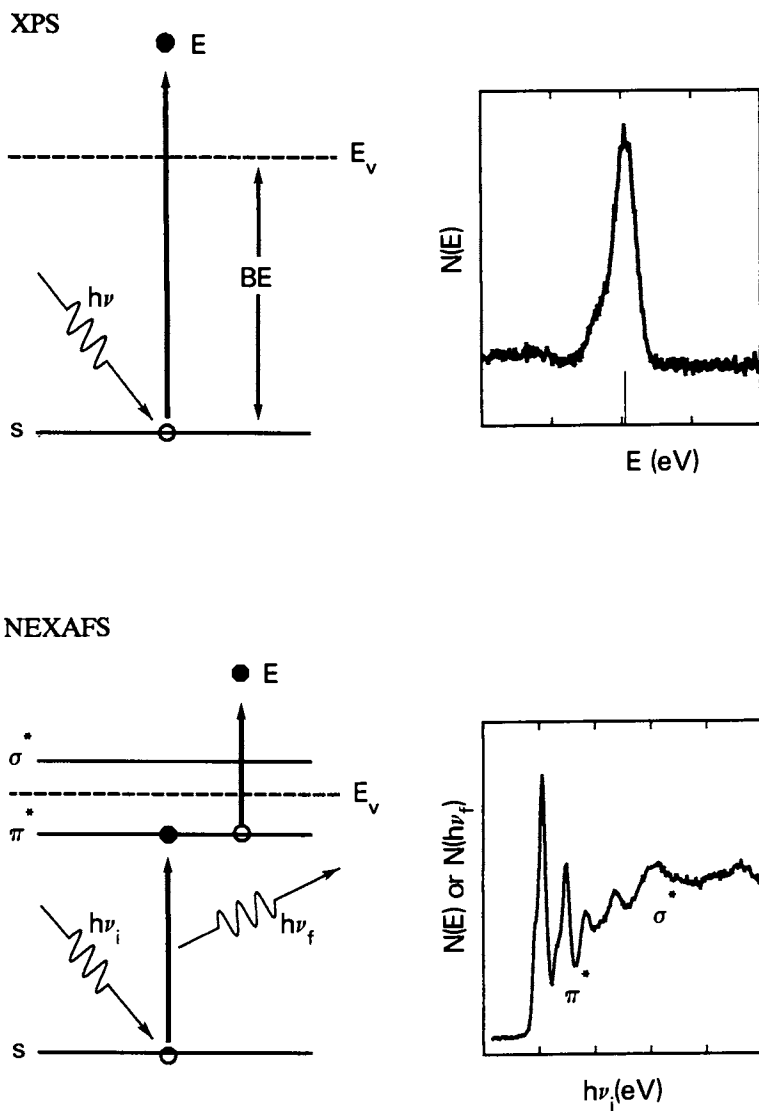
XPS

NEXAFS

Figure 1: Schematic representations and spectra for XPS and NEXAFS mechanisms.

bitals is to be determined, a polarized source and rotatable sample holder are required.   As with all photoelectron spectroscopies and surface studies, a UHV environment is essential.   Finally, an appropriate detector must be used.   For fluorescence detection this can be a Si(Li) or other narrow-energy-window x-ray detector.   For secondary electron collection a CMA, Channeltron or channel plates can be used, preferably with a large acceptance angle so that angle-dependent emission effects can be ignored.

For the studies presented in Sections IV and V, measurements were taken at IBM   Beamline U8B (12)   at the National Synchrotron Light Source. Monochromator energy resolution at the carbon K-edge was ~0.2 eV.   A display analyzer (13) with channel plates was used to detect secondary electrons in an 8 eV window centered at ~42 eV.   This energy was selected so that only the most surface-sensitive (minimum escape depth) electrons were detected.

NEXAFS spectra are taken by measuring the secondary electron yield as a function of incident photon energy from just below the edge to several tens of eV above it. (The oscillations in the edge structure at higher energies are EXAFS and are due to interference between photoelectrons emitted from an atom and those backscattered from neighboring atoms.)   The spectra must be normalized to the transmission function of the beamline optics.   This is essential for carbon NEXAFS spectra because optical surfaces are almost always coated with carbon contaminants which absorb light in the same energy region.   This "light curve" is a NEXAFS spectrum of a carbon-free material such as Si(111), gold, or a clean substrate in the case of chemisorption studies.   The material must not have XPS, UPS, Auger or NEXAFS transitions in the spectral window.   The normalized NEXAFS spectrum must also be calibrated in energy by comparison to a spectrum taken of a "standard", such as graphite for carbon K-edge NEXAFS.   If polarization studies are to be done, a series of spectra with varying angle of incidence are taken.   Curve fitting (14) and quantitative polarization analysis (15) are quite complicated and will not be discussed here.

The types of information that can be derived from NEXAFS spectra are summarized here and will be demonstrated by the examples in the next section.   First, as stated previously, changes in molecular orbitals can be detected as energy shifts (from changes in final state energy levels), broadening (from decreases in excited state lifetimes), and intensity changes (from changes in the transition probability to an excited state).   Second, it has been demonstrated (10) that for localized resonances the spectrum of a complex molecule can be analyzed as the sum of resonances from the individual functional groups contained in the molecule.   Molecules or polymers containing delocalized MO's, such as conjugated π systems, must be analyzed much more carefully.   Third, bond lengths can be empirically derived from positions of σ^* resonances (1-3) if the molecule is not too complex and if the σ bonds are localized. Fourth, molecular orientation of adsorbed species or drawn films can be determined by analyzing the dependence of π^* and σ^* resonance intensities on the angle between the electronic vector of the incident polarized photon beam and the substrate surface (4,11,15).

Other Work

D.A. Outka *et al.* have measured the carbon K-edge NEXAFS for a series of organic alcohols and carboxylic acids of increasing complexity (10).   In all but one case, each successive alcohol or acid spectrum contained features of the simpler alcohol or acid plus new features from the added functional group.   For example, the n-propanol spectrum contained a shape resonance for the C-C and C-O C1s→σ^* transitions (close in energy) and a C-H* resonance which is found at ~287 eV for all organic species containing hydrocarbon functional groups (6,8,9).   The allyl alcohol spectrum contained those features, plus π^* and σ^* resonances for the additional C=C double bond.   When the alkene group was substituted by an alkyne group in propargyl al-

cohol, the $\sigma*$ resonance shifted to higher energy. The effect of interaction between nearby π MO's was shown for the case of propiolic acid. The two normally degenerate p_x* and p_y* atomic orbitals on the carbon-carbon triple bond were split by the nearby carbonyl $\pi*$ MO. Thus, three $\pi*$ resonances appeared where normally only two might have been expected. Heating of the propargyl alcohol showed degradation of the alkyne $\pi*$ resonance and a small amount of conversion to alkene $\pi*$

J.A. Horsley *et al.* performed a study of gas phase, condensed and monolayer benzene on Pt(111) (4). In order to identify correctly the four features observed in the spectrum of the solid, they looked at the polarization dependence of the monolayer spectrum and performed a multiple scattering Xα MO calculation. The first two features, maximized at glancing incidence, were assigned to the first and second highest $\pi*$ MO's (e_{2u} and b_{2g}). The second two features were most intense for normal incidence and were assigned to the first and second-plus-third highest $\sigma*$ MO's (e_{2u} and $e_{2g} + a_{2g}$).

J. Stöhr *et al.* verified the $\pi*$ character of the C-H* resonance at ~287 eV by studying the polarization dependence of oriented polyethylene film (9). The C-H* resonance was maximized at glancing incidence (E perpendicular to the film surface and alkane chains). The C-C $\sigma*$ resonance was maximized at normal incidence (E parallel to the alkane chains). Detailed analysis of the polarization dependence was required since the alkane chain is not linear, but has 109° kinks in it because of the sp^3 C-C bond angle.

D. Outka *et al.* have studied the orientation of several Langmuir-Blodgett monolayers on oxidized Si(111) (16). By very detailed curve fitting and polarization dependence analysis they determined that arachidic acid ($CH_3(CH_2)_{18}CO_2H$) was not ordered, Cd arachidate was ordered normal to the substrate surface, and Ca arachidate was tilted 33° from the surface normal.

A recent study of poly(di-n-hexylsilane) films by V.R. McCrary *et al.* (17) measured the polarization dependent C1s and Si2p NEXAFS spectra, EXAFS, and UPS as a function of temperature. Above 42°C it was found that the hexyl side chains were disordered and that the Si backbone was partially disordered (no longer an all-trans configuration). Below 42°C there was coexistence of the disordered phase with the well-ordered (all-trans backbone and side chains) phase.

Metal-Polymer Studies

In order to investigate the chemical interaction between evaporated chromium and spun polyimide using NEXAFS spectroscopy it was necessary to analyze the spectra of several model polymers. These model polymers contained subsets of the many functional groups contained in poly(pyromellitimido oxydianiline) (PMDA-ODA PI). Figure 2 shows the structures and carbon K-edge NEXAFS spectra for three model polymers and PMDA-ODA PI. Details of the spectral assignments are given in reference 18. The poly(vinyl methyl ketone) (PVMK) was outgassed in UHV at room temperature. The poly(dimethyl phenylene oxide) (PMPO) was outgassed by heating in UHV. The polyimides were spun as polyamic acids and were outgassed and thermally imidized in UHV.

PMPO represents the ODA part of PMDA-ODA PI and has four $\pi*$ resonances at 285.5, 287.2, 289.2 and 290.6 eV. These result from transitions from C1s core level states of two different energies (carbon bonded to C and H, and carbon bonded to C and O or C and N) to the two lowest $\pi*$ MO's for the arene ring π system. PVMK contains a carbonyl group and has an intense, sharp carbon NEXAFS peak at 286.7 eV attributable to a C=O $\pi*$ resonance, and a smaller peak at 288.7 eV from the C-H* resonance. Poly(pyromellitimido 4,4'-methylene bis-cyclohexyl amine) (PMDA-MBCA PI) represents the PMDA part of PMDA-ODA PI without the added complication of any other π systems. As in the previously discussed case of propiolic acid, the arene and carbonyl $\pi*$ MO's on this polymer are in close enough proximity to interact and shift in energy. Thus, the arene $\pi*$ reso-
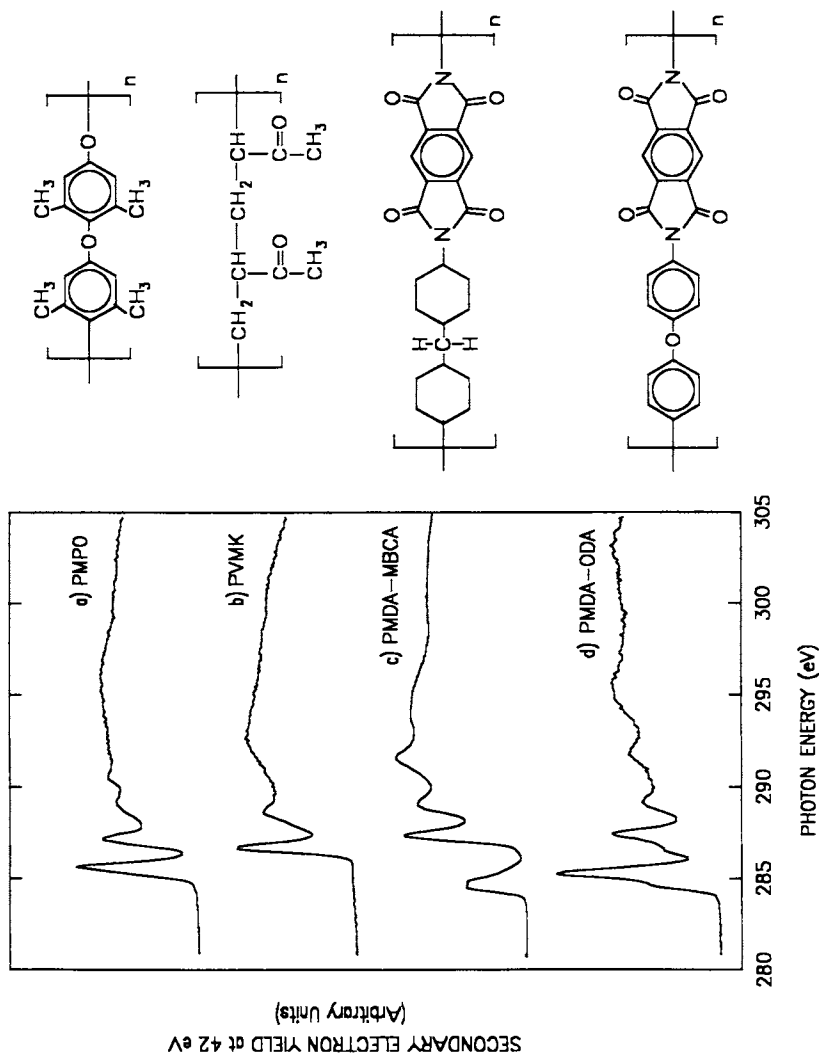
Figure 2: Protomer structures and carbon K-edge Nexafs spectra of a) poly(methyl phenylene oxide) or PMPO; b) poly(vinyl methyl ketone) or PVMK; c) PMDA-MBCA polyimide; and d) PMDA-ODA polyimide.

nance is shifted to lower energy (284.8 eV) than that expected, and the carbonyl π^* resonance is shifted to higher energy (287.4 eV). The C-H* resonance is also in this energy region. The third peak, at 289.1 eV is attributed to a second-lowest C=C π^* resonance and the fourth is the C-C σ^* resonance for the cyclohexyl ring carbon atoms.

The peaks in the PMDA-ODA PI spectrum can be assigned by adding together the spectra for PMPO and PMDA-MBCA PI. The shoulder at 284.8 eV is assigned to the π^* resonance for the PMDA arene ring. The peak at 285.2 eV and shoulder at 286.6 eV are transitions to the ODA π^* LUMO from the two different C1s core levels (carbon bonded to C and H, and carbon bonded to C and O or C and N). The carbonyl group π^* LUMO resonance appears at 287.4 eV. The peak at 289.2 contains contributions from PMDA and ODA second lowest C=C π^* orbitals. The remaining peaks are shape resonances.

Figure 3 shows the sequences of NEXAFS spectra for PMPO, PVMK and PI with increasing coverages of chromium. Cr metal was evaporated from a resistively heated tungsten basket, using a calibrated quartz crystal microbalance to monitor coverage. Coverages are given in Angstroms, such that one monolayer of close-packed Cr atoms has a thickness of 2.6 Å. The sequence of spectra for Cr on PMPO shows less than 5% change in relative peak intensity ratios within a given spectrum, and no shifts in energy. This implies little or no change in the polymer MO's and thus that no chemical bonding changes have occurred during early stages of metallization. The lack of any significant change discounts the formation of a Cr-arene organometallic complex because the intermixing of Cr 3d orbitals with arene π^* orbitals would produce additional features in the spectrum and broaden and probably shift the arene π^* resonance. Such features have been observed, using EELS, for $(c\text{-}C_6H_8)Fe(CO)_3$ [19] and bis-cyclopentadienyl transition metal complexes [20]. With increasing Cr coverages the NEXAFS spectra degrade as a result of attenuation by the overlayer and are "filled in" by contributions from the metal continuum states.

The sequence of spectra for PVMK show a marked relative depletion of carbonyl π^* peak intensity, implying that Cr strongly interacts with the carbonyl functional group. A small peak arises at ~285 eV, possibly due to the formation of graphite-like species.

Deposition of Cr onto PMDA-ODA PI results in significant intensity changes in the C1s→PMDA π^* and C=O π^* features. The difference spectrum of clean PI minus .04Å Cr/PI shows ~16% and 20% decreases in relative intensity, respectively. Again, Cr is interacting most strongly with the carbonyl groups on the PMDA part of PI. Because the π system on the PMDA part is delocalized, both the carbonyl and arene π systems are affected. Once again, there is no evidence for Cr-arene organometallic complex formation. The results from this NEXAFS study agree well with XPS studies on the same systems [18].

Polymer-Metal Studies

A study of the "inverse" situation of polymer-on-metal interaction was made recently, using a combination of core-level XPS and NEXAFS measurements [21]. Poly(amic acid) films were grown on clean, amorphous Cu and Cr substrates by codeposition of PMDA and ODA from resistively heated quartz cells under UHV conditions. The films were then annealed at ~200°C to promote imidization. The carbon NEXAFS results are shown in Figures 4 and 5. Figure 4a shows the spectrum for ~22Å of PAA on clean Cu. (The XPS spectra for this and a bulk film of PAA show no differences). The strong peak at 285 eV is at the resonance energy for transitions from the arene ring carbon atoms. The peak at 287 eV is attributed to the ODA ring π^* LUMO and to the amide carbonyl π^* LUMO. The peak at 288 eV is assigned to the carboxylic acid carbonyl π^*, as reported by Outka et al. [10]. Figure 4b shows the NEXAFS spectrum for the annealed film. It is quite similar to
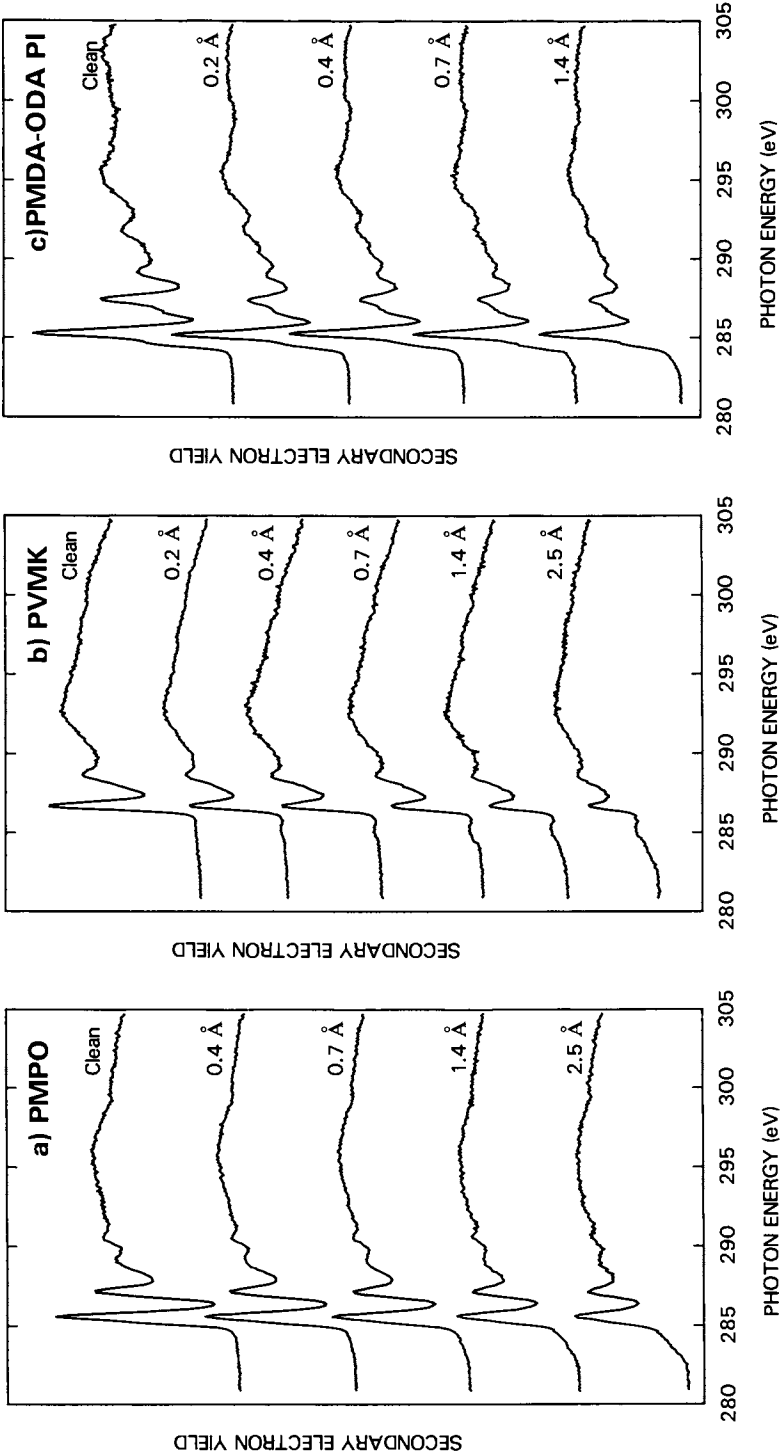
Figure 3: K-edge NEXAFS spectra of a)PMPO, b) PVMK, and c) PMDA-ODA PI as a function of increasing chromium coverage. Abscissa is partial electron yield, centered at 42 eV with a bandpass of 8 eV.
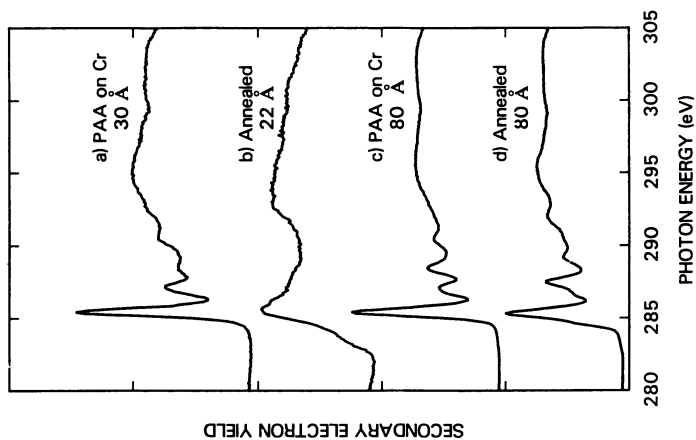
Figure 5: C K-edge NEXAFS spectra for a) a thin film of PAA grown on clean amorphous chromium; b) the annealed thin film; c) a thicker PAA film deposited over the annealed thin film; and d) the annealed thicker film.
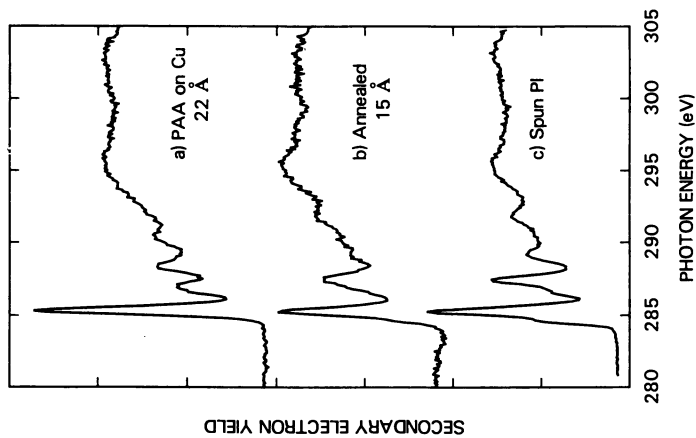

Figure 4: C K-edge NEXAFS spectra for a) a thin film of PAA grown on clean amorphous copper; b) the annealed thin film; and c) a spectrum of cured spun PMDA-ODA PI for comparison.

the spectrum for a spun polyimide film (Figure 4c) which is described in Section IV. There is perhaps some depletion in the carbonyl and PMDA ring π^* resonance intensities, in agreement with XPS results. One can conclude that PAA film grown on Cu surfaces may interact through the carbonyl groups, but that no significant molecular rearrangement or fragmentation occurs at the interface.

Figure 5 shows a sequence for PAA grown on a Cr surface. The $\sim$30Å PAA film spectrum differs from that in Figure 4a. There is strong disruption of the carbonyl groups. After annealing the spectrum bears no resemblance to that of PI. There is a loss of distinct π^* features, with some remnant of C=C π^* intensity remaining. A shoulder has grown in at low energy, perhaps implying the presence of carbide-like species, as concluded by XPS studies (21). Figures 5c and d show that a thicker film of PAA grows normally on top of this reacted interface, and imidizes to form PMDA-ODA PI.

Summary

The purpose of this paper is to introduce the technique of NEXAFS spectroscopy to scientists and engineers interested in the analysis of polymers and metal-polymer interfaces. NEXAFS is just coming into its own as a powerful tool for studying bonding interactions and molecular orientation of fairly complicated systems. By presenting background material and examples of applications to metal-polymer systems, it is hoped that the reader will be left with a basic understanding and an impression of the potential of this technique.

Acknowledgments

Literature Cited

1. Stöhr, J.; Gland, J.L.; Eberhardt, W.; Outka, D.; Madix, R.J.; Sette, F.; Koestner, R.J.; Doebler, U. Phys. Rev. Let. 1983, 51, 2414.

2. Stöhr, J.; Sette, F.; Johnson, A.L. Phys. Rev. Let. 1984, 53, (17), 1684.

3. Sette, F.; Stöhr, J.; Hitchcock, A.P. J. Chem. Phys. 1984, 81, (11), 4906.

4. Horsley, J.A.; Stöhr, J.; Hitchcock, A.P.; Newbury, D.C.; Johnson, A.L.; Sette, F. J. Chem. Phys. 1985, 83, (12), 6099.

5. Hitchcock, A.P.; Horsley, J.A.; Stöhr, J. J. Chem. Phys. 1986, 85, (9), 4835.

6. Hitchcock, A.P.; Newbury, D.C.; Ishii, I.; Stöhr, J.; Horsley, J.A.; Redwing, R.D.; Johnson, A.L.; Sette, F. J. Chem. Phys. 1986, 85, (9), 4849.

7. Johnson, A.L. Ph.D. Thesis, University of California, Berkeley, 1986, (LBL-20964).

8. Hitchcock, A.P.; Ishii, I. Electron Spectrosc. Rel. Phenom. 1987, 42, (1), 11.

9. Stöhr, J.; Outka, D.A.; Baberschke, K.; Arvanitis, D.; Horsley, J.A. Phys. Rev. B 1987, 36, (5), 2976.

10. Outka, D.A.; Stöhr, J.; Madix, R.J.; Rotermund, H.H.; Hermsmeier, B.; Solomon, J. Surf. Sci. 1987, 185, 53.

11. Stöhr, J.; Jaeger, R. Phys. Rev. B 1982, 26, (8), 4111.

12. Himpsel, F.J.; Jugnet, Y.; Eastman, D.E.; Donelon, J.J.; Grimm, D; Landgren, G.; Marx, A.; Morar, J.F.; Oden, C.; Pollak, R.A.; Schneir, J. Nuclear Instrum. and Methods 1984, 222, 107.

13. Eastman, D.E.; Donelon, J.J.; Hein, N.C.; Himpsel, F.J. Nuclear Instrum. and Methods 1980, 172, 327.

14. Outka, D.A.; Stöhr, J. J. Chem. Phys. 1988, 88, (6), 3539.

15. Stöhr, J.; Outka, D.A. Phys. Rev. B 1987, 36, 7891.

16. Outka, D.A.; Stöhr, J.; Rabe, J.P.; Swalen, J.D. J. Chem. Phys. 1988, 88, (6), 4076.

17. McCrary, V.R.; Sette, F.; Chen, C.T.; Lovinger, A.J.; Robin, M.B.; Stöhr, J.; Zeigler, J.M. J. Chem. Phys. 1988, 88, (9), 5925.

18. Jordan-Sweet, J.L.; Kovac, C.A.; Goldberg, M.J.; Morar, J.F. J. Chem. Phys. 1988, 89, (4), 2482.

19. Hitchcock, A.P.; Wen, A.T.; Rühl, E. J. Electron Spectrosc. (Proc. 4th Int. Conf. on Electron Spectroscopy), 1989.

20. Rühl, E; Hitchcock, A.P. J. Am. Chem. Soc. 1989, 111, 5069.

21. Kowalczyk, S.P.; Jordan-Sweet, J.L. Chem. Materials 1989, 1, 592.

Chapter 4

High-Resolution Electron Energy Loss Spectroscopy

Application to Polymer Surfaces and Polymer–Metal Interactions

Jean-Jacques Pireaux, Ch. Grégoire, M. Vermeersch, P. A. Thiry, M. Rei Vilar[1], and R. Caudano

Facultés Universitaires Notre-Dame de la Paix, Laboratoire Interdisciplinaire de Spectroscopie Electronique, Rue de Bruxelles 61, B–5000 Namur, Belgium

A few years ago, High Resolution Electron Energy Loss Spectroscopy (HREELS) - also named electron induced vibrational spectroscopy - has been successfully applied to characterize the composition and geometrical structure of polymer surfaces. In this review, the attributes of HREELS will be demonstrated and compared to the ones of other surface-sensitive spectroscopies. Special emphasis will be laid on the very unique information that can be obtained from the study of the incipient metallization stages of a well-defined polymer, i.e. a cured polyimide film.

It is now recognized that for the characterization of a material surface, it is of utmost importance to combine different surface sensitive techniques. This is certainly true also for the study of polymer surfaces, and for our better understanding of the interaction between evaporated metal atoms and a polymer.

X-ray photoelectron spectroscopy (XPS), SIMS (Secondary Ion Mass Spectroscopy) and nuclear-reaction-based analyses (like RBS - Rutherford Backscattering -, and PIXE - Proton Induced X-ray Emission) have already proven their complementary potentialities.

High Resolution Electron Energy Loss Spectroscopy has been "discovered" at about the same time as the previous cited techniques - the first reported experiment is related to a study of small molecules adsorbed on a (100)W surface and is dated from 1967 ($\underline{1}$). During the last 15 years, the characterization of adsorption states of molecules on metal and semiconductor surfaces was the principal attribute of HREELS : information on the elemental composition, on the chemistry, and the kinetics of surface reactions (versus temperature and/or time) were studied. One significant "plus" of HREELS is its ability to identify adsorption sites on a metal, by using the "dipole-selection rule" : it is therefore possible to gain information on the short-scale structure or morphology of a surface with HREELS.

The study of polymer surfaces would certainly greatly benefit from HREELS contributions, electron-induced vibrational spectroscopy being often presented as the surface counterpart of the classical optical infra-red and Raman spectroscopies. However, the first HREEL spectra from polymer surfaces were published only in 1985 for thin organic films ($\underline{2}$), in 1986 for a real insulating thick polyethylene

[1]Current address: LASIR–CNRS, Rue H. Dunant 2, F–94320 Thiais, France

sample (3), and in 1987, for true high resolution work presenting spectra similar in quality to IR ones (4-5) !

The reasons for this delay are probably manifold :

1° polymers, being anything else than clean metal or semiconductor single crystals, were probably frightening HREELS and UHV users ;

2° chemically and structurally, polymers are quite complicated and ill-defined materials ; from optical spectroscopies, one knows their vibrational fingerprints are very complex ;

3° most of the polymers are insulators : charging effects are expected to severely perturb HREELS experiments ;

4° being anything else than small molecules adsorbed on a metal, polymers will not benefit from the dipole-selection rule : quantification of HREELS results from polymers should start from a new or modified theory.

It is therefore understandable that the first HREELS measurements were performed on Langmuir-Blodgett ordered layers, thin polyimide films and conducting polymers (2). Nowadays, almost any polymer surface could be analyzed with HREELS.

The purpose of this review is threefold : 1° to briefly present the electron energy loss experiment ; 2° to demonstrate its attributes for polymers, as compared to the ones of other spectroscopies ; 3° to apply the potentialities of the spectroscopy to a study of the metallization of a polyimide (PMDA-ODA) film. Literature examples will be used for these illustrations.

The HREELS experiment

To exploit surface sensitivity, the experiment is performed in ultra-high vacuum, in the backscattering geometry (Figure 1) : the monochromatized electron beam directed towards the polymer surface ("in" beam) excites molecular vibrations : these energy losses are analyzed on the "outgoing" beam. The most useful information are collected when varying two parameters : the electron impact energy usually ranges from 1 to 10 eV, the scattering geometry (incident and collection angles θ_i, θ_r) is defined by rotating the analyzer (A) and/or the sample holder. In order to resolve the manifold of polymer vibrational bands, the highest instrumental resolving power is needed : however, even with a spectrometer capable of reaching 2.5 meV resolution (measured at full width at half max on the elastic peak, 1 meV = 8,066 cm^{-1}), the narrowest line width recorded up to now is about 7 meV, with current performance in the range of 10 to 14 meV (80 → 110 cm^{-1}). As will be shown later on, this allows one to resolve most of the vibrational bands, but not to the limit of detection of crystallinity or structural details, possible with IR spectroscopy.

Most organic polymers being insulators, charging problems on the material surface must be dominated in order to collect a meaningful vibrational spectrum ; this can be achieved in two ways : 1° by studying very thin (≈ 150 Å) polymer films, deposited onto a conducting substrate (2, 4-6) ; 2° by utilizing a particular "flood gun" accessory, tuned to deliver a defocussed beam of low intense current (< 1 µA) of high energy electrons (1 to 2 keV) (7,3). In the latter case, one has to monitor and avoid any polymer degradation caused by the auxiliary gun.

The attributes of HREELS

Sensitivity : an intensity-resolution compromise regarding IR spectroscopy. It is probably mandatory first to evidence that the HREELS spectroscopy allows one to record a useful vibrational spectrum, i.e. to detect at least the molecular groups

present on the polymer surface. Figure 2 combines several recordings from the same polyimide material : this PMDA-ODA was prepared as a thin (200 Å) film on a silicon wafer by spin coating and curing as usual (4). After introduction into the spectrometer, spectrum A (Figure 2) was recorded : even with an elastic peak (at zero loss energy : 0 cm^{-1}) presenting a "normal" resolution (in this case, 85 cm^{-1}), the spectrum is characterized by rather broad features : in fact, the poorly resolved bands do not allow the experimentalist to recognize a polyimide material ! However, when the same sample is heated *in vacuo* (500 to 530 K for several tens of minutes), all the vibrational bands appear much sharper (spectrum B, Figure 2). Now, about twenty vibrational bands are clearly distinguished as peaks, or shoulders. An IR absorption curve obtained from the same polymer (8) is helpful in the data interpretation and peak identification (Figure 2c). Without going into details (that are presented at length elsewhere (5)), we would just like to mention here that all the vibrational bands detected in the HREELS spectrum are seen on the IR absorption signal (and vice-versa). There is, indeed, a one-to-one correspondence between the electronic and photonic excited bands with - up to now - no systematic difference between the peak positions. However, it is very clear that the peak intensities as recorded by the two spectroscopies are very different ! This suggests - and we shall develop this point later on - that different excitation mechanisms, and thus different selection rules are governing HREELS and IR spectroscopy.

The polyimide data (Figure 2) allow us to point out to another ensemble of conclusions regarding HREELS results. 1° For polymers in general, the *intensity* ratio between the loss peak heights and the elastic peak is very high, much higher than for an adsorbate-substrate system where magnification factors in the range of 10^2 to 10^3 have to be used. There is therefore plenty of signal from a polymer surface ... but with a rather poor *resolution* ; 2° this in fact should not be a major concern for the experimentalist : Figure 2 proves that a measured resolution of 80 cm^{-1} indeed allows one to record a spectrum almost as good as an IR one ! 3° One notes moreover that HREELS is very surface sensitive, as it allows one to detect easily water adsorbed onto the polymer (Figure 2a) : at first sight, this might appear as a very good benefit ... counterbalanced by a severe drawback. For metal or semiconductor adsorption studies, it is indeed possible to prepare a "clean" substrate by heating, ion sputtering, etc. Cleaning procedures are not allowed for a polymer material, except a gentle heating. Thus, it might never be possible to study by HREELS a defined "clean" polymer surface. 4° Finally, we like to point out that HREELS spectra (Figure 2) show a very intense C-H stretching band, between 2800 and 3100 cm^{-1}. This is at variance with IR results : we shall specifically make use of this observation, keeping in mind at the same time that this is evidence that both electronic **and** photonic excited spectra are not governed by the same interaction mechanisms. The theoretical interpretation of HREELS should follow different schemes !

To summarize this section, we present HREELS as a new spectroscopy, with attributes similar to the IR ones, but with a very high surface sensitivity, and a different quantification procedure.

Surface characterization regarding other electron spectroscopies. To evidence specific attributes of HREELS to be compared to ESCA (XPS), UPS or AES ones, we chose to present (Figure 3) spectra recorded from polystyrenes (9). These thin film samples were made from normal and fully deuterated polymers. Immediately, it appears that HREELS is really capable of adding a new and unique dimension to electron surface analyses as :
1° hydrogen (and deuterium) is readily detected, through molecular vibrations, e.g.
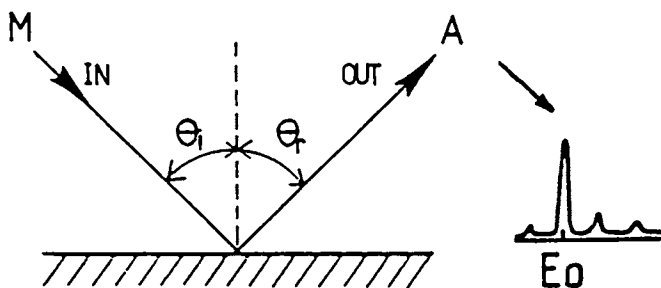
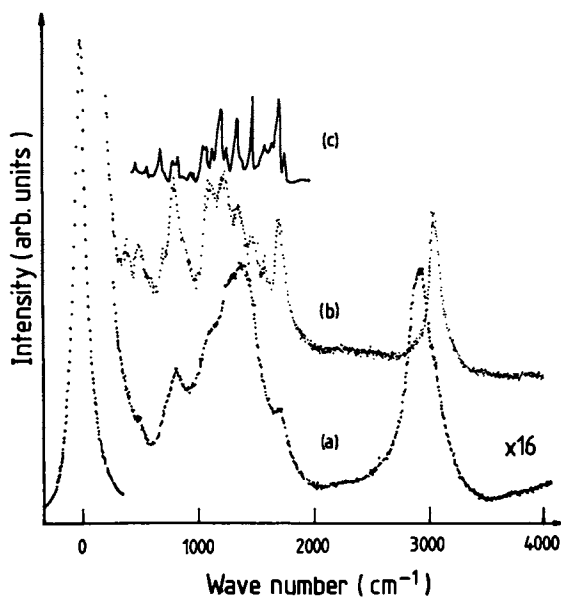Figure 1.   Schematized HREELS experiment, in the backscattering geometry.

Figure 2.   Vibrational fingerprints from a polyimide surface : (a) and
(b) electron induced spectra of a sample as introduced, and after heating *in
vacuo*, respectively ; (c) infrared optical absorption spectrum adapted from
Ref. 8.

of C-H$_x$ chemical groups on these specific polymers, but also of O-H or N-H functionalities ;

2° CH$_x$ species can be differentiated, as stretching bands of methyne, methylene and methyl groups in the 2800 to 3100 cm^{-1} region. Thus, HREELS allows a ready identification of aliphatic and aromatic species, as shown on Figure 3a : clearly, the v(C-H) band contains two structures at 2900 and 3040 cm^1, attributed to skeletal and phenyl C-H stretching, respectively. The v(C-D) stretching band around 2240 cm^{-1} can be deconvoluted in the same way, in accordance to IR band positions (9).

3° The loss region between 1000 and 2000 cm^{-1} contains bands related to deformation modes of the polymer : when studied in detail, these losses should provide similar to IR spectroscopy "molecular" information on the conformation, morphology, even crystallinity of the polymer chain. Some promising examples will be presented below.

Sensitivity and depth resolution. The use of a low energy electron beam to excite molecular vibrations physically guarantees a very high surface specificity (10).

As an example, Figure 3b shows that, for the fully deuterated polystyrene - thus containing no hydrogen anymore - CH stretching modes are still detected around 3000 cm^{-1}. Multiple excitations, combination modes or overtones cannot be excluded ; e.g. combination of the intense bands at 810 and 2240 cm^{-1} could explain the right-hand side peak, at the "phenyl-like" C-H stretch position (3000 cm^{-1}). But the peak at 2900 cm^{-1} is not attributed : as IR and proton NMR do not detect either hydrogen or contaminant in the deuterated polymer, we must conclude that the HREEL spectrum is evidence for : 1° terminating hydrogen atoms on the polymer chain, if chain ends are preferentially located at the surfaces. Indeed, an experiment with deuterated polystyrenes differing only by end groups produces different v(C-H) fingerprints (9) ; 2° slight surface contamination by aliphatic molecules during the film casting and/or handling. Presently, we favour the hypothesis of segregation of chain ends at the polymer surface, because this has been evidenced for polyethylene (3), and because polymers are thought - in comparison with metal and semiconductor surfaces - as the less reactive or more stable surfaces.

A possible application of the HREELS extreme surface sensitivity could be a differentiation of chemical groups present on a polymer surface when varying its tacticity. Again, by studying polystyrene, we discovered that "isotactic" films are mainly composed of phenyl rings, whereas the "atactic" ones expose equally their saturated skeleton and unsaturated pendent groups (9). As further evidence of this very attractive application of HREELS, Figure 4 reports spectra of polymethylmethacrylate films deposited on different metallic substrates : gold, aluminum and copper respectively (8). Focussing our attention on the C=O stretch band around 1710 cm^{-1}, we note that - everything else being ignored - this vibration is intense for the gold substrate (Figure 4a), for Al (b) also, but invisible for Cu (d). Moreover, on Al at low temperature (100 K), no v(C=O) stretch is detected (Figure 4c). Even if we are unable to quantify these results, we already have a good feeling that the polymer tacticity *and* the substrate nature might influence *for thin films* the average spatial conformation of the polymer monomeric unit at its very interface with the vacuum, during these HREELS experiments.

Therefore, HREELS is capable, like SIMS, of disclosing molecular, long-range information on the polymer surface. However, at this stage, it is fair enough to address our ignorance of the influence of the substrate on the vibrational response of a polymer thin film ! What are the effects of substrate *quality* - pure metal or with native oxide ? -, *roughness* on the atomic scale, and *polarizability* ? Authors (8,11) do feel these external parameters must be controlled and taken into account.
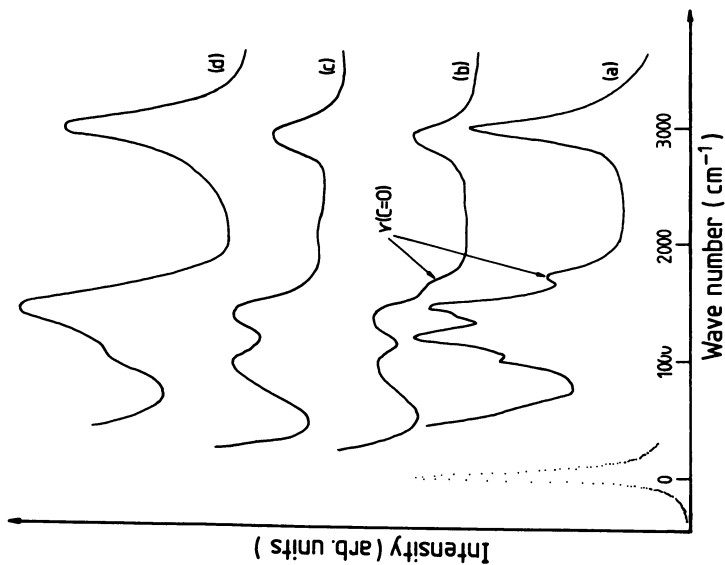
Figure 4. HREELS spectra of polymethylmethacrylate films deposited (a) on gold, (b) and (c) on aluminum, (d) on copper (the data for b through d are adapted from ref. 8). All data were collected at room temperature, except spectrum (c) (100 K).
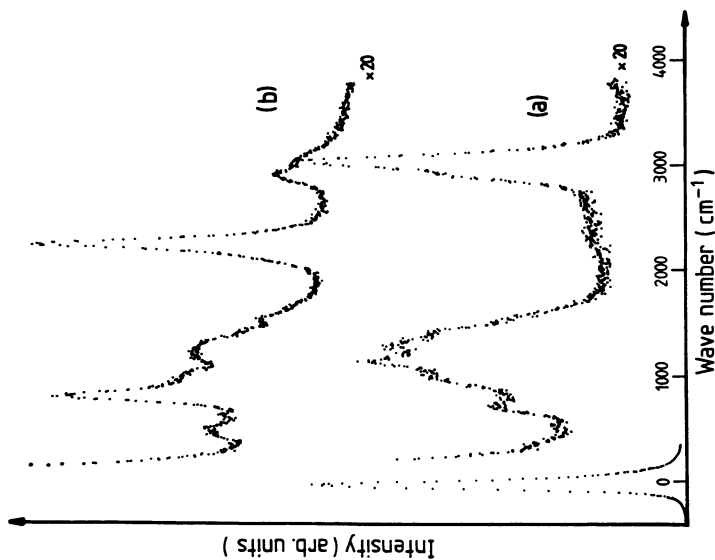

Figure 3. HREELS spectra of (a) 70% isotactic hydrogenated polystyrene, (b) atactic fully deuterated polystyrene.

Quantification. The proven success of HREELS in studying adsorbate-substrate systems is largely due to the very significant quantitative results gained on the substrate *coverage*, the adsorbate site *location*, and its *orientation* in the space. This is possible by using the dipolar theory, and the dipole selection rule imposed by the metallic substrate. It has been demonstrated (12) that polymers and polymer films behave and thus can be considered as condensed gases. However, there is a pronounced difference between (sub)monolayer coverages, and 100 to 200 Å thin polymer layers ! Referring to the questions asked in the previous paragraph, one can reformulate another more precise and crucial one : will the metallic substrates induce a dipole selection rule or will the electron beam solely interact with the polymer films ?

Facing the present lack of theoretical understanding of the phenomenon, there is at least one experimental test to assess a possible electron-polymer dipole coupling. The measurement of cross-section curves, i.e. vibrational band intensity versus electron impact energy, should produce a E^{-1} curve (13). Therefore, from the numerous vibrational bands clearly resolved on the clean polyimide spectrum (Figure 2b), three peaks were selected at 3060 cm^{-1}, 1720 cm^{-1} and 800 cm^{-1}, corresponding to ν(C-H), ν(C=O) vibrations and ring deformation modes respectively. Their intensities were monitored when varying the electron beam energy from 0.5 to 10 eV. Curves presented on Figure 5 are well approximated by straight lines, with slopes ranging from -1.5 to -2.0, i.e. significantly different from the factor -1 predicted for a pure dipole coupling (13). This observation suggests that no known symmetry or selection rule can now be applied, and that most probably low energy electrons are being scattered from polymer films by local impact interaction. No practical theory is thus now available to quantify the electron-induced vibrational spectra of polymers, and certainly research in this field is worthwhile and will be undertaken.

The metal-polyimide interface

The stake. The knowledge of the chemical reactions at the bonding interface between an evaporated metal layer and a polymer film is a research topic of interest to any scientist trying to improve adhesion in multilayers systems. For obvious reasons, *conventional infrared spectroscopy* cannot be of any help when studying metallized polymers since the light probe would be screened by the metal. When proceeding from the polymer side, conventional IR spectroscopy lacks the surface sensitivity to separate vibrational bands from the interface. As for *HREELS*, one could think of studying buried interfaces ($\approx$ 100 Å). Indeed, it has been shown that the electromagnetic field accompanying the probing electron can be coupled to phonon dipoles of a deep interface (14). However, we have shown here that for polymers, the dipolar interaction is most probably supplanted by another coupling mechanism. Being essentially of local nature, the electron excitation of a polymer vibrational band is *per se* restricted to the very surface of the material. Therefore, the sole practical way to study with HREELS a metallized polymer is to monitor polymer vibrational bands during (or sequentially with) the metal evaporation and condensation on its surface. Shifts or intensity modifications of vibrational bands during the incipient metal-polymer interface formation would teach the scientist at which site the metal atoms are landing and what kind of chemical reaction (if any) is developing.

The background. As an example, for polyimide in particular, and more precisely for PMDA-ODA, the key issue is the determination of the most reactive chemical groups of the monomeric unit : among other sites, the imide carbonyl (C=O) group and ring structures in the PMDA or ODA part are most often cited, depending on the metal used to cover the polyimide film. A priori, one can expect that metallic elements sensibly differing by their electronic structure (e.g. Al, with 3p electrons, Cr with 3d electrons or Cu with 4s electrons) would present different kinetic behaviour when reacting with PMDA-ODA, or different reaction sites, resulting in different values of adhesion test measurements. As for Cr bonding to polyimide, reaction with the imide carbonyl group (15a) and with the ring structures in PMDA (15b) have both been suggested by XPS results. The same spectroscopy allowed one to conclude that Cu interacts primarily with the PMDA segment (15c), ... or with the ODA part of a model molecule and with the PMDA one of another test system (15d). As for Al evaporation, synchrotron photoemission was used to discover that Al preferentially occupies planar imide rings, and that bonding occurs first at carbonyl sites (15e), what has been correlated by HREELS results (5), as it will be shown in the next section.

More recently, other data were published, still adding more confusion to the problem. First, an infrared (absorption reflection) spectroscopic study of Cr and Cu metallization of polyimide suggests that the carbonyl groups in the PMDA part are the primary reaction sites, with no complex formation on the aromatic rings. The changes were similar in nature (but not in intensity) for Cr and Cu (15f). On the other hand, on the basis of study of chemical reactions of Cr [$Cr^0(CO)_3(MeCN_3)$ reactant] with several polyimide model compounds, it was demonstrated that *neither* the carbonyl groups *nor* the anhydride ring are the thermodynamically preferred bonding sites. Cr^0 prefers to form π-arene complexes rather than react with oxygen functionalities. This study did not address, however, the question of relative kinetic accessibility of the different bonding sites of polyimide (15g). Finally, based on molecular orbital calculations, *simulations* of XPS data have shown that Cr located above the central ring of PMDA satisfactorily reproduces actual experimental data, provided it is assumed that reacted and unreacted PMDA/Cr species coexist. Other calculations of the *vibrational* band modifications induced by Cr deposition on PMDA show significant spectral changes mainly of the carbonyl stretches, and suggesting new HREELS measurements in the submonolayer coverage regime (15i).

The *HREELS* contribution : Al-polyimide *interaction* (5)

Using a UHV Knudsen cell to evaporate aluminum *in situ*, it was possible to reach a very low evaporation rate (0.1 to 1 Å/min), and consequently to study submonolayer coverage of the polyimide film. These PMDA-ODA layers (deposited on gold covered silicon wafers) were previously heated *in vacuo* to remove surface contaminants (Figure 2). From an extensive analysis (5), we choose to present one particular spectrum (Figure 6b), corresponding to about 10^{-1} of an aluminum layer (i.e. roughly $1.2 \; 10^{14}$ atoms/cm^2). This data is to be compared to the fingerprint of the clean surface (a), and for that purpose, assignments of the major features of the vibrational spectra are superimposed.

From right to left, the ν(C-H), ν(C=O), two ν(C$_6$H$_4$), ν(C-N), ν(C-O-C) and ν(OC$_2$)NC vibrational bands - measured respectively for the pure polymer at 3057, 1721, 1593 and 1488, 1379, 1247 and 1119 cm^{-1} - are clearly resolved, allowing us to note that some bands are affected, and others not, by the aluminum deposition. These effects appear much enhanced on Figure 6c presenting the
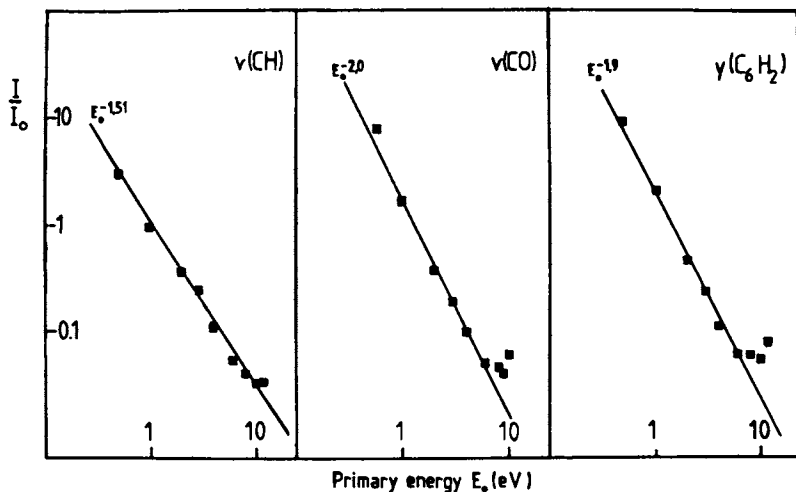
Figure 5. HREELS cross-section curves (peak height normalized to the elastic peak intensity) for the excitation of selected molecular vibrational bands of polyimide. The dielectric theory predicts a E^{-1} behaviour.
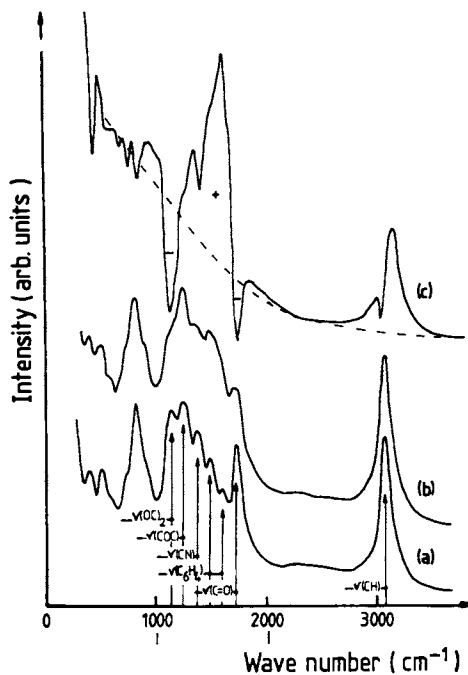

Figure 6. HREELS study of the aluminum-polyimide bonding : (a) clean polymer film ; (b) with about 1.2 10^{14} Al atoms/cm^2 ; enlarged difference spectrum (b-a).

difference spectrum (b-a), even if this spectrum is difficult to read, because the two original data presented a very different background slope. The two most severely *attenuated bands* are located at 1720 and 1120 cm^{-1}. They correspond to the carbonyl (C=O) stretch and the in-phase elongation of the two opposite carbonyls in the (C=O)$_2$NC entity. The interaction of the first evaporated Al atoms is thus clearly localized close to the C=O sites. Less intense is the simultaneous decrease of the v(C-N) band.

The *intensity increase* between 1600 and 1400 cm^{-1} is in fact attributed (a) to a gain of oscillators strengths of the v(C$_6$H$_4$) ring stretches, which might testify (b) of an intensity transfer of the two v(C=O) and v(C-N) bands (red and blue shifts respectively). The C-O-C ether linkages at about 1250 cm^{-1} are not affected at all by this first stage of the metallization.

Quite surprising in the difference spectrum (Fig. 6c) is the large increase in the stretching (C-H) band intensity, just above 3000 cm^{-1}. In a second analysis, it might perhaps be correlated to the vibrational intensity increase between 1400 and 1600 cm^{-1} (v (C$_6$H$_4$) bands), and the statu quo (or slight intensity decrease) of the v(C$_6$H$_2$) at 820 cm^{-1}. The six carbon ring atoms of the ODA segment behave differently than the PMDA arene CH groups ! We rationalize these observations in the following way : the first deposited Al atoms on the polyimide surface do interact preferentially with the carbonyl oxygen atoms ; due to the high electronic delocalization in the PMDA entity, C-N vibrational bands are also modified. As for the ODA part of the polymer, it is not touched by the incipient metallization (the C-O-C bonds remain intact). But, perhaps initiated by electronic cloud perturbation developing on PMDA, the conformation of the ODA rings is modified : the relative orientation of these C-H bonds flips in space, increasing the intensity of the v(C-H) stretching vibrational bond.

Summarizing, the very first Al atoms deposited onto the polyimide surface do interact electronically with the carbonyl PMDA electrons and induce a conformation change in the ODA entities.

The Cr-Polyimide interaction (2b,8,16)

In an early HREELS study of Cr deposition onto polyimide (2b,8), bonding interactions of the Cr atom affecting the carbonyl stretching vibrations were clearly evident. In a further attempt to gain more details on the chemistry developing at the metal-polymer interface, another preliminary set of spectra was recently collected during the metallization of a polyimide film deposited directly onto a silicon wafer (with its native oxide) (Fig. 7).

It is immediately evident (Fig. 7a) that this PMDA-ODA film spun onto Si presents an HREELS spectrum of poor quality (though the sample preparation was exactly similar for the recording of Fig. 6a and 7 a). The general shape of the polyimide vibrational spectrum is still recognizable, but all the bands are broadened, forbidding a clear identification of the chemical groups on the polymer surface. Approximately 1.5 and 4.5 10^{14} Cr atoms/cm^2 were evaporated on this sample (Fig. 7b and c) : this operation induced still a larger broadening of the whole HREELS spectrum, a modification of the general shape of the background and some slight changes in the vibrational bands : 1) the v(C-H) stretching band at $\pm$ 3000 cm^{-1} flattens and shifts to the red, as if v(C-H) aliphatic signal is present ; 2) no drastic attenuation of the v(C = O) stretching mode is detected, but the band might also shift to the red ; 3) the vibrational bands located around 1200 cm^{-1} are
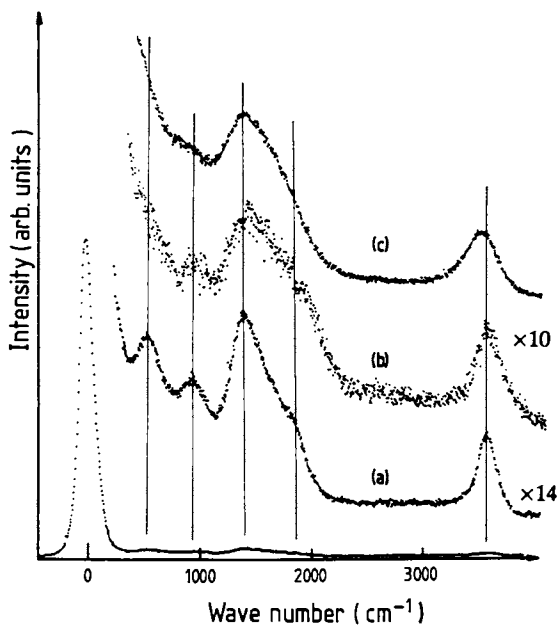
Figure 7. HREELS study o f the chronium-polyimide bonding : (a) clean polymer film, (b) with about 1.5 10^{14} and (c) 4.5 10^{14} Cr atoms/cm^2 respectively.

dramatically reduced in intensity ; 4) finally, the two structures at 400 and 750 cm^{-1} progressively disappear from the spectrum.

This behaviour of this Cr-polyimide interface is not mimicking the one of the Al deposition onto polyimide.

As the presented data are of rather poor quality, we would not like presently to discuss at length the problem ; we would prefer waiting for other sets of high resolution spectra that are scheduled for the near future (16)... However in the meantime, we studied the origin of the HREELS broadening (Fig.7), to discover that other authors (2b,8,11) already stressed upon an influence of the substrate : spectra of polymer films deposited onto a metallic substrate are of better quality than when deposited onto silicon or germanium.

It might be that the substrate-dependent broading testifies of a different anchoring of the polymer on the substrate, what could induce a different film structure, and thus a different chemistry when metallic atoms are evaporated onto the polymer. Some dielectric- structural-chemistry interrelations could explain the data presented above. Again, this will be the subject of further research.

Acknowledgments

Literature Cited

1. Propst, F.M.; Piper, T.C. J. Vac. Sci. Technol. 1967, 4, 53-56.
2. a) Wandass, J.H.; Gardella Jr., J.A. Surf. Sci. 1985, 150, L107-L114.
   b) Dinardo, N.J.; Demuth, J.E.; Clarke, T.C. Chem. Phys. Lett. 1985, 121, 239-244.
   c) Jennings, W.D.; Chottiner, G.S.; Natarajan, C.; Melo, A.V., Hoffman; R.W. O'Grady, W.E.; Lundström, I.; Salaneck, W.R. Apppl. Surf. Sci. 1985, 21, 80-94.
3. Pireaux, J.J.; Thiry, P.A.; Caudano, R.; Pfluger, P. J. Chem. Phys. 1986, 84, 6452-6457.
4. Pireaux, J.J.; Grégoire, Ch.; Thiry, P.A.; Caudano, R.; Clarke, T.C. J. Vac. Sci. Technol. 1987, A5, 598-607.
5. Pireaux, J.J.; Vermeersch, M.; Grégoire, Ch.; Thiry, P.A.; Caudano, R.; Clarke, T.C. J. Chem. Phys. 1988, 88, 3353-3362.
6. Pireaux, J.J.; Grégoire, Ch.; Vermeersch, M.; Thiry, P.A.; Caudano, R. Surf. Sci. 1987, 189/190, 903-912.
7. Liehr, M.; Thiry, P.A.; Pireaux, J.J.; Caudano, R. Phys. Rev. B 1986, 33, 5682-5697.
8. Dinardo, N.J.; Demuth, J.E.; Clarke, T.C. J. Chem. Phys. 1986, 85, 6739-6749; J. Vac. Sci. Technol., 1986, A4, 1050-1051
9. Rei Vilar, M.; Schott, M.; Pireaux, J.J.; Grégoire, Ch.; Thiry, P.A.; Caudano, R.; Lapp, A.; Botelho do Rego, A.M.; Lopes da Silva, J. Surf. Sci. 1987, 189/190, 927-934.
   Rei Vilar, M.; Schott, M.; Pireaux, J.J.; Grégoire, Ch.; Caudano, R.; Lapp, A.; Lopes da Silva, J.; Botelho do Rego, A.M. Surf. Sci. 1989, 211/212, 782-789.

10. Cartier, E.; Pfluger, P.; Pireaux, J.J.; Rei Vilar, M. Appl. Phys. 1987, A44, 43-53.
11. Wandass, J.H.; Gardella Jr., J.A. Langmuir 1986, 2, 543-548 ; 1987, 3, 183-188.
12. Pireaux, J.J.; Riga, J.; Thiry, P.A.; Caudano, R.; Verbist, J. Physica Scripta 1987, T13, 78-83.
13. Thiry, P.A.; Liehr, M.; Pireaux, J.J.; Caudano, R. Physica Scripta 1987, 35, 368-379.
14. Thiry, P.A.; Liehr, M., Pireaux, J.J.; Caudano, R. Surf. Sci. 1987, 189-190, 373-378.
15. a) Jordan, J.L.; Kovac; C.A.; Morar, J.F.; Pollak, R.A. Phys. Rev. B 1987, 36, 1369-1377.
    b) Haight, R.; White, R.C.; Silverman, B.D.; Ho, P.S. J. Vac. Sci. Technol. 1988, A6, 2188-2199.
    c) White, R.C.; Haight, R.; Silverman, B.D.; Ho, P.S. Appl. Phys. Lett. 1987, 51, 481-483.
    d) Sanda, P.N.; Bartha, J.W.; Clabes, J.G.; Jordan, J.L.; Feger, C.; Silverman, B.D.; Ho, P.S. J. Vac. Sci. Technol. 1986, A4, 1035-1038.
    e) Atanasoska, L.J.; Anderson, S.G.; Meyer, H.M., Lin, Z.; Weaver, J.H. J. Vac. Sci. Technol. 1987, A5, 3325-3333.
    f) Dunn, D.S.; Grant, J.L. J. Vac. Sci. Technol. 1989, A7, 253-255.
    g) Nandi, M.; Sen, A. Chem. of Mat. 1989, 1, 291-292.
    h) Rossi, A.R.; Sanda, P.N.; Silverman, B.D.; Ho, P.S. Organometallics 1987, 6, 580-585.
    i) Silverman B.D; Macromolecules 1989, 22, 3768-3776.
16. Pireaux, J.J.; Vermeersch, M.; Grégoire, Ch.; Caudano, R.; Ho, P. in preparation.

RECEIVED January 30, 1990

Chapter 5

Plasma- and Corona-Modified Polymer Surfaces
Characterization by Static Secondary Ion Mass Spectrometry

W. J. van Ooij[1] and R. S. Michael[2]

Department of Chemistry, Colorado School of Mines, Golden, CO 80401

The use of static SIMS for the characterization of surfaces of polypropylene (PP), PTFE and a PMDA-ODA type polyimide is described. Interfaces between evaporated copper or chromium films onto PTFE and polyimide were also analyzed. Some of the polymer substrates were modified by ion beams, corona discharge in air or plasma treatments in air, Ar and H_2. It is demonstrated that SIMS is highly complementary to XPS for the analysis of such modified surfaces, in that effects such as crosslinking, unsaturation and formation of low-molecular weight material at surfaces can be detected.

There are many different methods for modifying polymer surfaces to improve their adhesion and wetting properties. They include chemical etching and oxidation, ion bombardment, plasma treatments, flame treatment, mechanical abrasion and corona-discharge treatments (1,2). Especially flame and corona treatments are widely used for the modification of polyolefin surfaces to enhance, for instance, their printability. Despite the widespread use of such processes in industry, the understanding of the fundamental processes which occur at the polymer surface is very limited. This is undoubtedly due to the shallow depth to which the polymer is modified, typically 5 nm or less.

The application of modern surface analysis techniques, such as XPS, to the analysis of modified polymer surfaces, has demonstrated that in most of the above processes the polymer is oxidized. Many functional groups such as hydroxyl, carbonyl, ether, carboxyl, ester, peroxide, epoxide, etc., have been detected by direct XPS analysis or after derivatization of functional groups. The interaction between evaporated metal films and several of such functional groups has been clearly demonstrated (3).

Although XPS has provided a wealth of information on the surface chemistry of treated polymer surfaces, several possible processes are beyond the capabilities of the technique. Some of these are: crosslinking, formation of double bonds, reorientation of surface molecules and the formation of

[1]Current address: Armco Research & Technology, Middletown, OH 45043
[2]Current address: GE Plastics, Pittsfield, MA 01201

low-molecular weight material. Especially in processes which involve a free radical mechanism, such as corona discharge in the presence of air, reaction between oxygen and polymer radicals results in chain scission (4). This low-molecular weight material is highly oxidized and contains most of the incorporated oxygen functionalities. The presence of such material cannot be detected directly by XPS, but can be inferred from analyses of the surface before and after rinsing in water.

A surface analysis technique that has the potential to detect structural chemical changes in polymer surfaces, including low-molecular weight material formation, is static SIMS. Its capabilities for characterizing polymers by virtue of their fingerprint spectrum have been amply demonstrated in recent years (5,6). The technique is more surface sensitive than XPS and can detect structural differences, even in hydrocarbons (7). It is, therefore, highly complementary to XPS. Nevertheless, only very few applications to the study of modified polymer surfaces have been published. Among these are reports on SIMS analysis of flame-treated polypropylene and plasma-fluorinated polyolefin surfaces (8,9).

In this paper some applications of static SIMS to a variety of modified polymer surfaces are described. They include plasma treatments in reactive and inert gases, corona treatment in air, as well as thermal and ion beam modifications of polymer-metal interfaces. The examples presented and discussed here primarily serve to illustrate the capabilities of static SIMS for the study of such surfaces and interfaces. More detailed discussions of the actual chemical processes that proceed in several of the systems cited will be published elsewhere.

Experimental

Materials. Biaxially oriented polypropylene (PP) films of 50 μm thickness were obtained from 3M and have been described (9). PMDA-ODA (PI) was Kapton H polyimide from Dupont. Copper-plated PTFE films were obtained from Spire Corporation (Bedford, MA). They were prepared using the Ion Beam Enhanced Deposition (IBED) process in which a 100 nm thick Cu film was vapor-deposited onto a PTFE substrate in the presence of a beam of 400 eV Ar^+ ions of 25 μA/cm^2 (10). Shortly before SIMS analysis, the Cu film was removed slowly by peeling at 90° in ambient conditions. Metal-coated PI films were prepared by sputtering 50 nm Cr and 1 μm Cu onto a 50 μm thick Kapton film on both sides. Thermal annealing was performed in a vacuum chamber at 2x10^{-6} torr using a quartz lamp as the heating source. The samples were held for 15 min at the desired temperature and then cooled down to ambient temperature inside the chamber for about 2 hours. Just prior to SIMS analysis, the metal films were peeled slowly at 90° and then immediately introduced into the vacuum chamber of the instrument.

Plasma and Corona treatments. PP was treated in a glow discharge of air, Ar or H$_2$ at 820 V, 60 Hz and 13 Pa pressure for various lengths of time. The glass bell jar was cleaned by the glow discharge for several hours prior to exposure of the films (11). The treated films were exposed to the atmosphere for several hours and then analyzed. The PI films were plasma treated for several minutes in argon at 200 mbar, 40 V and 60 Hz. They were stored for two days in air before SIMS analysis. Corona treatment was performed on an industrial unit as described previously (4). Normalized energies of 0.8 J/cm^2 and 12.7 J/cm^2 were used and treatments at these energies were done at high and low relative humidities (>75% and <10%,

respectively). Spectra of the treated films were recorded within two hours after the treatment. Washing was done by rinsing for a few seconds in deionized water followed by drying in air. Contact angles were measured as described (4).

SIMS Analysis. The equipment and instrumental conditions have been described in detail (7,12). Mostly, a model 6300 Perkin Elmer spectrometer was used which was equipped with a 0-255 amu quadrupole mass analyzer. The primary beam of 4.5 keV Xe^+ and 60 pA current was rastered in a 2x2 mm^2 area. The total ion dose was not more than $3x10^{12}$ ions per cm^2, which is considered a practical limit for static conditions (5-7). Charge neutralization was done by means of 500 eV electrons. Spectral optimization has been described (7,12).

Some spectra were recorded on a non-commercial SIMS instrument designed and built at EG&G in Idaho Falls, ID. It has been described (13,14). Essentially, it is equipped with a primary source of SF_6 neutrals and anions and a 0-2000 amu quadrupole mass analyzer. Qualitatively, the spectra obtained were identical to those of the commercial instrument, but the secondary ion yield was higher and charge neutralization was not required.

Results and Discussion

Static SIMS of Metal-Polymer Interfaces. The adhesion of evaporated films of copper and gold to PTFE substrates can be improved markedly if the polymer is bombarded by low-energy Ar^+ ions prior to or simultaneously with the vapor deposition (10). SIMS spectra of the higher mass range of the Au-PTFE interface with and without the concomitant ion beam have been published (13). They indicated a higher yield of secondary ions containing at least six carbon atoms from both sides of the interface that had been treated with the ion beam. For both samples the spectra from the two matching sides were identical and in both cases these spectra were qualitatively also identical to that of the original PTFE, which showed, however, the same low yield of high mass fragments as that from the sample prepared without Ar^+ enhancement. No Au could be detected by SIMS on any of the four surfaces, although XPS analysis of the same samples indicated that the remaining PTFE film on both metal surfaces was less than 5 nm thick. Angular-dependent XPS analyses of these interfaces also showed that some roughening had occurred of the ion beam-treated interface.

These results suggest as a plausible mechanism for the ion beam adhesion enhancement a mechanical strengthening of the inherently weak surface layers of PTFE by crosslinking or by grafting of the linear, low-molecular weight surface molecules to the bulk of the polymer. The roughening aspect does not appear to be a major factor, since in that case some Au would have been exposed at the interface. This model implies that Au actually adheres to the PTFE by a chemical interaction, which can, however, not be detected by SIMS. This bond is stronger than the shear strength of the PTFE, with our without ion beam enhancement.

In order to verify this simple model, interfaces between vapor-deposited copper films and PTFE with and without ion beam enhancement were prepared and analyzed. Also, the PTFE substrate was treated in an AC argon plasma for 1-5 minutes and analyzed. The Cu-PTFE interface was identical to that between Au and PTFE and the increase of the higher mass ions was observed here, too. In these series of experiments reproduc-

ible and consistent differences in the low-mass regions were also observed. In Figures 1 and 2 the SIMS spectra are shown of PTFE before and following the plasma treatment, respectively. The intensities of the secondary ions $C_2F_4^+$, $C_3F_3^+$ and $C_3F_5^+$ increase with the length of the plasma treatment but they maintain their relative ratios. Figure 3 shows the difference spectrum of the metal sides of the Cu-PTFE interface with and without the ion beam enhancement. Essentially the same effect is observed as in the argon plasma treatment, viz., an increase of the same three ions as above in the ion-enhanced system. No other difference between the two interfaces was detected by SIMS and none of the four surfaces showed any sign of copper. Hence the two failure interfaces were identical to those observed for the Au-PTFE system.

We conclude from these results that the Au-PTFE and Cu-PTFE interfaces are essentially identical and that both fail cohesively upon peeling. The increase of peel strength must, therefore, be largely due to a strenghtening of the surface layers of the PTFE. This effect is the result of the argon ion bombardment, but the same effects are observed upon argon plasma treatment of the PTFE. It has been demonstrated before that bombardment of PTFE surface with energetic species results in better peel strengths of metal films and it has been postulated that this is due to a crosslinking of the surface layers (15), but such effects have not actually been demonstrated. XPS is not sensitive enough to detect the small decrease of CF_2 groups and increase of CF groups upon crosslinking. We feel that the increase of secondary ions $C_2F_4^+$, $C_3F_3^+$ and $C_3F_5^+$ in the SIMS spectra is an indication of increased crosslinking, although the effect can as yet not be quantified. Some evidence for this postulation is that all three fragments are highly unsaturated, as can be expected when C-C cross-links are created in the polymer. Very similar effects have been observed upon plasma treatments of polyethylene, i.e., in air, N_2 and H_2 (11,16). In such treatments the unsaturated secondary ions always increase, relative to the more saturated ones. In addition, the higher mass fragments, which are more branched, also increase in relative intensity. They are more stable than the linear ions of the same overall composition.

The interface formed between evaporated or sputtered metals and polyimides (PI) has been the subject of many studies and controversies. Although there is a concensus that at monolayer coverage the metal atoms mainly interact with the carbonyl oxygen atoms (3,17), the type of bonding and molecular interfacial arrangements between thick films and PI substrates is much less clear. This is caused by the fact that XPS has been the major tool for the characterization of the metal-polymer interface. By virtue of the rather long sampling depth of XPS, typically 5 nm in polymers, the interface can conveniently be studied in situ and non-destructively, as long as the metal film is not more than a few monolayers thick. This is not possible with SIMS. Therefore, we have recorded SIMS spectra of the interface between commercial PI films and metal layers of several microns thickness, i.e., such as actually used in devices. This enabled us to compare the composition of the fracture interface obtained by 90° peeling with the peel strength. As in the case of the Cu- and Au-PTFE systems, we have compared these results with those of the original PI and of PI films treated in Ar and He plasma's.

Unfortunately, PI of the PMDA-ODA type does not generate a highly characteristic static SIMS spectrum in either the positive or negative mode. A typical spectrum of a cleaned PI surface is shown in Figure 4. Spectra of many other commercial PI films have recently been published (18). Fragment 55 is $C_3H_3O^+$ formed by the carbonyl groups and two C atoms of
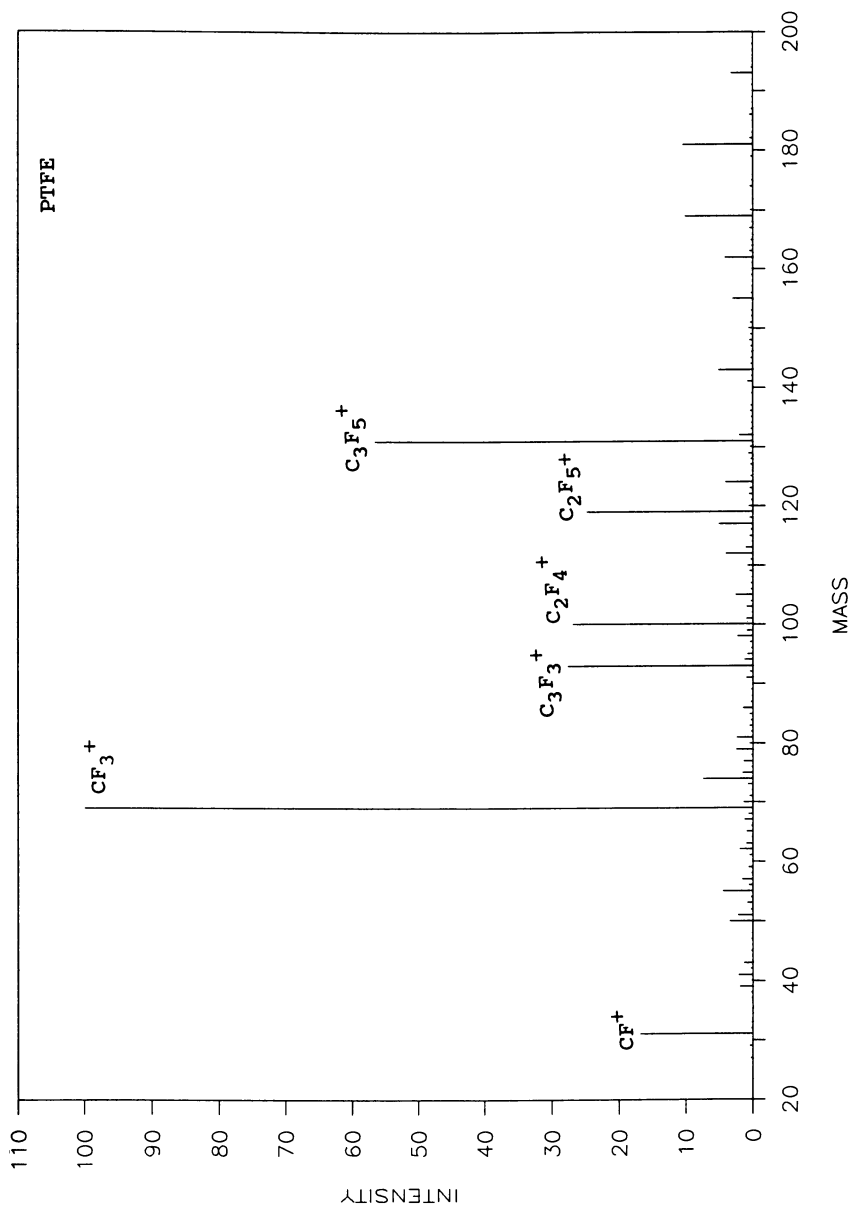
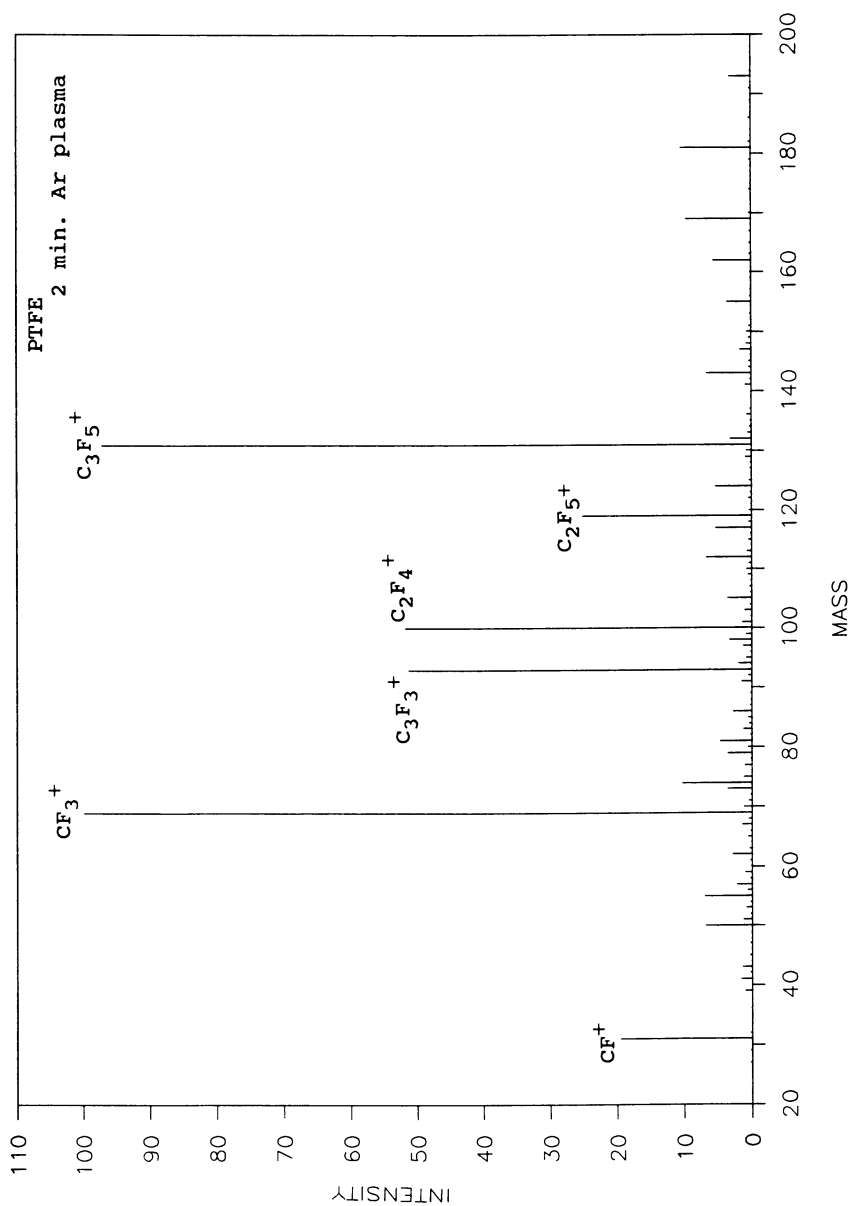Figure 1. Positive static SIMS spectrum of PTFE. Primary beam 10 keV, 10 pA SF_6.

Figure 2. Spectrum of PTFE after 2 min Ar plasma treatment. SIMS as in Fig.1. For plasma conditions, see text.
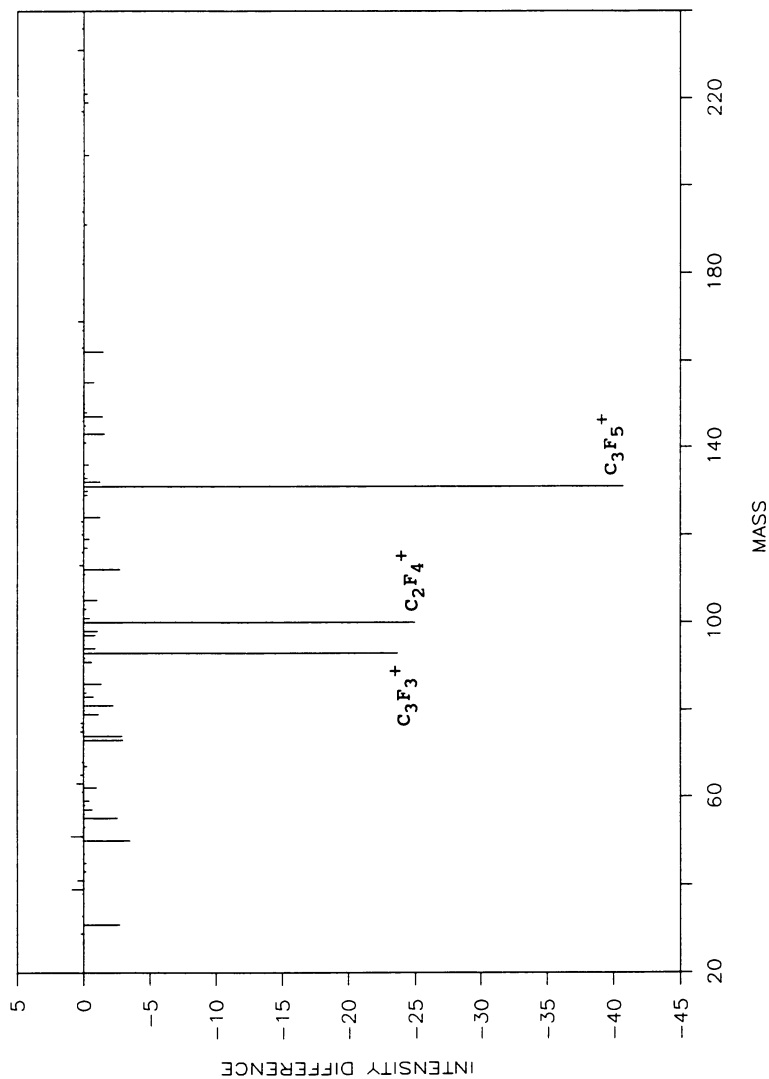
Figure 3. Difference spectrum between PTFE substrates of Cu-PTFE interfaces with and without Ar^+ bombardment in IBED process. SIMS as in Fig.1.
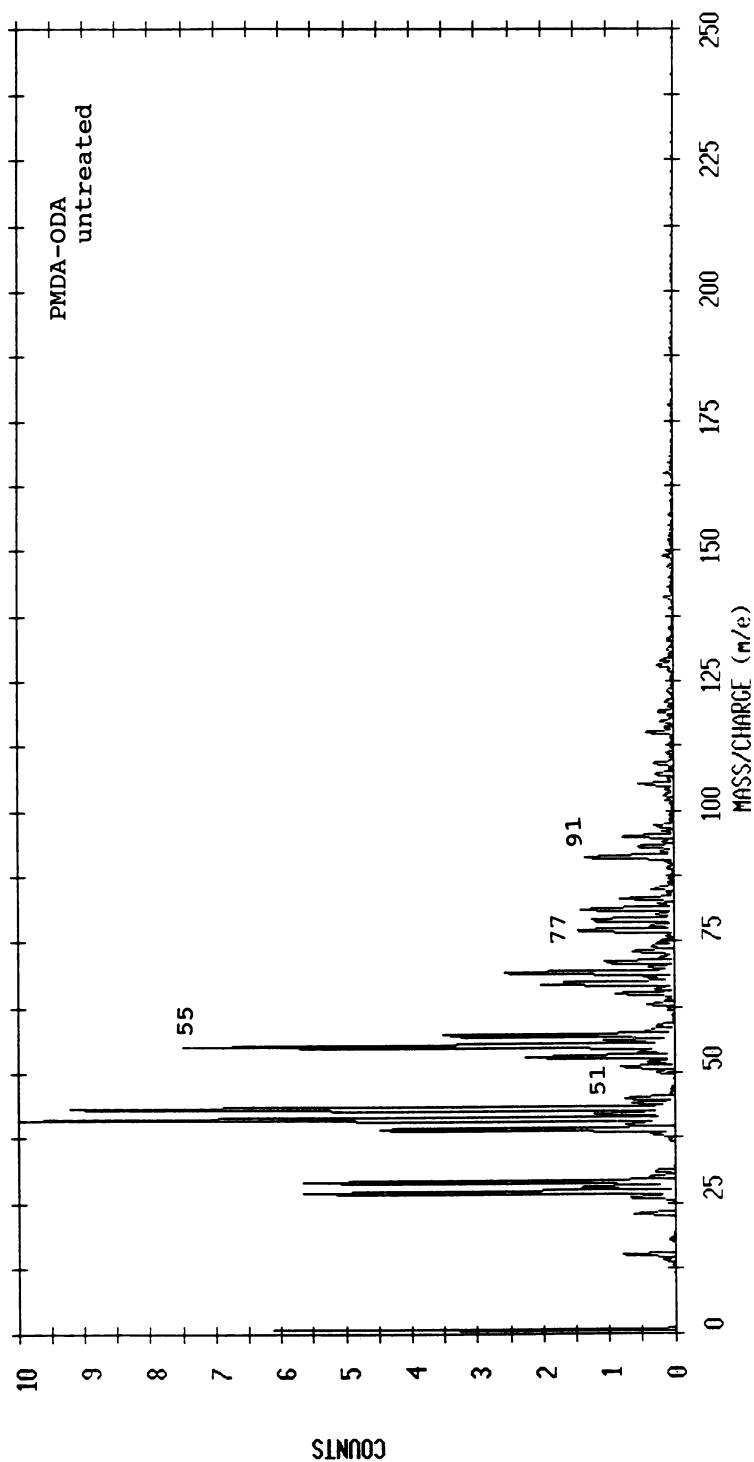
Figure 4. Positive static SIMS spectrum of cleaned PMDA-ODA (PI) film. Primary beam 4.5 keV, 60 pA Xe⁺. In all subsequent figures the same SIMS conditions were used.

the aromatic ring. The ion at 91 is an aromatic fragment. Other aromatic fragments are 12, 26, 37/38, 50/51, 62/63 and 77. In Figures 5a-d the SIMS spectra are shown of the polymer sides of Cr-PI interfaces after the metal film (50 nm Cr and 5 um Cu) was peeled off. Before peeling the interfaces had been annealed for 15 min at progressively higher temperatures. For all samples the metal sides were also analyzed. The spectra obtained from these surfaces were very similar to those of Figures 5a-d, indicating in all cases complete failure in an organic layer and not at the metal-polymer interface. XPS analysis of the peeled metal films suggested an average organic film thickness of 5 nm. So, here, too, the strength of the polymer surface layers determine the peel strength to a large extent.

In addition, the following conclusions can be drawn from the spectra shown in Figure 5.

1. No Cr or Cu is detected at any of the fracture surfaces except for the one annealed at 350°C. Here, Cr (52 amu) and Cu (63 and 65 amu) are both detected at the two sides of the interface. This must be interpreted as a diffusion of both metals into the polymer, as has been amply documented (17). The ions detected at 63/65 amu at the fractures surfaces of the samples annealed at lower temperatures are hydrocarbon ions, since they do not appear in the characteristic isotopic ratio of Cu ions.

2. The spectrum of the polymer side of the control is very similar to that of the untreated PI (Figure 4). No new peaks are observed, which suggests that no major chemical changes have taken place in the interface region. However, the intensities at masses 55 and 91 have decreased somewhat and those at 12, 15, 27, 50/51, 62/63 and of the entire C_2 cluster have increased to some extent. These changes indicate an increased unsaturation of the polymer in the interface region (7). The spectrum of the backside of the metal film showed the same trend.

3. The negative SIMS spectrum of untreated PI (not shown) always has some intensity at masses 26 (CN⁻) and 42 (CNO⁻), originating from the imide group. The spectrum of the backside of the metal film peeled off the control showed the usual low intensities of these ions. However, after annealing at 150 and 250°C, the intensities of these two ions had increased markedly. In contrast, the negative spectra of the corresponding polymer sides did not show increased intensities of these ions. The effect had disappeared after annealing at 350°C. Since CN⁻ and CNO⁻ ions are not formed by fully cured polyimides in appreciable amounts, but in high yields from polyamides and polyurethanes (5), this observation suggests a strong interaction of Cr atoms with carbonyl groups, resulting in a loosening of the bond between the carbonyl groups and the PMDA aromatic ring. That this is only observed on the metal side, indicates that the PI molecules with which the Cr film interacts are completely removed from the PI substrate. In this model, failure is between a thin layer of highly oriented PI molecules bonded to the Cr film via the carbonyl oxygen atoms and the bulk of the polymer.

The low intensities of the CN⁻ and CNO⁻ ions at the interface of the non-annealed sample (control) is indicative of a fracture interface which is somewhat deeper into the polymer. The Cr|O-C-N-bonds then escape detection by SIMS.

4. Comparison of the four spectra of the polymer sides (Figure 5) shows several interesting differences. After annealing at 150°C, the spectrum has changed drastically in that all fragments which are characteristic of aromatic molecules have strongly increased in intensity. In addition, high intensities at masses 45, 74 and 150 are now observed. We interpret the high yields of 'aromatic' fragments as indicative of a strong surface orientation of the
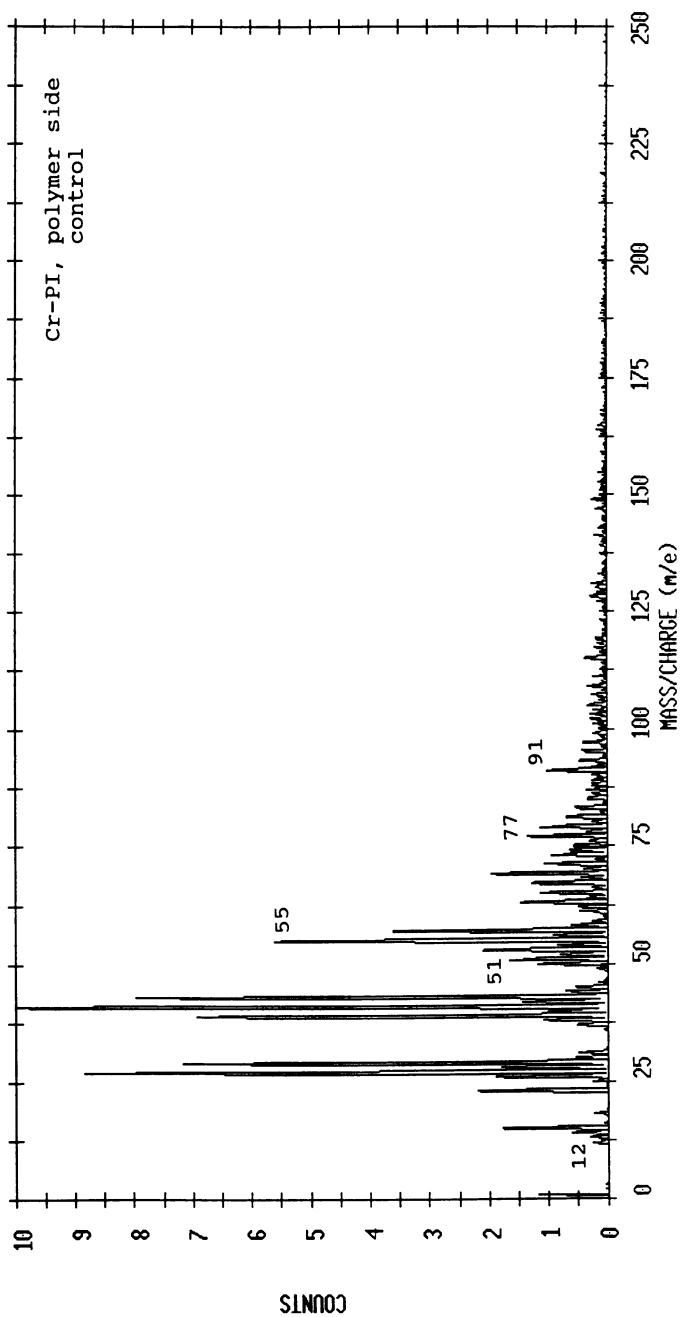
Figure 5A. Spectra of PI following peeling of sputtered films of 50 nm Cr and 5 μm Cu.
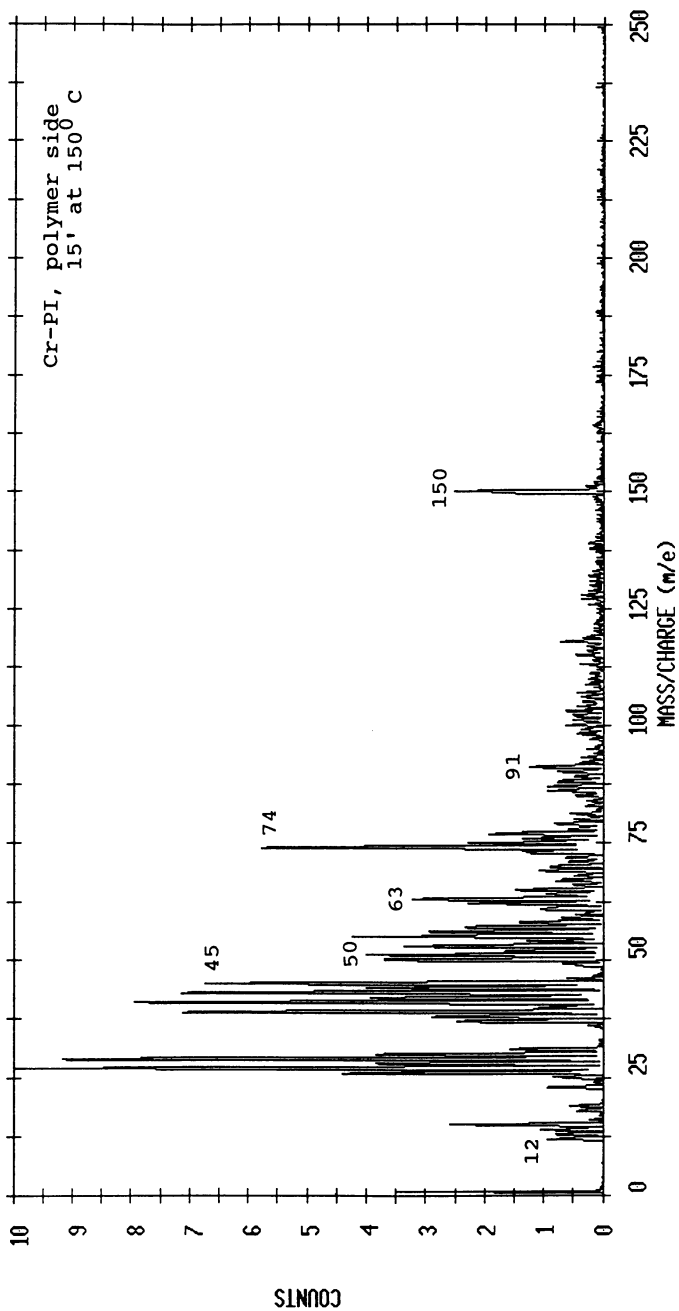
Figure 5B. Spectra of PI following peeling of sputtered films of 50 nm Cr and 5 μm Cu. The interface was annealed for 15 min at 150 °C.
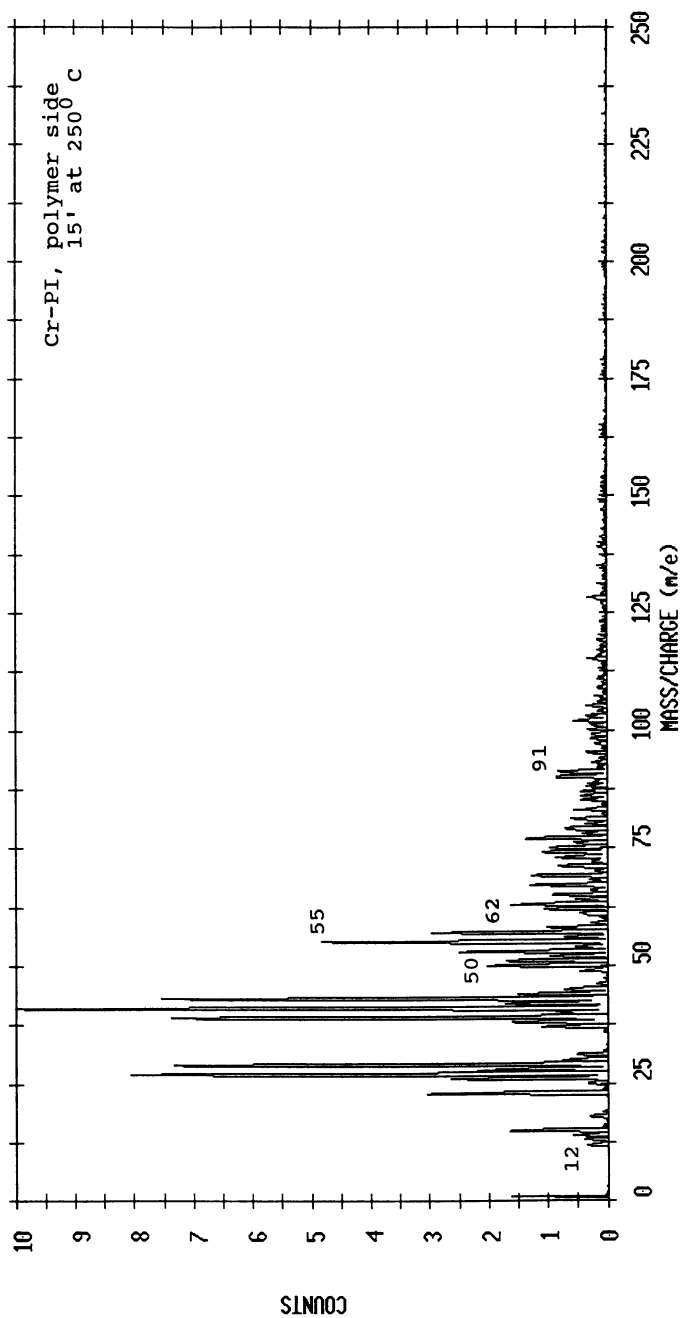
Figure 5C. Spectra of PI following peeling of sputtered films of 50 nm Cr and 5 μm Cu. The interface was annealed for 15 min at 250 °C.

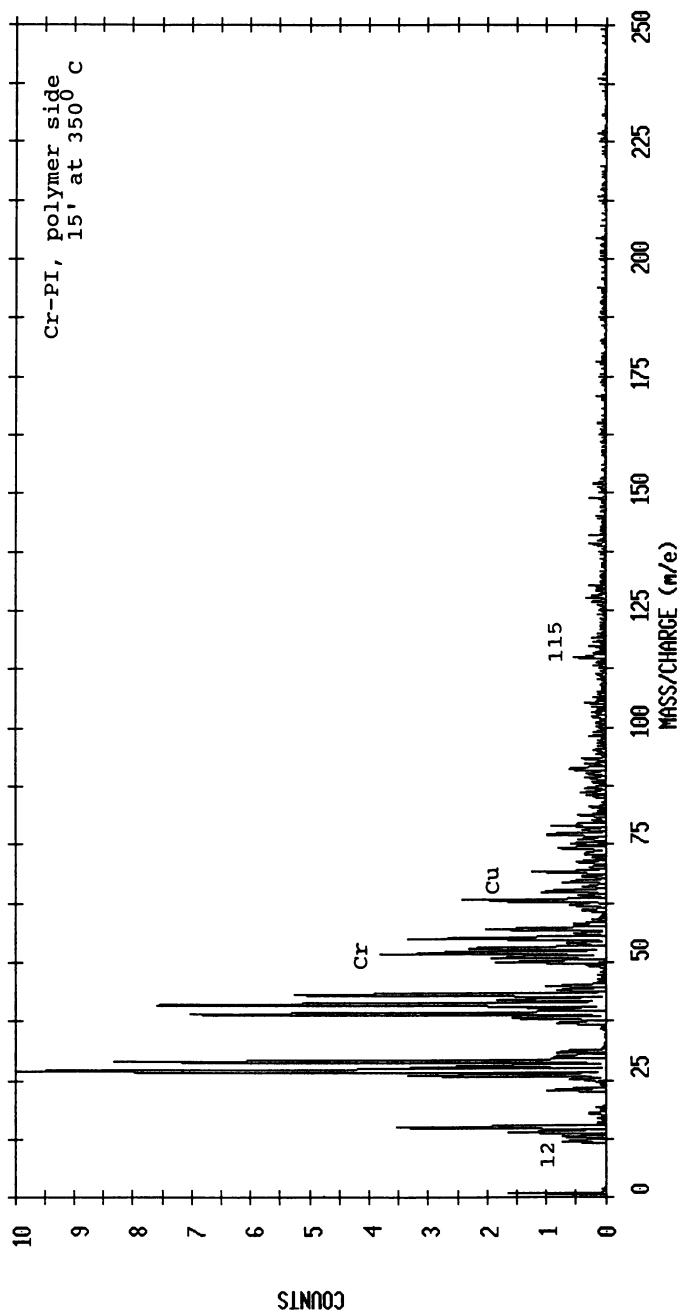Figure 5D. Spectra of PI following peeling of sputtered films of 50 nm Cr and 5 μm Cu. The interface was annealed for 15 min at 350 °C.

aromatic rings, as has previously also been observed for polyester (19).
This strong orientation is in agreement with the observation that annealing
of the Cr-PI sample resulted in high stress concentrations at the interface.
These are believed to be at least one of the causes of the observed reduc-
tion of the peel strength of the annealed samples (Van Ooij, W.J.; Yang,
C.H.; Chen, P.C., to be published).

   The most likely interpretation of the ions at masses 45, 74 and 150
are listed in Table I, along with many other peak identities. These peaks
show that hydroxyl groups are now present at the interface, i.e., the
carbonyl groups must have been reduced to some extent, possibly by a cata-
lytic effect of the Cr metal.

   It is important to note that polyamic acid and hydrolyzed PI form the
ion at mass 149 (see Table I) and not the ion at mass 150 (18). In plasma
treatments (see below) both 149 and 150 are formed.

   After annealing at 250°C the strong orientation of the aromatic rings
has largely disappeared and the spectrum resembles that of the original PI
again. Reduction effects are not observed here. The further reduction in
peel strength could thus be explained on the basis of a stress relaxation
due to the initiation of cracks in the interfacial region. It should be noted
that the metal film was still completely covered with organic material which
showed a strong interaction with the metal.

   Following annealing at 350°C, the polymer surface shows some signs
of decomposition (graphitization), e.g., by mass 12 and the high 27/29 ratio.
Both Cr and Cu are detected and the metal film is no longer completely
covered by organic material. In addition, the interaction between Cr and
the organic material is no longer observed and the total amount of oxygen,
as measured by the O^-/CH^- ratio, has decreased. This decomposition
explains the observed further reduction of the peel strength of the film.

   In order to obtain more information on the possible modes of decom-
position of PI, the films were also treated in Ar and He plasma's. Figure 6
shows the spectra obtained after 2 min treatment in Ar or He plasma,
respectively. After the Ar plasma the spectrum has changed markedly. New
peaks are at 18 (H_2O^+), 29 (COH^+), 44, 45, 74, and a series at 90, 102,
118, 130 and 149/150. The most likely identities are given in Table I.
They suggest that several bonds in the imide structure have been ruptured
and both amides and isocyanates have been formed. Especially the high
yield of 74 indicates that reduction of the carbonyl group has also occurred
in this treatment. Finally, the increased yield at mass 149 is indicative of
carboxylic acid formation. This may have occurred as a result of hydrolysis
during exposure to air following the treatment. The very high yield at mass
18, which is due to strongly adsorbed water, is in agreement with this
explanation. The carboxyl groups increase the hydrophylicity of the surface.

   At longer treatment times, e.g. 4 min, most of the new peaks in-
crease further, especially 90, 102 and 118. The intensities at 149 and 18
remain constant, whereas that of mass 74 drops sharply, indicating that 74
and 90 are not formed by the same reaction and that the degree of hydro-
lysis remains constant.

   After the He plasma treatment (Figure 6b), the effects are not the
same as in the Ar plasma. There is no increase at mass 149 and very little
at mass 18, indicating a less hydrophylic surface and less hydrolysis. A very
strong increase of 150 is now observed, similar to that shown in Figure 5b
for one of the Cr-PI interfaces. The formation of this suggests a combina-
tion of reduction of carbonyl groups and a rupture of one of the OC-N
bonds of the imide groupings. The high yield of mass 74 is also indicative
of reduction effects, as discussed before.

Table I. Peak Assignments in SIMS Spectra of Plasma-treated PI

Mass, amu	Proposed Structure
30	CH_3-NH^+
31	CH_2OH^+
32	$HO-NH^+$
42	$CH_2=CH-NH^+$
44	$C_2H_5-NH^+$
45	$COOH^+$, CH_3CHOH^+
46	$HO-CH_2-NH^+$
58	$C_3H_7-NH^+$
60	$CH_3CH(OH)NH^+$
74	$C_2H_5-CH(OH)NH^+$
88	$C_3H_7CH(OH)NH^+$
90	$\cdot R=N^{+\,*)}$
102	$NC-R^+$
118	$ONC-R^+$
130	$NC-R-CO^+$
148	$HOC-R-CONH^+$
149	$HOOC-R-CO^+$
150	$HOC-R-CH(OH)NH^+$

*) R is an aromatic ring, $-C_6H_4-$

PMDA-ODA
2 min. Ar plasma
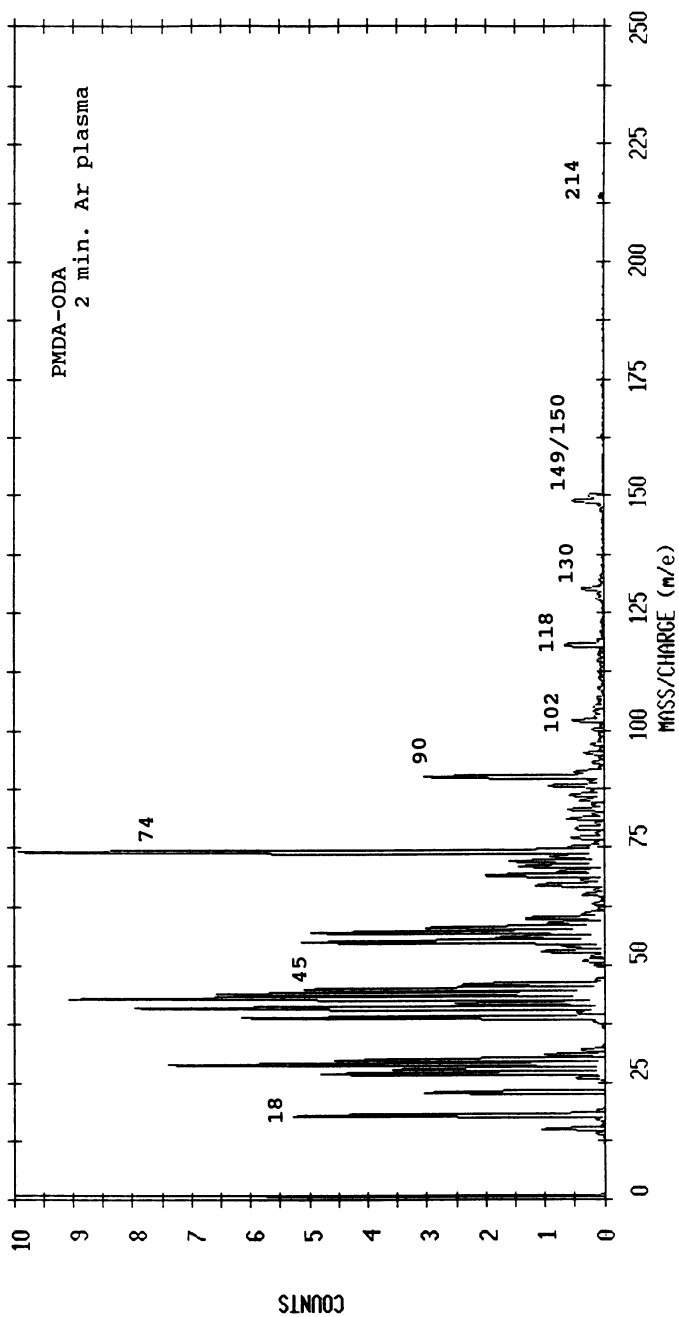
Figure 6A. Spectra of PI films modified for 2 min in AC plasma of Ar.

Figure 6B. Spectra of PI films modified for 2 min in AC plasma of He.

In summary, the analysis by static SIMS of PI surfaces modified by various treatments have provided evidence for chemical changes in the molecular structure. In all cases studied, changes could only be detected in the imide functionalities. Several bonds seem to be attacked in the plasma treatment. Remarkable is that the Ar plasma induces modifications which, upon subsequent exposure to the atmosphere, result in hydrolysis, followed by water adsorption. In the case of surface modification by vapor-deposition of chromium films, it was confirmed that the metal interacts mainly with carbonyl groups, as had long been demonstrated by XPS. However, static SIMS also provided some direct evidence for the development of interfacial shear stresses upon annealing of the metal-polymer films. Although chemical changes, such as reduction of the polymer, seem to take place as well, it is believed that these shear stresses are responsible for the reduction of the peel strength which was observed upon annealing. At rather moderate temperatures, i.e. 350°C, where the bulk of the polymer can still be expected to be stable, the onset of graphitization at the Cr-PI interface was observed. The metal-polymer bond is destroyed and Cr and Cu are observed to diffuse into the polymer. Both reduction effects and this graphitization reaction may have been catalyzed by the metal atoms.

Plasma vs. Corona Treatment of Polypropylene (PP). Corona treatments of polyolefins to modify their surfaces are very common in the polymer industry. The chemistry at such surfaces has been widely studied by XPS (4). It is generally assumed that corona treatments create abundant amounts of radicals which react with oxygen to form a hydroperoxide. This reacts further to eventually form crosslinks, oxidized products (ranging from hydroxyls to esters) with and without chain scission. The latter process is believed to lead to low-molecular weight material. There is some controversy over this material. Its role in determining the surface properties of the modified polymer is not completely understood. Its formation cannot be demonstrated directly by XPS, but only by comparing spectra before and after washing.

In this study we have compared the effects of a treatment of a simple polyolefin (PP) in a variety of AC plasma's with that of air corona. The primary purpose was to investigate, as in the first part of this paper, whether static SIMS can be used to increase the understanding of such modified surfaces. The actual chemistry that takes place at the surface of this and other polyolefins will be published in more detail elsewhere.

Figure 7 shows positive static SIMS spectra of PP before and after corona treatment and also following a brief rinse of the treated film in water. The spectrum of untreated PP is characterized by high yields of ions with mass 41, 55 and 69, which are probably C_3, C_4 and C_5 ions with the charge on the tertiary carbon atom and a double bond, although cyclic ions have also been proposed (7). The spectrum of the corona-treated film shows a high yield of mass 43. Several new ions with low intensities are also observed. These are probably oxygen-containing fragments. Mass 43 amu is also formed in high yields from polyvinyl alcohol and not from polyethers which form an ion at mass 45 (Van Ooij, W.J., Colorado School of Mines, unpublished data). It could thus indicate a hydroxyl or carbonyl group on the pendant methyl group or the tertiary carbon atom. The small yield of 45 ($COOH^+$) here may be indicative of a carboxyl group. The increase of hydrophylicity can be concluded from the presence of water (mass 18). Typical of corona-treatments in air is the appearance of a series of peaks in the spectrum at masses 120, 149, 167, 184, 211 and 226/227. Some of these are seen in Figure 7c. The peaks at mass 226/227 are the
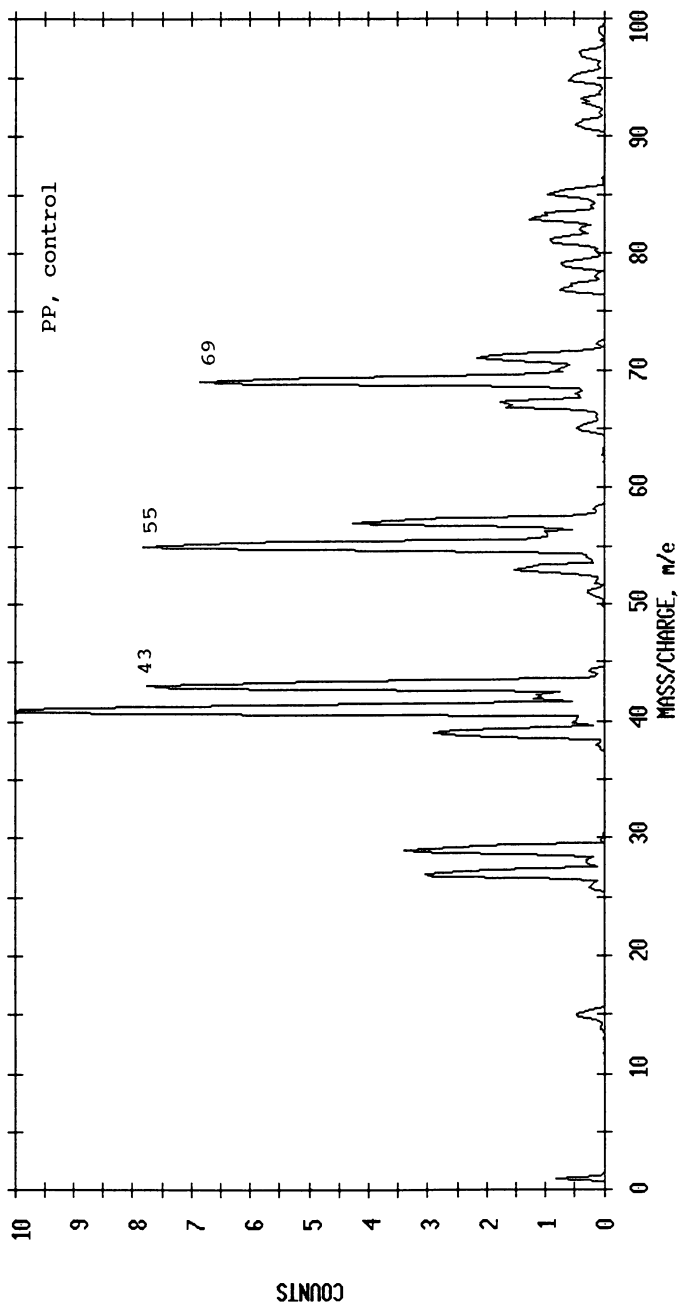
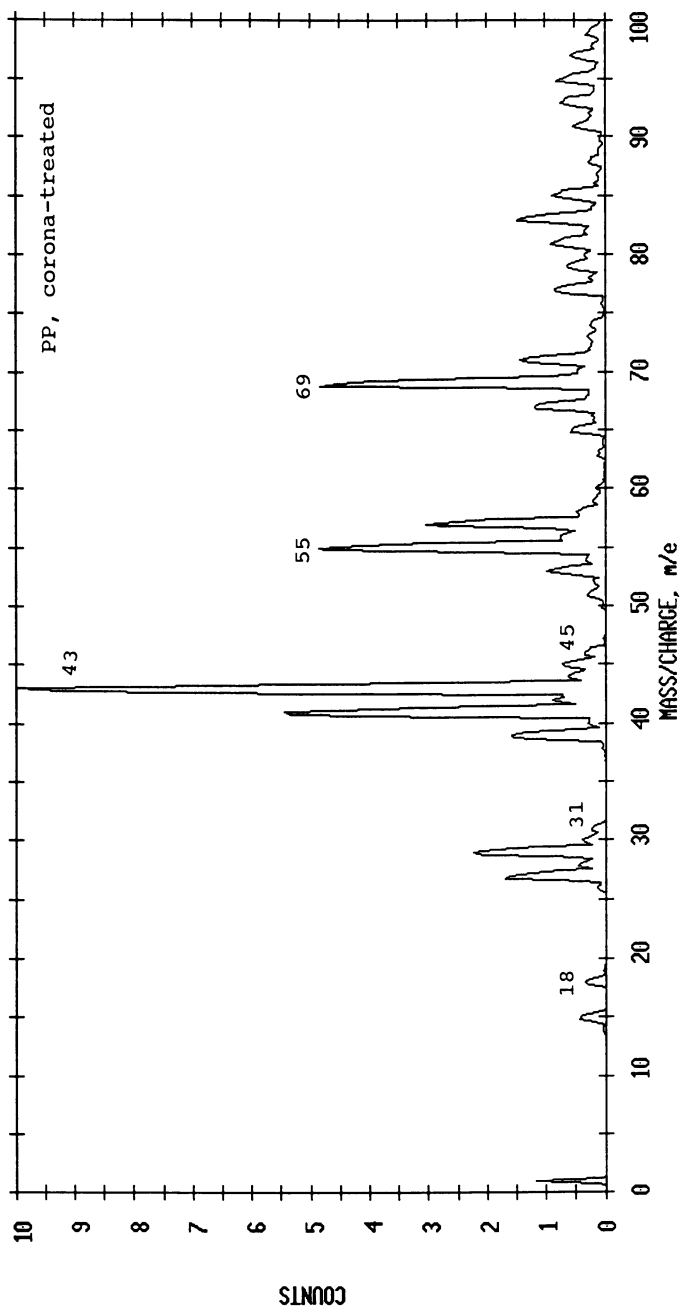Figure 7A. Spectra of polypropylene (PP) films before air corona treatment.

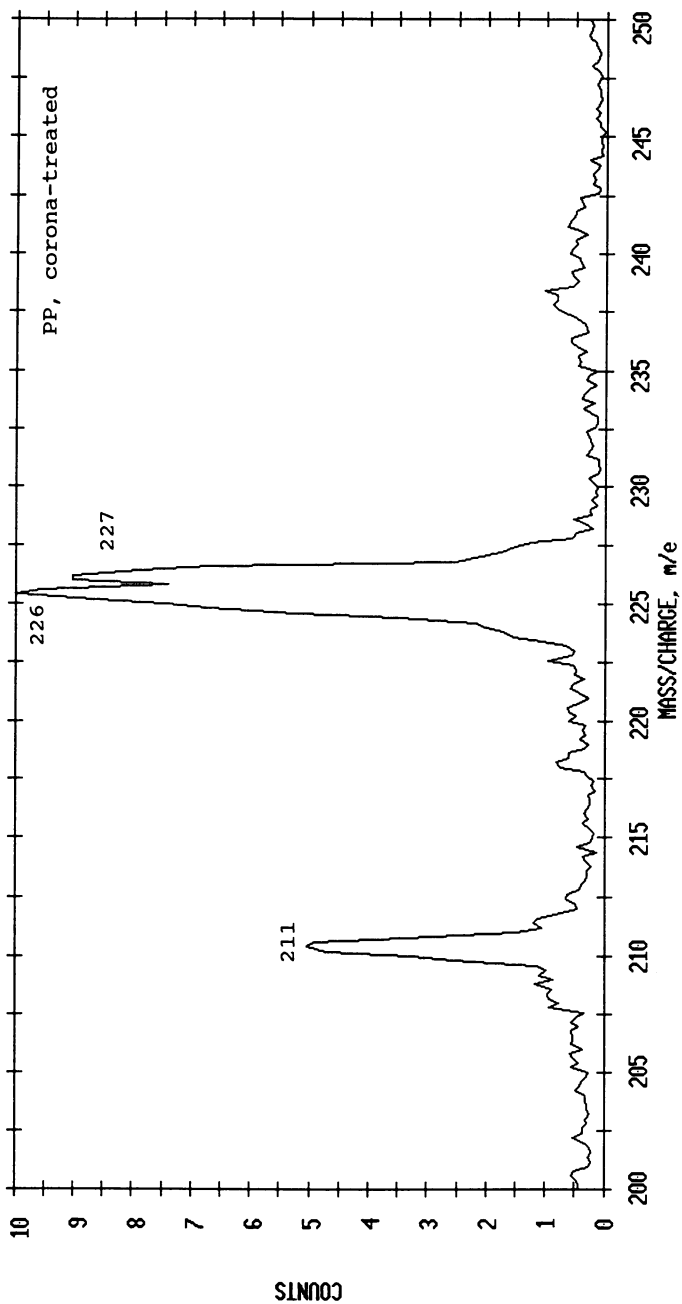Figure 7B. Spectra of polypropylene (PP) films after air corona treatment.

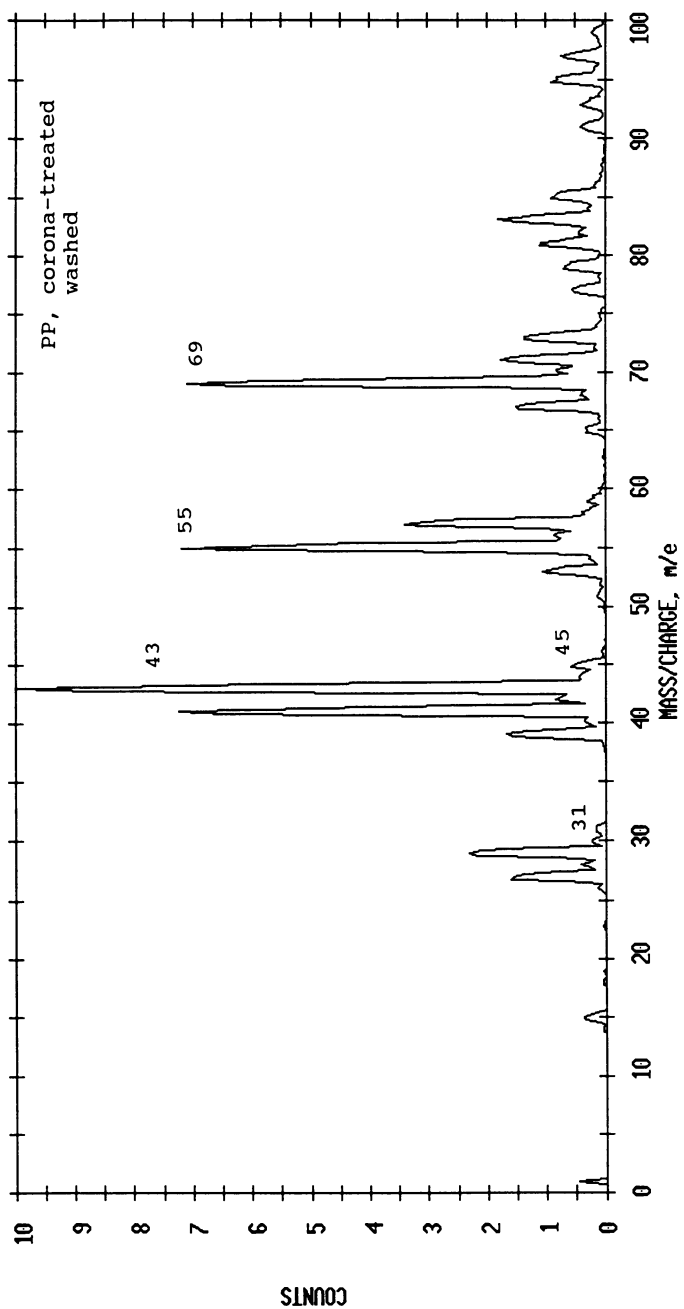Figure 7C. Spectra of polypropylene (PP) films after air corona treatment.

Figure 7D. Spectra of polypropylene (PP) films after washing corona-treated film in deionized water.

most intense peaks in the spectra. The intensity of the entire series is
dependent on the dose of the treatment, as is shown in Table II. After
rinsing the films briefly in water, all of these new peaks have completely
disappeared. The peak at mass 43 has also decreased strongly in intensity.
We interpret these series of peaks as the fragmentation pattern of a series
of low-molecular weight, highly oxidized material which is water-soluble.
Most of the oxygen that is incorporated in the treatment appears to be in
this material. However, after washing some oxygen remains. This is probably
the oxygen that reacts with the polymer without chain scission.

Table II. SIMS Peak Ratios of Air-Corona-Treated PP[*]

No.	Dose J/cm^2	R.H. %	184/41		27/29		109/27		16/13	
			fresh	washed	fresh	washed	fresh	washed	fresh	washed
1	12.7	10	0.17	0	1.38	1.46	0.29	0.29	1.18	0.57
2	12.7	75	0.04	0	1.73	1.58	0.79	0.38	0.76	0.55
3	0.8	10	0.10	0	1.34	1.50	0.36	0.34	1.59	0.79
4	0.8	75	0.01	0	1.41	1.72	0.51	0.31	0.94	0.57
5	0	-	0	0	1.10	1.10	0.15	0.15	0	0

[*])positive spectra except 16/13 ratio

It is remarkable that the series of peaks that appear after corona
treatment is also observed in corona treatment of other polymers, e.g.
polyester, polyethylene, and polystyrene. The nature of the low-molecular
weight material thus seems to be independent of the type of polymer, sug-
gesting a rather universal mechanism of formation. This mechanism is still
unclear, but a pertinent observation may be that at very short treatment
times the surfaces of many polymers indicate a high degree of unsaturation.
This is seen in Table II, which shows the ratio 27/29, which is a measure
of unsaturation. In corona as well as plasma treatments, the unsaturation
increases steeply and then decreases with increasing time or dose. It is thus
possible that many polymers initially form some sort of graphite-like
structure which then reacts at a slower rate with oxygen. This would explain
the similarity in the behavior of these polymers.
        In Figure 8 some spectra are shown of PP following plasma treat-
ments in air, argon and hydrogen. The spectrum obtained after hydrogen
treatment is the easiest to interpret. It shows only two differences as
compared with that of the original PP: a higher yield of all peaks contain-
ing eight or more C atoms, and an increase of the peak at mass 43. The
spectrum is virtually identical to that of the corona-treated PP after washing
(Figure 7d). No unsaturation or low-molecular weight material is observed.
Hence it seems that H_2 creates reactive sites in the polymer which either
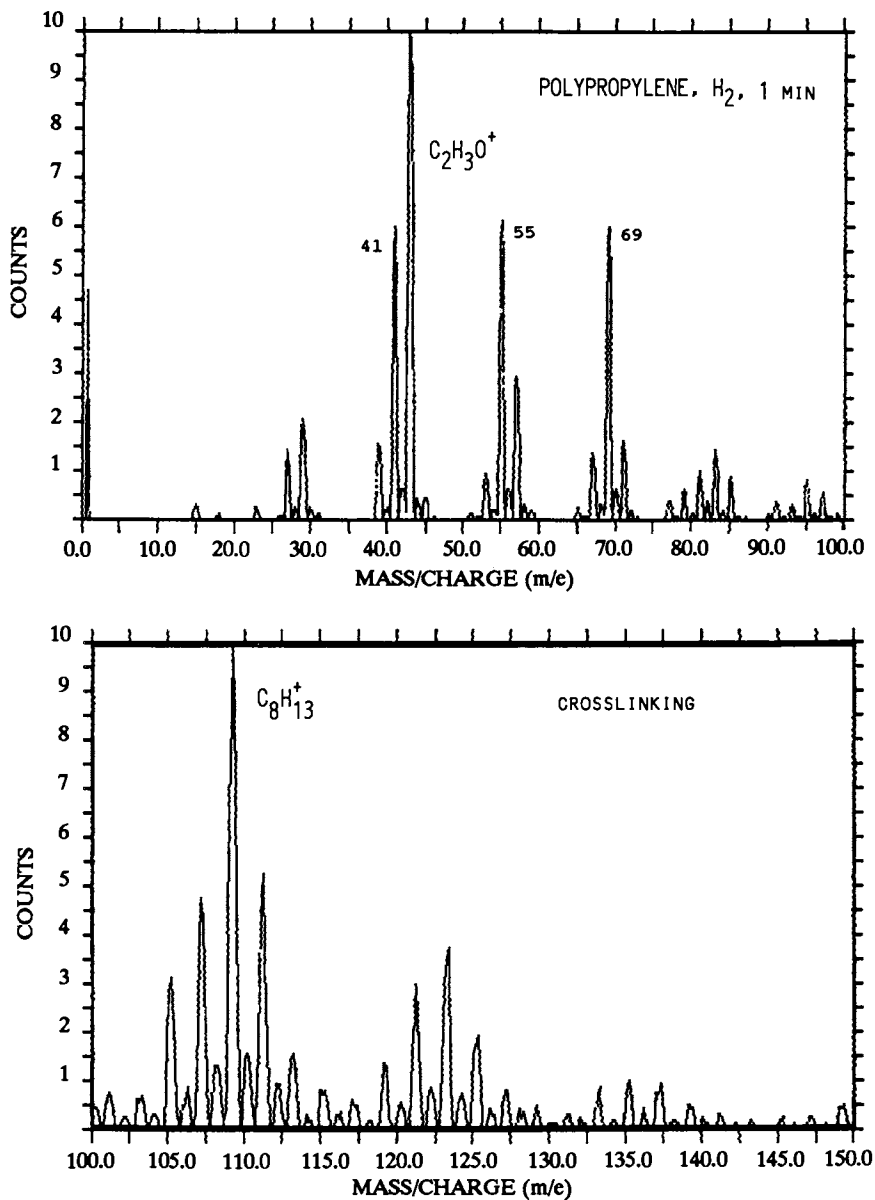crosslink or absorb oxygen upon exposure to the atmosphere. The surface

Figure 8A. Spectra of PP after AC plasma treatments for 1 min in hydrogen.
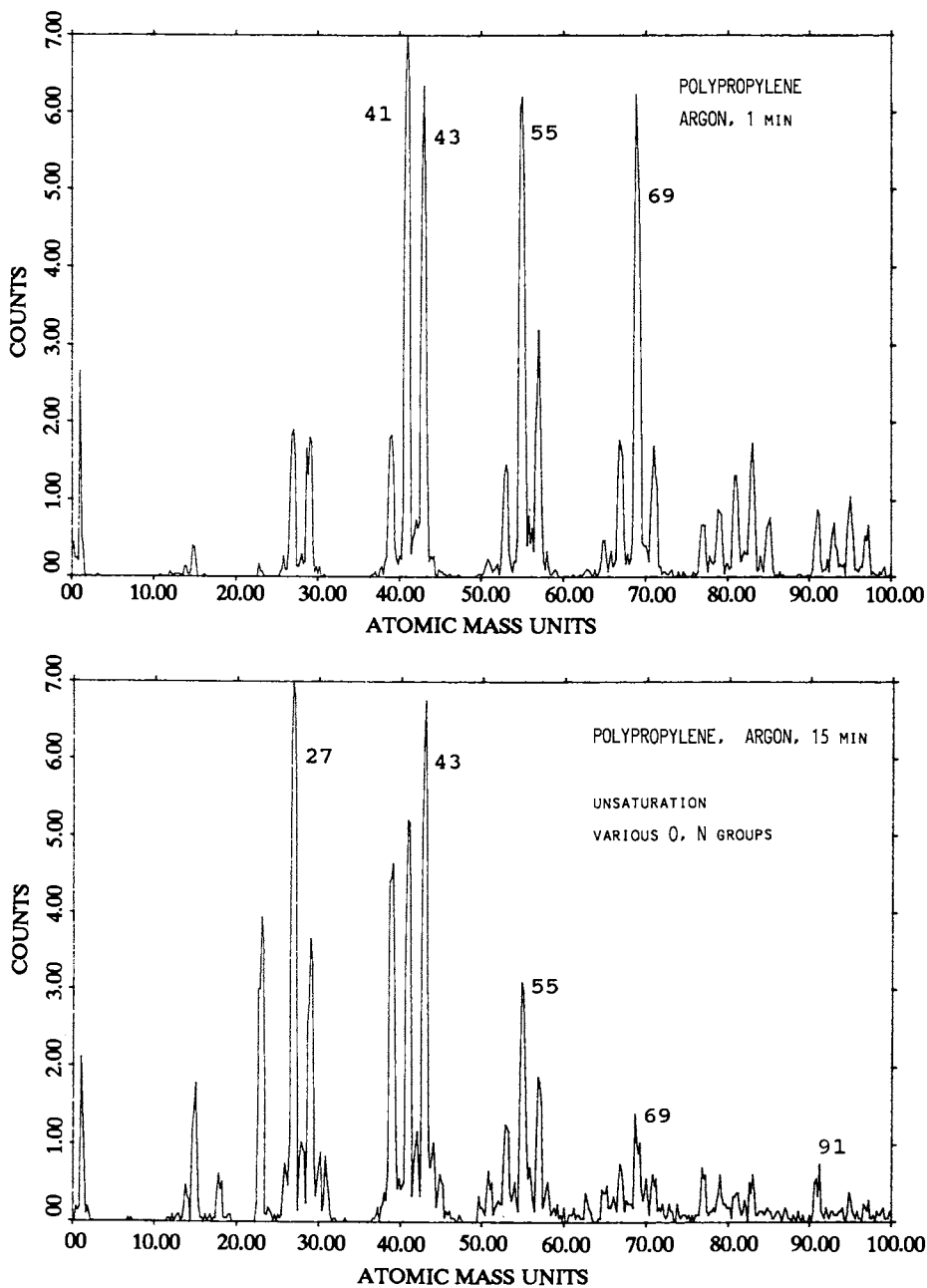
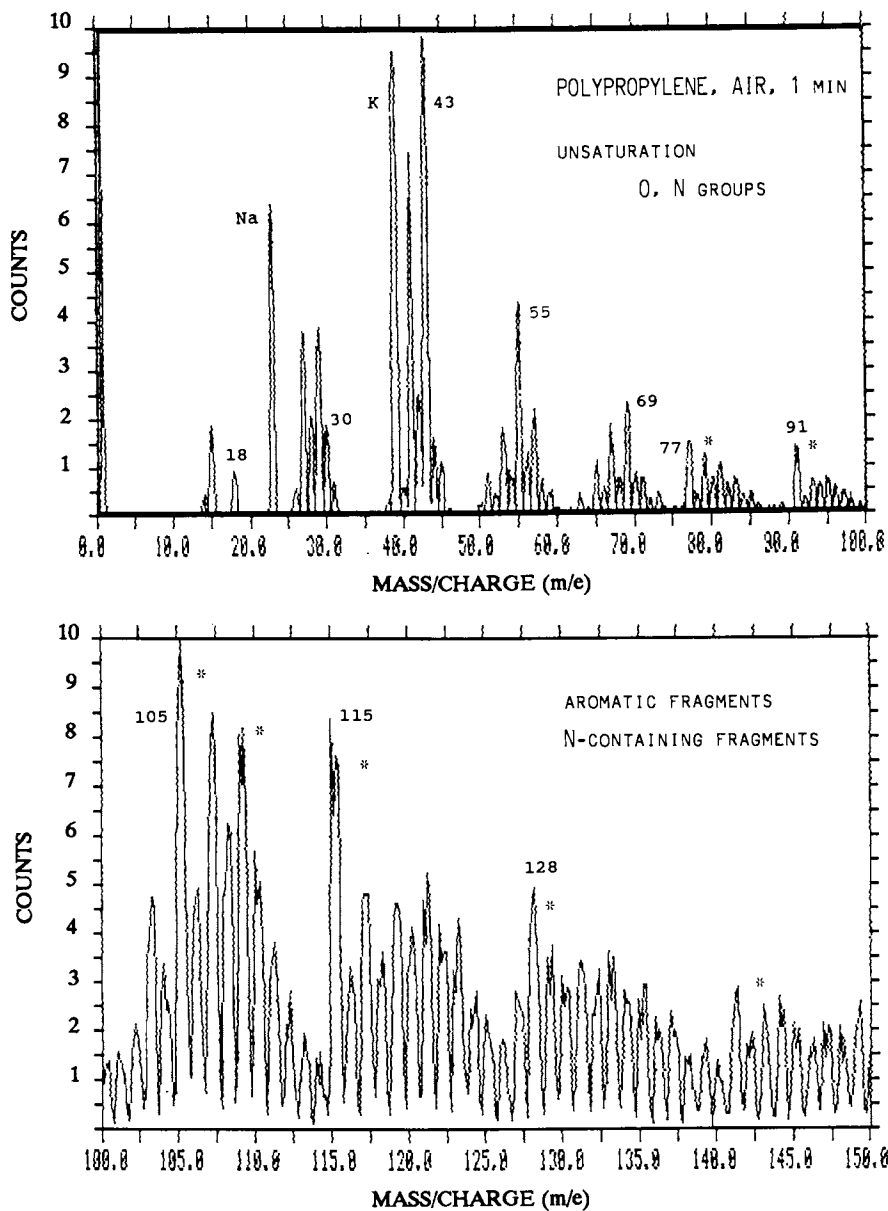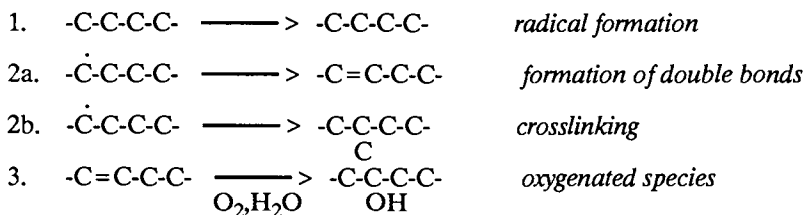Figure 8B. Spectra of PP after AC plasma treatments for 1 min in argon.

Figure 8C. Spectra of PP after AC plasma treatments for 1 min in air.

does not absorb water. The treatment, therefore, seems to induce the same reaction as that pathway in the corona which does not involve chain scission. Since the oxygen is absorbed after the treatment, this pathway probably does not involve the formation of a hydroperoxide.

The treatment in argon does not induce strong changes in the spectrum after short treatment times. After longer times, the main effect observed is a high degree of unsaturation in the surface. The amount of oxygen uptake after treatment is much less than for the hydrogen treatment. Following the air plasma, the spectrum has changed markedly (Figure 8c). The high intensities of Na^+ and K^+, typical of this treatment, are interpreted as indicative of etching of the polymer. A certain degree of unsaturation is still detected and the polymer has crosslinked to some extent (C_8/C_2 ratio). The even numbered peaks, starting at 28, are indicative of primary and secondary amines (12). Another interesting observation is that the spectrum does not change upon rinsing with water. The series of peaks which are interpreted as low-molecular weight compounds in corona treatments were never observed in plasma treatments, not even after much longer times.

The comparison of the spectra obtained after plasma or corona treatment in air, argon or hydrogen, suggest that, apart form the mechanism involving the formation of a hydroperoxide, another mechanism takes place which prevails in plasma but which also occurs in the corona treatment. This is summarized as follows:

1.   -C-C-C-C- ──────> -C-C-C-C-   *radical formation*

2a. -Ċ-C-C-C- ──────> -C=C-C-C-   *formation of double bonds*

2b. -Ċ-C-C-C- ──────> -C-C-C-C-   *crosslinking*
                                   C
3.   -C=C-C-C- ──────> -C-C-C-C-   *oxygenated species*
              O_2,H_2O OH

In H_2 plasma's reaction 3 occurs upon exposure to the atmosphere. Clearly, more work needs to be done before the surface chemistry of polymer modification can be more clearly understood. Static SIMS can play an important role in such studies.

Conclusions

The results presented here demonstrate that static SIMS has unique capabilities for the characterization of the surfaces of polymers that have been modified by metal deposition or by plasma or corona techniques. Especially, the introduction of unsaturation and crosslinking are aspects that in some polymers can be observed directly. The formation of low-molecular oxidized material that can be inferred from XPS studies, can also be observed directly. A limitation of the quadrupole-type instrument, which is still the most widely used, is its limited mass range and mass resolution. It can be expected that a considerably more detailed description of modified polymer surfaces can be obtained by application of the more powerful reflectron-type Time-of-Flight SIMS spectrometers, but such studies have, to date, not yet been published.

Acknowledgment

Literature Cited

1. Ashworth, V.; Grant, W.A.; Procter R.P.M., Eds.; Proc. Int. Conf. Modification of Surface Properties, Ion Implantation; Oxford Press, New York, 1987.
2. Baglin, J.E.E. In Surface and Colloid Science in Computer Technology; Mittal, K.L., Ed.; Plenum Press, New York, 1987, p 211.
3. Katnani, A.D.; Knoll, A.; Mycek, M.A. J. Adhesion Sci. Technol. 1989, 3, 441.
4. Strobel, M.; Dunatov, C.; Strobel, J.M.; Lyons, C.S.; Perron, S.J.; Morgen, M.C. J. Adhesion Sci. Technol. 1989, 3, 321.
5. Briggs, D. Surf. Interface Anal. 1986, 9, 391.
6. Van Ooij, W.J. Rubber Chem. Technol. 1989, 62, 656.
7. Van Ooij, W.J.; Brinkhuis, R.H.G. Surf. Interface Anal. 1988, 11, 430.
8. Garbassi, F.; Occhielo, E.; Brown, A. J. Mater. Sci. 1987, 22, 1450.
9. Van Ooij, W.J.; Michael, R.S. Mat. Res. Soc. Symp. Proc. 1988, 119, 285.
10. Loh, Ih-Houng; Hirvonen, J.K.; Martin, J.R.; Revesz, P.; Boyd, C. Mat. Res. Soc. Symp. Proc. 1988, 108, 241.
11. Van Ooij, W.J.; Brinkhuis, R.H.G.; Newman, J.G. In Secondary Ion Mass Spectrometry, SIMS VI; Benninghoven, A.; Huber, A.M.; Werner, H.W., Eds.; John Wiley & Sons: Chichester, UK, 1988; p 671.
12. Brinkhuis, R.H.G.; Van Ooij, W.J. Surf. Interface Anal. 1988, 11, 214.
13. Van Ooij, W.J. Materials Society Spring 1989 Meeting, San Diego, CA, April 24-28, 1989.
14. Appelhans, A.D.; Delmore, J.E. Anal. Chem. 1987, 59, 1685.
15. Ingemarsson, P.A.; Eriscsson, T.; Wappling, R.; Possnert, G. J. Adhesion Sci. Technol. 1989, 3, 503.
16. Van Ooij, W.J.; Brinkhuis, R.H.G.; Michael, R.S. 10th Symposium on Applied Surface Analysis, Denver, CO, April 27-29, 1988.
17. Paik, K.W.; Ruoff, A.L. J. Adhesion Sci. Technol. 1988, 2, 245.
18. Van Ooij, W.J. In Metallized Plastics 1: Fundamental and Applied Aspects; Mittal, K.L., Ed.; Plenum: New York, NY, 1990; p 171.
19. Van Ooij, W.J. Proc. Industry-University Advanced Materials Conf.; 1989, p 349.

Chapter 6

Depth Profiles of Thin Films and Interfaces by the Elastic Recoil Detection Technique

S. C. Gujrathi

Laboratoire de Physique Nucléaire and Groupe des Couches Minces, Université de Montréal, C.P. 6128, Succursale A, Montreal, Quebec H3C 3J7, Canada

An elastic recoil detection (ERD) technique, which also involves Rutherford forward scattering (RFS) and incorporates time-of-flight (TOF) principle for mass discrimination, is developed and successfully applied in the simultaneous "non-destructive" multielemental depth-profile studies of thin films and interfaces. In this technique, the light as well as medium mass elements are knocked out of the target by using energetic heavy ion beams obtained from the 6 MV Tandem accelerator. The mass separated energy spectra are deconvoluted into the depth profiles by using a newly developed computer analysis facility capable of yielding reliable atomic concentration ratios on routine basis without any a priori assumptions about the composition of an unknown target. The performance of the technique is illustrated through the results of some recent applications to a large number of targets such as Corning Glass 0211, silicon nitride and oxynitride films, borophosphoro silica glass, cobalt silicides and polyimide-metal interfaces. In several cases the quantitative results of ERD are compared with other material analysis methods, e.g. chemical analysis, energy dispersive X-ray analysis (EDX), X-ray photoelectron spectroscopy (XPS), etc. and found to be in very good agreement. The effects of beam dose on radiation sensitive films of polymers and polyimides are briefly discussed and a few methods to minimize them are suggested. Typical performance characteristics of the system using 30 MeV ^{35}Cl ions as beam probe are : 0.2 amu mass resolution in C region and ~ 0.7 amu in the Si-region, ~ 1 μm probing depth in Si, 80 - 100 Å surface resolution and 0.01 at. % minimum detection limit. Rapidly growing applications of this technique makes it a valuable complementary tool to other conventional analysis methods such as AES, ESCA and SIMS.

Modern technological developments and many fields of pure and applied research depend on the quantitative information about the spatial element distribution in thin solid layers and thin-film systems. For example, without the use of thin films the experimental studies on the physics of semiconductor are very difficult. Similarly the diffusion processes in solids, sandwich-like thin films structures in microelectronics, anti-reflecting or selectively transparent optical films, catalysts, coatings, composites - all rely on material properties on an atomic scale. The development of these new materials as well as the understanding of the basic physical and chemical properties that determine their specific characters are not possible without the knowledge of their compositional structure, in particular in the interface regions.

Modern material technology could not have progressed without the simultaneous advent of analysis techniques which can examine the surface and interface regions of solids. Several such techniques have been developed, and some of the most commonly used are: secondary ion mass spectrometry (SIMS), X-ray photoelectron spectroscopy (XPS) which is also known as electron spectroscopy for chemical analysis (ESCA), Auger electron spectroscopy (AES), particle induced X-ray emission (PIXE), nuclear reaction analysis (NRA), Rutherford backscattering spectrometry (RBS) and elastic recoil detection (ERD). Each technique has its own sets of advantages and disadvantages, and none capable of providing itself complete information on structure as a function of depth. In practice it is essential to apply more than one technique to perform the desired analytical tasks.

The energetic ion beam analysis techniques (PIXE, NRA, RBS and ERD) for accurate measurements of atomic composition and impurity concentrations in the near surface regions of solids have been now well established. The PIXE has an excellent sensitivity but has extremely poor depth resolution in routine depth profile analysis of thin films. The most commonly used ion beam analysis techniques are RBS and NRA. The RBS, which has several merits, e.g. ability to give absolute results, profile several elements simultaneously without the use of any standards, moderately good depth resolution, non-destructive, etc., becomes difficult or impractical when one want to profile light elements in the present of medium to heavy elements in the sample or substrate. One of the most difficult atomic species to profile but having enormous importance in many technological fields and specifically the polymer science is the hydrogen, for example, AES is insensitive to hydrogen while one can not use RBS because of its light mass. The commonly used technique is resonant nuclear reaction ^1H $(^{15}N, \alpha\gamma)$ ^{12}C at 6.4 MeV ^{15}N energy or ^1H $(^{19}F, \alpha\gamma)$ ^{16}O at either 6.4 MeV or 16.5 MeV ^{19}F energy near the surface. However, this technique suffers from several disadvantages, e.g. long measuring times, large ion dose requirement to obtain detailed profile, etc.

A very useful and powerful method to profile light elements including hydrogen in presence of medium to heavy elements is the ERD technique originally developed at the Université de Montréal which has several advantages over RBS. The original ERD technique

($\underline{1}$) is based on the ejection of the recoiled particles out of the sample in the forward direction by an energetic heavy ion beam. The measured energy spectra of these recoiled atoms can be related to their concentration profiles. The use of range foil in front of the energy detector to permit selective absorption of the various recoils introduces a few limitations in the application of the technique, e.g. deterioration of the energy resolution and hence the depth resolution, the limitation on the accessible depth in the depth profile information, etc. Indeed, the practical utility of the experimental set-up is enormously reduced in the region where overlapping spectra of various atoms are difficult to separate.

The drawbacks of the ERD using range foil for the mass discrimination have been removed by our group at the Université de Montréal in a very efficient way by using a time-of-flight (TOF) detection system ($\underline{2}$). Because RBS is now a relatively common and well established technique ($\underline{3}$), more emphasis is placed on the newly developed ERD-TOF facility. A brief description of our experimental facility as well as a newly developed versatile computer program ($\underline{4}$) capable of converting mass separated energy spectra into the depth profiles are given in the next section. Following that, some of the typical characteristics such as mass and depth resolution, sensitivity and quantitative reliability are illustrated through the applications of the technique to various thin films targets such as Corning Glass 0211, borophosphoro silica glass, silicon nitride and oxynitride, cobalt silicide and metal-polyimide interfaces. In the applications of ERD to the films of organic compounds one must be extra careful about the beam induced radiation effects. Some of these effects and a few possible solutions to minimize them have been pointed out.

Experimental Procedures .

Basic Principles in Nuclear Scattering . The basic principles of RBS and ERD could be briefly described using the schematic shown in Figure 1. The incident ion (Z_1), of mass M_1, and energy E_0 penetrates the target surface making an angle α and collides elastically with an atom (Z_2) of Mass M_2 situated at a depth x from the surface. After Coulomb scattering either the same mass M_1, emerges with energy E_1, or E'_1 from the surface (RBS) or it recoils mass M_2 with energy E_2 in the forward direction (ERD) making an angle β with the surface. Both the incident as well as outgoing ions suffer energy losses during their travel in the film that are proportional to their stopping powers which are energy and target (the film) composition dependent. The detected energies E_1 or E'_1, and E_2 are related to the incident ion mass M_1, and energy E_0 through the kinematic factors k_1 and k_2, respectively and the above mentioned energy losses. The expressions for k_1 and k_2 as well as Coulomb cross-sections σ_1 and σ_2 for RBS and ERD, respectively are given below.

$$k_1 = \left[\frac{\left(\mu^2 - \sin^2 \theta\right)^{1/2} + \cos \theta}{1 + \mu} \right]^2 \tag{1}$$

$$k_2 = \frac{4 \mu}{\left(1 + \mu\right)^2} \cos^3 \theta \tag{2}$$

$$\sigma_1 = \left(\frac{Z_1 Z_2 e^2}{4 E_0}\right)^2 \frac{4}{\sin^4 \theta} \frac{\left[\left(\mu^2 - \sin^2 \theta\right)^{1/2} + \mu \cos \theta\right]^2}{\mu \left(\mu^2 - \sin^2 \theta\right)^{1/2}} \tag{3}$$

$$\sigma_2 = \left(\frac{Z_1 Z_2 e^2}{4 E_0}\right)^2 \frac{4}{\cos^4 \theta} \left[\frac{1 + \mu}{\mu}\right]^2 \tag{4}$$

where $\mu = M_2/M_1$, θ is the scattering angle in the laboratory coordinate system and e is the electronic charge. Conventionally lighter ions such as protons and He, and θ approaching 180° are used in RBS in routine applications. However, use of heavier ions such as ^{12}C and ^{16}O are also increasing in selected applications because of their higher mass-resolution ability for heavier targets (5,6). From the kinematics of Coulomb scattering it is evident that when $M_1 \geq M_2$, there exists some critical angle $\theta_c \leq \pi/2$, where $\theta_c = \sin^{-1}(M_2/M_1)$, above which there are no RBS events. In ERD the detector has to be in the forward direction while the incident beam choice depends on several other factors including the recoils under investigation. In general the use of heavier ion beam (30-40 MeV ^{35}Cl or ^{40}Ar) permits to study several light and medium mass recoils using conventional charge particle detectors. When θ is less than θ_c the scattering of the incident beam in the direction of the detector is unavoidable, thus giving RBS (actually Rutherford forwarding scattering-RFS) events mixed with the recoils.

   The quantity of interest is the elemental concentration as a function of depth. The detected number of events are related to the concentration while their energies with respect to the maximum energy (surface energy) gives the depth information. These are discussed further in the depth profile analysis procedure described later.

   In ERD, from the consideration of various characteristics, e.g. maximum accessible depth, depth and mass resolution, detection sensitivity, etc, none of the experimental parameters, such as M_1, E_0, α, β, θ beam spot-size, and the detection solid angle Ω can be optimized without affecting the other. In our system, based on our needs as well as other anticipated applications, the overall choice of the ERD parameters are 30 MeV ^{35}Cl as the probing beam with $\theta = 30°$, $\alpha = \beta =$

15°, a beam size of 0.25 mm (width) x 2.0 mm (height) , and $\Omega = 10^{-4}$ sr. We are also equipped with conventional RBS, heavy ion RBS, PIXE, NRA and RBS-channeling facilities.

Experimental Arrangements in ERD . The ERD technique and the extended ERD with the TOF method used at the Université de Montréal have already been described in ref (1) and (2), respectively. Only a brief description is given below.

The schematics of the system used are shown in Figure 2. A well collimated incident ion beam strikes the target at glancing angle with the surface and the scattered incident ions as well as the recoils move in the forward direction toward a silicon surface barrier detector (SSBD). To profile hydrogen a range foil is used to stop all the ions except hydrogen as shown in Figure 2a. Another SSBD without absorber serves the purpose of normalization. In the ERD-TOF experiments the particles first pass through a thin (5-$10\mu g.cm^{-2}$) carbon foil as shown in Figure 2b. The secondary electrons emitted from the carbon foil are accelerated and then collected by a microchannel (MCP) detector which generate the first signal for the time measurement. The second time signal and the energy are obtained from a low resistivity cooled SSBD situated $\sim 70cm$ from the carbon foil. The mass M of the transiting ion is related to the particle energy E and the flight-time t through the relation

$$M = 2\, E t^2 / L^2 \qquad (5)$$

where L is the flight-length. The accurate determination of the energy is a difficult problem because of the non-linearity of the detector to various ions, the pulse-height defect phenomenon and the relatively poor resolution. As a first approximation the detector response is assumed to be linear and the mass is calculated event-by-event using the relation

$$M = 2\, (E_a + E_d)\, (T_a - T_d)^2 / L^2 \qquad (6)$$

where E_a is the apparent energy as given by the response curve for alpha particles; E_d is the pulse-height defect; T_a is the apparent time as given by the time-to-amplitude converter (TAC); and T_d represent various delays and walk corrections. The E_d and T_d parameters are known to be slowly varying functions of energy and mass. Our knowledge of these parameters in the regions encountered in the present ERD technique is incomplete and therefore, with our software, we treat these parameters as constants and adjust them to maximize the mass resolution in the chosen mass region. From Equation 5 the mass resolution can be readily deduced as:

$$\Delta M/M = [(\Delta E/E)^2 + (2\Delta T/T)^2 + (2\Delta L/L)^2]^{1/2} \qquad (7)$$
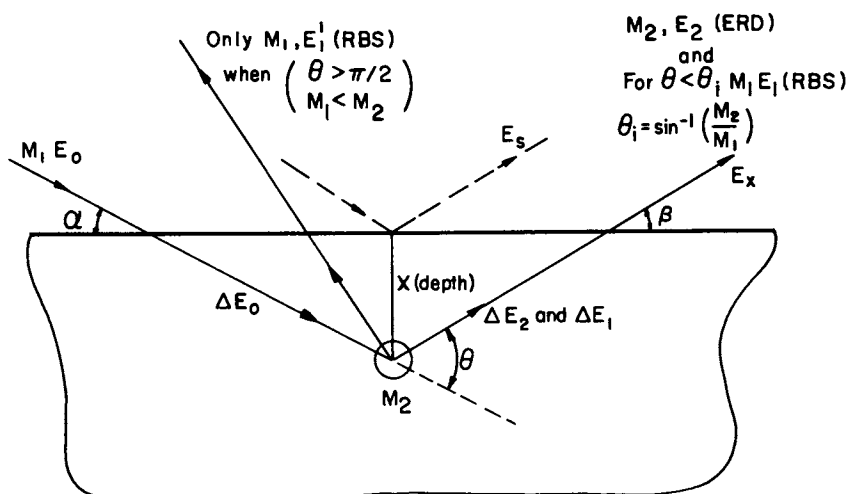
Figure 1. Schematic diagram of ERD and RFS nuclear scattering processes.
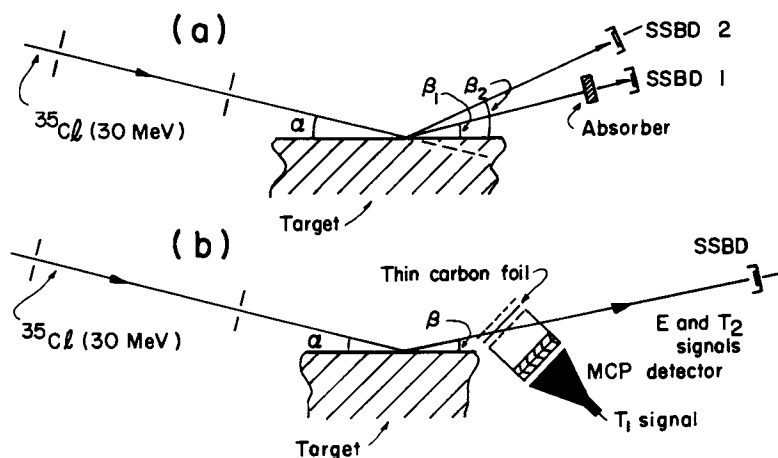
Figure 2. Schematics of the arrangements used in (a) ERD with absorber and (b) ERD-TOF, experiments.

where $\triangle E$, $\triangle T$ and $\triangle L$ are the variations in energy, flight-time and flight-path, respectively.

Depth Profile Analysis Procedure. By gating the mass-spectra the individual energy spectra of each mass is generated from the stored information. The next step is the deconvolution of the energy spectra according to the kinematics, cross-section, stopping powers and experimental conditions to produce depth profile for each element without any a priori assumptions about the composition of an unknown target (4). The depth deconvolution procedure is briefly discussed in the following.

Assume a target of uniform composition of two elements A and B as shown in Figure 3. It can be considered as a series of layers of partial thickness $\triangle x$. The mass separated energy spectra of the recoils of the two compositional elements are also schematically sketched. The highest energy in each spectrum corresponds to the scattering near the surface and the recoils from the inner depth appear at lower energies. In nuclear scattering analysis the natural and the most appropriate choice of the depth scale is in units of mass per unit area (e.g. μgcm^{-2}) because in most practical applications the physical density of the target is unknown. It should also be remembered that even in the layer structures or composites formed by the films of known densities, the interface region has unknown density which is changing as a function of depth. Consequently the stopping powers used in the calculation must be in density independent units (e.g. $keV\ cm^2\mu g^{-1}$).

In depth profile the quantity of interest is the concentration η, expressed in natural units (e.g. atoms $cm^2\mu g^{-1}$); it is related to the number of counts $\triangle C$ in a layer according to the relation

$$\triangle C = \sigma(E)\ \eta\ \triangle x\ \Omega\ Q \qquad (8)$$

where $\sigma(E)$ is the Coulomb cross-section at energy E referred to the surface of the layer according to the Equations 3 and 4, Ω is the detector solid angle, and Q is the total number of incident probing ions. For very thin films when the variations of the stopping powers are relatively very small, the total depth x can be calculated from the energy width (E_S-E) and the depth factor F using the equations

$$E_S - E = Fx \qquad (9)$$

$$F = \frac{k}{\sin \alpha}\left(\frac{dE}{dx}\right)_{in} + \frac{1}{\sin \beta}\left(\frac{dE}{dx}\right)_{out} \qquad (10)$$

where k is the kinematic factor (see Equations 1 and 2) and $(dE/dx)_{in}$ and $(dE/dx)_{out}$ are the stopping powers for the incident and outgoing ions, respectively. In general in many practical applications the
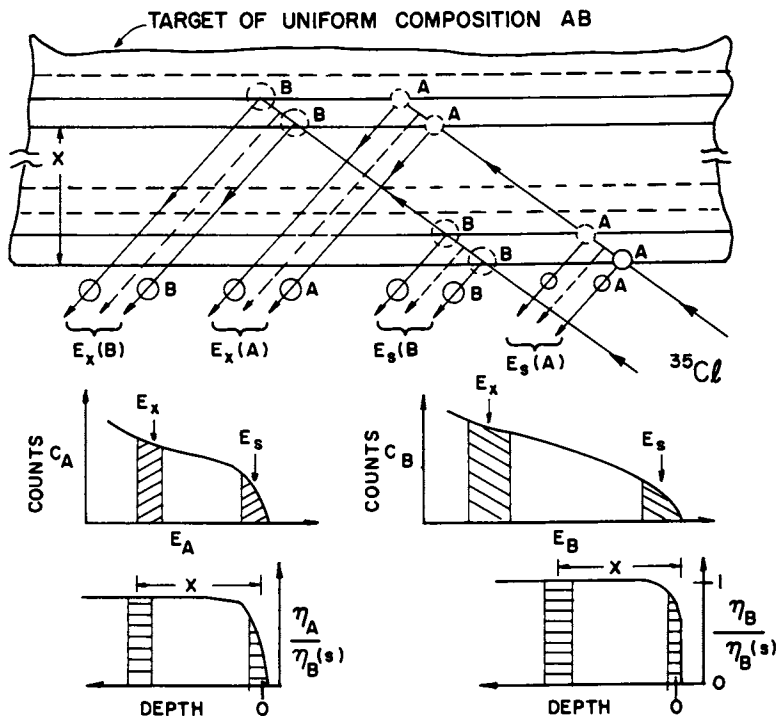
Figure 3. Schematics of the depth profiling approach for a sample of a homogeneous mixture of two monoisotopic elements A and B.

variations in the stopping powers are not negligible and therefore a complex computer program is required to evaluate the depth factors and the energies step by step at each layer.

We have developed the required sophisticated computer software in our laboratory. It is not a simulation program where some initial information regarding the sample is needed for the successful analysis. The basic approach involves the deduction of the depth represented by the counts at a certain energy by tracking back the recoil and tracing forward the projectile, from the surface in small fixed step sizes, applying stopping power formulas to change the energies until their ratio is the kinematic factor of the interaction: that the number of steps determines the depth. The required stopping power for each ion/target element combination is taken from the recent parametrization compilation given by Ziegler (7). In general these extrapolated values agree well with the available experimental energy loss measurements, the maximum deviation being less than 10%. Each element is profiled relative to a normalization window in the spectrum of a monitor element, which is usually the most abundant. Thus, for a specific layer in the target, the concentration of element A with respect to the concentration of element B near the surface can be readily obtained by using the Equation 8, e.g.

$$\frac{\Delta C_A}{\Delta C_B(s)} = \frac{\sigma_A}{\sigma_B} \frac{\eta_A}{\eta_B(s)} \frac{\Delta E_A}{\Delta E_B} \frac{F_B}{F_A} \frac{\Omega_A}{\Omega_B} \tag{11}$$

For an uniform composition of A and B one expects $\eta_B/\eta_B(s)$ equal to one as shown in Figure 3. There are several advantages of expressing the concentrations in the ratio form. Firstly, the need to know the incident ion dose Q is completely eliminated. In addition, if the elements A and B are detected in the same measurement, the Ω factors are also removed. Another practical advantage of the ratio method is the fact that the depth factor ratio F_A/F_B is relatively less sensitive to the gradual changes in the composition and the systematic errors in the energy loss parameters used in the calculation when a ratio is taken, the systematic changes in the numerator and the denominator tend to cancel each other.

The target material is generally of a more complex composition and in a definite layer structure (hence the interest); therefore, an iteration procedure is executed using Bragg's Law (8) which yields the stopping power of a complex target. The concentration of each element (from the initial calculations), at each step in depth, is used as weighting factor in the Bragg's Law calculation. The procedure is repeated with new profiles as weighting factors and generally converges after three iterations. Also since the calculation of the stopping power is done step by step, the iteration procedure automatically accounts for layer of different composition (such as thin layer of aluminium on top of polyimide). The program, to our knowledge first of its kind, is capable of handling a large number of multielement layers and is equipped

with a menu-driven database package which facilitates the manipulation and storage of data.

Applications of the ERD-TOF Technique

Corning Glass 0211. The performance of the ERD-TOF system to simultaneously depth-profile several light and medium mass elements can be illustrated by using a Corning Glass 0211 (used as glass-slide cover in optical microscopy) target. The chemical composition of this glass as specified by the manufacturer is given in Table I.

Table I. Composition of the Corning Glass 0211
as given by the Manufacturer

Component	Weight %
SiO_2	65
Al_2O_3	2
B_2O_3	9
Na_2O	7
K_2O	7
ZnO	7
TiO_2	3

By optimizing the E_d and T_d parameters in Equation 6 as well as neglecting the energy events below ~2.5 MeV a mass spectrum as shown in Figure 4a is obtained. The mass identifications are based on the mass calibrations obtained by using known single element targets and also the glass composition given in Table I. An excellent mass resolution for the observed elements up to ^{23}Na is clearly evident. For heavier masses the resolution deteriorates mainly because of the degradation of the SSBD energy resolution (see Equation 7). The weak ^{27}Al and ^{29}Si mass peaks are not resolved from the intense ^{28}Si. However, the strong ^{35}Cl peak is completely separated from the adjacent ^{30}Si and ^{39}K peaks. The Ti and Zn mass peaks have additional broadening of overlap effects because each of these elements has five stable isotopes with varying abundances. By setting gates on various mass peaks the corresponding energy spectra could be deconvoluted from the total recoil energy spectrum as shown in Figure 4b. The ^{35}Cl energy spectrum results from the Rutherford forward scattering of the incident beam from the various target elements having masses greater than 18 mass units and has been subtracted from the total energy spectrum to get the total recoil spectrum. Using the depth-profile program mentioned in the previous section, the individual recoil spectra were converted into the depth profiles. Figure 4c shows a composite depth profile plot in which the ordinate scale is expressed as weight percent for an ease in comparison. Each profile has been smoothed out using a special computer software routine in a piece-wise fashion based on the user defined layer structure to retain the evident structure in the transition regions. Nearly uniform depth
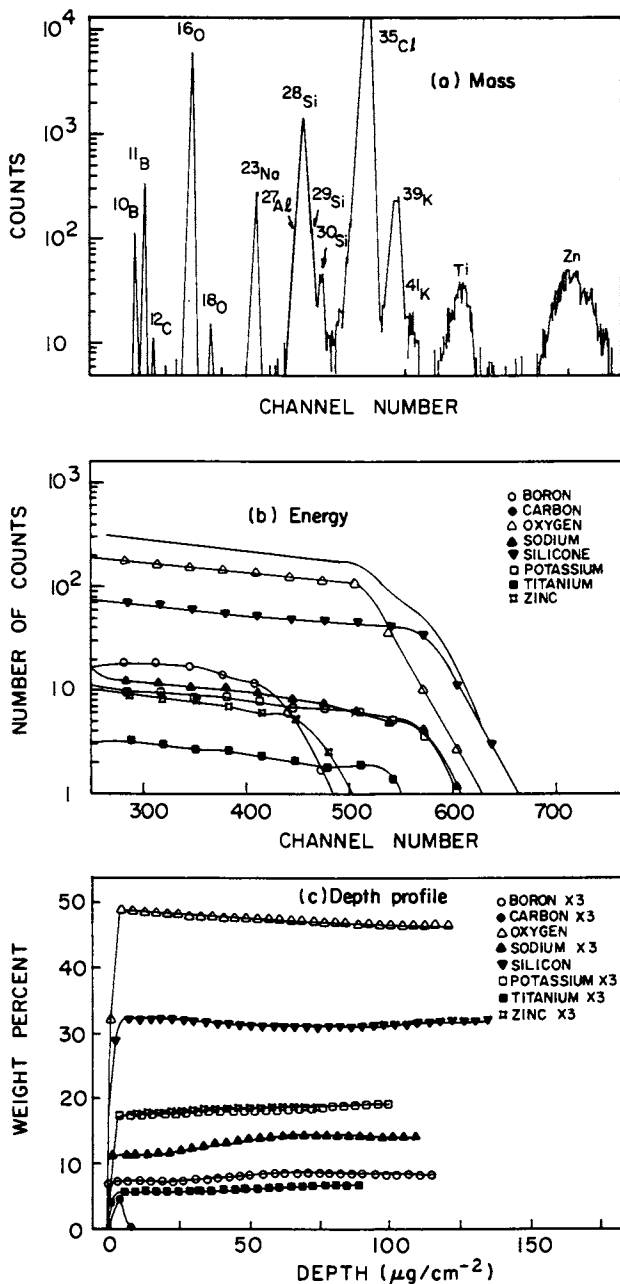
Figure 4. ERD-TOF results from a Corning Glass 0211 target: (a) mass spectrum, (b) mass separated energy spectra superimposed by total energy spectrum, and (c) composite depth profile of the observed elements.

distribution for nearly all the elements is consistent with the expected homogeneity of the material. In order to check the consistency of the results, the experiments were repeated after a period of two months using different targets of the same batch. As can be seen from the Table II, the reproducibility of the ERD results in two separate experiments is excellent. In addition, the measured concentrations of elements of the target are in very good agreement with the expected numbers deduced from the specified glass composition (see Table I). The experimental numbers given in Si column includes the Al contribution.

Table II. ERD Results Compared with the
Manufacturer's Specifications

| Elements | Weight% | | | Atomic% | | |
	ERD #1	#2	Manuf.	ERD #1	#2	Manuf.
B	2.67	2.74	2.83	5.16	5.22	5.21
O	47.20	47.37	47.33	61.56	61.02	61.94
Na	4.39	4.72	5.19	3.98	4.25	4.60
Al			1.06			0.79
Si	31.27	31.22	30.33	23.30	23.05	21.95
K	5.90	5.40	5.82	3.16	2.86	3.02
Ti	2.04	2.09	1.80	0.88	0.90	0.76
Zn	6.05	6.44	5.62	1.94	2.21	1.73

It seems that in ERD-TOF technique, the corning Glass 0211 can act as a suitable standard for not only the mass and energy calibrations but also for the relative concentrations of several elements. Further work on different Corning Glass samples to explore the feasibility of establishing their use as calibration standards in surface analysis techniques, such as ERD, SIMS, ESCA and AES, are in progress.

Borophosphoro-silica Glass. Thin films of borophosphoro silica glass films are extensively used in integrated circuits in silicon-based technology. One of the widely used methods to dope boron and phosphorous is achieved by adding their hydrides, phosphine (PH_3) or diborane (B_2H_6), to the silane (SiH_4) hydrogen gas mixture used in various vapour deposition techniques. The knowledge of the film composition including other impurities is very important in optimizing the fabrication conditions, such as gas flow rates, plasma frequency and power, and substrate temperature. The depth profiling by RBS technique has serious limitations as weak boron signal gets buried under the intense silicon background while phosphorous is not resolved from silicon. On the other hand the ERD-TOF technique not only readily and reliably gives depth profiles of boron and phosphorous

but can also quantify the presence of weak impurity elements such as hydrogen, carbon and nitrogen, if present.

Typical mass spectra in the carbon and silicon region obtained from a 0.9 μm thick borophosphoro silica glass are shown in Figure 5a. A mass resolution (full width at half maximum-fwhm) of 0.2 amu for ^{11}B and ~0.7 amu (fwhm) for ^{28}Si is clearly evident. Using the mass separated energy spectra and the deconvolution program the depth profiles of B and P can be deduced. In figure 5b the weight percent of B and P are plotted as a function of diborane flow rate keeping all other fabrication parameters constant. The concentrations of B were also obtained by using chemical methods and by wave length dispersive X-ray analysis (WDX). Similarly the P concentrations were deduced from the chemical analysis as well as energy dispersive X-ray analysis (EDX). These results are also shown in Figure 5b for comparison. A close correlation of the ERD results with the other methods of analysis is clearly evident. However, it must be noted that the WDX and the EDX are incapable of providing the depth profile information.

Silicon Nitride and Oxynitride Films. A systematic study of the chemical composition and the associated physico-chemical properties of the films produced by plasma enhanced chemical vapour deposition (PECVD) in a large volume microwave plasma reactor (LMP^R) has been an ongoing activity of our group since the past three years (9, 10). Thin dielectric layers of silicon compounds (P-SIN and Si_3N_4: H, P-SiO_2, P-SiON, a-Si:H) are of great importance in numerous Si and GaAs based microelectronics and macroelectronics applications. There are several critical fabrication parameters which affect the quality and the performance of the film. Of critical importance is the knowledge of correct chemical composition as a function of depth. The results to date have shown that the ERD method to be eminently applicable to study such films and the associated interfaces. Several of these films contain hydrogen as an unavoidable intrinsic impurity because of the basic conditions used in film fabrication processes (11), leading to the synthesis of new materials such as amorphous polysilane polymers (12) a-(SiH_2), or to the silane diimide (13) a-$Si(NH)_2$. Some times hydrogen is present due to deliberate preferential incorporation e.g. in PECVD amorphous hydrogenated (or deteriorated) silicon nitrides (14) such induced hydrogen is known to play the specific roles in film growth and structural properties. In many applications hydrogen is also found to be responsible for the degradation of the chemical stability and thereby of dielectric and other physical properties (15). The application of ERD using range foil to profile hydrogen is now well established (16-18). Although modified ERD-TOF technique (2) has higher depth resolution and accessible depth, it has a lower detection efficiency for hydrogen due to the limitations on the response characteristics of the MCP detector to protons. All the hydrogen concentrations reported in this article are based on the ERD technique using a range foil.

Figure 6a displays a typical composite atomic percent depth profile plot of all the observed elements from a ~ 1500Å thick layer of nearly
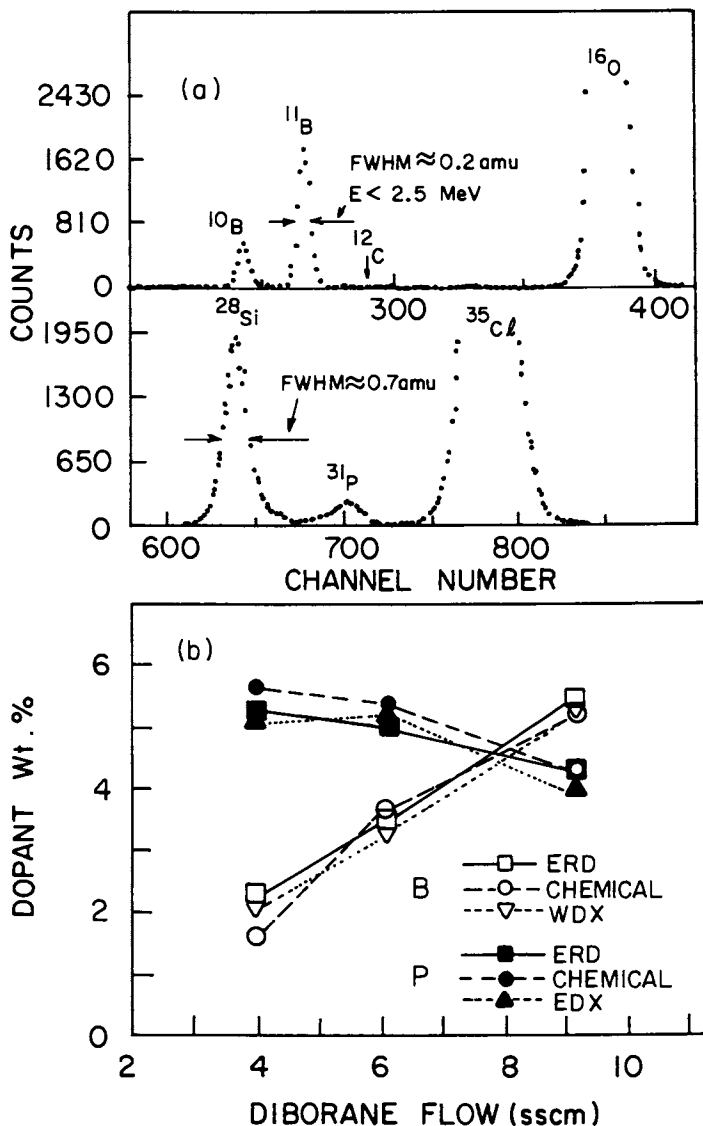
Figure 5.(a) Typical mass spectra of a 0.9μm borophosphoro silica glass (b) weight % concentrations of B and P compared with chemical analysis, EDX and WDX at various diboran flow rates.

stoichiometric PECVD a-Si$_3$N$_4$ on a silicon substrate precoated with a thin SiO$_2$ film. In order to illustrate the ability of the smoothing routine of the program the data points along with the fitted curve are shown only for the Si to avoid the complexity in the display. The O profile at the interface between the two layers matches extremely well with the falling edges of N and H as expected. The corresponding dip at the interface for Si however is not as sharp because of the effects of detector resolution and energy straggling. The surface C impurity is related to the interaction of the accelerated beam with the residual gas in the accelerator vacuum and can be easily reduced by using appropriate cold traps just before the target.

Figure 6b shows η_N/η_{Si} ratio as a function of [NH$_4$]/[SiH$_4$] gas ratio. The ERD results are based on the techniques described here while the XPS detections are based on A$_N$ $_{1s}$/A$_{Si}$ $_{2p}$ area ratio from core-level spectra of these films obtained either with the Al Kα or Mg Kα excitation lines. The refractive index results in the figure refers to the model dependent deductions of η_N/η_{Si} obtained by utilizing measured refractive index values using ellipsometry. For more specific details refer to our recent publication (19). At low gas ratios the agreement between the three measurements is quite satisfactory. Above [NH$_4$]/[SiH$_4$] = 1/2, the η_N/η_{Si} ratio from XPS and refractive index measurements are systematically higher and lower, respectively, than those determined by ERD. However, it has been shown (19) that the ERD results are most reliable in this stoichiometry range and the probable cause of any discrepancy is due to the limitations in other techniques e.g. in XPS it could be attributed to the variations in mean free path parameter λ used in the ratio calculation. Finally, the linear part of the log-log plot in Figure 7b corresponds to a square-root dependence of the η_N/η_{Si} ratio on the gas ratio covering 2/100 to 5/1 range.

In thin film applications ERD deserves a special merit worth mentioning. For the films of uniform composition the substrate whose density is known is also simultaneously profiled, the atomic densities (e.g. atoms/cm^3) of all the elements in the layer can be readily deduced by making use of the prior knowledge of the film thickness or the density. Indeed such quantitative results from ERD have been proved to be very useful in correlating other experimental and theoretical findings (19,20).

Cobalt Silicides. The interest in the study of metal silicides is growing at much faster rate because of their use as interconnects and contacts in semiconductor and VLSI technology. The silicides in general have lower resistivity than polysilicon and are able to withstand high annealing temperatures than most pure metal interconnects. In the development of the metal-silicide studies the most important quantities of interest are metal/Si ratio as a function of depth, the silicide film thickness and the identification and the quantification of any contaminants present. The conventional surface analysis techniques
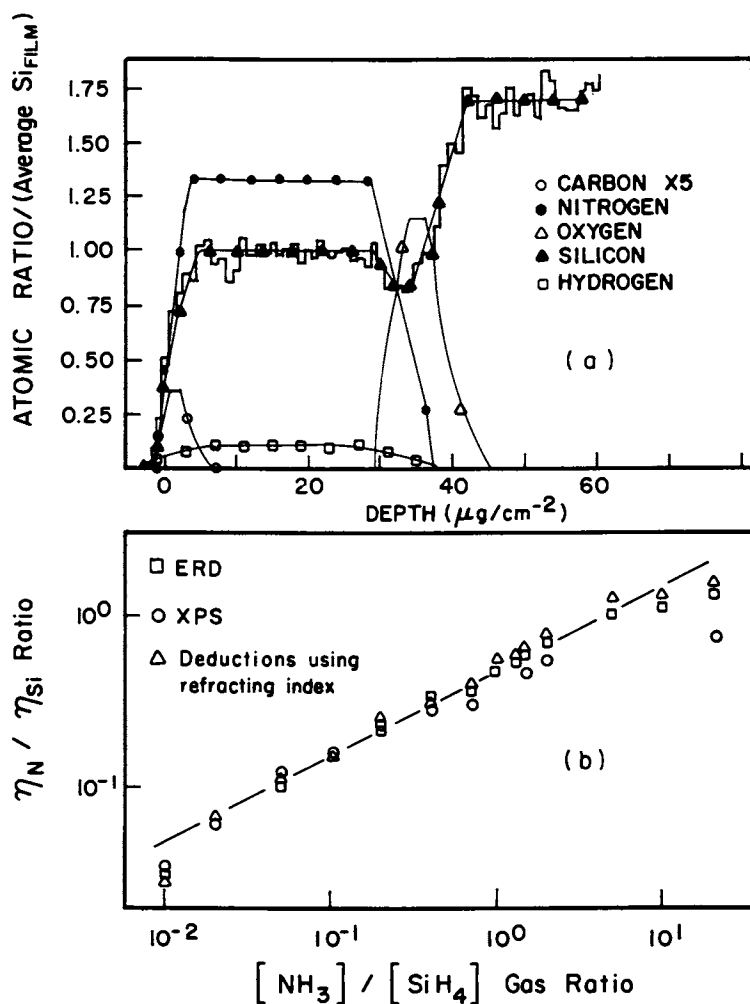
Figure 6.(a) Composite depth profile plot of a silicon nitride film on Si precoated with SiO_2. (b) η_N/η_{Si} ratio versus [NH3]/[SiH4] gas ratio for a-$Si_xN_yH_z$ PECVD film from ERD, XPS and the deduction based on measured refractive-index.

such as SIMS, XPS and AES require the use of ion sputtering for depth profiling. In such techniques the problems of experimental artifacts, e.g. preferential sputtering, sputter induced changes in the chemical bonds, etc. are inherent and unavoidable. These problems directly affect the yields. Sometimes one can overcome these limitations by using appropriate standards. However, in idealistic situations the required standards must be as close in composition as possible to silicide of interest. Unfortunately these standards are often hard to find if available at all. The standard-free nuclear scattering techniques such as RBS and ERD act as important complementary tools to other surface analysis methods. The technique described herein has added advantage over RBS of giving simultaneous information of light contaminants.

The results of a typical application in the study of cobalt silicide are displayed in Figure 7 in which the depth profiles of Si and Co are expressed as atomic ratios with respect to the average Co concentration in the film after it has been heat treated at various temperatures. The curves in Figure 7a result from a sample in which there is a Co film of ~ 585Å on pure Si wafer. It is now well-established that in the formation of metal silicide systems the initial changes in the composition occur at the interface without apparent changes at the sample surface. With the increase in the heat treatment one can then induce the effects including the phase changes in silicon throughout the film by appropriate combination of temperature and time duration. The curves in sections b, c and d of Figure 7 show the successive results after treatment at increasing temperature of appropriate duration. The initial tendency of formation of Co_2Si followed by the growth of the monosilicide phase CoSi and subsequent $CoSi_2$ can be easily visualized through these results. The increase in the film thicknesses are consistent with the changes in the physical densities of various phases.

Polyimide-Metal Interfaces. Several technological applications including semiconductor packaging and metallization demand a reliable and durable adhesion properties of the metal films. In the development of multilayer devices consist of alternating layers of metal and polyimides several reliable techniques are needed to study both thin films and their interfaces. The usefulness of the nuclear scattering techniques to study the metallization and the associated interfacial elemental diffusion processes under the effects of various temperature and humidity treatments on the metal-polyimide systems, such as Al, Cu, N, and Au on Du Pont Kapton type H have already been reported (21, 22). Only a couple of examples are presented here to illustrate the ERD application.

It is now well established that organic polymers are rather more sensitive to various ionizing radiations. In a recent study (23) it has been shown that the irradiation of polystyrene films by 20 MeV ^{28}Si beam results in ion-induced modifications of the sample because a significant quantity of H and C nuclei is released when the beam dose is increased above 10^{12} ions cm^{-2}. Similar effects of erosion of H and C profiles of plasma-polymerized hexamethydisilasene (HMDSN) thin

films were noted by our research group (24). However the corresponding Si profiles of HMDSN were found to be relatively stable under the beam doses studied.

In order to evaluate the effects of radiation damage on kapton substrate the H profile was studied systematically using lowest practical beam current of ~ 0.1 nA particle. Figure 8 shows the H concentration profile in Kapton from a composite spectrum taken at different spots on the target (curve a) and a spectrum taken at one spot (curve b), both the curves having the same integral dose. The horizontal line corresponds to the expected H concentration of 25.6 at.% based on the known Kapton composition $C_{22} H_{10} N_2 O_5$. In curve a, with an exception of a small bump near the depth of ~ $4 \mu gcm^{-2}$, the observed H concentration is nearly uniform and agrees with the expected value while the curve b clearly demonstrates an erosion up to a depth of 0.4μm. Further systematic studies reveal that the C concentration showed no detectable dependence on the beam current, instantaneous or integrated when the maximum dose was ~ 5×10^{13} ions cm^{-2} but both H and O concentrations relative to C always showed erosion effects similar to the ones shown in Figure 8b. By using low beam current of 1-2 nA particle and the dose less than 10^{13} ion cm^{-2}, all the depth profile spectra consistently showed the same structure.

As an example of polyimide-metal interface study consider the results displayed in Figure 9 in which part (a) shows a composite depth profile plot of Al, C and O elements form a target consisting of Al film on dry polyimide while (b) is the result of the Al film on hydrolyzed polyimide. A careful look at the interface region clearly demonstrate the mutual interpenetration of polyimide and metal. The evaporation of metal onto hydrolyzed polyimide surface increased interfacial mixing and metal tailing associated with the augmentation of the width. These changes may be attributed to the formation of mixed region at the interface. For more details one may refer to the reference (22).

An important application of ERD using ^{4}He beam to study proton and deuterium depth profiles in polymer-polymer diffusion studies has been recently well established (25-27). In these studies a significant contribution to the surface depth resolution comes from the straggling in the range foil Mylar absorber (10.6μm) needed for mass discrimination. In addition when hydrogen and deuterium energy spectra start overlapping there is a primary restriction on the measurable range of tracer diffusion coefficient D*. One can easily improve these limitations by using the ERD-TOF system described herein, albeit accepting a lower detection efficiency (~ 30%) for hydrogen (2). Recently we have been able to improve the H efficiency in our ERD-TOF set up to ~ 45% by optimizing the operational conditions of the MCP detector. Further experiments to increase the secondary electron yield from the carbon foil are promising.
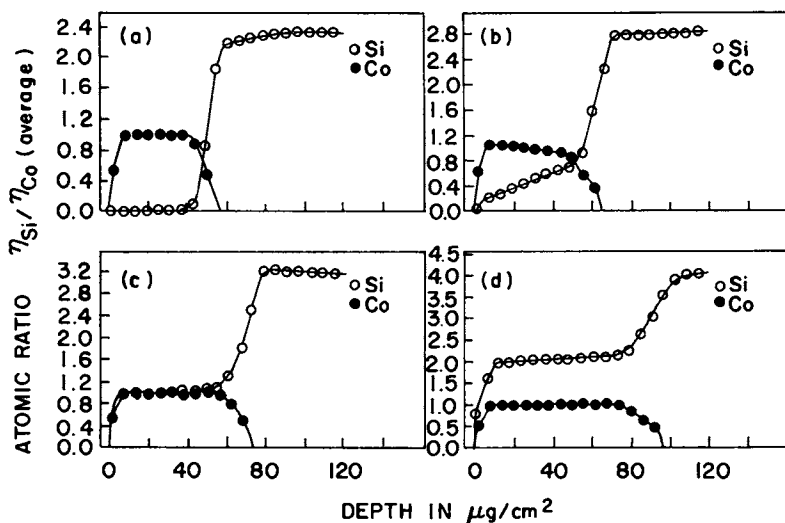
Figure 7. ERD application in the study of various phases of cobalt silicide. (a) Co film on Si, (b) ~ Co$_2$Si, (c) CoSi and (d) CoSi$_2$.
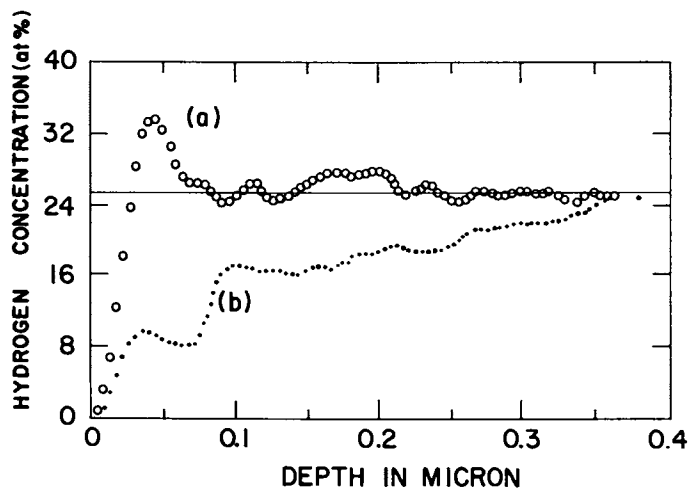
Figure 8. Hydrogen depth profile in Kapton (a) from a composite spectrum taken at different spots and (b) from a spectrum at one spot.
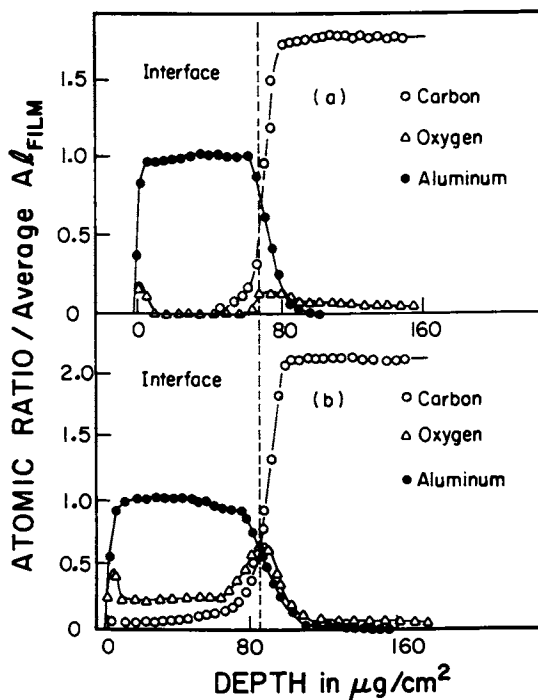
Figure 9. Composite depth profiles of Al, C, N and O from a target consisting of Al film on (a) dry and (b) hydrolized Kapton.

Operational Characteristics

The operational characteristics such as depth resolution, maximum accessible depth and minimum detection limit in ERD are highly subjective to each experiment condition. In our system with the conditions described in the experimental procedures section and assuming Si as the primary matrix for the target, the typical performance characteristics in routine applications are 80-100 Å depth resolution, ~ 1 μm maximum depth and about 0.1 at.% minimum detection limit. For more discussion of operation characteristics one may refer to our earlier work (2).

Conclusion

An ERD technique involving RFS and using 30 MeV ^{35}Cl ions as beam probe is described. The power and the utility of this quantitative method to simultaneously depth profile several light (including H) and medium mass elements are illustrated through a few examples form our routine applications. In nuclear scattering there is always the question of unavoidable radiation damage which is particularly more serious in the targets involving organic polymers and polyimides. However by adjusting suitable experimental conditions one can keep the damage effects to the minimum so as to obtain reliable depth profile information. The quantitative results of ERD are shown to be in good agreement with the corresponding results from other conventional surface analysis methods. Even though ERD is incapable of providing information about types of chemical bonding of the constituent atoms like ESCA and does not have the sensitivity of SIMS, it has the unique characteristics of providing simultaneous multielemental depth profiling information without destroying the target or using any external standards. It can act as a valuable complimentary surface analysis tool.

Acknowledgments

Literature Cited

1. L'Ecuyer, J.; Brassard, C.; Cardinal, C.; Chabbal, J.; Deschênes, L., Labrie, J.P.; Terreault, B.; Martel, J.G.; St.-Jacques, R. J. Appl. Phys. 1976, 47, 881.
2. Groleau, R.; Gujrathi, S.C.; Martin, J.P. Nucl. Instr. and Meth. 1983, 218, 11.
3. Chu, W.K.; Mayer, J.W.; Nicolet, M.-A. Backscattering Spectrometry; Academic Press, New York, 1978.

4. Oxorn, K.; Gujrathi, S.C.; Bultena, S.; Cliche, L.; Miskin, J. <u>Nucl. Instr. and Meth</u>. 1989, In press.
5. Peterson, S.C.; Ostling, M. <u>Nucl. Instr. and Meth</u>. 1984, <u>B4</u>, 88.
6. Yu, K.M.; Jaklevic, J.M.; Haller, E.E. <u>Nucl. Instr. and Meth</u>. 1985, <u>B10/11</u>, 606.
7. Ziegler, J.F., Biersack, J.P.; Littmark, U. <u>The stopping and range of ions in solids. Vol 1</u>, Pergamon Press, New York, 1985.
8. Feldman, L.C.; Mayer, J.W. <u>Fundamentals of Surface and Thin Film Analysis</u>, North-Holland, New York, 1986, p. 47.
9. Tessier, Yves; Klemberg-Sapieha, J.E.; Poulin-Dandurand, S.; Wertheimer, M.R.; Gujrathi, S.C.; <u>Can J. Phys</u>. 1987, <u>65</u>, 859.
10. Blain, S.; Klemberg-Sapieha, J.K.; Wertheimer, M.R.; Gujrathi S.C.; <u>Can. J. Phys</u>. 1989, <u>67</u>, 190.
11. Voke, N.; Kanicki, J. <u>Mater. Res. Soc. Symp. Proc</u>. 1986, <u>68</u>, 775.
12. Furukawa, S., Matsumoto, N.; Toriyama, T.; Yabumoto, N., <u>J. Appl. Phys</u>. 1985, <u>58</u>, 4658.
13. Tsu, D.V.; Lucovsky, G.; Mantini, M.J. <u>Phys. Rev</u>. 1986, <u>B33</u>, 9069.
14. Maeda, M., Nakamura, H. <u>J. Appl. Phys</u>. 1984, <u>55</u>, 3068-.
15. Flamm, D.L.; Ibbotson, D.E.; Chang, C.P. Mucha, J.A. <u>Proc. IUPAC Int. Symp. on Plasma Chemistry, ISPC 8</u>, Tokyo, Japan, Aug. 1987, p. 1124.
16. Brebner, J.L.; Cochrane, R.W., Groleau, R.; Gujrathi, S.C.; Keroack, D.; Lépine, Y.; Martin, J.-P.; Vanacek, M., Aktik, C.; Aktik, M.; Azelmad, A.; Currie, J.F.; Poulin-Dandurand, S.; Ranchous, B.; Sacher, E.; Tannous, C.; Wertheimer, M.R.; Yelon, A. <u>Can J. Phys</u>. 1985, <u>63</u>, 786.
17. Nagai, H.; Hayashi, S.; Aratani, M.; Nozaki, T.; Yanokura, M.; Kohno, I.; Kuboi, O.; Yatsurugi, Y. <u>Nucl. Instr. and Meth</u>. 1987, <u>B28</u>, 59.
18. Paszti, F.; Kotai, E.; Mezey, G.; Manuaba, A.; Pocs, L.; Hildebrandt, D.; Strusny, H. <u>Nucl. Instr. and Meth</u>. 1986, <u>B15</u>, 486.
19. Bustarret, E.; Bensouda, M.; Habrard, M.C.; Bruyère, J.C.; Poulin, S.; Gujrathi, S.C. <u>Phys. Rev</u>. 1988, 8171.
20. Rostaing, J.C.; Cros, Y.; Gujrathi, S.C.; Poulin-Dandurand, S. <u>J. Non-Cryst. Solids</u> (1987), <u>97 & 98</u>, 1051.
21. Currie, J.; Depelsenaire, P.; Groleau, R.; Sacher, E. <u>J. Colloid and Interface Sci</u>. 1984, <u>97</u>, 410.
22. Chauvin, C.; Sacher, E.; Yelon, A.; Groleau, R.; Gujrathi, S.C. in <u>Surface and Clloid Science in Computer Technology</u>; Mittal, K.L., Ed; plenum, New york, 1987, p 267.
23. Green, P.F.; Doyle, B.L. <u>Nucl. Instr. and Meth.</u>, 1986, <u>B18</u>, 64.
24. Groleau, R.; Currie, J.F.,; Wertheimer, M.R.; Klemberg-Sapieha, J.E. <u>Thin Solid Films</u>. 1986, <u>136</u>, 85.
25. Mills, P.J.; Green, P.F.; Palmstrøm, J.C.; Mayer, J.W.; Kramer, J.E. <u>Appl. Phys. Lett</u>. 1984, <u>45</u>, 957.
26. Green, P.F.; Mills, P.J.; Palmstrøm, J.C.; Mayer, J.W.; Kramer, J.E. <u>Phys. Rev. Lett</u>. 1984, <u>53</u>, 2145.
27. Green, P.F.; Mills, P.J.; Kramer, J.E. <u>Polymer</u>, 1986, <u>27</u>, 1063.

Chapter 7

Quantitative Trace Element Analysis by Proton-Induced X-ray Emission

A. J. Houdayer[1,3], P. F. Hinrichsen[1,4], and J.-P. Crine[2]

[1]Laboratoire de Physique Nucléaire, Université de Montréal, C.P. 6128, Succursale A, Montreal, Quebec H3C 3J7, Canada
[2]Hydro-Québec Recherche (IREQ), C.P. 1000, Varennes, Quebec J0L 2P0, Canada

The application of PIXE (Proton Induced X-Ray Emission) and micro-PIXE to quantitative analysis of impurities in polyethylene are described. The equipment, sources of background which affect the sensitivity and the precision of PIXE measurements are discussed for both thick and thin targets. A number of applications of micro-PIXE to the identification and location of trace elements in the "Trees" found in the polymer insulation of HV cables are presented.

PIXE (Proton Induced X-ray Emission) is a quantitative trace element analysis technique that combines the use of protons, or other heavy particles, to excite the characteristic X-rays of the trace elements in a sample with subsequent detection by an energy dispersive Si(Li) X-ray detector. This combination constitutes a very powerful technique for multi-elemental analysis with high sensitivity, and has been employed in a variety of different fields (1).

A brief discussion of the physical principles of PIXE as they relate to the background, sensitivity, and precision of the method will be presented. The design and performance of a typical experimental system will be illustrated by a description of both the conventional PIXE and micro-PIXE setups at the Laboratoire de Physique Nucléaire of the Université de Montréal.

The degradation processes known as "water treeing" and "electrical treeing" are major problems causing premature failure of underground high voltage cables.

[3]On leave from CEGEP André-Laurendeau, Montreal, Quebec H8N 2J4, Canada
[4]On leave from John Abbott College, Ste-Anne-de-Bellevue, Quebec H9X 3L9, Canada

Electrical trees are essentially breakdown channels whose size, typically 50 to 200 microns, together with the large variations in impurity concentrations in the surrounding polyethylene, makes the identification of the impurities associated with both kinds of trees very difficult by traditional techniques. The use of micro-PIXE for the location and analysis of trace elements in electrical and water trees found in the polyethylene insulation of high voltage cables will be described.

PIXE

When a sample is bombarded with protons they loose energy while slowing down in the target and ionize the target atoms which then emit their characteristic X-rays in a subsequent de-excitation process. The X-ray production cross section is thus a product of the ionization cross section, the fluorescent yield and the probability of transitions to fill the inner shell vacancy. The ionization cross section is predominantly Coulombic, and has a broad maximum when the velocity of the incident particle matches the orbital velocity of the electron (1). Thus for thin targets, i.e. targets for which the incident particle loses only a small fraction of its energy, the energy of the incident particle can be chosen so as to maximize the X-ray yield from a given element. The yield is generally adequate and for analysis of impurities it is the sensitivity or signal to noise ratio which depends on the inherent background which must be optimized.

The major sources of background in PIXE are bremsstrahlungen due to slowing down of both secondary electrons and the incident particles, and Compton scattered γ-rays from nuclear reactions in the target and the beam-defining slits etc. The latter is negligible at low bombarding energies and can be significantly reduced by appropriate design of the apparatus. The cross section for the production of bremsstrahlungen by the incident particles is given by

$$\frac{d\sigma}{dE_x} = C \frac{AZ^2Z_1^2}{EE_x} \left(\frac{Z}{A} - \frac{Z_1}{A_1} \right) \tag{1}$$

Where C is a constant, Z_1 and A_1 are the charge and mass of the target atom and Z, A and E are the charge mass and energy of the incident particle. It can be immediately seen that heavy projectiles significantly reduce the value of the term in the bracket(i.e. Z/A is almost the same for both the incident particle and target) and thus have a major advantage over electrons used in SEM.

The low energy background in PIXE, is due to secondary electron bremsstrahlungen the intensity of which are proportional to the characteristic X-rays, as both depend on the generation of vacancies in the electron

shells by the incident particles. Fortunately however the
energy of the secondary electrons is limited to $E_X >$
(4m/M) E, where m/M is the ratio of the electron to the
incident particle mass. Thus the choice of the incident
particle energy is a compromise between increasing the
production cross section and reducing the bremsstrahlung
background in the region of the characteristic X-rays from
the elements of interest. For thin targets the incident
particles are essentially monoenergetic, while for thick
targets (i.e. those which completely stop the incident
particles) the above expressions have to be integrated
over the particle energy as it traverses the target
material (2).

The optimum conditions for maximum PIXE sensitivity
with both thin targets (1), and thick targets (2) have
been extensively investigated and suggest that a thin
target sensitivity of 1 ppm can be achieved for elements
from Na to Pb. Optimum sensitivity can be achieved for a
wide range of elements by choosing two bombarding
energies, namely 1 MeV for Z = 11 to 26,(the response of
our detector is limited to Z > 10 by the beryllium
window), and 3.0 MeV which is high enough to excite the K
X-rays of elements up to Z = 50 and the L X-rays of
heavier elements, while not producing significant
background due to nuclear gamma radiation. The above
estimate of ppm sensitivity assumes the use of energy
dispersive Si(Li) X-ray detectors. Such detectors
typically have an energy resolution of FWHM = 150 eV at
5.9 keV. Improved resolution as well as increased solid
angle and exposure times can materially improve the
sensitivity. Recently wavelength dispersive detectors
have been used for PIXE (3) to improve the detector
resolution and hence the sensitivity, however at the
expense of solid angle.

For polyethylene samples the X-rays from the matrix
are absorbed by the beryllium window of the X-ray detector
and thus do not contribute to the background. However for
other samples, such as Si or GaAs semiconductors, the
characteristic X-rays of contaminants which fall in the
energy regions of the L and M X-rays of the matrix
elements are masked, see for example the spectrum from
H_2Pc shown in figure 1 in which the iodine L X-rays mask
the Ti K X-rays. Furthermore the response function of
Si(Li) X-ray detectors generally has a low energy tail
which can also contribute to the background for
characteristic X-rays below those of the matrix. Such
problems can often be overcome by the use of selective
filters (4).

The fact that neutron irradiation of hydrogen and
carbon produces no significant radioactivity makes Neutron
Activation Analysis (NAA) a very sensitive analytical
technique for detecting impurities in polymer cable
insulation and has been extensively used for this purpose.
It is therefore of some interest to compare PIXE with NAA.
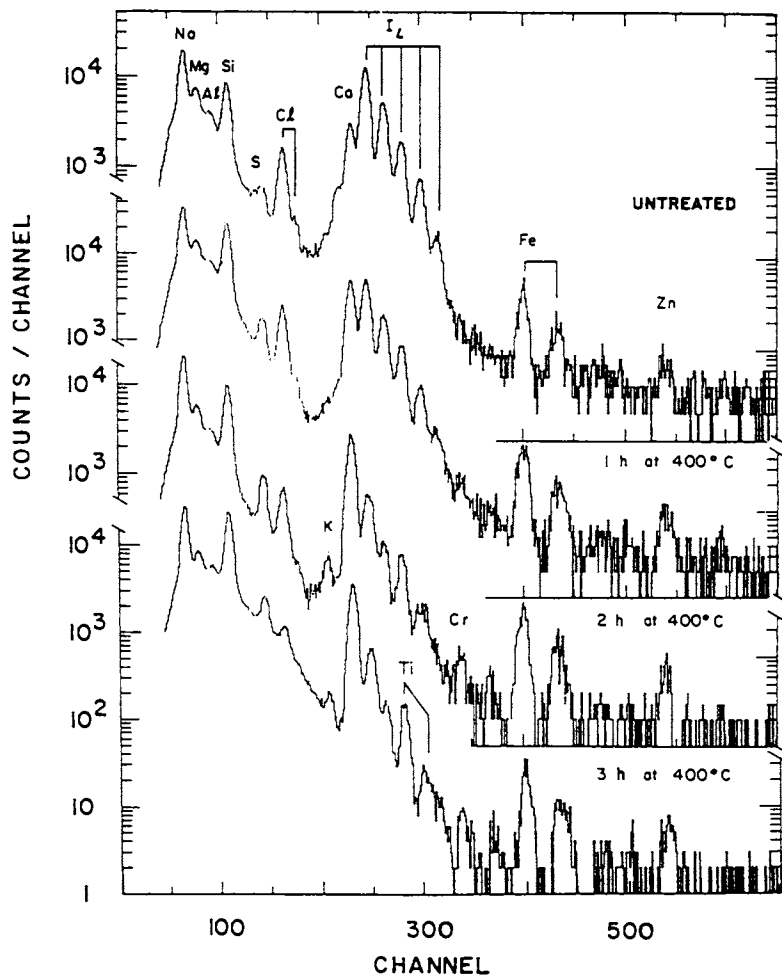
Figure 1. PIXE X-ray spectra from 1 MeV proton bombardments of an untreated sample of H_2Pc, and samples heat treated at 400 °C for 1, 2, and 3 hours respectively.

The sensitivity of NAA is limited by the statistics of the gamma ray background and of the signal which is proportional to the number of activated atoms and thus, for a given impurity concentration, to the quantity of sample irradiated. For many elements the sensitivity of NAA of 1 gram samples is superior to PIXE, however, NAA cannot detect some elements (such as lead) and is not very sensitive for others such as Si and Fe which are important contaminants of polyethylene insulation. Thus, the combination of NAA and PIXE allows one to estimate the concentration of a wide range of elements. Furthermore PIXE sensitivity is independent of the beam spot size, thus the use of a focused proton beam coupled with the short range of protons means that the sampled mass is typically a few nanograms, and therefore the absolute quantity of impurity which can be detected is very much lower than for NAA. Thus PIXE is unique, with sensitivity at the ppm level, for localized non-destructive multi-elemental analysis of nanogram samples. It might be thought that EDX with SEM, which can achieve much smaller beamspot sizes, could be even better, however, as pointed out above the bremsstrahlung background for EDX is about two orders of magnitude greater than for PIXE, and the sampled volume is limited by multiple scattering in the target rather than the spot size. The thick target MDLs (Minimum Detection Limits as defined in ref.(2)) for PIXE are compared with those for NAA of 1 g and 1 mg samples in figure 2 which shows that Micro-PIXE is ideal for the analysis of localized defects, such as water trees, the dimensions of which are mostly well below 1 mm. Furthermore micro-PIXE can provide detailed scans of the local impurity distributions (which are far from uniform).

Experimental Arrangements

PIXE Chamber. The PIXE setup used for rapid analysis of large numbers of samples is shown in figure 3. The Université de Montréal EN Tandem accelerator can provide proton beams of up to 100 nA and energy between 1 to 12 MeV on the target. The proton beam from the tandem is focussed by a pair of quadrupole lens and then passes through the deflection plates of the beam pulse pileup rejection system (not shown) before it is finally collimated to a 4 mm diameter spot on the target. The modified Kodak Carousel slide changer can accommodate up to 80 targets mounted on standard 2" x 2" slide mounts. For thin targets (i.e. targets which allow the beam to pass through them) the beam current is measured with a Faraday cup behind the targets, while for thick targets the beam is continuously sampled by a rotating vane. The protons backscattered by a gold layer on the vane are monitored by a surface barrier particle detector which is calibrated relative to the Faraday cup. A second particle detector is used to monitor the Rutherford Backscattered Spectrum (RBS) from the target which provides information
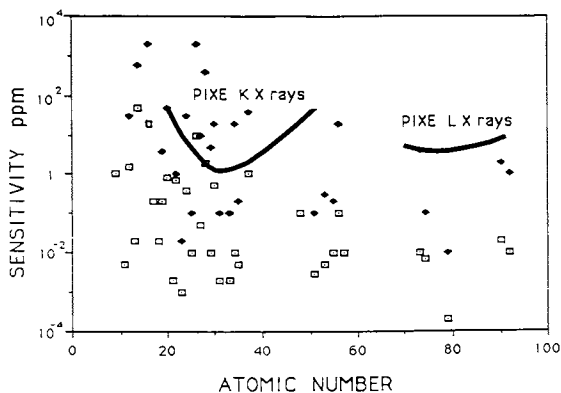
Figure 2. A comparison of the sensitivity of impurity detection in polyethylene cable insulation achieved with a) NAA of 1 mg samples, the solid points, b) NAA with 1 g samples, the open points and c) PIXE with 2.0 MeV protons, the two solid curves are for detection of the K and the L X-rays (data taken from ref. 2).
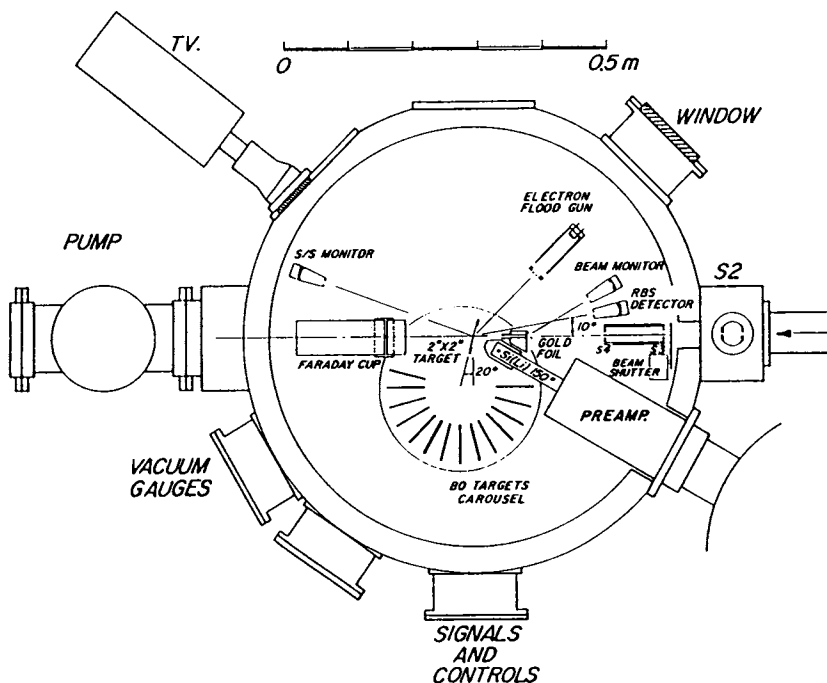
Figure 3. Diagram of the standard PIXE scattering chamber.

on light elements not accessible by PIXE. In order to reduce the bremsstrahlungen due to the charging of insulating targets an electron flood gun is used to continuously discharge the targets during irradiation.

The X-rays from the target are detected by a 12 mm^2 Si(Li) detector (energy resolution of 153 eV at 5.9 keV) which has a 12.7 micron beryllium window separating the detector cryostat from the target chamber vacuum. The pulses from the detector are shaped ($t_{dif} = t_{int} = 10$ μs) and then analyzed by a 1024 channel ADC. Pulse pileup, rather than available beam current or target damage can limit the data collection rate and produce spectral distortion. A beam deflection system is triggered by each detected X-ray and the proton beam is pulsed off during the pulse processing time. In this way the target is only irradiated while the Si(Li) detector is live. The time per sample is thus reduced and counting rates up to 2000 Hz can be used without significant spectral distortion.

Micro-PIXE. The major thrust of recent developments in the design of lens systems used for micro-PIXE has been towards ever increasing brightness and decreasing beam diameters (5,6). We believe however that much useful work can still be done using the 20 micron diameter beams produced by electrostatic quadrupole triplet lenses (7) which have the advantage that they are inexpensive and easy to operate. We have installed such a system on our 4.5 MV Dynamitron accelerator, see figure 4. The target chamber is a standard Dependex cross with six 4" diameter ports, which has been modified by the addition of two 1 in. diameter ports at ± 135^0 to the beam direction. A micromanipulator with computer controlled stepper motors is used for positioning the targets and for scanning the beam across them. The 30 sq mm Si(Li) detector (resolution FWHM = 154 eV for 5.9 KeV X rays), which has an 8 micron beryllium window, is mounted directly into the chamber vacuum through one of the 135^0 ports. This orientation reduces the bremsstrahlung background and provides flexibility in the orientation of the target. For reduction of the bremsstrahlungen due to charging of insulating targets (8) the second 135^0 ports is currently used for an electron flood gun. For RBS measurements two surface barrier detectors are mounted above and below the lens, at 158.5^0 the beam, and for simultaneous PIGE (Proton Induced gamma-ray Emission) measurements a Ge(Li) detector can be mounted in the 4" port adjacent to the Si(Li) detector.

Data Analysis. For both the macro- and micro-PIXE systems an on line display of the X-ray and RBS spectra is provided by an LSI 11/23, while detailed analysis of the RBS and PIXE spectra are performed using the programs RUMP (9) and MENUGF (10). The latter analyzes the 1024
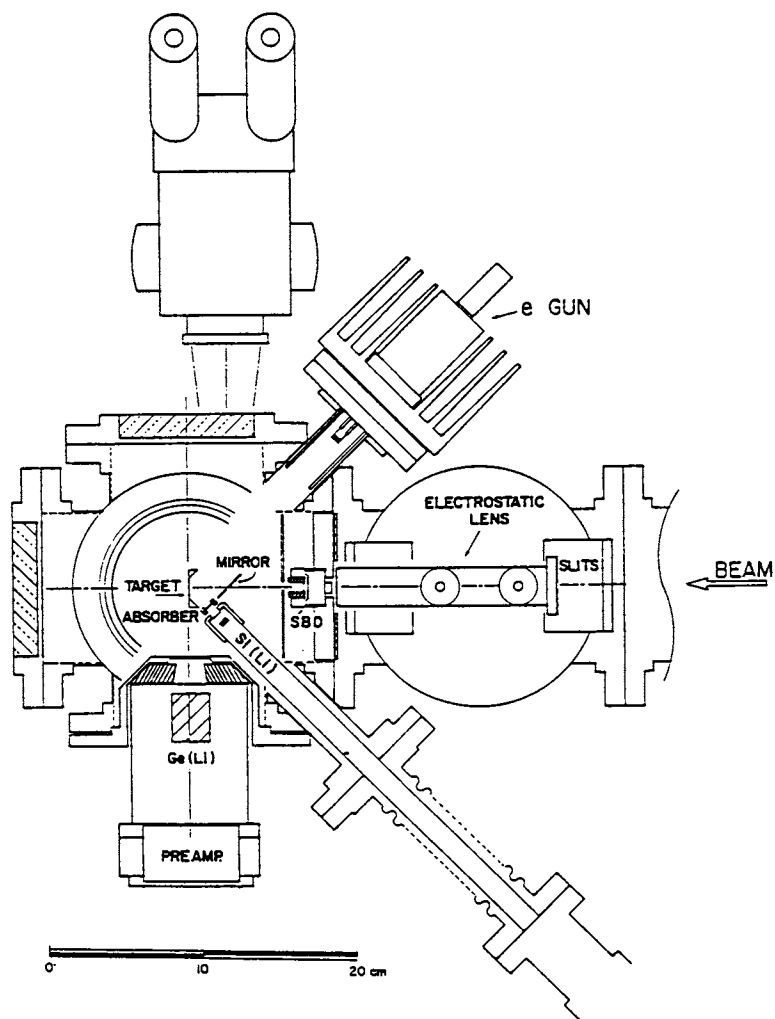
Figure 4. The electrostatic quadrupole triplet lens and target chamber used for micro PIXE showing: the 30 sq mm Si(Li) X-ray detector and the absorber ladder at 135°; the RBS detectors which are at 158° above and below the lens; the Ge(Li) PIGE detector and collimator; the electron flood gun; and the movable zoom microscope used for focusing and alignment of the beam.

channel X-ray spectra by first eliminating the continuous
background using a digital filter and then performing a
nonlinear least squares fit of Gaussian peaks to the
characteristic X-rays of up to 26 elements simultaneously.
    In order to calibrate the systems so that results can
be directly calculated in terms of the impurity
concentrations a set of standard thin foils of elements
from Na to Ba were irradiated with a known charge and the
absolute calibration in terms of the counts per μcoul per
μgm cm^{-2} of target material determined at proton
bombarding energies E_p = 1.0 and 3.0 MeV. If the major
constituents of the matrix are known, so that the energy
loss of the incident particles can be computed, the thick
target calibration can be deduced from this thin target
data. The yield as a function of depth is then derived
and corrections for self absorption in the target are made
by the program. This is a reliable procedure for
polyethylene, however, for complex matrix materials
fluorescence can enhance the yield and so it is advisable
to calibrate with thick standards which resemble the
material to be analyzed. A wide variety of such standards
are available and RBS and PIXE spectra of NBS liver, taken
to check our calibration, are shown in figure 5. The
agreement even for trace elements was found to be within
10 percent provided that the statistics were sufficient
for the program to clearly identify the peak.

Results

To illustrate the use of PIXE and micro-PIXE in the study
of breakdown phenomena in polyethylene high voltage cable
insulation and other related topics we will describe a few
typical measurements, first the study by standard PIXE of
impurities in the organic semiconductor H_2Pc and in the
carbon black semicon used in high voltage cables.
Examples of the use of the microbeam to study some
electrical and water trees as well as the diffusion of
impurities from the semicon into polyethylene under
typical electric field and humidity conditions will be
given.
    H_2Pc. Phthalocyanines are organic semiconductors
that strongly absorb visible light, and have been
extensively investigated for use in photovoltaic (11), and
photoelectrochemical cells (12). The results however were
somewhat inconsistent, and this was probably due to the
presence of impurities which were not always clearly
identified. Commercially available phthalocyanine was
analyzed in order to determine the trace elements present,
as well as the effect of heat treatment on the iodine
contamination. The X-ray spectra, for an accumulated
charge of 15 μC, from untreated and from H_2Pc purified for
1, 2, and 3 h at 400°C are shown in figure 1. Strong
lines from Na, Mg, Al, Si, S, Cl, Ca, Fe and Zn can be
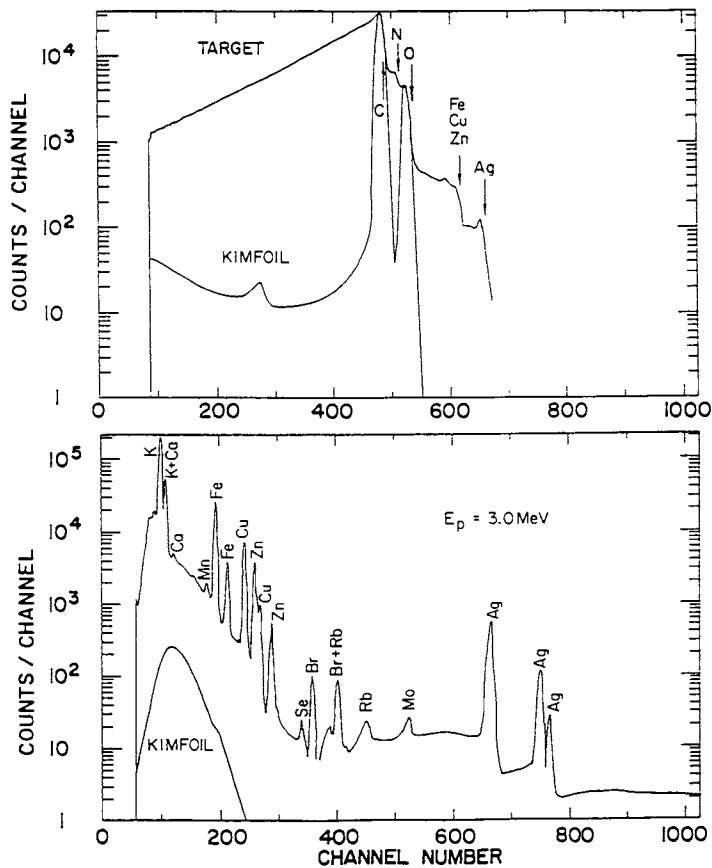
Figure 5. The PIXE and RBS spectra from a target of NBS standard liver mounted on a thin Kimfol backing.

seen in the untreated H_2Pc, however, the iodine (concentration 1.6%) which gives rise to the strong L X-rays in the energy region 3.9 to 4.8 keV, masks possible trace quantities of scandium, titanium and vanadium. Traces of titanium can however be clearly seen in the spectrum from the purified sample. The observed decrease in the impurity concentrations correlates with the electrical properties of the material (13).

Carbon Black Semicon. In high voltage extruded cables the polymeric insulation (mostly polyethylene and cross linked polyethylene) is located between two semiconductive shields consisting of polyethylene copolymers loaded with semiconductive carbon black which contains a significant mineral component. These minerals can migrate as ions into the clean insulation and can play a role in the deterioration of the cable. Three different semiconductive compounds were investigated by both NAA and PIXE. The X-ray spectra from the conventional semiconductive compound, the mar resistant semicon, and from two samples of the extra clean, super smooth semicon are shown in figure 6a to 6d respectively. The latter spectra illustrate the reduced mineral content of the extra clean material and that the remaining minerals, primarily Si and Ca, are distributed non-uniformly. The average concentrations derived from PIXE and NAA were in overall agreement and show that the conventional semiconductive compound contains a large number of mineral impurities which could potentially migrate into the polyethylene insulation.

Bow Tie Trees. An example of the use of the microbeam to investigate the contaminants in a bow tie tree in polyethylene insulation is presented in figure 7 which shows a) the spectrum from the center of the tree, b) the average of spectra from the insulation outside the tree and c) the difference spectrum. The latter clearly shows the presence of aluminum, possibly a shard from the manufacturing process, as well as excess sulphur, chlorine, potassium, calcium, copper and possibly iron.
    Another example are the micro-PIXE measurements which were made at 400 micron spacing along the axis of another "bow tie" tree which was microtomed along its axis. Both halves, A and B, were then analyzed. In addition to obtaining the impurity concentrations of a wide range of contaminants, a detailed mapping of the impurity distributions within the bow-tie tree and its surroundings was performed. The sum of the spectra from scans of sides A and B as well as individual spectra from the central region of this tree are shown in figure 8. Significant quantities of Na, Si, S, Cl, K, Ca, Ti, Cr and Fe were detected and the concentration of silicon showed large variations. The large difference in the Na, K and Ca concentrations observed at the centers of sides A and B, see figure 8, suggest rapid variations of the concentrations perpendicular to the microtome cut.
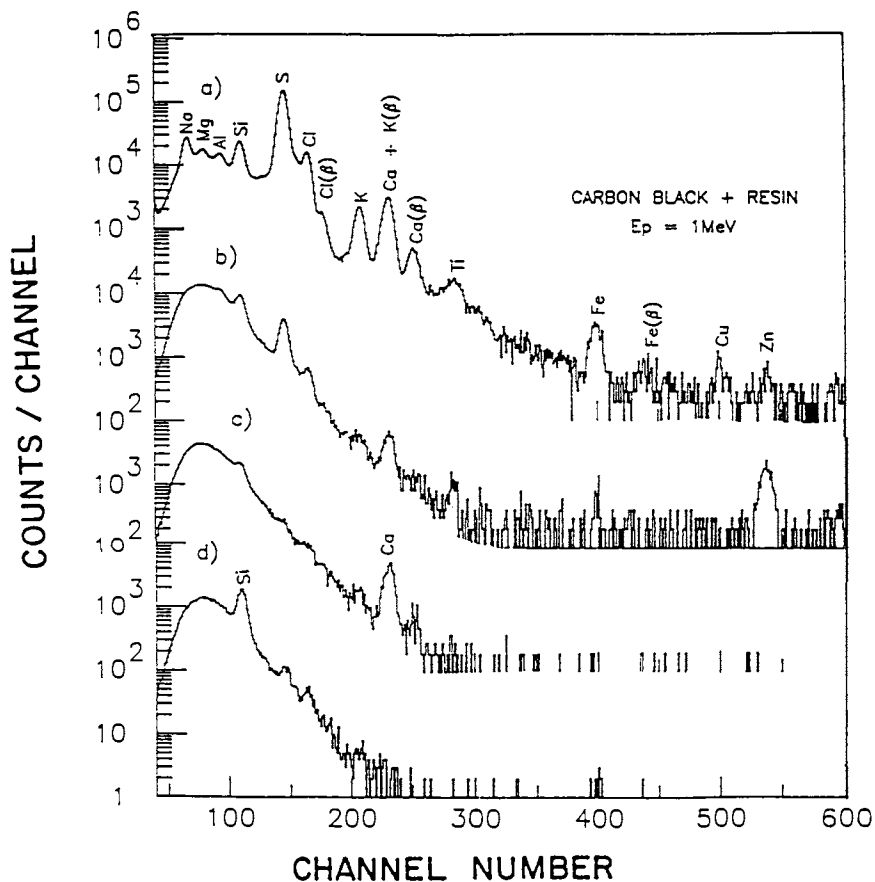
Figure 6. The X-ray spectra from 1.0 MeV proton bombardment of a) "furnace black," b) "mar resistant," and c) and d) two samples of the "extra clean super smooth" semiconductive compound. Note the improvement and the inhomogeneity of the remaining silicon and calcium.
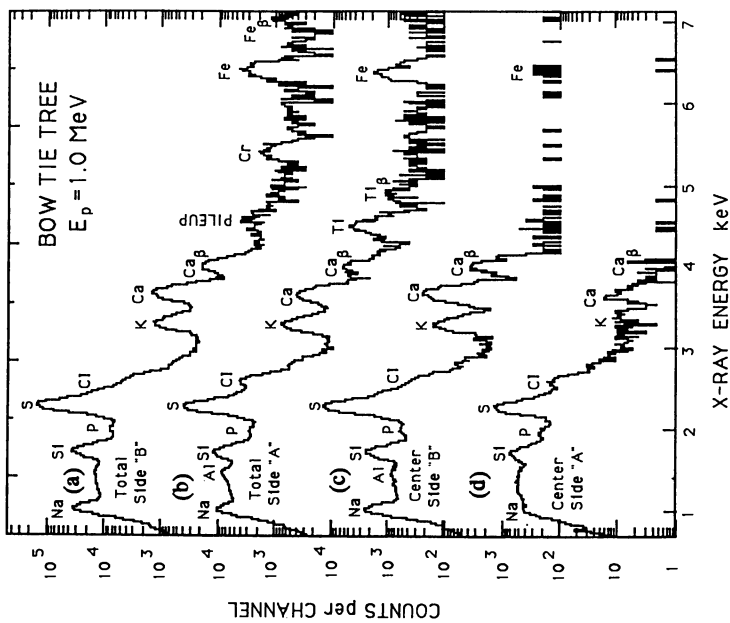
Figure 8. Micro-PIXE spectra from the bow tie tree; (a) summed over seven points along the axis on the side B of the bow tie tree; (b) summed over side A of the sample; (c) at the center of the tree side on side B; and (d) at the center of the tree on side A.
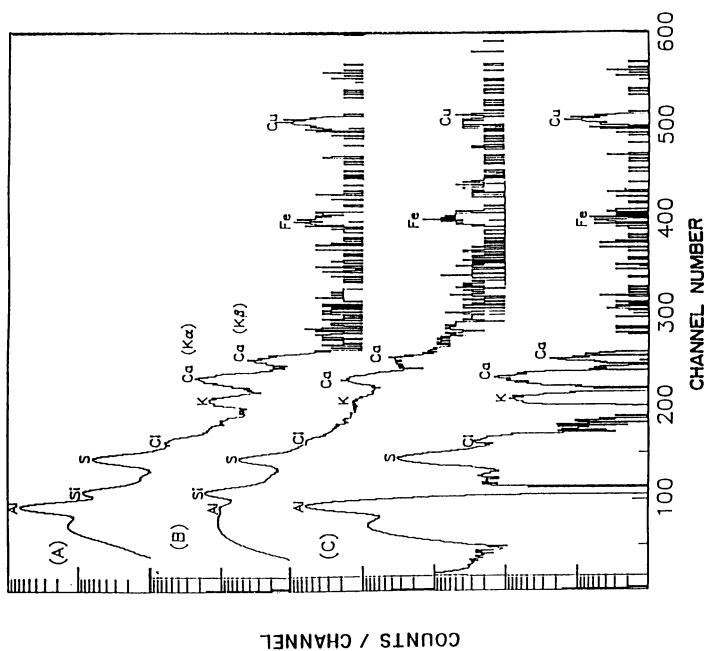
Figure 7. PIXE spectra from (A) the center of a bow tie tree; (B) the average of a few spectra from the surrounding insulation; and (C) the normalized difference spectrum which clearly shows the presence of excess Al, S, Cl, K, Ca, Cu, and possibly Fe.

Unfortunately PIXE does not have any significant depth resolution and thus does not provide any information on the impurity distribution in this dimension. Micro-PIXE data from this tree taken at Ep = 2.5 MeV confirmed the presence of K, Ca, Fe and Cu. This data also showed the presence of Zn and Pb, as well as 20 ppm of Ti at a single point near the center of the tree.

Electrical Trees. Results obtained with the microbeam at a proton bombarding energy of Ep = 1.0 MeV for many points on two adjacent electrical trees grown in a field aged cable are shown in figure 9 together with sketches of the electrical and water trees. The concentration of sulphur, which is presumably due to the added antioxidant, appears to be constant throughout both the electrical trees and the surrounding insulation. With the exception of one high concentration point this is also true for silicon. The origin of the uniformly distributed Si is most likely the catalyst used during polymerization but this could not account for the high concentration point which coincides with the peak in the concentrations of Al and Ca, see figure 9. The concentrations of Cl, Na, Mg, K and Ca vary by as much as two orders of magnitude, and these variations appear to be highly correlated, suggesting that these metals are present in the form of chlorides. The rapid decrease in the concentrations of these elements coincides with very large peaks in the Ca (1.5%), Si (0.5%), and Al (0.4%) concentrations, suggesting that some contaminant at this point may be the cause of the problem. The data for the two adjacent trees show little correlation. In the second tree the peak in the silicon concentration is 100 microns closer to the surface, with no corresponding Ca or Al peak.

Transport Studies. A systematic study of the transport of impurities from the semicon, which contains many impurities see figure 6a, into the polyethylene cable insulation under laboratory conditions which simulate those experienced by high voltage cables in service has been undertaken (A.Belhadfa, Ph.D. thesis, Université de Montréal, 1989). Batches of samples of virgin polyethylene, which were in intimate contact with commercial semicon and subjected to various electrical fields were stored at various temperatures for periods up to a few months. Some batches were kept dry while others were immersed in water. The distribution of impurities as a function of the distance from the interface was then measured with micro-PIXE. An example of the type of data which can be obtained is shown in figure 10. The virgin polyethylene from which the cable insulation is manufactured is seen to be very clean only containing Si, from the catalyst used in its manufacture and S from the added antioxidant. The impurities observed after two weeks are therefore clearly due to transport from the semicon. It is interesting to note the much higher
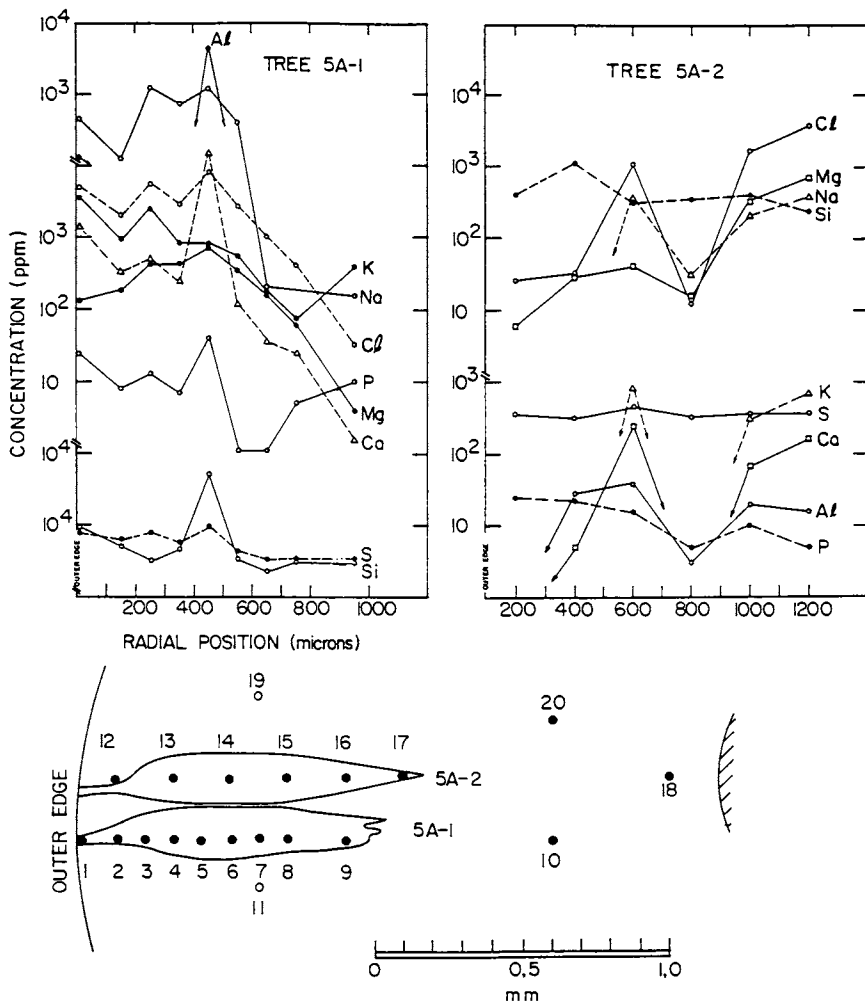
Figure 9. The radial concentration profiles for the impurities detected in two adjacent breakdown trees #5A-1 and 5A-2. Note the breaks in the logarithmic concentration scale and also the essentially constant concentration of sulphur in comparison with the large variations in the Na, Cl, K and Ca concentrations.
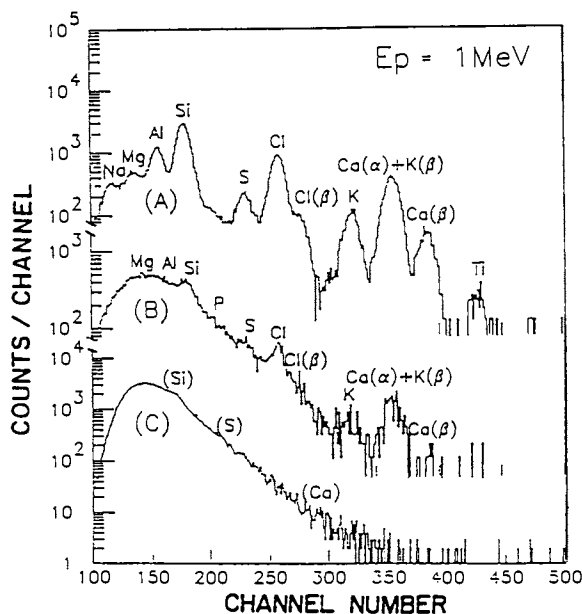
Figure 10.   Micro-PIXE spectra of polyethylene at a depth of 500 μm from the interface with a layer of semicon containing commercial carbon black, A) after two weeks in dry air at 55 °C, B) after two weeks immersed in water at 55 °C and C) the virgin polyethylene.

concentrations for the dry sample as compared with the sample kept immersed in water. This is presumably due to some leaching action of the water. These results will be published in detail elsewhere.

Conclusion

Micro-PIXE with a 20 micron beam spot has proved to be a versatile tool for investigations of water and electrical trees, as well as a variety of other samples. This system is simple to operate and does not require complex target preparation, so that multi-element surveys of a variety of samples can be rapidly performed.

More work remains to be done to better understand the role of impurities on water tree growth and we feel that micro-PIXE is a very powerful technique for such measurements since it has the required sensitivity and spatial resolution to provide detailed contour maps of the impurity concentrations, which can then be correlated with the visual tree. Our present micro-PIXE equipment with its 20 micron diameter beamspot is ideally suited for such measurements as it is very easy to use and provides online data. However, the use of only a few point measurements could miss essential components of the tree, and raster scans of the whole tree area would provide more complete information, and at the same time reduce beam induced damage.

Acknowledgments

Literature Cited

1. Johansson, S.A.E.; Johansson, T.B. Nucl. Instr. and Methods, 1976, 137, 473-478.
2. Teesdale, W.J.; Maxwell, J.A.; Perujo, A.; Campbell, J.L.; Van Der Zwan, 1.; Jackman, T.E. Nucl. Instr. and Methods, 1988, B35, 57-66.
3. Hamanaka, H.; Ohura, M.; Yamamoto, Y.; Morita, S.; Iwamura, K. Nucl. Instr. and Methods ,1988, B35, 75-79.
4. Michell, I.V.; Ziegler, J.F. Ion Beam Handbook for Materials Analysis Mayer, J.W.; Rimini, E., Eds., Academic Press Inc., New York, 1977, Ch. 5.
5. Grime, G.W.; Watt, F.; Chapman,J.R. Nucl. Instr. and Methods. 1987, B22, 1.
6. Legge, G.J.F. Nucl. Instr. and Methods ,1987, B22, 115.

7. Augustyniak, W.M.; Betteridge, D.; Brown, W.L. Nucl.Instr.and Methods , 1978, 149, 669-674.
8. Varier, K.M.; Nayak, A.K.; Mehta, G.K. Nucl. Instr. and Methods, 1985, B1, 671.
9. Doolittle, L. Nucl. Instr. and Methods ,1985, B9, 344-348.
10. Campbell, J.L.; Maenhaut, W.; Bombelka, E.; Clayton, E.; Malmqvist, K.; Maxwell, J.A.; Pallon, J.; Vandenhaute, J. Nucl. Instr. and Methods, 1986, B14, 204-220.
11. Shimura, M.; Baba, H. Denki Kagaku, 1982, 50, 678.
12. Marsan, B.; Bélanger, G.; Piron, D.L. Can J. Chem , 1985, 63, 1580.
13. Houdayer, A.; Hinrichsen, P.F.; Belhadfa, A.; Crine, J-P.; Marsan, B. J. Material Science, 1988, 23, 3854-3860.

Chapter 8

Trace Element Determination in Polymers by Neutron Activation

Gregory G. Kennedy

Energy Engineering Institute, École Polytechnique, C.P. 6079, Succursale A, Montreal, Quebec H3C 3A7, Canada

Neutron activation has been used to determine the concentrations of trace elements in polyethylene. A procedure has been optimized which involves three irradiations with a SLOWPOKE nuclear reactor and four counts with a gamma-ray spectrometer. Phosphorus is determined with beta-ray spectrometry. The detection limits, most of which are below one ppm, have been determined for 42 elements. The merits of the method are discussed in terms of sensitivity, accuracy, ease of use, interferences, and freedom from contamination.

In many laboratories that have access to a nuclear reactor, neutron activation is used for the chemical analysis of rocks, minerals, petroleum, biological tissues, alloys, etc., and the technique is well suited for the determination of the concentrations of trace elements in polymers. Neutron activation analysis was used by Given et al. (1) in their studies of water tree growth in polymeric insulation and by Wu and Chen (2) in their studies of dopant-polymer interactions in MoCl$_5$-doped polyacetylene films. In this work the principles of the method are described and the possibilities are illustrated by means of measurements carried out on polyethylene.

Description of the Method

Neutron activation analysis is a two-step technique (3). The sample to be analysed is first irradiated with the neutron flux of a nuclear reactor. The nuclei of a small but predictable fraction of the atoms of each element in the sample will capture neutrons and become radioactive. These will subsequently emit radiation at a time which depends on the half-life of the radioactive isotope. At the end of the pre-determined irradiation time the sample is removed from the reactor; it is now radioactive and the activity will decrease with time as the individual atoms emit radiation and

become stable. The principal kinds of radiation emitted are beta and gamma. The gamma-rays are the most interesting because each radioactive isotope emits gamma-rays of characteristic energy and a measurement of these energies permits the identification of the elements present.

The second step is the detection of the gamma-rays. The detector used is a germanium semiconductor. The sample is placed in front of the detector and a fraction of the gamma-rays emitted will strike the detector and give their energy to an electron in the germanium crystal by the photo-electric effect. This energy is converted to a voltage pulse whose amplitude is proportional to the gamma-ray energy. The signals from all the gamma-rays detected are stored in the memory of a multi-channel analyser to produce the spectrum, which is a record of the number of gamma-rays detected versus their energies. At the energies corresponding to the elements present in the sample we observe peaks, and the area of a peak is proportional to the amount of the element. The measurement gives the total amount of the element in the sample; this is divided by the sample weight to give the average concentration. This is a multi-element technique since several elements are detected in one measurement.

The technique is well suited to the analysis of polymers for a number of reasons. It offers high sensitivity for a large number of elements. Carbon and hydrogen are not readily activated by neutrons and thus do not interfere with the detection of trace elements. Both neutrons and gamma-rays are highly penetrating and therefore samples weighing up to one gram or more can be analysed without any special preparation and there are essentially no matrix effects (3,4).

Experiment

At the Ecole Polytechnique in Montreal we have routinely analysed many types of plastics over the last twelve years. In this work, polyethylene film from a commercially procured roll was analysed for trace elements in order to illustrate the possibilities of the technique. A one gram sample was cut from the sheet using a stainless steel blade and rolled into a cylinder 2.5 cm long and 0.7 cm diameter. It was placed in a plastic vial and irradiated in the neutron flux of the SLOWPOKE reactor (5) at the Ecole Polytechnique. The sample is shuttled to and from the reactor using a pneumatic system. Since the elements which we wish to detect have isotopes with half-lives varying from 11 seconds for fluorine to 5 years for cobalt, it was necessary to perform several measurements in order to optimize the conditions for groups of elements having similar half-lives. Thus the sample was irradiated three times with the reactor's maximum flux of 10^{12} neutrons/cm^2/s and counted four times with the gamma-ray detector. For each measurement an appropriate decay time, the time between irradiation and counting, was chosen. The times chosen for the four measurements are listed in Table I. The germanium detector used has a volume of 65 cm^3 and a resolution of 1.65 keV at 1332 keV and it is surrounded by 5 cm of lead shielding. To avoid contamination the sample was handled with clean polyethylene gloves. After irradiation and before counting it

was transferred into a new plastic vial so that elements in the vial were not detected.

Table I   Conditions for the four measurements

Method	Irradiation Time	Decay Time	Counting Time
a	20 seconds	3 seconds	20 seconds
b	10 minutes	1 minute	10 minutes
c	4 hours	18 hours	2 hours
d	4 hours	8 days	4 hours

Results

The spectrum obtained with method b is shown in Figure 1. The excellent energy resolution of the detector and the wide range of observed energies makes the identification of the elements and the calculation of the peak areas relatively simple. Peaks of 9 elements are visible above the Compton background. This background is due to gamma-rays which deposit only part of their energy in the detector. With measurements a,b,c and d only 12 elements were detected in this relatively clean material; their concentrations are listed in Table II. The concentrations were calculated by comparing the peak areas, obtained from the spectrum with a computer programme (6), with those of standards of each element irradiated and counted in a similar manner. It is not necessary to run standards with each analysis since the reactor neutron flux and the detector efficiency are known to be reproducible within 1% over long periods of time (7). The minor interferences between elements are well understood (8) and they have been corrected.

Table II   Trace elements detected in polyethylene film

Element	Concentration (μg/g)
sodium	0.25
magnesium	1.4
aluminum	5.1
sulfur	17.
chlorine	2.7
potassium	0.15
calcium	0.7
titanium	1.8
vanadium	0.07
manganese	0.005
zinc	1.6
bromine	0.009
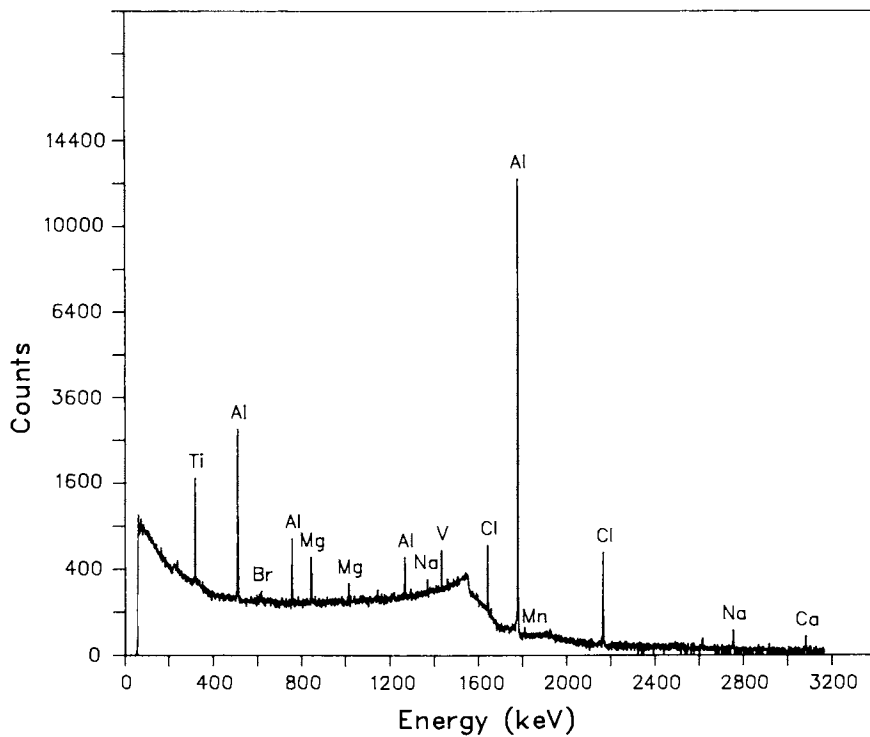
Figure 1.   Polyethylene gamma-ray spectrum obtained with method b.

Seven of the twelve elements detected here: Na, Al, Cl, K, Mn, Zn, and Br were also detected by Given et al. (1) in the polythene insulation of XLPE cable which failed in service. The other five were not detected, possibly because their neutron activation method for short-lived elements was not as sensitive as our method b. They also detected eleven other elements, probably because their material contained higher impurity concentrations, and they found that Na and Cl had migrated to regions containing water trees.

We have determined the detection limits for 42 elements which are often of interest in polymers; they are listed in Table III. The table also shows the conditions of the measurement which gives the lowest detection limit. The limit for a given element depends on the height of the Compton background at the energy of its peak. The detection limits were calculated according to Currie (9) as $3.29\sigma/S$, where σ is the uncertaintity in the peak area (one standard deviation) due to statistical fluctuations in the Compton background, and S is the sensitivity for that element, expressed in counts per microgram, as determined with a standard. Since the peak area is calculated by subtracting the counts in a background region from those in the peak region, σ is equal to 1.414 times the square-root of the number of counts in the background region. With the detection limit defined in this manner, in a sample containing an amount of the element equal to the detection limit, there is a 95% chance that the element will be reported as "detected".

In materials containing higher concentrations of elements emitting high-energy gamma-rays, the detection limits for many elements would be higher than those shown in Table III. They would also be higher in samples weighing much less than one gram. Since the total count-rate is low in the case of polyethylene and since the Compton background is due mainly to the activity of the sample (at least for methods a, b, and c), it can be shown that the detection limits increase as the inverse square-root of the sample weight. For example, in studies of elemental profiles in materials such as treed polyethylene cable insulation, samples weighing as little as one milligram may be analysed. Here, the detection limits would be approximately thirty times higher than those of Table III. With larger high-flux reactors, higher sensitivities and therefore lower detection limits can be achieved for many elements; the detection limits decrease approximately as the inverse square-root of the neutron flux. However, in some high-flux reactors the high temperatures prevailing in the irradiation sites prohibit long irradiations of polymers.

A special case in Table III is the element phosphorus, which is often of interest in polymers. Its radioactive isotope P-32 emits high-energy beta-rays but no gamma-rays. We detect it with a beta spectrometer employing a 0.6 cm thick plastic scintillator coupled to a photomultiplier tube. The one gram sample of polyethylene was too thick for the measurement of the beta-rays due to their lower penetrability. Thus, for this measurement, a sample 0.1 cm thick and 2 cm diameter was prepared after irradiation. Analysis of the beta spectrum permits the separation of the P-32 betas from other lower energy betas.

Table III   Detection limits in polyethylene

Element	Isotope	Half-life	Energy (keV)	Method	Detection Limit (μg/g)
Fluorine	F-20	11.0s	1633	a	1.
Sodium	Na-24	15.0h	1368	c	0.002
Magnesium	Mg-27	9.45m	1014	b	1.
Aluminum	Al-28	2.24m	1779	b	0.01
Silicon	Al-29	6.52m	1273	b	50.
Phosphorus	P-32	14.3d	beta	d	2.
Sulfur	S-37	5.05m	3102	b	10.
Chlorine	Cl-38	37.2m	2167	b	0.05
Argon	Ar-41	90.6m	1293	b	0.02
Potassium	K-42	12.4h	1524	c	0.05
Calcium	Ca-49	8.72m	3084	b	0.3
Scandium	Sc-46	83.8d	889	d	0.002
Titanium	Ti-51	5.76m	320	b	0.1
Vanadium	V-52	3.76m	1433	b	0.001
Chromium	Cr-51	27.0d	320	d	0.1
Manganese	Mn-56	2.85h	1811	b	0.002
Iron	Fe-59	44.6d	1099	d	5.
Cobalt	Co-60	5.27y	1173	d	0.05
Nickel	Co-58	71.3d	810	d	2.
Copper	Cu-66	5.10m	1039	b	0.05
Zinc	Zn-69	13.8h	439	c	0.05
Gallium	Ga-72	14.1h	834	c	0.001
Arsenic	As-76	26.0h	559	c	0.001
Selenium	Se-77	17.5s	162	a	0.003
Bromine	Br-82	35.5h	554	c	0.001
Rubidium	Rb-86	17.5d	1077	d	0.2
Strontium	Sr-87	2.81h	388	b	0.1
Molybdenum	Mo-99	66.0h	141	c	0.05
Silver	Ag-110	24.3s	658	a	0.01
Cadmium	Cd-115	53.5h	336	c	0.02
Indium	In-116	54.0m	1097	b	0.0002
Tin	Sn-125	9.70m	332	b	0.06
Antimony	Sb-122	65.3h	564	c	0.001
Iodine	I-128	25.0m	442	b	0.002
Cesium	Cs-134	2.90h	137	b	0.002
Barium	Ba-139	83.2m	166	b	0.1
Lanthanum	La-140	40.2h	1596	c	0.002
Tungsten	W-187	23.9h	686	c	0.001
Gold	Au-198	64.7h	412	c	0.0002
Mercury	Hg-197	64.1h	77	c	0.003
Thorium	Pa-233	27.7d	312	d	0.005
Uranium	U-239	23.5m	75	b	0.0005

Discussion and Conclusion

In studies where a knowledge of the diffusion of metallic ions in
polymers is important, one often wishes to measure a profile of the
concentration as a function of depth. Neutron activation cannot be
used to measure these profiles directly, but if the sample can be
cut into thin slices with a microtome, these can be analysed
individually to construct the profile. In our laboratory this
technique is used extensively to study the migration of ions into
the polyethylene insulation of high-voltage cables (10). These
impurities contribute to the degradation with use of the electrical
properties of the cable.
     For those who have access to the necessary equipment, neutron
activation analysis is a convenient method for the determination of
the average concentrations of trace elements in polymers. The fact
that very little sample preparation is necessary contributes to its
high reliability and reduces the risk of contamination to a
minimum. Accuracies of 5% or better can be achieved when the
concentrations are well above the detection limits. Analysis for
about a dozen elements can be completed in less than an hour. To
detect the elements with long-lived radioactive isotopes, about ten
days are needed. If a number of samples are to be analysed, they
can be irradiated simultaneously and counted sequentially using an
automatic sample changer.

Literature Cited

1. Given, M. J.; Crichton, B. H.; Farish, O. IEE Proceedings 1988,
   134, Pt. A, No. 9, 712-715.
2. Wu, H.-M.; Chen, S.-A. Synthetic Metals 1988, 26, 225-236.
3. De Soete, D.; Gijbels, R.; Hoste, J. Neutron Activation
   Analysis John Wiley and Sons Ltd.; New York, NY, 1972.
4. Zikovsky, L.; Nucl. Inst. Meth. in Phys. Res. 1984, B4, 421.
5. Kay, R. E.; Stevens-Guille, P. D.,; Hilborn, J. W.; Jervis, R.
   E. Int. J. Appl. Radiation Isotopes 1973 24, 509.
6. Kennedy, G.; Marcotte, J.; Zikovsky, L.; J. Radioanal. Nucl.
   Chem. 1987 110, 61.
7. Bergerioux, C.; Kennedy, G.; Zikovsky, L. J. Radioanal. Nucl.
   Chem. 1979, 50, 220.
8. Kennedy, G.; Galinier, J.-L.; Zikovsky, L. Canadian Journal of
   Chemistry 1986 64, No. 4, 790.
9. Currie, L. Anal. Chem. 1968 40, No. 3, 586.
10. Crine, J. P.; Pélissou, S.; St-Onge, H.; St-Pierre, J.;
    Kennedy G.; Houdayer, A.; Hinrichsen, P. Proc. Jicable Conf.
    Versailles, Sept. 1987 206.

Chapter 9

Morphology of Polymer Chains by Transmission Electron Microscopy

Yvon P. Carignan[1], Masanori Hara[2], and Frederic Cosandey[2]

[1]U.S. Army Armament Research, Development and Engineering Center, Picatinny Arsenal, NJ 07806–5000
[2]Department of Mechanics and Materials Science, Rutgers, The State University of New Jersey, Piscataway, NJ 08855–0909

Thin films of tagged (Iodinated) polystyrene dispersed in a polystyrene matrix have been studied by Transmission Electron Microscopy. Photomicrographs reveal the presence of random dark spots on an otherwise structureless background. These spots are interpreted as being the 2-D projection of the random coil chains of tagged polystyrene. Their count per unit area of the photomicrograph is directly proportional to the ratio of tagged polystyrene to polystyrene in the films. Varying the time of exposure under the electron beam (0 to 120 minutes) indicates that the polymer chains are not affected by the electron beam. Information is presented on the dimensions of the polymer coil and the occurrence of aggregation of the polymer chains at high mixing ratios (1:1) of the tagged polystyrene to polystyrene.

Great advances have been made in the study of polymers during the last twenty years principally because of the introduction and development of three techniques based on interference phenomena, namely, small-angle neutron (SANS), x-ray (SAXS) and light (SALS) scattering. The fraction of the radiation scattered is in SANS related to the nature of the scattering nucleus, in SAXS to the electron densities and in SALS to polarizabilities or refractive indices. These techniques have proven vital, from both experimental and theoretical points of view in addressing polymers either as homophase amorphous systems, heterophase amorphous or crystalline systems. For instance one of the most significant accomplishment in modern polymer science has been the confirmation of Flory's fundamental hypothesis through the application of SANS, namely, polymer chains exist as random coils in amorphous bulk polymers (1). Flory's hypothesis has been used extensively to explain various properties of amorphous polymers. One example of its successful application can be found in Kramer's work on the deformation behavior of glassy polymers, where he uses the end-to-end distance of the random coil as the basic parameter (2).

In spite of all the recent success which can be traced to the three techniques, SANS, SAXS, SALS, there are serious limitations in their scope ($\underline{3}$). For instance only average values, such as root-mean-square end-to-end distance and radius of gyration of a polymer chain can be extracted from these techniques. In other words, these techniques cannot provide information on the actual conformation or dimension of the individual polymer chain. Also since all three techniques are indirect, the analysis of the raw data is not straightforward and requires various manipulations and faith in existing theories to draw conclusions. Finally with regard to SANS, it must be noted that only a limited number of facilities in the U.S. have this capability, thus restricting its use.

In the present work we have taken the challenge of developing a direct technique which could provide the ultimate information on the actual morphology and dimensions of the individual polymer chains. We were convinced that if successful, an experimental technique which would give such detailed information on polymer chains would not only be received by researchers and technologists as a major breakthrough towards the simplification of their efforts in understanding and improving the performance of current and future polymeric materials but would also sort out the best, most realistic theory and model among the many being offered today to explain the properties of polymers.

Towards this objective, we have turned to the concept of mass thickness contrast microscopy, which could be exploited by tagging the polymer under study with a heavy atom, and after forming thin films of the tagged polymer dispersed in a matrix of untagged polymer, perform examination of the films by Transmission Electron Microscopy (TEM). Polystyrene (PS) was chosen as the polymer mainly because of its availability over a wide range of molecular weights (M_w - $1x10^4$ to $2x10^6$) and very low polydispersity ($M_w/M_n < 1.1$). Furthermore, PS has been over the years more scrutinized by both theoreticians and experimentalists than any other polymer in terms of its properties, conformation and dimensions. To enhance the contrast against the electron beam, the PS molecular chains were tagged with iodine atoms along the chain and these tagged PS chains were mixed with the starting PS for observation by TEM in the form of ultrathin films. Obviously, the visualization of the individual tagged polymer chains would be most appealing and convincing. An encouraging note as to the prospective success of our approach came from the work of Furuya et al ($\underline{4}$). These authors tagged the short rigid rodlike molecules with metal clusters at the chain ends to enhance contrast. By using STEM, they could observe spots from the contrast produced by the electron-dense clusters. We were nevertheless aware of the dangers for misinterpretation inherent to this type of approach. As pointed out by E.L. Thomas in his critical review on the "Transmission Electron Microscopy of Polymers" ($\underline{5}$), a number of papers have appeared in the literature which have completely misinterpreted the images seen via mass thickness contrast after tagging with a heavy atom.

EXPERIMENTAL

SYNTHESIS OF POLY(P-IODOSTYRENE). Poly(p-iodostyrene) or iodinated polystyrene (IPS) samples were prepared by iodination of polystyrene using the procedure described by Braun ($\underline{6}$). Polystyrene dissolved in

nitrobenzene was reacted with the mixture of iodine and iodic acid. The starting polystyrenes were polystyrene standards with narrow molecular weight distribution (M_w - $2x10^6$; M_w/M_n - 1.10). After the reaction was terminated, the polymer was recovered by precipitation into methanol. The products were then dissolved in a solvent mixture (benzene/methanol 90/10 v/v), freeze-dried, and dried under vacuum at room temperature for a week to remove the residual solvent. The iodine content of the samples was determined by elementary analysis. The relationship between the iodine content of the product and reaction time is shown in Fig. 1. The iodine content increases monotonically with increasing reaction time, as was pointed out by Braun. Also as shown in the figure, the molecular weight of the starting polystyrene (PS) has no effect on the rate of the iodination reaction. Therefore, we can use this calibration curve for preparing materials with the desired iodine content for PS of any molecular weight. Through viscosity (6) and light scattering measurements (10)it was established that the iodination reaction does not change the molecular weight of the starting polymer.

TRANSMISSION ELECTRON MICROSCOPY (TEM). The TEM study of the polymer films was conducted with a JEOL 100 CX-II microscope operating at 100 kV. The method of observation was based on the scattering contrast mechanism (7,8). As represented schematically in Fig. 2, the atomic scattering factor or the number of electrons scattered at a specific angle $\alpha°$ is directly related to the atomic number (Z) of the scattering atom. Therefore, polymer chains containing a heavy atom, such as iodine with Z—53 will scatter more electrons than the surrounding chains containing only light atoms (C,H,N...). A contrast will be obtained by blocking all the electrons scattered past a critical angle $\alpha°$ which is determined by the radius of the objective aperture (R) and the focal length of the objective lens (f) as shown in Fig. 3. Optimum contrast will be obtained for large f and small R. In this investigation the following parameters were used: f - 4.6mm and R - 10μm with iodine as the heavy atom.

THIN FILM SPECIMEN PREPARATION. Iodinated polystyrene (IPS) and polystyrene (PS) were dissolved separately in toluene at 0.5w% concentration. These two solutions were mixed to obtain a ratio of IPS to PS ranging from 1:1 to 1:100. For ratios below 1:100 the solution of IPS was further diluted by a factor of ten before mixing with the PS solution. The final solutions were stirred overnight before preparing the films.
      Thin film samples were cast on a glass slide and dried in a bell jar containing toluene vapor to decrease the evaporation rate. Thin films (about 1000Å) were formed in two hours. After solvent removal the films were cut on the glass slide into 2mm x 2mm squares before being dipped into distilled water. The thin films were picked up by copper grids and dried under vacuum for at least twenty-four hours before examination by TEM.

RESULTS AND DISCUSSION

The TEM results for an IPS:PS concentration ratio of 1:10 are given in Fig. 4. One observes a number of dark gray spots on an otherwise
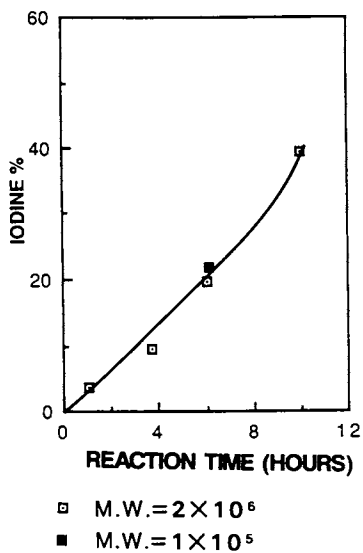
Fig.1   The iodine content in Iodopolystyrene as a function of
        reaction time.
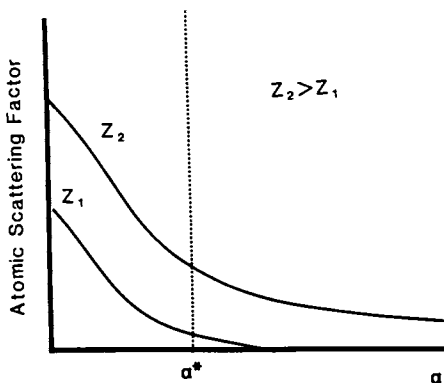
Fig.2   The atomic scattering factor as a function of the
        specific angle $\alpha°$
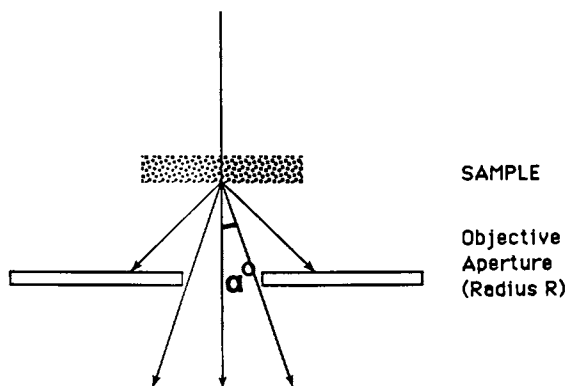
Fig.3   Relationship of critical angle $\alpha°$ to the radius of the objective aperture R.

Fig.4   TEM photomicrograph for Iodopolystyrene to polystyrene ratio of 1:10.

structureless gray background. We interpret these gray spots as representing the projection into 2-D space of the spherical volume occupied by random coiled IPS chains. This being the case, it would follow that reducing the (IPS:PS) ratio should correspondingly reduce the number (density) of spots on the photomicrographs. Indeed, as shown in Figs. 5 and 6 and listed in Table I the number of spots decreases accordingly, thus strengthening the argument that indeed we are observing 2-D projections of individual polymer chains of IPS.

Table I.   Density of Dark Gray Spots as a Function of IPS:PS Ratios

IPS:PS	Spots Count
1:10	40
1.20	20
1.50	7

By actually measuring the diameter of each spot on the photomicrograph (N=60) we have constructed the histogram shown in Fig. 7. A rough estimate of the average diameter of the spots is 650Å. Comparing this value with the value of 950Å calculated for PS of this molecular weight ($M_w = 2 \times 10^6$) in the unperturbed state, based on the random coil model suggests either; a) that our measurements of the gray spots are underestimating the actual size of the spots simply because the contrast within the spots gradually decreases from the center to the periphery thus making estimation of the true boundary of the spots very difficult; b) the IPS chains achieve a more compact coil configuration relative to the PS chains. However, previous work with IPS in the bulk using x-ray scattering (9,10) contradicts this hypothesis. This work has shown that the radius of gyration of IPS is in fact 6% greater than that of PS. Therefore, an increase in dimensions of IPS relative to PS is predicted in contrast to the 30% decrease observed in the present work; c) our results may simply confirm the theoretical predictions of Lindenmeyer (11), i.e., molecules exist in the more densely coiled conformations than the random coiled form.

At this point in time we tend to favor (a), i.e., our measurements are underestimating the actual size of the polymer coil simply because of the fading contrast and loss of sharpness at the boundary of the TEM image. Certainly more work is necessary to test the validity of this interpretation.

A number of other IPS:PS ratios were studied with IPS containing both 40% and 20% iodine as listed in Table II. When the ratio is as high as 1:1 we definitely observe aggregation of the IPS Chains (Fig. 8). No vestige of the single chains spots can be found. The average size of these aggregates is about sixty times the volume occupied by a single IPS chain.
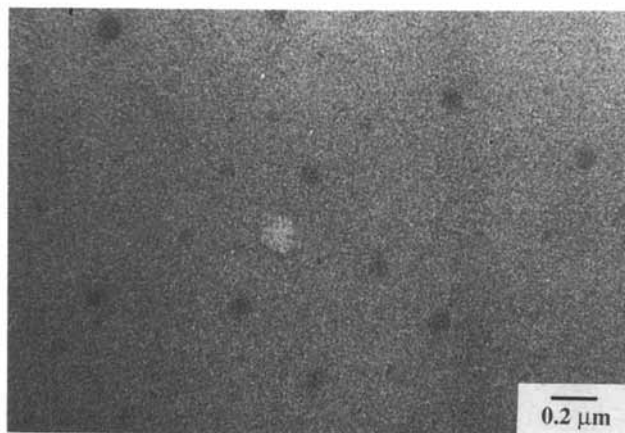
Fig.5   TEM photomicrograph for Iodopolystyrene to polystyrene
         ratio of 1:20.
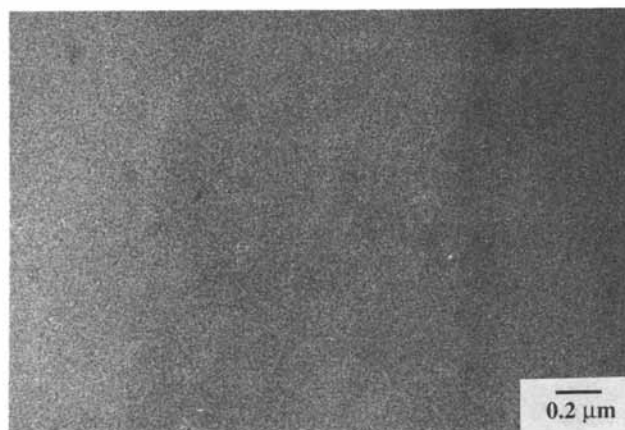
Fig.6   TEM photomicrograph for Iodopolystyrene to polystyrene
         ratio of 1:50.
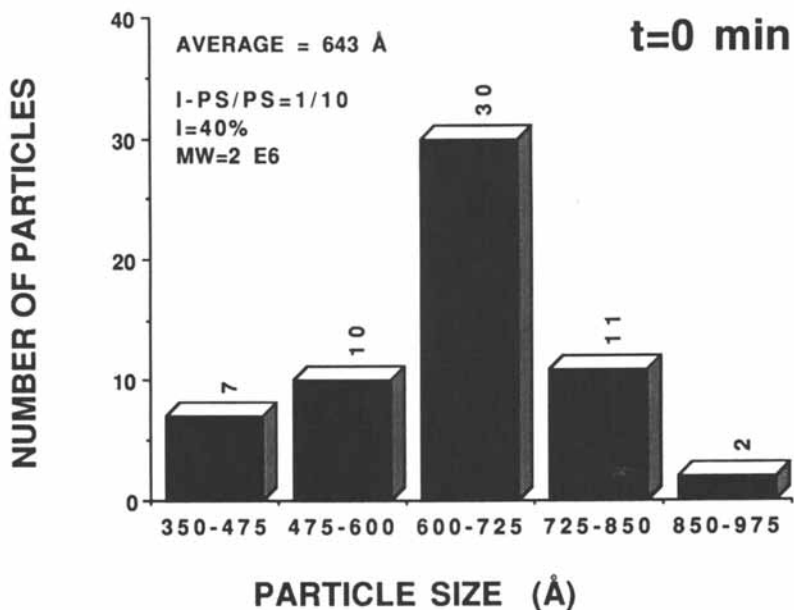
Fig.7   Particle size analysis from ratio 1:10 (Fig. 4).
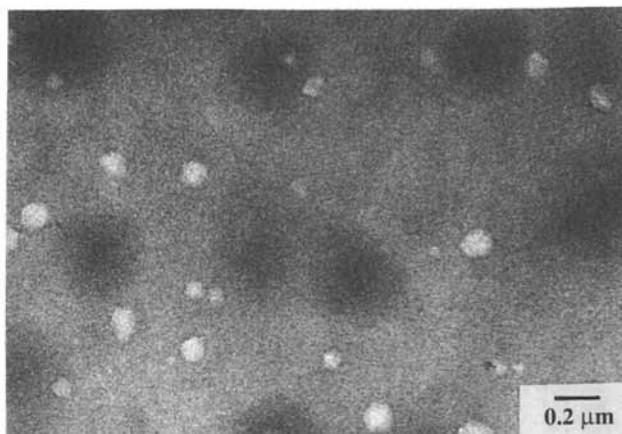
Fig.8   TEM photomicrograph for Iodopolystyrene to polystyrene
ratio of 1:1.

Table II. Summary of TEM results

Iodine Content	Mixing Ratios IPS:PS	Observations
40%	1:1	Phase Separated
	1:10	Random Coil
	1:20	Random Coil
	1:50	Random Coil
	1:100	No Structure
	1:1000	No Structure
20%	1:1	Phase Separated
	1:20	Random Coil
	1:50	No Structure
	1:100	No Structure
	1:1000	No Structure

Finally we have investigated the potential danger of polymer chain degradation by the energetic electron beam by examining any potential relationship between the sample exposure time to the electron beam and the average chain length of the polymer after exposure. As shown in Figs. 7,9, and 10 within the precision of our measurements it is concluded that no polymer degradation occurred under the conditions of these experiments.

CONCLUSIONS

This study demonstrates the significant potential of the approach of combining tagging of polymers followed by examination by TEM to provide direct information on the dimensions, conformation and shapes of individual polymer chains and the conditions under which the chains begin aggregating. The work described in this publication is essentially preliminary and further experiments are being conducted to test the scope of the technique. Such a procedure could be in principle extended to the study of morphological changes associated with interfacial interactions in multilayer systems.
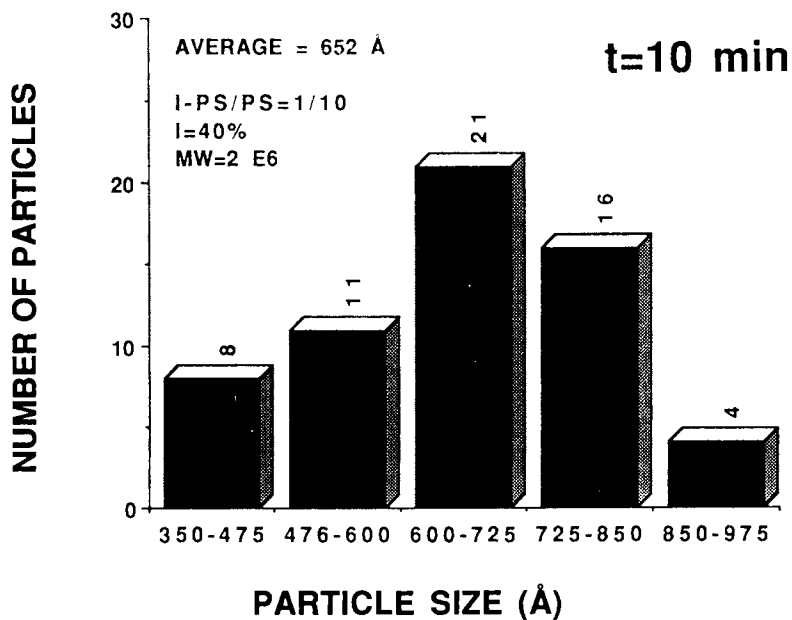
Fig.9   Particle size analysis for 10 minutes exposure time to electron beam.
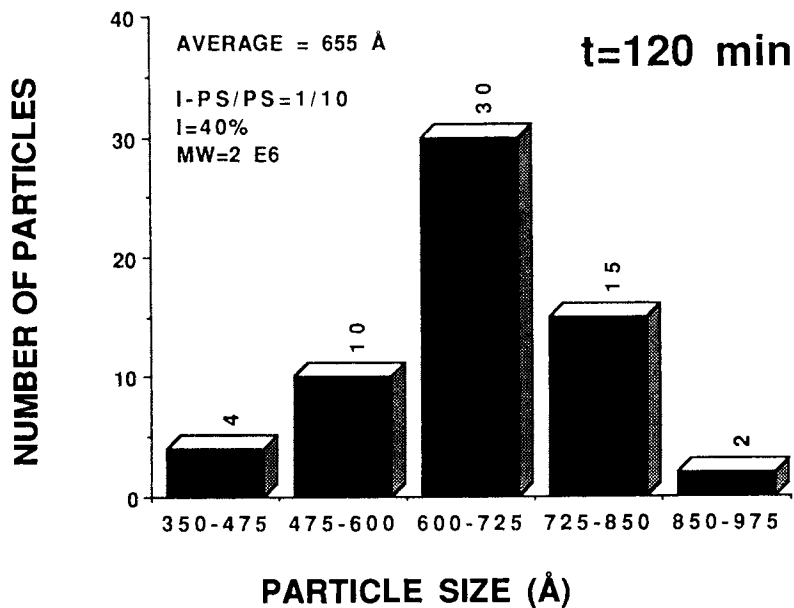
Fig.10 Particle size analysis for 120 minutes exposure time to electron beam.

LITERATURE CITED

1. Flory, P.J. "Principles of Polymer Chemistry": Cornell University Press: Ithaca 1971.
2. Kramer, E. J. Adv. Polym. Sci. 1983, 52/53, 1.
3. Higgins, J.S; and Stein, R.S. J. Appl. Cryst., 1978, 11, 346.
4. Furuya, F.R.; Miller, L.L.; Hainfeld, J.F.; Christopfel, W.C.; Kenny, P.W. J. Am. Chem. Soc., 1988, 110, 641.
5. Thomas, E. L.In Structure of Crystalline Polymers: Hall, I. ed.: Elsevier Applied Science: New York, 1984; Chapter 3.
6. Braun, D. Makromol. Chem., 1959, 30, 85.
7. Reimer, L. "Transmission Electron Microscopy"; Springer-Verlag: Berlin, 1984.
8. Henkee, C.S. In "Transmission Electron Microscopy"; Elsevier Applied Science: New York, 1988; Chapter 3.
9. Hayashi, H.; Hamada, F; Nakajima, A. Macromolecules, 1974, 7, 959.
10. Hayashi, H.; Hamada, F; Nakajima, A. Macromolecules, 1976,9, 543.
11. Lindenmeyer, P.H. J. Macromol. Sci., Phys., 1973, B8(1-2),361.

Chapter 10

Polymer Surface Modification
by Dual-Frequency Plasma Treatment

M. H. Bernier, J. E. Klemberg-Sapieha, L. Martinu, and M. R. Wertheimer

Groupe des Couches Minces and Department of Engineering Physics,
École Polytechnique, C.P. 6079, Succursale A, Montreal,
Quebec H3C 3A7, Canada

Several commercial polymers (polyethylene, polyimide,
polytetrafluoroethylene, polyvinylchloride and polycar-
bonate) have been treated by low temperature glow discharge
plasmas in various gases, namely NH_3, O_2, Ar, and CF_4.
These surface modifications were performed in "pure" micro-
wave (2.45 GHz, "single-mode") or in combined microwave/
radio frequency (2.45 GHz/13.56 MHz, "dual-frequency")
plasma. Important systematic changes of the surface com-
position, wettability, and adhesion of thin metal films
were observed for different substrate bias values, and
for the different gases. The modified surface-chemical
structure is correlated with contact angle hysteresis of
water drops; this helps to identify which surface charac-
teristics are connected with the wettability heterogeneity
and with adhesive bonding properties, and how they are
influenced by plasma-surface interactions.

Over the years, several methods have been developed to modify polymer
surfaces for improved adhesion, wettability, printability, dye-uptake
etc. These include wet-chemical treatments, and exposure to flames,
corona discharges, and glow discharge plasmas. Among these, low
pressure, low temperature nonequilibrium plasma treatment has proven
increasingly attractive for the treatment of polymer surfaces (1).
Due to inelastic collisions of electrons (typical energies 1 - 10 eV)
in low pressure (0.01 - 1 Torr) discharges, the plasma contains ions
in the same concentration as electrons, to preserve quasineutrality,
and neutral molecules, namely the original ground state parent gas
molecules and also chemically reactive species such as metastable
excited molecules and molecular fragments (free radicals). These
particles, and photons emitted from excited species, can interact
with the surfaces exposed to the plasma; depending mainly upon the
type of feed gas, this can result in deposition, etching (chemical
and/or ion-assisted), or modification of the surface structure and
surface-chemical composition ("grafting"). All these can drastically

alter the macroscopic surface properties such as wettability, and adhesion to other materials.

The effectiveness of a given plasma-assisted surface treatment depends primarily on the nature of the feed gas, and on a number of externally controllable parameters: pressure, power, gas flow rate, frequency of the electrical energy used to excite the discharge, reactor geometry, etc. These "external" variables, in turn, affect the "internal" plasma parameters which control the overall processes, namely the electron density n_e, the average electron energy $<E>$, the electron energy distribution function $f(E)$, and the plasma potential V_p.

Glow discharges may also be distinguished on the basis of the applied field frequency: it has recently been shown that microwave (MW) plasma produces high concentrations of chemical precursors in the gas phase, on account of a higher population of electrons in the energetic "tail" of the distribution function $f(E)$ (2). This leads, for example, to substantially higher deposition rates than at lower excitation frequencies (3), and to more efficient surface treatment, both in direct plasma exposure (4), and in "remote" reactors, where the surface is exposed to the plasma effluent downstream (5). On the other hand, processing at lower excitation frequencies (for example, radio-frequency RF) implicates enhanced interactions of charged species with surfaces exposed to the plasma (6). This results from ion bombardment caused by a larger difference between V_p and the surface potential V_s than is encountered in the case of MW plasma. In typical arrangements using parallel plate electrodes, the powered electrode (which is capacitively coupled to the RF power supply) develops a high negative DC self bias voltage V_s, owing to the much higher mobility of electrons in the plasma, compared with ions. The value of V_s can readily exceed several hundred volts, and it can be exploited for sputtering, reactive ion etching, and controlled ion-assisted deposition (7), to name but a few categories of technologically important processes.

Recently, the novel method termed "dual-frequency plasma deposition" has been used to demonstrate the growth of thin films with excellent properties, the deposition occurring at high rates near ambient temperature (8). In this method, MW energy provides a high concentration of precursors in the plasma, while RF power applied to the substrate creates a DC bias V_s, hence controlled bombardment by ions. In the present work we continue to investigate the beneficial effects of this dual-frequency approach, but this time for surface-modifying a series of commercial polymers in different feed gases. We study the effects of ion-induced surface bombardment by controlling V_s in a combined MW/RF discharge, for example, how it affects the surface composition, the surface wettability, and the adherence of thin, evaporated aluminum films.

EXPERIMENTAL METHODOLOGY

Surface treatments were carried out in the plasma apparatus illustrated schematically in Figure 1. The reactor contained a 15 cm diameter substrate holder/electrode facing a fused silica window,

alter the macroscopic surface properties such as wettability, and adhesion to other materials.

The effectiveness of a given plasma-assisted surface treatment depends primarily on the nature of the feed gas, and on a number of externally controllable parameters: pressure, power, gas flow rate, frequency of the electrical energy used to excite the discharge, reactor geometry, etc. These "external" variables, in turn, affect the "internal" plasma parameters which control the overall processes, namely the electron density n_e, the average electron energy $<E>$, the electron energy distribution function $f(E)$, and the plasma potential V_p.

Glow discharges may also be distinguished on the basis of the applied field frequency: it has recently been shown that microwave (MW) plasma produces high concentrations of chemical precursors in the gas phase, on account of a higher population of electrons in the energetic "tail" of the distribution function $f(E)$ (2). This leads, for example, to substantially higher deposition rates than at lower excitation frequencies (3), and to more efficient surface treatment, both in direct plasma exposure (4), and in "remote" reactors, where the surface is exposed to the plasma effluent downstream (5). On the other hand, processing at lower excitation frequencies (for example, radio-frequency RF) implicates enhanced interactions of charged species with surfaces exposed to the plasma (6). This results from ion bombardment caused by a larger difference between V_p and the surface potential V_s than is encountered in the case of MW plasma. In typical arrangements using parallel plate electrodes, the powered electrode (which is capacitively coupled to the RF power supply) develops a high negative DC self bias voltage V_s, owing to the much higher mobility of electrons in the plasma, compared with ions. The value of V_s can readily exceed several hundred volts, and it can be exploited for sputtering, reactive ion etching, and controlled ion-assisted deposition (7), to name but a few categories of technologically important processes.

Recently, the novel method termed "dual-frequency plasma deposition" has been used to demonstrate the growth of thin films with excellent properties, the deposition occurring at high rates near ambient temperature (8). In this method, MW energy provides a high concentration of precursors in the plasma, while RF power applied to the substrate creates a DC bias V_s, hence controlled bombardment by ions. In the present work we continue to investigate the beneficial effects of this dual-frequency approach, but this time for surface-modifying a series of commercial polymers in different feed gases. We study the effects of ion-induced surface bombardment by controlling V_s in a combined MW/RF discharge, for example, how it affects the surface composition, the surface wettability, and the adherence of thin, evaporated aluminum films.

EXPERIMENTAL METHODOLOGY

Surface treatments were carried out in the plasma apparatus illustrated schematically in Figure 1. The reactor contained a 15 cm diameter substrate holder/electrode facing a fused silica window,

Fig. 1: Schematic arrangement of the dual frequency plasma system for surface treatment of polymers.

through which MW (2.45 GHz) power was supplied from a slow wave applicator ($\underline{9}$). The substrate holder was capacitively coupled to an RF (13.56 MHz) generator, and the self-developed, negative DC substrate bias voltage V_s was measured (with reference to ground) using an RF choke. The reactor was turbomolecularly pumped to its base pressure prior to the experiments. Plasma treatments were performed in 10 sccm flows of NH_3, Ar, O_2 or CF_4 at a working pressure of 80 mTorr. The MW power was kept constant at 150 W in all experiments, while RF power (0 - 150 W), resulting in V_s values from 0 to -400 V, was adjusted separately for each polymer/gas combination. All samples were exposed to the plasma for 15 seconds.

The following commercial polymeric substrates have been investigated: low density polyethylene (PE, Dow Chemical Canada Inc.) polyimide (PI, DuPont Kapton H), polytetrafluoroethylene (PTFE, DuPont Teflon), polycarbonate (PC, Mobay Corp.) and surface-lubricated (with glycerol ester) polyvinylchloride (PVC, Canadian Occidental Petroleum Ltd). After plasma treatment, the samples were exposed to ambient atmosphere for 10 - 30 minutes while being transferred to the following analytical instrument for surface characterization: The surface chemical composition was determined by X-ray photoelectron spectroscopy (XPS) in a VG-ESCALAB 3MkII system using Mg - K_α radiation at 90° angle of incidence. The surface wettability was characterized by measuring the advancing (θ_a) and receding (θ_r) contact angles for water drops, using a micrometric syringe and a telescopic goniometer (Ramé-Hart, model NRL-C.A.). The measurement was repeated several times at different locations on each sample surface, and the average value was determined. The adhesion of a 250 nm thin evaporated aluminum film was evaluated using the well-known adhesive-tape peel-test ($\underline{10}$). The type 810 Scotch-brand tape was applied to the metallized polymer at constant pressure, then removed by peeling at a 90° angle. This was repeated at several different locations over the sample surface, and the observed adhesion was classified semi-quantitatively using a scale from 0 to 10: 0 designates poor adhesion, all metal removed, while 10 signifies excellent adhesion, no metal removed.

RESULTS and DISCUSSION

WETTABILITY and COMPOSITION - EFFECT of V_s

The effect of V_s on θ_a, θ_r, and on the atomic concentration ratios (ACR) at the surface has been investigated for all polymer/gas combinations. Since the results were found to differ principally on the basis of the various plasma treatments rather than based on the initial polymer structure, we present here for the sake of brevity only the data pertaining to PC and to PVC; these are shown in Figures 2 to 5. These graphs all show systematic variations in surface composition, and in the advancing and receding contact angles as a function of V_s, starting from $V_s = 0$ ("pure" MW plasma, with no applied RF power). The data points labelled "N" near the ordinate axis correspond to the clean, untreated, virgin polymer surface. We start by discussing the features common to these figures, before analysing specific cases separately.
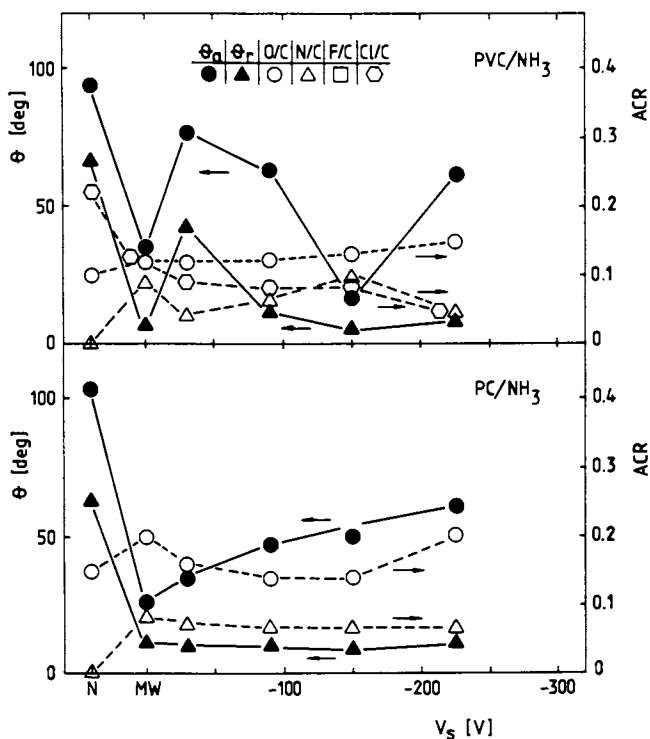
Fig. 2: Effect of substrates bias V_s on the surface characteristics of PVC and PC treated by NH_3 in MW/RF "dual-frequency" plasma: (●) advancing and (▲) receding contact angles; atomic concentration ratios (ACR): (○) O/C, (△) N/C, (⬡) Cℓ/C, (□) F/C.
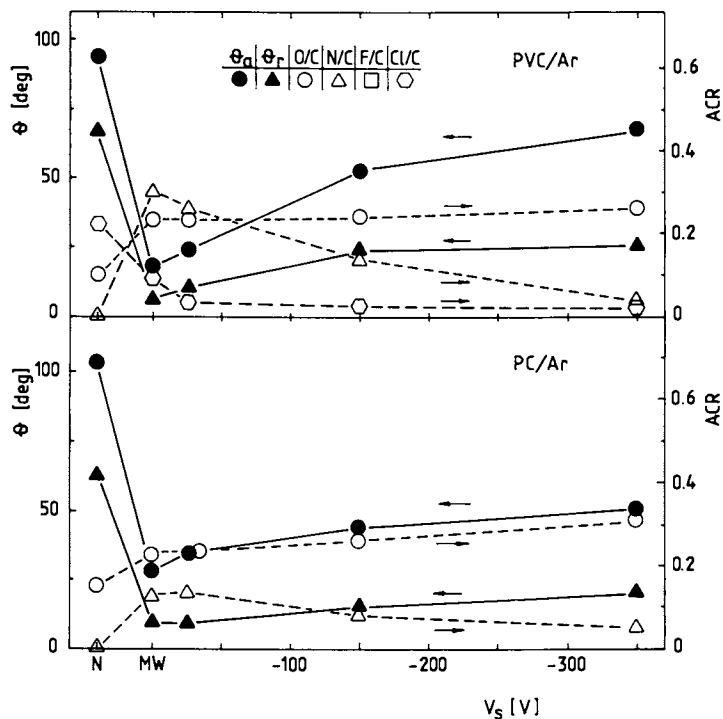
Fig. 3: Effect of substrate bias on the surface characteristics
of PVC and PC treated by Ar in MW/RF "dual-frequency-
mode" plasma.
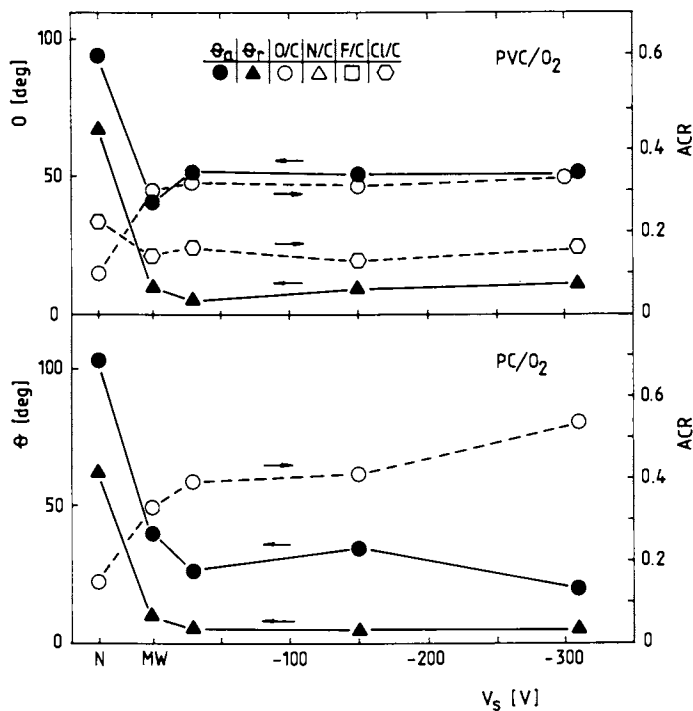
Fig. 4: Effect of substrate bias on the surface characteristics of PVC and PC treated by O_2 in MW/RF "dual-frequency" plasma.
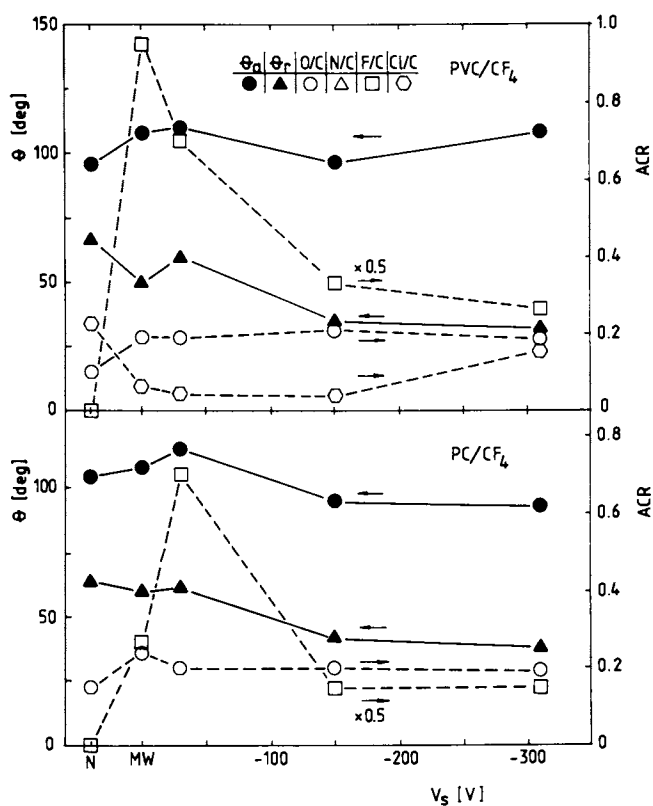
Fig. 5: Effect of substrate bias on the surface characteristics of PVC and PC treated by CF$_4$ in MW/RF "dual-frequency" plasma.

It is useful to consider the plasma-surface processes in terms of a mechanistic model involving the following steps:
 (i) initiation - creation of active precursors;
 (ii) propagation - reaction of precursors between each other or with the surface;
(iii) termination - formation of the final reaction product(s).

In plasma-chemical experiments of the present type, another reaction source must also be taken into account, namely (iv) post-treatment reactions, due to chemical interaction with constituents of the ambient atmosphere (oxygen and water vapor, in particular).

How are the above-mentioned steps influenced by increasing V_s? Let us distinguish four regimes, designated "A", "B", "C" and "D":

Regime "A": $V_s = 0$. The discharge is driven in the "pure" MW mode, an abundant source of active species in the gas phase. These diffuse to the polymer surface with which they react mostly by attachment. In this case ionic bombardment is very limited and low in energy because the insulating surface rapidly adopts a floating potential (usually a few volts positive with respect to ground).

Regime "B": $0 < |V_s| \lesssim |-50V|$. Applying some RF power to the substrate holder results in a negative V_s value of a few tens of volts, a potential drop which is restricted to a narrow (~1cm) "sheath" or "dark space" adjacent to the substrate. This causes the substrate surface to be bombarded by low energy positive ions, which drift into the sheath from the plasma. When the pressure is raised, energetic neutral species can also contribute increasingly, these being produced by recombination of ions. In regime "B" the attachment process is mainly affected by resputtering of incompletely reacted or of loosely bound species.

Regime "C": $|Vs| \gtrsim |-50V|$. A further increase in the RF power, hence in V_s, leads to enhanced activation in the gas phase, and to a more intense surface bombardment. On polymer surfaces, this can result in appreciable bond breakage, hence in the formation of high concentrations of active (free radical) sites which can react with gas phase species. Of course, enhanced sputtering and desorption, described above, also apply.

Another effect, "surface contamination", must also be taken into account: This may arise from residual gas and small leaks in the vacuum system, but a further possible source should not be overlooked, namely the following: Polymers are capable of entrapping appreciable amounts of gas in their free volume, and these molecules are released under the effect of vacuum and of particle bombardment. In the present experiments the polymers were deliberately not degassed before plasma treatment, as such a pretreatment would not likely be economical in an industrial plasma process. The released molecules, primarily air and water vapor, evidently can participate chemically during plasma treatment by intermixing with the feed gas molecules.

<u>Regime "D"</u>: Finally, after plasma treatment, free radical sites at
or near the polymer surface can remain active for extensive periods
of time (<u>11</u>). When the treated sample is subsequently exposed to
ambient atmosphere, these radicals can chemically react with atmos-
pheric constituents such as oxygen or water vapor. This certainly can
occur during the time interval while the sample is transferred
through atmosphere from the plasma reactor to the ESCALAB surface
instrument.

The general trends observed in Figures 2 to 5 can readily be ex-
plained in terms of the preceding model. The brief plasma exposure
(15 s) in the present experiments does not affect the surface mor-
phology (no roughening was observed by scanning microscopy), so that
contact angle changes can be assigned entirely to changes in surface
composition. In particular, the advancing and receding contact
angles are related to the surface concentrations of hydrophobic and
hydrophilic functional groups, respectively. This will be discussed
more explicitly in the following text. Thus, the contact angle hys-
teresis $(\theta_a - \theta_r)$, which can even be observed for the case of un-
treated polymer surfaces (see, for example, Figure 2), already
suggests the presence of a partly heterogeneous surface. We now
examine specific features of the various figures.

<u>NH$_3$ - plasma (Figure 2)</u>. The first remarkable feature is that far
more chemically bound oxygen appears after plasma treatment than is
present in both virgin polymers, PVC and PC. This may result either
from small leaks, from entrapped air or from "post-oxidation" (regime
"D"), or all three. In "pure" MW plasma ($V_s = 0$, regime "A") the
attachment of O and N containing groups is high, but it decreases in
regime "B". The maximum in N/C, near $V_s \sim -150$ V, presumably corre-
sponds to the optimum surface activation, while a further increase in
$|V_s|$ leads to the removal of N-containing groups. The chlorine con-
centration is reduced by plasma treatment, particularly by preferen-
tial sputtering at elevated V_s. It is noteworthy that θ_a and θ_r
appear to correlate with the N/C behaviour (see next section).

<u>Ar - plasma (Figure 3)</u>. Once again, oxygen uptake as discussed
above, is also seen to occur with Ar plasma treatment. For this
inert gas, one would expect the processes of regimes "C" and "D" to
dominate. Interestingly, the "contamination" by N is highest in pure
MW plasma (regime "A"), and it is seen to decrease under the effect
of ion bombardment. The oxygen content is almost constant, possibly
because O lost by sputtering (see above for N) is compensated by
enhanced reaction of the activated surface via process "D". As in
the case of NH$_3$ plasma, PVC is seen to lose Cℓ in Ar plasma.

<u>O$_2$ - plasma (Figure 4)</u>. In this case the surface oxidation is so
rapid and efficient, that no appreciable nitrogen incorporation is
observed. In fact, for PC the surface oxidation is seen to increase
with rising $|V_s|$. On the other hand, the Cℓ concentration of PVC
does not drop as much as in NH$_3$ or Ar plasma. Regarding contact
angle data, θ_a and θ_r values are seen to be mostly lower than for Ar
plasma treatment.

<u>CF₄ - plasma (Figure 5)</u>. As expected, CF_4 plasma treatment leads to dramatic effects; surface fluorination is seen to be very efficient in regimes "A" and "B", but the fluorine concentration drops rapidly at elevated $|V_s|$. The presence of hydrophobic CF_x groups maintains high θ_a values, as expected; θ_r decreases only slowly with increasing substrate bombardment, presumably due to the resulting surface cross-linking.

CONTACT ANGLE HYSTERESIS

We have attempted to correlate the contact angle hysteresis ($\theta_a - \theta_r$) with the surface composition. The most evident correlation has been found for the case of bound nitrogen, as illustrated in Figure 6, where θ_a and θ_r are plotted versus N/C for both PC and PVC. This suggests that the nitrogen-containing groups are the principal species responsible for surface wettability by water. In these terms, C-N groups represent the hydrophilic component, while C-H, C-F, and C-Cℓ groups represent the hydrophobic component. Our system then behaves in a way which agrees with a well-known model for a heterogeneous surface, first described by Johnson and Dettre (13). According to this model, θ_r decreases rapidly whenever a hydrophilic component is introduced. On the other hand, θ_a remains high until only a small portion of the surface remains hydrophobic. According to the data of Figure, 6 we can readily adjust the degree of water wettability, simply by controlling the substrate bias V_s for a given gas, pressure and flow rate.

METAL ADHESION

Our results regarding the adhesion of a thin, evaporated aluminum layer to the polymer surfaces are summarized in Table I, which uses the semiquantitative scale from 0 to 10 already described in the experimental section. The adhesion to untreated ("N") PVC and PC was found to be quite poor, and this is why we emphasize here the results pertaining to these two polymers. Table I permits one to distinguish the effects of different treatment gases and, for a given gas, the effect of varying V_s. For example, treatment in NH_3 plasma improves the adhesion to PVC only slightly, which strongly suggests that there exists no direct correlation between wettability and enhanced adhesion. Some improvement is observed for Ar plasma treatment, presumably due to the fact that the surfaces become more crosslinked, hence mechanically stronger. On the other hand, a large improvement in Aℓ adhesion is observed following O_2 plasma treatment for both PVC and PC. Indeed, O_2 plasma treatment has also been found by several other authors to improve Aℓ adhesion to other polymers not discussed here. An important contribution to this strong bond has been shown to originate from chemical linkages of the type C-O-Aℓ, which have been clearly and unambiguously demonstrated using various surface analytical techniques, particularly HREELS and XPS (14), and by ab-initio quantum-chemical calculations (15).

Finally, comparing the results for CF_4 plasma-treated PC and PVC, we note that substantial adhesion improvement occurs for the former but not for the latter. The fact that both treated surfaces become highly fluorinated and hydrophobic once again underscores the state-

Table I: Adhesion of Aluminum Films*

Polymer	Untreated	NH₃ MW	NH₃ Vₛ[V] -30	NH₃ Vₛ[V] -150	NH₃ Vₛ[V] -225	Ar MW	Ar Vₛ[V] -25	Ar Vₛ[V] -150	Ar Vₛ[V] -350	O₂ MW	O₂ Vₛ[V] -30	O₂ Vₛ[V] -150	O₂ Vₛ[V] -350	CF₄ MW	CF₄ Vₛ[V] -30	CF₄ Vₛ[V] -150	CF₄ Vₛ[V] -300
PC	1	7	5	4	9	7	5	6	9	10	10	10	10	9	10	10	10
PVC	0	3	6	4	1	10	2	3	3	10	10	10	10	2	1	1	9
PTFE	10	1	5	--	10	10	10	10	4	10	10	10	10	9	10	10	10
PI	10	--	10	10	10	10	9	7	4	10	10	10	10	9	8	8	9
PE	9	9	10	9	10	--	10	--	10	10	10	10	10	10	10	10	10

* 0 - 10 classification: "0" - no adhesion
"10" - excellent adhesion

ment above regarding apparent lack of correlation between wettabili-
ty and adhesion.

CONCLUSIONS

We have shown that dual-frequency (MW/RF) plasma treatment consti-
tutes an efficient new approach for surface modification of polymers.
An important parameter capable of controlling the surface composition
is the RF-induced substrate bias voltage, V_s. Surface-compositional
changes, in turn, can account for transitions from a dominantly
hydrophobic to a dominantly hydrophilic surface state, or vice versa;
indeed, treatments can be tailored to achieve a predetermined wetta-
bility state for a given surface. High V_s values also have the advan-
tage of reducing surface "contamination" by ion-induced sputtering of
weakly bound groups, and thereby promoting a mechanically strong
surface layer.

The surface wettability by water drops has been clearly linked with
the concentration of chemically bound nitrogen in the surface. Con-
versely, measurements of advancing and receding contact angles for
water can provide information regarding surface composition. On the
other hand, there appears to be little or no direct correlation be-
tween water wettability and adhesive strength of evaporated aluminum
films. Substantial improvement in adhesion of $A\ell$ to many polymers
can be achieved by O_2 plasma treatment of the polymer surface before
metallization. Other workers have shown this to result in chemical
linkages between the metal and polymer surface moieties.

The described dual-frequency plasma approach is very versatile and
can be applied for deposition, etching, or surface modification
merely by changing the operating parameters. This technology can
readily be scaled up to large-area industrial requirements.
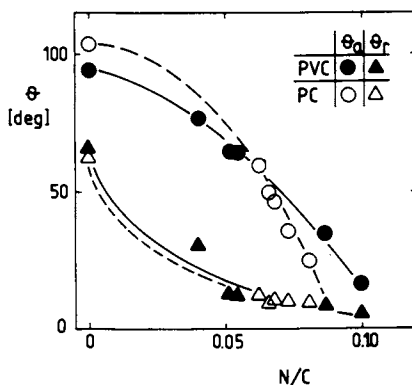
Fig. 6: Effect of the N/C XPS atomic concentration ratio on the
contact angle hysteresis: (O,●) advancing and (△,▲)
receding contact angles for PVC (●,▲) and PC (O,△).

Literature Cited

1. Clark, D.T.; Dilks, A.; Shuttleworth, D. In Polymer Surfaces,
   Clark,D.T.; Feast, W.J., Eds.; Wiley: New York, 1978, p. 185.
2. Wertheimer, M.R.; Moisan, M. J. Vac. Sci. Technol. A 1985, 3,
   2643.
3. Wertheimer, M.R.; Moisan, M.; Klemberg-Sapieha, J.E.; Claude, R.
   Pure Appl. Chem. 1988, 60, 815.
4. Neusch, M.; Kieser, J. Vacuum 1984, 34, 959.
5. Foerch, R.; McIntyre, N.S.; Sodhi, R.N.S.; Hunter, D.H. J. Appl.
   Polym. Sci. (in press).
6. Chapman, B. Glow Discharge Processes, Wiley: New York, 1980.
7. Biederman, H.; Martinu, L. In Plasma Deposition: The Treatment
   and Etching of Polymers, d'Agostino, R.; Ed.; Academic: New York,
   1990.
8. Martinu, L.; Klemberg-Sapieha, J.E.; Wertheimer, M.R. Appl. Phys.
   Lett. 1989, 54, 2645.
9. Wertheimer, M.R.; Klemberg-Sapieha, J.E.; Schreiber, H.P. Thin
   Solid Films 1984, 115, 109.
10. Strong, J. Rev. Sci. Instrum. 1945, 6, 97.
11. Yasuda, H. Plasma Polymerization; Academic: New York, 1985.
12. Martinu, L.; Pische, V.; d'Agostino, R., D-5, this volume.
13. Johnson, R.E.; Dettre, R.H. J. Phys. Chem. 1964, 68, 1744.
14. Pireaux, J.J., this volume; and Novis, Y.; Chtaib, M.;
    Degosserie, N.; Pireaux, J.J.; Caudano, R., this volume.
15. Selmani, A., this volume.

Chapter 11

Polyimide Surface Degradation

X-ray Photoelectron Spectroscopic Study Under UV-Pulsed Laser Irradiation

M. Chtaïb, E. M. Roberfroid, Y. Novis, Jean-Jacques Pireaux, and R. Caudano

Facultés Universitaires Notre-Dame de la Paix, Laboratoire Interdisciplinaire de Spectroscopie Electronique, Rue de Bruxelles 61, B–5000 Namur, Belgium

Polyimide surface modifications under UV ArF (λ = 193 nm) laser irradiation in air were studied by X-ray Photoelectron Spectroscopy (XPS). Several chemical transformations, the nature of which changed with fluence (energy per pulse and unit area), were evidenced at the polymer surface. A sharp decrease in the O/C and N/C signals was observed at fluence higher than $20mJ/cm^2$ and new carbon species appeared. At higher fluence (above 40 mJ/cm^2) complete denitrification took place and the chemical nature of the surface was completely modified.

During the last decade, there has been considerable interest in studying the interaction between ultraviolet radiation and polymers by the use of pulsed excimer laser (1–4). In fact, some attractive applications in microelectronics and surgery have been successfully implemented (5), and further informations about the different mechanisms (photochemistry, thermal effect...) involved at the polymer surface have been invoked in order to elucidate their relative contributions. More recently, the attention has been focused on this type of polymer surface modifications to improve some surface properties like the adhesion in metallized polymer structures.

Studies of polymers such as polymethylemethacrylate (PMMA), polyethylenetherephthalate (PET) and polytetrafluoroethylene (PTFE) revealed that the chemical surface changes depend considerably on the laser fluence , the nature of the environment surrounding the polymer during the treatments and the UV absorption coefficient of the polymer (6,7,8). It was found that the Ablative

PhotoDecomposition (APD) that occurs above a well-defined
ablation threshold usually leads to removal of polymer
material leaving a new fresh "clean" surface with the same
composition as the untreated material. However ,in the
case of PET   (8) both composition and structural
modifications occur even for fluences below the ablation
threshold.
    In this work, we present the effect of 193 nm pulsed UV
high intensity radiation on polyimide, a polymer well
known for its applications in solid-state technology
(thermal stability and dielectric properties). We have
used XPS in order to determine the evolution of chemical
surface composition versus laser fluence and have obtained
some attractive informations about these modifications
induced by UV laser radiation.

2. EXPERIMENTAL

    Polyimide KAPTON films were irradiated using a Lambda-
Physik EMG200 Excimer laser tuned to 193 nm radiation
(ArF). The samples were treated in air, at different
fluences; all received 10 shots at the repetition rate of
10 Hz. Surface analysis of the different samples was
performed using an ESCA-201 system (SSL) with an x-ray
microspot facility (150 μm).

3. RESULTS AND DISCUSSION

    Like most aromatic polymers, polyimide(fig. 1) absorbs
strongly UV radiation in the wavelength region below 200
nm (absorption coefficient a =4.10^5 cm^{-1}) (9). Therefore,
the penetration depth of the UV light in this material is
very small : about two thirds of the radiation intensity
is absorbed in the first 300 Å of the polyimide film.
    The XPS peak assignments were performed according to
literature   results   (10-12)   and   after   surface
characterization of untreated samples for comparison
purpose.
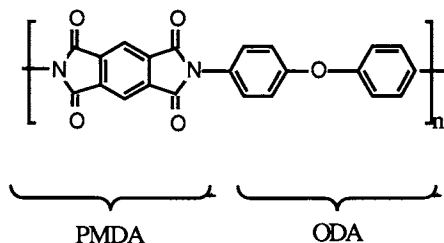
Fig. 1 : polyimide (PMDA-ODA)

The C1s core level signal of pristine polyimide (<u>fig: 2</u>) is composed of three peaks: At 285.0 eV (1) one sees a strong signal due to "pure" aromatic carbons (not bonded to N or O) in the ODA rings. The peak at 286.2 eV (2) is attributed to the other ODA carbons bonded to nitrogen and oxygen (<u>13,14</u>) as well as to those located in the central PMDA ring (<u>13</u>).   The last carbon peak on the high binding energy side at about 289.0 eV (3) is due to carbonyl groups C=O of the PMDA.

The O1s spectrum consists of two unresolved peaks : one centered at 532.3 eV due to carbonyl oxygen and the other at 533.7 eV due to oxygen atoms of the ether group (<u>fig:3</u>).

The N1s signal(<u>fig:4</u>) consists of a main peak at 400.8 eV due to nitrogen imide linking-up the two PMDA and ODA parts. The peak at 399 eV is probably fingerprinting some isoimide content into the material (<u>15</u>).

For fluences up to 15 mJ/cm^2, the intensities of different carbon features as well as those of oxygen and nitrogen remained constant. However minor fluctuations of the intensity ratios presented in <u>fig:5</u>, can be explained by the desorption of low molecular weight fragments stimulated even at low fluences. A similar tendency was pointed out for PET, another high absorbent polymer, in which case it has been attributed to a competitive mechanism between desorption of low molecular weight fragments and surface reaction with the ambient atmosphere (<u>8</u>).   For polyimide, further analysis is necessary to confirm this fact, but in the present work, we focus our attention on more drastic changes taking place at higher fluences (above 20mJ/cm^2). According to another study, the ablation threshold for polyimide with an ArF laser is about 25 mJ/cm^2 (9).

For fluences higher than 20 mJ/cm^2, a clear diminution of the relative concentration in oxygen and nitrogen is observed <u>(fig. 6)</u>. The O/C atomic ratio falls from 0.20 for the untreated polyimide to 0.04 at 40 mJ/cm^2 and is characteristic of an important deoxydation induced by the UV radiation.

These modifications are also visible in the C1s signal where the intensities of both peaks centered at 286.2 eV and 289.0 eV decrease considerably (<u>fig: 2c and 2d</u>).
other new peaks appeared in this XPS signal.   The one centered at 283.8 eV (peak 4) has been attributed to "graphite" type carbon or more precisely to cross-linked carbons chains coming from redeposited fragments of ablated polymeric material. The intensity of this signal is large and certainly contributes to an overestimated decrease in the N/C and O/C ratios. Peak(5) at around 287.2 eV suggests the presence of O-C-O and functionalities at the surface (<u>16</u>), while there are no such components in the structural formula (fig:1).   The
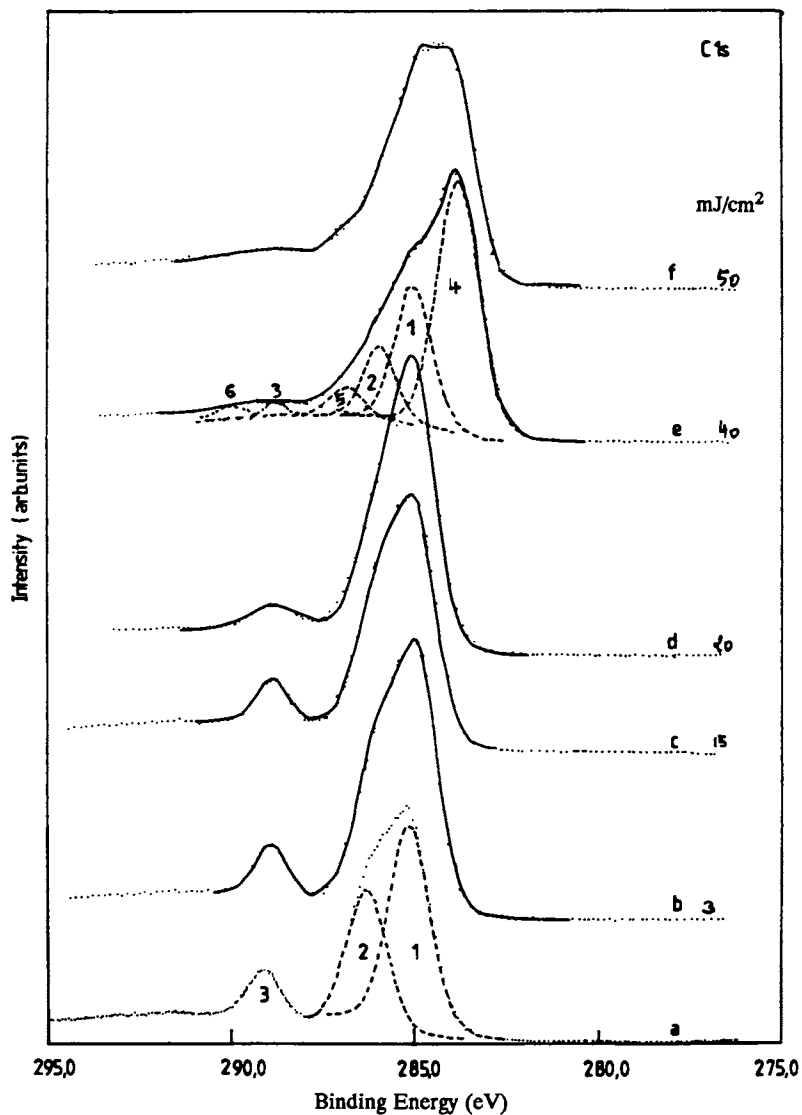
Fig. 2 : C1s spectra of treated polyimide at different fluences : reference(a), 3mJ/cm2(b), 15mJ/cm2(c), 20mJ/cm2(d), 40mJ/cm2(e), 50mJ/cm2(f).
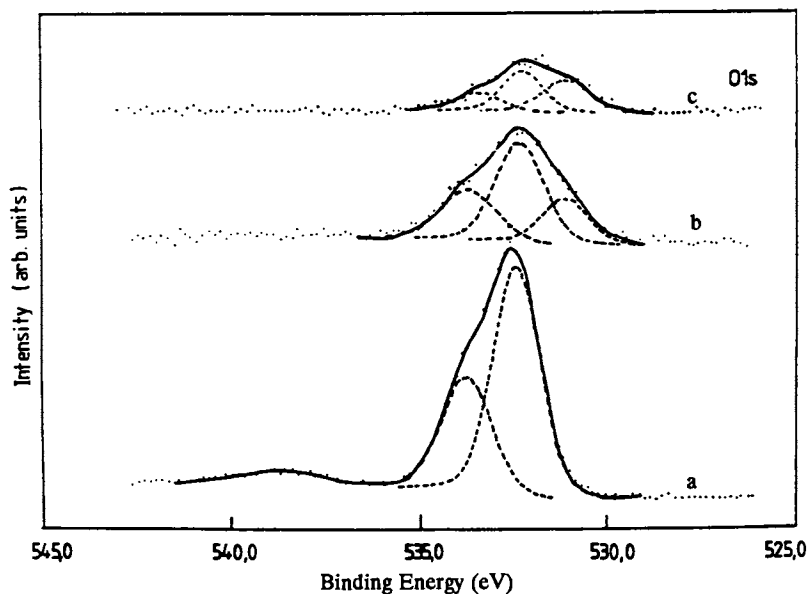
Fig.3 : O1s spectra of treated polyimide at different fluences : reference (a), 40mJ/cm^2(b), 70mJ/cm^2(c).
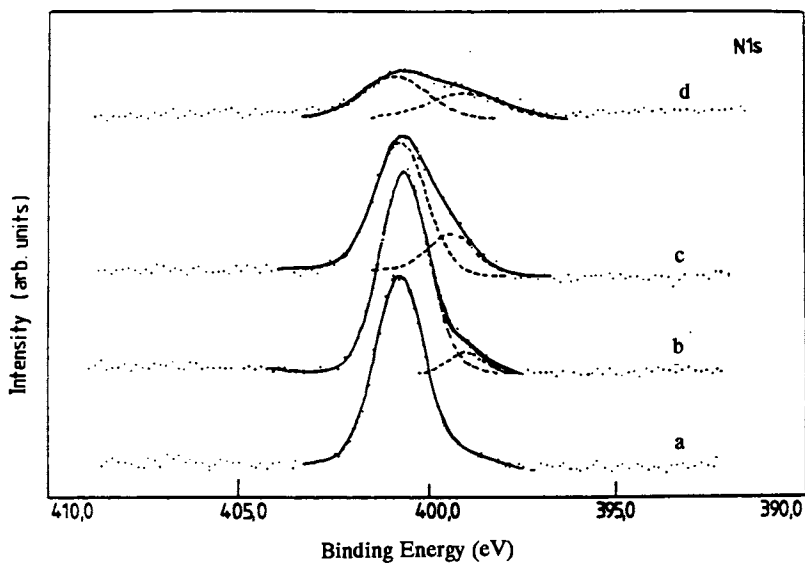
Fig. 4 : N1s spectrum of treated polyimide at different fluences : reference (a), 15mJ/cm^2 (b), 20mJ/cm^2 (c), 40mJ/cm^2 (d)
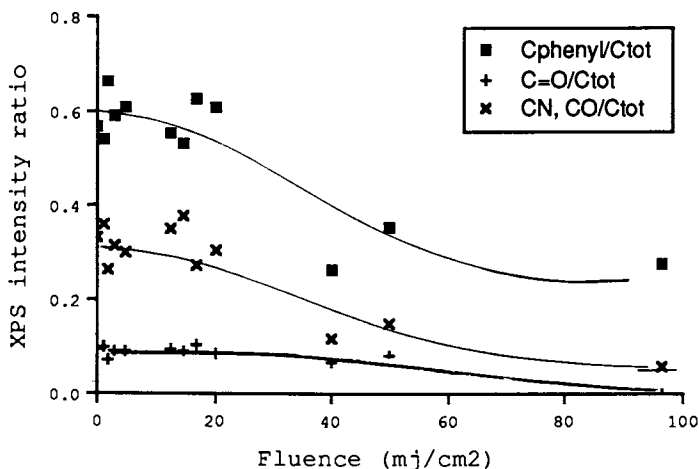
Fig. 5 : XPS intensity ratio of the different carbon species versus fluence.

small peak (6) at high binding energy (289.8eV) is tentatively assigned to carbon of HO-<u>C</u>=O type due to carboxylic functionalities formed at the surface.

At 40 mJ/cm^2 drastic changes are also observed in the oxygen signal (fig. 3). The intensities of the two peaks in the O1s region decrease at the same rate; but a new peak appears at low binding energy. This is consistent with the appearance of the carbon carboxylic peak (6).
the extra structure at low binding energy around 399 eV appears reinforced (fig. 4). Such a structure has been tentatively attributed to isoimide. However from another study(17), this peak was assigned to hydrogenated nitrogen or to C =N- (pyridin type) products resulting from the PI degradation. Hence it appears that UV radiation induces C-N bond rupture, creating nitrogen atoms with a chemical environment different from the ones of the PMDA ring (imides).

In addition to the decrease of the N integral intensity, there is also a change of its chemical nature. In fact the peak at 399 eV(isoimide) increases while the intensity of the imide peak (401.0 eV) (Fig:4) decreases during laser treatments (15 to 50 mJ/cm^2). The ratio N(399)/N(401) (fig.7) of these two peaks clearly shows an increase by a factor of 10 for fluences around 50mJ/cm^2. We noted that at very high fluence (96 mJ/cm^2), the N1s signal completely disappears.
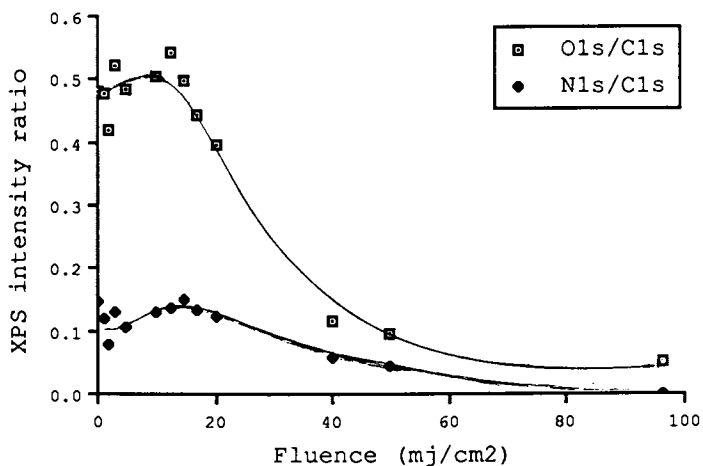
Fig. 6 : XPS intensity ratio of O1s/C1s and N1s/C1s versus fluence.
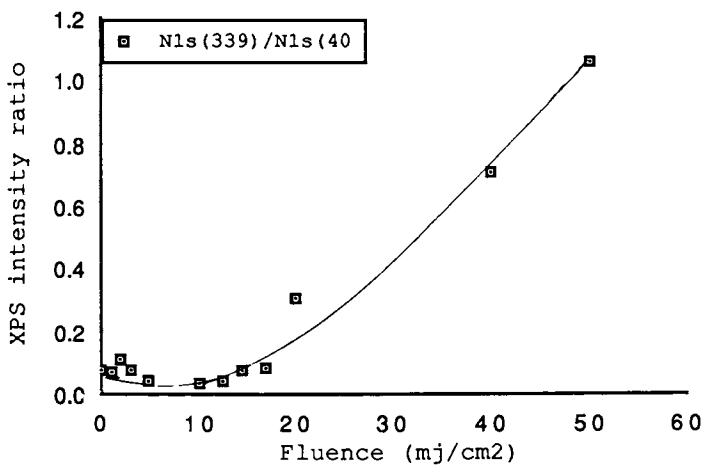
Fig. 7 : Ratio of the two peaks in the N1s region due to imide and iso-imide nitrogen versus fluence.

MODEL

The UV radiation induces the rupture of the imide ring, thus changing the neighbourhood of carbon and nitrogen via chemical reactions with ambient air (H_2O, N_2, O_2...). Beside the UV bond breaking a local increase of surface temperature, can also contribute by thermal damage to the appearence of carbon "graphite" at the surface.

From all these XPS informations in order to take into account the fact that after the laser treatments several species like isoimide, $C=N-$, $-CO$, $O-C-O$, and carboxylic groups are present at the surface of polyimide, we propose the following surface reaction under UV laser radiation above the ablation threshold in presence of air moisture:

isoimide
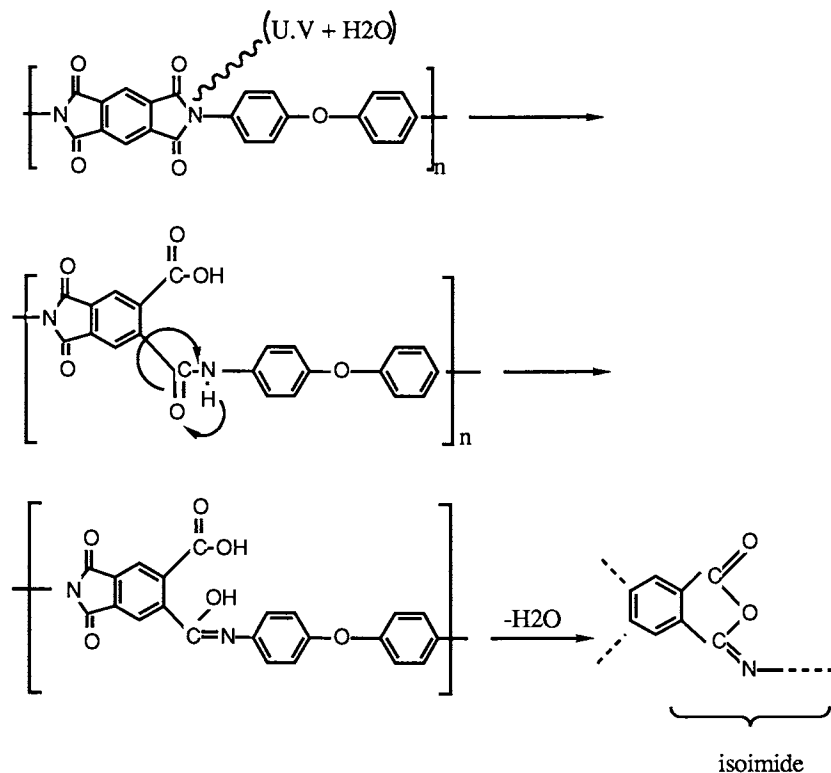
SUMMARY

The UV laser irradiation of polyimide in air leads to drastic changes in the polymer surface composition. At fluences under 40 mJ/cm^2, an oxygen and nitrogen depleted surface is created. At higher fluences, the radiation completely modifies the nature of the bonding between carbons, oxygen and nitrogen atoms and seems to induce new carboxylic functionalities and surface graphitization.

LITERATURE CITED

1. Srinivasan,R.; Mayne-Banton, V; Appl. Phys. Lett. 1982, 41, 6, 576
2. Srinivasan,R; Laser Processing and Diagnostics, 1984, 343, Springer-Verlag, Berlin, Heidelberg
3. Srinivasan, R; Leigh, W.J; J. Am.Chem. Soc.,1982 ,104, 6784
4. Znotruo,T.A.; Laser Focus, mai 1978, 54,
5. Srinivasan,R.; Science, 1987, 234, 559
6. Lazare, S; Srinivasan, R; J. Phys. Chem.,1986, 90, 2124
7. Burrell, M.C.; Liu, Y.S.; Cole, H.S., J. Vac. Sci. Technol., 1986 A4 (6)
8. Chtaïb, M; Roberfroid, E.M; Novis, Y; Pireaux, J.J.; Caudano, R, to be published in JVST (December 89)
9. Sutclife, E; Srinavasan, R., J. Appl. Phys., 1986, 60, 9
10. Philipp, H.R; Cole, H.S.; Liu, Y.S.; Sitnik, T.A., Appl. Phys. Lett., 1986, 48, 2, 192
11. Leary,H.J.; Campbell, D.S., Surf. Int. Anal., 1979, 4, 3
12. Lamb,R.N.; Baxter, J.; Grunze, M; Kong, C.W.,.Untertl,W.N, Langmuir, 1988, 4, 249
13. Baise,A.I.; Buchwahlr, P.L., In Conference on Polyimide; Mittal, K.L., Ed.; Ellenville, New York, 1982; p. 137
14. Peeling, J.; Clark, J.T., Polym. Degrad. Stabil.,1981, 3, 177
15. Leary H.J, Campbel D.S Surf. interface anal 1979 1 ,75
16. Momose, Y; Ikawa, K.; Satd, T., J. Appl. Polym. Sci., 1987, 33, 2715-2729
17. Anderson .S.G, Meyer.H.M .Atanasoska.L.J and Weaver.J.H, J.Vac.Sci.Technol. 1988 A6 38.

Chapter 12

Metal-Filled Polymers

Surface Modification by Plasma Deposition

L. Martinu[1], V. Pische[2], and R. d'Agostino[2]

[1]Groupe des Couches Minces and Département de Génie Physique, École Polytechnique, C.P. 6079, Succursale A, Montreal, Quebec H3C 3A7, Canada
[2]Dipartimento di Chimica, Universita di Bari, Via Amendola 173, 70126 Bari, Italy

Composite thin films consisting of gold grains incorporated in a fluorocarbon matrix were obtained by simultaneous plasma polymerization of a C_2F_6 monomer and sputtering of gold in an RF glow discharge. It is shown that increasing negative substrate bias voltage and substrate temperature very sensitively affect the film microstructure and properties, especially polymer crosslinking, gold concentration and surface contact angle hysteresis. XPS data and surface wettability measurements, closely related to the fluoropolymer crosslinking, are discussed in terms of plasma-surface interactions. Finally, metal-filled polymers with gradually varying characteristics, ranging from an insulating to a conducting regime, are described.

Metal-containing plasma polymer films are two-component composites formed by a conducting and an insulating constituent (for reviews, see 1,2). They are prepared by low pressure plasma deposition techniques. Their final properties depend on the individual characteristics of each component, but predominantly on their relative concentrations and microstructure. Three different regimes of film characteristics can be distinguished, depending on the amount of metal incorporated: (i) the dielectric regime: metal grains are dispersed in a matrix of plasma polymer; (ii) the transition regime: metal inclusions grow and form a maze network; this coincides with the percolation treshold at a critical metal volume fraction f_c; (iii) the metallic regime: plasma polymer inclusions are present inside a continuous metallic matrix.

Gold-doped plasma polymerized fluorocarbons (Au-PPFC) have been most frequently studied (3-8), but numerous other combinations have also been reported (1,2). For the Au-PPFC systems, f_c has been found to be ~ 0.40, at which the films' electrical conductivity abruptly changes by about 8 orders of magnitude (6,7). In the dielectric regime, the presence of metal clusters evokes an anomalous optical absorption around 550 nm (4,7). The optical and electrical properties

have been correlated with the gold concentration, grain diameters (typically 5-50 nm), and the cluster shapes (spherical or elipsoidal) (3,4,6,7). Because of optical selectivity, this type of films has been considered for applications such as coloured coatings or optical filters. Thermally induced changes in conductivity suggested applications for laser writing.

The present work is a continuation of our studies on Au-PPFC. We investigate the effects of film growth processes, influenced by different substrate biases, U_s, and substrate temperatures, T_s, on the film surface characteristics.

PLASMA PROCESSES in an RF-SYSTEM

Preparation of plasma polymer/metal films in low temperature nonequilibrium plasmas is generally based on a combination of two processes applied simultaneously:
a) plasma polymerization of an organic gas or vapour, and sputter-etching of a metallic target;
b) plasma polymerization and evaporation of the metal;
c) sputtering of a two-component target composed of a polymer and a metal.

The first approach (a) has been the one most frequently used: deposition occurs in a radio-frequency (RF) glow discharge at a typical pressure between 10 mTorr and 200 mTorr. The plasma is excited between two parallel electrodes: one is grounded, the other is capacitively coupled to an RF generator. In such an arrangement, a negative DC potential U_T develops automatically at the target electrode, due to the very high mobility of electrons compared with that of the ions (9). Positive ions which fall through the potential U_T, provoke physical sputtering, and they can promote ion-assisted etching of the target material. Free radicals formed in the plasma due to inelastic collisions of electrons with monomer molecules, are the principal precursor species responsible for the formation of plasma polymer.

The composite film grows on the grounded electrode when the sputter-etched metal and free radicals reach the substrate surface. The final metal concentration depends upon the rate at which the two components are generated, and this can be controlled by two means:

(i) by using different feed gas compositions at constant RF power; for example, an increase in the argon/fluorocarbon ratio leads to a decreased deposition rate of the polymeric component, and to an increase in the relative concentration of sputtered gold atoms in the gas phase;

(ii) by varying the RF power, hence the target bias voltage, at a constant feed gas composition; when increasing the input power and target bias above the threshold value for the given metal, the sputtering rate increases more rapidly than does the polymerization rate.

For both processes mentioned above, the bulk plasma characteristics (electron energy distribution function and plasma potential) are varied. It is thus difficult to distinguish whether the resulting film microstructure is controlled by processes in the plasma volume (for example different fragmentation of the monomer molecules) or by surface effects.

In this study, we control the film growth solely by substrate surface processes, by varying U_s and/or T_s, without affecting the bulk plasma parameters. This is possible when a third electrode, used as the substrate holder, is placed in the plasma system as shown in Fig. 1. A small amount of RF power delivered to this electrode results in a bias potential V_s which controls bombardment of the growing films by low energy ions. If the area of this third electrode is substantially smaller than that of the main RF electrode, its presence does not appreciably influence the plasma characteristics; this has recently been confirmed by actinometric optical emission spectroscopy (8).

EXPERIMENTAL DETAILS

The Au-PPFC films were deposited in a triode system shown schematically in Fig. 1. The powered main electrode (7 cm in diameter) was capacitively coupled to an RF (13.56 MHz) power supply, the opposing electrode (15 cm in diameter) was grounded, and the third electrode (3.6 cm in diameter) was located perpendicularly in the gap between the larger ones at the edge of the plasma zone. On it were placed the substrates for coating experiments.

The RF power was divided into two parts using a variable capacitor assembly. The negative potentials U_T and U_s were measured with respect to ground using an LC circuit. T_s was controlled by a thermostat system filled with ethylene glycol. The films were deposited under the following conditions: total power input, P = 200 W, U_T = -480 V, pressure P' = 130 mTorr; the total flow rate of feed gas mixture (87% C_2F_6, 13% H_2), F = 20 sccm. Gold, and in several experiments polytetrafluoroethylene (PTFE, Teflon), targets were placed on the main RF electrode.

The chemical structure and composition of films deposited onto the Aℓ substrates was determined by X-ray photoelectron spectroscopy (XPS) using a Perkin Elmer PHI 548 instrument. Measurement of advancing and receding water contact angles (α_a and α_r, to ± 3°) were carried out by the sessile drop technique, using a Ramé Hart contact angle goniometer (10).

RESULTS AND DISCUSSION

XPS ANALYSIS. The C(1s), F(1s), Au($4f_{5/2}$), and Au ($4f_{7/2}$) photoelectron energy lines were studied in particular. The effect of U_s and T_s on the C(1s) core level is shown in Figs. 2 and 3. The spectra may be deconvoluted into five overlaping peaks corresponding to different bonding configurations between carbon and fluorine. The binding energies due to C(284.5 eV), C-CF(286.9 eV), CF(289.0 eV),
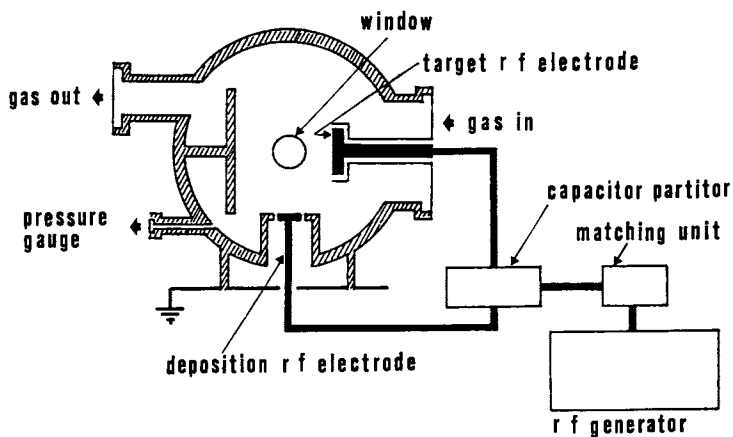
Fig. 1:   Schematic arrangement of the deposition system.
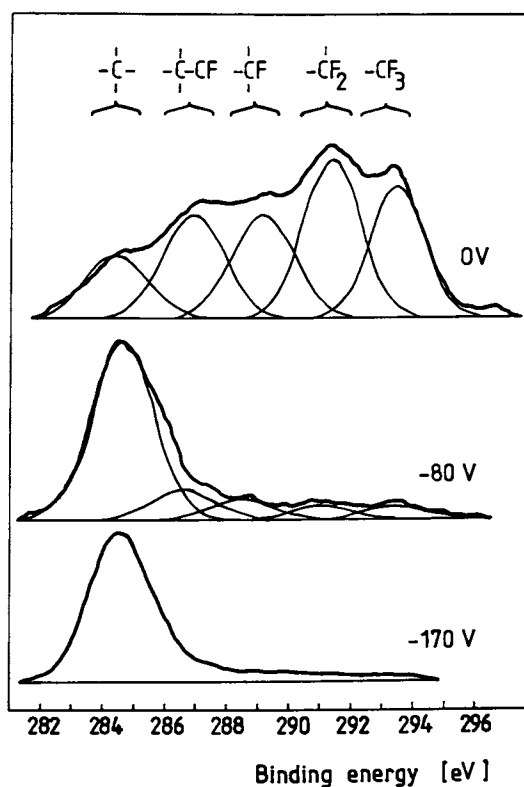
Fig. 2:   C(1s) core level spectra of Au-PPFC films deposited at
          T_s = 0°C and different U_s.

CF_2 (291.3 eV), and CF_3 (293.2 eV) are in good agreement with published data (11-13).

The peak near 284.5 eV coincides with both C-H and quaternary C photoemission signals. The amount of H bonded to C in films grown from C_2F_6/H_2 mixtures (at low H_2 concentration) is expected to be small (a few percent at most), in accord with our previous measurements (13).

Increasing U_s and T_s is seen to cause similar trends in the films' chemical structures: the fluorine concentration decreases leading to dominance of the peak at 284.5 eV. This behaviour is ascribed to bombardment of the growing film surface by low energy ions. Evidently, a rise in U_s increases the energy of impinging ions, leading to "sputter-damage" at the surface and C-F bond breakage resulting in a reduced F/C ratio. An increase in T_s results in enhanced surface mobility of the precursor species and in lower deposition rate of polymer, hence in prolonged exposure to plasma. As a consequence, the films are increasingly branched and crosslinked.

Lowering U_s and T_s causes a decrease in Au concentration (measured by XPS) in PPFC (8) that further results in smaller gold grain dimensions (3,7). In XPS studies on supported metal clusters deposited by evaporation, shifts in the binding energy and broadening of the spectral lines have been reported (14). For our films, the effect of gold concentration on the XPS characteristics is shown in Fig. 4. We plotted the difference between E_B for carbon and gold: E_B [C(1s)] - E_B [Au($5f_{7/2}$)] to eliminate the effects such as sample charging, and also the full width at half maximum (FWHM) for Au($5f_{7/2}$). The E_B values for the bulk materials are C(1s): 284.5 eV and Au($5f_{7/2}$): 83.8 eV.

At high c_{Au} (~ 20-30 at.%) no deviation from the E_B values for bulk C and Au were observed (see Fig. 4). Below 20 at.% Au the difference E_B(C) - E_B(Au) is seen to decrease (by about 0.7 eV at c_{Au} ~ 2 at.%), indicating a shift of the gold peak towards higher binding energies. Only a very slight increase in FWHM with decreasing c_{Au} was observed, partly on account of limited resolution of the spectrometer. We did not measure cluster sizes in this study, but from our previous work (3,7) we estimate that the grain diameters change from about 30-50 nm to about 1-10 nm in the described range.

The observed phenomena can be explained by relaxation processes in the condensed state (14). Grain size effects on the electron relaxation were observed also for optical behaviour of Au-PPFC films (4,5).

SURFACE WETTABILITY. Contact angles are plotted versus F/C and Au/C ratios in Figures 5 and 6, respectively. The value of the advancing contact angle, α_a ~ 110°, is comparable with that of "conventional" PTFE, and it decreases only slightly when F/C diminishes or Au/C rises. On the other hand, the receding contact angle α_r decreases rapidly with increasing C/F and Au/C. It can be seen that α_r is systematically higher for metal-free plasma polymer (i.e. when a PTFE target was used) than for gold-containing PPFC.
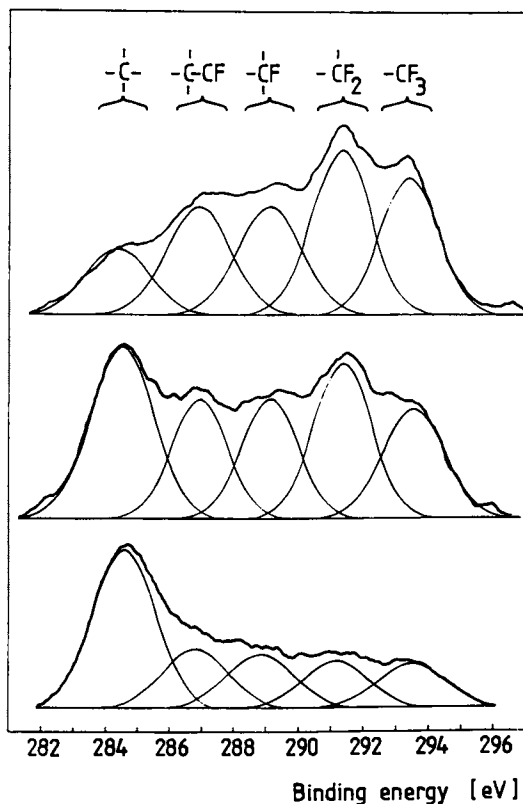
Fig. 3: C(1s) core level spectra of Au-PPFE deposited at $U_s = OV$ and different T_s.
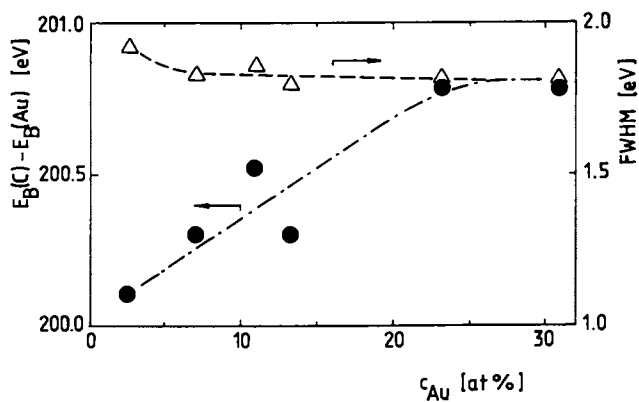
Fig. 4: Effect of gold concentration on the binding energy difference $E_B[C(1s)]-E_B[Au(5f_{7/2})]$ ($\bullet$), and on the full width in the half maximum (FWHM) ($\triangle$) of Au ($5f_{7/2}$) peaks in XPS spectra.
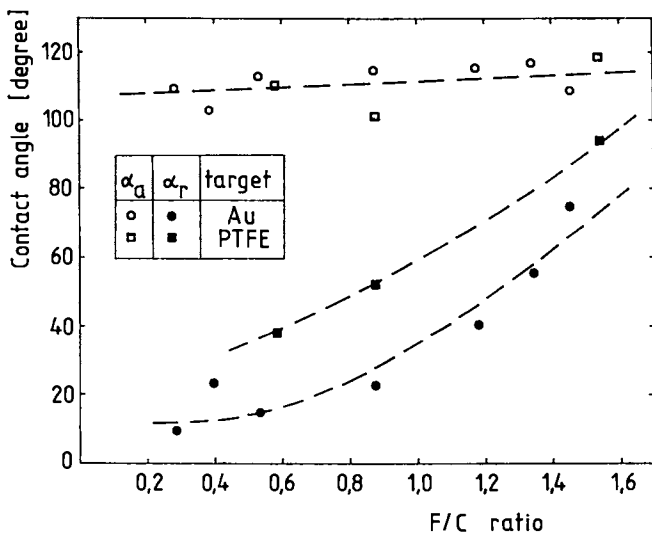
Fig. 5: Advancing and receding contact angles of Au-PPFC and
PPFC films versus F/C ratio.
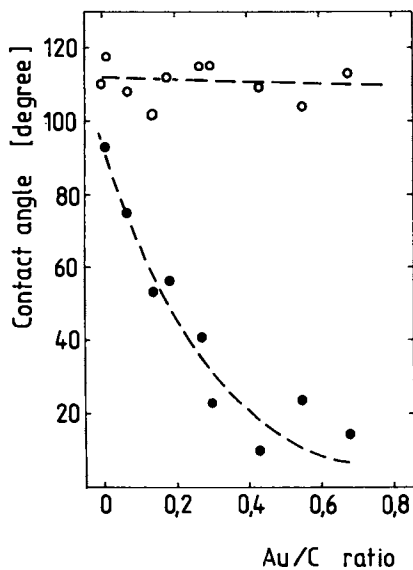
Fig. 6: Advancing (○) and receding (●) contact angles of
Au-PPFC films versus Au/C ratio.

These observations are in agreement with the model of a heterogeneous surface proposed by Johnson and Dettre(15). According to this model, α_r diminishes rapidly when a hydrophilic component is introduced at the surface. On the other hand, α_a remains high until only a small portion of the hydrophobic part persists, but it rapidly drops when the surface is nearly completely wettable. The contact angle hysteresis can therefore be considered as a measure of the surface heterogeneity. In agreement with our results, increasing Au/C or decreasing F/C represents introducing of the hydrophilic (high surface energy) constituent.

CONCLUDING REMARKS

Fluorocarbon monomer and gold were used as model materials to deposit composite thin films. It has been shown that the control of surface conditions by varying U_s and T_s can account for substantial changes in the polymeric structure (crosslinking) and also for the metal concentration as shown in ref. 8. In this way, the surface can be converted from a nonwettable, insulating state to a wettable, conductive one. The energy fluxes of species bombarding the growing layers are surmised to be responsible for these effects.

This approach can be applied generally with different monomer/metal combinations, for example, to prepare metal-filled hard carbon coatings. In this context, optical emission spectroscopy has been shown to be a very useful means for controlling the plasma process (1). The films' properties can be "tailored" over a broad range, including gradual variation in the direction perpendicular to the substrate. Potential applications exist in optics, electronics, decorative coatings an other areas. If a monomer with similar chemical composition as an underlying polymer substrate is chosen, the process can be used to produce strongly adhering metal coatings.

ACKNOWLEDGMENTS

REFERENCES

1. Biederman, H., Martinu, L., in "Plasma Deposition: The Treatment and Etching of Polymers", d'Agostino, R., Ed., Academic: New York, 1990.
2. Biederman, H., Martinu, L., Slavinska, D., and Chudacek, I., Pure Appl. Chem. 1988, 60, 607.
3. Martinu, L., Biederman, H., J. Vac. Sci. Technol. A 1985, 3, 2639.
4. Perrin, J., Despax, B., and Kay, E., Phys. Rev. B 1985, 32, 710.
5. Martinu, L., Thin Solid Films 1986, 140, 307.

6. Perrin, J., Despax, B., Hanchett, V., and Kay, E., <u>J. Vac. Sci.</u>
   <u>Technol.</u> A 1986, <u>4</u>, 46.
7. Martinu, L., <u>Solar Energy Materials</u> 1987, <u>15</u>, 21 and 135.
8. d'Agostino, R., Martinu, L., and Pische, V., <u>Plasma Chem. Plasma</u>
   <u>Process.</u>, submitted.
9. Chapman, B., <u>Glow Discharge Processes</u>, Wiley: New York, 1980.
10. Morra, M., Occhiello, E., and Garbassi, F., <u>J. Coll. Interf.</u>
    <u>Sci.</u>, in press.
11. Kay, E., and Dilks, A., <u>Thin Solid Films</u> 1981, <u>78</u>, 309.
12. Rice, D.W., and O'Kane, D.F., <u>J. Electrochem. Soc.</u> 1976, <u>123</u>,
    1308.
13. d'Agostino, R., Cramarossa, F., Fracassi, F., Desimoni, E.,
    Sabbatini, L., Zambonin, P.G., and Caporiccio, G., <u>Thin Solid</u>
    <u>Films</u> 1986, <u>143</u>, 163.
14. Mason, M.G., <u>Phys. Rev. B</u> 1983, <u>27</u>, 748.
15. Johnson, R.E., and Dettre, R.H., <u>J. Phys. Chem.</u> 1964, <u>68</u>, 1749.

Chapter 13

Wet-Process Surface Modification of Polyimides
Adhesion Improvement

Kang-Wook Lee and Steven P. Kowalczyk

T. J. Watson Research Center, IBM Corporation, Box 218, Yorktown Heights, NY 10598

Polyimide surface modification by a wet chemical process is described. Poly(pyromellitic dianhydride-oxydianiline) (PMDA-ODA) and poly(bisphenyl dianhydride-*para*-phenylenediamine) (BPDA-PDA) polyimide film surfaces are initially modified with KOH aqueous solution. These modified surfaces are further treated with aqueous HCl solution to protonate the ionic molecules. Modified surfaces are identified with X-ray photoelectron spectroscopy (XPS), external reflectance infrared (ER IR) spectroscopy, gravimetric analysis, contact angle and thickness measurement. Initial reaction with KOH transforms the polyimide surface to a potassium polyamate surface. The reaction of the polyamate surface with HCl yields a polyamic acid surface. Upon curing the modified surface, the starting polyimide surface is produced. The depth of modification, which is measured by a method using an absorbance-thickness relationship established with ellipsometry and ER IR, is controlled by the KOH reaction temperature and the reaction time. Surface topography and film thickness can be maintained while a strong polyimide-polyimide adhesion is achieved. Relationship between surface structure and adhesion is discussed.

Polymer surfaces are modified to obtain the desired surface properties without altering the bulk properties (1). One of the most desired properties is adhesion between polymers and other materials such as polymers, metals or ceramics (2). There are many techniques for polymer surface modification, but they can be divided into two major categories. One is a dry process in which the polymers are modified with vapor-phase reactive species that are

often plasma excited (3). The other is a wet process in which the polymers are modified in chemical solutions (4,5). The reactive species of the dry process are ions, radicals or electrons generated by electrical discharge, electron beam or laser irradiation. Since the radicals and the electrons are involved in the modification, the reactions are complicated and the products are not well understood. On the other hand, the reactive species of the wet process are acids, bases, electron donors, or electron acceptors in a solvent. If the reaction with small molecules in homogeneous solution is well-defined, there is a chance that the corresponding reaction occurs at the polymer surface. If a single functional group can be introduced to the surface, the relationship between the surface structure and the surface properties can be studied. The dry process can be applied to any polymer, but the wet process can be applied only to polymers which are insoluble in solvent.

In this work we are interested in polyimide surface modification by wet processes. Polyimides are employed as insulating layers in the fabrication of chips and chip carriers since they have good processability and excellent bulk properties such as low dielectric constant, high thermal stability, low moisture absorption, low thermal expansion, good mechanical properties, etc (6). It is useful to change only the surface properties without altering these bulk properties. It is known that the imide ring can be opened with a base such as an amine or an hydroxide (7). A polyimide such as poly(pyromellitic dianhydride-oxydianiline) (PMDA-ODA) reacts with KOH or NaOH to give a polyamate (potassium or sodium salt of polyamic acid) which is subsequently protonated with acid to give the corresponding polyamic acid (8). Upon curing at 230 °C or higher, the polyamic acid is converted back to polyimide.

SCHEME I

PMDA-ODA   Polyamate

Polyamic Acid   PMDA-ODA
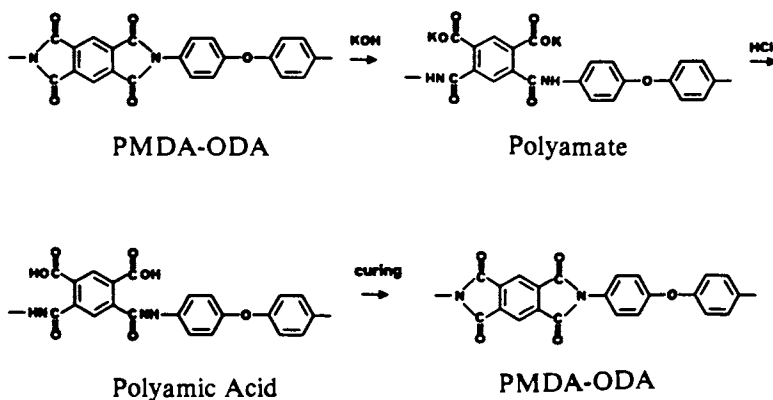
If the concentrated KOH solution is employed at high temperature, the base hydrolyzes the amide to cleave the chains. Thus the surface of the polyimide is etched (9). If the etching occurs up to a few microns of the surface, adhesion of metal to polymer is improved (10).

The depth of polymer surface modification generally ranges from a few tens Å to a few microns depending on the application purposes. For some industrial applications such as microelectronics and photoimaging, it is useful to maintain the surface topographical integrity within a few hundred Å. Thus the maximum modification depth should be within a few hundred Å. The depth is usually measured by X-ray photoelectron spectroscopy (XPS), Rutherford back scattering (RBS), forward recoil spectrometry (FRES) or infrared spectroscopy (IR). However, the depths in the range of 100 Å - 300 Å cannot be measured by either of these techniques since the sensitivities are out of range. The XPS sampling depth is less than 100 Å and the RBS sensitivity is around 300 Å. Thus there is an inaccessible zone between 100 Å and 300 Å. We have been able to measure the depth of modification from 100 Å up to 1000 Å using an absorbance-thickness relationship established with ellipsometry and external reflectance infrared spectroscopy (ER IR).

Here we report a wet surface modification of PMDA-ODA and poly-(bisphenyl dianhydride-*para*-phenylenediamine) (BPDA-PDA) with KOH or NaOH solution. The modified surfaces are identified with contact angles, XPS spectra and ER IR spectra. Polymer thickness and weight changes are also studied. The depth of modified layer is measured by a non-destructive technique using ER IR and ellipsometry. Relationship between surface structure and adhesion strength is discussed.

Experimental

Materials. Kapton H (PMDA-ODA) films (25 um), PMDA-ODA polyamic acid and BPDA-PDA polyamic acid were obtained from Du Pont. Upilex S (BPDA-PDA) films were purchased from Ube Chemicals. KOH, NaOH, HCl, 1-methyl-2-pyrrolidinone (NMP) and isopropanol were obtained from Aldrich.

Methods. Polyamic acid in NMP was spin-coated onto a Si or Quartz wafer (diameter = 2.25 inches) coated with Cr, and then cured to polyimide at 400 °C. The purpose of the 500-750-Å-thick layer of chromium is to enhance wettability and to give good reflectance to the Quartz wafer. Kapton H (PMDA-ODA) and Upilex S (BPDA-PDA) films were employed for gravimetric analysis. Around 5-um thick layers were used to measure the thickness change. The 100-1000-Å-thick layers were employed to obtain XPS and ER IR spectra. The samples for contact angle measurement, XPS and ER IR were dried under vacuum at ambient temperature for 12-24 h and the samples for gravimetric analysis were dried at 85 °C for 12 h. The samples for film thickness measurement were fully re-cured to polyimide.

Contact angle measurements were obtained with a Rame-Hart telescopic goniometer and a Gilmont syringe with a 24 gauge flat-tipped needle. Distilled water was used as the probe fluid. Dynamic advancing and receding angles were determined by measuring the tangent of the drop at the intersection of the air/drop/surface while adding (advancing) and withdrawing (receding) water to and from the drop. External reflectance infrared (ER IR) spectra were obtained under nitrogen using a Nicolet-710 FTIR spectrometer with a Harrick reflectance attachment. X-ray photoelectron spectra (XPS) were taken with a Surface Science Laboratories SSX-100 spectrometer with Al Kα excitation. Thicknesses of polyimide were measured with a Dek-Tak for thicknesses greater than 1000 Å and with a Waferscan ellipsometer equipped with a HeNe laser ($\lambda = 6328$ Å) for 100-1000 Å. The refractive index employed for PMDA-ODA is 1.73.

Modification Of PMDA-ODA. The polyimide samples were treated with 1 M KOH aqueous solution at 22 °C for 1 - 120 min depending on the purposes, followed by washing with water (2 x 3 min) and isopropanol (2 x 3 min). The samples were dried under vacuum at ambient temperature for 12 h. The resulting modified surface is potassium polyamate as identified by XPS and ER IR. The XPS survey spectrum displays a K2s peak at 379 eV and K2p doublet at 294 eV, and the ER IR spectrum exhibits the bands at 1668 (s), 1608 (s), 1540 (m), 1512 (m, sh), 1502 (s), 1411 (m) and 1369 (w) cm^{-1} in the range of 2000-1300 cm^{-1}. The potassium polyamate samples were treated with 0.2 M HCl aqueous solution at 22 °C for 5 min followed by washing with water (2 x 3 min) and isopropanol (2 x 3 min). The samples were dried under vacuum at ambient temperature for 12 h or at 80 °C for 12 h for gravimetric analysis. This modified surface is polyamic acid as identified by contact angle, XPS and ER IR. Thickness and weight changes of the films compared with the starting polyimide were also studied. The potassium peak in the XPS survey spectrum disappeared and the ER IR spectrum shows the bands at 1727 (s), 1668 (s), 1608 (m), 1540 (m), 1512 (m, sh), 1502 (s) and 1414 (m) cm^{-1} in the range of 2000-1300 cm^{-1}. Curing of the polyamic acid produces polyimide as identified by contact angle measurement, XPS and ER IR. All the analytical data are identical to those of the polyimide starting material.

Modification Of BPDA-PDA. The samples were treated with 1 M KOH aqueous solution at 22 or 50 °C for 1-90 min. The modified surface is potassium BPDA-PDA polyamate which is converted to polyamic acid by treatment with 0.2 M HCl aqueous solution at 22 °C for 5 min. The sample washing and drying procedures are similar to those for the PMDA-ODA modification.

Adhesion Measurement. The solution of polyamic acid was spin-coated onto a chromium-coated Si wafer and cured at 400 °C for 40 min. Thickness of the polyimide layer is approximately 6 um. A thin layer (200 Å) of gold was

sputter-coated onto one side (20% of the total area) of the polyimide sample to initiate peel (polyimide has poor adhesion to gold). The surface of the polyimide in the exposed area was modified to polyamic acid as described above. PMDA-ODA polyamic acid in NMP was spin-coated to the surface-modified polyimide film, and subsequently cured at 400 °C under nitrogen. Thickness of the adherate layer (peel layer) after curing is approximately 20 um and the width of the peel layer is 5 mm. The peel strengths were measured by 90° peel using an MTS with 25 um/sec peel rate. The reported values are the average of at least three measurements.

Results And Discussion

Surface Modification Of PMDA-ODA With KOH.
Polyamic acid solution in 1-methyl-2-pyrrolidinone (NMP) was spin-coated onto a Si or Quartz wafer and subsequently cured to polyimide. Since the polyimides cured at high temperature (350-400 °C) have good properties such as relatively low moisture absorption, low solvent swelling and good tensile properties (6), all the films in this work were cured at 400 °C under nitrogen. For the purpose of gravimetric analysis (11), Kapton H films, the chemical content of which is PMDA-ODA, were used. PMDA-ODA films were treated with 1 M KOH aqueous solution at 22 °C to give the corresponding potassium polyamate (potassium salt of polyamic acid). The excess of KOH was removed by washing with water (2 x 3 min). These samples without further washing and drying were used for the protonation reaction (discussed below). To identify the potassium polyamate surface by contact angle, XPS and ER IR, the samples were further further washed with isopropanol (2 x 3 min) and dried under vacuum. The water contact angles (advancing (Θa)/receding (Θr)) decreased from 85°/38° (on polyimide) to 23°/5°. The XPS survey spectrum displays new peaks due to potassium (Atomic Ratio Calcd for K/C: 0.09. Obsd: 0.02). Figure 1 shows the XPS C1s regions of polyimide and modified surfaces. The absolute binding energies are shifted due to charging and have not been corrected. We are interested in changes of the characteristic line shapes. There is only one carbonyl carbon peak (highest binding energy peak) of polyimide starting material (Figure 1a) since the polyimide carbonyls have the similar nuclear environments. But the spectrum (Figure 1b) corresponding to potassium polyamate surface exhibits two carbonyl carbon peaks since the binding energies of carboxylate carbon and amide carbon are different. Changes in the O1s spectra are consistent with the changes in the C1s spectra.

Thin layers (100-1000 Å) of polyimide on the substrate were prepared for external reflectance IR spectra and to measure the average depth of modification, which will be discussed in detail. Figure 2 displays the ER IR spectra of the 870-Å-thick polyimide and the modified samples in the range of 1900-1300 cm^{-1} which provide the most useful information for this re-
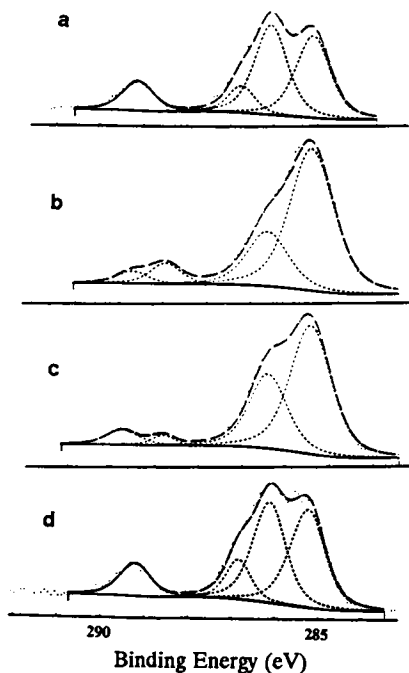
Figure 1. C1s XPS core-level spectra of (a) PMDA-ODA starting material, (b) potassium polyamate, (c) polyamic acid and (d) re-cured polyimide. The takeoff angle of electrons was 35° from the sample surface.
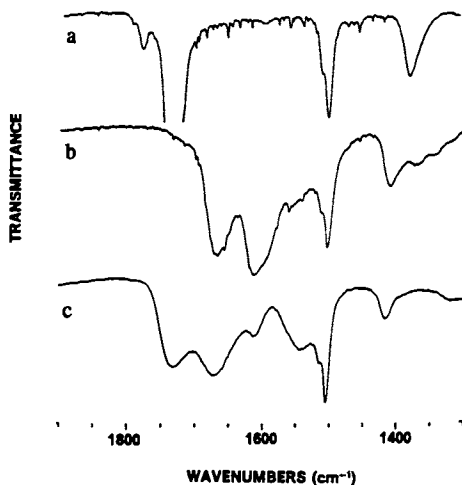
Figure 2. External reflectance IR spectra (a) PMDA-ODA polyimide, (b) potassium polyamate and (c) polyamic acid. The starting polyimide is 870 Å thick and the whole layer is modified. The IR incidence angle is 37° from the sample surface.

action. The external reflectance IR spectrum of PMDA-ODA (Figure 2a) displays the bands at 1778 (w), 1740 (vs), 1726 (w, sh), 1598 (vw), 1512 (m, sh), 1502 (s) and 1381 (m, br) cm^{-1}. The intensities of the external reflectance IR bands are slightly different from those of transmittance IR because of the orientation effects of vibrational modes (12). As shown in Figure 2a the strongest carbonyl stretching at 1740 cm^{-1} is the strongest absorption while in transmittance IR the ODA phenylene stretching at 1502 cm^{-1} is the strongest (the strongest carbonyl stretching band in transmittance IR appears at 1725 cm^{-1}). The whole layer of 870-Å-thick polyimide was modified to obtain a good IR spectrum. As shown in Figure 2b the imide carbonyl stretching at 1740 cm^{-1} (imide I band) and the imide II band at 1381 cm^{-1} completely disappeared. The peaks corresponding to PMDA-ODA polyamate are located at 1668 (s), 1608 (s), 1540 (m), 1512 (m), 1502 (s), 1411 (m) and 1369 (w) cm^{-1}. The peaks at 1668 and 1540 cm^{-1} correspond to the amide I and amide II bands, respectively. The peaks at 1608 and 1369 cm^{-1} are due to the carboxylate (asymmetric and symmetric stretching). It is noteworthy that Linde and Gleason (13) have observed the carboxylate bands at 1600 and 1390 cm^{-1} in the transmittance IR spectrum of the samples prepared by the reaction of polyamic acid (baked at 120 °C) with KOH. The peaks at 1512 and 1502 cm^{-1}, which are also observed in the polyimide spectrum, correspond to the phenylenes. The strong C-O-C (of ODA) stretching band appears at 1248 cm^{-1} (not shown in the figures).

Reaction Of Potassium PMDA-ODA Polyamate With Hydrochloric Acid. The samples treated with KOH and washed with water were protonated by treating with 0.2 M HCl aqueous solution at 22 °C for 5 min to yield a polyamic acid surface. The samples were washed with water (2 x 3 min) and isopropanol (2 x 3 min) and dried under vacuum. This modified surface was extensively analyzed since the polyamic acid surface is of great interest in electronic applications (14). Treatment with HCl does not modify the polyimide, but acidifies all of the potassium polyamate surface to the polyamic acid surface. The water contact angles increased from 23°(Θa)/5°(Θr) to 58°/8°, indicating that the surface became less polar. The polyamic acid surface is less polar than the potassium polyamate surface, thus these results are consistent with the proposed reaction shown in Scheme I.

A kinetic study using the water contact angles of the modified (to polyamic acid) surfaces was performed by changing the KOH reaction conditions since the contact angle provides us with information on the top monolayer (5 Å). The smaller the water contact angle is, the greater the wettability of the polyimide surface. The greater the wettability is, the stronger the polyimide adhesion. When the surface of the polyimide film was modified to polyamic acid, the water contact angles decreased to the

lowest values within a minute of KOH reaction and by subsequent acidification (Θa/Θr): 85°/38° (on polyimide), 56°/8.6°, 58°/7.5°, 62°/9.4°, and 60°/8.6° for control, 1, 5, 10 and 30 min reaction with KOH, respectively). The control reaction only skipped the treatment with KOH. Further reaction up to 4 h does not alter the receding contact angle, but it provides inconsistent advancing contact angle because the extensive reaction makes the surface rough (15). The receding contact angles, which are shown in Figure 3, are indicative of the surface wettability. As illustrated in Figure 3, the outermost layer of PMDA-ODA has been modified within a minute of KOH reaction, while the surface modification of BPDA-PDA is at least ten times slower at room temperature than that of PMDA-ODA (further discussed below).

Gravimetric analysis was performed on 6-cm^2 films after the two-step reaction (KOH-HCl). The condition of an HCl reaction is not a factor. The condition described here are on the KOH reaction. The weight keeps decreasing (less than 1 % for 10 min reaction with KOH and by subsequent acidification and 16 % for 4 h reaction) as the reaction progresses, but the thickness of the thin film layer does not change as much as the weight does. The thickness of the films are 4.87, 4.87, 4.82, 4.77 and 4.76 um for control, 10, 30, 60, and 240 min reaction with KOH, respectively (Figure 4). These results suggest that hydrolysis and etching of Kapton H films, which are used for gravimetric analysis, may proceed faster into the X-Y direction of the film than into the Z direction probably since the edge of the film may be more labile to saponification.

The potassium peaks in the XPS survey spectrum disappears. The shape of the XPS C1s spectrum (Figure 1c) is similar to that of polyamate and consistent with that of polyamic acid as is the O1s spectrum. The ER IR spectrum (Figure 2c) exhibits the bands at 1727 (s), 1668 (s), 1608 (m), 1540 (m), 1512 (m, sh), 1502 (s) and 1414 (m) cm^{-1}. The strong band at 1727 cm^{-1} corresponds to the carbonyl stretching of carboxylic acid. The peaks at 1668 and 1540 cm^{-1}, which are also observed with polyamate, correspond to amide I band (carbonyl stretching) and amide II band (coupling of C-N stretch and N-H deformation), respectively. The bands at 1512 and 1502 cm^{-1}, which also appear in the spectra of polyimide and polyamate, are due to the phenyl groups. Assignment of the 1414 cm^{-1} peak (also observed in the polyamate) is not clear, but it seems related to the C-N stretching (imide II band) at 1381 cm^{-1}. The intensity and the shape are similar. The vibrational mode of imide II band has been assigned (16,17). The C-O-C stretching of ODA has the similar wavenumber (1248 cm^{-1}) for polyimide, polyamate and polyamic acid.

Leary and Campbell (18) have reported that both carboxylic acid and amide of PMDA-ODA polyamic acid, which is baked at 120 °C to remove the NMP solvent, react with KOH. They have observed changes of carbonyl binding energies in the XPS spectra. On the other hand, in the

present work neither the carbonyl binding energies in the XPS spectra nor the amide carbonyl stretching band in the ER IR spectra have changed, indicating that no salt of amide is present at the modified surfaces. Even if the amide of polyamic acid reacts with KOH to give amide salt, the salt may be protonated in the washing stage (refer to experiment).

Surface Modification Of PMDA-ODA With NaOH And Acetic Acid. PMDA-ODA samples were treated with a 1.25 M NaOH aqueous solution at 22 °C for 1-10 min followed by protonating with 0.1 M acetic acid. The samples were washed and dried as previously described. Water contact angles, XPS spectrum and ER IR spectrum of the modified surface are typical of a polyamic acid surface, indicating that the reaction proceeds in the same way as described above. Upon curing the polyamic acid surface, the starting polyimide surface is produced. Contact angles and XPS Cls spectrum (Figure 1d) of the re-cured surface are exactly same as those of the starting polyimide.

Measurement Of Modification Depth With ER IR And Ellipsometer. For some industrial applications such as microelectronics and photoimaging, it is useful to modify the polymer surface deep enough to achieve good adhesion while minimizing the loss of polymer and maintaining the surface topography. As shown in Figure 4, the thickness of PMDA-ODA polyimide (5 um) remains unchanged when the polyimide was treated with 1 M KOH aqueous solution at 22 °C for 10 min. The topography of the modified surface also remains unchanged within the limit of SEM sensitivity while a strong polyimide-polyimide adhesion is achieved. To observe the loss of polymer thickness within a few tens Å, a very thin layer (260 Å) of polyimide was prepared by spin-coating a dilute PMDA-ODA polyamic acid solution in NMP onto a chromium-coated Si wafer. Thickness was measured with an ellipsometer. The thickness of PMDA-ODA, which is modified and re-cured to polyimide, remains unchanged.

We are interested in measuring the modification depth for the samples treated with 1 M KOH aqueous solution at 22 °C for 10 min since surface topography and film thickness remain unchanged under these reaction conditions. The modified layer is thicker than the XPS sampling depth (approximately 100 Å) since the XPS spectrum only displays the peaks due to the product. The RBS spectrum does not give a peak corresponding to potassium, so the modified layer is probably thinner than the limit of RBS sensitivity (approximately 300 Å). These results indicate that the modification depth is in the range of 100-300 Å which is an inaccessible zone for thickness measurement with usual techniques.

McCarthy and co-workers (19) have modified poly(chlorotrifluoroethylene) (PCTFE) and could estimate the modification depth using XPS and UV-Visible. First PCTFE is modified within the XPS sampling depth
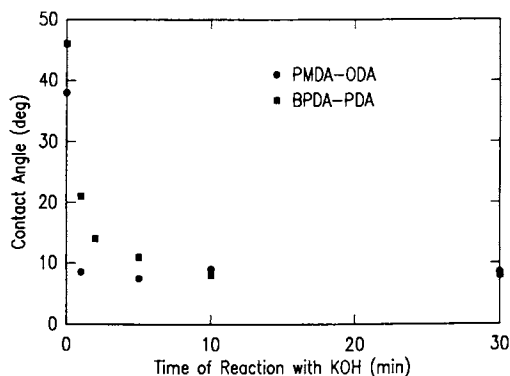
Figure 3. Receding contact angle vs. reaction time with KOH. The contact angles were measured on the samples modified with KOH at 22 °C and then treated with HCl.
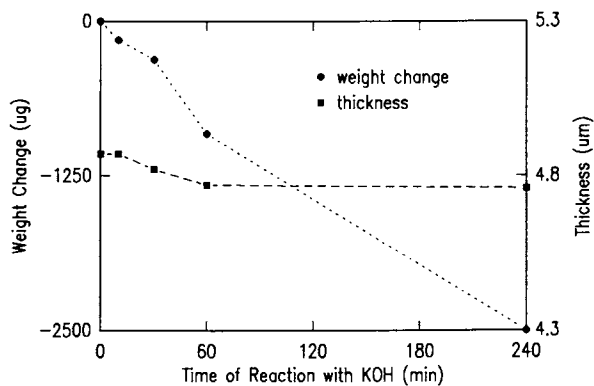
Figure 4. Variations of PMDA-ODA film weight and thickness by the reaction with KOH at 22 °C followed by acidification with HCl. The condition of the acidification reaction is not a factor.

and the modification depth is calculated by angle-resolved XPS technique. Then an UV-Visible absorbance corresponding to a modified surface with a known depth is measured. Assuming that the modification depth has a linear relationship with absorbance, they have estimated the depth by measuring an absorbance of a modified polymer. This technique can apply only to the case in which the modified surface has an isolated UV-Visible absorbance. However, the modified surface in this work does not have any isolated absorbance peak.

We have employed a method to measure the modification depth using an IR absorbance-thickness relationship established with ellipsometry and external reflectance infrared (ER IR) spectroscopy. Thin and uniform layers (100-1000 Å) of polyimide were prepared on the metal (chromium is used here to get good wettability of polyimide precursor) substrates, and then the film thicknesses and the absorbances of the imide carbonyl stretching were measured by ellipsometry and ER IR, respectively. The refractive index of PMDA-ODA employed here is 1.73. As shown in Figure 5, there is a linear relationship between the film thickness and the absorbance of carbonyl stretching at 1740 cm^{-1}. If the imide carbonyl absorbance of modified film is measured, the thickness of unmodified layer can be calculated. The depth of modification can be obtained by subtracting the thickness of remaining polyimide from the thickness of starting polymer. Figure 6 shows the ER IR spectra of the 260 Å-thick PMDA-ODA polyimides modified in an 1 M KOH aqueous solution for 0, 1 and 10 min. When the polymer reacted for 30 min, the imide carbonyl band completely disappeared (the IR spectrum is similar to one in Figure 2b). When the reaction time was 10 min, the absorbance of imide carbonyl is 0.0012 which corresponds to 30 Å in the thickness-absorbance relationship shown in Figure 5. Thus the modification depth for the 10 min reaction is approximately 230 (subtracted 30 from 260) Å. As long as an IR absorbance corresponding to a polymer can be measured, the thickness-absorbance relationship can be established using ellipsometry and ER IR. Thus the average depth of modification can be calculated by measuring the absorbances of starting polymer and modified polymer. We have not found a previous report on this method.

Polyimide-Polyimide Adhesion. To study polyimide-polyimide adhesion (10), a thin layer (200 Å) of gold was sputter-coated onto one side (20% of the total area) of the polyimide sample to initiate peel (polyimide has a poor adhesion to gold). The surface of the polyimide in the exposed area was modified to the polyamic acid surface. PMDA-ODA polyamic acid in NMP solvent was spin-coated to the surface-modified (to polyamic acid) polyimide film, and subsequently cured at 400 °C under nitrogen. Thickness of the adherate layer (peel layer) after curing is approximately 20 um and the width of the peel layers is 5 mm. The peel strengths were measured by 90° peel of the top polyimide layer. The failure occurs at the interface between
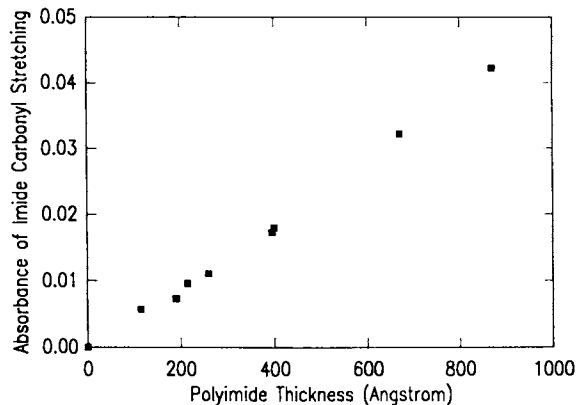
Figure 5. Relationship between PMDA-ODA polyimide thickness and imide carbonyl IR (1740 cm⁻¹) absorbance.
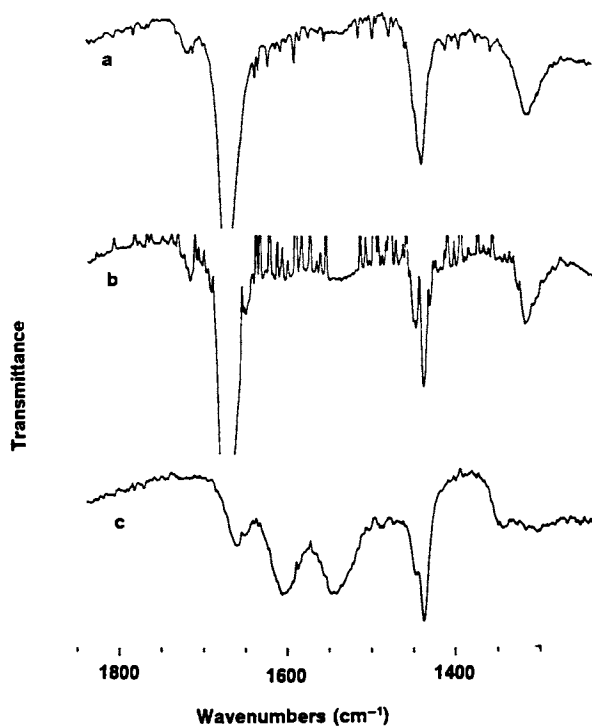
Figure 6. External reflectance IR spectra of the PMDA-ODA polyimides modified with 1 M KOH aqueous solution at 22 °C for (a) 0 min, (b) 1 min and (c) 10 min. The angle of IR incidence was 37 ° from the sample surface.

the top layer and the bottom layer (modified). It is an adhesive failure by one definition (there is no observable adherate polymer on the adherend by human eyes), but a cohesive failure by another definition (adherate polymer on the adherend is usually detected by a spectroscopic method such as XPS).

The peel strengths, which are indicative of adhesion strengths, depend on the time of reaction with KOH, but not on the acidifying condition. The peel strengths are 3, 40, 85 and 126 g/mm for control, 1, 5 and 10 min reaction with KOH, respectively. Once the outermost layer is modified to polyamic acid (1 min reaction with KOH and acidifying), the peel strength increases by more than 10 times. The deeper the modified layer is, the stronger the adhesion. These results suggest the following polymer surface structure-adhesion relationship. If the modified surface has a similar chemical structure as an incoming polymer (adherate), affinity between two phases is good and thus adhesion is strong. If the modified surface layer is amorphous like the polyamic acid layer in this work, an adherate polymer quickly diffuses into the amorphous layer (modified region) of an adherend. Subsequent curing induces interlocking of the polymer chains of adherend and adherate, and thus a strong adhesion is obtained. A possibility of transamidization between two polyamic acids (20) has been investigated, but no evidence for this chemistry has been obtained.

Surface Modification Of BPDA-PDA. Upon treatment with 1 M KOH at 50 °C, BPDA-PDA polyimide surface was converted to the corresponding potassium polyamate. Neutralization of the carboxylate surface gave polyamic acid surface which upon curing was transformed to polyimide. Neither potassium nor chlorine were detected with XPS. The evolution of the XPS C1s spectra (Figure 7) is different from that of PMDA-ODA due to the different numbers of phenyl groups in dianhydride and diamine repeat units. However, the shapes of carbonyl peaks are very similar. The spectra corresponding to polyamate (Figure 7b) and polyamic acid (Figure 8c) exhibit two carbonyl peaks since the modified surfaces have two different carbonyl groups: carboxylate and amide or carboxylic acid and amide. The ratio of two peaks is approximately 1:1.

We have studied kinetics using the contact angles of the polyamic acid surface which is formed by neutralization of the initially modified surface (potassium polyamate). The neutralizing condition is not a factor on the extent of modification. Thus upon the KOH-reaction times being changed, the contact angles of polyamic acid surfaces are measured. The water contact angles decrease relatively slowly for the KOH reaction at 22 °C. They are $\Theta a/\Theta r$ (unit: degree) = 79/46 (on polyimide), 58/21, 55/14, 55/11, 55/8, and 54/8 for control, 1, 2, 5, 10, and 30 min reaction with KOH, respectively. The receding contact angles are shown in Figure 3. It is noteworthy that the receding contact angles, which are indicative of the surface polarity, decrease more slowly than those of PMDA-ODA. Hydrolysis of
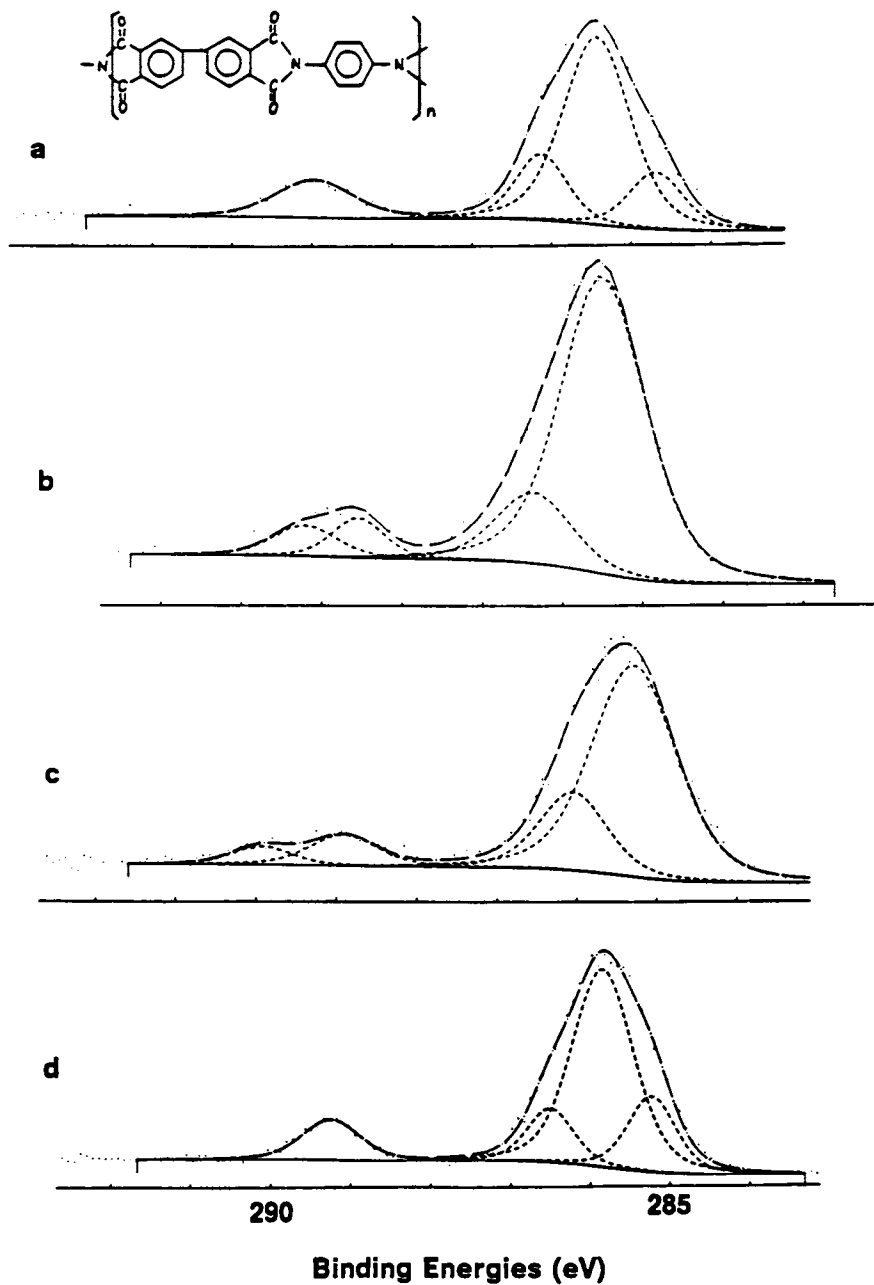
Figure 7. C1s XPS core-level spectra of (a) BPDA-PDA starting material, (b) potassium polyamate, (c) polyamic acid and (d) re-cured polyimide. The takeoff angle of electrons was 35° from the sample surface.

BPDA-PDA must be slower than that of PMDA-ODA probably due to higher ordering of BPDA-PDA and subsequently less diffusion of H_2O and KOH. If the KOH reaction temperature is raised, the reaction rate will be increased. When the modification is carried out at 50 °C, the contact angles are decreased to the lowest value ($\Theta a/\Theta r = 58°/7°$) within a minute. Film thickness and weight, as shown in Figure 8, remain essentially unchanged up to 2 h (5.12, 5.13, 5.11, 5.22, and 5.13 um for control, 10, 30, 60, and 120 min reaction, respectively).

Summary

Polyimide surface modification with KOH or NaOH aqueous solution is well defined. The reaction initially gives potassium or sodium polyamate which is then protonated with acid to yield polyamic acid. The outermost layer (5 Å) of PMDA-ODA can be completely modified within a minute of reaction in KOH solution. The depth of modification can be measured by a method using an absorbance-thickness relationship established with ellipsometry and external reflectance IR. The modification depth of PMDA-ODA treated with 1 M KOH aqueous solution at 22 °C for 10 min is approximately 230 Å. Surface topography and film thickness can be maintained while a strong
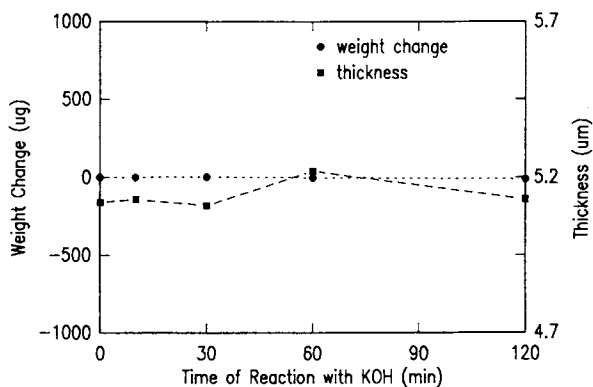
Figure 8. Variations of BPDA-PDA film weight and thickness by the reaction with KOH at 50 °C followed by acidification with HCl. The condition of the acidification reaction is not a factor.

polyimide-polyimide adhesion is achieved. The reaction of PMDA-ODA is much faster than that of BPDA-PDA. The reaction rate of BPDA-PDA is significantly enhanced by increasing the reaction temperature. Relationship between polymer surface structure and adhesion properties is understood to some extent.

Further reactions of the functional groups in the modified polyimide surface as well as adhesion experiments on BPDA-PDA are under investigation.

Acknowledgment

Literature Cited

1. (a) Clark, D.T.; Feast, W.J. Polymer Surfaces; John Wiley & Sons: NY, NY; 1978. (b) Feast, W.J.; Munro, H.S. Polymer Surfaces and Interfaces; John Wiley and Sons: NY, NY, 1987.

2. (a) Sharpe, L.H. Adhesion International 1987; Gordon and Breach: New York, 1987. (b) Wu, S Polymer Interface and Adhesion; Marcel Dekker: New York, 1982.

3. Chapman, B. Glow Discharge Processes; John Wiley & Sons: New York, 1980.

4. Whitesides and co-workers have studied surface modification of polyethylene by a wet method. Holmes-Farley, S.R.; Reamey, R.H.; McCarthy, T.J.; Deutch, J.; Whitesides, G.M. Langmuir 1985, 1, 725 and references therein.

5. McCarthy and co-workers have extensively investigated surface modification of polypropylene and fluorinated polymers. (a) Dias, A.J.; McCarthy, T.J. Macromolecules 1985, 18, 1826. (b) Costello, C.A.; McCarthy, T.J. Macromolecules 1987, 20, 2819. (c) Lee, K.-W.; McCarthy, T.J. Macromolecules 1988, 21, 309. (d) Lee, K.-W.; McCarthy, T.J. Macromolecules 1988, 21, 2318.

6. (a) Bessonov, M.I.; Koton, M.M.; Kudryavtsev, V.V.; Laius,L.A. Polyimides: Thermally Stable Polymers; Consultants Bureau: NY, NY, 1987. (b) Mittal, K.L. Ed. Polyimides; Plenum: NY, NY, 1982; vol 1 & 2.

7. A strong base attacks a cyclic imide to open the imide ring system, which is a modified "Ing-Manske" reaction. Ing, H.; Manske, R. J. Chem. Soc. 1926, 2348.

8. Nishizaki, N. "The hydrolysis of polypyromelliticimide", J. Chem. Soc. Jpn., Ind. Chem. Sec. 1966, 69, 1393.

9. (a) Kreuz et al., US Patent 4,426,253; Jan 17, 1984. (b) Lindsey, W.B. US Patent 3,361,589; Jan 2, 1968.

10. Good adhesion of metal to polyetherimide can be achieved where the polyetherimide is treated with KOH in ethanol. The depth of modification is in the um range. D. Foust presented at the International Symposium on Metallization of Polymers, Montreal, Canada, 1989.

11. McCarthy has introduced the gravimetric analysis to the surface identification. Refer to ref 5c and Bonafini, J.A.; Dias, A.J.; Guzdar, Z.A.; McCarthy, T.J. J. Polym. Sci.: Polym. Lett. Ed. 1985, 23, 33.

12. The vibrational mode perpendicular to the plane in ER IR gives stronger intensity than that parallel to the plane. (a) Allara, D. Macromolecules 1978, 11, 1215. (b) Rabolt, J.F.; Jurich, M.; Swalen, J.D. Appl. Spectrosc. 1985, 39, 269.

13. Linde, H.G.; Gleason, R.T. J. Polym. Sci.: Polymer Physics 1989, 26, 1485.

14. The polyamic acid surface has greater wettability than the polyimide surface.

15. When a liquid drop is advancing the surface while measuring the advancing contact angles, the drop stops forwarding at the valley and the hill of the rough surface giving the greater contact angle reading. As the drop passes the top of the hill, the smaller contact angle is read. (a) Wenzel, R.N. Ind. Eng. Chem. 1936, 28, 988. (b) Huh, C.; Mason, S.G. J. Colloid Interface Sci. 1977, 60, 11. (c) Busscher, H.J.; Van Pelt, A.W.J.; DeBoer, P.; DeJong, H.P.; Arends, J. Colloids and Surfaces 1984, 9, 319.

16. Ishida, H.; Wellinghoff, S.T.; Baer, E.; Koenig Macromolecules 1980, 13, 826.

17. Silverman, B.D. Macromolecules 1989, 22, 3768.

18. Laery, H.J.; Campbell, D.S. "ESCA Studies of Polyimide and Modified Polyimide Surfaces" Photon, Electron, and Ion Probes; ACS: Washington, DC, 1981.

19. Dias, A.J.; McCarthy, T.J. Macromolecules 1987, 20, 2068.

20. If the two different polyamic acid solutions were mixed and then cured, the glass transition temperatures of the cured polyimides are different from those corresponding to separately cured polyimides. These results are interpreted as transamidization which gives random co-polymer(s). C. Feger in Polymeric Materials for Electronic Packaging and Interconnections; J.H. Lupinski and R.S. Moore Eds; American Chemical Society: Washington, DC, 1989; p 114.

Chapter 14

Sensitivity of Plasma Fluorinated Polyimide and Poly(tetrafluoroethylene) to High-Energy Ion Beams During Rutherford Backscattering Spectroscopy

F. Emmi, L. J. Matienzo, D. C. VanHart, and J. J. Kaufman

Systems Technology Division, IBM Corporation, Endicott, NY 13760

Rutherford Backscattering Spectroscopy (RBS) is an
established technique for analysis of inorganic
materials. Recently, several applications of RBS on
polymer films have been reported; however, the effect
of ion beams on these surfaces has not been well
documented. RBS has been used to determine fluorine
distribution in polymers. Since ion beam irradiation
of polymers can induce chemical changes, instrumental
parameters need to be optimized to minimize damage.
    In this paper, plasma fluorinated PMDA-ODA films
and PTFE were studied to understand beam interactions
with the polymers as a function of irradiation time.
X-ray photoelectron spectroscopy (XPS), Fourier
transform infra-red spectroscopy (FTIR), scanning
electron microscopy (SEM) and RBS were used to
determine changes induced in the polymers by
irradiation.
    For PTFE, irradiation produced films which were
brittle and blistered; in contrast, the fluorinated
PMDA-ODA films only darkened and had no blisters.
Decomposition of these films resulted in defluorination
and formation of C=CF bonds. The damage to PTFE
extends to a depth approximately equal to the stopping
power of the ions in the polymer.

Polymer films are known to undergo changes under various types of
irradiation by either crosslinking or degradation reactions (1).
Studies have been performed which demonstrate how polymers are
affected by ions (2-6), electrons (7,8), x-rays (8,9), and UV light
irradiation (10-11). These interactions may produce changes in
optical (12), electrical (13), or chemical (12-14) properties of the
material.
    Polyimide films are extensively used in the microelectronic
industry as insulators for multilevel interconnect systems because of
their excellent thermal and electrical properties. In some cases,

these films can be etched, or modified by O_2-CF_4 plasmas to change
their properties. The interaction of the plasma with polyimides
results in different levels of fluorination that depend upon the gas
composition. In plasmas with high concentrations of CF_4, the
polyimide surface becomes highly fluorinated, with F/C ratios
approaching 2, similar to that for polytetrafluoroethylene (PTFE)
([15]).

An understanding of plasma etching mechanisms of polyimide in
O_2-CF_4 mixtures requires measurements of fluorine penetration.
Traditional analytical techniques, such as Ar+ ion etching performed
during SIMS or XPS analyses, can introduce erroneous results. As an
alternative, the use of Rutherford Backscattering Spectroscopy (RBS)
has been recently reported to be a viable technique to study fluorine
distribution in polyimide films ([16]). Although RBS is non-
destructive for most inorganic materials, beam interactions with
organic films occur during analysis ([3,17,18]). In order to study
metal diffusion into a fluoropolymer, or a surface-modified layer,
changes introduced by the analytical technique must be understood.
Polyimide (PMDA-ODA) exposed to ion beams in the energy region
between 1.9 and 3.6 MeV degrades by loss of carbonyl groups and the
formation of a carbon-rich surface ([3]). This degradation sequence
has also been observed for irradiation with Ar+ ions in the keV
energy range ([6,19]).

In this study, plasma fluorinated polyimide films of various
thicknesses were exposed to a 2 MeV He^{2+} ion beam at different doses
to determine beam effects. A thick PTFE film, irradiated under
similar conditions, was also examined; surface changes and fluorine
loss during RBS analysis were compared.

Experimental

Sample Preparation. PMDA-ODA polyimide films were prepared by spin
coating polyamic acid onto silicon wafers and curing to 360°C for
1 hour. The cured film thickness was approximately 10 μm. These
samples were treated downstream of an 85% CF_4-15% O_2 microwave plasma
for 30 minutes to produce a fluorinated layer, approximately 600Å
thick ([16]). Fluorinated layers less than 600Å thick were obtained by
additional treatment downstream from an O_2 rich (85%) microwave
plasma for various times. PTFE films (25 μm thick) were used as
received from E. I. duPont de Nemours Inc.

Instrumental Techniques. Ion beam irradiation of samples was
performed by focusing 2.1 MeV He^{2+} ions, using an Ionex Tandetron
accelerator, to a spot size of approximately 4 mm^2. Ion beam
currents were held constant at 10 nA. Radiation effects were
determined by varying the total charge on the sample between 0 and
20 μC. RBS spectra were collected with the samples at an angle of
45° with respect to the incident beam; additional instrumental
details can be found elsewhere ([20]). Spectral simulations were
performed using the RUMP method designed by Doolittle ([21]).

X-ray photoelectron spectroscopy (XPS) was used to analyze
polymer surfaces before and after ion beam irradiation. Data were
collected with a Surface Science SSX-100 spectrometer using Al Kα
x-rays in the high resolution mode with x-rays focused to a spot size

of 600 μm on the sample. Binding energies were referenced to the
adventitious C 1s line at 284.6 eV. SEM micrographs were obtained
with a Cambridge Instruments Stereoscan 250 Mark II electron
microscope after the sample had been coated with a 200Å layer of Pt.
Fourier transform infra-red (FTIR) spectra were collected in the
transmission mode using an IBM Instruments IR-44 spectrometer with a
spectral resolution of 4 cm^{-1}. Using a Bruker microscope attached to
the spectrometer, areas between 10 μm to 80 μm in diameter were
analyzed.

Results and Discussion

The use of helium ion beams for conventional RBS analysis allows the
detection of elements with atomic numbers greater than two; with
computer simulation, atomic ratios and distribution depths can be
calculated. Figure 1 shows RBS spectra for an untreated PTFE film
and a PMDA-ODA film after treatment in a CF_4 rich microwave plasma.
In the spectra, individual data points are represented by open
circles and the computer-simulated spectra are shown as solid lines.
For PTFE, only carbon and fluorine are observed; for the
plasma-treated polyimide film, carbon, oxygen, nitrogen and fluorine
are found. For a given set of experimental parameters, the
concentration and depth of an element in a sample determine the
spectral shape. For PTFE, fluorine is homogeneously distributed
throughout the film which results in a step-like signal. If the
fluorinated layer is thin, the fluorine signal appears as a peak, as
shown in Figure 1b.
        PMDA-ODA films, fluorinated for 30 minutes, were exposed
downstream of an O_2 rich microwave plasma for various times to reduce
the total amount of fluorine. Figure 2 compares the fluorine signal
intensities (10 μC total charge) collected after 0, 25, and 50
minutes of treatment. Using RBS, the initial fluorine thickness was
estimated to be 600Å, with a distribution profile representative of a
diffusion-controlled process (16). After treatments, the fluorine
signal intensity decreases to values below the resolution of the
instrument, thus not allowing for accurate distribution measurements.
These films were used to study changes induced by various irradiation
times.
        Fluorine losses occurring during analysis, as a function of
collected charge, were monitored by integrating fluorine counts
between channel numbers 180 and 210. Figure 3 displays the
integrated fluorine counts per 2.5 μC intervals for PTFE and the
fluorinated polyimide films. For each sample, the fluorine counts
were the highest initially, but they decreased with irradiation time,
approaching a constant value. The behavior of the fluorinated
polyimide films and PTFE were similar. Following ion irradiation,
the surfaces were studied using XPS. Analyses were performed on and
off irradiated areas; data were collected using a spot size which was
contained within the irradiated area.
        Figures 4a and 4b show the C 1s and F 1s regions, respectively,
for a polyimide film treated in a CF_4 rich plasma for 30 minutes.
The C 1s spectrum for the non-irradiated film shows an envelope
containing significant contributions from CF_x bonds in agreement with
previously reported data (15). After irradiation, a decrease in the
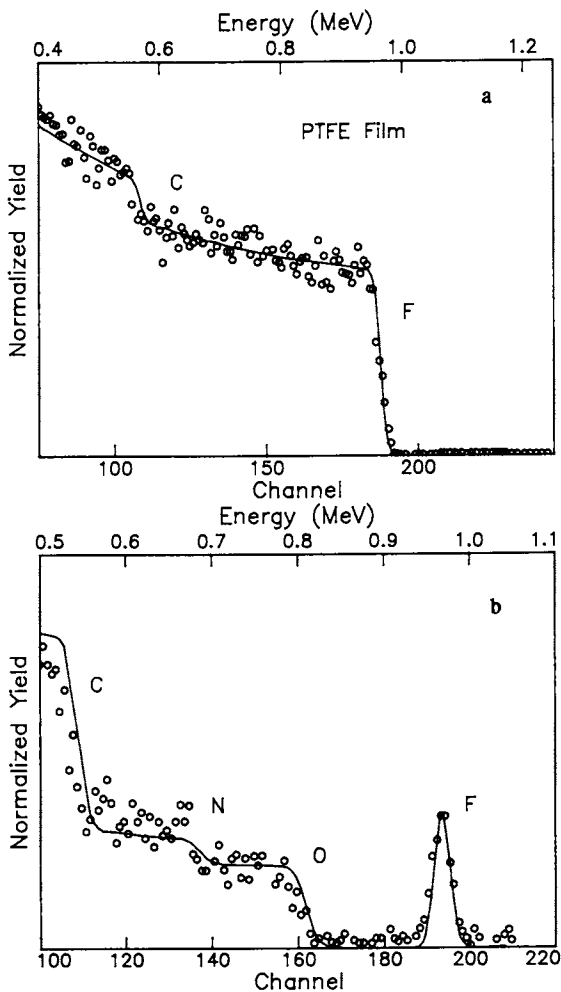
Figure 1. RBS Spectra of: (a) PTFE Film, and (b) PMDA-ODA film exposed 30 minutes to 85% CF_4/15% O_2 Plasma. Solid lines represent the simulated spectra.
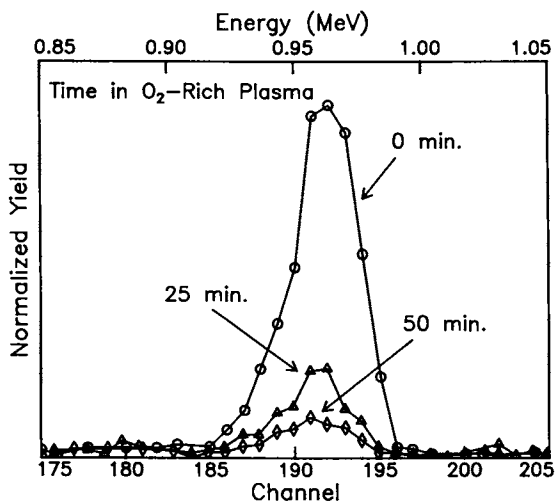
Figure 2. RBS signal intensity representative of fluorine distribution, as a function of time in O_2 rich plasma.
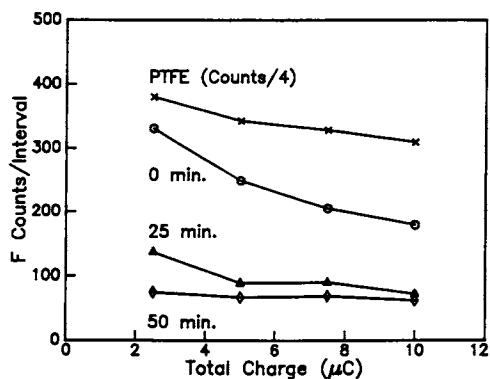
Figure 3. RBS fluorine intensity per 2.5 μC interval as a function of total charge for PTFE and fluorinated PMDA-ODA films. Given times represent exposure of films to an O_2 rich plasma.
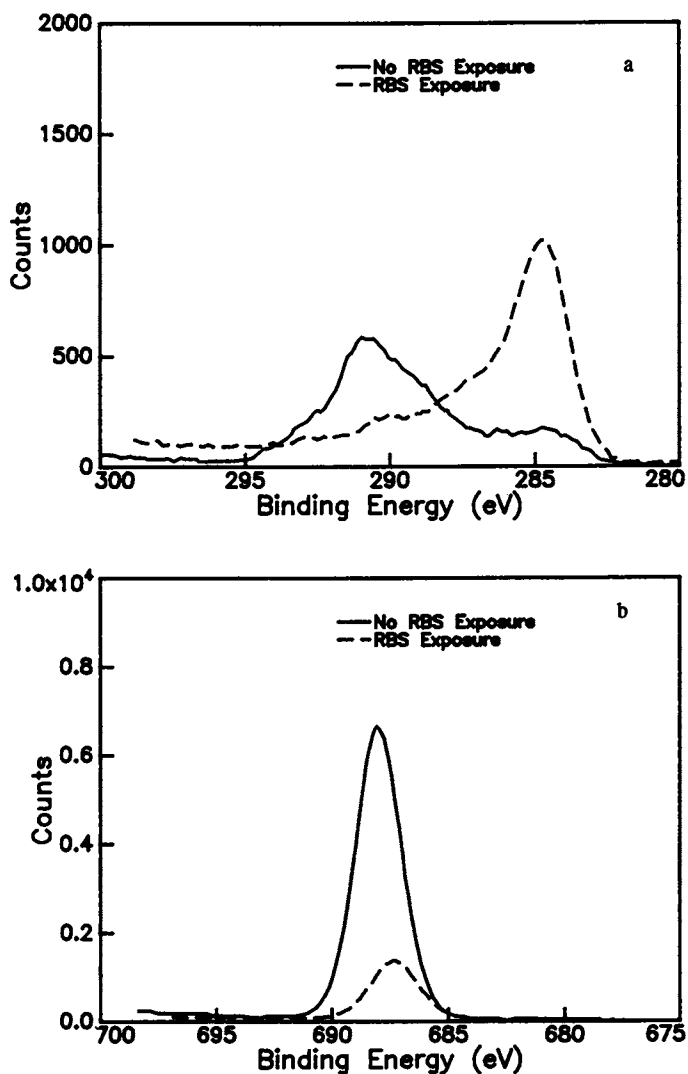
Figure 4.   (a) XPS C 1s spectra for plasma-fluorinated polyimide
before (solid line) and after (dashed line) He^2+ irradiation.
          (b) XPS F 1s spectra for plasma-fluorinated polyimide
before (solid line) and after (dashed line) He^2+ irradiation.

CF$_x$ peak intensity is observed, with a corresponding increase for carbon moeities at lower binding energies. A decrease of intensity was also observed in the F 1s spectrum following irradiation (see Figure 4b). The other plasma treated samples behaved in similar manner.

XPS results (C 1s and F 1s) obtained for PTFE are shown in Figures 5a and 5b on and off the irradiated areas. From the C 1s region, the intensity of the CF$_2$ peak was significantly reduced upon irradiation and, similar to the plasma-treated polyimide films, an increase was observed for carbon signals at lower binding energies. Fluorine loss was also detected in the F 1s spectrum, but the fluorine signal following irradiation was found to have a lower binding energy, possibly due to a change in the crosslinking density, as in the case of PVDF (22). The loss of surface fluorine due to ion irradiation, as determined using XPS, is shown in Table I; the amount of fluorine detected following irradiation was similar for all films. Additional work was performed on PTFE to gain further understanding of beam interactions with the polymer.

Table I. Atomic Concentration of F from XPS

Sample	Before RBS	After RBS[2]
0 min[1]	50	16
25 min[1]	45	17
50 min[1]	44	18
PTFE	65	15

[1]time in O$_2$-rich plasma
[2]10 μC total charge

Figure 6 shows atomic concentrations measured by XPS, on PTFE surfaces as a function of total charge during RBS analysis. With exposure time, the level of fluorine detected decreases from 65% to approximately 9%. Accompanying this loss of fluorine there is an increase in carbon levels. Oxygen is detected in all of the irradiated samples because of surface reactivity to air during transfer from the RBS chamber to the XPS instrument. The amount of oxygen increases with ion beam exposure, possibly due to a higher density of reactive surface sites.

Experiments to characterize the physical changes on irradiated areas were performed for plasma fluorinated polyimide and for PTFE samples; optical photographs of the damaged areas are shown in Figure 7. PTFE films develop blisters during He$^2+$ ion exposure, while the fluorinated polyimide samples only darken. The apparent darkening seen in the PTFE photograph results from light scattering by the blister surfaces. More detailed information on surface morphology was obtained using scanning electron microscopy (SEM).
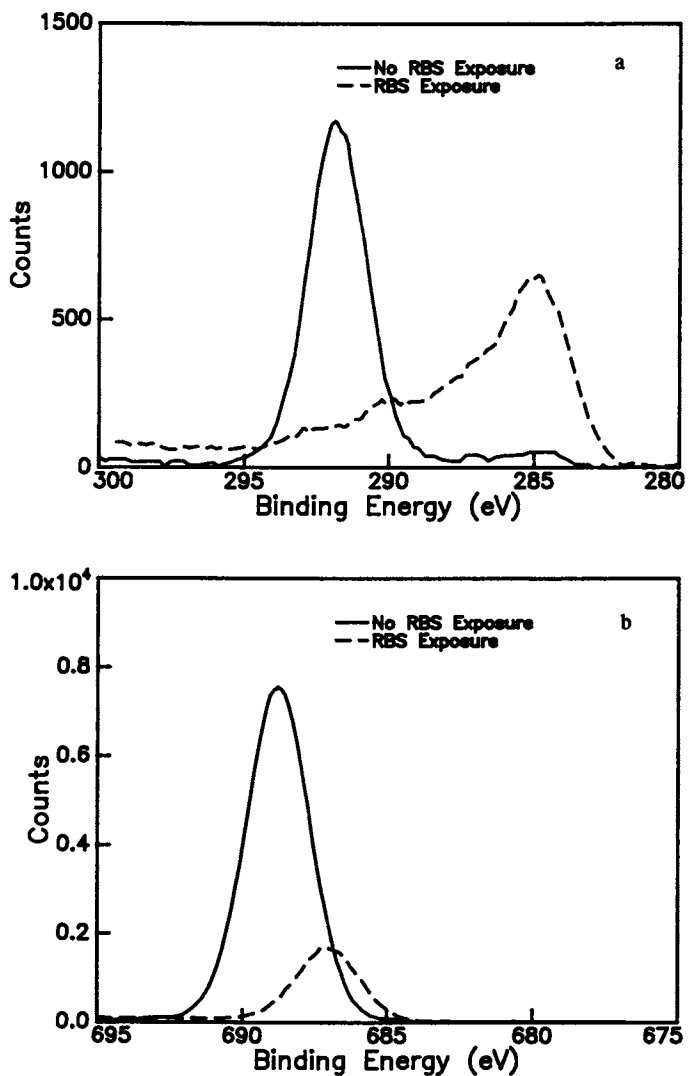
Figure 5. (a) XPS C 1s spectra for PTFE film before (solid line) and after (dashed line) He^{2+} irradiation.
         (b) XPS F 1s spectra for PTFE film before (solid line) and after (dashed line) He^{2+} irradiation.
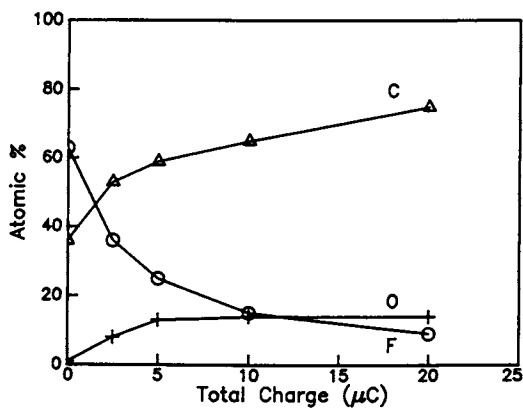
Figure 6. Atomic concentrations of PTFE surfaces (XPS) after different ion irradiation dosages (μC).
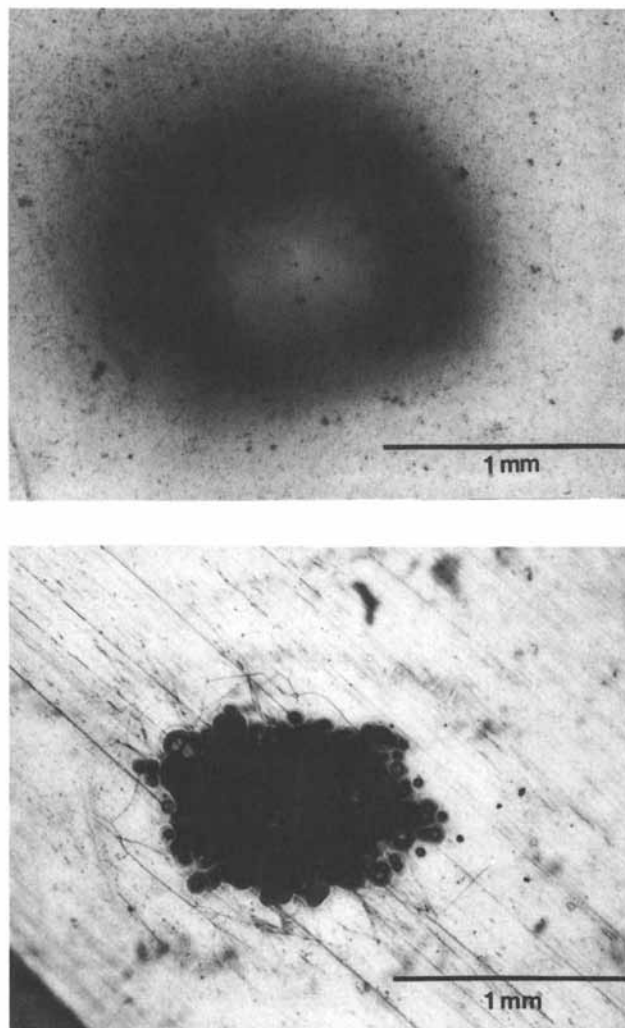
Figure 7.   Optical photographs of He^{2+} irradiated areas on plasma-fluorinated polyimide and PTFE films.

Figure 8 shows SEM images of PTFE following ion beam exposure. At
lower magnification (see Figure 8a), the appearance of the damaged
area resembles that of a brittle film. The higher magnification
photograph (see Figure 8b) shows areas which had blistered and
cracked; cracking may have occurred during sample transfer. From SEM
micrographs, the thickness of the blister wall is 6-7 μm.
Calculations, performed to estimate the depth of penetration of a
2.1 MeV He^{2+} ion beam at 45°, into PTFE, yielded a stopping power of
6 μm. The method used to determine the stopping power of the polymer
is described elsewhere (23). The calculated stopping power and the
measured depth of damage are approximately the same. The blisters
result from the evolution of volatile products during irradiation.
Volatile products, during exposure to x-ray or ion beams, have been
detected by mass spectrometry (9,24).

FTIR spectra were obtained from four areas of an irradiated
sample, as indicated in Figure 9. Peaks were only observed in the
region between 2000 and 800 cm^{-1}. Spectra 1 through 4 were collected
as follows: (1) outside the irradiated area, (2) through an intact
blister, (3) only through the bottom of the film after the top
portion of the blister had been removed, and (4) through the top
portion of the blister only.

The characteristic spectrum of a thick PTFE film (region 1)
shows an intense signal assigned to CF_2 stretching vibrations ca.,
1200 cm^{-1}. Changes observed in an irradiated area (region 2) include
broadening of the CF_2 stretching frequency region and the appearance
of a band at approximately 1720 cm^{-1}. This spectrum is a summation
of both the altered region and the bulk PTFE. The changes observed
in spectrum 2 are primarily from contributions of the altered layer
(region 4). The extent of damage appears to be confined within the
stopping power of the helium ions.

Information on the chemical changes, resulting from ion beam
irradiation, can be identified from spectrum 4. The broad signal at
about 1720 cm^{-1} is attributed to C=O and to C=CF type bonds (25).
C=O bonds likely develop by reaction of the exposed surface to air
during sample transfer from the irradiation chamber; C=CF bonds
develop during irradiation. In addition, the CF_2 vibration at around
1200 cm^{-1} broadens towards lower wavenumbers, indicative of
defluorination (26).

Conclusions

Ion irradiation of PTFE and plasma-fluorinated PMDA-ODA has been
performed under typical conditions of RBS analysis. Loss of fluorine
is observed on all films, especially at the start of irradiation.
Decomposition is introduced by the beam interaction with the polymer;
defluorination and formation of carbon-carbon double bonds are
detected by XPS and FTIR. For PTFE, irradiation produced films which
were brittle and blistered. The calculated stopping power for He^{2+}
ions and the experimentally measured depth of damage are
approximately the same.
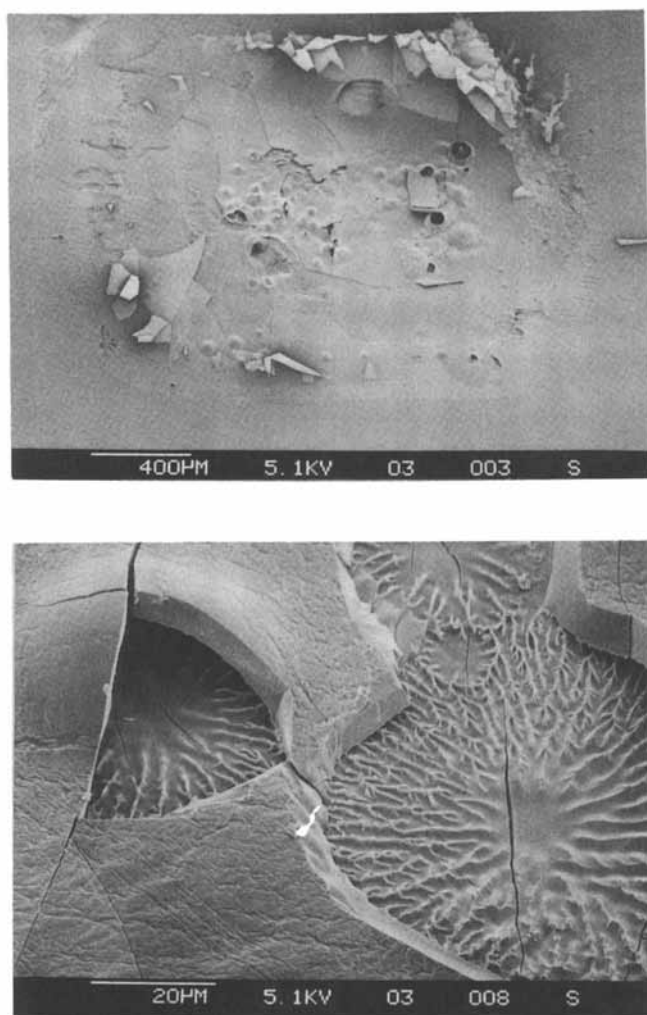
Figure 8. SEM micrographs of PTFE exposed to He^{2+} ions.
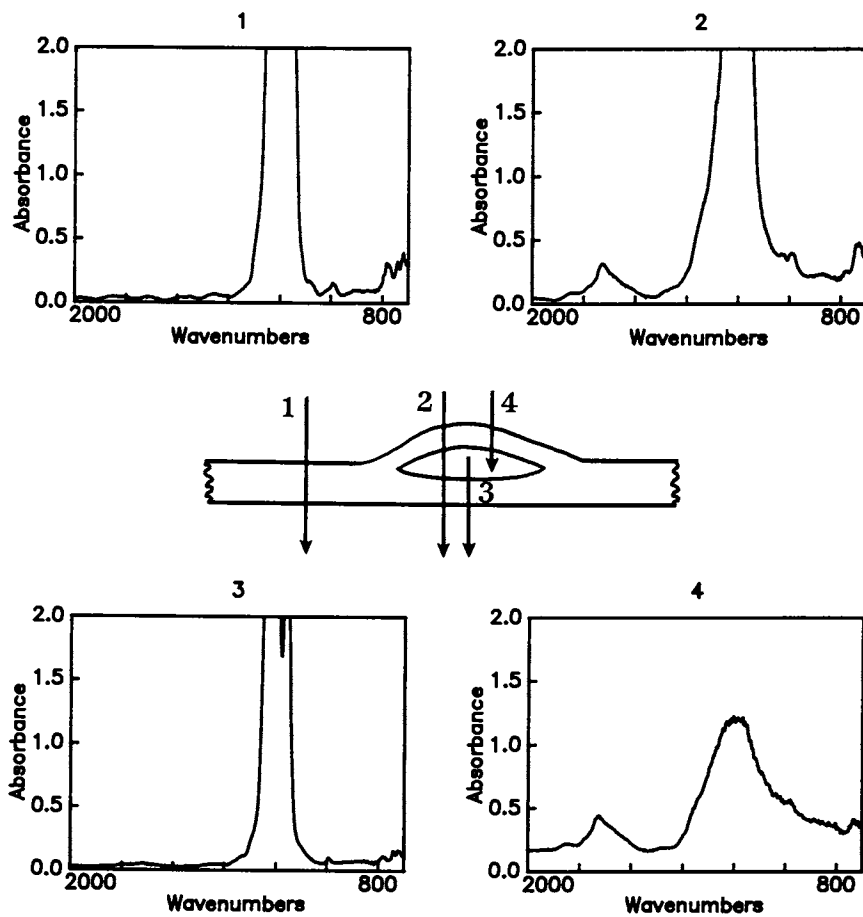
Figure 9.   Comparison of FTIR spectra obtained from different areas on PTFE film after irradiation.

Literature Cited

1. M. C. Wintersgill, Nucl. Instrum. Methods Phys. Res. B 1, 595 (1984).
2. T. Venkatesan, Nucl. Instrum. Methods Phys. Res. B 7/8, 461 (1985).
3. L. J. Matienzo, F. Emmi, D. C. VanHart, and T. P. Gall, J. Vac. Sci. Technol. A 7(3), 1784 (1989).
4. H. Ryssel, K. Haberger, and H. Kranz, J. Vac. Sci, Technol., 19(4), 1356 (1981).
5. E. H. Adem, S. J. Bean, C. M. Demanet, A. Le Moel, and J. P. Durand, Nucl. Instrum. Methods, Phys. Res. B32, 182 (1988).
6. B. J. Bachman and M. J. Vasile, J. Vac. Sci. Technol., A7, 2709 (1989).
7. D. T. Clark and W. J. Brennan, J. Electron Spec. Rel. Phenom., 41, 399 (1986).
8. H. Bolouri, J. M. R. MacAllister, R. A. Pethrick, and S. Affrossman, Appl. Surf. Sci., 24, 18 (1986).
9. D. R. Wheeler and S. V. Pepper, J. Vac. Sci., Technol., 20(2), 226 (1982).
10. Y. Momose, K. Ikawa, T. Sato, and S. Okazaki, Appl. Polym. Sci., 33, 2715 (1987).
11. F. D. Egitto and L. J. Matienzo, Polym. Degrad. Stab., in press.
12. T. Venkatesan, W. L. Brown, B. J. Wilkens, and C. T. Riemann, Nucl. Instrum. Methods Phys. Res. B 1, 605 (1984).
13. T. Hioki, S. Noda, M. Sugiura, M. Kateno, K. Yamada, and J. Kawamoto, Appl. Phys. Lett. 43, 30 (1983).
14. M. P. Zussman, S. Wood, L. C. Scala, J. Bartko, and A. Vincenz, J. Appl. Polym. Sci. 35, 2183 (1988).
15. F. D. Egitto, F. Emmi, R. S. Horwath, and V. Vukanovic, J. Vac. Sci. Technol. B3, 893 (1985).
16. L. J. Matienzo, F. Emmi, F. D. Egitto, D. C. VanHart, V. Vukanovic, and G. A. Takacs, J. Vac. Sci. Technol. A 6(3), 950 (1988).
17. F. Namavar and J. I. Budnick, Nucl. Instrum. Methods Phys. Res. B 15, 285 (1986).
18. S. J. Valenty, J. J. Chera, G. A. Smith, and W. Katz, J. Polym. Sci. Polym. Chem. Ed. 22, 3367 (1984).
19. D. Karpuzov, K. L. Kostov, E. Venkova, P. Kirova, I. Katardjiev, and G. Carter, Nucl. Instrum. Methods Phys. Res. B 39, 787 (1989).
20. P. J. Mills, C. P. Palmström, and E. J. Kramer, J. Mater. Sci. 21, 1491 (1986).
21. L. Doolittle, Nucl. Instrum. Methods B9, 344 (1985).
22. A. Fina, A. Le Moel, J. P. Durand, M. T. Valin, C. Le Gressus, E. Balanzat, J. M. Ramillon, and C. Darnez, Nucl. Instrum. Methods Phys. Res. B 42, 69 (1989).
23. L. C. Feldman and J. W. Mayer, in Fundamentals of Surface and Thin Film Analysis, Elsevier, New York, 1986.
24. L. Torrisi, L. Calcagno, and A. M. Foti, Nucl. Instrum. Methods, B32, 142 (1988).
25. R. Chaney and G. Barth, Fresenius Z. Anal. Chem., 329, 143 (1987).
26. L. J. Bellamy, The Infra-Red Spectra of Complex Molecules, Vol. 1, p. 369, Chapman and Hall, London, 1975.

Chapter 15

Surface Analysis of Polymers by Ionic Spectrometries

X-ray Photoelectron Spectroscopic Evaluation of Ion Bombardment Damages

Y. De Puydt, D. Leonard, and P. Bertrand

Université Catholique de Louvain, PCPM, 1 Place Croix du Sud, B–1348 Louvain La Neuve, Belgium

Polymethyl-methacrylate (PMMA) and Polyethylene terephthalate (PET) samples have been analyzed by two different ionic surface spectrometries: namely, ISS using 2 keV He ions and static SIMS using 4 kev Xe ions. The same techniques combined with XPS have been used in order to determine the ion doses leading to the lowest ion induced damages together with acceptable signal/noise ratios. It is shown that both the mass of the ion used for the analysis and the nature of the investigated polymer must be considered for the study of the ion induced damages.

Surface analyses of polymers have found an increased interest some years ago, with respect to important technological developments such as composite materials, adhesives, biocompatible materials, electronic materials... Moreover, various surface treatments have been applied to polymers in order to modify their physico-chemical properties such as adhesion, biocompatibility, dry etch resistance, electrical conductivity. In this way, the surface characterization of polymers using ionic spectrometries have retained our particular attention. Indeed, both ISS and SIMS have been demonstrated to be useful as analytical tools to solve applied problems related to the extreme surface (< 10Å) of polymers (1-4). However, the great sensitivity of polymers to ion induced damages (compared to inorganic materials) (5-7), has led to the use of so called 'static' analysis conditions. This means that the ion doses needed for the acquisition of ISS or SIMS spectra must be significantly lower than the dose required to cause damage to the polymer sample surface. In the present study, Polymethyl-methacrylate (PMMA) and Polyethylene terephthalate (PET) have been chosen for this purpose. Indeed, these two polymers have elemental composition very close to each other: $C_5H_8O_2$ for PMMA and $C_{10}H_8O_4$ for PET. This means for example that they have the same O/C stoichiometric ratio. Moreover, the carbonyl groups are found in the same amount relative to C-C and C-H bonds in the two polymers: the distinction between PMMA and PET is not obvious with a low resolution XPSpectrometer. Indeed, only the lower width of the neutral component (C-C / C-H) of the C_{1s} peak, as well as the presence of the shake-up component from the benzenic ring in PET, permit the distinction between PET and PMMA to be made from their XPS spectra. In an attempt to determine standard 'static' conditions for ISS and SIMS analyses of

polymer systems and to interpretate the corresponding ISS and SIMS results, the nature of the investigated polymers (PMMA and PET) as well as the mass, energy and dose of the ions used for the analysis (He and Xe) are considered.

<u>Experimental</u>

<u>Samples.</u> Polyethylene terephthalate (PET) samples are industrial (Mylar) biaxially oriented films (10 μm thick). Polymethyl-methacrylate (PMMA) has been spin coated on microscope glasses from a PMMA (1) / CH_2Cl_2 (9) solution, giving thin layers of a few hundred Å thickness.

Samples of about 1 cm^2 are fixed with double sided scotch tape on the sample holder (i.e. electrically insulated from the mass of the spectrometer); they are introduced without any cleaning procedure in the UHV analysis (ISS/SIMS) chamber where they are ion bombarded.

XPS and ISS analyses performed on all these samples, do not evidence any contaminant; only traces of alkaline contaminants (Na, K) are revealed by SIMS.

<u>Ion Bombardment Conditions.</u> A base pressure of 10^{-9} Torr is maintained in this chamber; the noble gas pressure (He, Xe) rises to about 10^{-7} Torr during the ion bombardment. The ion beam is rastered on (1.5 x 1.5) mm^2 areas at normal incidence: ^{4}He-2 keV ions are used for the ISS analysis when Xe-4 keV ions are used for SIMS. The incident ion current is measured with the aid of a moveable Faraday cup. Since the investigated samples are electrical insulators, charge neutralization is performed with low energy electrons (~ 10 eV) emitted from a heated W filament.

The ion doses for which the ion induced damages have been investigated by XPS are reported in Table I (the ion bombarded samples are exposed to air during the transfer to the XPS spectrometer).

Table I. He and Xe ion doses used for the XPS investigation
of ion induced damages

^{4}He-2keV (ions.cm^{-2})	Xe-4keV (ions.cm^{-2})
1.0 x 10^{14}	6.7 x 10^{13}
4.8 x 10^{14}	6.4 x 10^{14}
9.7 x 10^{14}	6.4 x 10^{15}
4.8 x 10^{15}	

<u>Analysis Conditions.</u> For the ISS analyses, the ion beam incidence is normal to the sample surface and the scattered ions are energy analyzed with a CMA in a full annular ring at 138° with respect to the incident beam direction. For the SIMS analyses, the sample is tilted until the ion beam incidence reaches 75° with respect to the surface normal. The secondary ions are first energy filtered before being mass discriminated in the quadrupole mass spectrometer. More details about both ISS and SIMS analyses are given in Table II.

The SIMS spectra are all obtained in the same way: a molecular peak (high mass > 100 amu peaks were preferred) characteristic of the investigated polymer sample is selected and the signal intensity is optimized by adjusting the first lens (extraction) potential. The time required for this procedure and the acquisition of one spectrum (160-10 amu) corresponds to a total ion dose less than 2.10^{13} ions/cm^2. The relative peak intensities for the same polymer are perfectly reproducible from one analysis to another, indicating that a good control of the

surface potential is obtained. It has also been verified that no signal from ionized residual gasses or from electron stimulated desorbed species is detected.

XPS analyses are performed on a Surface Science SSX-100 Model 206 photoelectron spectrometer. The analysis pressure is in the range of 1 to 5.10^{-9} Torr. Monochromated X-rays from an aluminium anode (hv = 1486.6 eV) powered at 10 keV and 5 nA, are focused on an area of 0.123 mm^2 centered on the previously ion bombarded areas. The photoelectrons are detected at an escape angle of 65° with respect to the sample normal. Charge compensation is performed with an electron flood gun (E_{e-} = 6 eV) together with a Nickel grid placed at about 1 mm above the samples. For all samples, low resolution (150 eV pass energy) spectra from 0-1000 eV are taken in order to verify the absence of contamination; furthermore, higher resolution (50 eV pass energy) spectra of 20 eV width and centered around the C_{1s} and O_{1s} lines are also accumulated. Under these conditions, the full width at half maximum of the $Au_{4f7/2}$ line is 0.9 eV. Binding energies are calculated with respect to the neutral component (C-C / C-H) of the C_{1s} line set at 284.6 eV.

Table II. Experimental details on the ionic spectrometers

	ISS	SIMS
Spectrometer	Kratos WG-541	Riber Q-156
Primary ion beam		
gas	$^4He^+$	Xe^+
energy	2 keV	4 keV
Sample current	10 nA	10 nA
Ion beam rastered area	1.5x1.5 mm^2	33 mm^2
Filament current for charge neutralization	2 A	2 A
scan region	0.2 to 0.6 E/E_o	160-10 amu
scan time	400 sec	102 sec

Results and Discussion

ISS Analyses. Figure 1 shows an ISS spectrum in the 0 to 0.6 E/E_o range obtained on PMMA with an ion dose of 10^{15} ions/cm^2. Besides a very intense peak at the low energy part of the spectrum, weak single scattering peaks are seen at the E/E_o energy ratios predicted by the binary elastic collision model: 0.29 for carbon and 0.41 for oxygen. The low energy peak has been observed for all the polymers investigated in our laboratory (PP, PMMA, PET and PTFE); its shape and intensity do not depend on the polymer nature. It is thought to be related to positive atomic and molecular sputtered ions: its energy distribution is indeed in good agreement with previous data obtained from organic materials (8). Moreover, its position depends on the sample surface potential.

The single scattering peaks are superimposed on the tail of this low energy peak and their intensities are very weak. As expected, an increase of the ion dose used for the ISS spectra accumulation improves the signal/noise ratio for the
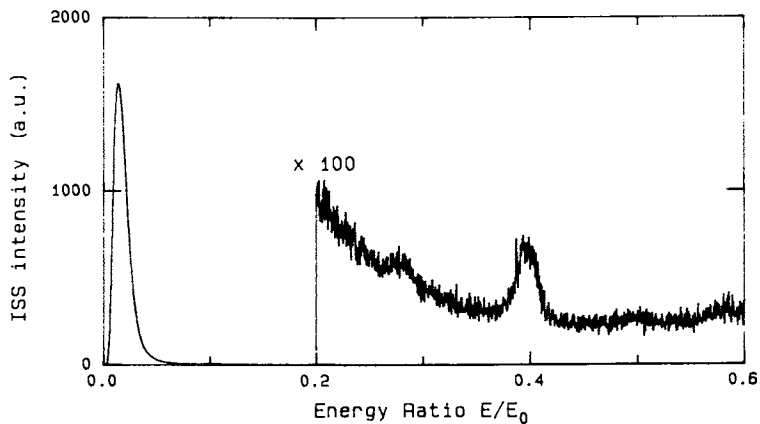
Figure 1. ISS spectrum of PMMA acquired with 10^{15} ^{4}He$^+$/cm^2 in the range of 0 to 0.6 E/E$_0$.

scattering peaks. The carbon signal appears to be very weak, proportional to the ion dose and quite independent on the nature of the polymer: indeed, the intensity variations of the carbon signal observed for the different polymers investigated are not significant. In contrast, the oxygen signal does not show the same behavior. First, the intensity of the oxygen signal is higher than the carbon one; then, it depends on both the polymer nature and the ion dose (Figure 2). The oxygen intensities measured for PMMA and PET with different He doses are reported in Table III together with the O/C ratios from the ISS and XPS analyses.

Table III. ISS and XPS data from PMMA and PET

^{4}He doses (ions/cm^2)	PMMA			PET		
	O_{ISS} *	O/C_{ISS}	O/C_{XPS}	O_{ISS} *	O/C_{ISS}	O/C_{XPS}
virgin			0.93			0.84
1×10^{14}	38	**	0.90	46	**	0.84
5×10^{14}	34	6.5	0.67	56	14.7	0.81
1×10^{15}	25	4.6	0.59	52	11.8	0.82
5×10^{15}	18	3.5	0.54	49	9.4	0.58

* *ISS intensities are reported to the ion doses used for the spectra accumulation ($\times 10^{12}$)*
** *no significant carbon signal has been observed for this dose*

The low carbon sensitivity of ISS on polymers has already been reported in the literature and has been attributed to the elastic shadowing of the carbon atoms by the heteroatoms (hydrogen, oxygen) present in the analyzed polymer (9). It appears therefore that these heteroatoms are on the topmost monolayer and that they prevent the direct scattering of the helium ions by the carbon atoms. This is fully consistent with the outermost surface layer sensitivity of the ISS technique. Moreover, this allows us to explain the low carbon intensity and the associated values of the O/C ratios measured by ISS (Table III) which are unexpectedly high by comparison with the bulk stoechiometric ratios which are 0.4 for both PMMA ($C_5H_8O_2$) and PET ($C_{10}H_8O_4$). Note that the difference in scattering cross section between carbon and oxygen, corrects the ISS O/C ratios by a factor less than 2 (not taken into account in Table III).

On the other hand, the ion dose dependance of the oxygen signal is indicative of some surface modifications occuring during the ion bombardment i.e. during the ISS analysis. These ion induced modifications are clearly illustrated by the XPS analyses performed on the ion bombarded samples: Figure 3 shows the evolution of the C_{1s} peak of PMMA and PET as a function of the He ion dose. For a He dose as low as 10^{14} ions/cm^2, XPS shows no significant change of the O/C atomic ratios but a broadening of the different peak components and, in the case of PET, a decrease of the aromatic shake-up from the benzenic ring are already observable. For higher He doses, a decrease of the oxygen containing functional groups is noted on the C_{1s} peak for both PMMA and PET.

The influence of the polymer nature is illustrated by the different degradation kinetics noted for PMMA and PET (see Table III and Figure 3): these may be explained considering the difference in ion sensitivity of the two polymers. Indeed, PMMA has been reported to be highly ion sensitive (5), when polymers containing aromatic moieties, such as PET, are known to be more ion resistant (6,10). Moreover, the oxygen containing group in PMMA is a pendant group which will be more easily sputtered than the carbonyl groups implied in the ester bonds in PET.
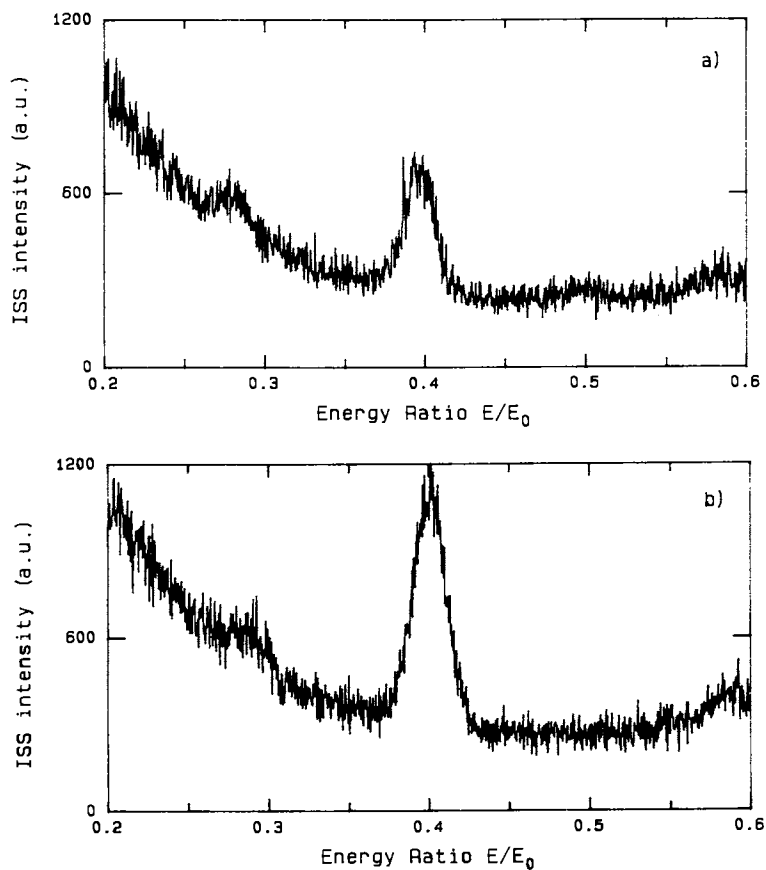
Figure 2. ISS spectra acquired with 10^{15} $^4He^+/cm^2$ in the range of 0.2 to 0.6 E/E_0 : (a) PMMA and (b) PET
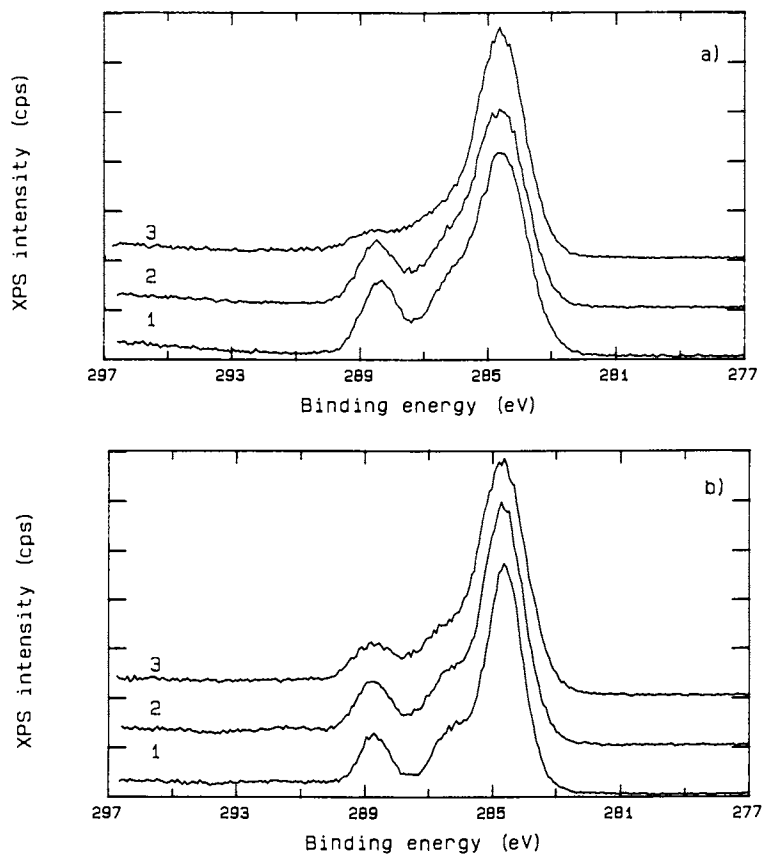
Figure 3. XPS spectra of (a) PMMA and (b) PET ; **1** = virgin, **2** = 10^{14} and **3** = 10^{15} ^{4}He$^+$/cm^2 bombarded

Static SIMS Analyses. Static SIMS spectra of PMMA and PET obtained with 2.10^{13} Xe^+/cm^2 are presented in Figure 4. They are totally comparable with already published spectra of the same polymers (3, 4, 8, 11). Figure 4 illustrates the greater molecular specificity of static SIMS compared to XPS.

Figure 5 shows the evolution as a function of the Xe ion dose, of the intensity ratios of peaks characteristic of PMMA (at 41 and 59 amu) and of PET (at 55 and 104 amu), as well as of ion induced degradation (at 91 amu): the maximum ion dose in Figure 5 corresponds to approximately the dose needed for the acquisition of one static SIMS spectrum under our experimental conditions. This indicates that the level of ion induced damages during the SIMS analyses remains acceptable as detected by the SIMS technique itself; note that XPS does not show any degradation features for such low Xe doses (see below). Moreover, Figure 6 shows that in the case of Xe bombardment the degradation proceeds faster for PET than for PMMA: the decrease in intensity of the characteristic peaks is more marked for PET.

For higher ion doses, the ion induced damages appear still clearly from the SIMS spectra of preirradiated samples with 6.10^{13} Xe^+/cm^2 (Figure 7): for PET, the characteristic peaks (at masses 104 and 149) have totally disappeared when for PMMA, they are still observed (at masses 59 and 69). Moreover, after Xe preirradiation of both PMMA and PET, peaks characteristic of ion induced degradation are observed at the masses 77, 91, 105, 115, 128, 141,... which correspond to the stabilized forms of unsaturated fragments (aromatics) resulting from the ion bombardment (11). Unsaturation induced by the ion bombardment is also observable from a shift in the relative intensities towards the low masses peaks within the C_x clusters: for example, the 27/29 ratio increases in the C_2 cluster (compare Figure 4 to Figure 7). Since no unsaturated or aromatic species are initially present in the PMMA backbone, these features are less marked for that polymer.

Finally, difference of ion induced degradation between PMMA and PET is also seen from the different evolution of the overall secondary ion yield with the preirradiation dose. Chain scission has been reported to be induced for PMMA (12) when crosslinking proceeds during the ion irradiation of PET (13). Moreover, reference to crosslinking has already been used to explain the decrease of secondary ion yield after ion bombardment (7): this may explain the greater decrease of the secondary ions intensity observed for PET, compared to PMMA.

The use of XPS to estimate the ion damages during the static SIMS analysis has appeared to be less interesting than in the case of ISS: the XPS sensitivity to the outermost surface is too low in order to detect the damages induced by the extremely low ion doses used for the static SIMS spectra acquisition. However, the static SIMS technique itself permits a direct evaluation of the ion induced damages (see above). For higher ion doses ($>10^{14}$ Xe^+/cm^2), the ion induced degradation is very similar for the He and Xe bombardment: the O/C decay observed for PMMA and PET is however more rapid in the case of the Xe bombardment. This may be explained by the difference between the XPS information depth and the range of Xe-4 keV ($\pm$ 100 Å) and He-2 keV ($\pm$ 300 Å) ions (14): the volume analyzed by XPS corresponds more to the volume disturbed by the Xe ions.

Conclusions

The PMMA and PET data show clearly the limitations of the ISS technique in providing the intrinsic composition of the outermost surface of polymers: no static conditions for ISS analysis on polymers has been achieved with acceptable signal/noise ratio. Nevertheless, it has been shown elsewhere (15,16) that ISS, used with other complementary surface techniques, may be helpful for solving practical problems related to the polymers surface. Static SIMS has been shown to be more suitable than ISS for the surface analysis of polymers. ISS and SSIMS
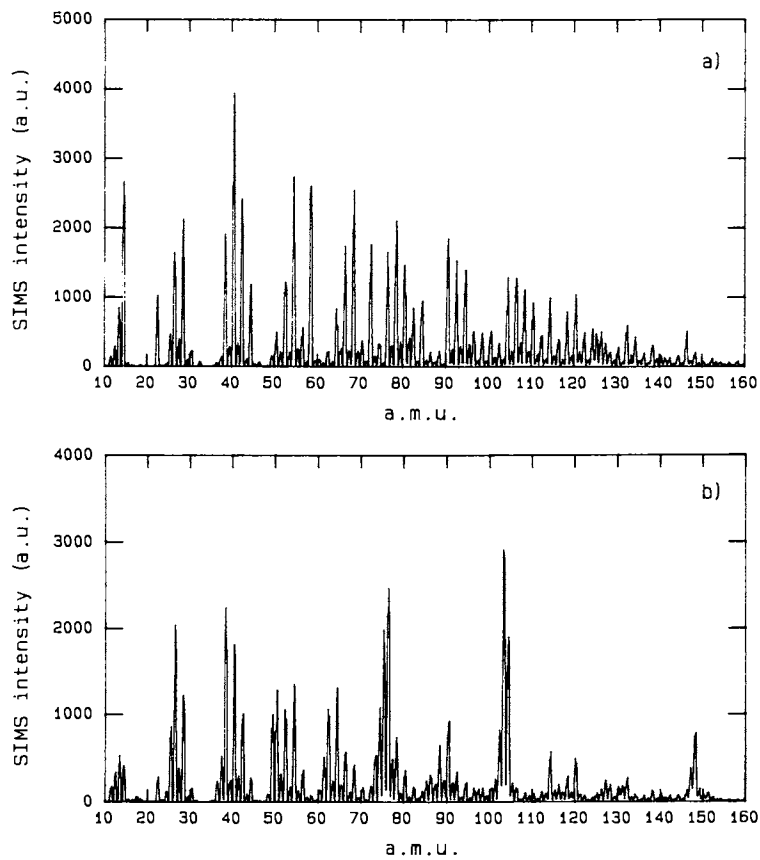
Figure 4. Static SIMS spectra acquired with less than 2.10^{13} Xe^+/cm^2 : (a) PMMA and (b) PET
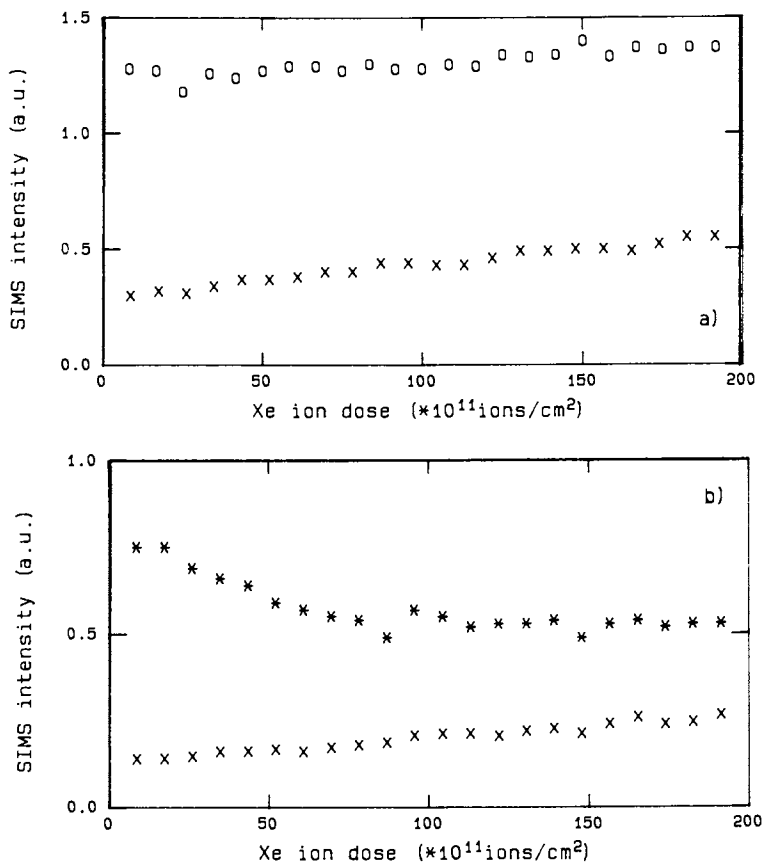
Figure 5. Evolution of the relative SIMS intensity ratios of peaks characteristic of (a) PMMA : o = 41/59, x = 91/59 and (b) PET : * = 55/104, x = 91/104
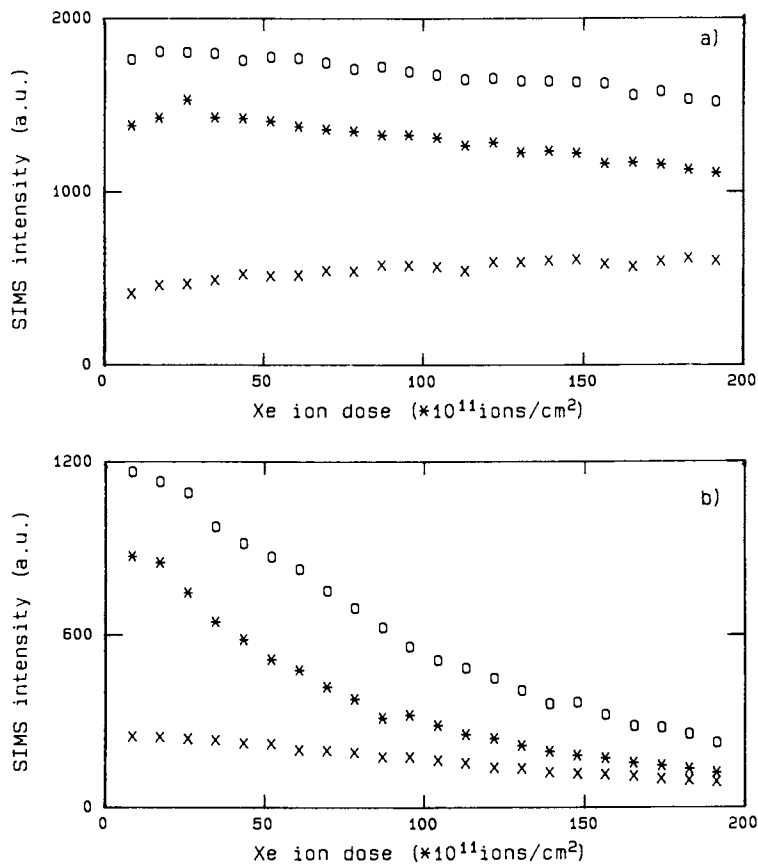
Figure 6. Evolution of the absolute SIMS intensities of peaks characteristic of (a) PMMA : o = 41, ∗ = 59, x = 91 and (b) PET : o = 104, ∗ = 55 and x = 91
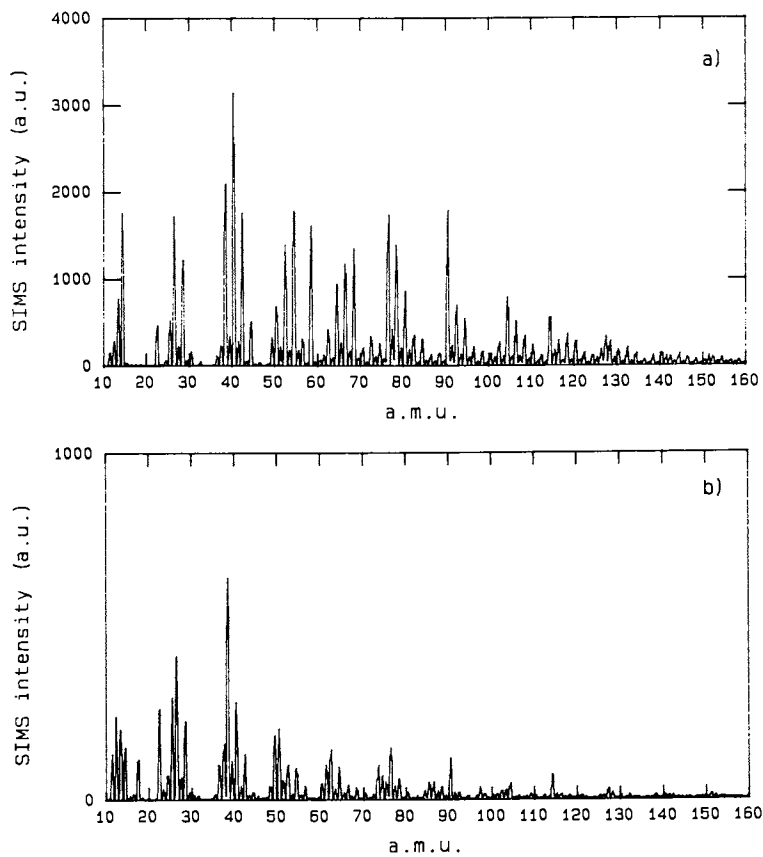
Figure 7. Static SIMS spectra of preirradiated (6.10^{13} Xe^+/cm^2) : (a) PMMA and (b) PET

have been used together with XPS as analytical tools for the study of the ion induced damages: differences in ion sensitivity between PMMA and PET have been outlined and explained considering the different chemical natures of these two polymers. ISS has shown that the He bombardment induces a preferential loss of the oxygen containing groups of PMMA by comparison to PET; SSIMS results have suggested that the Xe bombardment causes unsaturation less pronounced on PMMA than on PET. These results point out that both the nature of the investigated polymer and that of the ion used for the surface analyses must therefore be considered for the evaluation of ion induced damages.

Literature Cited

1.   Baun, W. L. Pure Appl. Chem. 1982, 54, 323.
2.   Gardella, J. A. Appl. Surf. Sci. 1988, 31, 72.
3.   Briggs, D. Surf. Interf. Anal. 1986, 9, 391.
4.   Briggs, D. British Polymer Journal 1989, 21, 3.
5.   Storp, S.; Holm, R. J. Electron. Spectrosc. Relat. Phenom. 1979, 16, 183.
6.   Ullevig, D. M.; Evans, J. F. Anal. Chem. 1980, 52, 1467.
7.   Briggs, D.; Hearn, M. J. Vacuum 1986, 36, 1005.
8.   Brown, A.; Vickerman, J. C. Surf. Interf. Anal. 1986, 8, 75.
9.   Hook, T. J.; Schmitt, R. L.; Gardella, J. A.; Salvati, L.; Chin, R. L.
     Anal. Chem. 1986, 58, 1285.
10. Charlesby, A. In Atomic radiation and polymers; Pergamon : N. Y. ,1960.
11. van Ooij, W. J.; Brinkhuis, R. H. G. Surf. Interf. Anal. 1988, 11, 430.
12. Venkatesan, T.; Calcagno, L.; Elman, B. S.; Foti G.
     In Ion beam modification of insulators; Mazzoldi, P. and Arnold, G. W.,
     Eds.; Elsevier: Amsterdam, 1987; p 322.
13. Reich, L.; Stivala, S. In Elements of polymers degradation;
     Mc Graw Hill Book Company: New York, 1971; p 38.
14. Biersack, J. P. In Ion beam modification of insulators;
     Mazzoldi, P. and Arnold, G. W., Eds.; Elsevier: Amsterdam, 1987; p 648.
15. De Puydt, Y.; Bertrand, P.; Lutgen, P. Surf. Interf. Anal. 1988, 12, 486.
16. De Puydt, Y.; Bertrand, P.; Novis, Y.; Caudano, R.; Feyder, G.; Lutgen, P.
     British Polymer Journal 1989, 21, 141.

Chapter 16

Thermal Stability of Electron-Irradiated Poly(tetrafluoroethylene)

X-ray Photoelectron and Mass Spectroscopic Study

Donald R. Wheeler and Stephen V. Pepper

Lewis Research Center, National Aeronautics and Space Administration, Cleveland, OH 44135

Polytetrafluoroethylene (PTFE) was subjected to 3 keV
electron bombardment and then heated in vacuum to
300 C. The behavior of the material as a function of
radiation dose and temperature was studied by x-ray
photoelectron spectroscopy (XPS) of the surface and
mass spectroscopy of the species evolved. Lightly dam-
aged material heated to 300 C evolved saturated fluoro-
carbon species, whereas unsaturated fluorocarbon
species were evolved from heavily damaged material.
After heating the heavily damaged material, those fea-
tures in the XPS spectrum that were associated with
damage diminished, giving the appearance that the radi-
ation damage had annealed. The observations were in-
terpreted by incorporating mass transport of severed
chain fragments and thermal decomposition of severely
damaged material into the branched and cross-linked
network model of irradiated PTFE. The apparent anneal-
ing of the radiation damage was due to covering of the
network by saturated fragments that easily diffused
through the decomposed material to the surface region
upon heating.

In many applications, polymers are exposed to radiation, high temper-
ature or a combination of both. Satellite thermal blankets, wiring
harnesses and components are irradiated on passage through the radia-
tion belts (1,2), while being exposed to the varying thermal environ-
ment of space. In the nuclear industry, materials suffer both in-
tense radiation and high temperature. U.V. radiation is known to
contribute to the surface modification of polymers during plasma
treatment (3) And in the electronics industry, electron, U.V. and
x-ray radiation are used to treat mask, insulator, packaging and
circuit board materials(4), all of which can be exposed to high temp-
eratures either during treatment or service. Polytetrafluoroethylene
(PTFE) is a candidate material in many of these applications because
of its superior thermal and chemical stability. However, its well
known sensitivity to radiation (5) limits its use in many cases. On

the other hand, low energy, high dose irradiation of PTFE can improve the adhesion of coatings (6) or inhibit the action of chemical etch treatments used to prepare the surface for coating (7). The latter effect has been proposed as a method for preparing printed circuits on PTFE substrates (8).

Thus, for many practical reasons, the behavior of irradiated PTFE during heating is of potential interest. The objective of this study was to use both X-ray photoelectron spectroscopy (XPS) and mass spectroscopy to examine the effects of temperatures from 20 C to 300 C on PTFE irradiated with 3 keV electrons.

EXPERIMENT

Apparatus. The experiments were performed in a vacuum system consisting of a preparation chamber and an analysis chamber separated by a gate valve. The preparation chamber was pumped by a 150 l/s turbo pump to a base pressure of 1×10^{-7} mbar. A quadrupole residual gas analyzer (RGA) was connected to the pumping line of the chamber. It did not have a direct line-of-sight to the specimen. Gases could be admitted to the chamber as desired through a variable leak valve. In the preparation chamber, the specimen could be mounted in a heatable support where it could be irradiated with an electron gun. A transfer device allowed the specimen to be moved to the analysis chamber without exposure to air.

The analysis chamber was equipped with diffusion and Ti-sublimation pumps and had a base pressure of 1×10^{-10} mbar It was also equipped with an RGA identical to the one on the preparation chamber. In this chamber the specimen could be analyzed by XPS and heated by a resistive element incorporated in the specimen mount. The temperature of the specimen was determined with an infrared pyrometer (9).

The unmonochromated x-ray source was Mg Kα. To minimize x-ray damage to the PTFE specimen (10), the source was operated at only 7.5 kV and 5 mA and was retracted as far from the specimen as possible. Under these conditions, no change in the C1s line of virgin PTFE could be detected after several hours of x-ray exposure, and more importantly, there was no detectable outgassing of the specimen at the 1×10^{-10} mbar level.

All spectra were obtained under the same conditions: Data were taken with the specimen normal at 80° to the axis of the analyzer input lens (grazing electron exit angle). The analyzed spot on the specimen was, then, 6 mm by 5 mm. The acceptance angle of the input lens was $\pm6^\circ$. The analyzer was a Vacuum Generators ESCALab Mk II operated with 0.5 eV resolution. Data were taken at 0.1 eV steps. The actual width of the C1s line from virgin PTFE was 1.6 eV as a result of the x-ray line width and differential charging of the specimen. The data were smoothed using a 15 point cubic-quartic Savitzky and Golay (11) algorithm, the x-ray satellites and a Shirley background were subtracted using computer routines available in the Vacuum Generators data analysis software. Only the treated data are presented here.

Specimens. The PTFE specimens used in all the experiments reported here were 76 μm thick sheets of pure, unsintered PTFE (Fluorglas #R-126, Fluorglas, Hoosick Falls, NY 12090). The material was mounted

on a 1 cm diameter, Mo sample stub. The stub's surface was ground on
SiC paper to give it a slight curvature and was then polished with 6
μm diamond paste. An oversize piece of the PTFE sheet was gently
stretched over the curved surface and fastened by wrapping a wire
around the shank of the stub. The stub was then heated in flowing
nitrogen until the PTFE film changed from white to clear. After
cooling, the PTFE sheet was in intimate contact with the heatable
stub. The fastening wire was removed and the excess PTFE sheet was
cut away with a scalpel. An area about 2 mm by 4 mm at the edge of
the specimen was painted with an isopropyl alcohol suspension of
graphite (DAG) to serve as the target of the infrared pyrometer dur-
ing temperature measurement (9).

Procedure. The experiment consisted of first irradiating the PTFE in
the preparation chamber, then either 1) heating in the analysis cham-
ber and acquiring XPS spectra after each temperature step or 2) heat-
ing in the preparation chamber and acquiring the mass spectrum of the
gas evolved from the damaged material. Each of these experiments was
separate, with new PTFE specimens used at each radiation damage level
and for XPS and RGA analysis. In the following sections, the proce-
dure used to condition the PTFE for the experiments is described,
first. Then the irradiation conditions are described. Finally, the
thermal treatment and details of the XPS and mass spectroscopy are
described.

Specimen Conditioning. The sample was first placed in the prepara-
tion chamber and heated to 350 C. During this first heating in
vacuum, there was normally some evolution of gas. The mass spectrum
of the gas closely matched that of the tetrafluorethylene monomer.
No gas was evolved during subsequent heating of the specimen to temp-
eratures below 350 C. An XPS spectrum of the specimen was obtained
to check its initial condition. The specimen prepared in this manner
exhibited only XPS features from F and C. The C1s line was a single
feature identical to the dashed peak labelled CF_2 in Figure 1. Its
binding energy was 397.0 eV to 397.2 eV below the F1s line, and the
ratio of the F1s to C1s peak areas, in our spectrometer, was 7.1±0.2.

Irradiation. Samples were irradiated with electrons in the prepara-
tion chamber. The electron accelerating voltage was 3 keV. The beam
current was 0.7 μA and was measured by directing the beam into a hole
in the sample support which was biased 30 volts positive. After the
beam current was stable, the specimen was placed on the support and
the beam was rastered over an area of 1.3 cm^2 which covered the en-
tire PTFE surface, and an absorbed-current image of the specimen was
displayed.
 It is likely that the specimen charged during irradiation either
due to embedded charge or excess secondary electron emission. How-
ever, charging was never severe enough to produce visible distortion
of the absorbed-current image, and the XPS spectrum was stable imme-
diately after irradiation. If charging of the specimen affected the
electron beam intensity, the effect was quite reproducible, since the
same changes in the XPS spectrum were observed for the same irradia-
tion times on many different specimens.

<u>Heating</u> <u>and</u> <u>X-ray</u> <u>Photoelectron</u> <u>Spectroscopy</u>. After irradiation for
the desired time, the specimen was moved to the analytical chamber
where it was heated in successive 50 C steps from 100 C to 300 C.
The desired temperature could be achieved in 3 to 5 min, and was
maintained for 20 min. During the first 5 min of heating there was a
rise in pressure in the system as gas was evolved from the specimen,
but by the end of the 20 min interval the pressure was close to the
background level. In preliminary experiments, it was determined that
any changes in the XPS spectrum were complete before the end of the
20 min of heating. Before heating and after each heating step, C1s
and F1s XPS spectra were obtained.

     Before irradiation, the XPS spectrum consisted of single C1s and
F1s lines. The C1s line occurred at approximately 292.0 eV binding
energy. It is by now well established that, on irradiation of PTFE,
the ratio of the F1s to the integrated C1s XPS intensities decreases
(<u>10-14</u>), while the C1s line develops a complex structure. Figure 1
shows the C1s line from PTFE irradiated for 100 min. Since the spec-
imens charged during analysis, and the degree of charging varied with
irradiation time and subsequent heating, the spectra were all shifted
to align the component of the C1s spectrum labelled CF_2 in Figure 1
and corresponding to unirradiated PTFE. The binding energy of that
peak has been set to 292.0 eV. The change in the spectrum consisted
of the growth of three components other than the original line. The
structure could, in fact, be fit reasonably well with four identical
Gauss-Lorentz lines as shown, in Figure 1. The width of the compo-
nent peaks varied from spectrum to spectrum, but was the same for all
components of one spectrum. The four components have previously been
assigned to carbon atoms in CF_3, CF_2 and CF groups and C with no pri-
mary fluorine bonds (<u>10,15</u>). In all the following results, the C1s
spectrum was characterized by the relative areas of these four compo-
nents and by the ratio of the F1s to C1s integrated peak areas.

<u>Heating</u> <u>and</u> <u>Mass</u> <u>Spectroscopy</u>. Specimens were prepared as described
above but using a Ni stub which had an attached thermocouple. The
specimens were placed on a heatable sample mount in the preparation
chamber and irradiated. The sample temperature was then raised at a
rate of 20 C/min to 30 C/min from 100 C to 300 C. The RGA continu-
ously recorded the spectral intensities at 19, 24, 31, 50, 69, 81,
93, 100 and 119 AMU.

     The mass spectra of several test gases were recorded in prelim-
inary experiments, so that they could be compared to the gas evolved
from the specimen. These test-gas spectra are shown in Table I. The
relative peak heights in the spectra were somewhat pressure depend-
ent, but the data in Table I were taken at approximately the same
pressure as the evolved gas. Table I shows two characteristic dif-
ferences between saturated and unsaturated fluorocarbons. First, the
69/31 ratio is greater than one for the saturated gases and less than
one for the unsaturated gas. Second, the m/e = 81 feature is absent
in the saturated gases but present in the unsaturated gas. The sam-
ple of gases in Table I is limited, however these features are also
characteristic of mass spectra reported in the literature (<u>16</u>).
Therefore, these two characteristics are used, here, to distinguish
saturated from unsaturated fluorocarbon gases evolved from PTFE.

Table I. Mass Spectra of Several Fluorocarbon Gases at 1×10^{-7} Torr, relative to the largest component in each test gas

m/e	Species	Test Gas			
		C_2F_6	C_3F_8	C_4F_{10}	C_2F_4
19	F	3.3	0.0	0.0	1.4
24	C_2	0.3	0.1	0.0	2.2
31	CF	48.5	31.1	26.1	100.0
50	CF_2	14.2	6.2	4.2	23.0
69	CF_3	100.0	100.0	100.0	1.7
81	C_2F_3	0.0	0.0	0.0	23.7
100	C_2F_4	0.2	1.8	2.2	6.5
119	C_2F_5	5.4	0.9	1.6	0.0

RESULTS

For surface analysis, the specimens were heated stepwise after irrad-
iation, and after each temperature an XPS spectrum was recorded.
These results are described first. Alternatively, irradiated PTFE
specimens were heated by ramping the temperature, as described above,
while the mass spectrum of the evolved gas was recorded. These re-
sults are described in the second section.

X-ray Photoelectron Spectra. Heating produced changes in both the
C1s structure and the F1s/C1s peak area ratio such that those fea-
tures associated with radiation damage were reduced. The change in
the C1s structure is illustrated in Figure 2 for a specimen irradiat-
ed 100 min. It is apparent that between 150 C and 200 C the compo-
nents of the line attributed to CF and C decreased relative to the
other two components. The result was a relative recovery of the CF_2
(undamaged) component and a change in the C1s line shape to one char-
acteristic of less damaged PTFE. This change in the CF_2 component
upon heating is shown for samples irradiated for other times in Fig-
ure 3. The recovery was only observed for irradiation times greater
than 30 min, while the samples irradiated for the shortest times may
have actually exhibited some decrease in CF_2 during the initial
stages of heating.
      The F1s/C1s peak area ratio increased on heating. This partial
recovery of the fluorine concentration is shown by the data of Figure
4 which shows that, like the change in the C1s structure, the change
in the F1s/C1s ratio began above 150 C, and only occurred for irradi-
ation times greater than 30 min.

Mass Spectra of Evolved Gas. The mass spectra of the gas evolved
while heating the irradiated PTFE varied with temperature and irradi-
ation time. Figure 5(a-d) shows the intensities of the mass spectro-
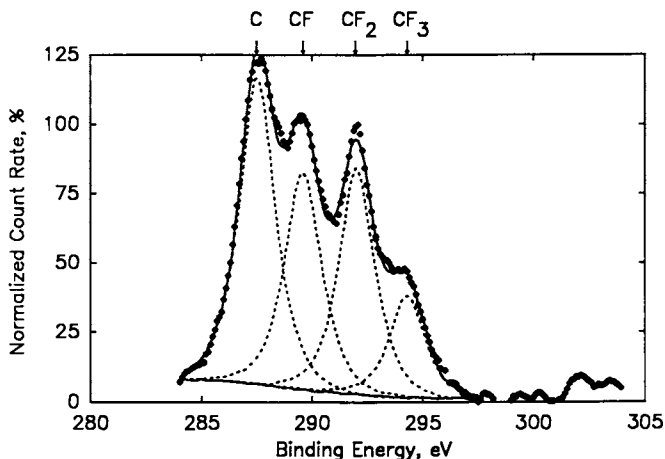
Figure 1. Four-component synthesis of C1s XPS feature from PTFE irradiated with 3 keV, 0.5 $\mu A/cm^2$ electrons for 100 min. Filled circles are original data; dotted curves are component peaks. Solid line is sum of component peaks. Shirley background is shown.
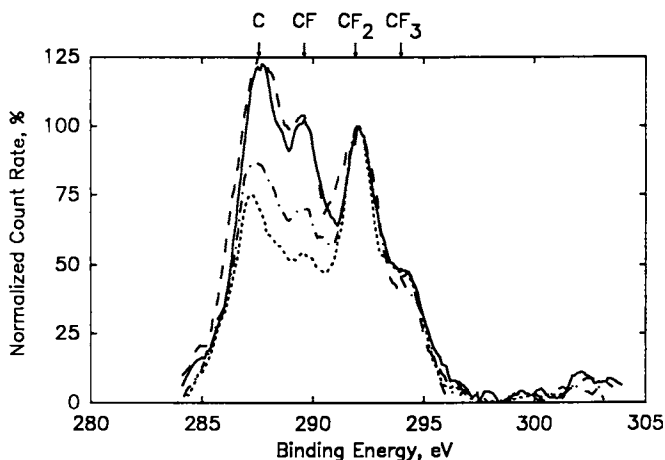
Figure 2. Effect of 20 min heating on C1s XPS feature from PTFE irradiated with 3 keV, 0.5 $\mu A/cm^2$ electrons for 100 min. Full line, no heating. Dashed line, 150 C. Dot-Dashed line, 200 C. Dotted line, 300 C.
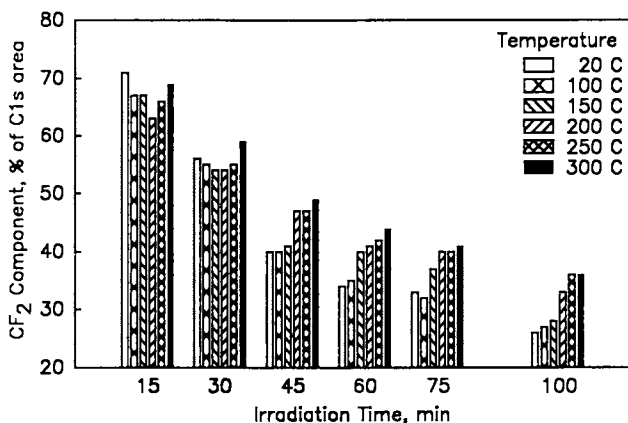
Figure 3. Relative area of the CF_2 component of the C1s XPS feature after stepwise heating of PTFE irradiated for various times with 3 keV, 0.5 $\mu A/cm^2$ electrons. Legend gives maximum temperature step achieved before taking XPS spectrum.
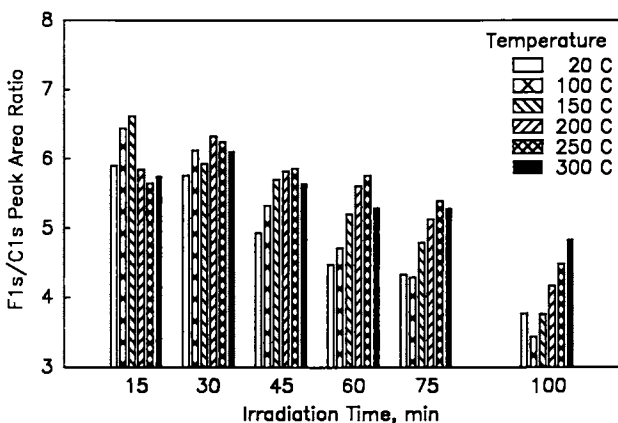
Figure 4. F1s/C1s XPS peak area ratio after stepwise heating of PTFE irradiated for various times with 3 keV, 0.5 $\mu A/cm^2$ electrons. Legend gives maximum temperature step achieved before taking XPS spectrum.
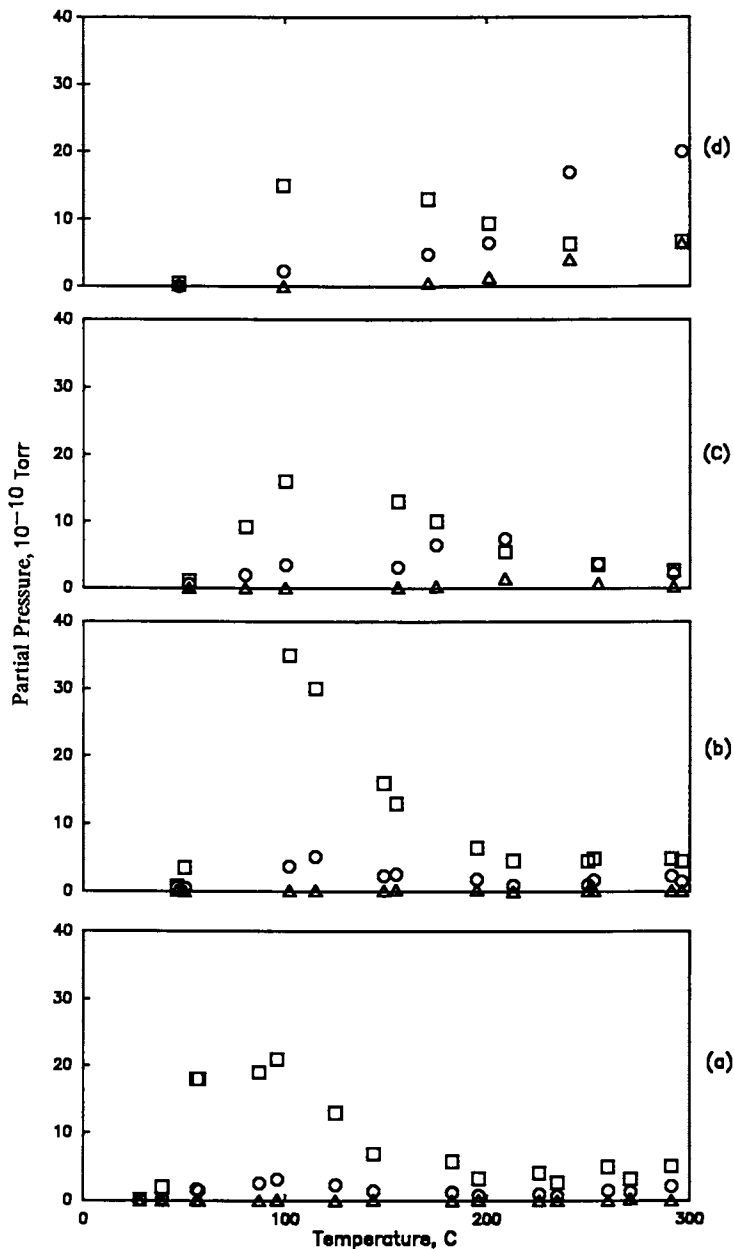
Figure 5.   Selected mass spectrometer peaks from gas evolved by PTFE irradiated for various times with 3 keV, 0.5 $\mu A/cm^2$ electrons while temperature increased at 25 C/min.   Squares, m/e = 69. Circles, m/e = 31.   Triangles, m/e = 81.   Irradiation times; (a) 15 min, (b) 30 min, (c) 60 min, (d) 100 min.

meter peaks for m/e = 31, 69 and 81 during heating of specimens which
had first been irradiated for times from 15 min to 100 min. At temp-
eratures below 150 C, the 69 component dominated and there was no 81
component. Therefore, the evolved gas consisted of saturated fluoro-
carbons. This gas was produced most rapidly from specimens irradiat-
ed 30 min or less. Above 150 C, the production of this type of gas
decreased. For the samples irradiated for 30 min or less there was
very little gas evolved at all at the higher temperatures.

However, as can be seen by comparing the partial pressures in
Figure 5(c) and 5(d) with those in Figure 5(a) and 5(b), samples ir-
radiated for more than 30 min did evolve gas, when heated above
150 C. The gas produced by these samples had a distinctly different
mass spectrum. The component at m/e = 31 was comparable to or larger
than that at m/e = 69, and an appreciable component at m/e = 81 was
produced. Selected values of the 31/69 ratio and the height of the
m/e = 81 peak are shown in Figure 6(a) and 6(b), respectively. The
selected irradiation times and temperatures are the same as those
used to present the XPS results in Figures 3 and 4. The 31/69 ratios
of Figure 6(a) and the amount of mass 81 indicated in Figure 6(b)
suggest that there was a significant amount of unsaturated fluoro-
carbon evolved from the samples irradiated longer than 30 min when
they were heated above 150 C.

DISCUSSION

It is useful to discuss these results within a model of the radia-
tion-damaged polymer. Our original report (10) on x-irradiation of
PTFE concluded that the damaged material was a highly cross-linked
and branched network. The new observations, reported here, permit
further elaboration of the model.

The techniques employed here permitted only limited observations
of a complex process. XPS samples the surface of the PTFE specimen,
but the nature of irradiated PTFE varies with depth and at each depth
is a function of irradiation time. Mass spectroscopy yields the time
dependence of gas evolved from the PTFE at various temperatures as
well as limited information on the molecular weights of the gas
species. However, these effects are a function of the rate of pro-
duction of the various species at each depth and the diffusion rates
of each species through the inhomogeneous material. Thus, the irrad-
iated PTFE system is too complex to allow a definitive model to be
based on the results presented here. However, we can suggest some
features of such a model by focusing on the lightly damaged PTFE
(15 min irradiation time) and the severely damaged material (100 min
irradiation time).

The evolution of saturated fluorocarbon gas upon heating is tak-
en as direct evidence of the presence of chain fragments in the dam-
aged PTFE. Figure 5 shows that more gas was produced, upon heating,
after 30 min irradiation than after 15 min, as would be expected if
the fragments are damage products, but the gas production decreased
for greater irradiation times. The simplest interpretation of these
observations is that saturated fragments were transported to the sur-
face where they were desorbed into the gas phase. At first, as the
damage increased, the supply of fragments also increased causing
greater gas production. However, with more severe damage, either all
the fragments were desorbed at room temperature, or they were trapped
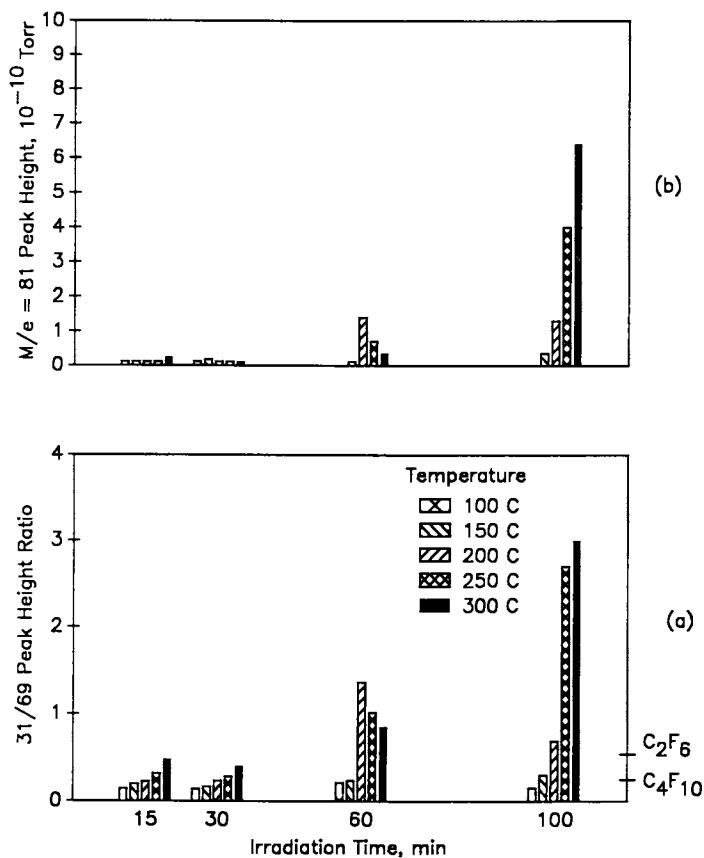
Figure 6. Ratio of 31/69 mass spectrometer peaks (a), and height
of m/e = 81 peak (b) at 50 C temperature intervals while PTFE
irradiated for various times is heated at 25 C/min. In (a)
reference values of the 31/69 ratio from Table I are shown.

in the network; the result, in either case, being a decrease in the production of saturated gas, upon heating.

Thus, it is to be expected that, with the saturated fragments all exhausted or trapped, the cross-linked and branched network that constitutes the most severely damaged material would be stable with temperature. Figures 5(d) and 6 show that, in fact, saturated gas production was reduced, and Figure 2 shows that up to 150 C the XPS C1s line was unchanged. However, when the temperature exceeded 150 C, there was a dramatic change: While lightly damaged material produced virtually no gas at these temperatures, the gas production from severely damaged PTFE increased. Also, the mass spectrum of the gas was characteristic of unsaturated rather than saturated fluorocarbons. Figures 2, 3 and 4 show that, simultaneous with this production of unsaturated gas, there was a substantial "recovery" of the XPS spectrum consisting of a relative increase in the CF_2 component of the C1s line and the F/C ratio and a decrease in the CF and C components of the C1s line.

The data presented here, while not definitive, permit some speculation on the mechanism of this apparent recovery of the irradiated PTFE. First note that unirradiated PTFE decomposes thermally at about 500 C by unzipping to release the monomer (16). Although the 31/69 ratio and the relative mass 81 intensity observed (Figure 6(a)) were much lower than that from the monomer (Table I), the gas produced here was almost certainly a mixture of saturated and unsaturated fragments. It seems likely that the unsaturated gas was a result of decomposition of the irradiated PTFE. Since unirradiated PTFE is thermally stable well above 300 C, it was presumably the damaged network that was susceptible to degradation in the 200 C to 300 C range observed here.

Loss of the severely damaged network at the surface could expose underlying, undamaged material to XPS analysis, thus accounting for the apparent recovery of the XPS spectrum. While this cannot be ruled out, it seems unlikely for two reasons: First, earlier observations (14) and dose-depth calculations (17) show that the severe damage due to 3 keV electrons extends far into the bulk of the PTFE. Transformation of that much bulk material into gaseous products would have produced far higher pressures than were observed here. Second, Figure 2 shows that although the CF and C components of the C1s line (characteristic of network material) decreased relative to the CF_2 component, the CF_3 component (characteristic of end goups) did not. This indicates that the material exposed was not undamaged material, because the CF_3 component was undetectable in XPS spectra of undamaged PTFE. A more likely explanation for the apparent recovery of the XPS spectrum is that breakdown of the dense network material released saturated fragments that had been trapped in and below the network. Release of untrapped, volatile, saturated fragments contributed to the observed release of gas, while migration of nonvolatile fragments to the surface caused the apparent recovery by covering the network material.

SUMMARY

The result of heating PTFE irradiated with 3 keV electrons has been
studied with XPS and RGA. The following observations have been made:
1. For low radiation doses the XPS spectrum was unchanged by heating
to 300 C, and saturated fluorocarbons were evolved from the surface.
2. For high dose and temperatures above 150 C, the XPS spectrum ex-
hibited an apparent recovery to that of a less damaged material.
3. Also at these temperatures and doses both saturated and
unsaturated fluorocarbon species were evolved from the surface.
       The following interpretation is suggested: Upon heating, frag-
ments trapped in the cross-linked structure became mobile and, to
some extent, volatile. When the structure was sufficiently radiation
damaged, it became thermally unstable and decomposed with a release
of both saturated and unsaturated fluorocarbons and the migration of
previously trapped fragments to the surface. These migrated frag-
ments covered the damaged network and lead to the appearance of par-
tial annealing in XPS spectrum of the surface.

LITERATURE CITED

1.   Pascale, J. V.; Herrmann, D. B.; Miner, R. J. *Modern Plastics*
      1963, *41*, 239
2.   Chan, King W.; Sawyer, Donald M.; Vette, James I. NASA
      TM-X-72611, 1977
3.   Clark, D. T.; Dilks, A. *J. Polymer Sci, Polymer Chem. Ed.* 1977,
      15, 2321-2345
4.   Krisnaswamy, J.; Li, l.; Collins, G. J. *J. Mater. Res.* 1988, *3*,
      1259-1267
5.   Chapiro, A. *Radiation Chemistry of Polymeric Systems*;
      Interscience: New York, NY, 1962; p 526ff
6.   Wheeler, D. R.; Pepper, S. V. *J. Vac. Sci. Technol.* 1982, *20*,
      442-443
7.   Rye, R. R. *J. Polymer Sci, Polymer Phys.* 1988 *26*, 2133-2144
8.   Rye, R. R.; Martinez, R. J. *J. Appl. Polymer Sci.* 1989, *37*,
      2529-2536
9.   Wheeler, D. R.; Jones, W. R.; Pepper, S. V. *J. Vac. Sci.
      Technol.* 1988, *A6*, 3166-3168
10.   Wheeler, D. R.; Pepper, S. V. *J. Vac. Sci. Technol.* 1982, *20*,
      226-232
11.   Seah, M. P.; Dench, W. A. *J. Elec. Spec.* 1989, *48*, 43-54
12.   Chaney, Robert; Barth, Günter *Fresnius Z. Anal. Chem.* 1987,
      329, 143-146
13.   Kelber, J. A.; Rogers, Jr., J. W.; Ward, S. J. *J. Mater. Res.*
      1986, *1*, 717-723
14.   Clark, D. T.; Brennan, W. J. *J. Elec. Spec.* 1986, *41*, 399-410
15.   Clark, D. T.; Feast, W. J. *J. Macromol. Sci. Rev. Macromol.
      Chem.* 1975, *C12*, 191
16.   Madorsky, S.L. *Thermal Degradation of Organic Polymers;*
      Interscience, New York, 1964, p. 130
17.   Kanaya, K.; Okayama, S. *J. Phys. D: Appl. Phys.* 1972, *5*, 43-58
18.   *Index of Mass Spectral Data, AMD-11*, Committee E-14 on Mass
      Spectrometry (American Society for Testing and Materials,
      Philadelphia, 1969)

Chapter 17

Novel Process for Surface Modification of Polyimide

N. L. D. Somasiri, T. A. Speckhard, and R. L. D. Zenner

Industrial and Electronic Sector Laboratory, 3M Company, St. Paul, MN 55144–1000

Surface modification (texturing) of polyimide through a metal clustering and migration process is reported. This process involves heat treatment of polyimide coated with a thin copper layer. Subsequent metallization of the textured surface leads to improved adhesion due to mechanical anchoring. Adhesion values of 7-10 lbs/in (ambient) and 4-6 lbs/in (after solder float) have been obtained.

Kapton polyimide has been widely used in the electronic industry because of its low dielectric constant, good mechanical properties and high thermal stability. Many applications require good adhesion between Kapton polyimide film and metal. Various processes to improve adhesion of metal to Kapton polyimide have been reported in the literature. DeAngelo et al., (1) describe a process to form metal oxides on the surface of polyimide to improve adhesion. Other efforts to improve adhesion of a metal layer involve roughening of the surface of polyimide substrate by methods such as cathodic sputtering (2), chemical attack (2, 5), and reactive ion etching (3, 4).

   Recently Krause et al., (6) have reported a novel method for metallizing Kapton polyimide utilizing an aqueous based reversible charge transfer process. The Kapton polyimide film is first reduced to the radical anion state (which exhibits a characteristic green color) in the absence of oxygen by exposure to a reducing agent. Upon immersion in certain metal salt solutions, the reduced polyimide acts as a reducing agent to deposit a thin film of metal on the polymer surface. The metal film that is deposited (e.g., copper) then serves as a seed layer for subsequent electroless and electrolytic plating to the desired metal film thickness. Adhesion values in excess of 6 lbs/in have been obtained under ambient conditions using this process but adhesion values fall to less than 1 lb/in when the samples are subjected to the solder float test at 280°C.

We have recently modified the Krause process by incorporating a heat treatment step which results in a novel process for surface texturing of Kapton polyimide (Somasiri, N. L. D.; Speckhard, T. A. U. S. Patent Applied For). When the textured polyimide is subsequently metallized, again using the Krause process, good adhesion is obtained after exposure to the solder float test.

Experimental

Kapton polyimide 300VN purchased from DuPont (Wilmington, Delaware) was reduced to a green colored film and a seed layer of copper (~80 Angstrom) was deposited as described by Krause et al., (6). After washing and drying in air, the seed copper coated Kapton polyimide was heated to 450°C in air for 3-5 minutes. More seed copper was deposited as described previously, and the thickness of copper was then increased to 2000 Angstrom by electroless copper plating (Cuposit CP-78, Shipley Chemical Co., Newton, MA). Final thickness of copper was increased to 1 mil (25 micron) by electroplating (Harshaw Cu-Tronix acid plating bath).

The electroplated metallized Kapton polyimide was initially dried in air and then dried at 135°C for one hour. The metal surface was masked with 1/16 inch wide 3M brand masking tape. Exposed metal was etched by immersing in aqueous 3M $FeCl_3$ solution. After thorough rinsing, the masking tapes were removed and 90° peel test was performed (using an Instron device) according to I.P.C. test method 650-2.4.9 Method A (7) in order to characterize the adhesive force between copper and Kapton polyimide. The material was then subjected to the solder float test (I.P.C. test method 650-2.4.9 Method C; ref. 7) and 90° adhesion was measured immediately and after 24 hours exposure to laboratory air (50% relative humidity) at room temperature.

Surface topography of Kapton polyimide as-received, seeded with copper, after the 450°C heat treatment, and after removal of copper oxide by acid etching was examined by scanning electron microscopy. Cross-sectional analysis of Kapton seeded with copper and after 450°C heat treatment was carried out by transmission electron microscopy.

Results and Discussion

We have discovered that heating Kapton polyimide with a seed coating of copper in air to 450°C leads to surface texturing. Scanning electron micrographs of Kapton polyimide, as-received, after seeding with copper, after 450°C heat treatment, and after removal of copper oxide by acid etching are shown in Figures 1a, b, c, and d, respectively. The as-received and copper coated films are smooth except for protrusions due to slip agent particles. After heating, the film exhibits a textured surface on the scale of about 0.5 micron. This roughness is due to the underlying polyimide and not metal oxide formation as can be seen in Figure 1d where the metal oxide has been etched away. Although at present the processes leading to the textured surface are not completely understood, preliminary experiments suggest that the copper atoms migrate and form clusters which then serve as catalytic sites for polyimide degradation. As shown in Figure 2, transmission electron micrographs of Kapton seeded with copper and after 450°C heat treatment reveal evidence for copper clustering. We have also observed a weakening of the copper signal in x-ray
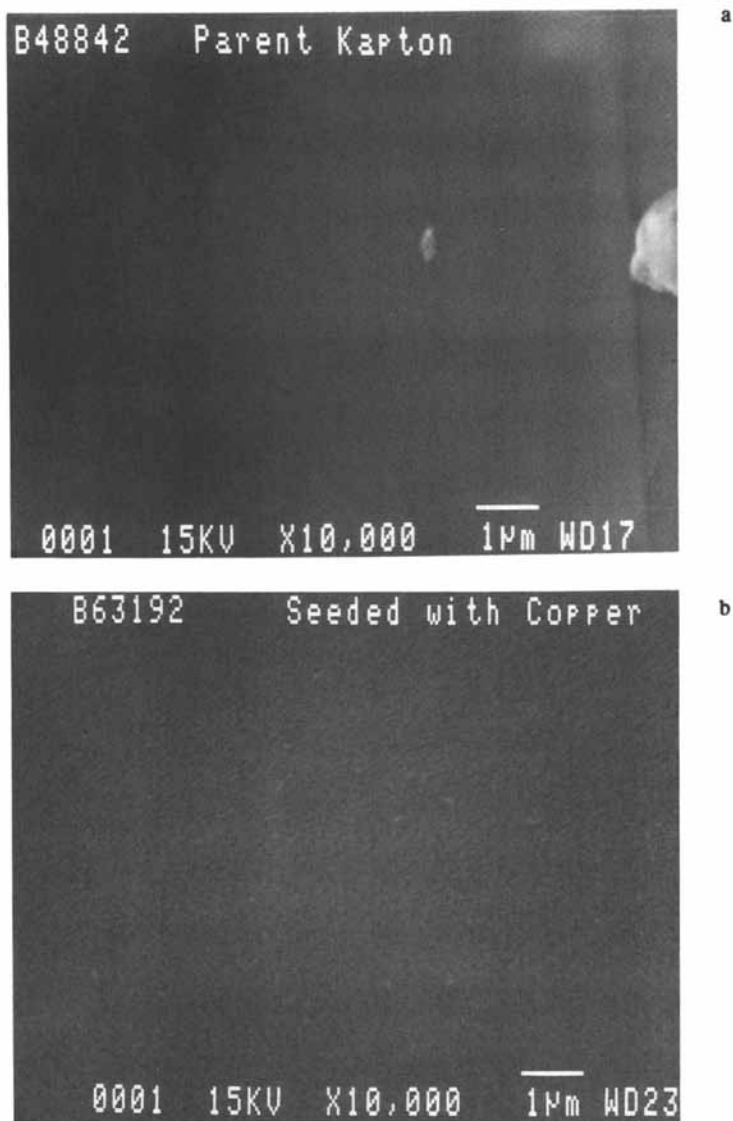
Figure 1. Scanning electron micrographs of Kapton polyimide: (a) as-received, (b) seeded with copper, (c) after 450°C heat treatment, and (d) after heat treatment and removal of all copper oxide.
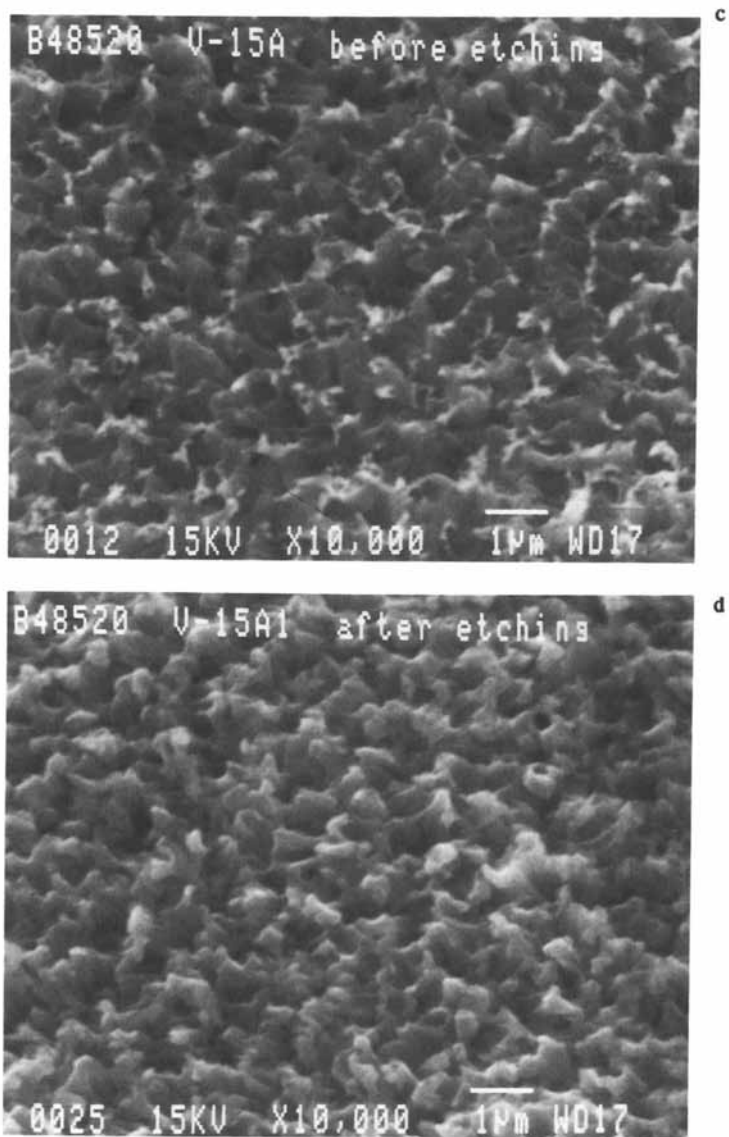
Figure 1 Continued.
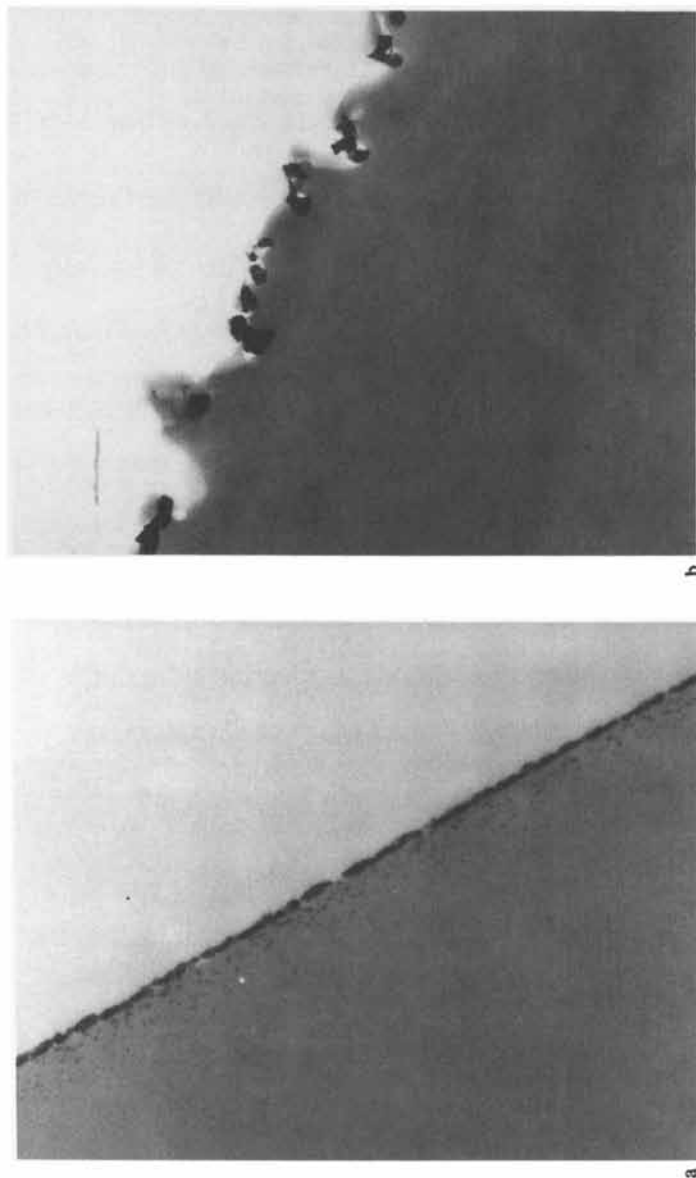
Figure 2. Transmission electron micrographs of Kapton polyimide (magnification 36000X): (a) seeded with copper and (b) after 450°C heat treatment.

photoelectron spectroscopic elemental analysis following treatments of 15, 75, and 135 seconds at 450°C further illustrating that copper migrates deeper into the Kapton.   In effect, the valleys in this "hill-and-valley" type morphology are created by preferential degradation of polyimide in the vicinity of copper/copper oxide clusters.   Some support for this mechanism can be found in the literature.   Ho et al., (8) have reported the formation of copper clusters when annealing copper coated polyimide to 300°C.   Copper is known to catalyze the thermal oxidation of polyethylene (9) and several metals such as silver (10), copper (10), and cobalt (11) have been reported to catalyze the thermal decomposition of polyimide.

When subject to 90° peel test, adhesion values of 7-10 lbs/in have been obtained under ambient conditions. Interestingly, the adhesion after the solder float test retained 4-6 lbs/in.   This high adhesion is believed to be primarily due to the mechanical interlocking facilitated by the textured Kapton polyimide.

Literature Cited

1.   DeAngelo, M. A.; Sharp, D. J.   U. S. Patent 3 562 005, 1971.
2.   Schoenaich, D. B.; Boeblingen P. F.; Gaertringen, W. K.; Schwerdt, F.; Thelen, U.; Holzgerlingen, T. V.   U. S. Patent 4 152 195, 1979.
3.   Ruoff, A. L.; Kramer, E. J.; Li, C. Y. IBM J. Res. Develop. 1988, 32(5), 626.
4.   Dunn, D. S.; Grant, J. L.; McClure, D. J. J. Vac. Sci. Technol. 1989, A7(3), 1712.
5.   Walsh, D. P.   U. S. Patent 4 806 395, 1989.
6.   Krause, L. J.; Rider, S. A.   U. S. Patent 4 710 03, 1987 .
7.   IPC Standard IPC-FC-FLX, The Institute for Interconnecting and Packaging Electronic Circuits, April, 1988.
8.   Ho, P. S.; Hahn, P. O.; Bartha, J. W.; Rubloff, G. W.; LeGowes, F. K.; Silverman, B. D. J. Vac. Sci. Technol. 1985, A3(3), 739.
9.   Chan, M. G.; Allara, D. L. Polymer Engineering and Science 1976, 14(1), 12.
10. Mittel, K. L. In Polyimides Synthesis, Characterization and Application; Plenum Press, New York, 1984; Vol. 2, p 871-887.
11. Anderson, S. G.; Meyer, III, H. M.; Weaver, J. H. J. Vac. Sci. Technol. 1988, A6(4), 2205.

Chapter 18

Reactions of Metal Atoms with Monomers and Polymers

Mark P. Andrews[1]

AT&T Bell Laboratories, Murray Hill, NJ 07974

Abstraction, reductive coupling, electron transfer, bond activ-
ation, oxidative addition, π-complexation, disproportionation
and metal cluster formation are some of the reactions that
occur when metal atoms interact with organic polymers and
small molecules. Examples of these reactions are provided
from the literature on the organometallic chemistry of free
atoms and coordination-deficient molecules. Past uses of
model compound studies to understand the early stages of
chromium metallization on polyimide are critiqued. New
evidence for reactions of chromium atoms with compounds
related to polyimides is given.

Organometallic compounds can be produced by direct reaction of metal atoms with organic
molecules. Some of this chemistry may be relevant to the earliest stages of metallization of a
polymer surface. An understanding of the physical and organometallic chemistry of metal atom
reactions with organic substrates may suggest new ways of viewing the metallization process. For
example, in the very early stages of polymer metallization the emerging interface might be
perceived as an evolving structure in which a polymer is converted first to an organometallic
surface, which later undergoes reactions with deposited metal atoms. If even in a limited way this
chemistry could be understood and simplified, new opportunities can be suggested for intervening in
the making of the adhesive bond; for it is well-known that metal atoms and clusters can selectively
activate organic functional groups (1). Once identified, selective activation might be exploited to
control specific surface adhesion processes.

Our intention in this Chapter is to sensitize surface scientists and others concerned with
understanding metal/polymer interfaces, to ways in which metal atoms can produce organometallic
chemistry. Much of the work reported in this Chapter is based on an established method called
metal vapor synthesis (MVS) or simply, vapor synthesis. Underlying the method is the rational use
of metal atoms and molecular high temperature species to prepare varieties of organometallic and
inorganic compounds, many of which may not be accessible by more conventional preparative
routes (2). Reduced steric restrictions and the high potential energy for reaction implicit in the free

[1]Current address: Department of Chemistry, McGill University, Montreal, Quebec H3A 2K6,
Canada

state of the atom or fragment often lead to low activation energy requirements for these kinds of reactions. MVS is similar to many industrial thin film processes for depositing highly reactive atomic and molecular species (3) to make thin films on polymers. Below we provide a short introduction to acquaint our readers with MVS and provide the experimental background necessary to understand how many of the compounds are prepared. Two recent articles review reactions of metal atoms with polymers (2,4).

Experimental

Large Scale Metal Vapor Syntheses. Detailed accounts of the technique have been given elsewhere (5). The principle of the method is simple. Vapors formed by resistive or electron beam heating are combined under vacuum with a co-reactant at a (cold) surface where products may be formed and isolated. Except when metal aggregates are desired, facile self-association reactions of the high-temperature species are suppressed to favor atom/co-reactant interactions. This is done with high pumping speeds, efficient furnace and refrigeration designs, and sensitive strategies for mixing and diluting reagents. Figure 1 shows a reactor (there are many varieties (5)) currently in use in our laboratory. The device is a 5 L Pyrex cryostat that can be evacuated to $\approx 10^{-7}$ Torr and rotated without breaking vacuum. Metals are evaporated with resistance electrodes or electrostatically focused, work-accelerated positive hearth dual electron guns (6). Transfer of gases, liquids and solids into and out of the apparatus is regulated by valves and cannulas connected to a high/low vacuum/inert gas manifold. When a cryogen like liquid nitrogen is raised about the flask, most gases introduced to the reactor can be frozen. As illustrated in the Figure, the electron gun deposits a layer of atoms into a pre-deposited layer of substrate on the inner top surface of the rotating flask. In this way, a laminate of solid accumulates. After melting the condensate, the products are isolated with standard inert atmosphere handling techniques (5). Similar preparations can be carried out in static glass reactors. These are large evacuable dewars that can be immersed in liquid nitrogen. The co-reactant is evaporated from an application-specific inlet tube and condensed with metal atoms and excess diluent on the reactor walls.

The rotatable reactor can also be used for reactions in fluids having suitably low ($\leq 10^{-3}$ Torr) vapor pressure. In this mode, metal atoms are evaporated upwards into the cold liquid, which is spun as a thin band on the inner surface of the flask. Reactions with dissolved polymers can then be studied. Specially designed electron gun sources can be operated, without static discharge, under these potentially high organic vapor pressure conditions (6). Run-to-run reproducibility is obtained by monitoring the metal atom deposition rate with a quartz crystal mass balance (thickness monitor).

Small Scale Metal Vapor Syntheses. Metal atom reactions can be studied on a microscopic scale with cryogenic matrix isolation and spectroscopy. Atoms, co-reactants and products are isolated in dilute form, usually in a rare gas solid, on a cold (< 15 K) optical window of a cryostat. Our understanding of macroscale MVS reactions in fluids have benefitted from adaptations of cryogenic matrix isolation for studies in liquids (7). For these experiments, a suitable optical window is cooled to the desired temperature and an aliquot of liquid (dissolved polymer, organic, inorganic or organometallic compound) is injected *via* vacuum microsyringe onto its surface. Metal atoms are quantitatively deposited into the fluid and reactions are monitored spectroscopically. This technique can be used to determine the fate of metal atoms deposited into thin, quiescent liquid films of polymers, oligomers or organic solute/solvent systems. Diffusion and kinetic experiments can be undertaken, together with feasibility studies related to product work-up, thermal and photo-stability. Examples of studies relevant to reactions with monomers and polymers will be given below.

Generalized Reactions of Metal Atoms

Scheme 1 depicts some of the outcomes possible (5) when a metal atom reacts with an organic molecule, which might be a monomer or a substituent on a polymer. Some of the more common reactions are generalized. Oxidative addition is relevant to insertion of a metal atom into a carbon-halogen bond, such as might be found in polyvinyl chloride or the monomer, allyl chloride, or

ROTATION DRIVE MOTOR

5 L PYREX FLASK

ELECTROSTATIC FOCUSING CAN

ATOM FLUX

HEARTH

QUARTZ CRYSTAL

EMITTER FILAMENT

CONDENSATION ZONE

VARIABLE TEMPERATURE CANNULA

TO VACUUM STATION

LIQUID NITROGEN TRANSFER TUBE

CRYOGENIC BLOCK

HEATED SHOWER HEAD FOR GAS DISPERSION

ELECTRICAL AND WATER CONNECTIONS

RETAINING COLLAR

ROTATABLE MAGNETIC FLUID VACUUM SEAL

STAINLESS STEEL FEEDTHROUGH

Figure 1. Dual electron gun rotatable reactor for condensed phase metal atom synthesis.

insertion of an atom into a carbon-hydrogen bond of ethane or polyethylene. Metals like titanium, chromium and aluminum are oxophilic, and capable of abstracting oxygen from ether, carbonyl and hydroxyl groups. Typical abstraction products are olefins and reductively coupled compounds. Some experimental conditions may generate ligand stabilized metal clusters. Electron transfer from alkali metal atoms to monomers like styrene or methylmethacrylate causes rapid anionic polymerization (8). In other cases, transfer from a transition metal to an electron acceptor can occur, as in the reaction of atomic Ni with tetracyanoquinodimethane (9). Silver atoms abstract iodine from CH_3I, but will substitute for iodine in reactions with $(CF_3)_2CFI$, giving $AgCF(CF_3)_2$. Disproportionation and ligand transfer occur when nickel atoms combine with tetrakis(allyl)tin to produce bis(allyl)Ni and colloidal tin. Many transition metals will form π-sandwich complexes by direct reaction of the atom with acyclic olefins, and with cyclic dienes, trienes and tetraenes. Simple orbital mixing processes, like those involving the early transition metals, Ti, V, Cr, Zr, Nb, Mo, Hf, Ta, and W, yield sandwich π-complexes with arenes (benzene, toluene, chlorobenzene, naphthalene, etc.) Similar complexes are produced when these metals combine with arene substituents on a polymer. Main chain and side chain mobility, functional group orientations and distributions, occluded solvents, monomer and polymer condensation products are some of the factors to be considered when comparing the chemistry of MVS with that at a polymer surface. In the following sections we examine several of these reactions, drawing parallels where it seems reasonable to do so, between the chemistry of small molecules and reactions at polymer surfaces.

Oxidative Addition. The process is defined as follows: reaction of a metal (complex) in which the formal oxidation state n of the metal, with an addendum, X-Y, to give a new complex, X-M-Y or similar, in which the formal oxidation state of the metal is increased to $n + 2$ (10). Oxidative addition of alkyl and aryl halides (RX and ArX) to Group 9 and 10 transition metals yields the structures, RMX and R_2M (plus MX_2 by disproportionation of RMX) (11, 12). These reactions work well with transition metal atoms if there is a possibility of initial coordination to the atom, as in the reaction of atomic nickel with allyl chloride (Scheme 2). Klabunde and co-workers have traced many reactions of nickel, palladium and platinum atoms with organic halides (3, 11). Product yields correlate directly with the availability of π-orbitals for initial coordination to the metal, and inversely with the strength of the carbon-halogen bond. Pt atoms react less efficiently than Ni or Pd atoms in organohalide oxidative additions, with Pd giving the most stable RMX species (13). Timms has found that high yields of oxidative addition reactions are obtained when a metal atom-carrier is prepared from a weak π-complex. Thus atomic palladium reacts with 1,2,3,4-tetramethyl-1,2-dichlorocyclobutene giving a palladium chloride dimer in 100 K toluene solutions. (14). An understanding of oxidative addition reactions of small molecule saturated halides and some aryl halides may provide a starting place for reasoning about reactions that occur at polyvinyl halide surfaces. RPdX and RNiX compounds formed from normal alkyl groups (R = CH_3, C_2H_5, $(CH_3)_3C$ and $(CH_3)_3CCH_2$) are extremely unstable, decomposing well below room temperature. Metal halides and hydrocarbon gases are evolved. To break alkyl fluoride bonds an electropositive metal is required (Ca, for example) having a high M-F bond strength. For these reasons RMX compounds developed at a polymer surface will also likely be thermally unstable, or may require aggressive conditions for formation. Free radicals from decomposition reactions might produce cross-linked surfaces. Mobilities, orientations and distributions of active functional groups at the polymer surface will be important here. Gaseous species can be expected from decompositions of pendant side-chain RMX species; there is some evidence that HPdX elimination is a decomposition pathway for C_2H_5PdX, with the HPdX capable of reducing RX to RH + PdX_2. Analogous reactions can be envisaged for polymers, but it is difficult to generalize because there are many different insertion and elimination mechanisms that exist for the wide variety of halides and metals involved in oxidative addition reactions.

Many oxidative addition complexes are stable because four and higher coordination inhibits decomposition via de-insertion and elimination. For benzylhalides that are pendant to a polymer main chain, compounds that exhibit $η^3$-bonding to the benzyl group are possible. The small molecule analog is the $η^3$-benzylpalladium chloride dimer. This complex is neither electronically nor coordinately saturated and is therefore not inert to ligand addition.
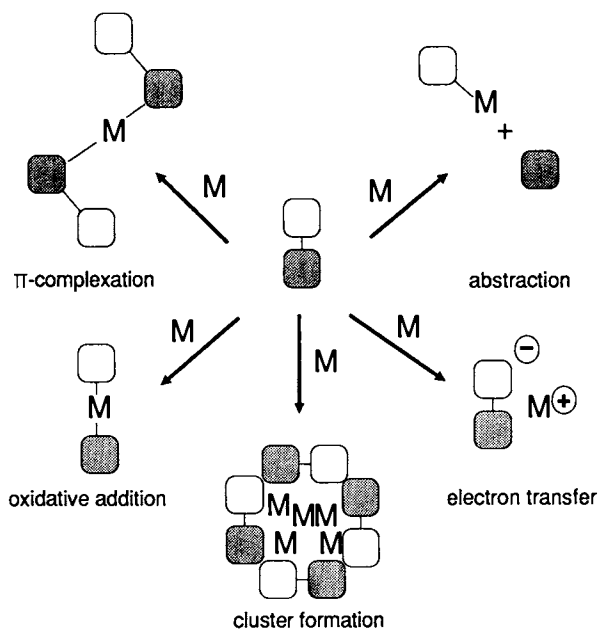
SCHEME 1
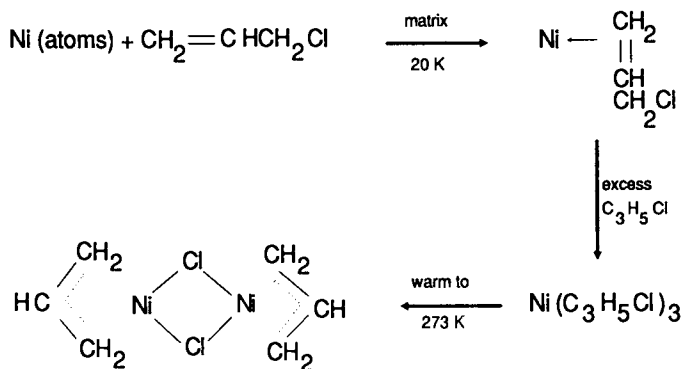
SCHEME 2

Abstraction and Reductive Coupling. These events are relevant to metal vapor depositions onto polymer surfaces rich in oxygen, active hydrogen and halides. Examples might include metal atom reactions with polyimides, polyesters, polyacrylates, hydroxylated polymers, halogen-containing polymers and polymers having carboxylic acids. Some abstraction reactions resulting from decomposition of oxidative addition products were described above. Different elements from the same Group have different reactions with the same substrate. For instance, dehalogenation and radical products are produced when alkyl halides are exposed to atoms from the copper triad. (15). Ethylbromide forms mainly n-butane from copper atoms, mainly ethane and ethene from Ag atoms, and all three organics in about equal amounts from atomic gold.

Studies of metal-polymer adhesion strength and photoemission (16) have shown that oxygen-containing polymers adhere strongly when metallized with electropositive metals like Ti, Cr, Ni and Al. Thermodynamic arguments suggest that metals with large negative free energies of gas phase oxidation form an interfacial oxide from reactions with the carbonyl oxygen atoms on polyimide (17). Recent high resolution photoemission studies of the interfacial reaction of Cr with polyimide and oxygen-rich model polymers seem to confirm that the carbonyl groups on the polymers are the initial targets of reaction (18). This is consistent with MVS studies that show that certain metal atoms are oxidized by ethers, epoxides, alcohols, ketones and aldehydes.

Deoxygenations can be classified as: (i) those in which oxygen is abstracted from the molecule, and (ii) those in which oxygen removal occurs together with intermolecular coupling. Gladysz et al. (19) have examined interactions of Ti, V, Cr, Co an Ni atoms with oxygen-containing substrates. When epoxides react with the metal vapors, alkenes are the major or exclusive products. Cyclohexanone and cycloheptanone are converted in low yield to reductively coupled and aldol products by atomic Cr, Co and Ni. Metal atoms disguised as formally zerovalent organometallic compounds will deposit colloids when contacted with carbonyl substrates. Colloidal titanium derived from bis(benzene)Ti (by MVS) will reductively couple ketones to olefins (20). This is an example of a chemical transformation on the active "surface" of metal aggregates.

Not surprisingly, metal atoms are more reactive than bulk metal towards protonic acids. Activated hydrogen in hydrocarbons like cyclopentadiene, can also be included in this group. With acids, chromium combines as a divalent salt if air is excluded, and as a trivalent salt if air is present (21). Not all reactions of metal atoms with oxygen sources lead to abstraction. Burkstrand has suggested that chelate-like complexes may form at the surface of an oxygen-containing polymer. He generalizes that increased adhesion strength correlates with the presence of such species. Indeed, reactions of acetylacetone with a range of first row transition metals yield known metal-acetylacetonate chelates (21).

Aluminum atom reactions are relevant to interfacial chemistry associated with aluminum-polyimide junctions. Al deposited under ultra high vacuum will reduce surface carbonyl functional groups (22). MVS co-condensation experiments show that besides ketones, aldehydes and epoxides, atomic aluminum will deoxygenate ethers. Chapter 7 of the monograph by Klabunde (12) includes tables of deoxygenation products of a variety of cyclic and acyclic ketones and ethers.

Chemical transformations caused by *metal clusters* should be considered in discussions of metal coverage studies on polymers. Bond activation by metal surfaces and clusters is well known. Although the MVS deoxygenation reactions have largely been attributed to individual metal atoms, undetected clusters and colloidal metal particles might participate in some cases. Clusters and minute metal particles produced by MVS methods can be aggressive towards carbon-oxygen and carbon-hydrogen bonds. For example, "pseudo-organometallic" powders are thought to develop from reactions of alkanes with Ni clusters that are formed at some stage in a low temperature MVS experiment. The powders contain large amounts of alkyl-, alkenyl-, and carbenoid (not carbide) C-H fragments (23). We have found that sub-100 Å iron particles grown in SF_6 matrices react with adventitious hydrocarbon. The particles self-decorate with a $-CF_2-$ polymer and surface carbides (24). The accumulation of carbide-like carbon species observed with increasing chromium coverage of polyimide may be linked to chemical bond activation by clusters of chromium (18).

<u>Simple Orbital Mixing Reactions: Π-Complexes.</u> This fertile area of metal atom chemistry has been systematically covered in the monographs by Klabunde (<u>12</u>) and by Blackborow and Young (<u>15</u>). Many kinds of unsaturation in a polymer can be attacked by metal atoms. Isolated and conjugated double bonds are susceptible to isomerization, cyclization, cross-linking, etc. Atoms of the first row transition series catalyze the isomerization of alkenes containing β-hydrogen (<u>25</u>). Aluminocyclopropane and aluminopropyl radical intermediates may be responsible for the dimerization products (hexanes) detected when Al reacts with propene in 77 K condensates (<u>26</u>). Apparently, Cr atoms polymerize butadiene to poly-1,2-butadiene (<u>27</u>), but they cross-link poly(butadiene-*co*-styrene) blocks in tetrahydrofuran solution (<u>28</u>). Mo or W give thermally and air stable tris(η⁴–butadiene)M (M=Mo, W) complexes (<u>29</u>). Since metal-hydrogen interactions are ubiquitous among the reactions of metal atoms with alkadienes having active hydrogens, there is reason to suppose that analogous transformations might occur on polymers. Coordination through the ligand π-system would ally the metal atom and the active hydrogen. Driving forces include increases in the coordination electron number of the complex; disproportionation to aromatic systems; disproportionation to 18-electron compounds; and isomerization to more stable species. All these reactions have been observed for small molecules, including monomers, but there have been no studies of such interactions on organic polymer hosts.

Benzene and its derivatives are the most important η⁶-arene (six-coordinated) ligands. When these are attached to Group 6 elements, they form the most intensively studied area of η⁶-ligand transition metal chemistry. Bis(benzene)chromium is perhaps the classic example of a sandwich compound made by combining Cr atoms and benzene at 77 K (Scheme 3) (<u>30</u>). A delicate balance of thermodynamic and kinetic stability determines the existence of chromium-arene sandwich complexes (<u>31</u>). Consider polystyrene in Scheme 4. We have separated the macromolecule into constituents that can react in various ways with different transition metal atoms. Condensation of Cr atoms with styrene in excess pentane in a static reactor at 77 K does not give the di–η⁶ compound. Instead, polystyrene is produced on warm-up (no molecular weight or yields reported), together with an infusible material in which Cr is apparently bound to the polymer. (Scheme 5, top). The insolubility of the latter may be caused by interchain cross-links formed by chromium bonded to phenyl groups on different chains. Soluble organometallic polymers are readily formed by evaporating Cr into cold solutions of polystyrene (<u>4</u>). Organometallic monomers of styrene and related olefins from MVS can also be polymerized to give organometallic polymers of π-complexes (<u>4</u>). Polymer bound species of the type (arene)CrL₃ (L = CO, PF₃) in Scheme 5 are isolated when a styrene/Cr condensate is warmed from 77 K under a blanket of the ligand. Iron atoms condensed with styrene under similar conditions produce low yields of polymer (ca. 1%) and no identifiable organometallic compounds. (η⁴–styrene)Fe(CO)₃, (η²–styrene)Fe(CO)₄ and Fe(CO)₅ can be isolated (Scheme 5, center) if the condensate is warmed in carbon monoxide atmosphere (<u>32</u>). No π-arene complexes of iron or nickel are known that are stable at room temperature. Nickel has a strong propensity to form π-allyl complexes, and this limits the preparation of η²-olefin nickel compounds. Scheme 5 (bottom), however, shows that (η²–styrene)₃Ni can be isolated from 77 K condensates. This compound decomposes at -20 °C, giving a black, air-stable polystyrene-nickel composite (<u>4</u>). A more stable derivative can be trapped as (bipy)Ni(η²–styrene) by adding bipyridyl to the condensate at temperatures below -30 °C. A similar compound can be made by the more traditional method of displacing ethene ligand with styrene,

$$ (C_2H_4)Ni(PPh_3)_2 \xrightarrow{\text{PhCH=CH}_2} (PPh_3)_2Ni(PhCH=CH_2) $$
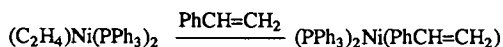
The Fischer-Hafner synthesis of sandwich compounds (<u>33</u>) does not permit functional groups to be incorporated into the arenes because of side reactions with the Lewis acid catalyst (Friedel-Crafts reducing conditions). This is not the case when metal atoms are used directly. Many metal-arene complexes have been identified that contain F, Cl, CH₃O, R₂N and CO₂R substituents. It is reasonable to assume that polymer-bound phenyl substituents containing these functional groups will yield similar sandwich complexes.
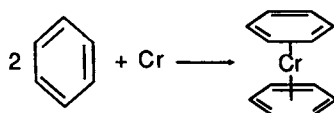
SCHEME 3

POLYSTYRENE

SCHEME 4

L = CO, PF$_3$
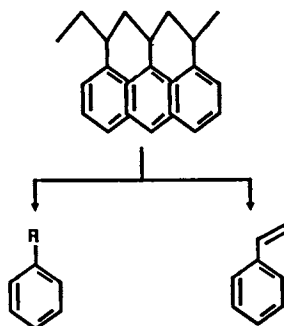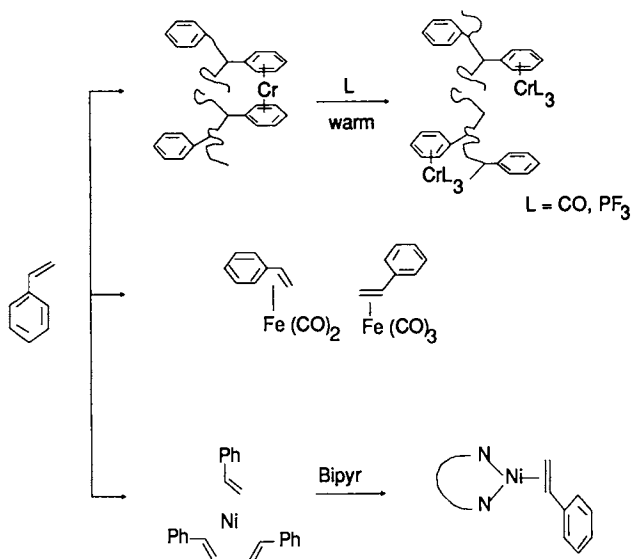
SCHEME 5

Bonding of the metal atom to the ring is responsible for an extensive chemistry at the arene ligand or metal center. Attachment of the metal atom to the arene can have several effects: (i) activation of the ring to nucleophilic attack; (ii) enhancement of aryl-H acidity; (iii) steric inhibition of attack on functional groups from one side or the other of the ring. In chromium-arene compounds, transmission of substituent effects across the ring is reduced, probably because of loss of aromatic character (34). Electrophilic attack at the ring is unlikely, but nucleophilic substitution occurs when a good leaving group is present (35). Incorporation of fluorine atoms into the arene rings of π-complexes raises the acidity of arene protons, which undergo facile metallation. Functionalized chromium-arene molecules can be made from the metallate (36). Oxidative stability is enhanced by certain combinations of fluorine atoms and trifluoromethyl groups. The chemistry of π-complexes of other early transition metals has been studied and that of molybdenum and tungsten has been elaborated into a spectrum of transformations that includes substitution at the metal center and activation of the phenyl ring in ways unique to the central metal atom (37). Finally, $(arene)_2M$ (M= Zr, Hf) 16-electron complexes will coordinate a 2-electron donor like trimethylphosphine to the metal atom, demonstrating another driving force for reaction at the metal center.

It is tempting to suppose from these findings that similar kinds of compounds and bond activation might occur when metal atoms react with the phenyl substituents of polymers. Indeed there is an analogous chemistry of Group 4-6 atoms with various phenyl-rich homopolymers and copolymers (4). Polystyrene is partially converted to a sandwich-bearing organometallic polymer on reaction with chromium atoms (38). In spite of evidence that chromium can react with monoenes and dienes (39) the phenyl group is selected exclusively in block copolymers of styrene with isoprene (40). (Air oxidation of the product deposits minute Cr_2O_3 inclusions in the polymer. This type of oxidation may perhaps be seen as an early manifestation of interfacial oxide formation developed from a discrete organometallic compound, rather than from an abstraction process.) The most extensively studied reactions have been those of metal atoms with phenyl derivatives of liquid dimethyl siloxane polymers (Scheme 6) (4). The thermal stability of some bis(arene)metal complexes derived from the poly(methylphenylsiloxane)s exceeds that of analogous compounds not bonded to polymer (38). Here also, coordination of a metal atom activates ring substituents. The phenyl-silicon bond is resistant to hydrolysis in the uncomplexed polymers, yet in Cr/poly(methylphenylsiloxane) it can be slowly cleaved by methanol at 25 °C. After partial oxidation, the carbon-silicon bond becomes even more labile, and rapid hydrolytic cleavage occurs when traces of water are present (38).

Apart from the metal atom aggregation reactions described below, bis(arene)metal complexes of the early transition metals are resistant to ligand displacement. The rings on the corresponding bis(naphthalene)metal species (41) are by, contrast, labile. Polymer-supported analogs of these naphthalene compounds with vanadium and chromium are known (42), but Ti atoms attack the polymer at the silicon ether linkage. These and other hybrid polymers can be further modified once the metal atom is incorporated. Thus α-methyl naphthalene is displaced from the hybrid organometallic polymer shown in Scheme 7 (43).

The free or polymer-bound bis(arene)metal complex can also react with metal atoms. Francis et al. (44) first published evidence that the siloxane-bound π-complexes are converted to dimers and higher nuclearity clusters by additional metal atoms. Their experiments were conducted on quiescent thin liquid films of polymer applied to the optical window of a cryotip (see above, Small Scale Syntheses). Low nuclearity polymer-encapsulated molecules of Ti_n, V_n, Cr_n and Mo_n (n = 2-5) were inferred from quantitative studies of the metal atom aggregation process. The initial reaction appears to occur as follows:

$$ML_2 + M \rightarrow M_2L_2$$
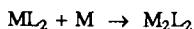
Support for this step was obtained by us in experiments where M was shown to add directly to bis(arene)metal complexes to give M_2L_2 (45, 46). Maximum nuclearity and stability of these species depends on the element, atom deposition rate, temperature and the type of arene. Mono-alkyl and -silyl substituted arenes give compounds that are unstable above 0°C. On the other hand, single crystals of a related triple-decker sandwich of mesitylene and chromium have been obtained (47).

M = Ti, V, Cr, Mo, W
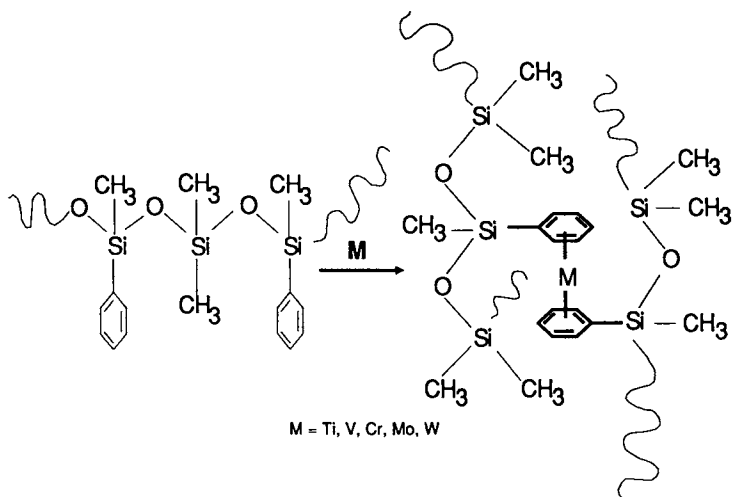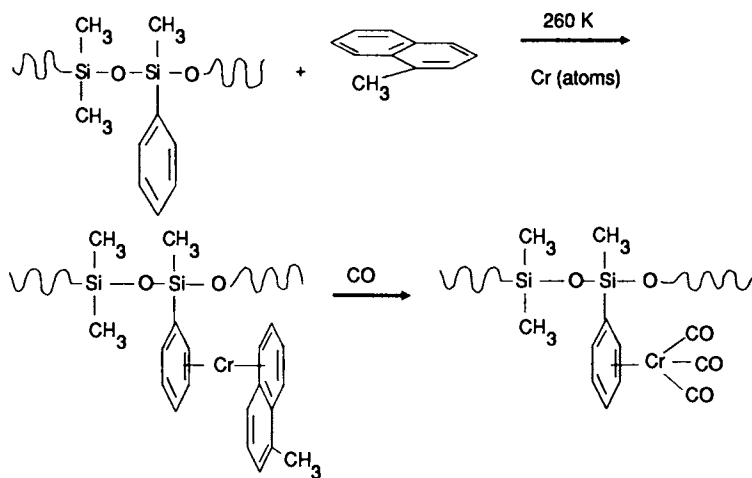
SCHEME 6

SCHEME 7

The constituents are arranged in an alternating way, Mes/Cr/Mes/Cr/Mes. In general, liquid phase addition reactions occur at a metal site, pre-formed in a support medium that contains arene functionalities (48). Free arene substituents and organometallic π-complexes can therefore trap a diffusing metal atom. Under well-defined conditions, such reactions are favored over competing metal atom polymerizations.

The evolution and decomposition of metal clusters in the polysiloxanes has been quantified (49), and a diffusion-plus-reaction model for cluster growth at the surface and in the near sub-surface region of a polymer film has been developed (50). Collectively, the studies show that organometallic chemistry at the polymer/vacuum interface can have profound effects on both the dynamics of polymer chains at the surface and the evolution of low nuclearity clusters (50, 51).

The ability of π-arene metal complexes to coordinate additional metal atoms may be significant in the early stages of metallization of some phenyl-rich polymers. At the lowest coverages of say chromium on polystyrene, $(arene)_2Cr$ may be formed. With continued accumulation of metal these compounds may rapidly convert to thermally unstable organometallic cluster species that eventually expel the metal core.

Summarizing, low nuclearity clusters of metal atoms are stabilized under specific conditions of temperature and metal loading in arene-functionalized polymeric and oligomeric hosts. Critical for growth and stabilization of species containing more than two atoms in the same complex are polymers having a high degree of mobility at the reaction temperature, initial coordination of a metal atom to form a stable sandwich complex, and the simultaneous development of a network of chains cross-linked by metal atoms through the formation of these sandwich complexes.

Π-Interactions at Polymer Surfaces

What evidence is there for metal atom/π-arene interactions at polymer surfaces? Some researchers have argued that open-faced sandwich complexes of chromium may exist in the low and intermediate metal coverage regimes on polyimides such as pyromellitic dianhydride-4,4′-oxydianiline polyimide (PMDA-ODA). Chromium is important as an adhesion promoter when layered between PMDA-ODA and another metal like copper or nickel (52). For Cu/polyimide or Ni/polyimide interfaces no significant reaction occurs on deposition of the metal, either at room temperature or at elevated temperatures. For depositions of chromium on polyimide, chemical changes are strong within the polymer chain and Cr/polyimide intermixing is small (52). In contrast, metals like Cr, Ni and Cu evaporated onto polystyrene, generally exhibit poor adhesion. The reasons for the low adhesive strength are not clear. Complexation of Ni or Cu to the phenyl ring will be weak; however, barring kinetic effects, a chromium atom ought to form a π-complex at the surface of low Cr coverage polystyrene. The XPS studies of White and co-workers (53) show that there is preferential ordering (>75%) of phenyl groups at the polystyrene surface. Although the existence of a bis(arene)Cr compound implies strict conditions on the inter-ring distance be satisfied, open-faced sandwich compounds might also exist, or co-exist with bis(arene)M species at the surface. Convincing evidence for an open-faced complex exists only for the C_{6v} η^6-benzenevanadium compound, first isolated at 12 K in argon matrices, and described fully by Andrews et al. (54). Ideally, this compound might be viewed as the chemical outcome of bringing a single metal atom into contact with a phenyl-rich polymer surface. It is worth detailing the electronic structure of benzenevanadium to clarify later arguments about the electronic structure of postulated $(\eta^6$-PMDA)Cr.

The vanadium atom sits on the principal six-fold axis above the six-member ring. Proof for this structure comes from electronic absorption, infrared, Raman and electron paramagnetic resonance (epr) spectroscopy. The epr spectrum displayed in Figure 2 is most informative. (Similar data have been obtained for reactions of hexafluorobenzene with vanadium in argon (54)). Vanadium has a nuclear spin, $I=7/2$, which produces an 8-line vanadium hyperfine spectrum. Epr spectra for benzene/argon dilutions of 1/250 and 1/50 (V/Ar $\approx 1/10^4$) are recorded in Figure 2A and B, respectively. The outcome of annealing the 1/50 matrix is represented in 2C. Selected vanadium hyperfine lines showing proton superhyperfine are provided as inserts a and b. The most important features are (i) the presence of eight vanadium hyperfine lines (rigid limit) belonging to the
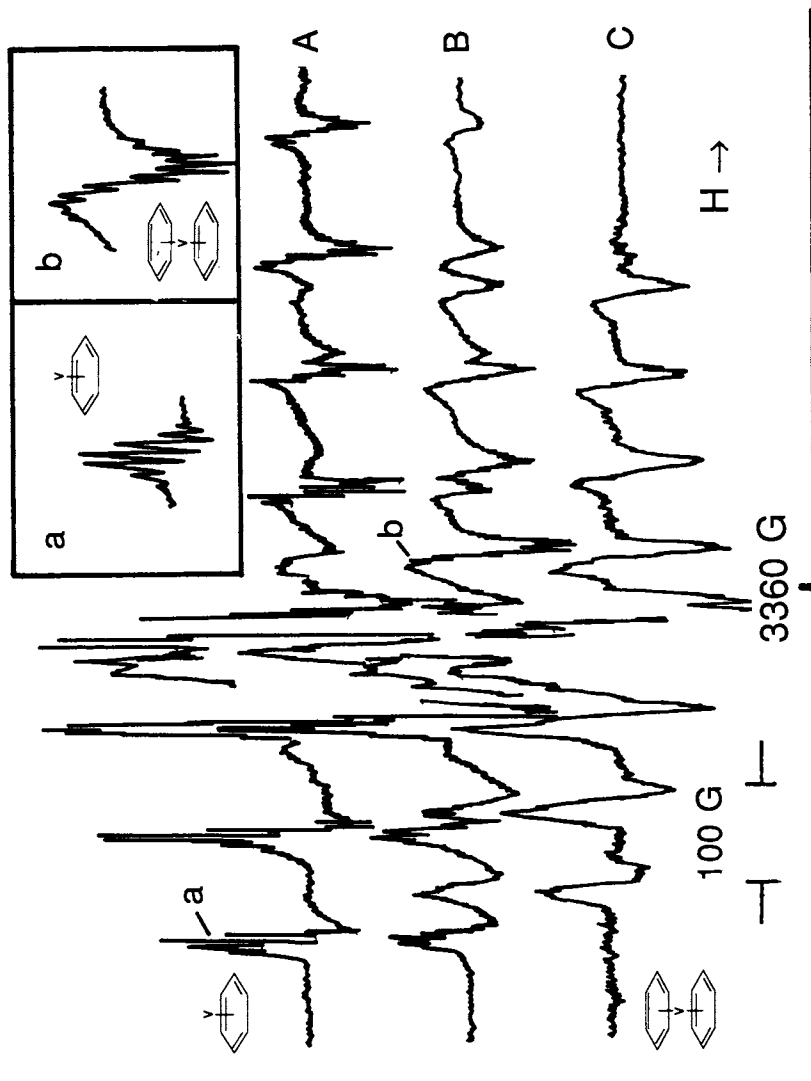
Figure 2. 12 K epr spectra of open-faced vanadiumbenzene sandwich and bis(benzene)vanadium sandwich complexes in solid argon. See text for details.

sandwich complex, $(C_6H_6)_2V$ in 1/50 but not 1/250 dilution matrices; (ii) emergence of eight new vanadium hyperfine lines (rigid limit) coexisting with those of the sandwich complex at the 1/50 dilution, but standing alone at 1/250 C_6H_6/Ar; (iii) formation of $(C_6H_6)_2V$ at the expense of $(C_6H_6)V$ molecules when the 1/50 matrices are annealed to 40 K; and (iv) resolved proton superhyperfine splitting for both species. The thirteen-line and seven-line couplings for the bis(arene) and mono(arene)vanadium complexes, respectively, are diagnostic of an interaction of an unpaired electron with twelve and six equivalent protons. The complicated signal near 3300 G belongs to hydrocarbon radicals trapped after cracking of benzene on the hot vanadium filament. Observation of resolved proton superhyperfine implies spacious multiple substitutional trapping sites in argon for both types of molecules, and facile rotation of them about their C_6 molecular axis. Computer simulation of these spectra, combined with uv-visible electronic, infrared absorption spectroscopy and theoretical calculations all support a C_{6v} $^2A_1$ ground state symmetry for the open-faced sandwich. This is illustrated in the energy level diagram shown in Figure 3. The unpaired electron, which is non-bonding, is located in the $6a_1$ molecular orbital. This MO has largely vanadium d_{z^2} character. Bonding involves a synergism that includes transfer of electron density from the occupied 2p π-system of benzene (e_{1g} level) to the formally empty d_{xz},d_{yz} orbitals of vanadium ($4e_1$ molecular orbital); and back-transfer of charge from the $d_{x^2-y^2}$, d_{xy} orbitals of vanadium in $(C_6H_6)V$ ($3e_2$ level) to the benzene antibonding orbitals. Similar electronic structures will obtain for chromium, titanium and other early transition metals with benzene. Apart from lifting orbital degeneracies due to reductions in symmetry, this electronic structure should carry over to alkyl-substituted benzene. We have in mind the phenyl substituents of polystyrene. The electronic structure of $(\eta^6-PMDA)Cr$ will differ (*vide infra*).

Burkstrand has used XPS (16) to probe the electronic structure of chromium overlayers on polystyrene. He found that the bulk value of the Cr $2p_{3/2}$ core energy was reached when the metal coverage was much less than one monolayer. Evidently, the bond between Cr and the polymer is not strong enough to reduce the migration of metal atoms on the surface. This is somewhat surprising because of the expected thermodynamic stability of the chromium-arene complex. Mean bond disruption enthalpies (D(M-Arene)) are about 150-170 kJ-mol^{-1} (55). Although from Burkstrand's experiments the carbon 1s core levels showed no measurable changes apart from attenuation caused by increasing metal coverage, the XPS peak width for Cr on polystyrene decreased with decreasing coverage, contrary to expectation. These results are interesting, and we might ask if there is something peculiar to the polymer surface that prevents π-arene complexes from forming. The data of White (53), suggest that phenyl groups concentrate at a polystyrene surface, but little is known about their orientation and distribution. That the polymer is *macroscopically* rigid may be unimportant for the reaction. Chromium atoms can react with (macroscopically) solid surfaces. Experiments by Lagowski (56) show that bis(η^6-arene)chromium compounds are produced from reacting chromium atoms directly with solid substrates at 77 K in the absence of any solvent. Effects of chain mobility and microviscosity at the surface might be probed by depositing chromium onto polystyrene films heated above its glass transition temperature (T_g). Evidence (49, 50) suggests that π-arene complexes ought to form under these conditions. The efficiency of the reaction could be followed as the film was gradually cooled through T_g. It would also be useful to calibrate XPS data against small molecule and polystyrene-supported bis(arene)Cr compounds to study this problem further. Perhaps the results on metal clustering in the polysiloxanes contain a clue to the poor adhesion of chromium on polystyrene, and Burkstrand's XPS data (16). If π-complexes are initially formed they may be quickly converted by the additional Cr to weaken the Cr-arene interaction, causing extrusion of Cr from the rings and aggregation to multimers at the surface of the film.

Metal Atom Reactions with Polyimides, A Critique of Model Compound Studies

Interpretations of the early stages of metallization of PMDA-ODA are controversial, but the data are more extensive than for polystyrene. PMDA-ODA has been featured for use in integrated circuit fabrication and lately, for mapping the engineering (57), physics and chemistry of polymer metallization (58). Many analysts of XPS, ultraviolet photoelectron spectroscopy (UPS), near edge
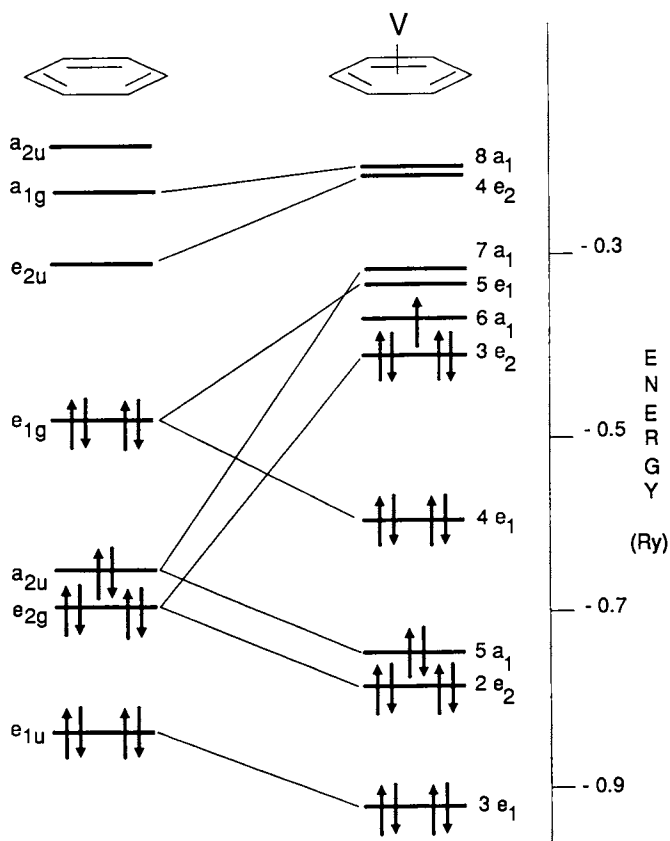
Figure 3. Energy level diagram for an open-faced vanadiumbenzene sandwich complex in C_{6v} symmetry.

x-ray absorption fine structure (NEXAFS), and electron energy loss spectroscopy (EELS) have identified PMDA as the most reactive monomer repeat unit and the primary site of reaction with deposited metal (58). PMDA-ODA films that have been reduced electrochemically or by *in situ* cesium deposition, show strong similarity in XPS to low Cr coverage polymide films (58e). The findings appear to substantiate a mechanism involving initial electron transfer. Solution phase organometallic experiments show that reduction occurs at the PMDA carbonyl group. In contrast, theoretical studies (59). of possible bonding modes between chromium and PMDA-ODA have rationalized XPS core level spectra by invoking π-arene complexes of Cr/PMDA-ODA like benzenevanadium, rather than carbonyl group reduction A critical summary of the literature will be helpful to understand the surface organometallic chemistry involved here (60-62).

Reduction of the PMDA Carbonyl Group. Two-step reduction of polyimide yields first a radical anion at reduction potential -0.72 V vs. SCE, and then a dianion at a reduction potential of -1.38 V vs. SCE (58e, 62). Admittedly, it is difficult to compare the electrochemical reduction of polyimide in solution to the reduction of a polyimide surface by a gas-phase reducing agent (atomic chromium); however, chromium is sufficiently reducing to generate the radical anion polyimide species (58c). Surface studies of Clabes *et al.* and others (58) on chromium coated PMDA-ODA films give a consistent picture of chemical reduction at the carbonyl group of PMDA. This view accords with analyses of electronic absorption, infrared and spectroelectrochemical studies of PMDA-like model compounds (58e, 62). Molecules like N,N'-di-n-pentyl pyromellitimide and 4,4'-diphenoxyphenyl pyromellitimide have one and two electron reduction potentials similar to those of cured PMDA-ODA (61). This shows that when charge is donated into the lowest unoccupied molecular orbital of PMDA the inherent chemistry (reduction) is not altered on going from the polymer surface to the solution phase. As we show below, the electronic wavefunctions corresponding to the ground and first excited states of the monomeric and polymeric anions are strongly localized on the pyromellitic diimide group. Clabes and co-workers contend that this ensures that the chemistry of PMDA will be independent of its ODA neighbor, and one is justified in extrapolating the chemistry of model compounds, and related cryogenic matrix isolation, solution phase and metal atom synthetic work to the polymer (62). Note that although the PMDA/ODA monomer units can be viewed to be chemically independent, the outcome at the interface might ultimately be under kinetic control of the polymer.

PMDA-ODA and the Issue of π-Arene Complex Formation. Some studies have tried to identify chromium-arene complexes with PMDA and ODA. Kinetics and thermodynamics should favor Cr atom reaction with the diamine ODA portion of PMDA-ODA as opposed to the anhydride PMDA portion of the polymer. Stoichiometrically, the ODA unit offers two arene rings as Cr atom targets for every one ring of PMDA. Formation of π-complexes with the ODA portion would be expected on kinetic grounds alone, provided two properly oriented monomer molecules were available. Thermodynamics also favors reaction at ODA. Arenes substituted with amine or methoxy groups will form more stable complexes with chromium than with arenes conjugated with carbonyl groups (63, 64). For example, bis(benzophenone)Cr can be made only in trace amounts by direct metal atom synthesis from benzophenone (65). On the other hand, acylation of bis(benzene)Cr gives bis(benzophenone)Cr in 30% yield (66); however, the compound undergoes autogenic deoxygenative reductive coupling in which the central Cr(0) atom plays the role of the coupling agent. This phenomenon reflects, among other things, the oxophilicity of the element.

    In theoretical and experimental studies of XPS and vibrational spectra, Rossi (67), Ho (59) and Silverman (68) have advocated open-faced PMDA sandwich π-complexes, where the Cr atom is located on the principal molecular axis above the central arene ring. Formation of such species implies an unusually high selectivity of chromium for the *arene* part of the PMDA group, despite kinetic and thermodynamic considerations to the contrary. Ho *et al.* also claim that chromium prefers these PMDA binding sites over ODA *up to nearly monolayer coverages of metal* (59).

    As interesting as the Rossi-Ho-Silverman argument is, the PMDA/Cr open-faced sandwich should perhaps be viewed as a putative model for low coverage PMDA-ODA. Were open-faced π-complexes to form they would most likely do so at the lowest Cr coverages, provided (i) there were little or no competition with the ODA portion to form bis(ODA)Cr compounds; (ii) significant metal

atom diffusion and aggregation were precluded; (iii) the half-sandwich species were sufficiently long-lived; and (iv) there were no reduction of the carbonyl group. Coordinately unsaturated half sandwich complexes of benzene or hexafluorobenzene are extremely reactive (54). By extension, a half-sandwich complex of Cr with PMDA would probably not survive long enough to be detected with XPS or HREELS, even under high vacuum. Water from the imidization process (69), unconverted carboxylic acid, amine and dioxygen would react rapidly with the exposed Cr atom. Exposure of low coverage Cr/PMDA-ODA films to CO has failed to produce (arene)Cr(CO)₃ complexes. This argues against the existence of any long-lived PMDA/Cr open-faced sandwich complex (62), despite opposing claims by Ho *et al.* (59). But these claims are based on theoretical modeling and interpretations of high resolution XPS and UPS spectra that make little physical or chemical sense. In the first place, at chromium coverages up to nearly a monolayer it is unreasonable to expect that metal atoms would position themselves, without aggregation, exclusively above PMDA units. That they would do so as coordinately unsaturated organometallic compounds, in complete violation of the "eighteen electron" rule (10), requires extraordinary kinetics. Such selectivity implies existence of deep potential wells for binding chromium, since otherwise atoms would recombine on the polymer surface or form bis(arene)M complexes. Second, their interpretation means that Cr shows an unusual predilection for the π-system of the PMDA unit. Yet molybdenum atoms, whose reactivity parallels that of chromium, show little inclination to discriminate among different organic arenes when forming π-compounds in mixed arene experiments (70). Finally, established chemistry shows π-sandwich formation with metal atoms to be a low activation energy, orbital mixing process. Ho's restricted potential energy surface search provides no basis for concluding that the lowest energy states of the system can be represented by chromium coordinated above the 5- or 6-membered rings of PMDA alone (59). Indeed, in a later publication on the subject Rossi, Ho and Silverman (67) abandoned a model with Cr located above the imide 5-member ring.

If the issue of π-complex formation with PMDA-ODA polyimide seems confused, the results of model compound studies have, in places, exacerbated the problem. Several research groups have turned to reactions of formally zerovalent chromium to model the chemistry of PMDA-ODA/Cr (58e, 60, 62) The studies assume that the chemistry of atomic Cr and of certain chromium carbonyl complexes is coextensive. Since atomic chromium has not been available as a benchtop reagent, popular sources of formally zerovalent chromium, disguised as Cr(CO)₆ and (CH₃CN)₃Cr(CO)₃, have been used. These compounds readily form (arene)Cr(CO)₃ complexes (71).

When Goldberg *et al.* (58e) attempted to synthesize (arene)Cr(CO)₃ molecules by reacting chromium carbonyls with N,N'-di-n-butyl pyromellitimide, (PMDA-BA) only the one-electron reduction product of PMDA-BA was obtained. The reactions were done under conditions that should have favored formation of the (PMDA-BA)Cr(CO)₃ complex. Nandi and Sen (60) combined (CH₃CN)₃Cr(CO)₃ with the compounds shown in Scheme 8 They found no evidence for reduction of the *phthalimide* moiety (reaction at oxygen). (Arene)Cr(CO)₃ π-complexes were formed with phthalimide arene, N-substituted and ODA-like arenes. They concluded that Cr(0) prefers to form π-arene complexes (even with electron deficient rings) rather than react with oxygen functionalities. The *thermodynamically* preferred binding site for Cr(0) in PMDA-ODA polyimide is, in their view, not PMDA but ODA. Nandi and Sen pointed out that their study did not address the question of kinetic accessibility of different binding sites on PMDA-ODA. They conceded that Cr atoms may well bind to the carbonyl groups on the polymide, should that group be more accessible. In light of published surface studies we must then ask what their findings *do* contribute to understanding the polyimide/metal bond. As a probe of the organometallic chemistry of PMDA-ODA polyimide *via* model compounds, the study by Nandi and Sen is flawed. N-substituted pyromellitimide, *not* N-substituted phthalimide, is a model for PMDA. At -1.33 V, the reduction potentials of N-substituted phthalimides are too high to permit the molecules to be reduced by (CH₃CN)₃Cr(CO)₃ (58e, 61). (Those of N-substituted pyromellitimides are the same as PMDA-ODA polyimide, -0.70 V (61).)

There are additional reasons why the (arene)Cr(CO)₃ compounds can be misleading as models for PMDA-ODA polyimide/Cr interactions. Formation of (arene)Cr(CO)₃ compounds of model PMDA or ODA systems suggests that π-complexes can be formed at the polyimide surface in the early stages of metal deposition. But the (arene)chromium(tricarbonyl) complexes can give little additional chemical or physical insight into surface phenomena because the properties of

bis(arene)Cr complexes differ from those of (arene)Cr(CO)$_3$ complexes (71). The carbonyl ligand is a better π-acid than is arene. It is the presence of the carbonyl ligands in (arene)Cr(CO)$_3$ compounds that confers unusual reactivity on the latter. Only the (arene)Cr(tricarbonyl) compounds presently show a rich organometallic chemistry based on nucleophilic and electrophilic substitution at the arene. The tricarbonyl compounds are usually resistant to oxidation by O$_2$, whereas most bis(arene)Cr compounds are not. The presence of bis(arene)Cr complexes of PMDA-ODA will affect the micro-dynamical properties of the polymer chains at the surface in ways that (arene)Cr(CO)$_3$ cannot because each bis(arene)Cr complex produces an intra- or inter-molecular cross-link. Finally, XPS core level shifts determined from PMDA-, phthalimide-, or ODA-Cr(CO)$_3$ model compounds like those of Nandi and Sen will be meaningless for comparison with the real polyimide. Accumulation of charge density on the carbonyl ligands will produce arene-carbon, carbonyl-carbon, and carbonyl-oxygen core level shifts that differ from those for the symmetric sandwich compounds. Bis(arene)Cr model compounds relevant to PMDA-ODA are necessary to calibrate XPS experiments concerned with low surface coverage Cr on polyimide. In summary, it is only the chemistry of mono- and bis(arene)Cr complexes, *should they exist at polyimide interface*, that may be relevant to adhesion. The following section gives a preliminary report of some chromium *atom* reactions with PMDA-ODA functional group analogs.

Reactions of Cr Atoms with ODA Analogs

Since reactions of Cr can often be conducted when the ring is substituted with potentially competing functional groups, it is surprising that no evidence for π-complexes with ODA has been found in the surface studies of PMDA-ODA/Cr. We sought first to determine if ODA-like molecules would form isolable π-complexes with chromium. 4-phenoxyaniline and phenyl ether were selected for reaction with atomic Cr. In separate experiments each compound was co-condensed with thermally evaporated chromium in an evacuated spinning glass reactor, cooled to 77 K.

Atomic Cr does indeed react with phenyl ether to yield a dark green, air-sensitive π-complex. Results of elemental analysis, high resolution mass spectrometry, ^{1}H nmr and epr are consistent with the formulation. Epr confirms that the di-η^6 complex has pseudo-axial symmetry. Air oxidation of a green, diamagnetic 2-methyltetrahydrofuran (2-MTHF) solution of the molecule gives a yellow liquid whose epr spectrum is shown in Figure 4. The room temperature signal consists of a resonance located at g = 1.9857. Superimposed hyperfine structure ($<A> = 3.5 \times 10^{-4}$ cm^{-1}) of 11 equally spaced transitions results from interaction of a single unpaired electron with 10 magnetically equivalent hydrogen atoms. At 4.2 K in 2-MTHF glass, the parallel and perpendicular components of the g-tensor are different enough to be resolved. The epr parameters are typical of π-arene chromium complexes (72, 73).

4-Phenoxyaniline offers two sites for π-complex formation, and the possibility of three different products on reaction with atomic chromium. The metal atom experiment can give kinetically controlled products. Owing to the two donor substituents, NH$_2$ and OC$_6$H$_5$, ring A in Scheme 8 is more electron rich than ring B. So far we have been able to isolate only the compound having the Cr atom bound to the less electron rich ring, B. Other organometallic compounds are present in the unpurified product. These may be isomers.

The metal atom reactions with phenyl ether and 4-phenoxyaniline establish that there is no electronic reason why π-complexes of Cr with ODA in PMDA-ODA should not form. Mindful that these studies are still preliminary, our finding for 4-phenoxyaniline/Cr contrasts with that by Nandi and Sen (60). They observed ring A to be the exclusive binding site for Cr(CO)$_3$ derived from Cr(CO)$_3$(CH$_3$CN)$_3$, explaining the result on thermodynamic grounds. Their experiment failed to distinguish possible kinetic products of reaction of arene with the chromium carbonyl.
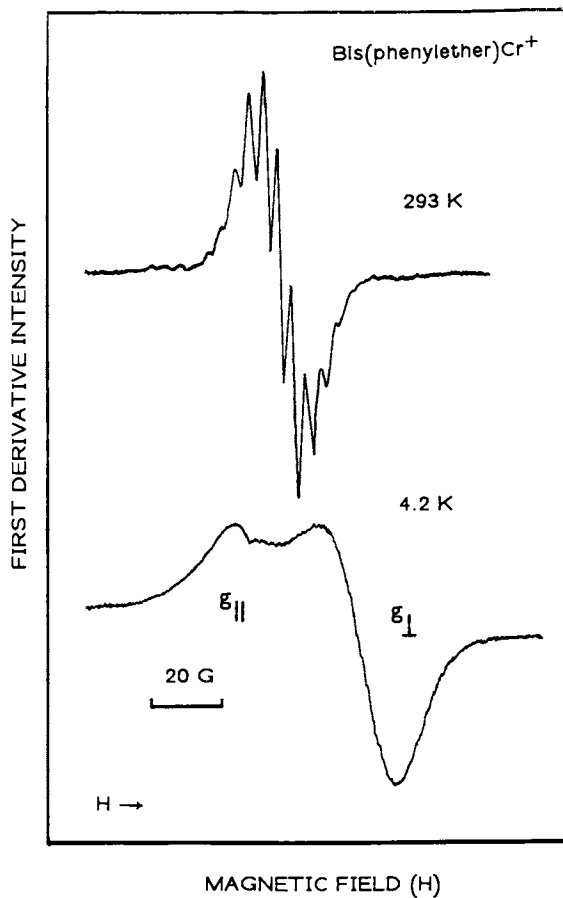
Figure 4. Epr spectrum of bis(phenyl ether)Cr$^+$ in 2-MTHF solution at room temperature and 4.2 K.

Reactions of Cr with Imides and Related Compounds

Nandi and Sen observed (Scheme 8) that $Cr(CO)_3$ bound to both rings A and B with a 2:1 preference for ring B in the phthalimide derivative (2). We were unable to isolate any organometallic π-complexes from reactions of Cr atoms with the phthalimides (2). Regardless of the conditions, experiments with chromium vapors yielded only chromium metal, complex mixtures of organic compounds derived from the phthalimides, and unreacted phthalimide. Since we were unable to isolate a complex having Cr bound to ring B in compound (2), we looked more closely for evidence of reaction elsewhere on the molecule. The carbonyl moiety of the imide group is a good candidate for study because of the precedent for its reduction (58c,e, 61, 62). Our preliminary studies with di-n-butyl pyromellitimide show that chromium vapors reduce the carbonyl group. When Cr is deposited into 2-MTHF solutions of di-n-butyl pyromellitimide the fluid gradually turns dark blue-green. The experiment was conducted under conditions that would also allow formation of the π-arene complex. The electronic absorption spectrum of the fluid at 180 K under argon is shown in Figure 5. The spectrum is similar to one recorded by Mazur (61) and Goldberg et al. (62) for electrochemical reduction of di-n-pentyl pyromellitimide. When exposed to air, the solution re-oxidizes to neutral di-n-butyl pyromellitimide.

To explore the reduction process further, a theoretical study of pyromellitic diimide as a model for imidized PMDA was undertaken. The geometry was adopted from the crystal structure determination by Bulgarovskaya and co-workers (74). Density functional theory was used to calculate the energy level distribution and charge densities for the D_{2h} molecule. The result is displayed in Figure 6. Correlations with the upper levels of benzene are also shown to give a simplified picture of the nodal character of the central arene ring in the diimide. The acceptor orbital for electron reduction can be readily identified with the $2a_u$ virtual level near -0.52 Ry. This level is delocalized only over four of the central arene-carbon atoms, the carbonyl-carbon and oxygen atoms. The largest orbital amplitude occurs at the four carbons of the arene ring. There is also amplitude at the oxygen atoms with somewhat smaller amplitude at the carbonyl carbons. This result justifies our earlier statements the electronic wavefunctions corresponding to the ground and first excited states of the monomer and polymer anions are strongly localized on the pyromellitic diimide group. This ensures that the chemistry of PMDA will be independent of its ODA neighbor, and in this sense one is justified in extrapolating the chemistry of model compounds, and related cryogenic matrix isolation, solution phase and metal atom synthetic work

With this energy level diagram before us we can understand how a chromium atom might be bonded when located directly above the arene portion of PMDA. In PMDA/CR the $2a_u$ orbital is correctly phase-matched to mix with the d_{xy} level of Cr. This fact has already been pointed out by Rossi (67) and Silverman (68). Figure 5 details the spin manifold of the PMDA levels lying between the "benzene"-like $1bsub3g$, $2b_{2g}$ and $2b_{1u}$ molecular orbitals. We can anticipate the synergic nature of the PMDA-arene/Cr bonding interaction. Recall that for a given C-6 ring charge density is donated in a forward manner from the occupied π-system of the arene into acceptor d-π ($d_{xz,yz}$) orbitals on the metal center. The accumulated charge is reduced by back-donation that occurs from the metal atom to the formally empty anti-bonding π-system of the arene. In the language of pseudo-axial ligand field theory, it is the d-δ set of orbitals ($d_{x^2-y^2}$, d_{xy}) that donates charge back to the arene. The $d_{xz,yz}$ orbitals of chromium will participate as acceptor orbitals the same way in PMDA as they do in the open-faced benzene complexes, but the occupied $d_{x^2-y^2}$ and d_{xy} levels cannot donate charge density as effectively to PMDA. To understand this, note that the $4e_{2u}$ π^* levels of benzene split in D_{2h} PMDA into a high lying $4b_{1u}$ and lower lying $2a_u$ level. In benzenechromium the low lying e_{2u} antibonding level of benzene interacts strongly with both orbitals of the degenerate d-δ set. In PMDA, the $4b_{1u}$ level is too high in energy to interact strongly with the chromium $d_{x^2-y^2}$ orbital.

PMDA   ODA

1   2

$$R = \left[O-\bigcirc\kern-1.2em\textcircled{c}\, , H\, , Et\, , t\text{-}Bu \right.$$
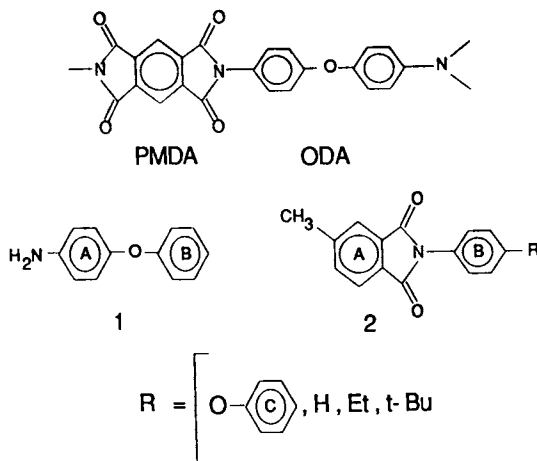
SCHEME 8
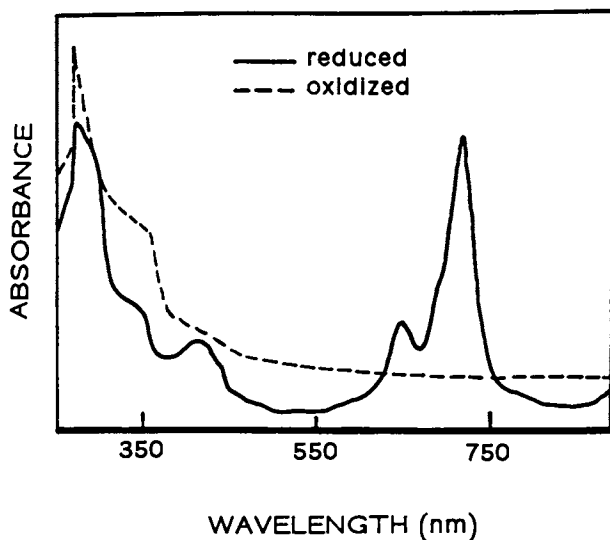
Figure 5. Electronic absorption spectrum of the product of reaction between Cr and di-*n*-pentyl pyromellitic diimide under argon at 180 K and after exposure to air.
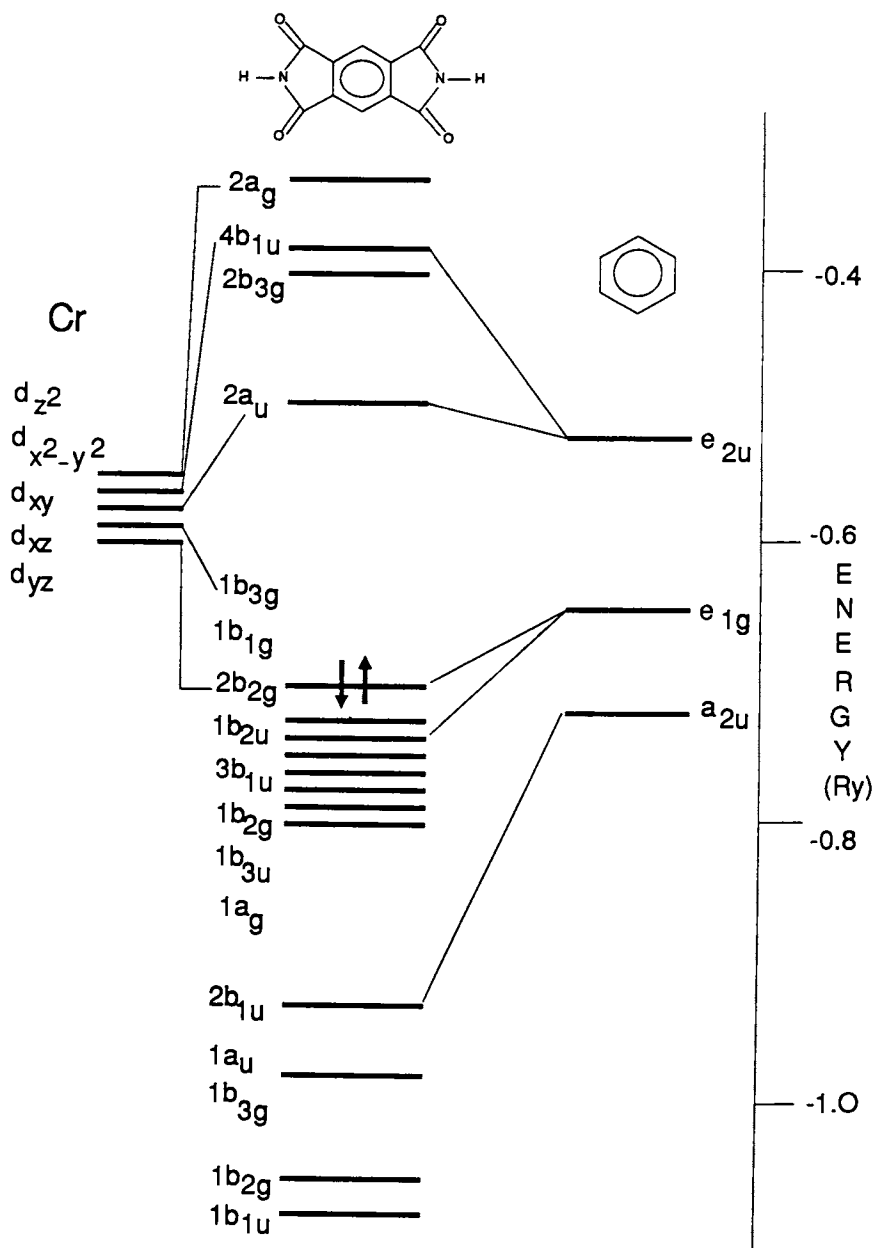
Figure 6. Energy level distribution for pyromellitic diimide. The highest occupied molecular orbital is the $1b_{3g}$. The chromium levels are supplied to show only how they can interact by symmetry with the orbitals on pyromellitic diimide.

Literature Cited

[1]   Yamamoto, A. Organotransition Metal Chemistry John Wiley and Sons: New York, 1986.
[2]   Andrews, M. P.; Ozin, G. A. Chem. Materials 1989, 1, 174.
[3]   Thin Films from Free Atoms and Particles; Klabunde, K. J., Ed.; Academic Press: New York, 1985.
[4]   Andrews, M. P. in Encyclopedia of Polymer Science and Engineering; 2nd Ed., Wiley: New York, 1987, Vol. 9, p 623, and references cited therein.
[5]   Andrews, M. P. In Experimental Organometallic Chemistry; ; Wayda, A. L.; Darensbourg, M. Y.; Eds.; ACS Symposium Series; American Chemical Society: Washington, DC, 1987; Vol 357, p 158; Klabunde, K. J. Chemistry of Free Atoms and Particles; Academic Press: New York, 1980; Blackborow, J. R.; Young, D. Metal Vapour Synthesis in Organometallic Chemistry; Springer-Verlag: New York, 1979.
[6]   Ozin, G. A.; Andrews, M. P.; Francis, C. G.; Huber, H. X.; Molnar, K. Inorg. Chem. 1990, 20, 201.
[7]   Ozin, G. A.; Francis, C. G.; Huber, H. X.; Andrews, M. P.; Nazar, L. F. J. Am. Chem. Soc. 1981, 103, 2453; Ozin, G. A.; Francis, C. G.; Huber, H. X.; Nazar, L. F. Inorg. Chem. 1981, 20, 3635.
[8]   Heffner, S. A.; Andrews, M. P.; Galvin, M. E. Polym. Commun. 1988, 29, 335.
[9]   Klabunde, K. J. Ann. New York Acad. Sci. 1977, 295, 83.
[10] Pearson, A. J. Metallo-organic Chemistry; Wiley: New York, 1985, p 29.
[11] Klabunde, K. J.; Anderson, B. B.; Neuenschwander, K. Inorg. Chem. 1980, 19, 3719.
[12] Klabunde, K. J. Chemistry of Free Atoms and Particles; Academic Press: New York, 1980.
[13] Lin, S. T.; Klabunde, K. J. Inorg. Chem. 1985, 24, 1961.
[14] Timms, P. L. Proc. Roy. Soc. Ser A 1984, 396, 1.
[15] Blackborow; J. R.; Young, D. Metal Vapour Synthesis in Organometallic Chemistry; Springer-Verlag: Berlin, 1979.
[16] Burkstrand, J. M. J. Appl. Phys. 1981, 52, 4795; ibid., Phys. Rev. 1979, B20, 4853; ibid., J. Vac. Sci. Vac. Technol. 1982, 20, 440.
[17] Chou, N. J.; Dong, D. W.; Kim, J.; Liu, A. C. J. Electrochem. Soc. 1984, 131, 2335.
[18] Jordan, J. L.; Kovac, C. A.; Morar, J. F.; Pollak, R. A. Phys. Rev. 1987, B36, 1369.
[19] Gladysz, J. A.; Fulcher, J. G.; Togashi, S. J. Org. Chem. 1976, 41, 3647; Togashi, S.; Fulcher, J. G.; Cho, B. R.; Hasegawa, M.; Gladysz, J. A. J. Org. Chem. 1980, 45, 3044.
[20] Ledon, H.; Tkatchenko, I.; Young, D. Tetrahedron Lett. 1979, 173.
[21] Koerner von Gustorf, E. A.; Jaenicke, O.; Wolfbeis, O.; Eady, C. R. Angew. Chem. Int. Ed. Engl. 1975, 14, 278; Skell, P. S.; McGlinchey, M. J. ibid., 195.
[22] Nuzzo, R. G.; Wong, Y.-H.; Schwartz, G. P. Langmuir 1987, 3, 1136.
[23] Davis, S. C.; Klabunde, K. J. J. Am. Chem. Soc. 1978, 100, 5973.
[24] Andrews, M. P.; Lamberti, V. E. Amer. Chem. Soc. Meeting, New Orleans, LA, 1987.
[25] Skell, P. S. U.S. Government Report, AFOSR-75-0200, 1975.
[26] Skell, P. S.; McGlinchey, M. J. Angew. Chem. Int. Ed. Engl. 1975, 14, 195, and references cited therein.
[27] Young, D.; Green, M. L. H. J. Appl. Chem. Biotechnol. 1975, 25, 641.
[28] Andrews, M. P.; Galvin, M. E.; Heffner, S. A., unpublished results.
[29] Skell, P. S.; Van Dam, E. M.; Silvon, M. P. J. Am. Chem. Soc. 1974, 96, 626.
[30] Timms, P. L. Chem. Commun. 1969, 1033.
[31] Nguyen Hao; McGlinchey, M. J. J. Organomet. Chem. 1978, 161, 381.
[32] Blackborow, J. R.; Eady, C. R.; von Gustorf, K.; Scrivanti, A.; Wolfbeis, O. J. Organomet. Chem. 1976, 108, C32.
[33] Fischer, E. O.; Hafner, W. Z. Naturforsch. 1955, 10B, 665.
[34] Graves, V; Lagowski, J. J. Inorg. Chem. 1976, 15, 577; Graves, V.; Lagowski, J. J. J. Organomet. Chem. 1976, 120, 397.
[35] Tan, T.-S.; McGlinchey, M. J. J. Am. Chem. Soc. 1976, 98, 2271.
[36] Tan, H.-S.; McGlinchey, M. J. J. Chem. Soc., Chem. Commun. 1976, 155; Agarwal, A.; Tan, H.-S.; McGlinchey, M. J. J. Organomet. Chem. 1978, 141, 85.
[37] Canestari, M.; Green, M. L. H.; Izquierdo, I. J. Chem. Soc., Dalton Trans. 1984; Cloke, F. G. N.; Green, M. L. H.; Morris, G. E. J. Chem. Soc., Chem. Commun. 1978, 72.
[38] Francis, C. F.; Timms, P. L. J. Chem. Soc., Dalton Trans. 1980, 1402.

[39] Skell, P.; Williams-Smith, D. L.; McGlinchey, M. J. J. Am. Chem. Soc. 1973, 95, 3337.
[40] Andrews, M. P.; Galvin, M. E. Heffner, S. H. Mat. Res. Symp. Proc. 1989, 131, 21.
[41] Kundig, E. P.; Timms, P. L. J. Chem. Soc. Chem. Commun. 1977, 912.
[42] Francis, C. G.; Moran, P. D.; Spare, N. J. Organometallics 1985, 4, 1958.
[43] Francis, C. G.; Ozin, G. A. J. Macromol. Sci. 1981, 16, 167.
[44] Francis, C. G.; Huber, H. X.; Ozin, G. A. Inorg. Chem. 1980, 19, 214.
[45] Ozin, G. A.; Andrews, M. P. Angew. Chem. Int. Ed. Engl. 1982, 1255;
      Angew. Chem. 1982, 94, 402.
[46] Andrews, M. P.; Ozin, G. A. J. Phys. Chem. 1986, 90, 1245.
[47] Lamanna, W. M.; Gleason, W. B.; Britton, D. Organometallics 1987, 6, 1583.
[48] Andrews, M. P.; Ozin, G. A. Inorg. Chem. 1986, 25, 2587.
[49] Andrews, M. P.; Ozin, G. A. J. Phys. Chem. 1986, 90, 3353; Andrews, M. P.; Ozin, G. A.
      J. Phys. Chem. 1986, 90, 3140.
[50] Andrews, M. P.; Ozin, G. A. J. Phys. Chem. 1986, 90, 2938.
[51] Andrews, M. P.; Ozin, G. A. J. Phys. Chem. 1986, 90, 3140; Andrews, M. P.; Ozin, G. A.
      Inorg. Chem. 1986, 25, 2587; Andrews, M. P.; Ozin, G. A.; Francis, C. G.
      In Inorganic Syntheses; Holt, S. L., Jr., Ed.; Wiley: New York, 1983; Vol. 22., p 116.
[52] Hahn, P. O.; Rubloff, G. W.; Bartha, J. W.; LeGoues, F.; Tromp, R.; Ho, P. S.
      Mater. Res. Soc. Symp. 1985, 40, 251.
[53] Akhter, S.; Fahlquist, L.; White, J. M.; Hardegree, E. L. Appl. Surf. Sci. 1989, 37, 406.
[54] Andrews, M. P.; Mattar, S. M.; Ozin, G. A. J. Phys. Chem. 1986, 90, 744; Ozin, G. A.;
      Andrews, M. P.; Mattar, S. M.; McIntosh, D. F. J. Am. Chem. Soc. 1983, 105, 6170.
[55] Pilcher, G.; Skinner, H. A. In The Chemistry of the Metal-Carbon Bond;
       Hartley, F. R.; Patai, S., Eds.; Wiley: New York, 1982, Ch. 2.
[56] Markle, R. J.; Pettijohn, T. M.; Lagowski, J. J. Organometallics 1985, 4, 1529.
[57] Faupel, F.; Yang, C. H.; Chen, S. T.; Ho, P. S. J. Appl. Phys. 1989, 65, 1911.
[58] (a) Jordan, J.L.; Kovac, C. A.; Morar, J. F.; Pollak, R. A. Phys. Rev. 1987, B20, 1369; (b)
      Chou, N. J.; Dong, D. W.; Kim, J.; Liu, A. C. J. Electrochem. Soc. 1984, 131, 2335; (c)
      Chou, N. J.; Tang, C. H. J. Vac. Sci. Technol. 1984, A2, 751; (d) Hahn, P. O.; Rubloff, G.
      W.; Bartha, J. W.; LeGoues, F.; Tromp, R.; Ho, P. S.
      Mater. Res. Soc. Symp. Proc. 1985, 40, 247; (e) Clabes, J. G.; Goldberg, M. J.; Viehbeck,
      A.; Kovac, C. A. J. Vac. Sci. Vac. Technol. 1988, 6, 991.
[59] White, R. C.; Haight, R.; Silverman, B. D.; Ho, P. S. Appl. Phys. Lett. 1987, 51, 481.
[60] Sen, A.; Nandi, M. Chem. Mater. 1989, 1, 291.
[61] Mazur, S.; Lugg, P. S.; Yarnitzky, C. J. Electrochem. Soc. 1987, 134, 346.
[62] Clabes, J. C.; Goldberg, M. J.; Viehbeck, A.; Kovac, C. A.
      J. Vac. Sci. Vac. Technol. 1988, A6, 985.
[63] Goldberg, M. J.; Clabes, J. G.; Kovac, C. A. J. Vac. Sci. Vac. Technol. 1988, A6, 991.
[64] Travkin, N. N.; Rumyantseva, V. P.; Gribov, B. G. J. Gen. Chem. USSR 1971, 41, 1929,
      and references cited therein.
[65] Elschenbroich, C.; Heck, J.; Stohler, F. Organometallics 1982, 1, 1399.
[66] Elschenbroich, C.; Bilger, E; Heck, J.; Stohler, F.; Heinzer, J. Chem. Ber. 1984, 117, 23.
[67] Rossi, A. R.; Sanda, P. N.; Silverman, B. D.; Ho, P. S. Organometallics 1987, 6, 580.
[68] Silverman, B. S. Macromolecules 1989, 22, 3768.
[69] Hahn, P. O.; Rubloff, G. W.; Ho, P. S. J. Vac. Sci. Vac. Technol. 1984, A2, 756.
[70] Wilburn, B. E.; Skell, P. S. J. Am. Chem. Soc. 1982, 104, 6989.
[71] Davis, R; Kane-McGuire, L. A. P. In Comprehensive Organometallic Chemistry; Wilkinson,
      G. Stone, F. G. A. S.; Abel, E. W., Eds.; Pergamon, New York, 1982; Vol. 3, Ch 26;
      Sneeden, R. P. A. Organochromium Compounds; Academic: New York, 1975.
[72] Elschenbroich, Ch.; Mockel, R.; Zenneck, U.; Clack, D. W. Ber. Bunsenges. Phys. Chem.
      1979, 83, 1008.
[73] Elschenbroich, Ch.; Heck, J. J. Am. Chem. Soc. 1979, 101, 6773.
[74] Bulgarovskaya, I. V.; Novakovskaya, L. A.; Zvonkova, Z. V. Sov. Phys. Crystallogr. 1976,
      21, 285.

Chapter 19

Reactions of Metal Powders with Organic Polymers

John Delmonte

Delsen Testing Laboratories, Glendale, CA 91201

Metal powders are comingled with liquid epoxy
polymers and with finely divided low density
polyethylene (LDPE). The mixtures are exposed to
temperatures exceeding the decomposition of the
organic polymers, but below the melting point of
the metal. Observations were made of the
polymer-metal mixtures with the aid of a
differential scanning calorimeter (D.S.C.).
Commercial grades of powdered iron, copper and
aluminum were used. Significant differences
among the metals are reported in studies of the
exotherm "spikes" which were generated. Data are
reported on samples in the presence of air, as
well as in the presence of an inert gas (Argon).
Thermal decomposition of the subject epoxy was
lowered most in the presence of iron, and less
with copper, followed by aluminum. Metal powders
influenced the D.S.C. curves of LPDE when
conducted in air,but had little effect in the
presence of Argon.

Interaction between metals and polymers are usually
assessed from data on the performance of polymer
adhesives and coatings upon metal surfaces. High
temperature operations and environmental aging processes
may produce instability, observed in discoloration of the
organic film or by the loss of adhesive strength of the
metal and the polymers. In many polymer-metal systems
chemical bonds are formed that involve metal-oxygen-
carbon complexes. The oxygen source may be the
atmosphere, oxide on the metal surface, or from the
polymer (1). The degradation of polyethylene on copper is
illustrative of polymer oxidation involving long-range

interface effects (2). The formation of novel organometallic compounds by the reaction of finely divided metal powders represents a powerful tool for chemical synthesis (3). Studies have been conducted on the bonding to cold-rolled steel and electro-galvanized steel with epoxy dicyanamide adhesives, using changes in infrared spectra to suggest interfacial chemistry (4). The effect of the degradation of polyacrylamide in the presence of iron or oxygen has also been reported (5).

This paper will disclose a simple procedure for identifying potential problem areas by subjecting combinations of two or more diverse materials to high temperature gradients. Both thermoplastic and thermosetting polymers will display high chemical reactivity as they are exposed to temperatures approaching their decomposition. The sensing of this reactivity is obtained with precision on a differential scanning calorimeter.

Thermoplastic polymers will begin to soften with increasing temperature and thermally decompose into lower molecular weight fractions. It is probable that the more volatile, lower m.w. polymers will demonstrate greater tendency for chemical interaction with the metal surfaces. An increasing temperature gradient may also induce homopolymerization of low m.w. polymers. Interactions will also be influenced by atmospheric oxygen and hence in the tests which follow: comparisons are made between air and inert gas exposure.

In this paper the principal information is developed on liquid DER332 epoxy (Dow's Bisphenol A of diglycidylether) and (a finely divided low density polyethylene). Several finely divided metals; iron, copper and aluminum were blended with equal volumes of the above mentioned polymers. These were exposed during high temperature gradients in the presence of atmospheric oxygen and argon gas. In general, the ASTM screen mesh size for the Al,Cu, and Fe powders used were in the 100 to 200 mesh size. Preliminary studies indicated that this finer mesh sizes yielded slightly lower decomposition temperatures of the polymer, though this paper focuses more upon the large difference observed between the three metal powders selected. It is recognized that interactions are concerned with relationships between colonies of organic molecules (if a powdered consistency) or low molecular weight liquid/organic polymers, with molecular colonies of metallic elements at their outermost interfaces. In these tests the following metal powders were used:

A. MD-201 - Aluminum Company of America.
B. Copper Powder - C-112 of U.S. Bronze Co.
C. Iron Powder - MH-100 of Hoeganaes Co.

PROCEDURE
A modified differential scanning calorimeter was used in

the tests to facilitate the rapid removal of volatiles or
gaseous products which might evolve during the course of
the experiments. The basic Perkin-Elmer D.S.C. apparatus
and recording system used was Model - 2C. This apparatus
is sensitive to the thermal behavior of small samples
when using aluminum pans or cups (1/2 cm. diameter).
Sample sizes were generally in the range of 10 to 70
milligrams - depending on the volumetric loading of the
more dense metallic component. The small sample size
promoted confidence in the exotherm or endotherm data,
because of the proximity of the thermocouple sensing
device on the cup. Procedures were standardized as far as
possible to permit comparisons between diverse material
combinations. The metal powders and polymers used in
these test were commercial grades without further
laboratory purification.

RESULTS

Figures 1 and 2 illustrated the D.S.C. scans for the base
epoxy resin DER-332 alone and in combination with 50%
volume concentration of Al, Cu, and Fe. The metal filled
specimens yielded sharp exotherm "spikes" which were
interpreted as evidence of chemical reactions. There is a
definite temperature associated with the exothermic
"spike" of each metal. Sharp "spikes" were not in
evidence for the basic neat resin. The depth of the
exotherm was greatest for Fe, followed by Cu and Al.
Increasing the volume percentage of Fe increased the
depth of the "spike", while decreasing the volume
percentage of Fe to less than 50%, decreased the depth of
the spike, with only minor differences of the temperature
at which the exo "spike" occurred.
   The reference base was established as a common
denominator for achieving a uniform heat input to the
specimens to maintain 20°C. temperature gradient per
minute, the sharpness of the exotherm "spike" was more
evident at a 20°C. gradient. As endo and exotherm
reactions began to take place after decomposition of the
polymer commenced above 300°C., the heat inputs to the
specimens were overshadowed by chemical reactions.
However, the profiles of the D.S.C. curves were
consistent and identified with a specific metal-epoxy
combination. Results in air and in argon are
significantly different in their D.S.C. profiles as would
be expected form the potential oxidizing effect of air.
See Table I.
   For comparison purposes Figure 3 illustrates the
recorded weight loss of the DER 332 and the 50% Ep-Cu
mixture at a 20°C. per minute rise in temperature. Most
of the epoxy resin has decomposed and disappeared above
360°C. Without question more meaningful data has been
generated in the above use of the D.S.C. apparatus. The
D.S.C. curves suggest the presence of interactions above
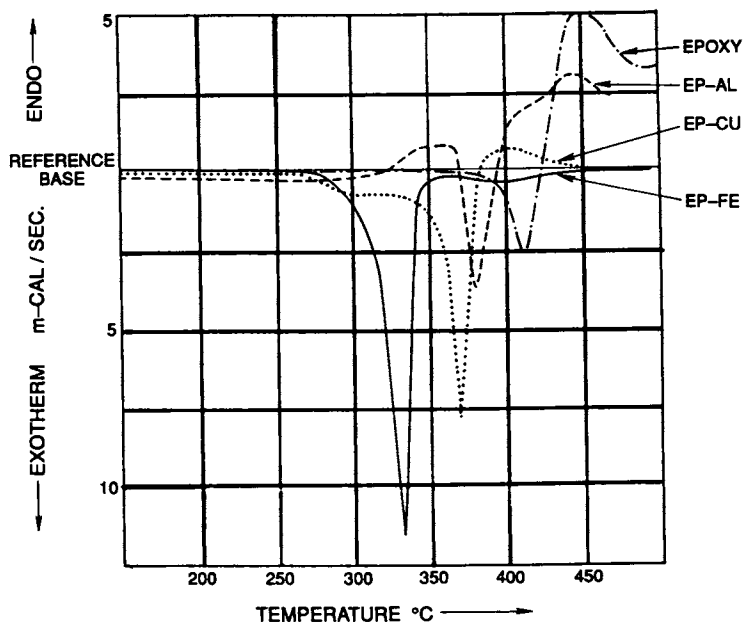
Figure 1. D.S.C. Scans of Epoxy and Combinations with
Al, Cu, and Fe (In Argon).
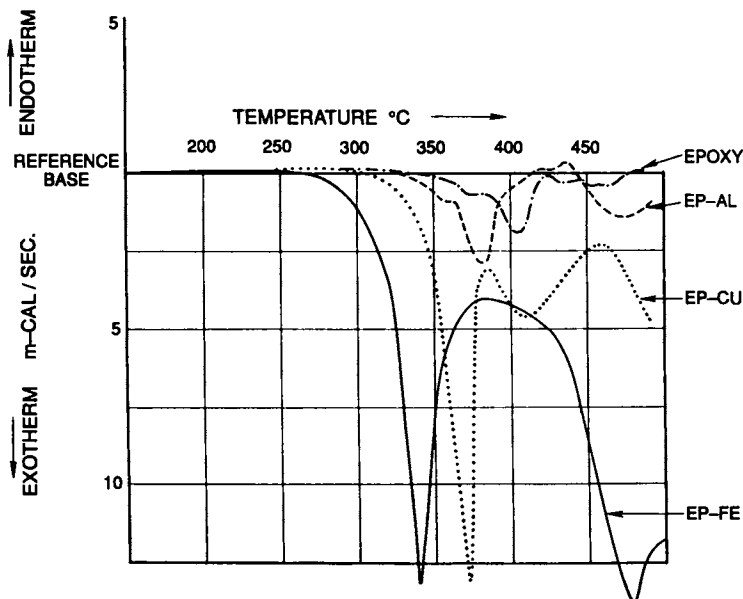
Figure 2. D.S.C. Scans of Epoxy and Combinations with
Al, Cu, and Fe (In Air).

Table I. Principal D.S.C. Exotherms
of Figures 1 and 2

In Air	Specimen	In Argon
Approx.401˚C.	Base Epoxy	Approx.409˚C.
341˚C.	EP-Fe	332˚C.
370˚C.	Ep-Cu	369˚C.
372˚C.	Ep-Al	379˚C.
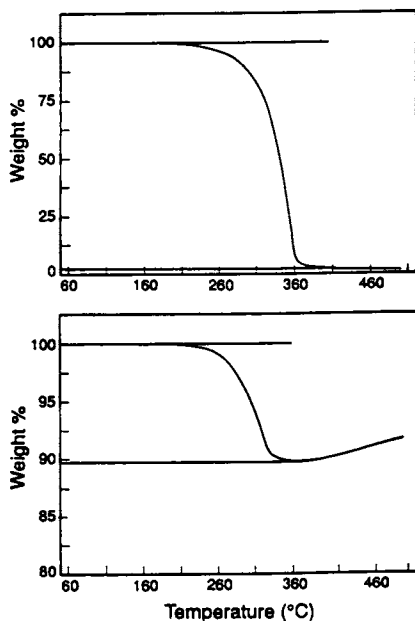
Figure 3. Weight Loss of Epoxy and Weight Loss of Epoxy
and 50% Vol. of Cu.

the decomposition temperature of the epoxy polymer.
Further data were obtained on samples of low density
polyethylene (LPDE) mixtures with metal powders. LDPE is
generally considered inert to many chemicals. When high
temperature gradients of 20°C. per minute were applied to
mixtures of LDPE and metal powders, it was found that
closely identical D.S.C. curves were obtained in argon
gas. From the data for LDPE, LDPE-Fe, LDPE-Cu, and LDPE-
Al, the 50% Fe/LDPE was selected for illustration in
Figure 4. On the other hand, when tests were performed in
air, widely dissimilar data were obtained See Figure 5.
The presence of oxygen produces untoward effects on the
decomposition of LDPE in the presence of Al, Cu, and Fe.
It was noted that the profiles of these curves were
repeatable. Many unexplained reactions occurred during
polymer decomposition in the presence of metal powders.

CONCLUSIONS

1. The data provided by Metal-polymer D.S.C. curves
   provide new insight on high temperature reactions.
2. The precise temperatures for the exothermic "spikes"
   of the D.S.C. curves for epoxy-metal powders in both
   air and oxygen suggest new reactions not previously
   reported.
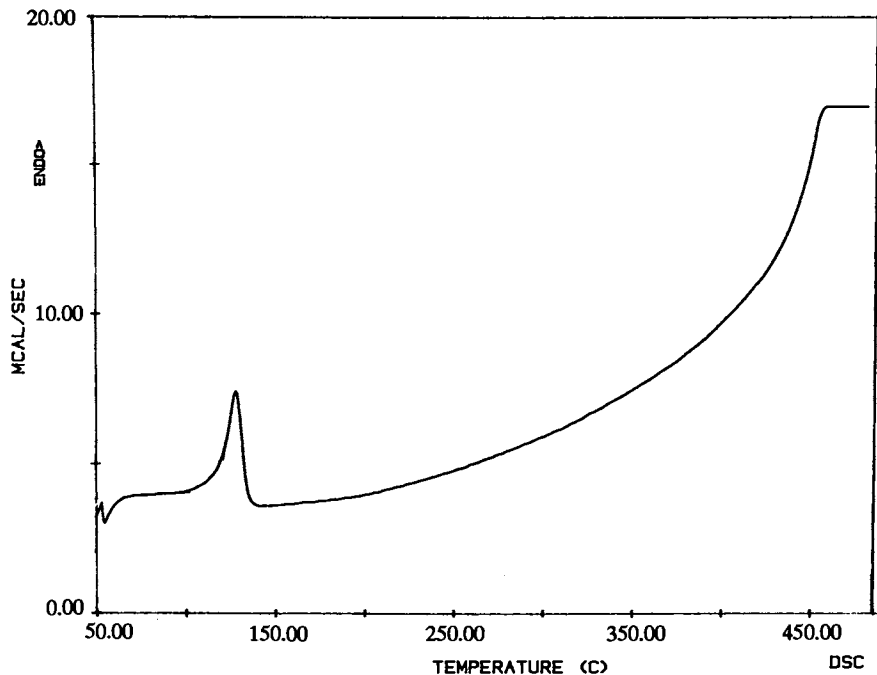
Figure 4. D.S.C. Scan of LDPE and in Combination with
50% Vol. of Cu. (In Argon).
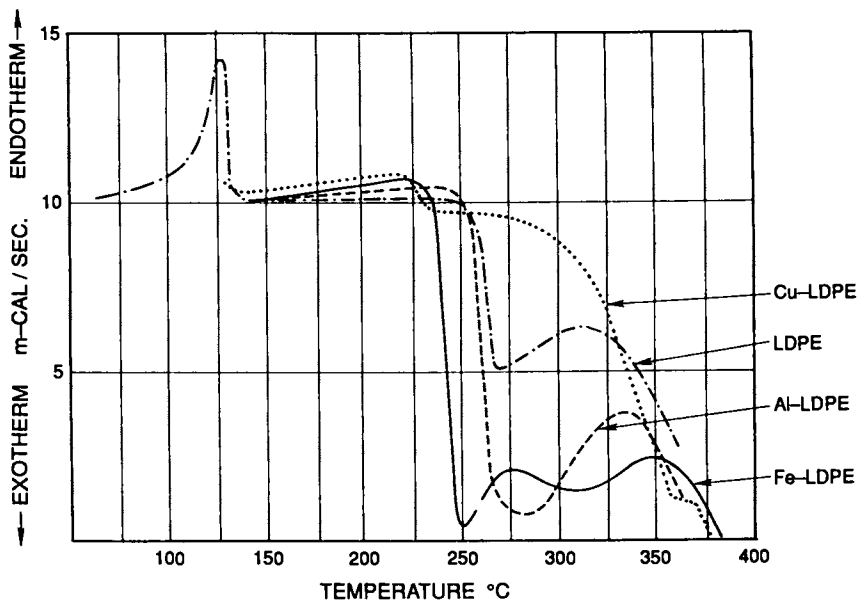
Figure 5. D.S.C. Scans of LDPE and Combinations with
Al, Cu, and Fe, (In Air).

Literature Cited

1. Leidheiser, H. Jr. and Deck, P. Science 2 Sept. 1988,
   241, 1176.
2. Chan, M. and Allara, D.L. Polym. Eng. Sci. 1974, 4,
   12.
3. Rieke, R. Science 8 Dec. 1989, 246, 1260.
4. Carter, R.O., Dickie, R.A., and Holubka, J.W. Journal
   Polymeric Materials, Science and Engrg. 1988, 58, 55.
5. Francois, J. et al. ACS Polymer Preprints 1987, 28,
   694.

Chapter 20

Reaction During the Sputtering of Metals onto Polyimide

A. Domingue[1], L. Dignard-Bailey[1,3], Edward Sacher[1], A. Yelon[1], and T. H. Ellis[2]

[1]Groupe des Couches Minces and Département de Génie Physique, École Polytechnique, C.P. 6079, Succursale A, Montreal, Quebec H3C 3A7, Canada
[2]Département de Chimie, Université de Montréal, C.P. 6128, Succursale A, Montreal, Quebec H3C 3J7, Canada

X-ray photoelectron spectroscopy has been used to study the metal polyimide interface formed during room temperature metal deposition. Several mono-layers of Al, Au and Cu were sputter-deposited onto cured polyimide, to a thickness which permitted the observation of both polyimide and metal peaks. Deconvolution of core-level C1s, N1s and O1s polyimide peaks and Al2p, Au4f and $Cu2p_{3/2}$ metal overlayer peaks has demonstrated that chemical reaction occurs at the carbonyl sites for all these metals under the conditions used. In addition, the aromatic nature of the molecular structure at the interface is believed to decrease while the percentage of an isoimide-like component increases.

The polyimides, unusually strong, versatile and stable insulating polymers, have acquired increasingly important roles in the thin film industry as high performance material coatings and dielectric layers necessary for the demanding conditions experienced by special high technology devices such as multilayer microelectronic structures (1-4). The long term mechanical stability of such devices depends greatly on the adhesion experienced at the metal-polymer interface and, as a result, the development of a metal-polyimide interface with enhanced stability and reliability has become an important industrial objective. Interfacial adhesion had been previously believed to be a consequence of a combination of mechanical intermixing, interfacial mixing of phases and intrinsic effects at the interface (5-7). The depth-profile characteristics of the metal-polyimide interface have been shown, in fact, to vary with the vapor-deposited metal utilized; however, this has not been sufficient to justify the amount of interfacial adhesion actually observed (8). There are also specific interfacial interactions, a

[3]Current address: Metals Technology Laboratories, Canada Centre for Minerals & Energy Technology, Ottawa, Ontario K1A 0G1, Canada

consequence of the intrinsic properties of the interface, which are strongly implicated and they influence the durability and strength of adhesion. Of these interactions (chemical, electrostatic and molecular), it is the presence of chemical bonds at the interface, providing the strongest adhesive links, which are best suited to withstand current processing techniques (3,9).

In order to monitor the progress of interfacial reactions occurring during the metallization of cured polyimide, x-ray photoemission spectroscopy (XPS or ESCA) was used to reveal electronic core-levels indicative of the environment at the interface and adjacent regions. Evidence of chemical reaction would include the appearance of new peaks with characteristic binding energies (chemical shifts) representative of new or altered chemical states of the element. We can thus ascertain the formation of metal-oxygen chelate complexes (1).

Previous studies have shown that a trend exists in the behavior of some evaporated metals on polyimide surfaces: x-ray and ultraviolet photoelectron (XPS, UPS) as well as high resolution electron energy loss (HREELS) measurements have indicated that while for some metals such as aluminum, titanium and chromium there is bond formation with the PMDA carbonyl oxygen of the polyimide (2, 10-13), other metals such as copper, palladium and gold undergo little reaction or interaction (10,12,14,15). It has, however, since been postulated that metals, in order to adhere well at all to a polymer under a wide variety of conditions, must form metal- polymer bonds (10).

Deposition of metals can proceed via thermal evaporation which produces low energy vaporized atoms which condense onto the sample surface. The heat of condensation liberated, 300 - 450 kJ per mole (16,17), is high enough for reaction to occur between metal and polymer (18) but is restricted to those metal species which are the most highly reactive; analysis of interfacial species in the literature is minimal. In contrast to evaporation, sputter-deposited "hot" metal atoms have significantly higher average energies (at least ten times greater (18), which results in more extensive interfacial reaction (1) and, thus, produces more clearly measurable changes, as observed in this study. The potentially damaging effects of significant substrate heating during sputter-deposition are minimized by using low deposition rates (19). The substantially increased adhesion obtained with sputter-deposited metal-polymer interfaces has resulted in the growing importance of metal sputtering for the deposition of thin metal films on polymers (1).

EXPERIMENTAL

Core level spectra were acquired in a Vacuum Generators dual chamber UHV system. This consists of the ESCALAB Mk II electron spectrometer run by the SURFSOFT data acquisition and manipulation program (20) on an AT-type microcomputer, an analyzer chamber for taking the measurements and a preparation chamber for sample introduction and treatment. The samples were transferred directly from the preparation chamber to the analysis chamber. The data were obtained with the analyzer operating at 20 eV pass energy in the constant analyzer energy mode, using non-monochromatized Mg Kα (1253.6 eV) radiation. The experimental resolution was 0.80 eV FWHM. Operating

pressures in the analysis chamber never exceeded 5×10^{-10} torr. The system possesses an argon ion gun facility for sample cleaning and sputtering, and has provision for sample heating in vacuo. Metal depositions were carried out in the preparation chamber by bombarding the metal targets with 6 kV (for Al) and 3 kV (for Au and Cu) argon ions at a background pressure of 5×10^{-6} torr. The samples were positioned on the transfer system railing at some distance from the metal target and well out of the way of the sputter beam (preliminary studies showed no detectable degradation of the samples by the beam at this position). Such conditions resulted in metal film deposition thicknesses of approximately 20 Å after 30 minutes. The metals used (Al, Au, Cu) were of 99.99% purity (Alfa). All gases used were of ultra high purity (Linde).

The polyimide thin film samples wre prepared by spin coating an approximately 2 μm film of electronic grade PMDA-ODA polyamic acid precursor (Dupont PI-2545) onto a 3" silicon wafer. This film was dried under vacuum at 85 °C for several hours and cured at 350 °C in the preparation chamber for 30 minutes.

Reactions occurring at the interface during sputtering were monitored using the C1s, O1s, N1s and appropriate metal electronic core levels (21-24). Analysis was carried out at 85° from normal (grazing angle), thereby probing the core levels at the interface. After background subtraction (Shirley), the core level spectra were fit with 70% Gaussian, 30% Lorentzian peaks in order to highlight the various contributions. There was only a slight charge-induced spectral shift for the thin film samples and this was readily compensated for by referencing the polyimide aromatic peak to -285.0 eV binding energy.

RESULTS AND DISCUSSION

POLYIMIDE. The XPS spectra of thin films of clean, cured PMDA-ODA polyimide (Fig. 1), examined prior to metal deposition, display core level contributions and peak intensity ratios in agreement with those generally observed for the cured polyimide film surfaces (21,25) (Figs. 2a-c and Table I). The relative contributions from the major carbon 1s peaks (Fig. 2a) representing the various components of the PMDA-ODA polymer repeat unit, conform to previous assignments (25) and include the PMDA imide carbonyl carbon peak (peak 2), the peak representing the ODA aromatic ring carbons not bound to oxygen or nitrogen (peak 4), the peak representing unresolved contributions from remaining carbons in the structure (peak 3) and the broad aromatic $\pi - \pi^*$ shake-up contributions (peak 1). The small extra peak, observed at lower binding energy (peak 5), is generally not accounted for (except as a peak asymmetry) (21) and we shall not elaborate on it in this discussion. These are all in excellent agreement with the literature (25). The relative contributions of the major oxygen 1s peaks (Fig. 2b) originating from the ether (peak 1) and carbonyl oxygens (peak 2) demonstrate the non-stoichiometric nature of cured polyimide film surfaces evident in a carbonyl-ether ratio of less than the 4:1 ratio theoretically expected (21,25,26). A third, very weak peak at lower energy is not identified. The N1s spectrum (Fig. 2c) is, characteristically, dominated by the band corresponding to the imide nitrogen (peak 2). It also displays a small unidentified peak at

Table I. Cured Polyimide Film

Spectrum	Peak	Position/Shift (eV)	%Area (exptl)	%Area (theor.)	Origin
C1s	1	-291.5/-6.5	3.7	-	$\pi-\pi^*$
	2	+289.1/-4.1	11.0	18.2	C=O
	3	-286.1/-1.1	49.3	45.4	C-O
					C-N
					C-C=O
	4	-285.0/ 0.0	34.9	36.4	aromatic
	5	-283.4/+1.6	1.1	-	-
O1s	1	-533.7/-1.3	29.6	20.0	ether
	2	-532.4/ 0.0	68.3	80.0	carbonyl
	3	-530.7/+1.7	2.1	-	-
N1s	1	-402.7/-1.7	4.8	-	-
	2	-401.0/ 0.0	91.9	100.0	imide
	3	-399.3/+1.7	3.3	-	isoimide

higher binding energy (peak 1), as well as a lower energy component (peak 3) not accounted for in the bulk structure but generally believed to be due to the presence of isoimide structures (25); this structural isomer of polyimide is generally believed to be the reason for the carbonyl deficiency observed (22,25).

ALUMINUM. A chemical reaction is known to occur when aluminum is deposited via evaporation onto polyimide (27). Sputter-deposition produces similar effects on the core levels (Figs. 3a-c, 4a) (Table II). This includes a significant reduction of the carbonyl C1s peak intensity (peak 2 in Fig. 3a) and reduction the O1s carbonyl peak intensity (peak 2 in Fig. 3b). This is generally explained as a consequence of the selective reaction occurring at the carbonyl sites at the surfaces (14,28). The limited nature of the reaction, possibly due to changes in site activity (13), is underlined by the reduction in C1s carbonyl peak intensity which does not exceed approximately 50% of the original signal (peak 2 in Fig. 3a). This agrees with the suggestion that only one half of the carbonyls available undergo reaction with aluminum atoms (10). There is also a reduction in the C1s $\pi - \pi^*$ contribution (peak 1 in Fig. 3a) which can be attributed to a reduction in electron delocalization in the PMDA or ODA structures (loss of aromatic character). The other carbon peaks maintain their relative intensities, however, and this shows that the polyimide structure is generally retained after sputter-deposition of the aluminum. The presence of any carbides, typically exhibiting C1s binding energy peaks below 284 eV, can possibly account for peak 5 in Fig. 2a but the absence of a concurrent high energy carbide peak (~79.8 eV) (29) in the Al2p core level spectrum (Fig. 4a) precludes this possibility. There appear to
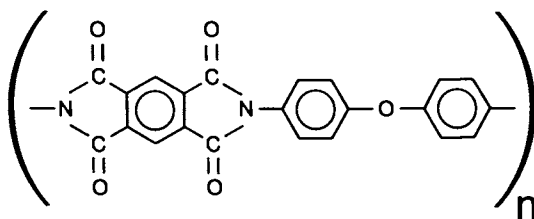
Fig. 1: PMDA-ODA polyimide repeat unit.
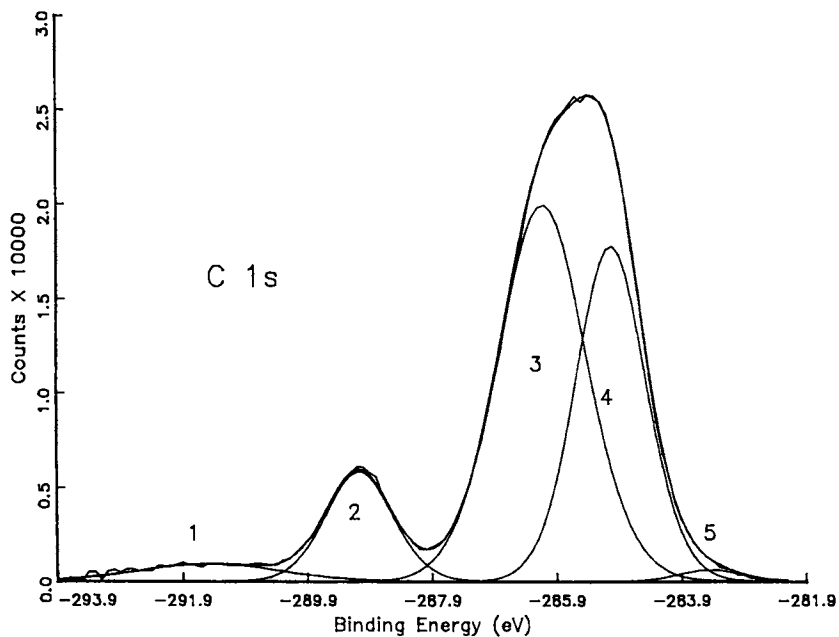
Fig. 2a: XPS spectra of cured polyimide film: C 1s spectrum.
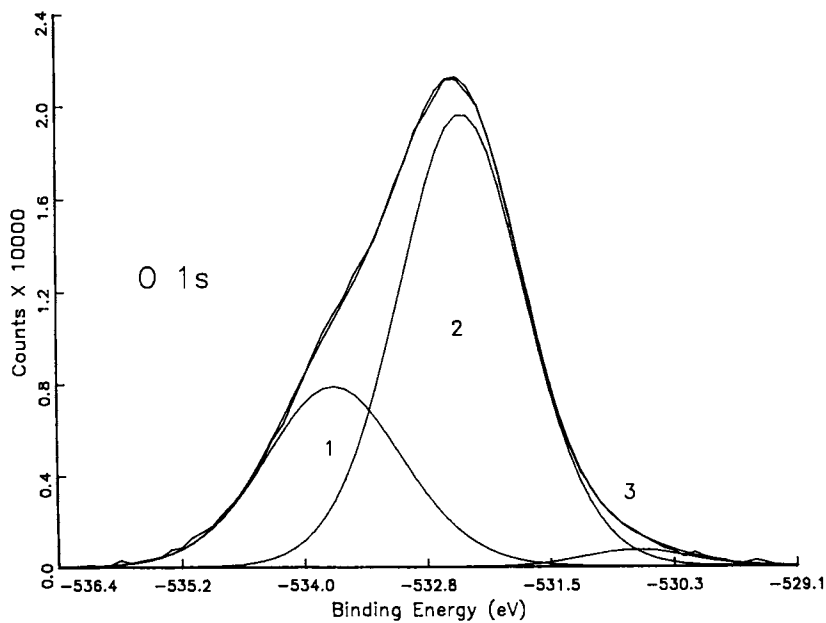
Fig. 2b: XPS spectra of cured polyimide film: O 1s spectrum.
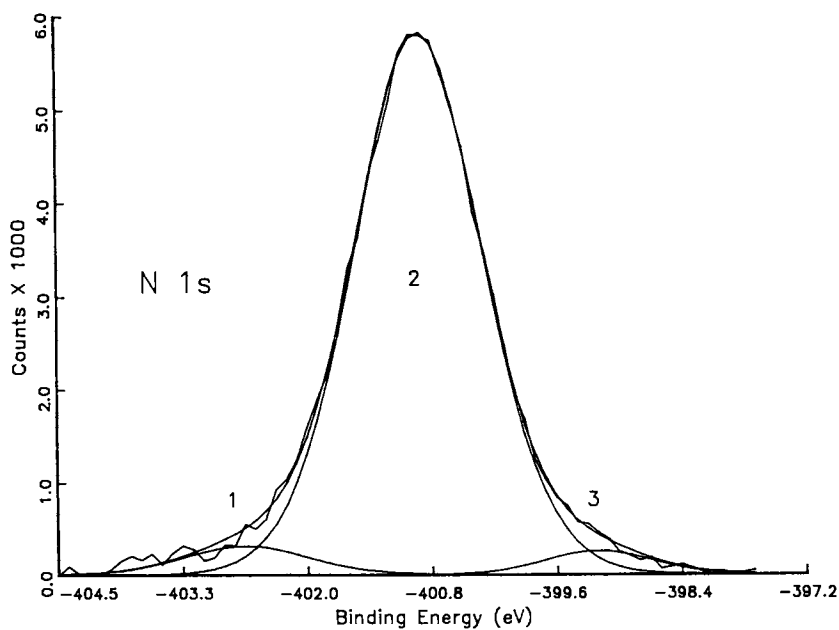
Fig. 2c: XPS spectra of cured polyimide film: N 1s spectrum.

Table II. Aluminum on Polyimide

Spectrum	Peak	Position/Shift (eV)	%Area	Origin
C1s	1	-291.3/-6.3	1.0	$\pi-\pi^*$
	2	-289.0/-4.0	7.3	C=O
	3	-285.9/-0.9	50.8	C-O
				C-N
				C-C=O
	4	-285.0/ 0.0	37.5	aromatic
	5	-283.3/+1.7	3.4	-
O1s	1	-535.0/-2.5	1.6	-
	2	-533.7/-1.2	27.9	ether
	3	-532.5/ 0.0	50.2	carbonyl
	4	-530.8/+1.7	8.5	-
	5	-531.8/+0.7	11.8	-
N1s	1	-402.7/-1.8	2.1	-
	2	-400.9/ 0.0	69.6	imide
	3	-399.2/+1.7	28.3	isoimide
Al2p	1	-76.8/-4.3	4.0	higher oxidation state
	2	-75.7/-3.2	20.3	higher oxidation state
	3	-74.8/-2.3	75.7	higher oxidation state
	5	-72.5/ 0.0	0.0	elemental
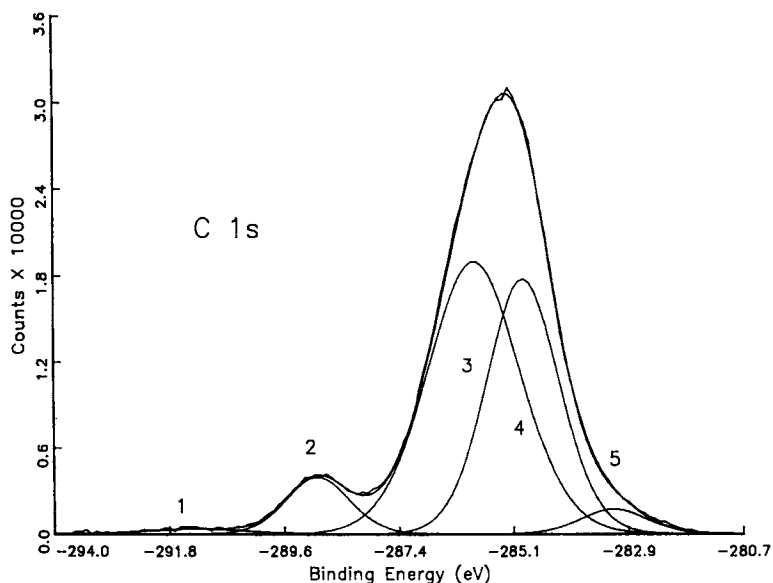
Fig. 3a: XPS spectra of polyimide with sputter-deposited aluminum: C 1s spectrum.
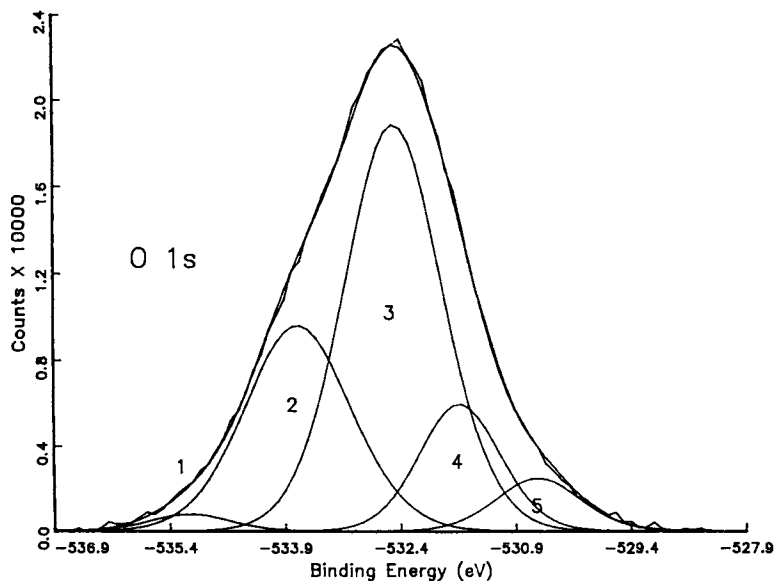
Fig. 3b: XPS spectra of polyimide with sputter-deposited aluminum: O 1s spectrum.
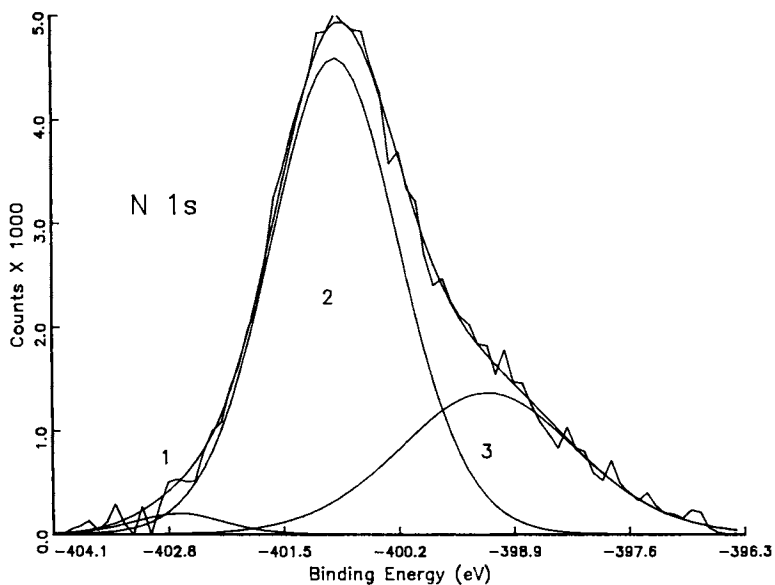
Fig. 3c: XPS spectra of polyimide with sputter-deposited aluminum: N 1s spectrum.

be only slight changes in the O1s spectrum (Fig. 3b). However,
detailed analysis shows that several new components can now
distinguished at lower energies (Peaks 4 and 5). They can be
associated with the appearance of Al-O species (10,27,30) at the
surface. In addition, the N1s spectrum (Fig. 3c) is now observed to
display an important increase in intensity in the region
corresponding to the appearance of isoimide-like components (peak
3). This suggests a significant modification of the polymer
structure. Thus far, it has been fairly obvious that the deposition
of sputtered aluminum onto polyimide produces a strong interaction
between the metal atoms and carbonyl groups. We now see, however,
that there is also evidence of structural reorganization at the
surface during deposition. This may be due to heat released at the
interface or via the insertion of metal atoms into the substrate.
The isomerization of polyimide to isoimide-like structures may help
to explain the greatly reduced aromatic character of the polymer at
the interface. The characteristic chemical shifts observed in the
Al2p spectrum (Fig. 4a) indicate that the aluminum deposited on the
polyimide now exists entirely as a series of oxidized species at the
surface (peaks 1, 2 and 3) similar to those already observed by
Atanasoska et al. (12), on polyimide with low Al coverage (0.5 - 2
Å. This agrees with the formation of an Al-O-C complex, presumably
in several different environments. A charge delocalization from
oxygen to carbon concurrent with reaction is usually suggested to
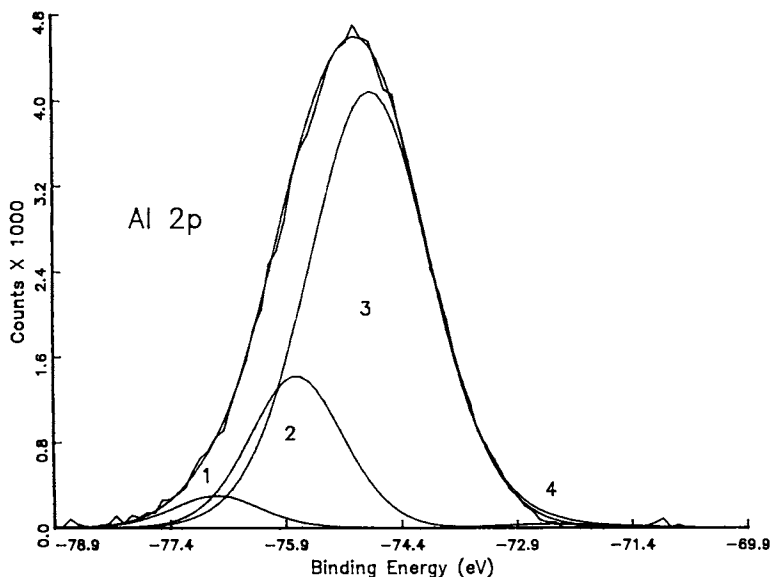
Fig. 4a: XPS spectra of metal electronic core levels present in polyimide treated with
sputter-deposited metals: Al 2p spectrum.
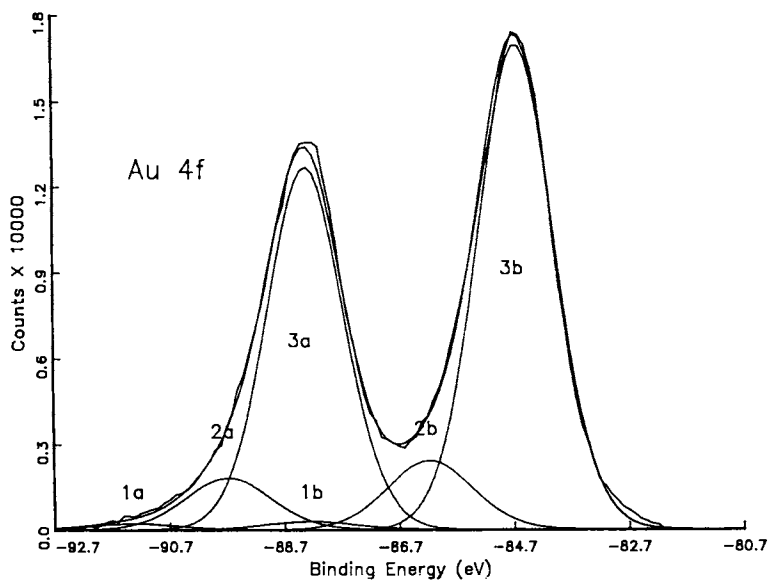
Fig. 4b: XPS spectra of metal electronic core levels present in polyimide treated with sputter-deposited metals: Au 4f spectrum.
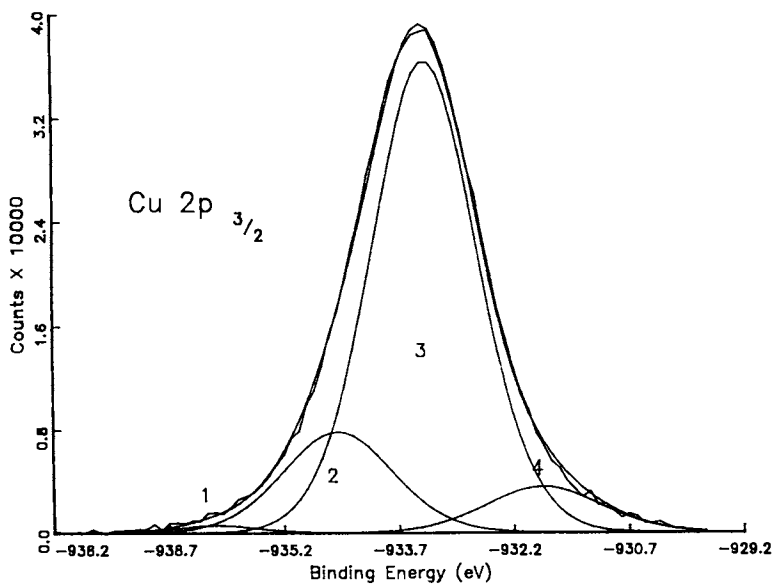
Fig. 4c: XPS spectra of metal electronic core levels present in polyimide treated with sputter-deposited metals: Cu $2p_{3/2}$ spectrum.

explain the absence of an expected O1s chemical shift. No signal
from metallic aluminum (peak 4) is observed. The aluminum has thus
totally reacted with the polymer. This can be explained by the
diffusion of the depositing aluminum into the polymer substrate.
This has previously been suggested to occur in this system (27) and
it agrees with findings from nuclear scattering studies which have
shown that an extensive penetration of the metal into the bulk
occurs (8).
GOLD. The deposition of gold onto polyimide (Fig. 4b and Table IV)
is also observed to reduce the carbonyl C1s peak intensity (peak 2
of C1s in Table III) as well as that of the aromatic π - π^* C1s
(peak 1 of C1s), an effect analogous to that observed for the
aluminum-polyimide system. New components also appear at lower
energies in the O1s spectrum and there is an isoimide-like component
in the N1s spectrum (peak 3). Gold is not generally known to exist
in a stable complex form (marginal chemical reactivity) and is

Table III. Gold on Polyimide

Spectrum	Peak	Position/Shift (eV)	%Area	Origin
C1s	1	-291.7/-6.7	0.9	π-π^*
	2	-289.0/-4.0	9.3	C=O
	3	-286.0/-1.0	51.0	C-O
				C-N
				C-C=O
	4	-285.0/ 0.0	38.0	aromatic
	5	-283.4/+1.6	0.9	-
O1s	1	-534.9/-2.4	1.6	-
	2	-533.7/-1.2	28.2	ether
	3	-532.5/ 0.0	54.8	carbonyl
	4	-531.5/+1.0	11.1	-
	5	-530.4/+2.1	4.3	-
N1s	1	-402.7/-1.8	2.5	-
	2	-400.9/ 0.0	77.5	imide
	3	-399.4/+1.5	19.9	isoimide
Au4f$_{5/2}$	1a	-91.4/-3.1	0.7*	+3
	2a	-89.7/-1.4	5.9	+1
	3a	-88.3/ 0.0	36.1	elemental
Au4f$_{7/2}$	1b	-88.3/-3.7	1.0	+3
	2b	-86.2/-1.6	7.8	+1
	3b	-84.6/ 0.0	48.5	elemental

*Au4f peak area ratios (5/2:7/2) are expected to be 0.75.
They are found to be 0.70 (Au^{+3}), 0.76 (Au^{+1}) and 0.74 (Au^o)

believed to exhibit poor adhesion with polymers at room temperature
(6). In the gold-polyimide system, the interface is also generally
believed to be free of any measureable chemical interactions (29).
Observations by Chauvin et al. have shown, however, that the
adhesive strength of this interface varies with treatment
(hydration) (8). Interfacial intermixing (none occurs with gold) (8)
or mixed-phase effects cannot account for this behaviour. We have
observed that shifts in the various core levels occur after the
deposition of gold (low coverage) onto the polyimide surface via
sputtering. The deposited gold remains mostly in metallic form and
does not penetrate into the bulk, in agreement with nuclear
scattering results (8), but the gold 4f core level spectrum (Fig.
4b) cannot be adequately represented when only peaks of metallic
gold are used exclusively (peaks 3a and 3b). Peaks with the chemical
shift of Au^{1+} (peaks 2a and 2b) must also be included in order to
obtain a reasonably satisfactory fit. An even better fit is obtained
by including Au^{3+} (peaks 1a and 1b). This fit is kept consistent
with theoretical 4f peak area ratios and reported binding energy
values for Au^{1+} and Au^{3+} species (31). It clearly indicates that
gold is present at the interface in several characteristic oxidation
states (32). This would explain the low energy O1s components (Au-O
species), which cannot be accounted for by an electron injection
process at the interface or by random peak shifts (33). In
coparison, a similar process is reported to occur with palladium,
which, although also considered "unreactive", undergoes some
reaction, oxidizing when sputtered onto polyester (34).

COPPER. The deposition of copper on polyimide (Table IV) produces
results similar to the previous systems. There is depletion of the
carbonyl and π - π^* C1s peaks and a similar quantity of isoimide
component is produced. In addition, there is a significant change in
O1s peak intensities, including the appearance of low energy
components similar to the other systems and associated with Cu-O
species (23). The Cu $2p_{3/2}$ core levels (Fig. 4c) show the presence
of several oxidation states. Therefore, reactions also occur with
copper, despite generally held assumptions of marginal chemical
reactivity (15,27,35,36). Most of the copper deposited remains in
the metallic state, in agreement with the nuclear scattering
results, which show that diffusion into the bulk occurs only upon
subsequent heating (8).

CONCLUSIONS

A comparison of changes occuring in C1s, N1s and O1s core level
spectra for the systems examined can be emphasized by overlapping
their area-normalized spectra and reveals interesting parallels. The
effects observed for all the metals examined in this study are very
similar. There is, in all cases, a loss in relative intensities for
the π - π^* and carbonyl peaks of the C1s spectra (Fig. 5a). There
are also comparable changes occurring at both lower and intermediate
binding energies (~-287.5 and -283.0 eV). The N1s spectra (Fig. 5c)
show comparable decreases in imide intensity and increases in
isoimide intensity. Correspondingly, a loss of carbonyl intensities
is observed in the O1s spectra (Fig. 5b), along with the appearance
of the new lower energy peaks which can be associated with the
appearance of metal-oxygen species at the interface (10,

Table IV. Copper on Polyimide

Spectrum	Peak	Position/Shift (eV)	%Area	Origin
C1s	1	-291.4/-6.4	1.6	π-π
	2	-289.0/-4.0	9.5	C=O
	3	-286.1/-1.1	45.7	C-O
				C-N
				C-C=O
	4	-285.0/0.0	41.9	aromatic
	5	-283.4/+1.6	1.3	-
O1s	1	-535.0/-2.5	1.4	-
	2	-533.7/-1.2	27.4	ether
	3	-532.5/ 0.0	54.3	carbonyl
	4	-531.6/+0.9	12.7	-
	5	-530.5/+2.0	4.3	-
N1s	1	-402.7/-1.8	2.5	-
	2	-400.9/ 0.0	79.9	imide
	3	-399.2/+1.7	19.9	isoimide
Cu2p$_{3/2}$	1	-936.1/-2.7	0.9	higher oxidation state
	2	-934.5/-1.1	16.7	higher oxidation state
	3	-933.4/ 0.0	74.4	elemental
	4	-931.9/+1.5	8.0	-
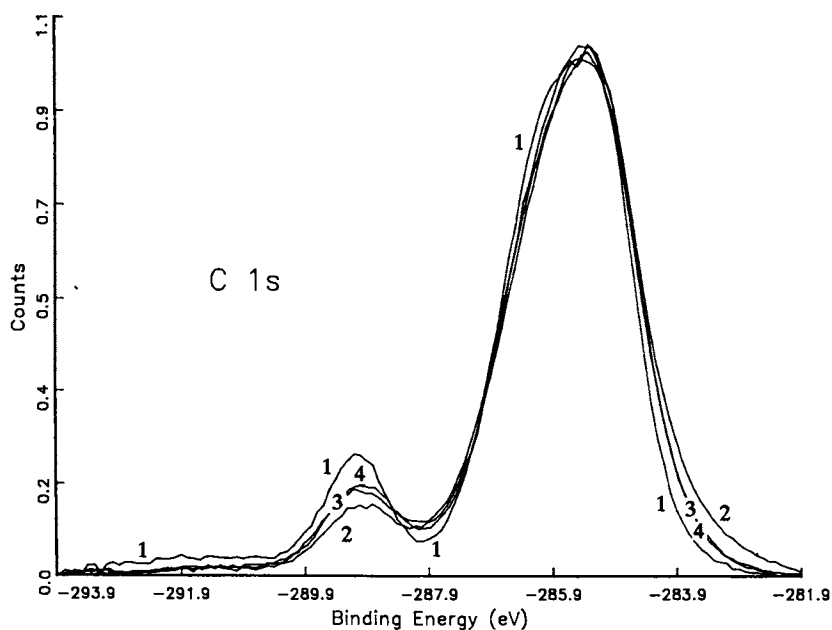
Fig. 5a: Overlapping spectra of non-metallized and metallized polyimide: C 1s spectra. 1 = Untreated; 2 = wt. Al; 3 = wt. Au; 4 = wt. Cu.
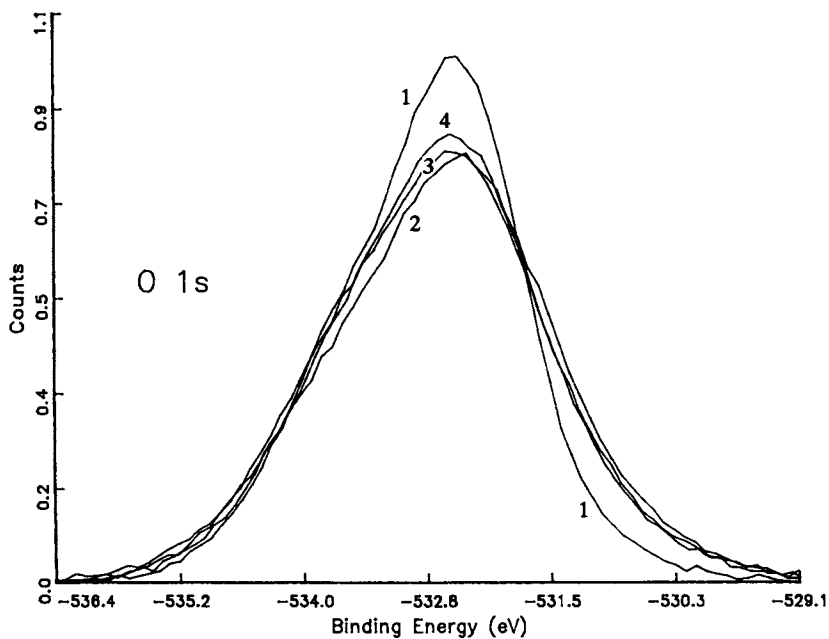
Fig. 5b: Overlapping spectra of non-metallized and metallized polyimide: O 1s spectra. 1 = Untreated; 2 = wt. Al; 3 = wt. Au; 4 = wt. Cu.
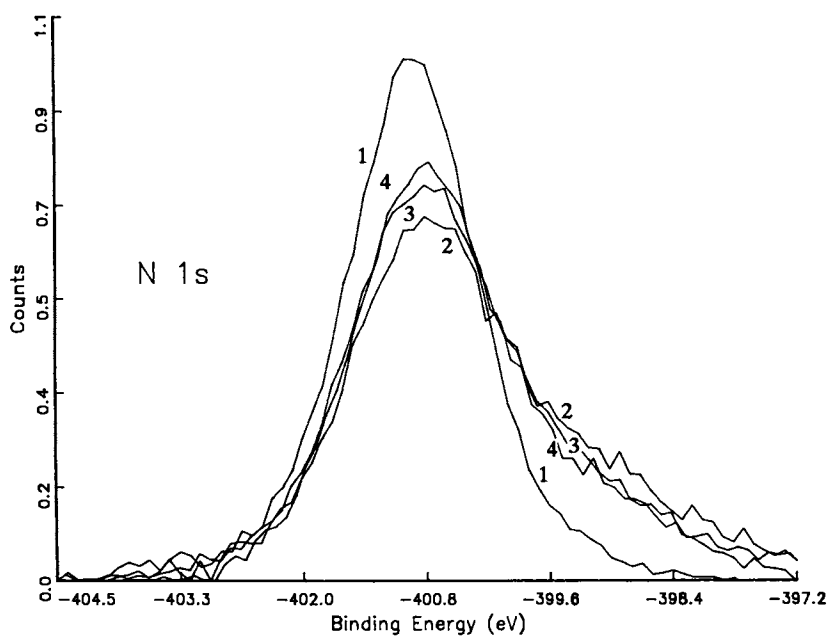
Fig. 5c: Overlapping spectra of non-metallized and metallized polyimide: N 1s spectra. 1 = Untreated; 2 = wt. Al; 3 = wt. Au; 4 = wt. Cu.

23,27,30,31). It seems that, in all cases, the initial reaction occurs preferentially at the PMDA carbonyl oxygen. Subsequent reactions which may occur at other sites, eg., the PMDA aromatic ring, the ODA aromatic ring (13), were not observed. There also was no evidence of any significant metal-carbon bond formation (28) in these systems. Thus, a variety of sputtered metals, including gold, are found to be capable of reacting with polyimide when deposited at room temperature. In contrast to previous studies of evaporated films which indicate no reactions with gold or copper, the reaction between metal and polymer is extensive on sputter-deposition due to the greater energies of the metallic species under these conditions. The reactions observed occur preferentially at carbonyl sites, the extents of which vary with the sputtered metal and conditions used. We have seen no evidence of metal reaction at any other site. The extra energy also produces important changes in the surface polymer structure including, possibly, the formation of isoimide-like components.

ACKNOWLEDGMENTS

LITERATURE CITED

1. Burkstrand, J.M J. Vac. Sci. Technol., 1982, 21, 70.
2. Dunn, D.S.; Grant J.L. J. Vac. Sci. Technol., 1989, A7, 253.
3. Chou, N.J.; Tang C.H. J. Vac. Sci. Technol., 1984, A2, 751.
4. Sroog, C.E. J. Polym. Sci.: Macromol. Rev., 1976, 11, 161.
5. Burkstrand, J.M. J. Appl. Phys., 1981, 52, 4795.
6. Burkstrand, J.M. J. Vac. Sci. Technol., 1982, 20, 440.
7. Chou, N.J.; Dong, D.W.; Kim, J.; Liu, A.C. J. Electrochem. Soc., 1984, 131, 2335.
8. Chauvin, C.; Sacher, E.; Yelon, A.; Groleau, R.; Gujrathi, S. in Surface and Colloid Science in Computer Technology, K.L. Mittal, Ed., Plenum, N.Y., 1987; p. 267.
9. Chou, N.J.; Tang, C.H. in Surface and Colloid Science in Computer Technology, K.L. Mittal, Ed., Plenum, N.Y., 1987. p. 287.
10. Pireaux, J.J.; Vermeersh, M.; Gregoire, C.; Thiry, P.A.; Caudano, R.; Clarke, T.C. J. Chem. Phys., 1988, 88, 3353.
11. Jordan, J.L.; Kovac, C.A.; Morar, J.F.; Pollack, R.A. Phys. Rev. B, 1987, 36, 1369.
12. Atanasoska, Lj.; Anderson, S.G.; Meyer, H.M.; Lin, Z.; Weaver, J.H. J. Vac. Sci. Technol., 1988, A5, 3325.
13. Selmani, A. J.Vac. Sci. Technol., 1990, A8, 123.
14. Bartha, J.W.; Hahn, P.O.; LeGoues, F.; Ho, P.S. J. Vac. Sci. Technol., 1985, A3, 1390.
15. White, R.C.; Haight, R.; Silverman, B.D.; Ho, P.S. Appl. Phys. Lett., 1987, 51, 482.

16. Honig, R.E. <u>RCA Reviews</u>, 1957, <u>18</u>, 195.
17. <u>CRC Handbook of Chemistry and Physics</u>, 69th ed., R.C. Weast, Ed., CRC Press, Boca Raton, FL, 1988-89; p. F-188.
18. Currie, J.F.; Depelsenaire, P.; Groleau, R.; Sacher, E. <u>J. Colloid Interface Sci.</u>, 1984, <u>97</u>, 410.
19. Pargellis, A.N. <u>J. Vac. Sci. Technol.</u>, 1989, <u>A7</u>, 27.
20. Surface Software, Inc., Montreal, Quebec, Canada.
21. Leary, H.J., Jr.; Campbell, D.S. <u>ACS Symp. Ser.</u>, 1981, <u>162</u>, 419.
22. Kiang, K.S.; Salaneck, W.R.; Aksay, I.A. <u>Solid State Commun.</u>, 1976, <u>19</u>, 329.
23. Burkstrand, J.M. <u>Appl. Phys. Lett.</u>, 1978, <u>33</u>, 387.
24. Wagner, C.D.; Riggs, W.M.; Davis, L.E.; Mouler, J.F.; Muilenberg, G.E. <u>Handbook of X-ray photoelectron Spectroscopy</u>, Perkin-Elmer, Eden Prairie, MN, 1978.
25. Baise, A.I.; Buchwalter, P.L. in <u>Polyimides</u>, K. Mittal, Ed., Plenum, New York, Vol. 1, 1984; p. 537.
26. Leary, H.J., Jr.; Campbell, D.S. <u>Surf. Interface Anal.</u>, <u>1</u>, 75 1980.
27. Ho, P.S.; Hahn, P.O.; Bartha, J.W.; Rubloff, G.W.; LeGoues, F.K.; Silverman, B.D. <u>J. Vac. Sci. Technol.</u>, 1988, <u>A3</u>, 739.
28. Nuzzo, R.G.; Wong, Y.H.; Schwartz, G.P. <u>Langmuir</u>, 1987, <u>3</u>, 1136.
29. Meyer, H.M., III; Anderson, S.G.; Atanasoska, Lj.; Weaver, J.H. <u>J. Vac. Sci. Technol.</u>, 1988, <u>A6</u>, 1002.
30. Thomas, J.H., III; Bryson, C.E., III; Pampalone, T.R. <u>Surf. Interface Anal.</u>, 1989, <u>14</u>, 39.
31. Pireaux, J.J.; Liehr, M.; Thiry, P.A.; Delrue, J.P.; Caudano, R. <u>Surf. Sci.</u>, 1984, <u>141</u>, 221.
32. Meyer, H.M., III; Anderson, S.G.; Atanasoska, Lj.; Weaver, J.H. <u>J. Vac. Sci. Technol.</u>, 1988, <u>A6</u>, 30.
33. Dinardo, N.J.; Demuth, J.E.; Clarke, T.C. <u>Chem. Phys. Lett.</u>, 1985, <u>121</u>, 239.
34. Soeda, F.; Hayashi, K.; Ishitani, A. <u>J. Electron Spectrosc. Relat. Phenom.</u>, 1982, <u>27</u>, 205.
35. Hahn, P.O.; Rubloff, G.W.; Bartha, J.W.; LeGoues, F.; Ho, P.S. <u>Mater. Res. Soc. Symp. Proc.</u>, 1985, <u>40</u>, 251.
36. Haight, R.; White, R.C.; Silverman, B.D.; Ho, P.S. <u>J. Vac. Sci. Technol.</u>, 1988, <u>A6</u>, 2188.

Chapter 21

Aluminum—Polyester Corrosion

An X-ray Photoelectron Spectroscopic Study

M. Chtaïb[1], Y. Novis[1], R. Caudano[1], P. Lutgen[2], and G. Feyder[2]

[1]Facultés Universitaires Notre-Dame de la Paix, Laboratoire
Interdisciplinaire de Spectroscopie Electronique, Rue de Bruxelles 61,
B–5000 Namur, Belgium
[2]E. I. du Pont de Nemours and Company, Luxembourg

Metallized polymers are used nowadays in numerous industrial applications (food packaging, capacitors, magnetic tapes etc...). The adhesion and the durability of metal/polymer systems represent the most important concepts that concern many research groups (1-3). Obviously, any aggressive medium which corrodes the metal film will be directly related to some loss of adhesion and durability. The aim of this work is to investigate the influence of corrosive environments on aluminum layers evaporated onto PET film and especially on both the Al surface and interface.

Metallized Mylar® was soaked in bidistilled water for three weeks before the XPS profiling. A dry sample was also analyzed for comparison purposes. The profile of the treated film showed the growth of stoichiometric Al_2O_3 on the surface of the Al film .

Furthermore, a Mylar® film was contaminated on purpose with NaCl and dried in air before metallization. XPS results revealed a clear chemical reaction at the interface between Al and NaCl. The growth of Al on NaCl crystals was seen to be responsible for the appearance of a large number of pin-holes and cracks in the samples.

Results

Water corrosion

From Fig. 1, one clearly sees that the XPS profiles of both oxygen and Al are drastically changed when the sample was soaked in water (21 days). At the uppermost surface, there is a thin layer of carbon contamination above large aluminum oxide consisting of 3 layers of different composition.
- The first oxide layer (120 Å) has 40% Al and 60% O : Al_2O_3
- The second one (80 Å) has 50% Al and 50% O : AlO (AlOH hydroxyde)
- The third part (175 Å) of the Al oxide represents a diffusion layer with deficient oxygen composition : Al_xO_y (y smaller than x).
By opposition to the treated film, the reference sample has a much thinner oxide layer (native oxide of ≈ 60 Å) and an Al concentration in the bulk close to 95% .
- The 3-dimensional spectra of Fig. 2 display the Al2p core level. The peak at low binding energy is due to Al in the metallic state while the broad peak is due to Al^{3+} (Al_2O_3). Since this peak is too wide, we invoke for this feature a convolution of Al^{3+} peak with a peak due to other oxide species like AlOH.
- Spectra of Al2p recorded at the interface confirm a slight increase of the oxide peak at the interface for the sample soaked in water. It appears from these results that water intrusion into Al native oxide causes the Al to converts to an hydroxyde with an accompanying change of the metal film composition and morphology.

NaCl corrosion

A Mylar® film was contaminated with NaCl and dried in air before metallization. XPS profiles were carried out in different areas of these samples. Observations by optical microscope were also made in reflexion and transmission modes.
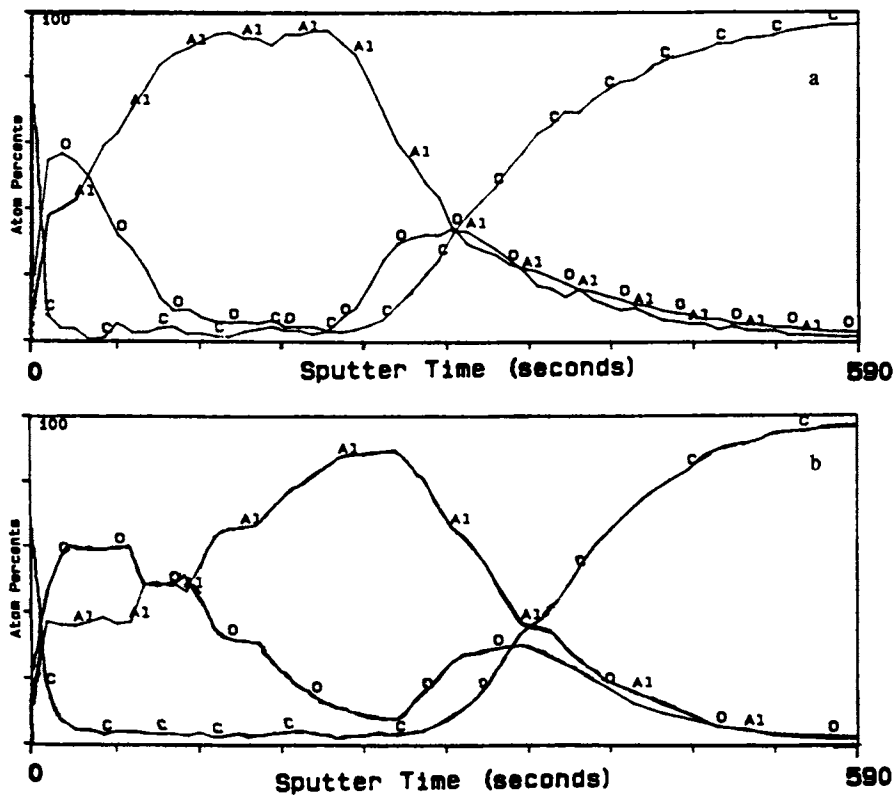
Fig. 1   XPS profiles of Al, O, and C. (a) dry sample, (b) wet sample
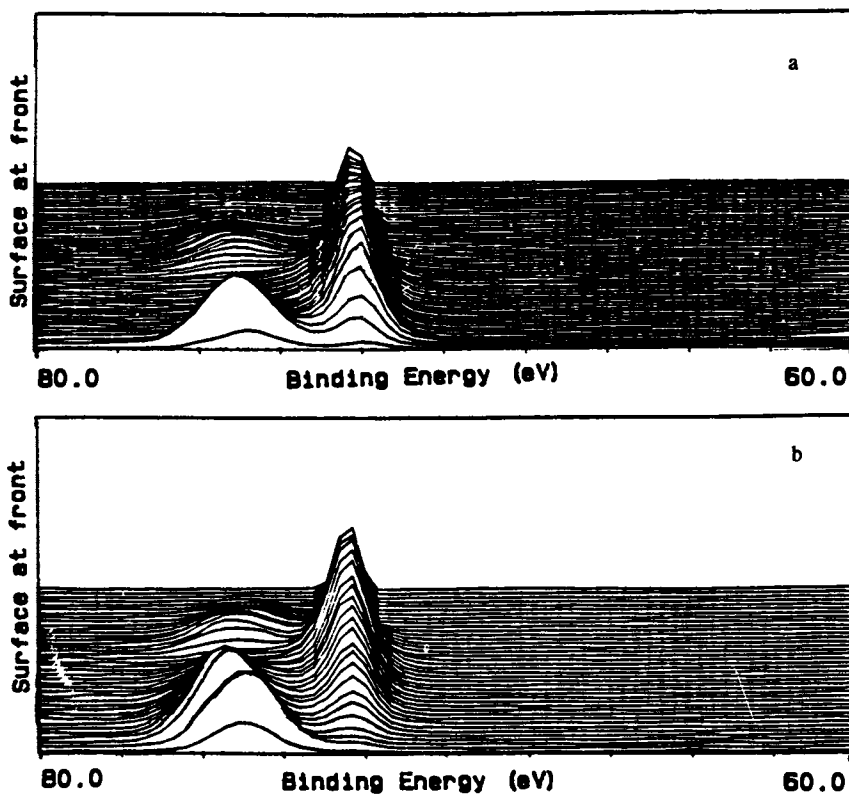
Fig. 2   Al2p core levels versus etching depth (a)
              Ref.sample, (b) wet sample

The XPS profiles were performed on white spots visible in the NaCl contaminated sample. As one can see from the profiles presented in Fig. 3, the Al surface of the NaCl contaminated sample does not present major differences compared to the surface of the reference sample. However, drastic changes between the two samples are observed at the interface and in the bulk of Al :

Firstly : The Al concentration falls from 98 atomic % in the reference sample to around 80% in the contaminated sample. Also a large amount of oxygen and carbon are detected in this latter sample.

Secondly, the Cl signal in the second profile of Fig. 3 fingerprints the presence of NaCl . This latter seems to be located at the interface.

The optical microscope picture obtained from the NaCl contaminated sample exhibits a well oriented growth of Al in some areas of the sample (Fig.4). When performing the XPS profile in these regions, the ion etching reveals the presence of the NaCl inside the crater shown in Fig.5. The two pictures of Fig.6a (reflected light) and Fig.6b (transmitted light) were obtained from the same region of the film. The dark side of the Fig.6b (transmitted light) is due to the region of the aluminized polyester which is almost free of NaCl while the bright spots of this picture are due to the Al cracks matches the locations of the crystals observed in reflection mode (Fig.6a). This means that the corrosion of aluminum takes place where the NaCl crystals are present.

Discussion and conclusion

We have studied the effect of water and sodium chloride (NaCl) on aluminized Mylar. We suggest that the reaction between water and both aluminum and its native oxide is an important step leading to the corrosion of the metallic
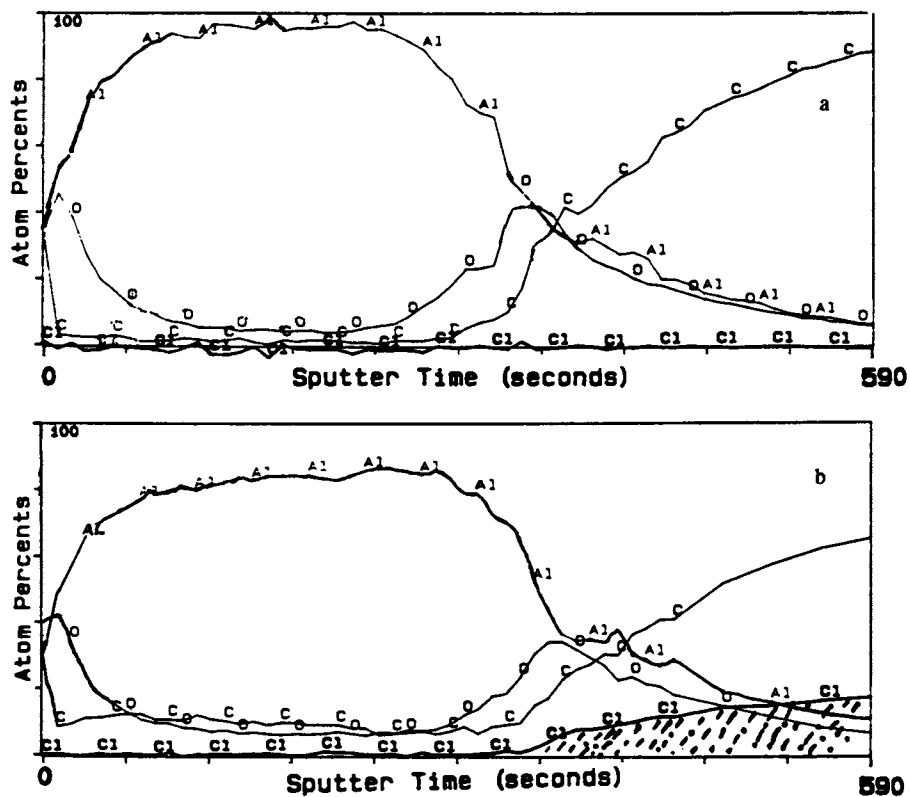
Fig. 3   XPS profiles of Al, O, C and Cl
          (a) Ref. sample, (b) contaminated sample (NaCl)

Fig. 4   Picture of Al/Mylar contaminated with NaCl
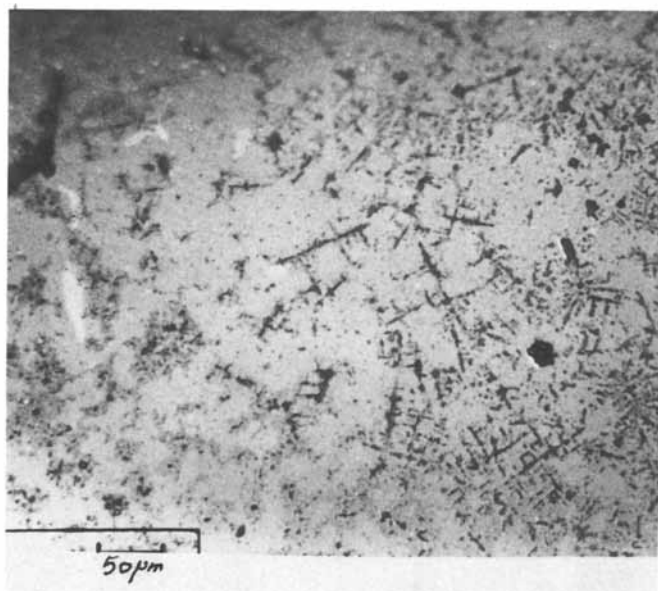
Fig. 5   Picture of NaCl cristals inside the crater.
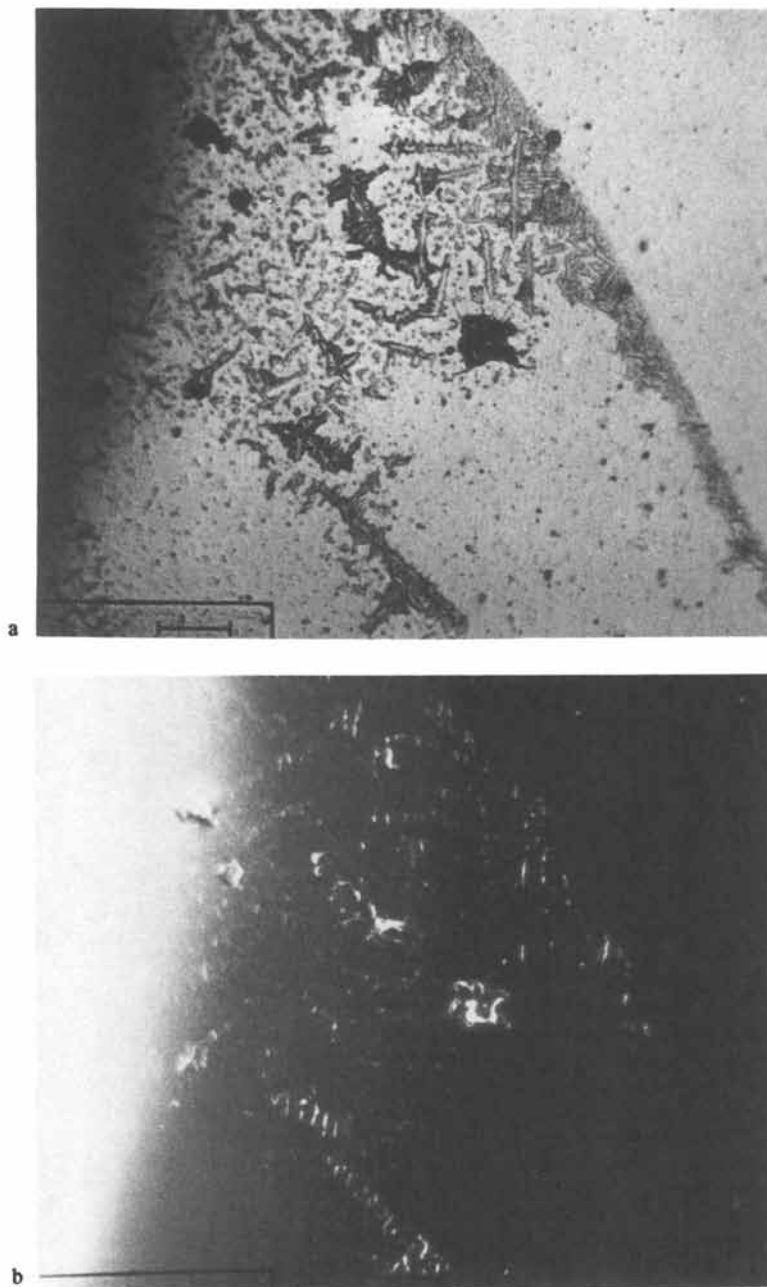
Fig. 6   Picture of same contaminated area. (a)
              reflected light, (b) transmitted light.

film. Even though, the Al native oxide provides protective
barrier. It appeared that the moisture intrusion via the
oxide porosity comes in contact with the aluminum metal and
causes its hydratation by a reaction of this type (4)

$$2 \ Al + 4 \ H_2O \rightarrow 2 \ AlOOH + 3 \ H_2\uparrow$$
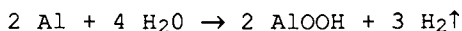
On the other hand, the presence of NaCl contaminant in
aluminized polyester interface can react with Al and leads
to the appearance of pin-holes and cracks in the metallic
layer.

Acknowledgments

Literature cited

1. _Industrial Adhesion Problems_, ed. by D.M. Brews and D.
   Briggs, Chapter 4, Orbital Press, Oxford, 1985.
2. De Koven, B.M.; Hagano, P.L., _Appl. Surf. Sci._ 1986, _27_,
   199.
3. Mittal, K.L., _J. Vac. Sci. Technol._ 1976, _13_, 19.
4. Venables, J.D.; _J. Mat. Sci._ 1984, _19_, 2431-2453.

Chapter 22

Metal–Polyimide Interfaces Characterized by Secondary Ion Mass Spectroscopy

B. K. Furman, S. Purushothaman, E. Castellani, S. Renick, and D. Neugroshl

T. J. Watson Research Center, IBM Corporation, Box 218, Yorktown Heights, NY 10598

The effects of deposition process conditions and post-deposition annealing on the adhesion of electron beam evaporated Ti, Zr, Cu, and Cr to fully cured polyimide have been characterized by Secondary Ion Mass Spectrometry (SIMS) , Auger Spectroscopy and mechanical peel testing. Mechanical peel testing was used to evaluate the relative strength of metal-polyimide adhesion and it's subsequent degradation, as a function of deposition conditions, and post processing . Auger and SIMS analysis provided complementary characterization of peel failure loci and interfaces associated with observed failure . SIMS analysis of as-deposited metal films was also used to characterize impurity levels, both metallic and gaseous, incorporated throughout the metal during deposition. SIMS was also used to characterize the absorption and redistribution of water during processing, using isotopically enriched water exposure. Together these techniques provide a us with a comprehensive understanding of factors influencing metal/polyimide adhesion degradation . Two modes of degradation are reported in this study.

One mode results in the reduction of peel strengths by 25-35% to 45-55 g/mm. This is characterized, through Auger analysis, as a cohesive failure in the polyimide. This region has been identified by SIMS as reactive to isotopically tagged water,suggesting, that the reaction of water with the damaged polyimide decreases the polyimide strength in this area. The observed reaction of water in the region directly below the metal interface is consistent with mechanical weakening of this region during thermal or T&H processing. This is further supported by the fact that similar samples ,identically annealed without exposure to water vapor in air show little or no degradation in peel strengths.

A more dramatic failure results in peel strengths of 0-10 g/mm and is characterized as an adhesive failure at the polyimide/metal oxide interface.This was the only failure mode observed in Ti and Zr films. Isotopically tagged water used with SIMS analysis shows that on annealing water reacts with the Ti with oxygen segregating to the metal/polyimide interface and hydrogen penetrating into the bulk of the Ti, in these samples.

Similar results were observed for samples exposed to light RF sputter cleaning and a Cr adhesion layer. SIMS identified a Cr-oxide region to be enriched in O^{18} if samples are exposed to H_2O water prior to annealing. Extending the time used to ramp the sample to higher temperatures has been demonstrated to delay this interface failure. Again no degradation is observed if samples are not exposed to air prior to thermal processing. In this case we propose that the water absorbed in the polyimide segregates at the metal/polyimide interface and reacts with the metal during the elevated temperature annealing resulting in the formation of an oxygen rich region at the interface and loss of adhesion.

Polymeric materials are increasingly being used as dielectrics in microelectronic applications [1,2]. Among the various polymeric materials being explored and used most is polyimide primarily because of its low dielectric constant , ability to withstand elevated temperatures and resistance to solvents when fully cured. One of the major challenges in building a reliable metal/polymer structure is the adhesion between the metal and the polymer. Numerous studies are reported in the literature where adhesion between metals and polyimide has been examined [3,4,5]. Many of these studies focus on understanding the chemistry of the bonding process between sub-monolayer additions of the metal atoms onto a clean as-cured polyimide surface inside a UHV system. Although such studies provide valuable insight into the fundamental aspects of metal/polyimide bonding under very idealized conditions, they are not necessarily applicable in total to the situation encountered in a practical metal/polyimide structure.

Commonly UHV systems are not used for metal deposition and gaseous impurities can be incorporated into the metal/polyimide interface. In addition, polyimide surfaces are subjected to in situ precleaning using energetic inert ions from a plasma or an ion gun to remove contaminant layers induced from prior processing and/or storage. It has been recently shown that this can lead to significant alterations in the polymer surface [6,7] and incorporation of metallic impurities. The details of the bonding process and hence the adhesion will no doubt be affected by such treatments. Further, metal/polyimide structures of practical interest experience thermal and ambient exposures after deposition as a result of subsequent process steps. Answers to such process related issues are not readily deducible from the fundamental studies. Accordingly, one needs to study metal/polyimide adhesion on samples fabricated under realistic processing environments and subjected to thermal and ambient exposures to understand the relevant issues. In this paper, we address metal/polyimide adhesion from this point of view. Using thin film peel stripes of evaporated onto in situ sputter cleaned polyimide samples under high vacuum process conditions (10^{-7} Torr to 10^{-6} Torr), we have performed peel strength measurements to characterize adhesion and surface analysis of the peel failure surfaces to understand the failure mechanisms. From the data on the as-deposited samples as well as those annealed at 350°C in N_2 or forming gas, we propose a mechanism for the observed adhesion degradation after annealing.The model is based on the premise that water absorbed by the polyimide during processing or from the ambient can react with the damaged region of the polyimide or the metal adhesion layer resulting in adhesion degradation. The model was critically tested by using isotopically tagged water exposure of the polyimide and SIMS, to track the source of the oxygen as well as by an in situ annealing experiment that precluded water absorption and hence the suspected source of oxygen in the polyimide. The results from these experiments support the proposed adhesion degradation mechanism.

EXPERIMENTAL DETAILS

Substrates used for this study were 57 mm silicon wafers which were spin coated with a 5 μm layer of commercial polyimide (PMDA-ODA based) which was fully cured in a flowing nitrogen ambient to a maximum temperature of 400°C. A 200 nm edge coating of Copper was applied on top of the polyimide to act as a peel initiating release layer. Prior to metal deposition, the polyimide surface was sputter cleaned in situ in an RF Ar^+ plasma to remove surface contaminants and to normalize the surface conditions on all the samples studied. Two general conditions were used: 50 W,10 min. and 200W. for 30 min. . These conditions represent the forward power applied to the plasma for a given time. Since these conditions are system dependent they can be better compared using by there resulting etch rates of Silicon dioxide.The above conditions represent etch rates of 15 and 200 nm/min respectively.

After RF sputter etching the substrates were heated to 90°C or 150°C and peel strips of 10 or 50 nm Ti,Zr,Cr,Cu/8μm Cu thickness were then electron beam evaporated without

breaking vacuum on these wafers, through Cu coated stainless steel masks with 1.6mm wide slits in them. A chamber pressure of either low 10^{-7} Torr or low 10^{-6} Torr was achieved just prior to the onset of metal deposition, to investigate the effect of background pressure on adhesion. The wafers were stored in dry nitrogen after deposition until they were removed for peel testing or annealing. 90° peel testing was done in a mini-peel tester at a peel rate of 4.5 mm/s and peel forces were measured using a Sensotec compact load cell that was calibrated to a sensitivity of 50 g/volt. Peel strengths in g/mm were obtained from the peel force traces over peel lengths of at least 30 mm and by averaging the results from at least two to three peels per condition. Some of the wafers were annealed at 350°C in a tube furnace in a flowing ambient of N_2 or forming gas for 30 minutes and peel tested to evaluate the effect of such an exposure.

Surface analysis was carried out on the peeled metal strips as well as the substrate side of the peel failure to characterize the failure loci. Auger analyses were performed using a Physical Electronics (PHI) Model 595 Scanning Auger Spectrometer. A 3 keV electron beam with a 50 nA beam current was used for the analysis of fracture surfaces and elemental depth profiles. A 2 keV Ar^+ ion beam was used for depth profiling. For SIMS analysis, a CAMECA IMS 3F Ion Microscope was used. Depth profiles were obtained by monitoring negative secondary ions of H, D, O^{18}, O^{16} while sputtering with 10 keV Cs^+ ions. Mass surveys and Cu distributions were obtained using 12.5 keV O_2^+ primary ions while detecting positive secondary ions. Typical beam currents were 0.5 μA rastered over an area of 250 x 250 μm. Average sputtering rates were 2.5 nm/s., determined by measuring the crater depth after sputtering .

RESULTS AND DISCUSSION

Table 1 shows the effect of sputter cleaning, metal, and post deposition annealing on peel strength. In all cases ,except Cu ,as-deposited samples were observed to fracture cohesively within the polyimide 10-20 nm below the metal adhesion layer. The strength and depth of the fracture showed little difference regardless of metal deposited. It was noted that poor adhesion was observed if no in situ cleaning preceded metal deposition and that differences in cohesive peel strengths were observed when RF sputter parameters were changed. SIMS surface surveys of as-received and RF sputtered polyimide are shown in figure 1. These results identified that our in-situ "clean" was indeed more complex than the simple removal of surface contaminants and polyimide . In fact metal ions coated onto the walls of the evaporator were being implanted into the near surface region of the polyimide. The level and species of metal are observed to influence the initial peel strength and subsequent thermal degradation rate. To establish consistency within our experiments the evaporation chamber was pre-coated with 200nm of Cu prior to RF sputter cleaning polyimide samples. Figure 2 shows a SIMS in-depth profile of the Cu incorporated during in-situ RF sputter cleaning. Auger analysis has also quantified the level of Cu as 5 % Atomic approximately 5-10 nm deep in the polyimide. This Cu appears innocuous to the as deposited cohesive strength of the polyimide in that similar levels of Cr or low level metal impurity levels with Ar ion beam treatment all result in similar strength cohesive separation when peeled. It was noted that the dose of Ar ion bombardment and resulting damage to the polyimide did effect as-deposited strength. In general low dose bombardment results in higher as-deposited peel strengths . At higher doses no additional degradation is observed because we are sputter etching the polyimide while propagating a constant damage zone ahead of the surface being etched. In this study we have chosen conditions of high dose to eliminate run to run variations which can be observed with low dose exposure as well as the enhanced thermal degradation observed at low dose exposure, as will be discussed later in this paper.

Table I. Metal–Polyimide Peel Strengths

Adhesion Layer	RF Sputter Clean		As Deposited		Anneal[a]		In Situ Anneal[b]	
	Power (W)	Time (min)	Peel Strength (g/mm)	Failure Interface	Peel Strength (g/mm)	Failure Interface	Peel Strength (g/mm)	Failure Interface
Ti	200	30	53–68	Pl–Pl	0	Ti–Pl	60–70	Pl–Pl
Zr	200	30	75–80	Pl–Pl	0	Zr–Pl	—	—
Cu	none	none	0–5	Cu–Pl	20	Cu–Pl	—	—
Cr	200	30	73–78	Pl–Pl	35–45	Pl–Pl	70–80	Pl–Pl
Cr	50	10	70–85	Pl–Pl	10–30	mix	70–80	Pl–Pl

[a] 30 min, 350 °C, F. G.
[b] 30 min, 350 °C, no air, H_2O.
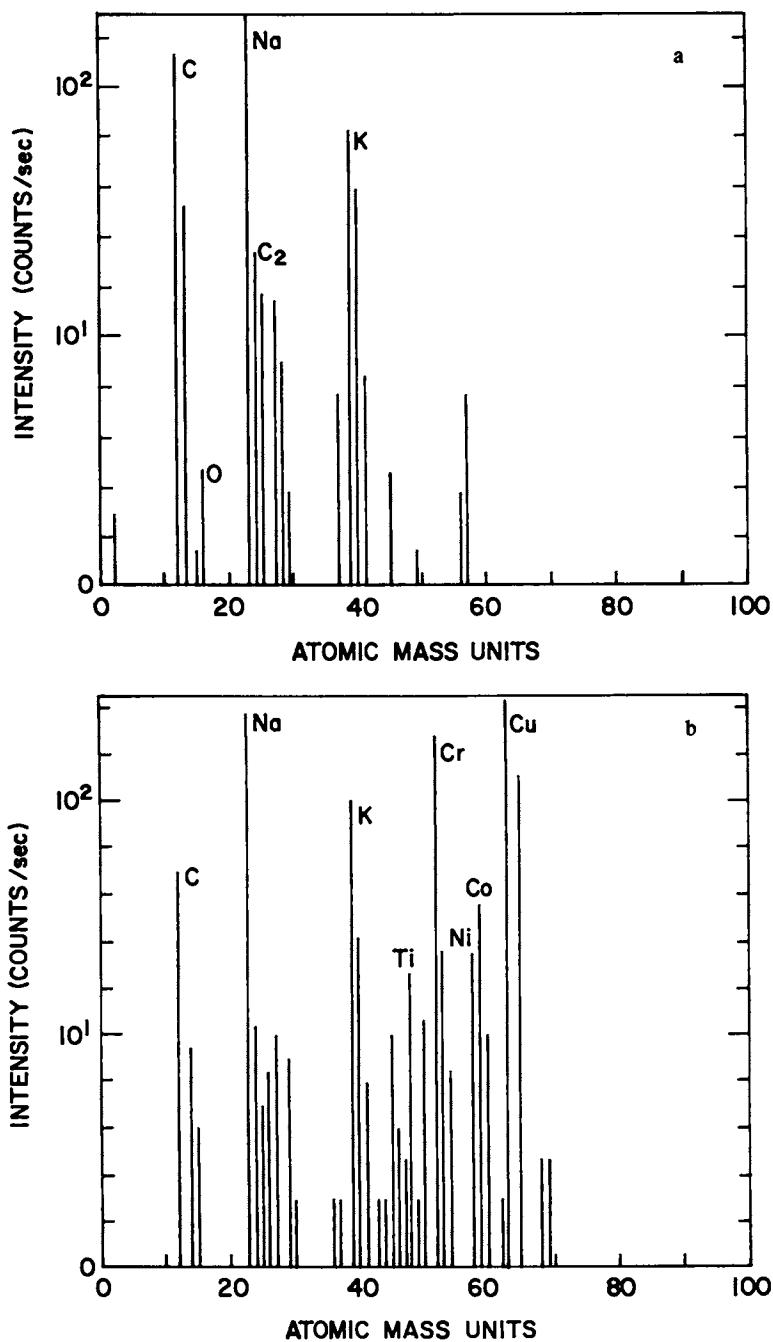
Figure 1. SIMS Surface surveys of (a) as-recieved polyimide and (b) after RF sputter cleaning in Ar ion plasma (200W,30min)
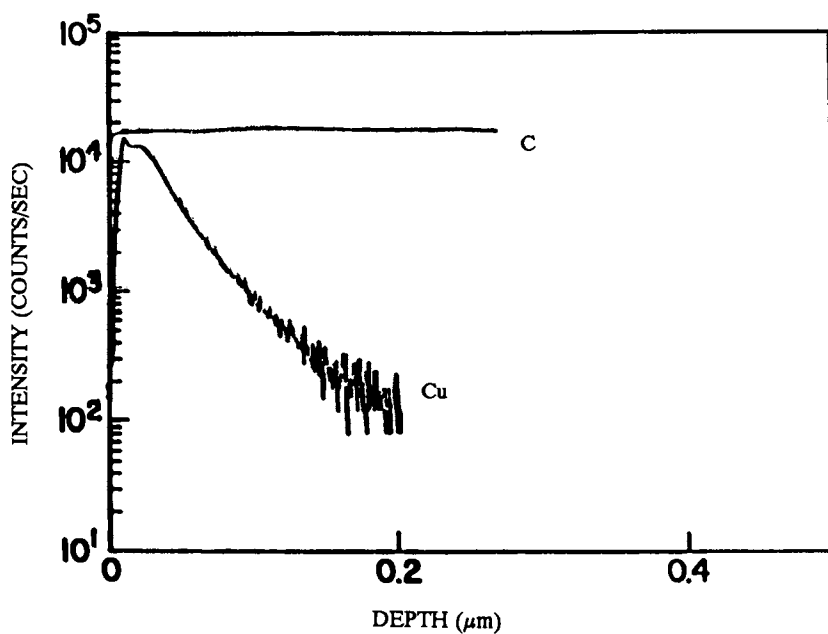
Figure 2. SIMS in depth profile of carbon (polyimide) and Copper introduced during RF sputter cleaning.

As-deposited Ti/Cu peel strips yielded peel strengths of 53-68 g/mm . After the 350°C annealing the peel strengths dropped to a zero value independent of the deposition conditions and the annealing ambient employed. Figure 3 shows Auger spectra of the resulting peel fracture surfaces. On the metal peel surface of the sample peeled in the as-deposited condition, only C, O and N characteristic of a cohesive failure in the polyimide are observed. Subsequent Auger depth profiling, shown in Figure 4(a) indicates that the peel failure occurs within the polyimide approximately 5-10 nm below the Ti/polyimide interface. In the sample peeled after annealing, the metal side of the fracture surface shows high levels of Ti and O indicative of an adhesive failure between the polyimide and an oxidized Ti layer (Figues 3b and 4b). Auger analysis of the polyimide side of this fracture shows no Ti present confirming, that adhesive failure has occured. Similar results were obtained for both nitrogen and forming gas annealing ambient. Auger depth profiling into the Ti film of the peel strips showed that little or no polyimide is present and the oxygen extends from this fracture surface up towards the Ti/Cu interface after annealing in either ambient.

In order to verify if this oxygen was due to absorbed water within the polyimides, experiments were done by exposing the polyimide to H_2O^{18} either before or after the metal deposition, followed by 350°C annealing and depth profile analysis. Thus, one can clearly trace the ingress and migration of absorbed water by monitoring the distributions of O^{18} by SIMS and distinguish these from the oxygen associated with the polyimide substrate as these would be O^{16} . High mass resolution and energy offsets wer used to verify the 18 amu peak was indeed elemental and not a molecular peak from H_2O^{16} Further, these latter mass peaks also would serve as internal standards for surface analysis of the isotopic mass peaks thus helping in eliminating artifacts associated with depth profiling by sputter etching. SIMS results shown in figure 5 indicate that there is a region of absorbed tagged water within the polyimide directly below the Ti after exposure to tagged water. After subsequent annealing at 350°C, the distribution of O^{18} (associated with absorbed tagged water) is observed to sharpen and localize at the Ti/polyimide, . These samples differ from peel strips previously discussed ,in that the top copper layer is significantly thinner to allow in-depth profiling from the metal side without significant interface distortion . SIMS depth profiles of strips peeled from the polyimide ,similar to those shown in Figure 4 except exposed to tagged water are shown in Figure 6. Films just exposed to tagged water and peeled show little or no O^{18} enrichment, Figure 6(a), while the exposed, annealed and peeled sample indicates O^{18} enrichment at the Ti/polyimide interface, Figure 6(b). These results identify that the high oxygen observed by Auger analysis at the fracture surface was originally present as water absorbed within the polyimide and not from the polyimide itself or ambient effects.

From the above results it is clear that the observed degradation of adhesion of Ti to polyimide is a result of the reaction of the water absorbed in polyimide with Ti during the elevated temperature anneals. A few weight percent water is known to be absorbed in polyimides within a very short time on exposure to any ambient bearing humidity [8]. It appears that the absorbed water segregates under the Ti/polyimide interface, see Figure 5. On annealing, the water reacts with the Ti at the interface most probably forming an oxide. We hypothesize that this oxide formation either chemically or physically disrupts the metal-polyimde bonds since adhesive failure results. A schematic representation of this experiment is shown in Figure 7.

In order to verify this claim and to definitively establish the role of absorbed water in the polyimide, the following experiment was performed. Ti/ thick Cu peel strips were deposited on polyimide coated substrates as before, but the vacuum chamber was purged with dry N_2 or forming gas after completing the deposition and the samples were annealed at 350°C, in situ.
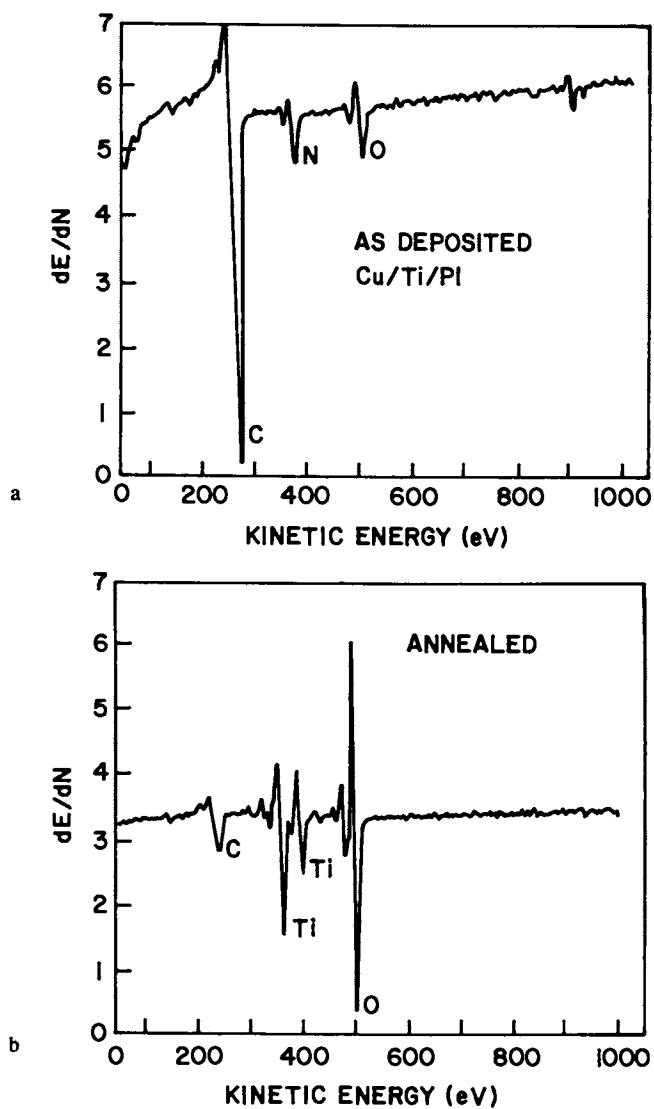
Figure 3. Auger spectra of Ti/Cu strip surfaces peeled from polyimide: (a) as-deposited (b) after 350°C forming gas anneal (200W,30min RF).
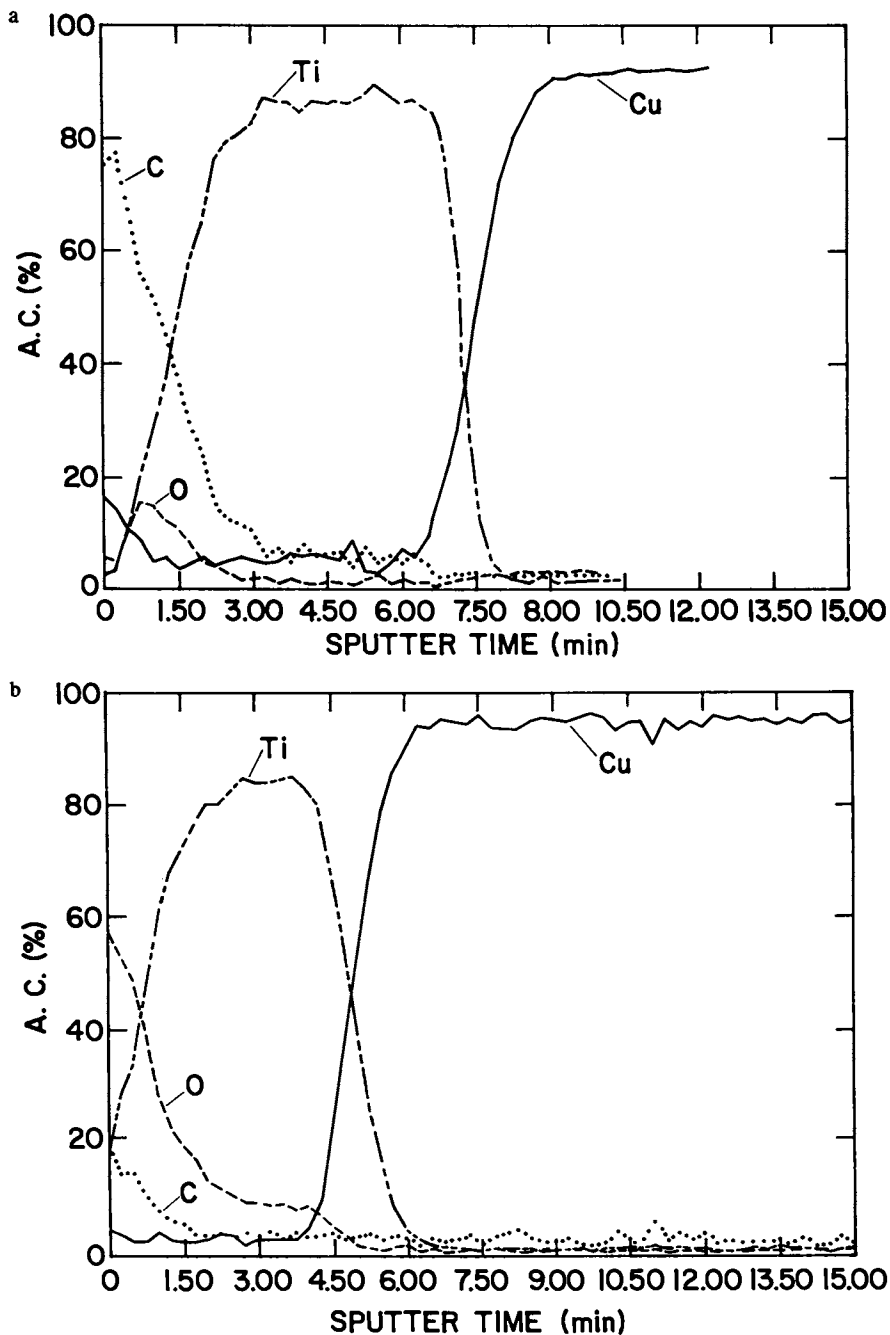
Figure 4. Auger depth profiles of Ti/Cu strip peeled from polyimide: (a) as-deposited and (b) after 350°C forming gas anneal (200W, 30min RF)
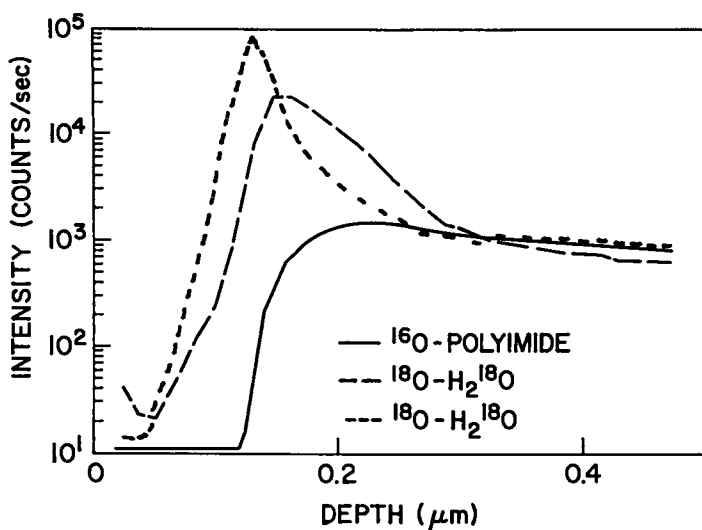
Figure 5. SIMS depth profiles of Ti/thin Cu films on polyimide: as deposited, showing O^{18} from polyimide and ambient humidity exposure; exposed to H_2O^{18} and annealed in nitrogen at 350 °C.
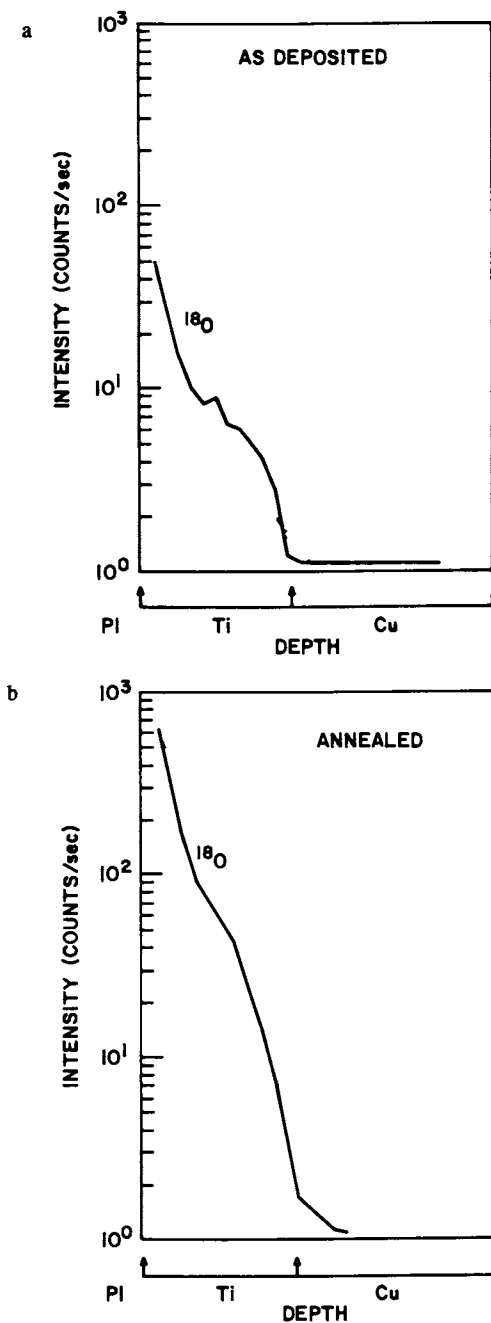
Figure 6. SIMS depth profiles of Ti/thick Cu peel strip surfaces originally deposited on polyimide, exposed to &h2o18 and peeled (a) as-deposited and (b) after 350°C forming gas anneal (200W,30min RF)
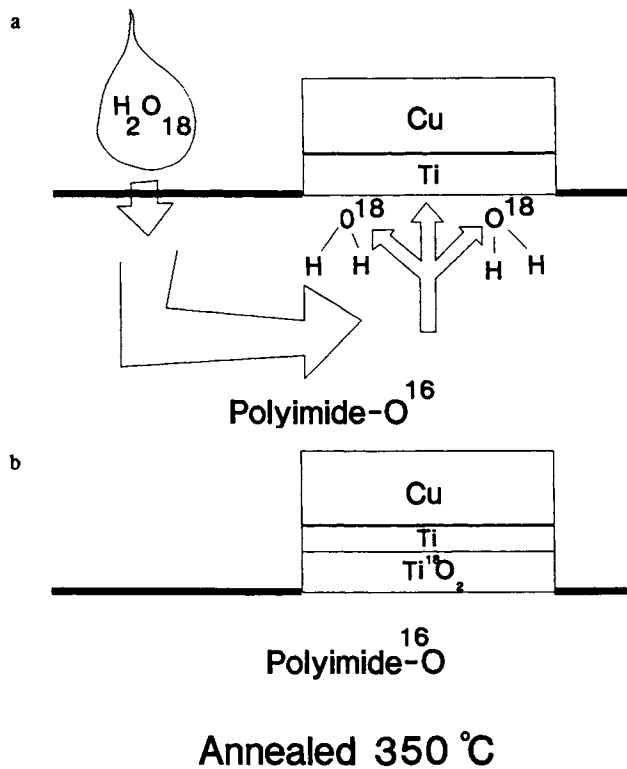
Figure 7. Schematic representation of (a) isotopic water absorption and (b) redistribution after anneal.

Since the parts were never exposed to ambient air prior to annealing, water absorption in the polyimide was precluded. Peel strengths and peel failure loci chemistry in these in situ annealed samples were similar to those of samples peel tested in the as-deposited condition. This conclusively demonstrates that the presence of absorbed water in the polyimide prior to elevated temperature annealing is essential for the thermal degradation of Ti/polyimide adhesion. Attempt to "dry" sample prior to high temperature annealing fails to eliminate this moisture induce degradation of the metal/polyimide interface   In the case of Cr however, surface pretreatment has been shown to significantly retard the rate at which water absorbed within the polyimide can react with the Cr/polyimide interface . SIMS results with isotopically tagged water are shown in Figure 8 for thin Cr/Cu deposited on polyimide. It should be noted that O^{18} profile in Figure 8a differs slightly from Figure 5a. This may be due to differences in the oxygen yield at the interface which can be influenced by the metal layer (Cr vs Ti) over the polyimide. Auger analysis indicated no differences in oxygen distributions between samples. Prior to Cr deposition the polyimide was in-situ sputter cleaned for 30 minutes at 200 W for all samples except the one shown in Figure 8(d) which saw a low dose clean of 10 minutes at 50W. Similar to the experiment described previously for Ti, Figure 8(a) represents the naturally occurring O^{18} distribution in the polyimide. Figure 8(b) is observed after the sample is soaked for 1hour in H_2O^{18} or exposed to H_2O^{18} vapor for 48 hours. We observe a significant (200x) increase in the O^{18} level in the region of Cr/polyimide interface. These results indicate that this region may be capable of gettering water from the bulk of the polyimide. Since no adhesion degradation occurs after the soaking only it is unlikely that significant chemical reaction has occurred at this time. In addition, similar distributions are obtained for D_2O supporting the hypothesis that only absorption and segregation has occurred . If we in-situ sputter clean at high dose as described earlier ,expose to H_2O^{18} and anneal we see no significant penetration or reaction of the O^{18} into the Cr,but a significant level remaining within the polyimide in the region whose cohesive strength has degraded 25-35%, Figure 8c. These results indicate that the water has reacted with the polyimide resulting in mechanical weakening of this region. This is further supported by the fact that if identical samples are subjected to "dry" thermal processing no degradation is observed. In addition similar degradation is observed for long exposure to humid environment at elevated temperature (1000 hr 85 C 70% RH) . In contrast, if the polyimide surface is exposed to a short sputter clean at low power (50W,10') prior to Cr deposition, significant Cr/polyimide adhesion degradation occurs similar to Ti samples. Figure 8(d) shows the O^{18} distribution in a similarly treated sample. In this case 50x levels of O^{18} are observed in the Cr layer compared to the 30 minute 200W sample. Auger analysis confirmed that this corresponds to significant levels of Oxygen (50-60 % At.) within the Cr and accounts for the catastrophic failure at the Cr /Polyimide interface. The exact mechanism of the effect of in-situ sputter cleaning on the kinetics of Cr/polyimide adhesion degradation is still a topic of research. Two potential contributor's are the role of trace metals such Cu introduced during RF cleaning and modification of the polyimide during ion bombardment. Experiments to identify their individual and/or synergistic effect on water diffusion across the metal /polyimide interface and their ability to getter and thus minimize the amount of water available for reaction.

CONCLUSIONS

SIMS has been shown to provide information on trace impurities and isotopic distributions applied to the study of metal/polyimide adhesion. Combined with Auger and mechanical results a more precise understanding of the effects of thin film of processing on adhesion has been obtained. In the case of Titanium ,very good adhesion to sputter cleaned polyimide in the as-deposited condition was observed. However, on subsequent thermal exposure at 350°C for 30 minutes in either N_2 or forming gas the adhesion degrades to zero. This degradation is a result of the reaction of the water absorbed in the polyimide with the Ti during
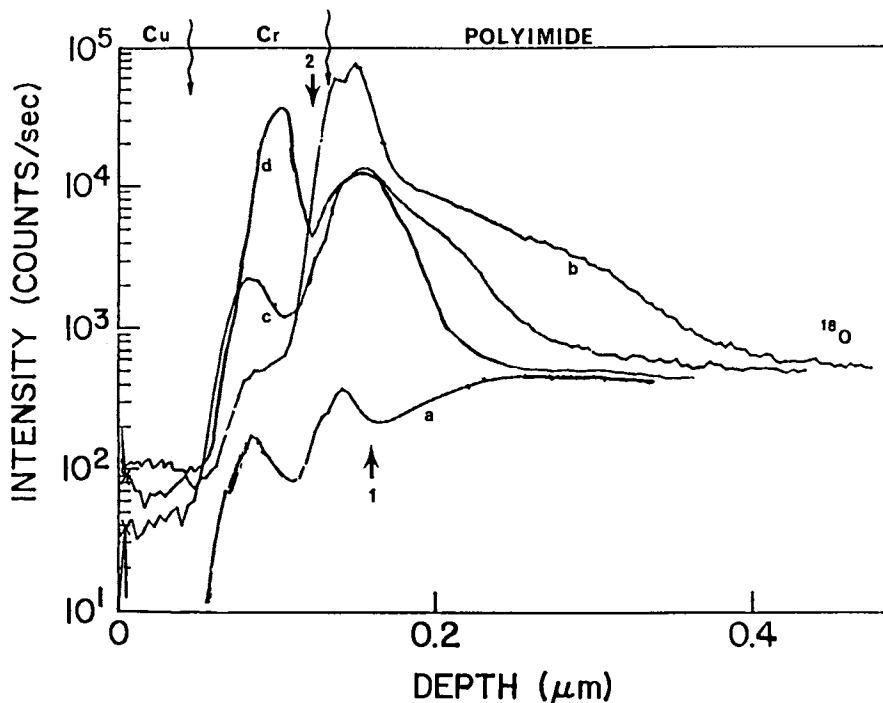
Figure 8. SIMS depth profiles of Cr/thin Cu films on polyimide: (a) as deposited, showing O^{18} from ambient humidity exposure (normalized for isotopic abundance); (b) exposed to H_2O^{18} and (c) exposed to H_2O^{18} and annealed in forming gas at 350 °C (200 W, 30 min RF) and (d) exposed to H_2O^{18} and annealed in forming gas at 350° (50 W, 10 min RF).

annealing to form an oxygen rich Ti layer (most probably a form of titanium oxide) at the Ti/polyimide interface. Similar results are observed for Zirconium . In the case of chromium where the reaction kinetics appears slower than Ti and Zr ,we have found that surface pre-treatment of the polyimide prior to Cr deposition can significantly alter the rate of metal/polyimide degradation. Details asto the role of metallic impurities and a modified polyimide layer in retarding water reaction with the metal/polyimide interface are still under study.

ACKNOWLEDGMENT

REFERENCES

1. M.Terasawa, S.Minami and J.Rubin, *Int. J. Hybrid Microelectron., vol. 6, 1983*, pp. 607-615.
2. T.Watari and H. Murano, *IEEE Trans. Compon. Hybrids Manuf. Technol., CHMT-8 , No. 4, 1985*, 462-467.
3. N.J.Chou and C.H.Tang, *J. Vac. Sci. Technol. A, vol.2(2), 1984*, pp.751-755.
4. P.S.Ho, P.O.Hahn, J.W.Bartha, G.W.Rubloff, F.K.LeGoues and B.D.Silverman, *J. Vac. Sci. Technol. A, vol.3(3), 1985*, pp.739-745.
5. F.Ohuchi and S.C.Freilich, *J. Vac. Sci. Technol. A, vol.4(3), 1986*, pp.1039-1045.
6. W.E.Vanderlinde, P.J.Mills, E.J.Kramer and A.L.Ruoff, *J. Vac. Sci. Technol. B, vol. 3(5), 1985*, pp.1362-1364.
7. P.Bodo and J.E. Sundgren, *Sur. and Int. Anal., vol.9, 1986*, pp.437-440.
8. E.Sacher and J.R.Susko, *J. Appl. Polym. Sci., 23 , 1979*, pp. 2355-2364

Chapter 23

Model Systems for Polyimide-on-Copper Interface

S. Stafström[1], P. Bodö[1], W. R. Salaneck[1], and J. L. Brédas[2]

[1]Department of Physics, Linköping University, S–581 83 Linköping, Sweden
[2]Service de Chimie des Matériaux Nouveaux, Université de Mons, Département des Matériaux et Procédés, 7000 Mons, Belgium

We present results from theoretical studies of diformimide- and methyl-diformimide-on-copper, chosen as a model for the phthalimide- and methyl-phthalimide-on-copper interfaces, respectively. *Ab initio* Hartree-Fock calculations are performed to derive the geometrical and electronic structure of these systems. Valence band spectra obtained from ultraviolet photoelectron spectroscopy (UPS) are presented for mono- and multi-layers of phthalimide- and methyl-phthalimide-on-copper. The theoretical results are used to interpret these spectra. It is shown that the phthalimide molecules interacting with the copper surface, adhere primarily through reaction at the nitrogen sites, which simultaneously lose their hydrogen atoms. Methyl-diformimide on copper is a model for the interaction at the methyl-phthalimide-on-copper interface. The methyl group in this case is assumed to remain at the original position on the molecule. The ligand-copper inter-action is found to take place primaryly between the nitrogen lone pair and Cu 4s orbitals. This type of interaction is, however, considerably weaker than for phthalimide-on-copper. The different interaction patterns observed for the phthalimide- and methyl-phthalimide-on-copper interfaces are discussed in relation to the polyimide-on-copper interface.

Thin films of polymers are becoming important for micro-
electronic applications. Processable polymer films consti-
tute ideal insulating materials between wiring networks in
multilevel VLSI packing technology (1-2). At present, poly-
imide is the most commonly used polymer in such applica-
tions. Understanding of the interaction between the polymer
and the electroactive components is essential in this
context. In particular, for insulating polymers, the adhe-
sion to a metallic substrate is of great importance. Much
effort has been made in trying to relate fundamental inter-
facial chemistry to adhesion in order to find a way to
control adhesion in an intelligent way (3-7).

The properties of the polyimide-metal interface are
different depending on whether the polymer is applied to a
metallic substrate or whether the metal is deposited on the
polymer. That a different interfacial chemistry occurs in
these two situations is clearly demonstrated by a greater
adhesion strength for polyimide on a metal than for the
metal on polyimide (8-9). It is extremely difficult, how-
ever, to prepare for study an ideal interface consisting of
one or two monolayers of polyimide on a clean metal sub-
strate. Therefore, most of the studies of the polyimide-
metal interface are restricted those involving vapor-
deposited metals on polyimide.

To get around the difficulties involved in preparing for
study an interface consisting of a monolayer of polyimide
on a metal substrate, vapor-deposited components of poly-
imide (9-11) and model molecules for parts of the polyimide
(11-12) on metals have been studied recently. Due to the
limited size of these model molecules, they can be vapor-
deposited in monolayers on the surface of clean metallic
substrate in an ultra high vacuum system. In this way,
useful information concerning the initial interface forma-
tion of (parts of) polyimide on a metal surface can be
obtained.

In this article, we present the results of a theoretical
study of two molecules, which model polyimide, interacting
with a cluster of copper atoms. These molecules are
phthalimide (pim) and methyl-phthalimide (mpim). The
chemical structures of phthalimide (pim), methyl-
phthalimide (mpim), and polyimide (PI) are shown in Figure
1. The model molecules represent the carbonyl- and
nitrogen-containing part of PI. It is well known from
earlier work that both the carbonyl groups and the nitrogen
atom react strongly with metals. In particular, it has been
shown that copper, in general, often associates with
nitrogen atoms in certain organo-metallic molecules (13).
The theoretical results are based on *ab initio* Hartree-
Fock calculations on pim and mpim, as well on subsystems of
these molecules representing the most important part in the
interaction with the copper cluster. Results are presented
for the optimized geometry and the density of valence
states (DOVS). The DOVS is used to interpret the results of

ultraviolet (He II) photoelectron spectroscopy, or UPS, of
pim and mpim vapor-deposited on clean polycrystalline
copper substrates.

Results from Core-Level Studies of Phthalimide-on-Copper.

Recently, we have presented results of a study of core
level X-ray photoelectron spectroscopy (XPS) of the
pim/copper interface (12). These previous studies involve a
comparison between the electronic properties of a stable
adsorbate of pim on the copper substrate and those of a
thick (50 Å), multilayer film of pim on copper. The
essential features of the XPS core level spectra presented
in ref. 12 are the following: The C(1s) level is split into
two major peaks with an intensity ratio of 6:2. The high
intensity peak corresponds to the 6 carbon atoms in the
benzene ring, whereas the peak with lower intensity
corresponds to the 2 carbonyl carbons. In the monolayer
case, the carbonyl carbon atoms experience a chemical shift
toward lower binding energy by about 1.2 eV relative to the
multilayer film. The benzene ring carbons remain
essentially unaffected, which indicates that the 6 membered
ring of the pim molecule does not interact significantly
with the copper substrate. The chemical shifts of the O(1s)
and N(1s) peaks, upon going from the monolayer to the
multilayer, are about 0.9 eV and 2.2 eV, respectively. An
analysis of the XPS spectra indicates that the nitrogen
atoms are the primary reaction sites with the copper
substrate (12). The exceptionally large chemical shift for
this type of systems is explained via a scenario in which,
simultaneously to the formation of the N-Cu bonds, the N-H
bond is broken.
   By analyzing the XPS intensities for normal and grazing
exit of electrons from the sample surface it was concluded
that the pim molecules are lying approximately flat on the
copper surface. Note that this orientation of the pim
molecule in principle allows for a considerable interaction
between the benzene ring and the copper surface. However,
it is known from earlier studies that the benzene UPS
valence band remains essentially unaltered when benzene is
deposited on a copper surface (13). No evidence for a
strong π-electron-copper interaction is thus observed
despite the fact that the benzene molecule is believed to
lie flat on the copper surface. Hence, the observation of
only minor chemical shifts in the 1s levels of the benzene
ring carbons is consistent with the proposed orientation
(12) of pim on the copper surface.

Results from Core-Level Studies of Methyl-phthalimde-on-Copper.

Core level XPS studies of adsorbates of mpim on poly-
crystalline copper substrates show a double peak structure

for the nitrogen, carbonyl carbon, and oxygen 1s levels
(14). The major peaks for these levels remain unshifted
compared to the multilayer sample, whereas the additional
minor peaks appear at lower binding energies. The energies
of the minor peaks are very close to the energies observed
for the corresponding levels of the adsorbates of pim on
copper. This result indicates that some mpim molecules
interact with the copper surface in the same way as for
pim, whereas other mpim molecules remain intact. In our
studies of mpim we will exclusively analyze a type of
interaction for which the methyl group remains bonded to
the molecule. Since the case for which the methyl group is
released is identical to the case of pim-on-copper, this
type of interaction is already included in the study of
pim. The differences in interactions between the pim-Cu and
mpim-Cu interfaces will be discussed in more detail in
section 4.

Computational Details

The theoretical results presented in this article are all
based on *ab initio* self-consistent field (SCF) Hartree-Fock
calculations (15). The SCF wavefunctions are expanded in a
basis of atomic orbitals (AO's). The AO's are expressed in
terms of contracted Gaussian functions. In order for the
basis set to be well-balanced, a similar contraction
pattern is used for all atoms involved. The particular
contraction pattern utilized here is of split-valence type.
The parameters entering the Gaussian functions as well as
the contraction pattern are taken from ref. 16. The C, N,
and O basis sets are (3s2p) contractions of a (7s4p)
primitive set. The H basis set composition is (4s) con-
tracted into (2s). The Cu basis set starts with a (13s7p4d)
primitive set and adds one function to the 4p region with
exponent 0.09. The contraction yields a basis set (5s3p2d).

The Model System for Phthalimide-on-Copper

Since the pim and mpim molecules are quite large, any *ab
initio* calculation including a cluster of metal atoms will
necessarily be very tedious. Therefore, it is desirable to
model the ligands by a subsystem which includes only the
part that is primarily involved in the interaction with the
copper surface. As mentioned in the introduction, data from
XPS core level spectroscopy show that the nitrogen atom is
the primary reaction site in the interaction between pim
and a copper surface, and that the effect of this inter-
action does not extend significantly into the benzene
moiety of the pim molecule. Therefore, we chose as a model
system for pim the molecule: $NH(CHO)_2$ (di-formimide, see
Figure 1). As will be shown in the next section, the el-
ectronic structure of this model molecule has an electronic
structure which very much resembles that of the imide part

of pim. It is expected, therefore, that the results ob-
tained for this model molecule, concerning the interaction
with copper, also hold for pim.

   Due to the relatively large sized systems included in
this study (metal ligand complexes) we are unable to extend
the calculations to correlated wave-functions. However,
studies on small ligands, like CO, interacting with metal
clusters, show qualitative agreement between the SCF method
and methods involving correlated wave-functions (17).

Partial Density of Valence States

Both pim and the model system NH(CHO)$_2$ have C$_{2v}$ symmetry.
Taking into account the symmetry restrictions of this point
group, a full geometry optimization is performed. A com-
parison between the structural and electronic properties of
the two systems is presented in section 3. The comparison
is made more direct by comparing the partial DOVS of the
imide group of the two molecules. This quantity is obtained
by weighting the contributions from each molecular orbital
(MO) to the DOVS by a factor which is proportional to the
content of a particular subset of AO's, g, to the MO (in
this case g consists of all valence AO's of the imide group
NH(CO)$_2$). The weighting factor, I$_n$(g), is defined in the
following way:

$$I_n(g) = \sum_{p,q \in g} C_{pn} S_{pq} C_{qn} \qquad (1)$$

where C$_{pn}$ is the coefficient for the pth atomic orbital of
molecular orbital n in the LCAO expansion of the MO's, and
S$_{pq}$ is the overlap matrix element. Since the molecular
orbitals are normalized, the sum of the partial DOVS over
all subsets of atomic orbitals yields the total DOVS.

The Copper Cluster in the case of Phthalimide

It has been shown from studies of the copper-CO system,
that clusters of five and nine copper atoms produce similar
interaction features (17), whereas limiting the cluster to
one copper atom only is too severe an approximation to the
copper surface. Based on these findings, a Cu$_5$ system is
chosen to represent the copper surface in the study of pim-
on-copper. The Cu$_5$ cluster is a square pyramid with Cu-Cu
distances taken from bulk data. Pim is placed on top of the
pyramid with the nitrogen atom pointing towards the top
copper atom (see Figure 2). This orientation is based on
the result of XPS core level spectroscopy, showing that the
nitrogen atom is the primary reaction site with the copper
surface. The nitrogen atom is restricted to lie on the
fourfold axis of the Cu$_5$ cluster and the ligand is oriented

Polyimide
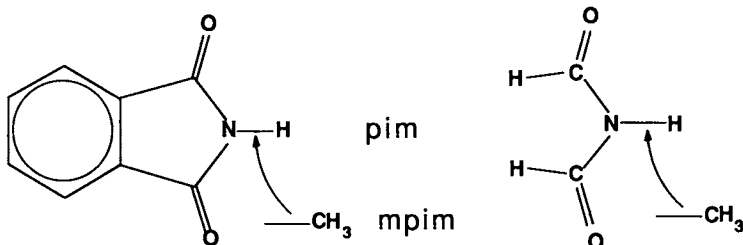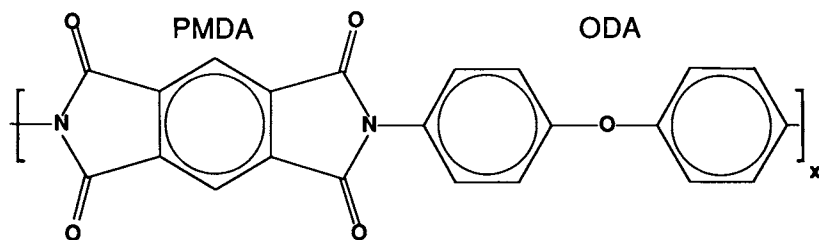
Figure 1. Chemical structure of a polyimide (PI) unit cell (top), phthalimide (pim) and methyl-phthalimide (mpim) (bottom, left), and the model systems NH(CHO)$_2$ and NCH$_3$(CHO)$_2$ (bottom, right).
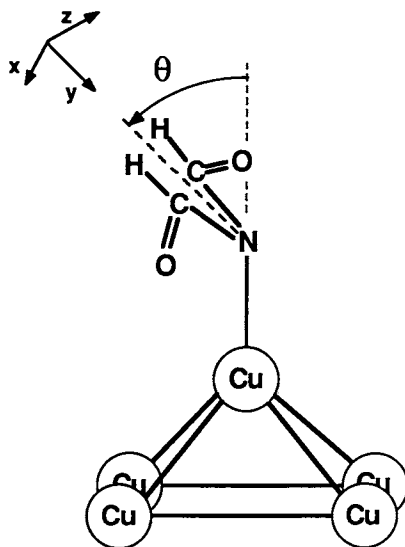
Figure 2. The N(CHO)$_2$-Cu$_5$ cluster.

relative to the copper cluster in such a way that the whole
system has σ symmetry with the mirror plane parallel to the
yz-plane (see Figure 2). With these restrictions in the
metal-to-ligand orientation, we optimize the Cu-N distance
and the angle between the ligand plane and the xz-plane,
denoted θ in Figure 2, as well as all bond lengths and bond
angles of the N(CHO)$_2$ molecule. The results of this
calculation are presented in section 4.

Model System for Metyl-phthalimide-on-Copper

As discussed above, the studies of the mpim-on-copper
interface presented here treat the methyl group as re-
maining bonded to the rest of the molecule, in contrast to
the case of pim for which the hydrogen is released from the
nitrogen atom upon interaction with copper. With the methyl
group still attached to the imide nitrogen, the metal-
ligand interaction is weaker for the mpim-on-copper system
than for the pim-on-copper system. Since the chemical
shifts give no indication of a preferred reaction site, the
choice of a model system for mpim interacting with copper
is less obvious. However, photoemission studies of mole-
cules on surfaces, including a variety of metal surfaces,
usually show large shifts in binding energy for lone pair
orbitals, indicating that the interaction primarily takes
place at lone pair sites. In order to investigate the
changes in the UPS valence band spectrum of mpim due to
interactions with a copper surface we take as model mole-
cule for mpim, NCH$_3$(CHO)$_2$. In this molecule, all the lone
pair orbitals of mpim, namely those at the nitrogen and
oxygen sites, are included but the benzene ring is omitted.
This is the same type of approximation as taken for the
pim-copper interface which makes comparative studies
between the two systems possible.
    Results from geometry optimizations and electronic
structure calculations on mpim and NCH$_3$(CHO)$_2$ (both having
σ symmetry), including comparison of the partial DOVS for
the NCH$_3$(CO)$_2$ group, are presented in section 3.

The Copper Cluster in the case of Metyl-Phthalimide

 Assuming that mpim lies approximately flat on the copper
surface, we select two different orientations of NCH$_3$(CHO)$_2$
relative to the copper cluster, one for which the nitrogen
atom is considered as the primary reaction site (see Figure
3a) and another for which the carbonyl groups are put on
top of Cu atoms (see Figure 3b). In order to make compara-
tive studies between these two structures, we include a
cluster of four copper atoms in the studies of the mpim-
copper interface. The Cu$_4$ cluster is the tetrahedron shown
in Figure 3. The Cu-Cu distances are taken from bulk data.
In optimizing the geometry of the two configurations, we

found no stable value for ligand–Cu distance. Instead we
fix the distance between the Cu cluster and the ligand. For
the structure shown in Figure 3a, we set the N–Cu bond
length to 2.3 Å, which is the value optimized for the N–Cu
distance in NH_3–Cu_5 (18). We have also performed calcul-
ations for other values of the N–Cu distance and found that
the electronic properties of the ligand are quite insen-
sitive to variations in this parameter. With the N–Cu dis-
tance fixed, we have optimized the angles θ, α and β, de-
fined in Figure 3a. Except for the β angle, no optimization
of the ligand geometry is performed. The geometrical param-
eters for $NCH_3(CHO)_2$ are fixed to those optimized in the
case of the free molecule. This simplification is based on
the fact that the Cu–ligand interaction is much weaker in
this system than in the previously discussed $N(CHO)_2$–Cu_5
system.
    To study the type of interaction obtained when the car-
bonyl groups are close to copper, we consider the arrange-
ment shown in Figure 3b, where the Cu_4 cluster has been
rotated 90° compared to the previous arrangement. The two
lower Cu atoms now coincide with the mirror plane of the
ligand and the top Cu atoms are close to the oxygen atoms.
No optimization of the geometrical parameters that deter-
mine the ligand-to-copper orientation is performed in this
case. Instead, the Cu_4 cluster is oriented relative to the
ligand in such a way that the two topmost Cu atoms lie
precisely below the C=O bond. The C–Cu and O–Cu distances
are fixed to 2.28 Å and 2.49 Å, respectively. The N–Cu
distance is in this case 2.63 Å. The geometrical parameters
for $NCH_3(CHO)_2$ are fixed to those optimized in the case of
the free molecule and the angles θ and α are put to 90°.
Like for the structure displayed in Figure 3a, these sim-
plifications are rationalized by the fact that the inter-
actions between $NCH_3(CHO)_2$ and the copper cluster are weak.

Results for Isolated Molecules

In this section, the experimental UPS (He II photons) va-
lence band spectra for pim and mpim are presented together
with convoluted DOVS spectra for pim and mpim, and their
respective model systems, $NH(CHO)_2$, and $NCH_3(CHO)_2$. The
theoretical results are used to interpret the experimental
spectra. We will also show that the model systems have
electronic and geometrical properties very similar to those
of the pim and mpim molecules, respectively.

Phthalimide

The UPS valence band spectrum for a multilayer (50 Å thick)
pim film is shown in Figure 4, together with the convoluted
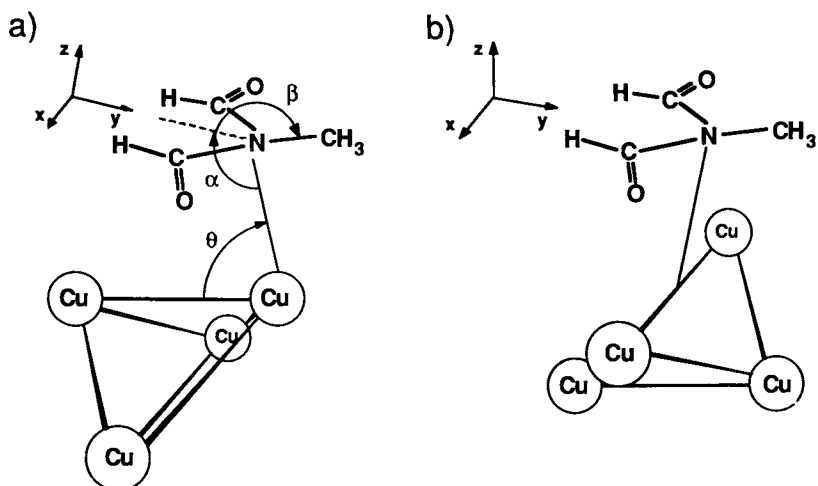
Figure 3. The $NCH_3(CHO)_2-Cu_4$ cluster: a) orientation when the nitrogen is close to Cu and b) orientation when the carbonyl group is close to Cu.
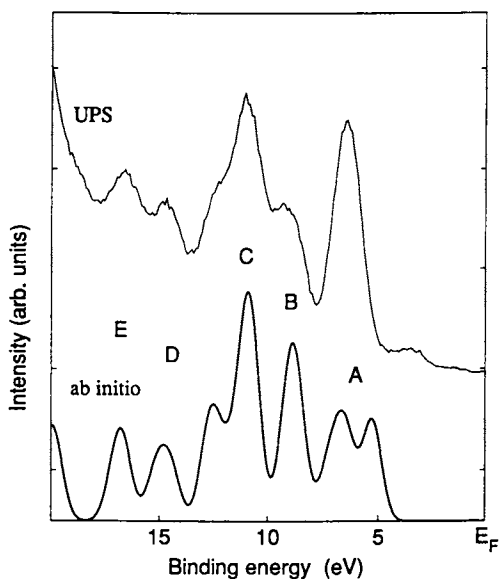
Figure 4. UPS valence band spectra for multilayer film of pim on copper (top) and the theoretically calculated DOVS for pim (bottom).

DOVS spectrum of an isolated pim molecule obtained from an *ab initio* calculation including geometry optimization. The two spectra are remarkably similar, which makes an inter- pretation of the experimental peaks in terms of specific molecular orbitals (MO's) very fruitful.

Starting from the low binding energy side we find a single, quite broad peak (peak A), 7 eV below the Fermi level in the experimental spectrum (The small shoulder at the low binding energy side of this peak is due to Cu 3d electrons from the substrate). The theoretical result shows two peaks around this energy. The one at the lowest binding energy is due to two π-orbitals localized to the benzene moiety, whereas the other peak contains three MO's, one nitrogen lone pair orbital (π) and two oxygen lone pair orbitals (σ). The reason for the discrepancy between the experimental and theoretical spectra is not clear to us. It should be noted that the same splitting is observed in calculations using a minimal basis set.

Peak B in the theoretical spectrum (at 9 eV) derives its strength from 4 MO's, two π-orbitals localized to the C=O unit (bonding) and the benzene moiety, respectively. The two σ-orbitals associated with this peak are localized mostly to the benzene moiety. The main peak at 10 eV (peak C) is found to be strongly dominated by delocalized σ- orbitals. The shoulder at the high binding energy side of this peak contains two molecular orbitals, one that is delocalized over the whole molecule and another strongly localized to the N-H bond. Peaks D and E, finally, contain two σ-orbitals each. The D-peak MO's are rather delocal- ized, whereas for peak E, there is one molecular orbital localized mainly to the benzene ring and another strongly localized to the N-H group.

Comparison between Phthalimide and $NH(CHO)_2$

In order to examine to what extent the model molecule, $NH(CHO)_2$, reproduces the valence electronic properties of the nitrogen-carbonyl part of pim, we compare the partial DOVS spectrum for the imide part of these two molecules (see Figure 5, the spectra are normalized in such a way that the maximum peak has the same height in both cases). Indeed, the two spectra are remarkably similar. In par- ticular, we calculate the relative difference in LCAO coefficients for the nitrogen lone pair orbital in peak A of the two systems to be less than 3%. The only major difference between the two spectra is a stabilization of the D peak in going to the pim molecule. This behavior is understood from the fact that in pim, the orbitals of peak D are delocalized over both the imide- and the benzene moieties, whereas in $NH(CHO)_2$ they are forced to be localized to the imide moiety.

The common geometrical parameters of pim and $NH(CHO)_2$ are found to be in close agreement. The C-N, C=O, and N-H bonds are optimized to be 1.391 Å, 1.213 Å, and 0.999 Å in pim and 1.377 Å, 1.212 Å, and 1.005 Å in $NH(CHO)_2$. The bond angles C-N-C and O-C-N are optimized to be 114° and 126° in pim and 124° and 124° in $NH(CHO)_2$. The shorter C-N bond in the model molecule is consistent with the observation of a slightly larger $C\ 2p_z$-$N\ 2p_z$ bond order in $NH(CHO)_2$ as compared to pim. This increase in bond order is a compensation for the loss of correction bond order to the benzene ring not present in the model system.

Methyl-phthalimide

The UPS valence band spectrum for a multilayer mpim film is shown in Figure 6, together with the convoluted DOVS spectrum of an isolated mpim molecule obtained from an *ab initio* calculation including geometry optimization. The equalities in structure between pim and mpim produce only minor differences in the DOVS for these molecules (compare Figures 4 and 6). Therefore, the assignments made above for pim also hold in the case of mpim. The increase in intensity of peak B, compared to what is observed for pim, is found to be due to s-bonding carbon-hydrogen molecular orbitals of the methyl group. The shoulder at the high binding energy side of peak C observed for pim is also less pronounced in the case of mpim. We recall that this peak is partially due to a molecular orbital localized to the N-H bond. Upon formation of the N-C bond instead, the corresponding molecular orbital appears closer to the maximum of peak C. Indeed, this behavior is also observed experimentally (compare Figures 4 and 6). The additional, low intensity peaks in the region of peaks D and E, observed both theoretically and experimentally, are also due to the mixing of the methyl group orbitals with those of the pim moiety.

Comparison between Methyl-phthalimide and $NCH_3(CHO)_2$.

The local DOVS spectra arising from the $NCH_3(CO)_2$ group, common to both mpim and $NCH_3(CHO)_2$, show the same type of agreement that was previously observed between $NH(CHO)_2$ and pim. This indicates that the electronic properties of $NCH_3(CHO)_2$ represent well those of the $NCH_3(CO)_2$ group of mpim.

The common geometrical parameters of mpim and $NCH_3(CHO)_2$ (both having σ symmetry) are also found to be in close agreement. The C-N, C=O, and N-C bonds are optimized to be 1.392 Å, 1.216 Å, and 1.454 Å in mpim and 1.379 Å, 1.213 Å, and 1.466 Å in $NCH_3(CHO)_2$. The bond angles C-N-C and O-C-N are optimized to be 112° and 125° in mpim and 120° and 124°
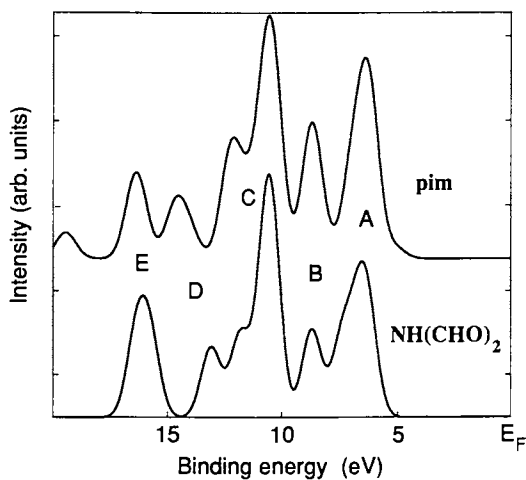
Figure 5. Partial density of states for the imide group of pim (top) and $NH(CHO)_2$ (bottom).
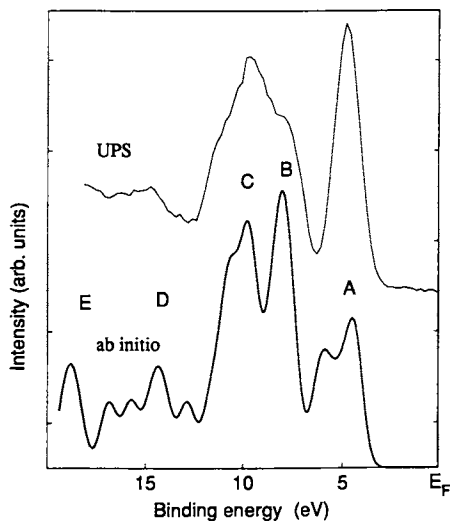
Figure 6. UPS valence band spectra for multilayer film of mpim on copper (top) and the theoretically calculated DOVS for mpim (bottom).

in $NCH_3(CHO)_2$. The methyl carbon is co-planar with the
phthalimide (or imide) part of the molecule, which, as in
the case of pim and $NH(CHO)_2$, produces an sp^2 hybridization
of the nitrogen AO's with the lone pair occupying the N p_z
orbital.

Results for Metal-Ligand Systems

Phthalimide-On-Copper

Based on the findings from XPS studies, namely that the pim
molecules interacting with the copper surface adhere pri-
marily through reaction at the nitrogen sites (see above),
we have studied the model system $N(CHO)_2-Cu_5$ (see Figure
2). The optimized geometry and the DOVS for this system are
presented here together with the experimental UPS valence
band spectrum for an adsorbate of pim on copper.

The angle θ, giving the orientation of the ligand
relative to the Cu_5 cluster, was optimized and found to be
$0°$. This result indicates that the ligand is directed
normal to the copper surface. (The Cu_5 cluster can be
regarded as modelling a Cu(100) surface) This finding is
seemingly in contradiction with the results of angular
dependent XPS studies of the pim-copper interface, which
indicate that pim lies approximately flat on a poly-
crystalline copper surface. However, since the copper
surface in these experiments was polycrystalline, it is
less meaningful to refer the orientation of the Cu_5 cluster
to the normal of the surface (12). Furthermore, the
presence of the benzene ring in the experimentally studied
pim molecule might also produce additional interactions
with the copper surface that can influence the value of θ.

The knowledge of how the pim-Cu interaction depends on
the value of θ can be extended by performing calculations
with the θ angle fixed to different values. Here, we
consider three different values of θ, namely; $0°$, $60°$, and
$90°$. The last value represents an orientation where the
ligand is _parallel_ to the base plane of the Cu pyramid.
Values for optimized bond lengths and bond angles of the
ligand, and for the N-Cu bond length in these three cases
are presented in Table 1. Clearly, the N-C and N-Cu bond
show a strong q dependence, whereas the C=O bond is less
affected. The larger N-C distance in the case of $\theta=90°$ is
understood from the fact that the hybridized N $2s,2p_y$
orbital, that for $\theta=0°$ participates in the bond with Cu,
in this case mixes with the corresponding orbitals of the
neighboring carbon atoms. The mixing occurs in an _anti-
bonding_ fashion, which weakens the N-C bond.

Table I. Carbon-nitrogen (C-N), carbon-oxygen (C=O), and nitrogen-copper (N-Cu) bond-lengths (in Å) for Cu_5-N(CHO)$_2$ for three different values of θ, and the C-N and C=O bond lengths for the isolated NH(CHO)$_2$ molecule.

| | Cu_5-N(CHO)$_2$ | | | NH(CHO)$_2$ |
	$\theta=0°$	$\theta=60°$	$\theta=90°$	
C-N	1.344	1.360	1.378	1.377
C=O	1.234	1.229	1.224	1.212
N-Cu	1.910	1.966	2.078	

Bond-Order Analysis

By performing a Mulliken population analysis we obtain the bond orders for the various chemical bonds in the system. The bond order provides us with information about the strength of the chemical bond as well as the bonding/anti-bonding characteristics. In particular, for the N-Cu bond order in the case of $\theta=0°$ we find bonding contributions from mixing of the N 2s,2p$_y$ orbitals with the Cu 4p$_y$ orbital, but anti-bonding contributions from mixing of the N 2p$_y$ orbital with the Cu 4s orbital. In the case of $\theta=90°$, the situation is different. With the z-direction defined to be normal to the plane of the molecule (see Figure 2), the nonvanishing N-Cu bond orders come from mixing of the N 2s,2p$_z$ and Cu 4s,4p$_z$ orbitals. The Cu 4p$_z$ orbital is observed to participate in bonding MO's whereas the Cu 4s orbital mixes with the nitrogen orbitals in an anti-bonding fashion.

The UPS valence band spectrum for a monolayer (adsorbate) of pim on a polycrystalline copper surface is shown in Figure 7, together with the corresponding spectrum for the multilayer sample, previously displayed in Figure 4. The changes in the emission spectrum of pim in going from multilayer to monolayer samples are the following. Peak A shifts slightly towards lower binding energies, widens and overlaps with the strong peak of the Cu 3d states, peak B grows in intensity, peak C looses the shoulder at the high binding energy side and decreases in intensity. The D and E region peaks shift to lower binding energies and a new emission peak is observed between peaks D and E.

Density of Valence States

Figure 8 shows the theoretically calculated partial DOVS
for the <u>imide part</u> of the $N(CHO)_2$-Cu_5 system. The result
displayed is for $\theta=0°$, i.e., the ground state value of θ
for the model system. In fact, the DOVS is shown to be
quite insensitive to changes in θ, as will be discussed
further below. For comparison, the DOVS for the imide part
of the $NH(CHO)_2$ molecule is also included. The differences
between these two theoretical spectra should correspond to
the differences observed between the UPS valence band
spectra for mono- and multilayer samples of pim, i.e., the
spectra shown in Figure 7. Indeed, we observe changes in
the DOVS in going from the free model molecule to the model
system interacting with copper, that are very similar to
the changes observed experimentally in going from multi-
layer samples to adsorbates. The differences observed
between the lower and upper curves of Figure 8 are summa-
rized as follows: peak B grows in intensity compared to
peak C, the shoulder at the high binding energy side of
peak C is no longer observed, and an additional peak is
observed between peaks D and E.
   Starting from the high binding energy side, the MO
responsible for the additional structure between peaks D
and E (at 14.4 eV) originates from a MO in peak E of the
free molecule. This MO has a strong N $2s,2p_y$-H 1s bonding
character. Replacing the hydrogen atom by the Cu cluster
destabilizes this state and a MO involving a N $2s,2p_y$-Cu 3d
mixing (anti-bonding) is formed instead. For $\theta=90°$, the
corresponding MO contains the N 2s-Cu 3d orbitals and
appears in this case at 14.7 eV. The shoulder at the high
binding energy side of peak C (at 11.8 eV) in $NH(CHO)_2$ (see
Figure 8, bottom) is due to a strong N $2p_y$-H 1s bonding
orbital, which in the ligand-copper system is replaced by
an anti-bonding N $2p_y$-Cu 4s MO ($\theta=0°$). This replacement de-
stabilizes the molecular orbital, which appears at 9.3 eV
instead. For $\theta=90°$, the situation is quite different since
there is essentially no overlap between the N $2p_y$ orbital
and the copper system. As discussed above, the N $2p_y$ orbi-
tal mixes with different atomic orbitals of the ligand
instead. The increase in intensity of the peak B is par-
tially due to the molecular orbital shifted to 9.3 eV, but
also arises from some mixing of Cu 3d orbitals with ligand
orbitals causing a shift of states from peak C to peak B
(for both $\theta=90°$ and $\theta=90°$).
   It is apparent from the discussion above that the DOVS
is not sensitive enough to changes in θ, and can therefore
not be used directly to determine the ligand-to-copper
orientation. From the experimental point of view, a well
defined and flat surface is needed in order for a unique
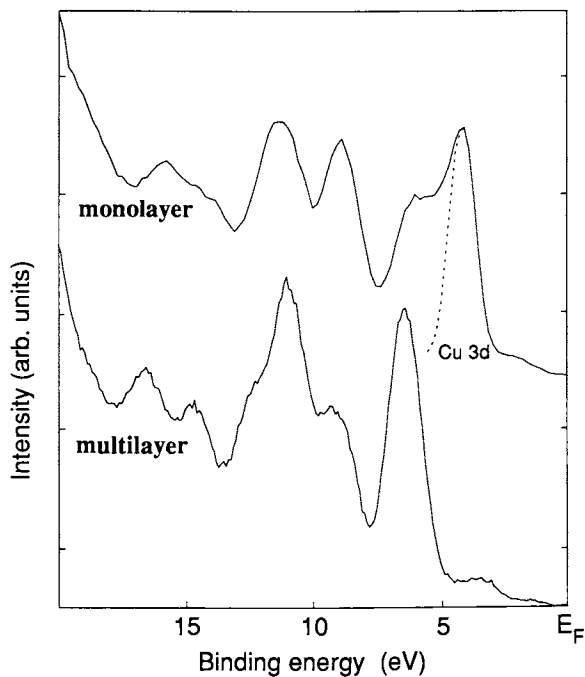
Figure 7. UPS valence band spectra for multilayer (bottom) and monolayer (top) films of pim on copper.
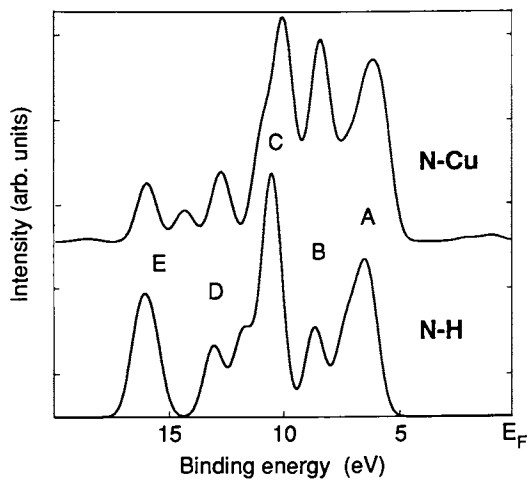
Figure 8. Partial density of states for the imide group of $NH(CHO)_2$ (bottom) and $N(CHO)_2-Cu_5$ (top).

orientation of pim on copper to be achieved. With such a
surface, angular resolved photoemission studies can be
performed and compared with cross-section modulated DOVS in
order to determine the θ angle, as well as other geometri-
cal parameters of the pim-to-copper orientation. We have
initiated such studies and hope to report on results in the
near future. In addition to photoemission studies, vibra-
tional spectroscopy should prove to be a sensitive tech-
nique since we have shown that the geometrical parameters
of pim are quite sensitive to changes in θ.

Methyl-phthalimide-on-Copper

The UPS valence band spectrum for a monolayer (adsorbate)
of mpim on polycrystalline copper is shown in Figure 9,
together with the corresponding spectrum for the multilayer
sample, previously displayed in Figure 6. The spectrum of
the adsorbate is shown to be dominated by the Cu 3d peak.
The major change that is observed in going from multilayer
to monolayer samples is a slight decrease in the intensity
of peak C compared to the other peaks. Otherwise, the
general broadening of all peaks together with the very
minor differences between the two spectra makes it diffi-
cult to extract information concerning the effects on the
valence electronic structure of mpim due to interactions
with the copper surface.
    The DOVS corresponding to the structures of the
$NCH_3(CHO)_2$-Cu_4 system displayed in Figure 3a and 3b are
shown in Figure 10. The corresponding spectrum for the free
molecule is also included (Figure 10, bottom). The experi-
mental observation of no major differences between the
valence band spectra for the mono- and multilayer samples
is confirmed theoretically. The two different orientations
of the Cu_4 cluster relative to the ligand produce very
similar DOVS. This shows that, independent on orientation,
the interactions between mpim and copper (or between
$NCH_3(CHO)_2$ and Cu_4) are weak compared to the inter-actions
at the pim-copper interface. From the Mulliken population
analysis, we find significant bond order (anti-bonding) for
the orientation of nitrogen close to Cu (Figure 3a) only to
occur between the N $2p_z$ and Cu 4s orbitals. Mixing of the N
$2p_z$-Cu 4s orbitals is also observed to dominate the bond
order for the case of Cu close to the C=O group (Figure
3b). None of the AO's of the carbonyl group show large
mixing with the Cu AO's. Thus, even though the Cu is more
distant from the nitrogen atom than the carbonyl group, the
main interactions still take place at the nitrogen site.
This is probably due to the lone pair character of the MO
involving the N $2p_z$ AO. Of course, the particular geometry
included in our study does not permit close interactions
between the lone pair of oxygen and the copper cluster.
However, since the oxygen lone pairs are directed mainly
along the x-axis in the molecular plane (see Figures 3a and
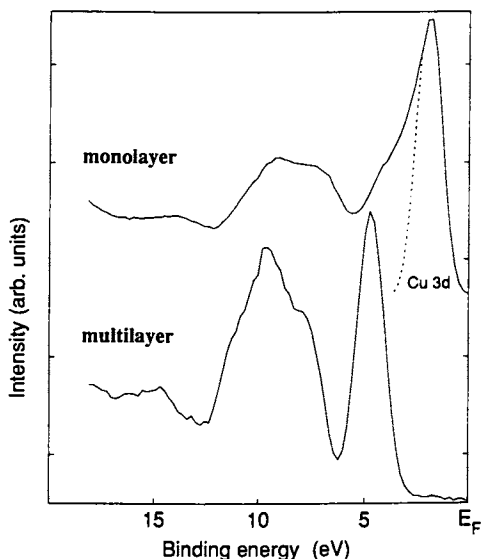
Figure 9. UPS valence band spectra for multilayer (bottom) and monolayer (top) films of mpim on copper.
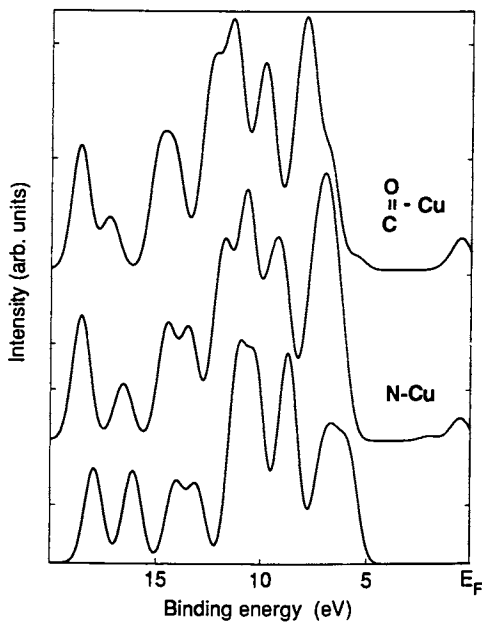
Figure 10. Partial density of states for the methyl-imide group. The bottom spectrum shows the result for $NCH_3(CHO)_2$ and the middle and topmost spectra are for $NCH_3(CHO)_2-Cu_4$. with the orientation shown in Figures 3a and 3b, respectively.

b), a strong interaction between them and the copper atoms
requires an arrangement where the x-axis is perpendicular
to the copper surface.

Summary and Conclusions

The UPS valence band spectra of multilayer and monolayer
samples of phthalimide (pim) and methyl-phthalimide (mpim)
on copper have been compared with the calculated DOVS for
corresponding systems. Very good agreement is found between
theory and experiment for all the systems included in this
study. This made it possible to interpret the features
appearing in the UPS spectra in terms of specific molecular
orbitals. Furthermore, by analyzing the MO's, the nature of
the ligand-metal bonding is uncovered.
   By comparing the spectrum for the stable adsorbate
(monolayer) with the spectrum for the pim multilayer, we
are able to derive useful information concerning the inter-
facial chemistry. From a comparison with the theoretical
DOVS for a molecule modelling pim, $NH(CHO)_2$, it is clear
that the nitrogen atom is the primary reaction site with
the copper surface, and that in the adsorbate, the hydrogen
atom bound to the nitrogen atom is removed. The breaking of
the N-H bond is observed to be the main cause of the
changes appearing in the DOVS whereas the particular way in
which pim interacts with Cu has litte influence. This is
clearly shown by the insensitivity of the DOVS to varia-
tions in the orientation between the ligand and the copper
cluster. In contrast, we observe a strong orientational
dependence in the ligand N-C bond which suggests that
vibrational studies should be very useful in determining
the orientation of pim on a copper surface.
   The interfacial interactions in the case of mpim on
copper, for which the methyl group is assumed to remain
bonded to the rest of the molecule, are found to be much
weaker than the interactions at the pim/copper interface.
This is confirmed by the very small differences between the
DOVS for the molecule modelling mpim, $NCH_3(CHO)_2$, and the
DOVS for the same molecule interacting with a copper
cluster. Furthermore, two different orientations of the
copper cluster relative to mpim, one for which the N-Cu
distance is the shortest Cu-ligand distance, and another
for which the C=O-to-Cu distance is shortest, show approxi-
mately the same interaction pattern, namely, the N lone
pair dominates the mpim-copper interaction. It should be
stressed that our consideration that the methyl group
remains bonded to the rest of the mpim (or the $NCH_3(CHO)_2$)
molecule upon interaction with a copper surface is still an
assumption, introduced to obtain a different interaction
pattern than for the case of pim-on-copper. The agreement
between theory and experiment, however, suggests that this
assumption is sound.
   The two different types of interactions that have stud-
ied here should be discussed in relation with the interac-

tions taking place at the polyimide-on-copper interface.
The bond between the imide nitrogen and the benzene ring of
the ODA part of polyimide is considerably stronger than the
N–H bond in pim. However, recent XPS core level studies of
adsorbates of benzen-phthalimide on a copper surface indi-
cate that the corresponding N–C bond in this system is
broken (15). Therefore, it might be the case that if the
imide nitrogen of polyimide comes close enough to the
copper surface, the polymer chain is broken up at the
nitrogen site and the interfacial interaction is of the
same type as that for pim-on-copper. If this does not
occur, the interaction at the nitrogen site will be con-
siderably weaker and of the same type as that observed for
the $NCH_3(CHO)_2-Cu_4$ system. In contrast, it has been shown
that the vapor deposition of copper upon polyimide results
in a primary reaction between the carbonyl oxygen and the
copper atoms (19).

Acknowledgments

Literature sited

1. See for example Polyimides, Mittal K. L., Ed. Plenum
   Press: New York, 1984; Vols. 1 and 2.
2. Jensen R. J.; Cummings J. P.; Vora H., IEEE 1984,
   CHMT7, 384.
3. Chou N. J.; Dong D. W.; Kim J.; Liu A. C., J.
   Electrochem. Soc. 1984 131, 2335.
4. Ohuchi F. S.; Freilich S. C., J. Vac. Sci. Technol.
   1986, A4, 1039.
5. Jordan J. L.; Kovac C. A.; Morar J. F.; Pollak R. A.,
   Phys. Rev. 1987, B36, 1369.
6. White R. C.; Haight R.; Silverman B. D.; Ho P. S.,
   Appl. Phys. Lett. 1987, 51, 481.
7. Goldberg M. J.; Clabes J. G.; Kovac C. A., J. Vac. Sci.
   Technol. 1988, A6, 981.
8. Kim Y. H.; Kim J.; Walker G. F.; Feger C.; Kowalczyk S.
   P., J. Adhes. Sci.Technol. 1988, 2, 95.
9. Kowalczyk S. P.; Kim Y. H.; Walker G. F., Appl. Phys.
   Lett. 1988, 52, 375.
10. Kowalczyk S. P.; Jordan-Sweet J. L., Chemistry of
    Materials 1989, 1, 592.
11. Grunze M.; Lamb R. N., Chem. Phys. Lett. (1987) 133,
    283.

12. Salaneck W.R.; Stafström S.; Brédas J. L.; Andersson
    S.; Bodö P.; Kowalczyk S. P.; Ritsko J.J., J. Vac.
    Sci. Technol. 1988 A6, 3134.
13. Cotton F.A.; Wilkinson G., Advanced Inorganic
    Chemistry, 4th Ed., Wiley Interscience: New York,
    1980.
14. Bodö P.; Salaneck W. R.; Stafström S.; Uvdahl K., This
    volume.
15. The HF equations are solved using the Gaussian-86
    program obtained from the Carnegie-Mellon Quantum
    Chemistry Publishing Unit, Pittsburgh PA, 1984.
16. Gaussian Basis Sets for Molecular Calculations,
    Huzinaga S., Ed. Elsevier: Amsterdam, 1984.
17. Hermann K.; Bagus P. S.; Bauschlicher C. W., Phys. Rev.
    1984, B30, 7313.
18. Bagus P. S.;. Hermann K; Bauschlicher C. W., J. Chem.
    Phys. 1984 81, 1966.
19. Ho P. S.; Hahn P. O.; Bartha J. W.; Rubloff G. W.;
    LeGoues F. K.; Silverman B. D., J. Vac. Sci. Technol.
    1985 A3, 739.

Chapter 24

Polyimide—Copper Interface

Model Study Using Photoelectron Spectroscopy

P. Bodö, K. Uvdal, S. Stafström, and W. R. Salaneck

Department of Physics, Linköping University, S–581 83 Linköping, Sweden

As an approach to a better understanding of adhesion
mechanisms between polyimide and copper, we have
studied the interaction between a set of model
molecules for a polyimide and vapor deposited
polycrystalline copper. Thin films and adsorbates of
benzene, phthalimide, methyl-phthalimide, benzene-
phthalimide, and malonamid, which are representative
of separate parts of the polyimide repeat unit, were
deposited *in situ* on clean copper and examined by
means of X-ray and Ultraviolet photoelectron
spectroscopy (XPS and UPS). In contrast to the
previously observed bonding to the carbonyl oxygen in
polyimide, as Cu is deposited on polyimide, our
results show that most of these polyimide model
molecules bond to Cu, through electron transfer, with
the imide nitrogen atom as the primary reaction site.

For a number of years, polymers such as polyimide, have been
subjected to widespread research, because of their increasing
importance as dielectric materials for the fabrication of
microelectronic devices (1). In particular, the adhesion of metal or
polyimide films deposited on polyimide substrates and *vice versa*, is
of considerable importance in most applications, and many studies
ranging from adhesion testing to detailed spectroscopic analysis of
interfaces have been reported previously (2,3,4,5,6).
    The problem of adhesion between a polymer and a metal is
strongly dependent on the specific type of polymer and metal
involved, as well as on the deposition process under which the
interface between the two is formed. In order to improve adhesion,
different pretreatment methods can be used, but the development of
such techniques requires detailed information about metal-polymer
interfaces. Particularly, in the case of thin metal films deposited
by physical vapor deposition (PVD) in ultra high vaccum (UHV), X-ray
and ultraviolet photoelectron spectroscopy (XPS and UPS) have been
used to obtain chemical information about initial film growth modes,

interfacial reactions, and effects of substrate pretreatment
(2,3,6,7).
     The reverse situation, with polyimide deposited on metals,
however, has not been studied to the same extent as metals-on-
polyimide. The lack of such information is partly due to the problem
of preparing polyimide films, in UHV, thin enough (monolayers) for
interfacial studies with, e.g., XPS and UPS. Using XPS, the mean
free path of electrons is typically 20-30 Å, and hence one has to be
able to prepare films thinner than that in order to gain information
about the interface. Usually, polyimide is deposited by spin
coating, a technique performed in air and not very suitable for
making such extremely thin films. If it is desirable to compare the
results of studies of the interface between a polyimide and metals
with those of metal films vapor deposited on polyimide, then the
polyimide deposition process should be performed in UHV in order to
keep the metal substrate clean and free from oxide layers. Metal
films grown by evaporation on polyimide do not have any oxide layer
facing the polyimide surface. However, if instead the purpose is to
compare *in situ* UHV-studies with those of polyimide films on metals
(prepared in air), oxidized metal substrates are prefered.
Polyimide, and polymers in general, can not be deposited by
conventional physical vapor deposition (PVD) techniques, without
loosing their original structure. However, polyimide films can be
prepared *in situ* in UHV by co-evaporation of oxydianiline (ODA) and
pyromellitic dianhydride (PMDA) with subsequent heat curing (8).
Using this technique, Grunze *et al.* (9) demonstrated that the
adhesion of such a polyimide film to a silver surface involves
chemical bonding to fragmented PMDA and/or ODA chemisorbed on the
substrate. Furthermore, Kowalczyk *et al.* (10), using Cr and Cu
substrates, have also observed fragmentaion at the interface, and
suggest, in the case of Cu, an interaction between polyamic acid and
Cu via carbonyl groups resulting in a carboxylic complex.
     In order make an effort to bring the polyimide-metal adhesion
problem to an even more fundamental level, we have previously
proposed that **model molecules**, chosen as representative of selected
parts of the polyimide repeat unit, may be used to predict the
chemical and electronic structure of interfaces between polyimides
and metals (12). Relatively small model molecules can be vapor
deposited *in situ* under UHV conditions to form monolayer films upon
atomically clean metal substrates, and detailed information about
chemical bonding, charge transfer and molecular orientation can be
determined, and even site-specific interactions may be recognized.
The result of such studies can also be expected to be relevant in
comparison with the results of studies of metal-polymer interfaces.
Another very important advantage with this **model molecule** approach
is the possibility to apply a more reliable theoretical analysis to
the data, which is very difficult when studying complex polymers
such as polyimide.
     In this report we use XPS to compare the interfacial
interactions for a set of **model molecules** for polyimide, deposited
in UHV upon vapor-deposited polycrystalline copper substrates.

Experimental

The copper substrates used were films grown by physical vapor-

deposition on optically flat Si(100) wafers. When mounted in the spectrometer system, which has a separate sample preparation compartment, the copper surfaces were cleaned, immediately before model molecule deposition, by sputtering with 5 keV Ne$^+$ ions, until the surface was free from oxygen and carbon according to XPS.

The model molecules which are solid at room temperature (except for benzene), were evaporated from a source consisted of a borosilicate glass container with a small opening, like the design of a Knudsen cell. The source was mounted inside a heatable and coolable copper shaft, that could be inserted to the vaccum system through a load-lock arrangement. Upon heating, the pressure was allowed to rise from below 10^{-10} Torr up to $\approx$ 5 x 10^{-9} Torr, and then rapid cooling of the copper shaft was started. After the copper shaft was cold, but before the cooling reduced the evaporation rate of the molecules, the substrate, held at a low temperature, was exposed to the molecule source. Benzene was deposited by introducing benzene vapor into the vaccum system through a leak valve in a gas-handling system, using a dosing tube arrangement. The resulting average film thickness was estimated by observing the attenuation of the XPS Cu 3p intensity, and using the value of Clark *et al* (13) for the effective elastic mean free path of electrons at 1.15 keV in typical hydrocarbons, 23 ± 2 Å.

XPS spectra were recorded using unmonochromatized Mg K$^\alpha$ radiation (1253.6 eV), and an unmonochromatized He-resonance lamp was used for ultraviolet photoelectron spectroscopy (UPS). XPS spectra were taken with an analyzer resolution of 0.2 eV, and the net resolution measured as the full width at half-maximum (FWHM) of Au 4f(7/2) was 0.9 eV. The spectrometer is of our own construction and is, e.g., designed to provide optimum angle-dependent XPS or XPS(θ) (12,14). For high θ-values, the photoelectrons leave the sample surface near the grazing angel, and due to the limited escape depth of the electrons, this is a "surface sensitive" mode. In the "bulk sensitive" mode, for low θ-values, the photoelectrons exit near the surface normal, and hence more information from the "bulk" of the sample is obtained (15).

The spectra taken of adsorbates have all been corrected for an overall binding energy shift relative to thin film spectra, which is due to a shift in the work function Φ. This shift, $\Delta\Phi$, can be determined from the cutoff of the secondary electron energy distribution in the UPS valence band spectra. The exact value of the work function shift (typically $\Delta\Phi \approx 0.4$ eV) is, however, not critical for the discussion below. We focus only binding energy shifts, which are of importance for the interpretation of the data discussed below.

Results and Discussion

The results are based on measurements using the following polyimide model molecules; Benzene (BE), phthalimide (PIM), methyl-phthalimide (MPIM), benzene-phthalimide (BPIM), and malonamide (MAM). The geometrical structure of these model molecules and, for comparsion, a polyimide (PI) of the type PMDA/ODA, are shown in Figure 1.

In the following we will refer to "thin films" and "adsorbates" of these model molecules. Our thin films have a thickness in the

range of 30 - 50 Å. The XPS and UPS measurements of these films
reflect "bulk" properties of the molecules, since in this case there
is essentailly no contribution to the spectra from the
film/substrate interface. The thin films are prepared and maintained
by keeping the substrate at a relatively low temperature, typically
≈ 210 K. The adsorbates, on the other hand, consist of approximately
a molecular monolayer, remaining on the substrate after temperature
has been raised to a level (depending upon each individual molecule)
where the overlayers in a thin film evaporate. Further increase in
temperature then resulted in evaporation of the adsorbate.

Benzene. The XPS C 1s spectra obtained from a thin film (upper
spectrum), with a thickness of aproximately 45 Å, and an adsorbate
(lower spectrum) of benzene are shown in Figure 2. The spectrum from
the thin film shows a symmetric peak having a binding energy of
284.9 eV and a small shake up satellite, typical for π-bonded
systems, with its maximum at about 291.8 eV. As benzene becomes an
adsorbate, consisting of roughly a monolayer, the main peak broadens
somewhat but there is no binding energy shift observed. However, the
shake up feature has almost disappeared and there is an overall
increase in the background intensity on the high binding energy side
of the main peak. The loss of the shake up peak is probably due to
core-hole screening by electrons near the Fermi level in the metal
substrate (16). The UPS valence band spectrum for the adsorbate
remains essentially the same as that of a thin film, with the
expectation of a slight work function change. These results indicate
that the benzene molecule remains intact upon adsorption, and the
adsorbate is weakly bond to the polycrystalline copper surface.
Thus, we can not expect the other model molecules in this study to
have any strong interaction with the Cu surface via the benzene
ring.

Phthalimide. The C 1s spectrum for a thin film of PIM (lower
spectrum), shown in Figure 3, has two well resolved peaks with a
relative intensity ratio of about 6:2, corresponing to the six
carbon atoms in the ring and to the two carbonyl carbons,
respectively. As going from a thin film (lower spectrum) to an
adsorbate (upper spectrum), with an estimated thickness of about 3
Å, the carbonyl carbon peak exhibits a shift of ≈ 1.2 eV towards a
lower binding energy relative to the ring carbon peak. The ring
carbon peak remains at about the same binding energy. The 0 1s peak
is also shifted towards a lower binding energy as the PIM thin film
is reduced to an adsorbate, as shown in Figure 3. This 0 1s shift is
≈ 0.9 eV, which is somewhat lower than that for the carbonyl C 1s
peak. The N 1s level, shown in Figure 3, experiences the largest
binding energy shift, ≈ 2.2 eV, of the three core levels.
      According to these observed chemical shifts in the core levels,
with the largest shift in the N 1s peak, followed by the C 1s
carbonyl carbon, the smallest in the 0 1s, and almost no shift in
the C 1s ring carbon peak, we infer that electronic charge is
transferred from the Cu substrate to the PIM molecule, and the net
charge is delocalized over the N atom and the two carbonyl groups.
By using the XPS chemical shifts and the charge potential model of
Siegbahn *et al* (11) to calculate the net charge distribution, as
described previously, we verify that the N atom is the primary
reaction site for the PIM adsorbate (12).
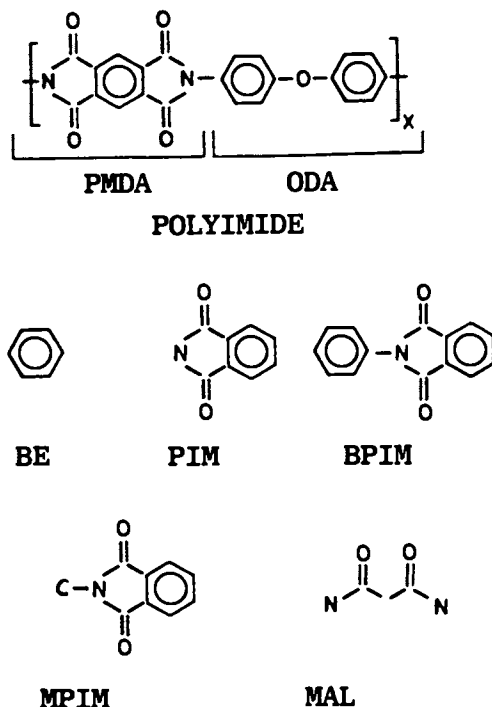
Figure 1. Chemical structure of PMDA/ODA polyimide (PI)
monomer unit, benzene (BE), phthalimide (PIM), benzene-
phthalimide (BPIM), methyl-phthalimide (MPIM), and malonamid
(MAM).

BINDING ENERGY (eV)
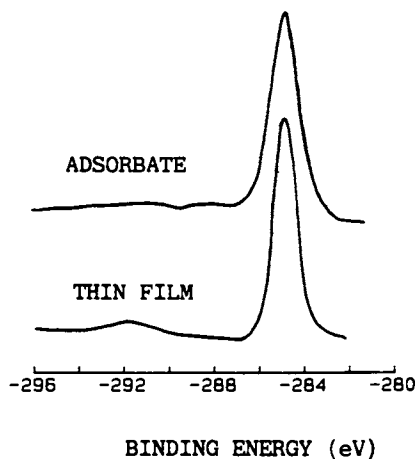
Figure 2. C 1s XPS core level spectra of benzene on copper.

The middle spectra for each core level in Figure 3, show a
state where slightly more than a single layer of PIM are present at
the Cu surface. The observed shifts for the adsorbate are present
even for this partial second layer, but just a part of each peak has
shifted from the thin film to the adsorbate position. The middle C
1s spectrum shows, for example, two distuingishable carbonyl C 1s
peaks. Therefore, these spectra reflect PIM in two different states,
one interacting at the interface, and one non-interacting in the
partial second layer, which is equivalent to the spectra of the
(bulk) thin film. The C 1s peak corresponding to the carbonyl
carbon, the O 1s, and the N 1s spectra consist of two different
peaks, one shifted and one unshifted relative to the bulk state.
Furthermore, the two double state spectra for the N 1s level in
Figure 3 are recorded in the surface sensitive and bulk sensitive
mode, respectively. In the surface sensitive mode, where the
electron take off angle $\theta \approx 80°$, the contribution to the N 1s
spectrum is predominantly from nitrogen atoms in the outermost non-
interacting molecules. Thus, we conclude that only the first
molecular layer, closest to the Cu surface, experiences the electron
charge transfer, i.e., interacts with the Cu surface. For near
normal exit, $\theta = 0°$, the intensity in the shifted N 1s peak becomes
stronger. (The large sloping background, appearing especially for
the adsorbate, comes from a nearby X-ray induced copper LMV Auger
spectrum. There are, however, no Cu Auger peaks, which enterfere
with the N 1s XPS peaks.) This double state behaviour, when there is
a little more than a monoloayer of PIM adsorbed on the Cu surface,
shows that only the first molecular layer of PIM interacts with the
Cu surface.

Benzene-phthalimide (BPIM). The C 1s, O 1s and N 1s spectra of BPIM
on Cu are shown in Figure 4. The lower spectra corresponding to a
thin film of BPIM are similar to those of a thin film of PIM,
except for a relatively smaller carbonyl carbon peak as expected.
The ring-carbon to carbonyl-carbon intensity ratio is now 12:2,
because of the additional benzene ring. The upper spectra are
recorded for a BPIM adsorbate having an estimated average thickness
of about 2 Å, i.e., somewhat less than a monolayer. For this BPIM
adsorbate we observe about the same kind of chemical shifts as those
for PIM. These shifts are for BPIM estimated to be, $\Delta C1s \approx 1.0$,
$\Delta O1s \approx 0.9$, and $\Delta N1s \approx 2.3$ eV, indicating that BPIM interacts with the
Cu surface in a similar way as does PIM. As a consequence of this
interaction, the bond between the imide nitrogen and the benzene
ring in BPIM has to be broken, otherwise it is not reasonable to
expect these particular large shifts. Although, the chemical shifts
are similar to those of PIM, the spectra for PIM and BPIM adsorbates
are not identical, which would be the result if all benzene rings
desorb from the surface and the remaining (PIM) molecules interact
with the Cu surface. A comparsion of the intensity ratios of the
core levels for the thin film with those for the adsorbate,
indicates that much of the nitrogen and considerable amounts of
oxygen have dissapeared due to degradation. At present, such a
degradation behaviour of BPIM is under further investigation. The
middle spectra of BPIM in Figure 4 also show a mixed interacting and
non-interacting state like that observed for PIM. This double state
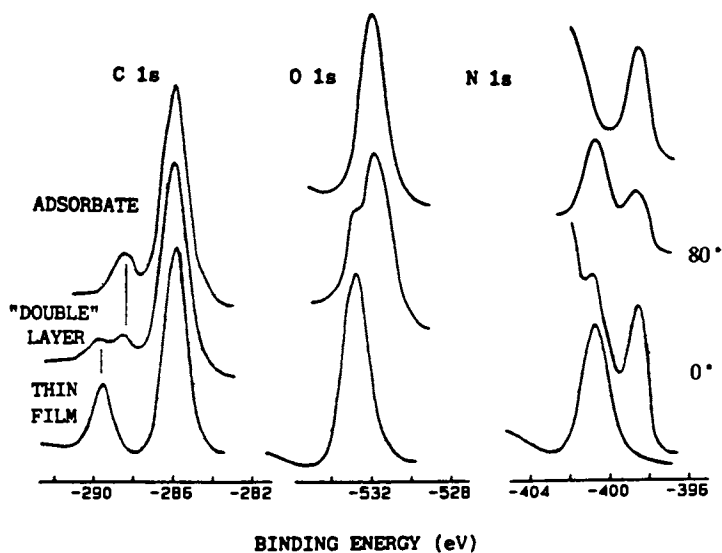
Figure 3. C 1s, O 1s, and N 1s XPS spectra of phthalimide (PIM) on copper.
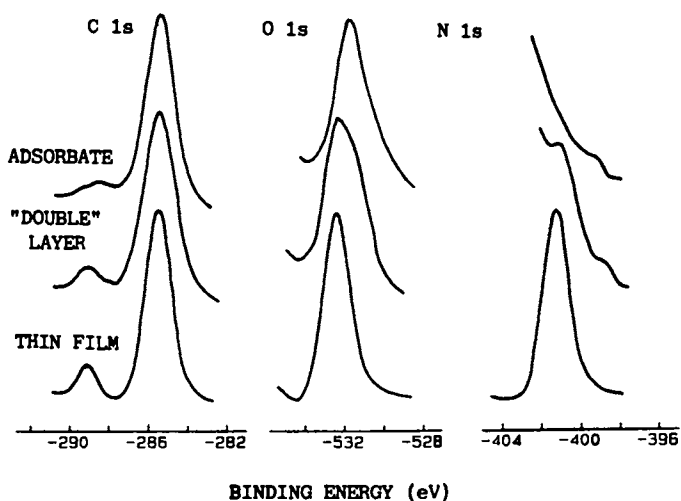
Figure 4. C 1s, O 1s, and N 1s XPS spectra of benzene-phthalimide (BPIM) on copper.

adsorbate of BPIM was achieved by a short heating, which, in the
case of PIM, would have resulted in a single layer adsorbate only
interacting with the Cu surface, i.e., no double state. The breaking
of the bond between the imide nitrogen and the benzene ring
obviously requires a certain amount of energy, and the charge
transfer interaction with the Cu surface does not show up as "easy"
as for PIM. However, at the present, we do not have enough data to
make a detailed comparsion between the BPIM-Cu and PIM-Cu
interaction that is followed by substrate heating.

Methyl-phthalimide (MPIM). The results obtained for MPIM are very
much the same as those for BPIM. The C 1s of the carbonyl carbon, O
1s, and N 1s peaks shift with about the same amount as for BPIM and
PIM. The binding energy shifts are estimated to ΔC1s$\approx$1.2, ΔO1s$\approx$1.0,
and ΔN1s$\approx$2.2 eV. Thus, the results imply that MPIM interacts with
the Cu surface in the same way as BPIM (and PIM) through electron
charge transfer with the N atom being the primary reaction site. In
this case the methyl group must be removed from the molecule by
breaking the bond between the imide nitrogen and the methyl group in
MPIM. A comparison of the intensity ratios of the core levels,
however, shows a loss of N and O, similar to the behaviour of BPIM.

Malomamide (MAM). The MAM molecule is somewhat different from the
other model molecules used in this study. MAM contains two amid
bonds, while PIM, BPIM and MPIM contain imide bonds. Therefore, it
still is useful to compare the adsorption of MAM and its interaction
with the Cu surface with the behaviour of the imide model molecules.
      The C 1s, O 1s, and N 1s spectra of MAM are shown in Figure 5.
Among the lower spectra, obtained from a thin film, the C 1s
spectrum shows a relatively high contribution from carbonyl carbons.
The carbonyl-to-aliphatic carbon intensity ratio is about 2:1 as
expected. In the form of an adsorbate (about 4 Å thick), upper
spectra in Figure 5, the same type of shifts are observed for MAM as
for the imide molecules. In this case they are estimated to be
ΔC1s$\approx$1.4, ΔO1s$\approx$0.7, and ΔN1s$\approx$2.2 eV. However, as an adsorbate, MAM
shows two peaks in the N 1s spectrum, one unshifted and one shifted
relative to the thin film case. This indicates that only one of the
two NH$_2$ end groups interacts with the Cu surface. We therefore infer
that even MAM interacts with the Cu surface through electron charge
transfer, with one N atom being the primarily reaction site. Angle-
dependent, XPS(θ), data of the adsorbate, show an increased
contributionen from the non-interacting NH$_2$ group to the N 1s
spectrum in the surface sensitive mode, i.e., indicating that the
MAM molecule stands up (at an unknown angle) on the Cu surface.

Theoretical study. Along with the XPS measurements of the model
molecules interacting with Cu, UPS was used to record the
corresponding valence band spectra. In order to interpret these
valence band spectra a theoretical study based on *ab initio* self-
consistent field (SCF) Hartree-Fock calculations has been made for
the case of PIM and MPIM on copper. The results of this theoretical
study, which are published in a separate report (17), show good
agreement between theoretical and experimental data, and strongly
support the core level results indicating that the nitrogen atom is
the primary reaction site for the interaction with copper. It was
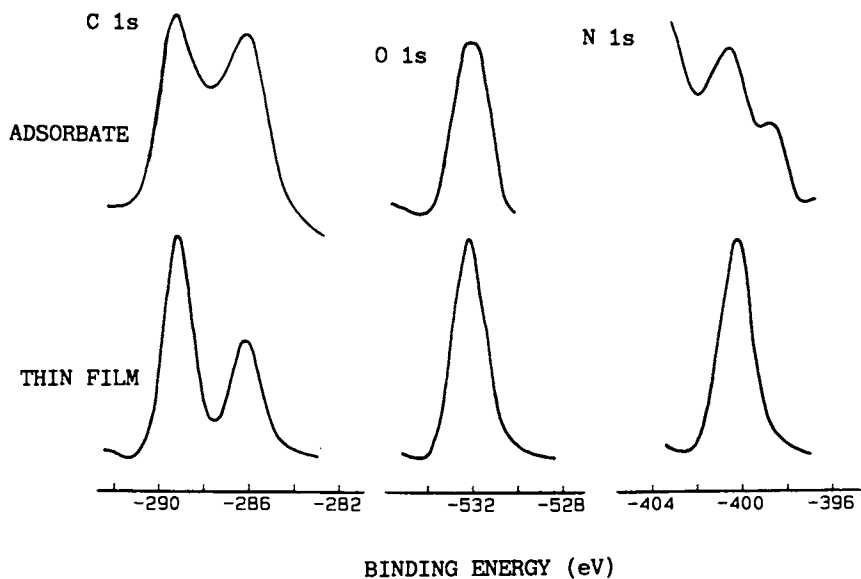
Figure 5.   C 1s, O 1s, and N 1s XPS spectra of methyl-
phthalimide (MPIM) on copper.

also concluded from this other study that there is only a very weak
interaction between MPIM and Cu, different from that between PIM and
Cu, if the methyl group remains bonded to the MPIM molecule.

Summary and Conclusions

In this study, we have used a set of polyimide model molecules to
obtain information about possible interactions at the polyimide
copper interface. Benzene, phthalimide (PIM), benzene-phthalimide
(BPIM), methyl-phthalimide (MPIM), and malonamid (MAM) were
deposited in ultrahigh vacuum (UHV) onto clean polycrystalline
copper substrates, and the measurements were performed by means of
XPS and UPS.

   Except for benzene, all the model molecules studied show a
similar behaviour as adsorbates on the copper surface. According to
the observed binding energy shifts in the C 1s, O 1s, and N 1s core
level spectra, as well as to the theoretical interpretaion of
valence band spectra, we conclude that these model molecules
interact with the copper surface through electron charge transfer
from the copper to the various molecules, with the nitrogen atom as
the primary reaction site. This charge transfer is found to occur
only in the first molecular layer closest to the substrate surface.
This interaction via the nitrogen atom implies that the imide
hydrogen is dissociated from PIM, the benzene group from BPIM, and
the methyl group from MPIM.

   For both vapor-deposited copper-on-polyimide, and polyimide
deposited on copper, it has been reported that the carbonyl oxygen
is the primary reaction site responsible for the interface
interaction (3,10). In contrast, results of our study show that
interface bonding between copper and polyimide also could occur at
the imide nitrogen site as a result of breaking the bond between the
imide nitrogen of PMDA and the benzene ring of ODA. In order to
further investigate details about model molecule interactions with
the Cu (and other metal) surface and evaluate their relevance for
predicting possible bonding mechanisms at polyimide/metal
interfaces, we suggest even more careful investigations of model
molecules adsorbed upon metal surfaces.

Acknowledgments

Literature Cited

1. See, for example, Polyimides; Mittal, K.L., Ed; Plenum: New
    York, 1984; Vols. 1 and 2.
2. Bodö, P.; Sundgren, J.-E. J. Vac. Sci. Technol. A 1988, 6,
    2396.
3. Ho, P.S.; Hahn, P.O.; Bartha, J.W.; Rubloff, G.W.; LeGoues,
    F.K.; Silverman, B.D.; J. Vac. Sci. Technol. A 1985, 3, 739.
4. Jordan, J.L.; Sanda, P.N.; Morar, J.F.; Kovac, C.A.; Himpsel,
    F.J.; Pollak, R.A.; J. Vac. Technol. A 1986, 4, 1046.

5. Oh, T.S.; Kowalczyk, S.P.; Hunt, D.J.; Kim, J.; J. Adhesion Sci. Technol., in press.
6. Ohuchi, F.S.; Freilich, S.C.; J. Vac. Sci. Technol. A 1986, 4, 1039.
7. Bodö, P.; Sundgren, J.-E.; J. Appl. Phys. 1986, 60, 1161.
8. Salem, J.R.; Sequeda, F.O.; Duran, J.; Lee, W.Y.; Yang, R.M.; J. Vac. Sci. Technol. A 1986, 4, 369.
9. Grunze, M.; Lamb, R.N.; Chem. Phys. Lett. 1987, 133, 283.
10. Kowalczyk, S.P.; Jordan-Sweet, J.L.; Chemistry of Materials, in press.
11. Siegbahn, K.; Nordling, C.; Johansson, G.; Hedman, J.; Heden, P.F.; Hamrin, K.; Gelius, V.; Bergmark, T.; Verme, L.O.; Manne, R.; Baer, Y.; ESCA Applied to Free Molecules; North-Holland: Amsterdam, 1969
12. Salaneck, W.R.; Stafström, S.; Brédas, J.L.; Andersson, S.; Bodö, P.; Kowalczyk, S.P.; Ritsko, J.J.; J. Vac. Sci. Technol. A 1988, 6, 3134.
13. Clark, D.T.; Dilks, A.; Shuttleworth, D.; J. Electron Spectrosc. Phenom. 1978, 14, 247.
14. Salaneck, W.R.; Bergman, R.; Sundgren, J.-E.; Rockett, A.; Greene, J.E.; Surf. Sci. 1988, 198, 461.
15. Fadley, C.S.; Bergström, S.A.L. In Electron Spectroscopy; Shirley, D.A., Ed.; North-Holland: Amsterdam, 1972; p 23.
16. Sinjic, M.; Physica Sripta 1980, 21, 561.
17. Stafström, S.; Bodö, P.; Salaneck, W.R.; Brédas, J.L.; see these proceedings.

Chapter 25

Aluminum–Polyimide Interface

A. Selmani

Department of Chemical Engineering, École Polytechnique, C.P. 6079,
Succursale A, Montreal, Quebec H3C 3A7, Canada

We use an ab-initio local spin density method to in-
vestigate the aluminum/polyimide interface at low
coverage. We found in agreement with XPS and EELS
experiments, that the aluminum atom bonds to the
carbonyl group. Our calculations suggest a for-
mation of a linear C-O-Al complex. We calculated
core levels chemical shifts and vibrational fre-
quencies in the vicinity of the carbonyl group.
The results are satisfactory. We finally suggest a
mechanism of the bonding of aluminum to polyimide
at medium coverage. This mechanism explains many
features not yet resolved by experimentalists.

In recent years, polyimides (PI) have attained great importance
in the microelectronics industry. They are used as thin layers
of insulation between wiring networks in multilevel
very-large-scale integration packages. For these purposes,
there is a need to understand the properties of the polymer
surface and of polymer-metal interfaces. An understanding of
the relationship between chemical bonding and adhesion may
provide new possibilities for the optimization of metal-polymer
adhesion (1-3). The interaction of various metals with
polyimides has been investigated using several different surface
science techniques. X-ray photoelectron spectroscopy (XPS),
(4-11), in particular, has been used to investigate the
chemistry of thin metal films deposited on the surface of a much
thicker polyimide phase. The main conclusions of these studies
are: i) The carbonyl groups are the most reactive sites on the
polyimide surfaces. ii) There are two distinct classes of
metals studied. The first do not produce a change in the
binding energies of carbonyl groups (4, 6, 8). These include
such elements as Cu and Ag. The second bond to the carbonyl
group, but without breaking the C-O bond (Cr, Ti, Ni, Al) (4,
7-11). These studies yielded measurements of electronic core
level shifts, which we shall compare with those obtained with

our calculations. High resolution electron energy loss spectroscopy (HREELS) has also been used (12-15) to characterize clean polymer surfaces (12) and to study the interface of polyimide with evaporated chromium, palladium and aluminum (13-15). These measurements of vibrational spectra led to the conclusion that chromium and aluminum bond to the carbonyl group, in agreement with XPS results. Palladium was found to behave like copper and silver. We shall discuss below some vibrational frequencies observed for the Al/PI system. In this paper, we use a quantum chemistry approach to contribute to the understanding of metal-polyimide interfaces. We shall focus on the interaction of aluminum atoms with a polyimide monomer. Using the ab-initio LCGTO-LSD (Linear Combination of Gaussian Type Orbitals-Local Spin Density), we will investigate aluminum-polyimide bonding at the most important site and compare the core level chemical shifts and vibrational frequencies with those obtained with XPS and HREELS.

Model and method of calculations

The repeat unit of poly (4,4' oxydiphenyl pyromellitimide) is shown in Fig.1. It consists of two portions, pyromellitic dianhydride (PMDA) and oxydiphenyl amide (ODA), indicated in the figure. In order to model the interaction of aluminum atoms with the polyimide surface, we consider only the PMDA part of the monomer with hydrogens to saturate the nitrogen atoms (Fig. 2). This approach is justified by the fact that only PMDA contains carbonyl groups, and by the fact that we are interested mainly in low metal coverage. We know from XPS (4-11) and EELS (13-15) experiments that the first deposited metals interact with carbonyl groups. Further, there is no indication that the PMDA phenyl group or the ODA participate directly in the interaction. To simplify the calculations, we use a C_2 symmetry by considering two aluminum atoms adsorbed simultaneously on the PMDA fragment (Fig. 2). In this study we employed the LCGTO-LSD-VWN (Vosko, Wilk, Nusair exchange-correlation potential) method (16). This ab-initio method, which takes into account most of the correlations in the system, gives, in the case of small molecules, results which compare with those obtained with the best CI methods (see, for example, ref. (16,17). It has been also widely used in the study of adsorption of atoms and small molecules on well ordered metallic and semiconductor surfaces (18,19). The informations it provides, such as adsorption geometries and energies, compares very well with that obtained by surface analysis techniques. Beside the fact that it provides better results than the ab initio Hartree Fock method, it is less time consuming, which makes it more suitable for the study of large systems. At the technical level, the drawback presently is that the gradient techniques which help in the energy optimization process are not yet implemented in the program and that makes the task very difficult to achieve for more than one degree of freedom, especially for complexes whose calculations are very time consuming. Since we are interested in the chemical shifts of

core levels, we treated all the electrons of all the atoms explicitly. The orbital and auxiliary basis sets were optimized by reference to numerical LSD VWN (20) atomic calculations described elsewhere (21). In Table I, we present the pattern of these basis sets of the five atoms, C, O, N, H and Al. The PMDA bond angles and distances used in these calculations are taken from X-ray diffraction (22). For the lowest coverage, we are interested mainly in the carbonyl group region. For this purpose, we considered the bonding of an Al atom at five different sites, indicated as 1-5 in Fig. 3. The positions 1, 2 and 3 correspond to bonding, respectively, at the carbon atom, in between the carbon and the oxygen atoms and at the oxygen atom. Positions 4 and 5 correspond, respectively, to an O-Al axis having an angle α equal to 45° and 0° with respect to the C-O axis. For each of the five positions, the distance of the Al from the C=O is optimized, to yield the highest binding energy.

Table I. The pattern of basis sets used in the present work. It is described as follows: For orbital basis sets, C: (521/41) means that the basis set for carbon contains 8 s basis functions, contracted to 3, (521), and 6 p basis functions, contracted to 2, (41). For auxiliary basis sets, C: (622/522) means that, there are 6 s basis functions, 2 for p and 2 for d. The first part (622) concerns charge density, and the second part (522) the exchange-correlation. Exponents and coefficients will be sent upon request

	Orbital basis sets	Auxiliary basis sets
C	(521/41)	(622/522)
O	(521/41)	(622/522)
N	(521/41)	(622/522)
Al	(5321/521)	(934/934)
H	(5/0/0)	(1/1)

Results and Discussion

The optimum binding energies for each of the five positions described above are shown in Table II. It is clear that the formation of C-O-Al complex (position 5, $\alpha = 0°$) is favored. The Al-O distance is found to be 1.80 A. (We should stress here that the C-O distance is not reoptimized after bonding to Al.) In Table 2, we also show the vibrational frequency calculated, using the harmonic oscillator approximation, for the Al-O streching in position 5. Its value is 890 cm^{-1}. Pireaux et al (15), using HREELS techniques to study the Al/PI interaction, found that the vibration at 1720 cm^{-1} associated with C = O gradually weakens with increasing Al deposition, and that a broad peak develops near 800 cm^{-1}. We believe, thus, that the Al-O vibration accounts, at least in part, for the increase in
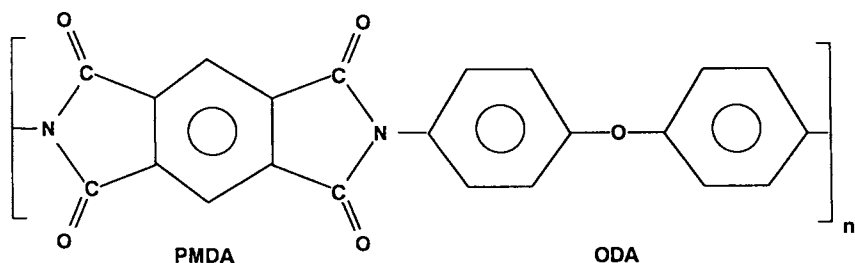
PMDA   ODA

Fig. 1: The repeat unit of polyimide (PMDA-ODA).
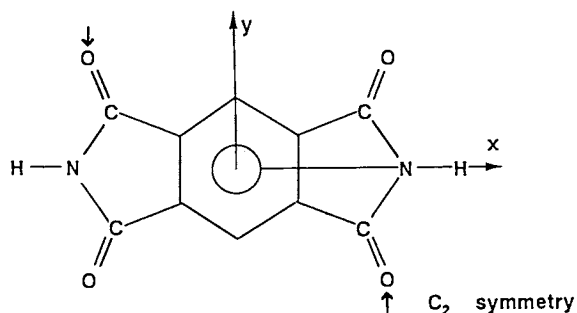
C_2 symmetry

Fig. 2: The model chosen to study the interaction of Al with carbonyl group. To keep the C_2 symmetry, we adsorb simultaneously two Al atoms as indicated by the arrows.
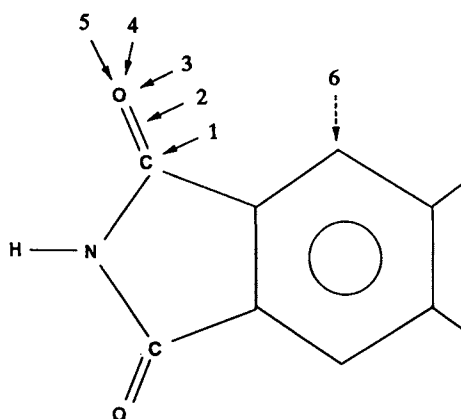
Fig. 3: Arrows indicate sites where Al is adsorbed.

intensity observed around 800 cm^{-1}. Let us now examine the core levels. Treating the PMDA alone, we calculated binding energies of the C_{1s} and O_{1s} levels for the C and O in the carbonyl group to be respectively 271.10 and 507.10 eV. The XPS values reported by Bartha et al (9) for the same levels in the PI system are 288.8 and 533 eV (for the carbonyl group). The comparison of the absolute values of binding energies is meaningless since our model represents only the PMDA part of the whole monomer. After the bonding of Al to O in its preferred position ($\alpha = 0°$), we calculated the C_{1s}, O_{1s} and Al_{2p} chemical shifts. The C_{1s} is shifted by .94 eV to lower binding energies, while O_{1s} and Al_{2p} are shifted to higher binding energies by .64 and .90 eV, respectively. Bartha et al (9) found the same tendencies, though the values are not the same. The calculated and XPS results are summarized in Table III. The relaxation effects at the atomic levels should cancel out when we calculate the chemical shifts, but we recall again that the geometry of the molecule in the vicinity of the reacted carbonyl groups was not reoptimized after Al binding. This contributes to the difference in the values of the chemical shifts (~.5 eV). We therefore conclude that the agreement between theory and experiment is reasonably satisfactory.

At higher aluminum coverage, we show, in Fig.4, how a second active site for Al may be created, due to electronic rearrangements subsequent to the creation of the C-O-Al group. The possibility of the existence of a second active site is supported by the fact that only half the carbonyl groups react with Al atoms. Pireaux et al (15) observed that the intensity of carbonyl group peak is only reduced by half and not shifted from its position before aluminum deposition. The authors propose two possible explanations: i) Due to the morphology of the polymer surface, two C=O bonds are buried below the surface and

Table II. Binding energies, (Al-O) or (Al-C) distances and vibrational frequencies of Al on (PMDA) at different positions corresponding to those of Fig. 2

position	binding energy eV	Al-O or Al-C distance (A)	vibrational frequency cm^{-1}
1	1.43		
2	1.44		
3	1.62		
4	2.0	(Al-O)1.85	
5	2.5	(Al-O)1.80	890
6	1.7	(Al-C)2.10	503

Table III. XPS and calculated core levels in (eV) and their chemical shifts. The minus sign in the chemical shift numbers indicates that the levels are shifted to higher binding energies

	C_{1s}		O_{1s}		Al_{2p}	
	XPS[a]	calcul.	XPS[a]	calcul.	XPS[a]	calcul.
Al	-	-	-	-	72.3	69.5
(PMDA)	288.8	271.10	533	507.1	-	-
Al/(PMDA)	287.1	270.16	533	507.77	73.8	70.43
Chem. shift	1.7	0.94	0	-0.64	-1.5	-0.9

a) XPS data on Al/PI system from ref. 9.

not directly available to the aluminum reaction. ii) Due to electronic delocalization caused by a first "Al-0-C" bond formation, the symmetric C=0 site in the imide has lost part of its chemical reactivity. We believe that the first explanation

is not plausible. Even if the remaining C=0 bonds are buried below the surface, if their chemical potential is unchanged and if they remain the most active sites at the surface, they will attract the evaporated aluminum atoms. However, the creation of a second active site due to electronic delocalization would lead aluminum to bond to this second site (if it is chemically the most active site) rather than bonding to the remaining C=0 bonds.

To estimate the aluminum bonding at this site, called position 6 (Fig. 3), we bonded Al to the carbon of the PMDA phenyl, and we optimized the C-Al distance. We found that this site gives a binding energy of 1.7 eV (Table II). The vibrational frequency corresponding to this bond is estimated to be 503 cm^{-1}. This value would be higher if we had considered the optimization of both the Al and H bonded to the phenyl carbon. We thus suggest that this vibration could also contribute to the intensity in the region of 800 cm^{-1}. It is obvious that we suppose that the ODA does not play any important role in the low and medium coverage. Following our model, the creation of a second active site on the phenyl group carbon and bonding of aluminum to it would create an aliphatic carbon and lead to a decrease of aromaticity. We believe that the peak observed in HREELS (15) at medium coverage at 2900 cm^{-1} (not assigned) is due to a C-H streching of the induced aliphatic carbon where the second aluminum is bonded. This model is also supported by the decrease of the C_{1s} aromatic carbon peak observed in XPS spectra (9)
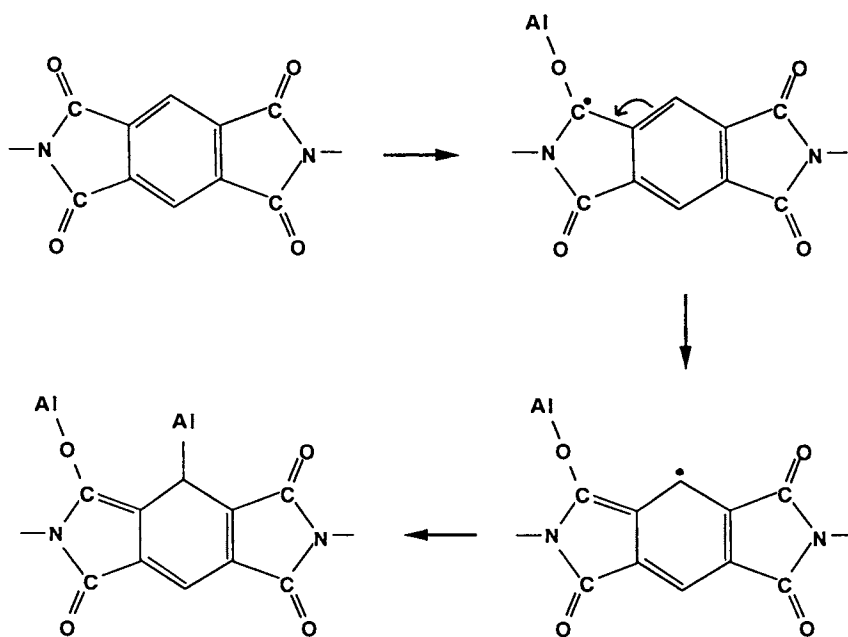
Fig. 4: Suggested mechanism for the adsorption of Al on polyimide surface. The dot on the carbon is not a radical but indicates an increase of electronic density.

during aluminum deposition and a simultaneous increase of the C_{1s} peak at lower energy which, we believe, corresponds to the aliphatic carbon. As we mentioned in the text, we did not reoptimize the C=O bonds after bonding aluminum atoms to them. To support our model, a complete calculation using the gradient techniques to study the whole electronic reorganization of the monomer, is being performed. This study also includes the investigation of chromum and copper metal atoms.

Conclusion

The model we have chosen to study the aluminum-polyimide interface is satisfactory. We found, using the LCGTO-LSD-VWN method, that the formation of a linear C-O-Al complex has the highest binding energy in the vicinity of the carbonyl group. A comparison of the calculated vibrational frequencies and core level chemical shifts compares well with those obtained by HREELS and XPS. We suggest a mechanism of the adsorption of Al to polyimide surfaces by assuming that the ODA fragment does not play any important role at low coverages.

1. Polymer Materials for Electronics Applications, ACS Symp. Ser. 184 (1982)
2. Polyimide-Synthesis, characterization and Applications, Vol. 1, Ed. K.L. Mittal, Plenum (1984).
3. Wilson, A.M., Thin Solid Films, 83 (1981) 145.
4. Chou N.J. and Tang C.H., J. Vac. Sci. Technol. A, 2 (1984) 751.
5. Jordan J.L., Sanda P.N., Morar J.F., Kovac C.A., Himpsel F.J. and Polak R.A., J. Vac. Sci. Technol., A, 4 (1986) 1046.
6. Sanda P.N., Bartha J.W., Clabes J.G., Jordan J.L., Feger C., Silverman B.D., and Ho P.S. J. Vac. Sci. Technol., A, 4 (1986) 1035.
7. Jordan J.L., Kovac C.A., Morar J.F. and Pollak P.A., Phys. Rev. 3, 36 (1987) 1369.
8. Ho P.S., Hahn P.O., Bartha J.W., Rubloff G.W., Legones F.K. and Silverman B.D., J. Vac. Sci. Technol. A, 3 (1985) 739.
9. Bartha J.W., Hahn P.O., LeGoues F. and Ho P.S., J. Vac. Sci. Technol. A3 (1985) 1390.
10. Atanasoska L., Anderson S.G., Meyer H.M. III, Lin Z., and Weaver J.H., J. Vac. Sci. Technol. A5 (1987) 3325.
11. Ohuchi F.S. and Freilich S.C., J. Vac. Sci. Technol. A, 4 (1986) 1039.

12. Pireaux J.J., Gregoire C., Vermeersh M.,   Thiry   P.A   and
    Caudano R., <u>Surface Sci</u>. 189/190 (1987) 903.
13. Dinardo N.J., Demuth J.E.,   and Clarke T.C., <u>Chem. Phys.</u>
    <u>Lett</u>. 121 (1985) 239.
14. Dinardo N.J., Demuth J.E. and Clarke T.C., <u>J. Vac. Sci.</u>
    <u>Technol</u>. A4 (1986) 1050.
15. Pireaux J.J., Vermeersh M., Grégoire C., Thiry P.A. and
    Caudano R., <u>J. Chem. Phys</u>. 88 (1988) 3353.
16. Salahub D.R., in <u>Ab initio Methods in Quantum chemistry Part</u>
    II, Advances in chemical Physics, Vol. 69, edited by Lawley
    K.P., (Wiley-Interscience, chichester, 1987) pp. 447-520.
17. Selmani A. and Salahub D.R., <u>J. Chem. Phys</u>. 89 (1988) 1529.
18. Salahub D.R., in <u>Contributions of clusters physics to Mate-</u>
    <u>rials Science and Technology</u>, Eds. Davenas J. and Rabette
    P., (Nijhoff, Amsterdam, 1986).
19. Selmani A., Salahub D.R., and Yelon A., <u>Surface Sci</u>. 202
    (1988) 269.
20. Vosko S.H., Wilk L. and Nusaïr M., <u>Can. J. Phys</u>. 58,
    (1980) 1200.
21. Andzelm J., Radzio E. and Salahub D.R., <u>J. Comp. Chem</u>. <u>6</u>,
    (1985) 520.
22. Takahashi N., Yoon D.Y., and Parrish W., <u>Macromolecules</u>,
    17 (1984) 2583.

Chapter 26

Solventless Polyamic Acid

Consequences for Reactivity with Metals

T. Strunskus[1], M. Grunze[2], and S. Gnanarajan[3]

[1]Laboratory for Surface Science & Technology, Sawyer Research Center, University of Maine, Orono, ME 04469
[2]Angewandte Physikalische Chemie, Universität Heidelberg, Im Neuenheimer Feld 253, 6900 Heidelberg, Federal Republic of Germany
[3]Department of Physics, University of Jaffna, Therunelvely, Jaffna, Sri Lanka

In this article we discuss the core level spectra of solventless prepared poly (N,N'-(p,p'-oxydiphenylene) pyromellitamic acid) or PMDA/ODA polyamic acid (PAA) films with particular emphasis on the chemical composition and on the O1s and C1s "shake up" transitions. Both vapor deposited polyamic acid and the resulting polyimide films show an excess of oxydianiline (ODA) and a deficiency of carbonyl groups. A qualitative analysis of the "shake up" transitions on the O1s and C1s core holes indicate that polyamic acid is in a non-planar conformation. A shoulder in the N1s band at higher binding energy was assigned to positively charged nitrogen and we concluded that a proton is trans-ferred from the amic acid group onto the nitrogen atom of unreacted oxydianiline. The amic acid group of the molecule is the primary site of interaction with evaporated gold atoms and with bulk silver surfaces. In the case of polyamic acid and polyimide films on polycrystalline silver Infrared-Absorption Reflection experiments indicate that the interfacial bonding is achieved via silver carboxylate linkages.

Polyamic acids (PAA's) are the precursor molecules in the formation of polyimides (PI), a class of high temperature polymers widely used in microelectronic applications. Due to their favorable combination of thermal stability, chemical resistance and easy processibility they are replacing ceramic materials in microelectronic applications. Typically, PI's are processed in their polyamic acid precursor state. The polyamic acid is formed through polycondensation of an aromatic dianhydride with an aromatic diamine by dissolving and mixing the monomeric materials in a highly polar organic solvent (usually N-methyl pyrrolidone (NMP)). The obtained PAA solution is then spin deposited onto the substrate and the solvent is evaporated. Imidization to PI is achieved by subsequent heating in an inert atmosphere at temperatures up to 350°C.

Curing and imidization of PAA obtained from solution has been investigated by Feger et al. [1]. They demonstrated that complexation of PAA by the solvent NMP has a marked influence on imidization. Only at temperatures high enough for decomplexation and for breaking the remaining hydrogen bonds between PAA and NMP can the highly reactive free groups react to form imide or, in a reverse reaction, to form anhydride. Decomplexation precedes imidization and anhydride formation. Only in the case of excess NMP in the solution, decomplexation occurs simultaneously with imidization and anhydride formation [1]. An important role of the solvent is to facilitate a high mobility of the polyamic acid moieties and the conformal changes to allow imidization.

Alternatively PAA can be obtained without solvent by vapor deposition polymerization as described first by Salem et al. [2]. In this technique the dianhydride pyromellitic and the dianhydride diamine (4,4'-oxidianiline) are codeposited onto a substrate, where they react to form PAA. Again the transformation to Polyimide is obtained by subsequent heating to temperatures up to 350°C. By comparison to spun on films, initial interaction of the polymer with the substrate occurs in the uncomplexed PAA state. The chemical interaction between PAA and the metal establishes the adhesion of the final polyimide film. This is discussed in this communication for evaporated gold cluster and bulk silver surfaces.

The x-ray photoelectron spectra for both dissolved and solventless polyamic acid have been reported in the literature [2-8]. It has been noted previously by us [5-7], that the spectra for solventless PAA and PI exhibit a pronounced deficiency for the C1s and O1s carbonyl emission. This, together with an analysis of the N1s lineshape and the O1s and C1s shake up features, allows us to derive conclusions on the chemical nature of solventless polyamic acid and to explain it's high reactivity towards metals as discussed below.

Experimental

The gold substrates for the vapor deposition experiments were obtained by evaporation from a tungsten basket onto freshly cleaved mica sheets. The gold overlayers were sufficiently thick (d > 8 nm) to suppress completely the photoemission signal from the underlying mica substrate. Vapor deposition of crystalline PMDA (pyromellitic dianhydride) and ODA (4,4'-oxydianiline) (Aldrich Gold Label) was carried out in the preparation chamber using small quartz test tubes heated resistively with a tantalum wire wrapped around them. Sublimation temperatures were measured by type K thermocouples inserted through the front end of each tube. The temperatures were adjusted to give approximately equal fluxes of PMDA and ODA to the surface. The base pressure of the preparation chamber was in the 10^{-9} mbar range; during deposition the pressure rise was in the 10^{-6} mbar range. After dosing, the samples were transferred in vacuo into the analysis chamber. XPS measurements were performed with a Mg K_α anode operated at 100 W. The spectra are calibrated against the Au 4f 7/2 emission

with an electron binding energy (BE) of 84.0 eV. No charging corrections were applied. All spectra presented here were recorded with an experimental resolution of 0.9 eV.

The Infrared spectra were recorded with a specially constructed evacuable infrared reflection spectrometer using conventional optics and a grating monochromator. The evacuated spectrometer ($p < 10^{-3}$ mbar) was attached to a small UHV chamber using calcium-fluoride windows. The small UHV chamber was part of a larger surface analysis system. The polymer films were produced in the vacuum system by vapor deposition and analyzed in ultra-high vacuum without exposure to air.

Results and discussion

1) Polyamic acid

In the following section we focus on some specific features in the core level spectra of polyamic acid and relate them to chemical and structural models for polyamic acid.

a) Carbonyl deficiency in PAA and PI films

Codeposition of PMDA and ODA onto a substrate held at room temperature leads to the formation of polyamic acid (PAA) [5-7]. Since the reactive sticking coefficient of PMDA and ODA forming PAA is substantially larger than for the sticking of the monomers on the bare metal surface, the initial interaction will be predominantly between PAA and the metal. The XPS spectra of the C1s region directly after dosing the gold substrate and after various curing stages are displayed in figure 1a to 1e. The corresponding spectra of the O1s region are shown in figure 2a to 2e. The film thickness of the PAA film (fig. 1a) was 8.8 nm as determined from the attenuation of the gold substrate using $\lambda = 2.2$ nm as the electron mean free path for the Au 4f emission at 1170 eV kinetic energy [9]. The lineshapes for PAA as well as for the intermediate curing stages and the final PI film are in good agreement with data reported previously by us and others [2-8].

The main band in the C1s emission around 285 eV binding energy arises from emission of the carbon atoms in the phenyl rings. The features at higher binding energies ($E_B > 288$ eV) in the C1s emission are due to C=O double bonded carbon in carbonyl groups and "shake up" transitions due to π-π* excitations in both the aromatic ring systems and in the carbonyl groups. A detailed assignment of the C1s emission for polyamic acid and for polyimide has been reported previously [2-8].

From a semi-quantitative analysis as described elsewhere [6] we obtain an O:N:C ratio of 4.7:2.6:22 compared with the stochiometric ratio of 7:2:22 (normalized to 22 carbon atoms per polyamic acid (or polyimide) repeat unit). Considering the contributions of the ODA and the PMDA monomers to the nitrogen to carbon (N:C) ratio the composition of the polyamic acid can be calculated independent of the degree of imidization. Using this method we obtain a monomer distribution of 66% ODA to 34% PMDA compared with a 50% to 50% distribution expected for stochiometric
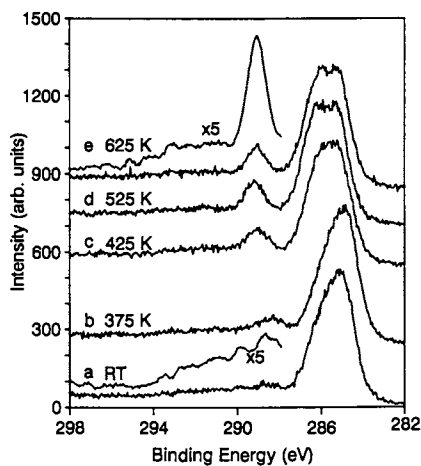
Figure 1: C1s XPS spectra of codeposited PMDA and ODA on a mica supported gold substrate
a) after deposition at room temperature (PAA) 8.8 nm
b) heated to 100°C for 30 min
c) heated to 150°C for 30 min
d) heated to 250°C for 30 min
e) heated to 350°C for 30 min (PI) 7.1 nm
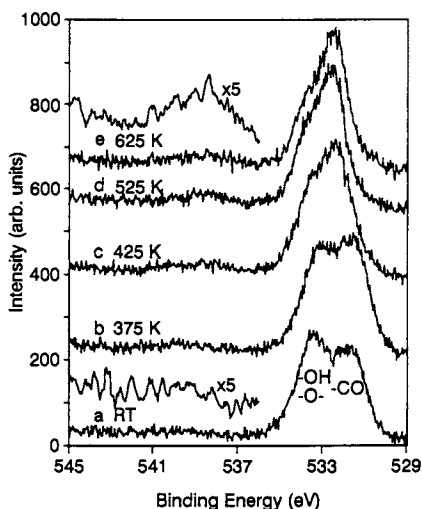
Figure 2: O1s XPS spectra of codeposited PMDA and ODA on a mica supported gold substrate
a) after deposition at room temperature (PAA) 8.8 nm
b) heated to 100°C for 30 min
c) heated to 150°C for 30 min
d) heated to 250°C for 30 min
e) heated to 350°C for 30 min (PI) 7.1 nm

polyamic acid (or polyimide). Upon stepwise heating to 350 C most of the excess ODA is desorbed resulting in a polyimide film with an O:N:C ratio of 4.5:2.1:22 (compared with the stochiometric ratio for polyimide of 5:2:22), corresponding to a monomer distribution of 53% ODA to 47% PMDA as calculated from the N:C ratio.

   The integrated intensity of the carbonyl carbon emission relative to the integrated phenyl carbon emission for polyamic acid (around 289 eV in figure 1a) and for polyimide (at 289.0 eV in figure 1e) after correction for the excess ODA is only 3.4:18 and 3.5:18, respectively, i. e. too small to account for four carbonyl groups per PAA or PI repeat unit. (The integral for the carbonyl groups in polyamic acid was obtained by integrating over the combined carbonyl and shake up region and subtracting the shake up intensity as observed in polyimide). Adding to the carbonyl and phenyl intensity the fraction of shake up intensity as observed in Pyromellitic dianhydride (PMDA) and in Oxydianiline (ODA) i.e. 7.8% (PMDA carbonyl), 10.8% (PMDA phenyl) and 6.2% (ODA phenyl), respectively [27], does not change the carbonyl to phenyl intensity ratios of polyamic acid and polyimide significantly. However, if the fraction of the shake up intensity is higher for the carbonyl groups in PAA or PI than it is in PMDA, we underestimate the carbonyl intensity, if it is lower, the carbonyl intensity could be too high. Taking these uncertainties into account, no quantitative conclusions about the carbonyl deficiencies can be drawn from the C1s spectra alone.

   The O1s emission of polyamic acid in figure 2a shows a broad doublet around 533 eV. This arises from the carbonyl group emission (lower binding energy) and the hydroxyl and ether oxygen photoemission (higher binding energy) [2,5-7]. The disappearance of the hydroxyl groups due to the formation and desorption of water during the curing process can be clearly seen in figure 2 for the various curing stages. A detailed discussion of the assignment of the bands for the O1s emission of PI (fig. 2e) has been given by Haight et al. [10].

   From the deconvoluted O1s spectra (not shown here) we obtain 47% carbonyl oxygen contribution in PAA and a 72% contribution of carbonyl oxygen to the total oxygen content in polyimide (both corrected for excess ODA). Depending on the degree of imidization the expected carbonyl oxygen contribution should increase to 80% for full imidization. If 90% "imidization" is assumed in the polyimide shown in fig. 2e, we obtain a deficit of 0.5 carbonyl oxygen atoms per PI repeat unit (consistent with the C1s data). We note, that we can not distinguish between complete imidization plus trapping of water and incomplete imidization. Thus the actual degree of imidization can be higher than the 90% given above.

   "Incomplete" imidization is further supported by the following considerations: When the amount of ODA monomer in the PI film is calculated from the nitrogen to carbon (N:C) ratio (result independent of the degree of imidization) and the oxygen to carbon (O:C) and the oxygen to nitrogen (O:N) ratio (results depend on the degree of imidization), respectively, a portion of 53% ODA (and 47% PMDA) is obtained from each calculation, and thus the results are in very good agreement with each other. Lower or higher degrees of imidization would give carbonyl oxygen deficiencies in the O1s spectra from zero and up to 1.1 oxygen atoms per PI repeat unit, respectively, but

inconsistent results are obtained when the amount of ODA in the film for the corresponding degree of imidization is calculated from the three ratios mentioned above. In summary there appears to be a 12-15% deficiency of C=O double bonded carbon and oxygen atoms in vapor deposited PAA and PI films.

Higher carbonyl deficiencies have been reported for spin coated polyamic acid [4,8] and polyimide films [4,8,10-12]. The carbonyl group deficiency for spin coated polyimide films has been discussed by Atanasoska et al. [11]. They attribute it to the formation of isoimide groups (as high as 25%), but they also note that there is some contradictory evidence. It is known, for instance, that isoimide groups irreversibly transform to imide groups upon heating to 300°C [13] and only a few percent isoimide are indicated in infra-red spectra of polyimide films [2,13].

A loss of carbonyl groups during imidization can be ruled out, since it is not consistent with the nitrogen to carbon (N:C) ratio in polyimide. Also, no loss of carbonyl groups is found in the case of PMDA multilayer condensation at room temperature and one expects that the carbonyl groups are stabilized by the reaction with ODA. This is supported by the fact that the PMDA loses carbonyl groups at temperatures exceeding 373 K, whereas no loss of carbonyl groups in the PI is observed up to 673 K [15].

Considering the excess of ODA, and apparent deficit of carbonyl C1s intensity found in vapor deposited polyamic acid [5-7], we propose a reaction as shown in Figure 3. The nucleophilic attack of an ODA amino group (3B) at a carbonyl group of PMDA (3A) is accompanied by opening of the PMDA anhydride ring leading to a "protonated" positively charged amide nitrogen and a negatively charged carboxylate group (3C). In the carboxylate group the carbon-oxygen bond order is reduced as compared to a carbonyl group and the C1s binding energy will be shifted to lower values, resulting in a too low carbonyl C1s intensity, when peak areas are compared. Since the amino nitrogen of oxydianiline is the center of highest basicity (highest proton affinity) in the system, an ammonium salt can be formed through the transfer of a proton from the amide group onto an amino group of free oxydianiline (3D). This ionic form is most likely further stabilized by intra- or intermolecular hydrogen bonding (not shown in figure 3). The transfer of a proton within the molecule leads to the formation of the neutral form of polyamic acid (3E).

Further evidence for a proton transfer comes from the N1s spectra in figure 4, showing the amino nitrogen in a thin ODA film (4.8 nm) evaporated at room temperature onto a gold substrate (4a), the N1s spectrum of polyamic acid (4b) and the N1s spectrum taken after imidization and curing at 350°C (4c). The N1s spectrum of polyamic acid shows a high binding energy shoulder, interpreted by us as positively charged nitrogen. This assignment is in agreement with similar assignments made by Clark et al. [14] in a study of amino acids, dipeptides and polypeptides. Deconvolution of the N1s peak into 3 gaussians gives an intensity distribution of 82%:18% between the main peak (2 gaussians) and the high binding energy shoulder (1 gaussian), respectively. With an ODA to PMDA ratio of 66%:34% (as calculated from the N:C ratio) this corresponds to a situation were 35% of the acid groups are in the carboxy-
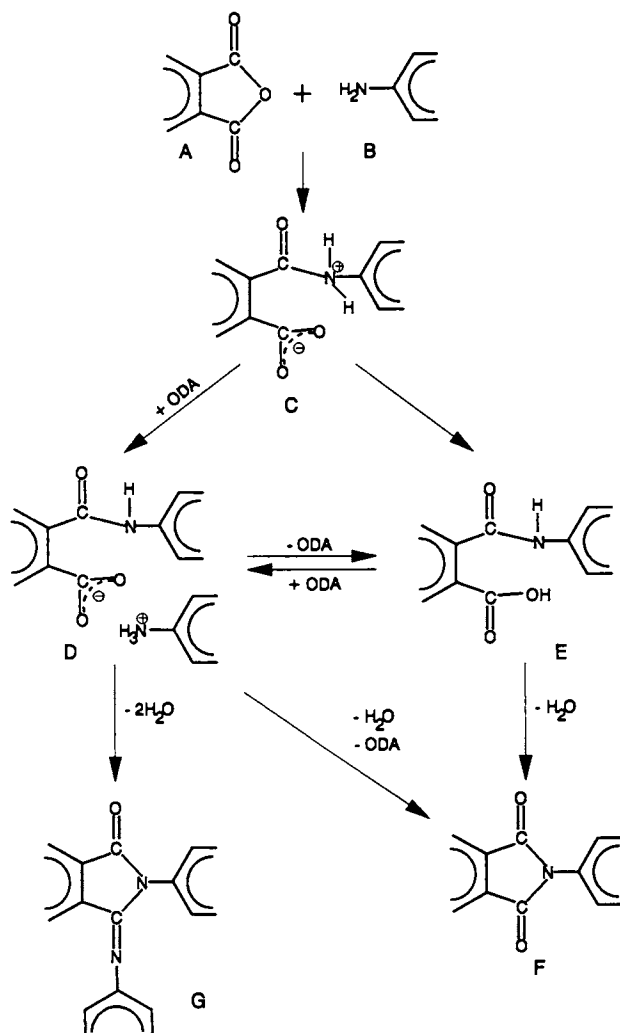
Figure 3: Schematic Diagram for the reaction of ODA with PMDA
A PMDA; **B** ODA; **C** Ionic form of PAA (intermediate state); **D** Ammonium salt formation in PAA; **E** Neutral form of PAA; **F** PI; **G** Branching of PAA due to reaction with a second ODA monomer
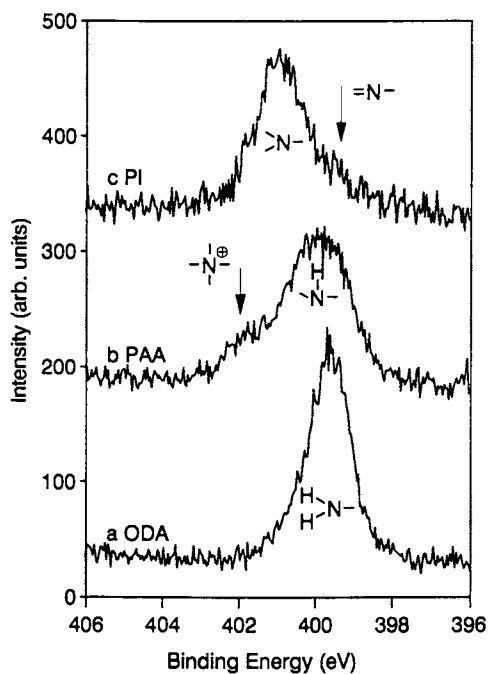
Figure 4: N1s XPS spectra (on a mica supported gold substrate)
a) Oxydianiline (ODA) thickness 4.9 nm
b) Polyamic acid (PAA) thickness 8.8 nm
c) Polyimide (PI) thickness 7.1 nm

late form. This implies that only one of the two amino groups in excess ODA is protonated and forms an ammonium salt.

If the fraction of acid groups which are in the carboxylate form (35%) do not contribute to the carbonyl intensity, a carbonyl deficiency of 0.7 carbonyl groups per polyamic acid repeat unit follows from the model in fig. 3 for PAA. This is close to the 0.6 we found in the analysis of the C1s core level data.

Whereas the proton transfer does not effect the stochiometry of the final PI when water is eliminated in the imidization reaction (fig. 3F), addition of an excess ODA molecule to polyamic acid could lead to the imine type crosslink formation schematically shown in figure 3G. This would lead to a deficiency of carbonyl oxygen atoms for vapor deposited polyimide and is consistent with our analysis. Mack et al. [16] proposed imine crosslink formation from their Raman spectroscopic studies for vapor deposited polyimides with excess ODA. In accordance with this model we attribute the low binding energy shoulder in the polyimide N1s line (figure 4c) to double bonded nitrogen species. However, the model gives no explanation for the carbonyl deficiency found in spin deposited polyamic acid and polyimide. In this case no excess of ODA is observed and only a very weak shoulder has been reported for the N1s line [4,11].

b) Shake up features in PAA and PI

Analysis of the region around 539 eV in figure 2, where the π-π* shake up satellite of the carbonyl oxygen emission occurs provides additional information about polyamic acid. The intensity in this region increases upon curing as shown by the enlarged scale spectra (compare figs. 2a and 2e). The areas under the weak shake up features were measured using a linear baseline. In defining the baseline a lot of care must be taken. It was chosen in a way that the integrals obtained for the "flat" regions next to the shake up features were vanishing. Deviations of the "true" background from this background under the shake up feature will give rise to some error in the integrated intensities (estimated by the error bars in fig. 5).

The integrated intensities of the oxygen π-π* shake up emission and its energy relative to the O1s carbonyl emission (determined from the deconvoluted spectra not shown here) are plotted in figure 5 for various curing stages. Obviously, there is a correlation between the intensity and the corresponding energy of the O1s shake up. We note, that the effect of imidization on the C1s shake up region is substantially less pronounced (compare figs. 1a and 1e).

Qualitatively these spectral changes during imidization can be understood by considering the origin of satellite structures in core level photoemission spectra. The creation of a core hole is accompanied by excitations of valence electrons from occupied states into unoccupied (nonbonding or anti-bonding) orbitals. The energy of these transitions, in our case the π-π* transition in the PMDA part of PAA and PI, depends on the localization of both the highest occupied molecular orbital (HOMO) and the lowest unoccupied molecular orbital (LUMO) within the molecule. Depending on the localization the (predominantly) electrostatic interaction with the core hole i.e. screen-

ing of the core hole, is different. Accordingly, the energy of the transition can be larger (when the HOMO is more strongly affected by the core hole) or smaller (in case the LUMO is localized around the core hole) than the excitation energy in the neutral molecule. In extreme cases, such as nitroaniline, the LUMO is pulled below the HOMO in the electrostatic field of the core hole, leading to negative shake up energies in molecules [17]. The spatial distribution or localization of the HOMO and LUMO with respect to the core hole also determines the intensity of the shake up. As discussed by Cederbaum and coworkers [18], the more localized the LUMO is towards the core hole, the smaller is the shake up energy due to the stronger electrostatic interaction and the higher is the intensity. This assumes, of course, that the HOMO is located further away from the core hole experiencing a smaller electrostatic attraction.

Haight et al. [10] performed *ab initio* calculations to determine the localization of the HOMO and LUMO in the PMDA part of polyimide to explain the spectral changes in their core level spectra when chromium is adsorbed on PI. The LUMO exhibits a much greater orbital amplitude on the carbonyl oxygen than on the carbonyl carbon atoms. There is no significant LUMO amplitude on the nitrogen or on the carbon atoms in the central phenyl ring bonded to hydrogen, some amplitude is found on the carbonyl carbon atom next-nearest neighbor carbon atoms. Accordingly, any changes in charge density on the carbonyl groups would effect predominantly the π^* orbital located around the oxygen atom, but due to the conjugation of the π electron system in a planar molecule the charge density would be affected also on the central phenyl ring and this would effect the C1s π-π^* shake up transition. However, in the case when the system is not planar, conjugation is not possible, separating the p electron systems of the carbonyl groups from that of the central phenyl ring. The HOMO and LUMO are expected to be localized mainly on the central phenyl ring and the interaction with the O1s core hole would be strongly reduced, lowering the intensity of the O1s shake up and increasing the energy of the π-π^* transition due to a smaller conjugated system.

Curing of polyamic acid effects the shake up region in the C1s and O1s core hole spectra differently. Major changes are observed only for the O1s core hole data. This demonstrates that the carbonyl groups and the central phenyl ring in polyamic acid are not conjugated and thus not planar. A non-planar geometry of the PMDA moiety in polyamic acid is also supported by theoretical considerations presented by S. Kowalczyk et al. [19]. During imidization there must be a transition of the PMDA part of the molecule from non-planar non-conjugated in polyamic acid to planar conjugated in polyimide. A "quasi continuous" transition via conformations with an increasing degree of coplanarity and conjugation and corresponding π-π^* transitions is suggested by the almost constant half-width of the shake up transition in polyamic acid and polyimide. The half-width of the O1s shakeups in the PAA/PI system is about twice the value found for the planar PMDA molecule (~1.1 eV), which indicates that for a given curing state different conformations in PAA contribute to the O1s shake up satellite.

Changes in the shake up intensity in the C1s and O1s spectra have been observed in the case of chromium deposition on fully cured PI and are interpreted as a charge transfer from the chromium atoms into the PMDA part of the polyimide [10,20,21]. Even at low coverage of one chromium atom for every three PI repeat units there are drastic changes in the XPS lineshapes and both the C1s and O1s shake up intensity are reduced. The phenyl emission shifts from higher to lower binding energy leading to a lineshape qualitatively in agreement with the lineshape observed for PAA and the carbonyl C1s intensity is reduced substantially. In the O1s and N1s spectra broadening of the peaks and for the O1s a split into a doublet has been found for increasing chromium coverages.

The spectral changes occurring upon chromium adsorption on polyimide were interpreted by Haight et al. [10] by a model in which the chromium atom adsorbs over the PMDA phenyl ring and donates charge into the lowest unoccupied molecular orbital (LUMO) of the coplanar system. This will lead to a shift of the C1s phenyl carbon emission to lower binding energies due to increased screening of the core hole and to reduction of the carbonyl bond order thus leading to a decrease in the characteristic carbonyl intensity.

A different interpretation is favoured for the chromium on polyimide data by Jordan et al. [21], who propose that initial attack of chromium and charge transfer occurs on the carbonyl moiety. Since the charge transferred from the metal is distributed over the planar PMDA moiety of the polyimide, the core level spectra by themselves will not allow a distinction between the two models proposed. However, a careful analysis of the shake up features in the C1s, O1s and N1s core hole spectra might reveal the initial binding site when the amplitude distributions of the LUMO's and HOMO's in the system relative to the created core hole are considered.

2) Interaction of Polyamic acid with metals

In the following we will present some data on the interaction of polyamic acid with metals which demonstrates the high reactivity of the carboxyl group in solventless PAA.

a) Gold

Sub monolayer evaporation of gold onto a polyamic acid with excess PMDA at room temperature leads to shifting of the PAA core level spectra to higher binding energies by ca. 0.8 eV, to broadening of the C1s and O1s spectra, and a further reduction of the carbonyl C1s intensity and the O1s shake up intensity (not shown here) [15]. As shown in fig. 6, the high binding energy shoulder on the N1s emission is strongly suppressed. The uniform shift of the core levels to higher binding energy can be explained by charging of the surface layer due to photoionized gold atoms and clusters leading to a change in the charge balance of the non-conducting polyamic acid film. This charging effect, which will vary across the surface and leads to differential charging, can also account for the broadening of the C1s and O1s emission. The changes in the N1s spectra, together with a further reduction of the O1s shake up in-
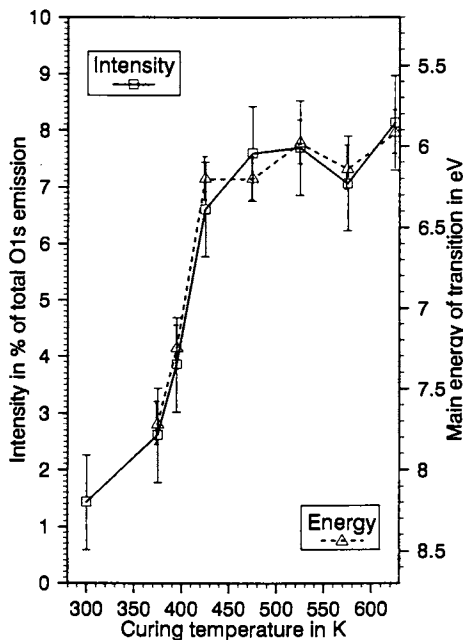
Figure 5: Plot of the integrated O1s "shake-up" intensity (left y-axis) from fig. 2 and energy in eV (right y-axis) relative to the O1s carbonyl emission at various curing temperatures. Error bars are estimated.
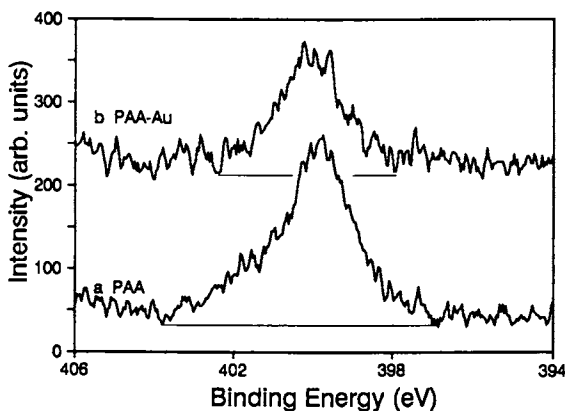
Figure 6: N1s XPS spectra of a thick polyamic acid film
a) before and b) after deposition of less than a monolayer gold

tensity (not shown here), however, indicate that the gold atoms preferentially interact with the amic acid part of the molecule. It can be speculated that gold clusters stabilize the carboxylic acid group in substitution for positively charged ammonium groups.

b) Silver

The experimental procedures and x-ray photoemission results for the preparation of ultrathin (d = 1.1 nm) polyimide films on polycrystalline silver by co-condensation of PMDA and ODA are described elsewhere [5]. In that work our XPS results suggested that the polyimide chains bond to the silver surface via a carboxylate type bonding. This conclusion was derived from an analysis of the results obtained for the interaction of the monomers (PMDA and ODA) and of the resulting ultra-thin polyimide film. Due to the relatively larger thickness of the polyamic acid films as compared to the monomer adsorbate phases and the polyimide film, no conclusions were possible about the reaction of the polyamic acid with the silver substrate.

In figure 7 we show Infrared-Reflection Absorption data for a thin polyamic acid film (a), a thin polyimide film (b) (after curing the PAA film of spectra a) and a thick (d > 10 nm) polyimide film (c) on a polycrystalline silver surface. Transmission and reflection infrared absorption spectra of thick (d > 1000 nm) spun-on polyamic acid and polyimide films have been reported previously [22-24]. Salem et al. [2] presented in their pioneering paper the infrared transmission spectra for vapor deposited polyamic acid and polyimide. Except for the relative intensities between the individual absorption bands, our results for a thick polyimide film (Fig. 7c) are identical to those for spun-on and vapor deposited films, showing the unresolved symmetric and asymmetric (strong) $v_{C=O}$ stretches between 1700-1800 cm^{-1}, the $v_{1,3}$ (1,4-C_6H_4) ring mode at 1504 cm^{-1}, the $v_{(C-N)}$ imide mode at 1385 cm^{-1}, the v_{C-O-C} stretch mode at 1245 cm^{-1}, and the $v(OC)_2NC$ (imide III) mode at 1117 cm^{-1}. A full discussion of the mode assignments is given in the literature [24].

The differences in relative intensities between the bands in our work and those of others as mentioned above have been discussed previously [25] and is due to the preferred alignment of the polyimide chains parallel to the surface plane.

In a grazing incidence (θ = 85 with respect to the surface normal) infrared reflection experiment the light is almost completely p-polarized at the surface and the electric field is strongly enhanced [26]. Further, due to the dipole-image dipole interaction of the oscillators only those modes will absorb light which have a dynamic dipole component perpendicular to the surface plane. Thus, in the surface near region those modes fulfilling the above requirements will be strongly enhanced. Accordingly, the polymer/metal interface will dominate the reflection infrared absorption spectra in experiments where films are sufficiently thin not to show a strong bulk signal. To which distance away from the metal the surface enhancement of the electric field and the dipole image-dipole interaction will dominate the reflection spectrum is not known and subject of a present study.
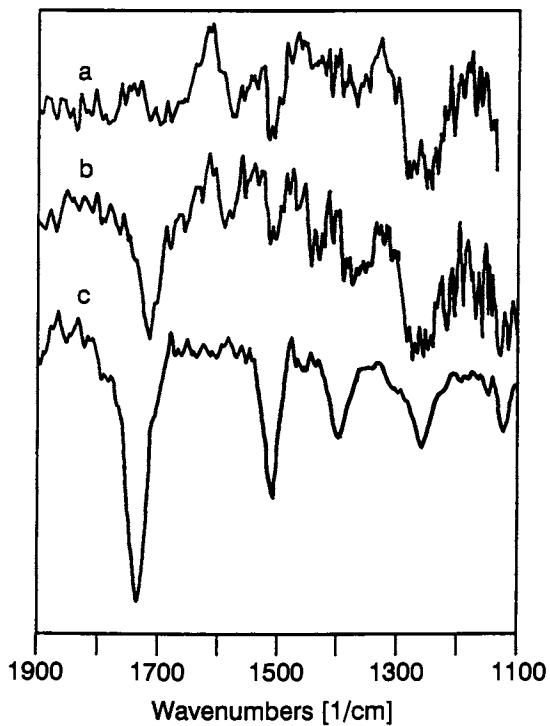
Figure 7: Infrared Reflection Absorption spectra of
a) a thin polyamic acid film on polycrystalline silver
b) a thin polyimide film obtained from a) after curing
c) a thick polyimide film

The spectrum of polyamic acid (7a) is dominated by the imide bands between 1200-1300 cm^{-1} and the $v_{1,3}$ (1,4-C_6H_4) ring mode at 1504 cm^{-1}. We note, that there is no pronounced band around 1660 cm^{-1} where we expect the $v_{C=O}$ stretch in carboxylic acid, there is rather a broad background absorption indicative of carbonyl groups in different chemical environments. At 1540 cm^{-1} we expect the N-H bending mode and around 1390 cm^{-1} the amide stretch frequency in PAA.

In silver acetate ($CH_3COO^-Ag^+$) two strong absorption bands are found at 1580 cm^{-1} and 1395 cm^{-1} for the asymmetric and symmetric $v_{(COO^-)}$ stretch. This corresponds to the wavenumber range where we also find absorption intensity for the thin PAA film on silver not present in thick polyamic acid films. We therefore propose, that some fraction of the polyamic acid interacts with the silver substrate via carboxylate type bonds. Intensity appearing in the asymmetric $v_{(COO^-)}$ stretch region as well as in the symmetric stretch region would indicate that the carboxylate is present in a mono-dentate form, since for a bidentate configuration we expect only to see the symmetric stretch, which has a dynamic dipole moment perpendicular to the surface. However, these spectra were taken on a polycrystalline silver surface and are too noisy to allow a quantitative interpretation.

The interaction of the polyimide chains via carboxylate type bonds is however clearly evident in spectra 7b for the cured polyimide film on polycrystalline silver. In addition to the characteristic vibrational modes of bulk polyimide we find two strong bands at 1600 cm^{-1} and 1440 cm^{-1} not present in the bulk spectra in the thick film (7c). These are interpreted as arising from the polyimide-silver carboxylate type interface bonding as discussed above for polyamic acid. The presence of both the asymmetric and symmetric $v_{(COO^-)}$ stretch could again be due to a preferential monodentate bonding configuration or to the polycrystalline nature of the substrate.

These results demonstrate, that the amic acid site in polyamic acid facilitates the adhesive bond between polyimide and silver as suggested by x-ray photoelectron results reported elsewhere [7].

Summary

Vapor deposited polyamic acid and polyimide films show both an excess of ODA and a deficiency of carbonyl groups. In the case of polyamic acid the excess of ODA leads to the formation of ammonium-carboxylate groups. The C1s emission of the carboxylate groups is shifted to lower binding energy and does not contribute to the typical C1s carbonyl emission, leading to a deficiency of carbonyl groups in a quantitative analysis. The presence of a high binding energy shoulder in the N1s emission in polyamic acid is consequently attributed to positively charged nitrogen in the ammonium groups. Upon curing to polyimide a portion of the excess ODA gets chemically bonded to the imide ring through imine type bonds, leading to a deficiency in the C1s

and O1s carbonyl group emission and a low binding energy shoulder in the N1s core hole spectra. Based on the analysis of the shake up intensity on the O1s and C1s core hole emission we concluded that polyamic acid is in a non-planar conformation and that the conformation changes upon curing quasi continuously to a planar polyimide conformation. The carboxyl moiety of PAA acts as a preferential interaction site between polyamic acid and metal atoms (Au) or bulk metal surfaces (Ag) and thus facilitates adhesion between the two materials.

References

1.   Brekner, M. J.;Feger, C. J. Polym. Sci. Polym. Chem. Ed., 1987, 25, 2005 and 2479.
2.   Salem, J. R.; Sequeda, F. O.; Duran, J.; Lee, W. Y.; Yang, R. M. J. Vac. Sci. Technol., 1986, A4(3), 369.
3.   Leary, H. J.; Campbell, D. S. In Photon, Electron and Ion Probes of Polymer Structure and Properties; Dwight, D. W.; Fabish, T.J.; Thomas, H. R., Eds.; ACS Symposium Series 16; American Chemical Society: Washington, DC 1981, p.419.
4.   Leary, H. J.; Campbell, D. S. Surf. Interface Anal., 1979, 1, 75.
5.   Grunze, M.; Lamb, R. N. Chem. Phys. Letts., 1987, 133, 283.
6.   Lamb, R. N.; Baxter, J.; Grunze, M.; Kong, C. W.; Unertl, W. N. Langmuir, 1988, 4, 249.
7.   Grunze, M.; Lamb, R. N. Surf. Sci. 1988, 204, 183.
8.   Silverman, B. D.; Bartha, J. W.; Clabes, J. G.; Ho, P. S.; Rossi, H. R. J. Polym. Sci. Polym. Chem. A 1986, 24, 3325.
9.   Clark, D. T.; Thomas, H. R. J. Polym. Sci. Polym. Chem. Ed., 1977, 15, 2843.
10.   Haight, R.; White, R. C.; Silverman, B. D.; Ho, P. S. J. Vac. Sci. Technol. 1988, A6(4), 2188.
11.   Atanasoska, Lj.; Anderson, S. G.; Meyer III, H. M.; Zhangda Lin; Weaver, J. H. J. Vac. Sci. Technol. 1987, A5(6), 3325.
12.   Buchwalter, P. L.; Baise, A. I. in Polyimides, Synthesis, Characterization and Applications, Mittal, K. L., ed. Vol. 1 (Plenum, New York 1983).
13.   Zurakovska-Orszagh, J. Eur. Polym. J. 1979, 15, 409.
14.   Clark, D. T.; Peeling, J.; Colling, L. Biochim. Biophys. Acta. 1976, 453, 533.

15. Strunkus, T. Diplomarbeit, Univ. Heidelberg, Heidelberg, 1988.

16. Mack, R. G.; Patterson, H. H.; Cook, M. R.; Carlin, C. M. J. Polym. Sci., Polym. Let. Ed., 1989, 27, 25.

17. Domcke, W.; Cederbaum, L. S.; Schirmer, J.; von Niessen, W. Phys. Rev. Letts. 1979, 42, 1237.

18. Schirmer, J.; Angonoa, G.; Cederbaum, L. S. Z. Phys. D 1987, 5, 253.

19. Kowalczyk, S.; Stafstroem, S.; Bredas, J. L.; Salanek, W. R.; Jordan-Sweet, J. L. preprint.

20. Clabes, J. G.; Goldberg, M. J.; Viehbeck, A.; Kovac, C. A. J. Vac. Sci. Technol. A 1988, 6(3), 985.

21. Jordan, J. L.; Kovac, C. A.; Morar, J. F.; Pollak, R. A. Phys. Rev. B 1987, 36, 1237.

22. Burrell, M. C.; Codella, P. J.; Fontana, J. A.; Cheva, J. J.; McConnel, M. D. J. Vac. Sci. Technol. A 1989, 7, 55.

23. Shih, D.-Y.; Paraszczak, J.; Klymko, N.; Flitsch, R.; Nunes, S.; Lewis, J.; Yang, C.; Cataldo, J.; McGouey, R.; Graham, W.; Serino, R.; Galligan, E. J. Vac. Sci. Technol. A 1989, 7 (3), 1402.

24. Ishida, H.; Wellinghoff, S. T.; Bauer, E; Koenig, L. L. Macromolecules 1980, 13, 826.

25. Grunze, M.; Unertl, W. N.; Gnanarajan, S.; French, J. Mat. Res. Soc. Symp. Proc. Vol. 108, 1988, p 189.

26. Pearce, H. A.; Sheppard, N. Surface Sci. 1976, 59.

27. Strunkus, T.; Grunze, M. unpublished results.

Chapter 27

Characterization of the Poly(ether ether ketone)–Copper Interface
Preliminary Electron Spectroscopy for Chemical Analysis

R. D. McElhaney, D. G. Castner, and B. D. Ratner

Department of Chemical Engineering and Center for Bioengineering, BF–10, University of Washington, Seattle, WA 98195

Poly(ether ether ketone) (PEEK) is a polymer used in carbon fiber reinforced composites. In addition, PEEK has been proposed for use in medical devices(1). The desirable physical properties of PEEK are its relative insolubility, thermal stability, and toughness.

Due to its insolubility, it is necessary to process PEEK thermally(2). However, it has also been shown that degradation of PEEK occurs when processing molds have copper surfaces(3,4). This degradation occurred in the presence of air, but not in a nitrogen environment.

Electron spectroscopy for chemical analysis (ESCA) studies were undertaken in order to characterize the PEEK/copper interactions that occur on Cu(0), Cu(I), and Cu(II) surfaces.

Experimental

ESCA data were collected on a Surface Science SSX-100 ESCA spectrometer. This instrument generates aluminum K_α X-rays, which are then monochromatized and focused onto a 150-1000 μm oval spot. Electron pass energies of 25 eV (high resolution) or 150 eV (low resolution) were used. Low resolution was used to determine atomic percentages, while high resolution was used to acquire chemical state information. For nonconductive samples, an electron flood gun was used to neutralize surface charging. Binding energies (BEs) were corrected by shifting the aliphatic C1s peak to 285.0 eV. The spectrometer was equipped with a variable temperature stage permitting control of the sample temperature from that of liquid nitrogen to 450°C.

Puratronic grade CuO [Cu(II)] and 99.9999% pure Cu(0) disks (9 mm diameter) were obtained from Johnson Matthey, Inc. Cu(I) powder (Cu$_2$O, 99.5% pure) was obtained from Morton Thiokol, Inc. Cu(II) disks were produced by heating Xe$^+$ etched copper to 600°C in an atmospheric muffle

furnace for 15 min. ESCA analysis indicated a 100% Cu(II) surface was produced by this treatment. Heating Cu(II) disks to 300°C under 10^{-8} torr vacuum produced nearly complete reduction to Cu(I).

PEEK powder, low MW-Grade 450 P (Batch SPG-9-33P), was manufactured by ICI, Ltd. For a bulk PEEK sample, wafers were produced by heating the powder to 300°C between aluminum sheets and applying a pressure of 5 metric tons in a Carver press. ESCA analysis of the pressed PEEK wafers consistently yielded surface compositions that were similar to the expected bulk composition. However, an occasional trace of fluorine was detected. A typical analysis is shown in Table I.

Table I. PEEK Composition

	Atomic Percent	
Element	*XPS*	*Bulk*
Carbon	86.7	86.4
Oxygen	13.3	13.6
Fluorine	trace	----

To monitor both the copper and the polymer species during a PEEK/copper interface reaction, a PEEK overlayer thinner than 80 Å, the approximate sampling depth of ESCA, was required. Centrifugal casting (3000 rpm for 15 sec) of an extract of PEEK in hexafluoroisopropanol (HFIP) onto copper disks proved successful for obtaining samples on which both PEEK and copper species could be detected by ESCA. The extract was obtained by passing a 20-30 wt. % suspension of PEEK in HFIP through a 0.5 μm Teflon filter. The solubility of a representative fraction of the PEEK in HFIP was verified by IR analysis. Comparison of the IR spectra from a PEEK/KBr pellet and the evaporated filtration product indicated identical spectra.

Results

Pure Component Reference Spectra. An ESCA C1s spectrum of the pressed PEEK wafer is shown in Figure 1a. An ESCA O1s spectrum of the pressed PEEK wafer is shown in Figure 1b. The C1s spectrum can be resolved into peak components indicative of hydrocarbon-type environments (285.0 eV), carbons singly bound to oxygen (at approximately 286.5 eV), and a distinctly resolved peak indicative of carbon in a ketone environment at 287.3 eV. Since this $\underline{C}$=O peak is expected at 288.0 eV, this suggests delocalization of electron density along the backbone chain. The PEEK surface stoichiometry is as expected (see Table I). This further supports the idea that the $\underline{C}$=O peak is

shifted due to unique electron distribution and not because of a surface reaction of the carbonyl group. The O1s spectrum shows two peaks, oxygen in single bond environments and oxygen doubly bonded to carbon. A more detailed analysis of these spectra will be presented in a future paper.

Copper spectra obtained are similar to those found elsewhere in the literature(5,6). Cu(II) is easily differentiated from Cu(I) and Cu(0) by the Cu $2p_{3/2}$ peak (Figure 2). Cu(II) has a higher BE (933.7 eV versus 932.5 eV) and, more significantly, a large shakeup satellite centered at 942.5 eV. The small shakeup satellite and high BE Cu 2p shoulder in the Cu(I) spectrum is attributed to surface oxidation of Cu(I) from exposure of the sample to laboratory air. Differentiation of Cu(I) from Cu(0) is achieved through analysis of the Cu Auger lines (Figure 3). The Cu L_3VV peak BE of Cu(I) (569.9 eV) is 1.9 eV higher than that of Cu(0) (568.0).

PEEK on Copper(0). PEEK is thermally stable on metallic copper under vacuum. Upon heating to temperatures in excess of 350°C, metallic copper does not induce significant changes in the PEEK/copper spectra (Figures 4-6). Those changes that occur between 30-200°C can be attributed to the desorption of contaminants and the conversion of Cu(I) to Cu(0). The Cu(I) is present because of a short exposure (3-4 min) to the laboratory environment between Xe^+ etching and spin casting. Above 200°C, the spectra indicate only PEEK and Cu(0) are present.

PEEK on Copper(I). In contrast to the PEEK/Cu(0) experiments, the amount of PEEK on Cu(I) changes significantly with heating. From 100°C to 300°C, there is a decrease in the amount of carbon and a corresponding increase in the Cu(I) level (Figure 7). Elemental spectra indicate the disappearance of PEEK (Figure 8). In particular, note the decrease in the C1s spectrum signal-to-noise with increasing temperature, an indication of substantial loss of carbon. If the elemental composition changes were due to decomposition, pronounced changes in the ESCA line shapes would be expected. This was not observed. Throughout the heating cycle, the copper oxidation state is unchanged and the distinguishing high resolution C1s PEEK features are retained.

Copper(II). Upon heating the Cu(II) specimen in the vacuum chamber from 100°C to 300°C, ESCA suggests that there is a desorption of surface contaminants and a gradual conversion of Cu(II) to Cu(I) (Figure 9). High resolution ESCA spectra provide additional support for the copper reduction. These spectra will be presented elsewhere. When removed from the vacuum, the heated sample had a reddish brown color, similar to the Cu_2O standard.

PEEK on Copper(II). In contrast to the PEEK on Cu(I), PEEK on Cu(II) did not significantly change in composition from 100-250°C. Between 250°C and 300°C, an abrupt compositional change was noted. This change was marked by a large increase in Cu(I) and the disappearance of carbon. High resolution ESCA spectra suggest that there is a sharp reduction of Cu(II) and the desorption and/or decomposition of PEEK above 250°C.
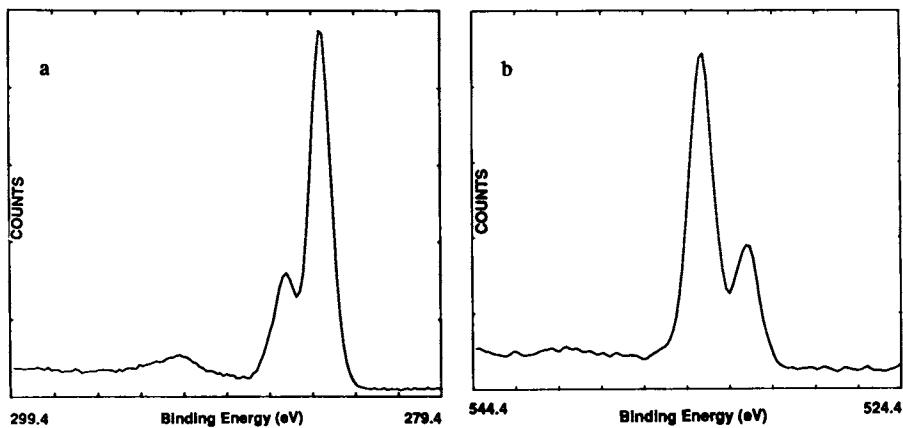
Figure 1. (a) ESCA C1s spectrum of a pressed PEEK wafer and (b) ESCA O1s spectrum of a pressed PEEK wafer.
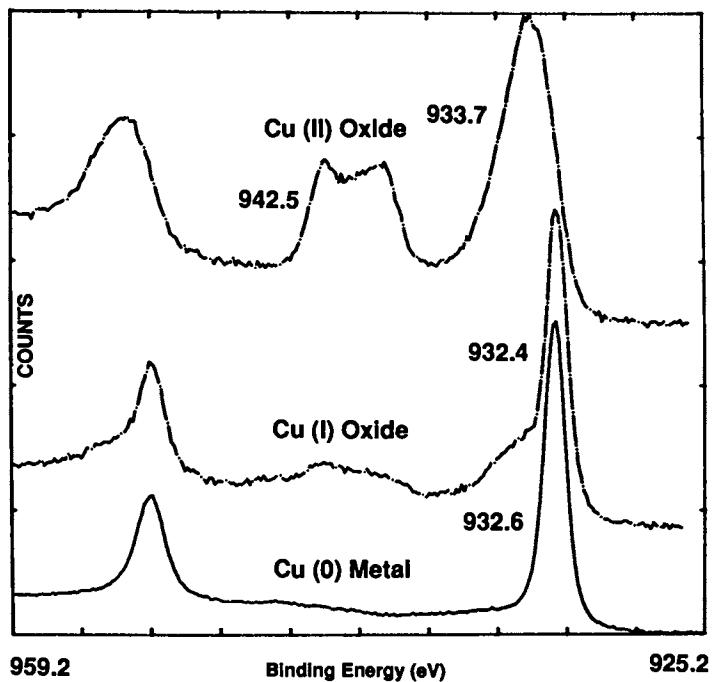
Figure 2. ESCA Cu 2p spectra of Cu(0), Cu(I), and Cu(II).
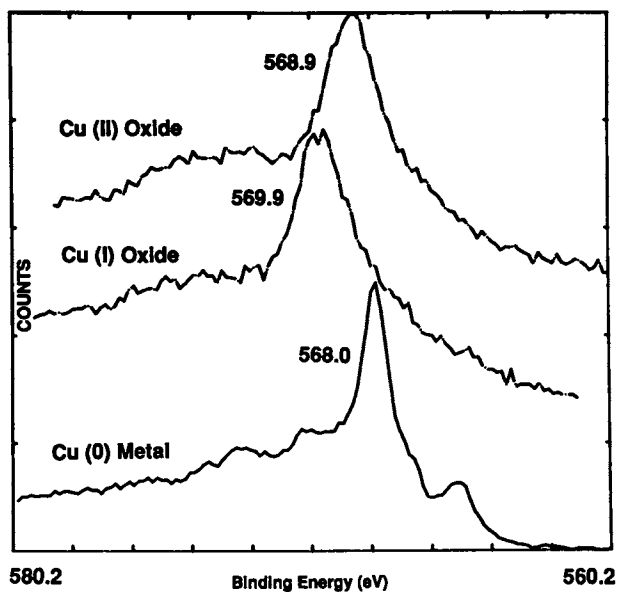
Figure 3. The X-ray induced Auger L_3VV spectra for Cu(0), Cu(I), and Cu(II).
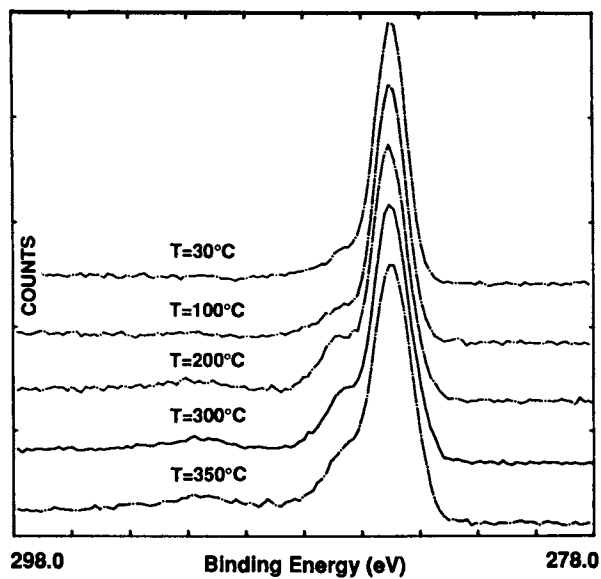
Figure 4. ESCA C1s spectra for a thin, solvent-deposited film of PEEK on copper metal at temperatures from 30°C to 350°C.
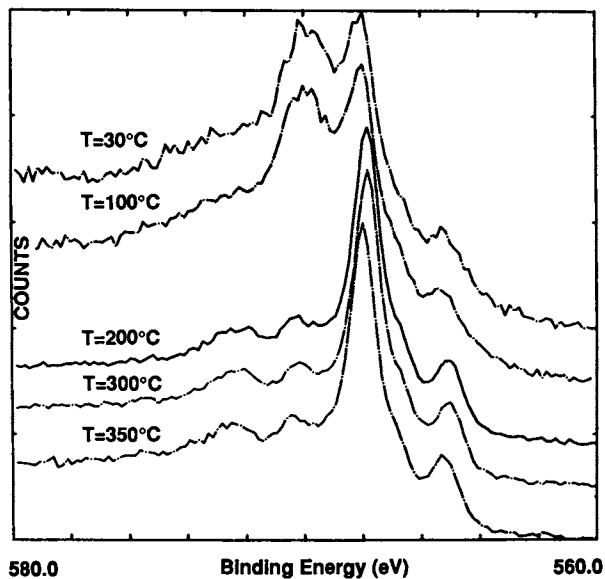
Figure 5. The X-ray induced Auger L_3VV spectra for a thin, solvent-deposited film of PEEK on copper metal at temperatures from 30°C to 350°C.
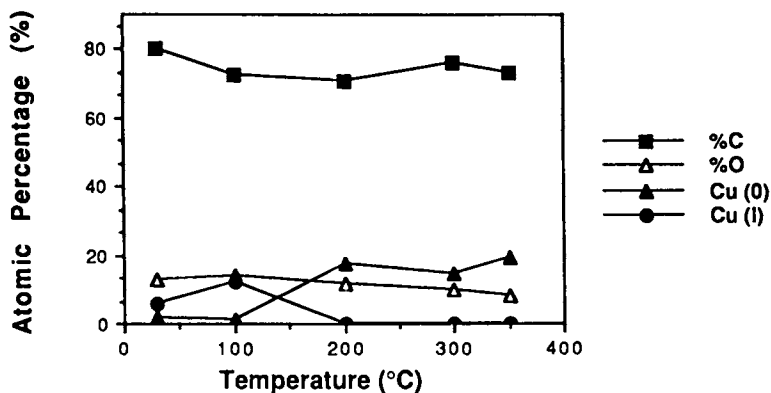
Figure 6. ESCA composition data for a thin, solvent-deposited film of PEEK on copper metal at temperatures from 30°C to 350°C.
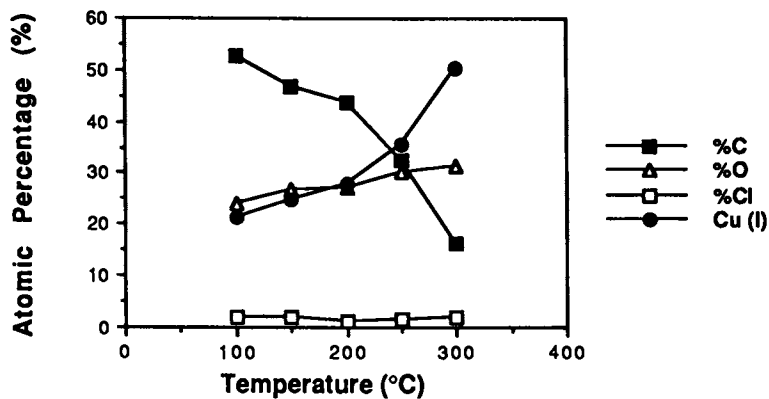
Figure 7. ESCA composition data for a thin, solvent-deposited film of PEEK on Cu(I) at temperatures from 100°C to 300°C.
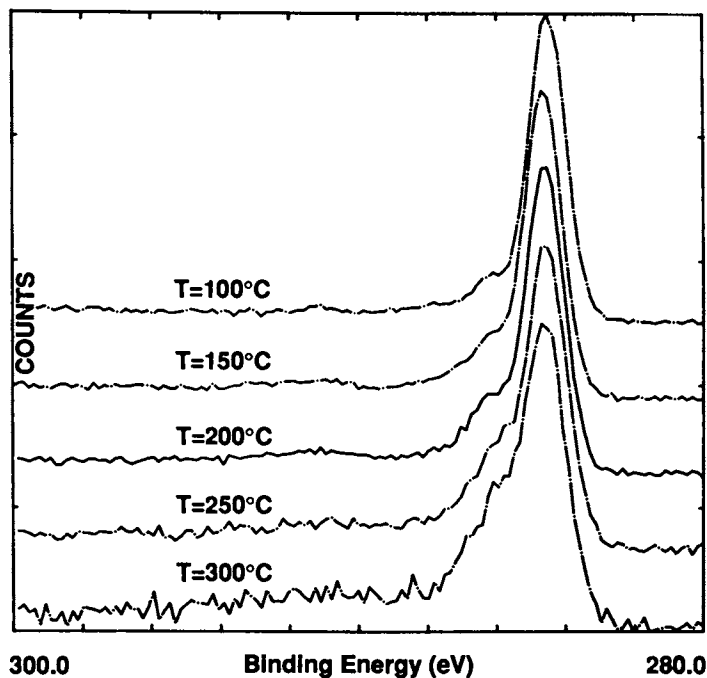
Figure 8. ESCA C1s spectra for a thin, solvent-deposited film of PEEK on Cu(I) at temperatures from 100°C to 300°C.

Cu(II) Standard
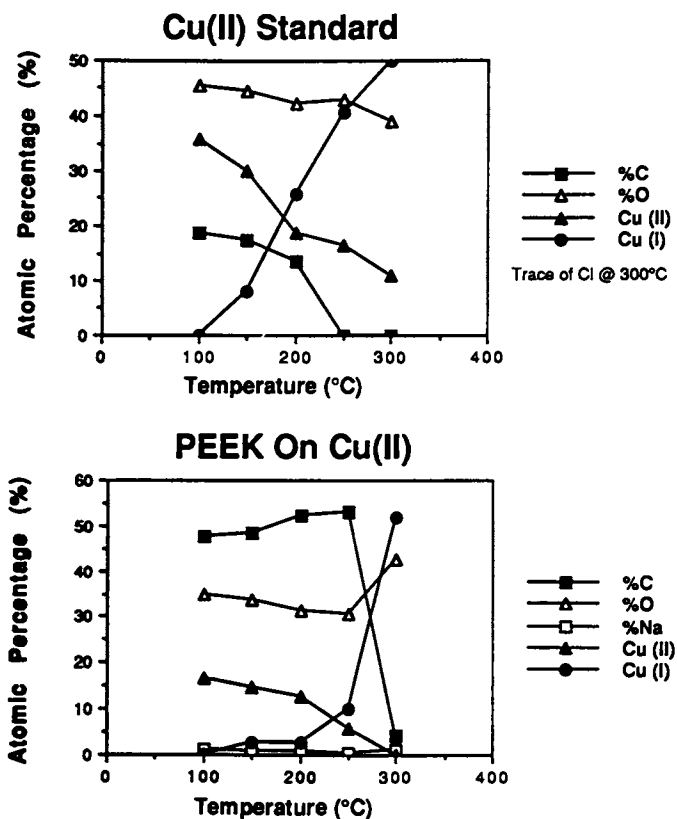
PEEK On Cu(II)

Figure 9. ESCA composition data for a thin, solvent-deposited film of PEEK on Cu(II) at temperatures from 100°C to 300°C. Data for the Cu(II) substrate without the PEEK overlayer are shown for comparison.

Discussion

Degradation of PEEK in the presence of copper appears to be catalyzed by Cu(II) or the reduction of Cu(II) to Cu(I). Metallic copper does not catalyze the decomposition of PEEK. On metallic copper, the PEEK remains intact to at least 350°C. Cu(I) does not show a strong interaction with PEEK. PEEK loss from the Cu(I) surface, possibly due to desorption, is apparent below 300°C. Up to 250°C, Cu(II) retains the PEEK in a manner similar to the metallic copper. However, there is a marked loss of PEEK on Cu(II) near 250°C and a reduction in the copper oxidation state. These two observations suggest that chemical reaction is occurring.

Mechanistic interpretation of the PEEK/Cu(II) degradation is difficult, based upon the data obtained. Possibly, a specific combination of Cu(I) and Cu(II) at the surface catalyzes the reaction. It can also be hypothesized that our PEEK/Cu(II) observations represent desorption of PEEK from Cu(I) after

reduction of Cu(II). This, however, is not supported by the PEEK/Cu(I) results, which indicate some PEEK remains on Cu(I) after heating to 300°C.

The results of Prime(4) and of Velisaris and Seferis(3) document the thermal decomposition of PEEK under atmospheric pressure and at temperatures just above the PEEK melting point (342°C). The decomposition we observe for the PEEK/Cu(II) system occurs below 300°C. This difference in decomposition temperature may be related to the pressure regime under which the experiments were performed (ultrahigh vacuum condition versus atmospheric pressure).

Additional experiments are required in order to clarify the processes occurring. In particular, the kinetics of changes in the PEEK and copper species must be measured. Also, additional high resolution C1s spectra (and a detailed analysis of the spectra of low molecular weight model compounds for PEEK) will help to clarify the chemical changes occurring in the PEEK. The coupling of a mass spectrometer to the vacuum chamber during the thermal treatment will assist in determining the identity of desorbing species.

Conclusions

The primary interest in PEEK polymer is for the fabrication of tough, durable objects. The results presented here may offer insights useful in processing PEEK and preventing surface degradation. There is also considerable interest in metal-organic interfaces with regard to medical implants. Studies on fundamental aspects of metal-catalyzed reaction of organics at interfaces may offer insights into the corrosion of metals in the body environment, protein adsorption to metals, and the integration of metals to bone (osteointegration).

Acknowledgments

Literature Cited

1. Williams, D. F.; McNamara, A.; Turner, R. M. *J. Mater. Sci. Letters* **1987**, *6*, 188-190.
2. Lovinger, A. J.; Davis, D. D. *Macromolecules* **1986**, *19*, 1861-1867.
3. Velisaris, C. N.; Seferis, J. C. "Thermal Processing and Characterization of Polyetheretherketone (PEEK) Matrices," *Plastics 85*, Proceedings of the SPE 43rd Annual Technical Conference and Exhibition, 1985.
4. Prime, B. R. *J. Polym. Sci.* **1986**, *25*, 641-644.
5. McIntyre, N. S.; Cook, M. G., *Analyt. Chem.* **1975**, *47(13)*, 2208-2213.
6. Panzar, G.; Egbert, B.; Schmidt, H. P. *Surface Science* **1985**, *151*, 400-408.

Chapter 28

Langmuir Blodgett Film–Metal Interfaces

Static Secondary Ion Mass Spectrometry and Electron Spectroscopy for Chemical Analysis

Paula A. Cornelio and Joseph A. Gardella, Jr.

Department of Chemistry, State University of New York at Buffalo, Buffalo, NY 14214

The chemistry which occurs at metal-polymer interfaces can be modelled using Langmuir Blodgett monomolecular films on metal surfaces. Studies using ESCA and static SIMS show the effects of surface chemistry and morphology of the substrate on the formation of complete overlayers and the interaction with the interfacial layer. Quantitative analysis allows the identification of surface impurities. In addition, the ability to provide quantitative information from static SIMS molecular ion signals allows for the possibility of kinetic probes of surface polymer degradation and crosslinking.

The metal polymer interface can be studied in a variety of ways using surface science methods. Recently, much emphasis has been placed on the understanding of the initial stages of metallization of polymers. In particular, the role of metal-organic interactions as they relate to the fundamentals of adhesion mechanisms are of interest. One experimental approach is to examine the first monolayers of metal as they are deposited on a polymer surface (1), i.e the polymer is the substrate. However, the organic polymer-metal interface may be studied in the opposite perspective, via understanding the roles of organic molecular or macromolecular structure and chemistry of the metal surface _qua_ substrate (2). In the present paper, recent ion and electron spectroscopic studies of the

interaction of organic and polymeric interfaces with polycrystalline metal surface will be presented. The particular focus has been the use of Langmuir Blodgett (LB) films (3) as model organic and polymeric layers.

In this review results from two surface science methods are presented. Electron Spectroscopy for Chemical Analysis (ESCA or XPS) is a widely used method for the study of organic and polymeric surfaces, metal corrosion and passivation studies and metallization of polymers (1a). However, one major accent of our work has been the development of complementary ion beam methods for polymer surface analysis. Of the techniques deriving from ion beam interactions, Secondary Ion Mass Spectrometry (SIMS), used as a surface analytical method, has many advantages over electron spectroscopies. Such benefits include superior elemental sensitivity with a ppm to ppb detection limit, the ability to detect molecular secondary ions which are directly related to the molecular structure, surface compositional sensitivity due in part to the matrix sensitivity of secondary emission, and mass spectrometric isotopic sensitivity. The major difficulties which limit routine analysis with SIMS include sample damage due to sputtering, a poor understanding of the relationship between matrix dependent secondary emission and molecular surface composition, and difficulty in obtaining reproducible, accurate quantitative molecular information. Thus, we have worked to overcome the limitations for quantitation, and the present work will report the results of these studies.

The consideration of the simplest and most widely used atomic ion SIMS experiments are complicated by quantitative difficulties. Anderson and Hinthorne (4) have shown that the atomic ion yields of different elements contained in a single matrix can vary over several orders of magnitude. This so-called substrate matrix effect has complicated quantitation with SIMS, since the absolute ion yield depends upon some electron exchange process between the departing secondary ion and the substrate surface (5). An additional problem in quantitative SIMS is sampling. SIMS is a destructive technique; it is impossible to obtain measurements from the same volume more than once. The reproducibility is determined by analyzing different spots under the same conditions. Therefore, a true measure of random uncertainty requires that the sample be homogeneous. Lack of surface homogeneity introduces large errors which are analytically related to improper sampling (6).

Various empirical calculation methods to standardize atomic ion quantitation have been proposed, however

Morrison has shown that even these are irreproducible (6). Relative quantitation of atomic ions has been quite successful, with sensitivity factor approaches the most widely used (7). However, no such treatment has been available for molecular ions in static or low damage SIMS owing to the difficulty of detection and low signal levels. In addition, the inability to reproduce molecular ion emission is related to instrumental factors, irreproducibility of samples, and the role of surface chemistry. An advance in the use of static SIMS could be made with a suitable method for quantitation. The present paper will discuss such an approach as it applies to surface chemistry of metal-organic systems.

In addition to matrix effects and quantitation, a simpler qualitative question must be asked. How does ionization occur during the momentum transfer process and how is this ionization affected by changes in surface composition? One approach to study molecular ion formation mechanisms has been to use Langmuir-Blodgett films as model systems, where molecular orientation can be controlled (3). The hierarchy of possible models which have been investigated include: mono-and multimolecular stearic acid and barium stearate films on Ag, Au, and Ge supporting substrates, as well as pure and mixed mono- and multi- molecular arachidic and behenic acid films on Ag. In addition, monolayer films of LB polymers and polymerizable films have been of continuing interest (3). These studies have addressed the interaction of thin organic overlayers with various substrate matrices and the effect of substrate morphology on the production of secondary ions, the effective sampling depth, and the extent of ion induced damage to the LB film.

In order to evaluate surface chemistry and stability of the films, ESCA studies were undertaken to confirm the stoichiometry and the degree of homogeneity. ESCA analysis of a layered system is complicated by attenuation of signal contribution from the substrate. Many previous studies of LB films by ESCA have been accomplished with the goal of measurement of sampling depth in ESCA (8-10). The photoemission intensity from underlying atoms is attenuated by overlayers. The sampling depth of the ESCA experiment is then intimately related to this attenuation phenomenon if the analysis involves a heterogeneous sample. The inelastic mean free path (IMFP) is defined as the mean distance traversed by an electron in a solid, between its ejection from the bound state and its participation in an inelastic scattering event. Seah and Dench (11) have tabulated results and derived an empirical model for IMFP and sampling depths as a function of the IMFP

for both inorganic and organic species. Building up
multiple layers of known thickness and density using LB
films is also an important means to study the sampling
depth and buried interfaces of importance in the
organic/metal system.

Experimental

A full description of the SIMS and ESCA instruments can
be found in previous papers (3). Briefly, the SIMS
experiments were carried out on a modified Leybold
Heraeus LHS 10 SIMS 100 quadrupole instrument. A cold
cathode ion source producing Ar^+ ions at current
densities of less than 1 nA/cm^2 and dosages of less
than 10^{12} ions/cm^2 was used as the source. Secondary
ions were mass filtered by the quadrupole and detected
by an off axis discrete dynode Kramer multiplier.
Signals are then averaged via pulse shaping and
counting directly by an IBM PC based SIMS control unit
also described previously. Quadrupole scan control and
rapid signal averaging is achieved via this unit. Base
pressure of the instrument is typically 5 x 10^{-10}
millibar. ESCA measurements were made using a Surface
Science Instruments model 206 ESCA with mono-
chromatized Al Kα radiation focussed to spot sizes of
typically 300 μm. Measurements reported represent the
average of at least four replicates on three separate
preparations of each sample for both ESCA and SIMS.
Reproducibility in ESCA is $\pm$ 5% RSD.

Langmuir Blodgett films were produced with a KSV model
2200 Langmuir trough in a laminar flow hood. The
trough is stabilized on a vibration isolation table.
Fatty acids (Stearic Acid (SA), Arachidic Acid (AA) and
Behenic Acid (BA) {Sigma, chromatographic grade (>99%
purity)}) were dissolved in benzene solution (1 mg/ml)
and instilled onto the trough substrate water (triple
distilled in quartz) via a microsyringe. Force-area
isotherms were measured for each sample. Films were
compressed to close packed two dimensional solid
conditions (typically 20 Å^2/molecule = 25 dynes/cm
surface pressure) and transferred to radio frequency
glow discharged silver, gold (3) or germanium
substrates. Y type deposition, i.e. the orientation of
the hydrophilic head at the surface with alternating
tail -tail and head-head stacking was used. Acceptable
transfer ratios were 1.00 $\pm$ 0.08. Coverage homogeneity
was verified via water contact angles and via the
observation of the shape of the meniscus. Substrate
chemistry and morphology will be discussed in the
results and discussion.

Results and Discussion

To validate the stoichiometry and stability of the
films studied by SIMS, AA and BA LB films were analyzed
by ESCA.   First, the materials were analyzed as
standards in pure powder form to determine the oxygen
sensitivity factor (relative to carbon equal to 1) and
guarantee the stoichiometry of the materials under X-
Ray and vacuum.   This evaluates elemental composition.
Functional group concentration can be accomplished
using peak fitting methods on the carbon 1s line; the
ratio of (CH_x) to COO can be determined.   For arachidic
acid and behenic acid this ratio is expected to be 19:1
and 21:1, respectively.   Further guarantee can be
evaluated using the oxygen 1s line and achieving a 1:1
ratio between the two forms of oxygen.   In addition, if
a carboxylate has been formed, then the two forms of
oxygen will become equivalent and coalesce to a single
line.   The ESCA analysis of standard materials is
summarized in Table 1.   This shows that under the
analysis conditions used, the materials are stable in
the bulk to X-Ray and vacuum.   However, perfect
stoichiometry is not achieved in each of the samples as
the atomic ratios appear to be systematically high.
This indicates either excess carbon (in the form of
slight amounts of contaminant) or a systematic bias in
the oxygen atomic sensitivity factor (since this system
ratios all sensitivity factors to carbon as 1).   The
latter explanation can be eliminated via comparison to
peak fitting results in Table 1.   Since the ratio of
CH_x to oxidized carbon species is slightly high, and
the internal oxygen ratios are within error of 1:1, it
seems reasonable to assume that slightly high amounts
of hydrocarbon based impurity at the surface of the
powder are responsible for the error in the powder
standards.   Further, X-Ray damage seems to be
negligible.   Long term time based studies shows little
change in composition over time until extreme (> 9
hours) exposures under the monochromatized X-Ray are
reached.

Table 1 ESCA Analysis of Standards

Sample	C/O	$\underline{C}H_x/\underline{C}OO$	C–$\underline{O}$/C=$\underline{O}$
		Experimental Ratios (Theory)	
Behenic Acid	12.6 (11)	21.8 (21)	0.97 (1)
Arachidic Acid	12.9 (10)	19.4 (19)	0.97 (1)

However, even with the slight amounts of impurity,
these data provide reasonable reference for those from
the LB films and the substrate blanks.

Table 2 reports data from analysis of LB films prepared on silver substrates used for the SIMS studies performed below. The "blank" silver surface (as prepared by detergent and chemical cleaning, rinsing and glow discharge cleaning and suitable exposure in the purified trough water (3b)) presents a surface which is rough silver oxide, with low levels of oxidized carbon contamination. Upon transfer of a single layer of fatty acid, it is evident that the coverage is not thick enough to attenuate silver photoemission intensity. Further, intensity from the existing carbon contamination on the substrate is still detectable as a deviation from the ideal carbon ratio and the presence of C-O. Also, the oxygen signal from the silver oxide and contaminant oxide is present in the oxygen 1s spectrum. However total attenuation can be achieved with a thickness somewhere between the equivalent thickness of five layers of arachidic ($\equiv$ 136.5 Å) and behenic acids ($\equiv$ 149.3 Å). When silver signal is fully attenuated as is the case for five layers of behenic acid, then the value for the carbon to oxygen ratio is equivalent to the value for the powder standard and within error limits of stoichiometry. This is also the case for films of thicker values than the five layers, up to eleven layers, which have been prepared.

Table 2 ESCA Analysis of LB Films

Sample	Experimental Ratios (Theory)		
	C/O	C/Ag	$\underline{C}H_x/\underline{C}O/\underline{C}OO$[1]
1 AA/Ag[2]	15.0	2.75	26/1.6/1 (19/0/1)
3 AA/Ag	10.1	9.80	na
5 AA/Ag	9.83	----	na
5 BA/Ag	12.2	----	na
11 AA/Ag	12.6	----	22/0/1 (19/0/1)

Key: na = not available

Notes

[1] $\underline{C}O$ type carbon should not be present in pure fatty acid compound. This is indicative of surface impurity.

[2] Silver oxide was detected in oxygen 1s envelope at low binding energy. Oxygen ratios exclusive of this surface silver oxide were within 5% error of 1/1 C-$\underline{O}$/C==$\underline{O}$.

This basis for evaluation of the films allows firmer understanding of the role of the substrate chemistry and morphology in the interpretation of SIMS results discussed below. Neutral fatty acid films are less stable than ion exchanged and stabilized films, using Cd^{+2}, Ca^{+2} or Ba^{+2}. However, these films are more sensitive to surface chemistry, and so defects in structure are expected. However, structural defects aside, the morphology of the rough silver surface is not completely attenuated until five layers of behenic acid are transferred. This implies either fully physically covering the roughness (3b), the so-called "carpet effect" does not occur until this coverage, or that the sampling depth is such that the silver signal can still be produced through defects or through attenuation. This problem has been discussed in previous ESCA studies of LB films, and these films were not chosen for continuity or full coverage, but for chemical reasons. Thus, the base of knowledge is extremely important to interpret SIMS data, but better coverage can and has been achieved using smoother substates and more stable LB film molecules or polymers. Results from those systems are currently under study.

One important chemical result from the ESCA studies involves the formation of surface carboxylates. Upon transfer of the monolayer to silver, the formation of a carboxylate could be detected by the production of a single peak in the oxygen 1s line due to equivalent oxygens in the carboxylate structure. Since the oxygen spectrum of the monolayer yields near stoichiometric C-O/C==O ratio of 1, the carboxylate is not detectable. Studies with monolayer films of cadmium arachidate indicated detectability of the carboxylate as a single carbon 1s peak. The lack of the formation of this interfacial carboxylate indicates the strength (or weakness) of surface chemistry which occurs on this silver surface as prepared.

Turning to SIMS analysis of the same systems, previous work conducted by Wandass, Schmitt and Gardella (3b) indicated evidence for both "matrix" (i.e. substrate surface chemistry) and "structural" (i.e. short range order in the LB film) dependence of $(M+H)^+$ emission from stearic acid LB layers on Ag, Au, and Ge. In particular, $(M+H)^+$ emission was not observed for a single monolayer on Ag, where the molecular orientation positions the carboxylic acid towards the reactive, oxidized Ag surface. However, $(M+H)^+$ emission from a stearic acid monolayer on both Au and Ge was observed. The results indicated that $(M+H)^+$ emission is influenced by the type of interaction/complexation

between the carboxylic acid moiety of the fatty acid and the oxide layer of the substrate. The less reactive Au substrate was thought to set up weak physisorptive bonding between the fatty acid carboxylic group and the Au surface, thus yielding favorable intermolecular proton transfer. Furthermore, although complexation between the the stearic acid "head" and the high energy RF plasma treated Ge was anticipated, $(M+H)^+$ ion emission was observed for a single monolayer on Ge.

Correlations were proposed between the rate of signal decrease as a function of ion dosage and ion stability. Wandass and Gardella investigated the intensity of $(M+H)^+$ emission for 15 layers of stearic acid on Ag as a function of ion dosage and observed an 80% decrease in the absolute signal intensity within the first 5 minutes of analysis (3). The protonation of a weak carboxylic acid should yield a relatively unstable resonance structure. The rapid drop in intensity with ion dosage may be indicative of either the thermodynamic instability of the ion or the disruption of structure which mediates against the production of $(M+H)^+$ ions. Such a simple structure may be envisioned as the head to head configuration of multiple layers in the Y configuration promoting close range based intermolecular protron transfer. Disruption of the structure would decrease the opportunity for such an ion formation mechanism to occur.

To test these possibilities, secondary molecular ion emission from arachidic (AA) and behenic (BA) acids cast directly onto equivalently prepared silver substrates from solution was compared to the secondary ion emission from LB films of equivalent molecular concentrations (i.e. molecules/cm^2) to determine the effect of orientation in molecular ion formation. The qualitative results are summarized in Table 3. For single LB layers of AA and BA on Ag, no $(M+H)^+$ emission is observed, as was previously reported for stearate, oleate and linolenic systems (3a). The Ag cationized molecular species, $(M+Ag)^+$ and $(M-H+2Ag)^+$, are observed for both solution cast and LB monolayers on Ag, as well as $(M-H)^-$. For 5 LB layers of AA on Ag (5 AA/Ag), the protonated molecular ion $(M+H)^+$ as well as the neutral loss of water $(M+H-H_2O)^+$ is observed. $(M+Ag)^+$ emission is observed, but $(M-H+2Ag)^+$ was completely attenuated. $(M-H)^-$ emission is also weak for 5 LB AA/Ag. For 5 LB BA/Ag, only $(M+H)^+$ is observed. $(M+H-H_2O)^+$ overlaps with Ag_3^+ cluster ion. Neither molecular ions from Ag cationization of BA nor $(M-H)^-$ is observed. For single monolayers of AA solution deposited monolayers of AA on Ag, only $(M+Ag)^+$, $(M-H+2Ag)^+$, and $(M-H)^-$ are observed,

qualitatively the same as the LB film. However, for 5 monolayer equivalent solution deposition of AA on Ag, no $(M+H)^+$ ion signal is observed. However, Ag cationization of the AA molecule and $(M-H)^-$ is observed.

In order to characterize the extent of ion induced damage and the effect of attenuation of molecular emission by overlayer coverage a series of mixed multilayer systems were fabricated. The overall sample thickness was 5 LB layers (approx. 140 Å), consisting of 4 layers of arachidic acid and 1 layer of behenic acid. Five permutations are then possible by altering the position of the behenic acid layer with respect to the substrate. The positive and negative SIMS results are summarized in Table 4. These results suggest that the molecular ions from different mechanisms result from different depths.

Focussing directly on the results from the BA related molecular ions, it can be proposed that the $(M+H)^+$ originates from structurally limited positions within the top (closest to air interface) three monolayers. Since it is more chemically stable, the $(M-H)^-$ ion may be assumed to be more representative of the total amount of BA present. But, as layer thickness increases and the distance between the molecule and the metal surface increases, the probability of formation of $(M-H)^-$ decreases. Ag cationization to produce molecular ions is thought to be dependent on emission of a neutral species from the top two layers and the presence of a requisite amount of gas (or selvedge) phase silver ions for coordination in this region. Since multiple layers attenuate (although at five layers not completely) the silver ion signal from these surfaces, the amount of silver is limited, and this affects the probability of formation of these ions. The clear result is that for BA, only when the BA is in the topmost (airfacing) layer are both conditions met. Thus the effective sampling depth of this ion is one monolayer in the assembly.

The use of SIMS to obtain quantitative information has traditionally been recognized as a very difficult task complicated by the fact that internal standards and sensitivity factors cannot be applied universally. One approach, which has met with some success in dynamic SIMS, is the construction of a depth profile of implanted dopant (of known total dopant dosage) and then to relate the integrated area under the depth profile curve to the total concentration of dopant. This allows determination of concentration at any

Table 3 Qualitative SIMS Molecular Ion Results
for LB Films

		Molecular Ions Detected			
Sample	$(M+H)^+$	$(M+H-H_2O)^+$	$(M+Ag)^+$	$(M-H+2Ag)^+$	$(M-H)^-$
1 SA/Ag	no	no	yes	yes	yes
5 SA/Ag	yes(w)	yes(w)	yes	yes	yes
1 AA/Ag	no	no	yes	yes(w)	yes
5 AA/Ag	yes	yes	yes(w)	no	yes
5 AA/Ag (soln cast)	no	no	yes	yes	yes
1 BA/Ag	no	no	yes	yes(w)	yes
5 BA/Ag	yes	yes(o)	no	no	no

Key: (w) = weak signal (o) = overlap with interference
(soln cast) = cast from solution (not LB film)

Table 4 Qualitative SIMS Results from Five
LB Layer Alternating Layer Experiment

	Molecular Ions Detected					
Sample	$(M+H)^+$		$(M+Ag)^+$		$(M-H)^-$	
	AA	BA	AA	BA	AA	BA
4AA-1BA/Ag	yes(s)	no	no	no	yes	yes(w)
3AA-1BA-1AA/Ag	yes(s)	no	no	no	yes	yes(w)
2AA-1BA-2AA/Ag	yes(s)	yes	yes	no	yes	yes(w)
1AA-1BA-3AA/Ag	yes(s)	no	yes(s)	no	yes	yes
1BA-4AA/Ag	yes(s)	yes	yes	yes	yes	yes(s)

Key: (s) = strong (w) = weak intensity

particular point on the depth scale (12). The total integrated peak intensity approach applied to the quantitation of molecular secondary ions has been investigated by Clark and Gardella (13). Ag^+ emission has been successfully employed as an internal ratio standard for quantitation of 1-DOPA, 5,6 dihydroxyindole, and dopamine as solution deposited thin films on Ag. In the present work, we extend this approach to quantitation of pure arachidic acid LB multilayers deposited onto Ag. The ratio of $(M+H)^+$/Ag intensities was integrated over a specific ion dosage ($5 - 70 \times 10^{12}$ ions/cm^2) and this integrated peak ratio was found to non-linear with increased LB layer thickness. The ratio increased from 3 to 5 layers, and then decreased, with the value for 9 layers lower than that of 3. Some explanations for the non-linearity can be proposed: First, Ag^+ emission is attenuated by increased LB overlayer coverage, and emission is completely lost for analysis of 11 AA/Ag (with 4kV primary ions, at higher primary ion energy (30kV), Ag ion emission and cationization is observed). Thus, Ag is obviously an inappropriate internal indicator for normalizing the absolute molecular ion intensity. While Ag ion ratioing was successful in the earlier study (13), coverages above close packed monolayers were not verified for the positive ions probed. Further, none of the positive ions probed in the earlier study were dependent on surface processes for formation, these were structurally stable ions, at much higher absolute ion yields. As discussed above, $(M+H)^+$ emission from a fatty acid requires the protonation of a weak acid which is thermodynamically disfavored and results in an unstable resonance structure. $(M+H)^+$ emission is not representative of the amount of material present because of a disfavored formation mechanism. More $(M+H)^+$ ions simply cannot be formed even though the surface concentration of arachidic acid increased from 1.5×10^{15} to 4.5×10^{15} molecules/cm^2 ($3 - 9$ layers of AA/Ag). Third, the mechanism of $(M+H)^+$ emission is dependent upon structure. No increase in $(M+H)^+$ emission is observed since the ion beam implantation has disrupted the structural integrity of the LB film, precluding further $(M+H)^+$ formation. Thus, if structural integrity is important in the formation of $(M+H)^+$ from fatty acid thin films (since microsyringe casting of concentrations equivalent to three, five and eleven monolayers results in no detectable $(M+H)^+$) then the first several LB layers may not contribute equally to the overall $(M+H)^+$ signal.

In order to demonstrate the potential of other approaches to quantitation of LB films a series of mixed fatty acid monolayers was prepared in which the

molar concentration ratio of the two fatty acids was
known.   Experimentally, the molecular secondary
emission of (M-H)$^-$ and (M+Ag)$^+$ from the two fatty
acids was monitored as a function of ion dosage and the
ratio of experimentally measured molecular emission
compared to the actual molar ratio of the two fatty
acids within the monomolecular film. In this way, one
fatty acid acts as an internal standard, taking the
place of the internal indicator, Ag . The intensity of
the molecular emissions was integrated over a specific
ion dosage (5.0 - 70 x 10^{12} ions/cm^2).   When this
"internal standard" approach is used in conjunction
with the total integrated peak intensities, a linear
correlation between the experimental ratio of secondary
emissions from BA and AA and the actual molar
concentration is obtained. The results are shown in
Figures 1 and 2. Comparison between normalization to
an "internal standard" (i.e., BA/AA) and normalization
to an "internal indicator" (i.e., Ag$^+$) leads to the
conclusion that normalization of either BA or AA
(M+Ag)$^+$ peak area to Ag$^+$ results in increased error.
Two explanations can be proposed: First, Ag$^+$ is not
representative of the state of the ionized surface, or,
second, the formation of (M+Ag)$^+$ involves an
intermediate cationization step, while some of the Ag$^+$
escapes the selvege and reaches the detector, other Ag$^+$
ions take part in molecular cationization. The amount
of Ag$^+$ that escapes does not relate to the amount
involved in cationization in a way that can be
expressed precisely as a ratio (M+Ag)$^+$/Ag$^+$.   The
linear correlation coefficient for quantitative
analysis using (M-H)$^-$ emission was 0.9734 and the
average relative standard deviation for 4 measurements
was 12%.   The linear correlation coefficient for
quantitative analysis conducted using (M+Ag)$^+$ emission
was 0.9948 and the average relative standard deviation
for 5 measurements was 13%.   The accuracy of the
measurements using (M-H)$^-$ ranged from 19 - 32 percent
relative error and 0.4 - 60 percent relative error
using (M+Ag)$^+$.   Note that another aspect of the
validity of this approach lies in the fact that the
slope of the line is equal to unity, which must be the
case for this particular analysis if the ratioed ion
intensities are directly related to concentrations.

Conclusions

The study of LB films by ESCA and SIMS provides some
important lessons for the metal polymer interface. The
surface chemistry of polycrystalline silver is active
enough to effect the protonation process to form
molecular ions. Yet, the chemistry is not sufficient
to completely deprotonate the fatty acids and produce
carboxylate salts with the silver as counter ion. The
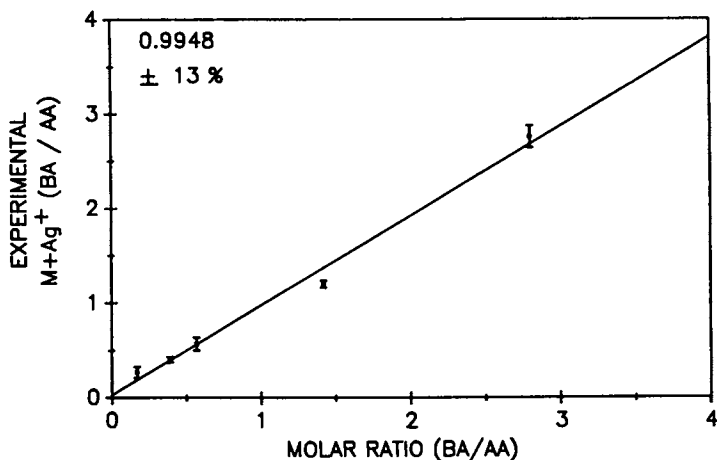
Figure 1. Plot of Integrated (M+Ag)$^+$ ion signal for Behenic Acid ratioed to that for Arachidic Acid Langmuir Blodgett monolayers of mixed composition. Correlation Coefficient = 0.9948 $\pm$ 13%RSD. Slope = 0.964 (Theory = 1) Intercept = 0.0192 (Theory = 0).
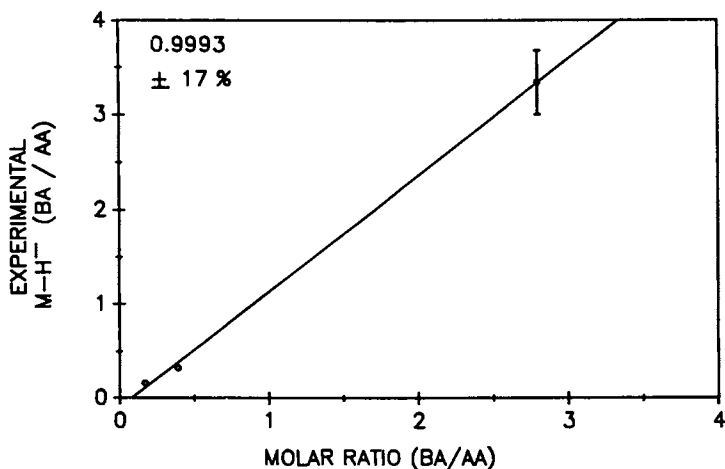
Figure 2. Plot of Integrated (M-H)$^-$ ion signal for Behenic Acid ratioed to that for Arachidic Acid Langmuir Blodgett monolayers of mixed composition. Correlation Coefficient = 0.9993 $\pm$ 17%RSD. Slope = 1.28 (Theory = 1) Intercept = 0.115 (Theory = 0).

ability to provide quantitative analysis of mixed
molecular species should allow the development of the
ability to provide quantitative kinetics of surface
reactions such as crosslinking and other degradations
which occur upon metallization. Finally, the ability
to address surface contaminants of all types is an
important problem. It is likely that low molecular
weight contamination plays a significant role in
adhesion phenomena between metal/polymer interfaces.
The ability to evaluate hidden or buried interfaces
between these materials is a major future challenge.

Literature Cited

1a. Burkstrand, J. M. J. Appl. Phys. 1981, 52, 4795.
 b. DiNardo, N. J.; Demuth, J. E.; Clarke, T. C. Chem.
     Phys. Lett. 1985, 121, 239.
 c. Pireaux, J. J.; Vermeersch, M.; Grégoire, Ch.;
     Thiry, P. A.; Caudano, R.; Clarke, T. C. J. Chem.
     Phys. 1988, 88, 3353.
2.   Grunze, M.; Lamb, R. N. Surface Science 1988, 204,
     183.
3a. Wandass, J. H., III; Gardella, J. A., Jr. J. Am.
     Chem. Soc. 1985, 107, 6192.
 b. Wandass, J. H., III; Schmitt, R. L.; Gardella, J.
     A., Jr. Appl. Surf. Sci. 1989, 40, 85.
 c. Hook, K. J.; Gardella, J. A., Jr. J. Vac. Sci.
     Technol. 1989, A7, 1795.
 d. Cornelio, P. A.; Gardella, J. A., Jr. J. Vac. Sci.
     Technol. 1990, A8, in press.
4.   Anderson, C. A.; Hinthorne, J. R. Anal. Chem. 1973,
     45, 1421.

5. Benninghoven, A.; Rudenauer, F. G.; Werner, H. W. In <u>Secondary Ion Mass Spectrometry: Basic Concepts, Instrumental Aspects and Trends</u> Elving, P. J., Winefordner, J. D., Kolthoff, I. M. Eds.; John Wiley and Sons: New York, 1987.
6. Rudat, M. A.; Morrison, G. H. <u>Anal. Chem.</u> 1979, <u>51</u>, 1179.
7. Brenna, J. T.; Morrison, G. H. <u>Anal. Chem.</u> 1986, <u>58</u>, 1675.
8. Brundle, C. R.; Hopster, H.; Swalen, J. D. <u>J. Chem. Phys.</u> 1979, <u>70</u>, 5190.
9. Hall, S. M.; Andrade, J. D.; Ma, S. M.; King, R. N. <u>J. Elec. Spec. Relat. Phenom.</u> 1979, <u>17</u>, 181.
10. Hupfer, B.; Schupp, H.; Andrade, J. D.; Ringsdorf, J. <u>J. Elec. Spec. Relat. Phenom.</u> 1981, <u>23</u>, 103.
11. Seah, M. P.; Dench, W. A. <u>Surf. Int. Anal.</u> 1979, <u>1</u>, 2.
12. Werner, H. W.; Boudewijn, P. R. <u>Vacuum</u> 1984, <u>34</u>, 83.
13. Clark, M. B., Jr.; Gardella, J. A., Jr. <u>Anal. Chem.</u> 1990, <u>62(8)</u>, 870-5.

Chapter 29

Redox Seeding and Electroless Metallization of Polyimides

A. Viehbeck[1], C. A. Kovac[1], S. L. Buchwalter[1], M. J. Goldberg[1], and S. L. Tisdale[2]

[1]T. J. Watson Research Center, IBM Corporation, Box 218, Yorktown Heights, NY 10598
[2]Systems Technology Division, IBM Corporation, Endicott, NY 13760

This paper describes a process for activating polyimide surfaces for electroless metal plating. A thin surface region of a polyimide film can be electrochemically reduced when contacted with certain reducing agent solutions. The electroactivity of polyimides is used to mediate electron transfer for depositing catalytic metal (e.g., Pd, Pt, Ni, Cu) seeds onto the polymer surface. The proposed metal deposition mechanism presented is based on results obtained from cyclic voltammetric, UV-visible, and Rutherford backscattering analysis of reduced and metallized polyimide films. This process allows blanket and full-additive metallization of polymeric materials for electronic device fabrication.

Polyimides are widely used in the electronics industry as dielectric and passivation films *(1)*. The metallization of polyimides is an important concern in VLSI packaging applications because of demands for increased wiring density, greater reliability, and lower processing costs *(2)*. The integrity of the metal/polymer interface also must be maintained during device fabrication and use. Strong adhesive forces can be developed on polyimides by evaporation or sputtering of electropositive metals such as Cr, Ti, and Ni *(3)*. Metal plating methods used in printed circuit board fabrication offer cost advantages over vacuum metallization techniques *(4)*. However, conventional surface activation processes for catalyzing electroless plating are often inadequate for use with unfilled materials and smooth surfaces resulting in poor adhesion or nonuniform deposits.

Polyimides have excellent dielectric strength and a low dielectric constant, but in certain electrolyte solutions they can electrochemically transport electronic and ionic charge. Haushalter and Krause *(5)* first reported that Kapton polyimide films derived from 1,2,4,5-pyromellitic dianhydride (PMDA) and 4,4'-oxydianiline (ODA) undergo reversible reduction/oxidation (redox) reactions in electrolyte solutions. Mazur et al., *(6)* presented a detailed study of the electrochemical properties of chemically imidized aromatic PMDA-derived polyimides and model compounds in nonaqueous solutions. Thin films of thermally

cured PMDA-ODA polyimide on electrodes have been shown to be electroactive in aqueous electrolyte solutions *(7)*. Viehbeck et. al., have recently reported on an investigation of the redox properties and effects of charge delocalization for different polyimides and imide model compounds in aprotic solutions *(8)*.

It has been shown that electroactive polymer films on electrodes can mediate electron transfer for metal deposition *(9-11)*. Haushalter and Krause *(5)* have described the treatment of PMDA-ODA films with highly reactive Zintl complexes (e.g., Sn_9^{-4}, $SnTe_4^{-4}$) to yield an intercalated material able to reduce ions of platinum, palladium and silver at the film surface. Mazur et al., *(12)* reported the deposition of conductive Ag, Cu, and Au metal interlayers within a PMDA-ODA film by electrochemical reduction.

This paper describes a new seeding process for electroless metallization of polyimides and other electroactive polymers. Polyimide films can be reduced electrochemically at an electrode surface or by contact with an appropriate reducing agent in an electrolyte solution. In the latter case, only the outer surface of the film undergoes reduction. Once the polyimide surface is reduced it then can mediate electron transfer to metal ions or metal complexes in solution causing metal to be deposited at the surface with concurrent reoxidation of the polyimide. The deposition of metals such as Pd, Pt, Ni, and Cu renders the surface active towards further metal deposition from conventional electroless metal plating baths. Well-adhering metal films can be formed on polyimides by this method. The main process steps for blanket metallization of a polyimide film, illustrated in Scheme I, involve polymer reduction, metal seeding, and electroless metal plating. Specific details of each process step are provided in the discussion below.

Experimental

Starting materials and solvents were purchased from Aldrich Chemical Co.; acetonitrile (ACN), N,N-dimethylformamide (DMF), and N-methyl-2-pyrrolidone (NMP) were obtained anhydrous in Sure/Seal bottles and used as received. The polyamic acid of PMDA-ODA (2545 Pyralin) was supplied by DuPont. The soluble polyimide XU-218, derived from 3,3′,4,4′-benzophenone tetracarboxylic dianhydride (BTDA) and diamino-1,1,3-trimethyl-3-phenylindan isomers (DAPI) was purchased from Ciba-Geigy Corp. The acetylene termi-nated imide oligomer powder (Thermid MC-600) derived from BTDA, aminophenylacetylene, and 1,3-bis (2-aminophenoxy) benzene (APB) was obtained from National Starch and Chemical Company. Kapton Type H (PMDA-ODA) films were obtained from DuPont Co., Apical polyimide films were obtained from Allied Corp., and Upilex Type-S and Type-R polyimide films derived from 3,3′,4,4′-biphenyl tetracarboxylic dianhydride (BPDA) plus *p*-phenylenediamine (PDA) and ODA, respectively were obtained from ICI Americas Inc.

Synthesis of Polymers. Polyamic acid solutions were prepared by condensation of the aromatic anhydride and amine in N,N-dimethylacetamide (DMAc). Polyimide modified electrodes were made by casting or spin coating the precursor polyamic acid solution onto stainless steel or platinum substrates. Imidization was achieved by either heating the films to 400°C for 60 min or through a chemical dehydration process involving immersion in a 1:1 mixture of acetic anhydride and pyridine *(6)*. BTDA-DAPI films were made by casting from a DMAc solution and heating to 100°C.

Electrochemical and Spectroscopic Methods. Cyclic voltammetry (CV) was done using a con-ventional three-compartment cell with the anode and cathode compartments separated by a fine porosity fritted glass disk. All experiments were done under a nitrogen blanket at

1. REDUCE SURFACE

2. DEPOSIT SEED

3. METALLIZE

POLYIMIDE FILM

ELECTROLYTE SOLN

REDUCING AGENT

REDUCED SURFACE LAYER

SEEDING SOLUTION

Pd(II)

Pd METAL DEPOSIT

ELECTROLESS METAL
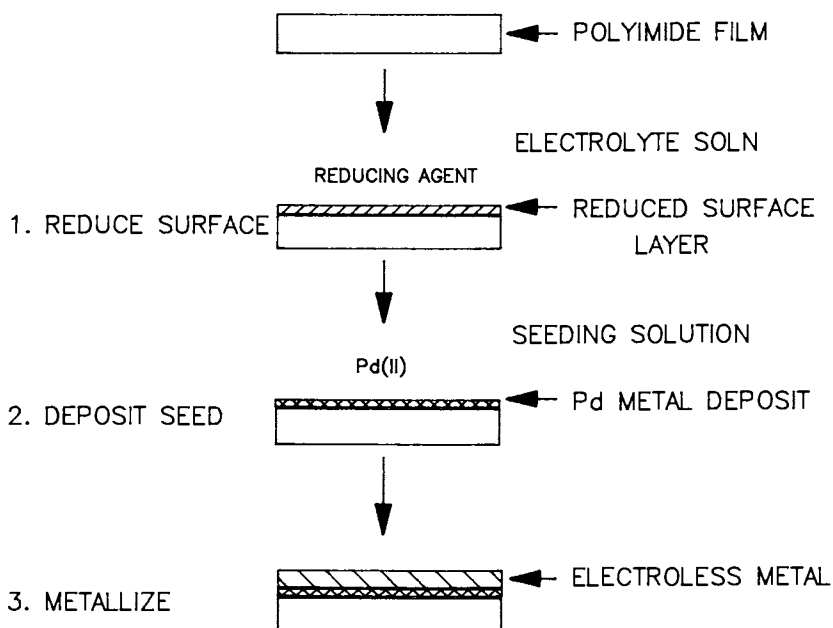
Scheme I. Process Steps for Redox-Mediated Metallization of Polyimides.

$23 \pm 2°C$, and referenced against the saturated calomel electrode (SCE). Solutions were made from anhydrous solvents and 0.1 M tetrabutylammonium tetrafluoroborate (TBAFB) as supporting electrolyte unless otherwise stated. Electroless plating solutions were prepared fresh prior to use. UV-Visible measurements were made using an HP 8452A (Hewlett-Packard) diode array spectrophotometer. Surface ATR-IR spectra were obtained on an IBM Instruments IR44 Fourier transform spectrometer using a KRS-5 (45°) crystal. Rutherford back-scattering was done using 2.3MeV, $10\mu C$ He$^+$ ions.

Results and Discussion

Electrochemical Reduction of Polyimides. Polyimides can undergo reversible reduction / oxidation reactions at an electrode surface in an electrolyte solution. The cyclic voltammetric response for a PMDA-ODA film on an electrode surface is shown in Figure 1(a) along with a CV for N,N'-di(n-butyl)pyromellitimide model compound in solution; Figure 1(b). The redox reactions of the imide functional group involves a one electron reduction to a radical-anion form (green colored) and a second reduction producing the dianion form (red-violet colored). The reduction of polyimide films occurs with electron injection into the polymer at the electrode interface with simultaneous uptake of counter-ions (cations) for charge balance. These cations are supplied by the electrolyte and enter the film at the polyimide/solution interface. The redox mechanism for PMDA-derived imides has been proposed previously *(5, 6)*.

A list of redox potentials for the first ($^1E^0$), second ($^2E^0$), and third ($^3E^0$) electron reduction couples for different polyimide films is provided in Table I. The potentials were measured by cyclic voltammetry of polyimide films on an electrode surface and represent the average of the cathodic and anodic peak potential for the respective redox couple.

Table I. Redox Potentials for Polyimide Films

Polyimide[a]	Potential vs. SCE		
	$^1E^0$	$^2E^0$	$^3E^0$
BPDA-ODA (PI2611)	-1.37	-1.58	---
HFPA-ODA (PI2566)	-1.35	-1.49	---
BTDA-DAPI (XU-218)	-1.04	-1.24	-1.74
BTDA-APB (Thermid 630)	-1.01	-1.29	-1.80
PMDA-ODA (PI2545)	-0.79	-1.33	---
PMDA-HDA [b]	-0.78	-1.60	---
PMDA-MCA [c]	-0.80	-1.44	---
NTDA-ODA	-0.64	-1.03	---

[a] CV's run in 0.1 M TBAFB/ACN, at 50 mV/sec.
[b] HDA = hexamethylenediamine
[c] MCA = methylene-bis-cyclohexylamine

The proposed reduction process for 1,4,5,8-naphthalene tetracarboxylic dianhydride (NTDA)-, PMDA-, and BPDA-polyimides involves two sequential one-electron transfers to generate the radical-anion and dianion states respectively. In the case of BPDA-polymers, the formation of a diradical-dianion on the second reduction might be more energetically favored over the
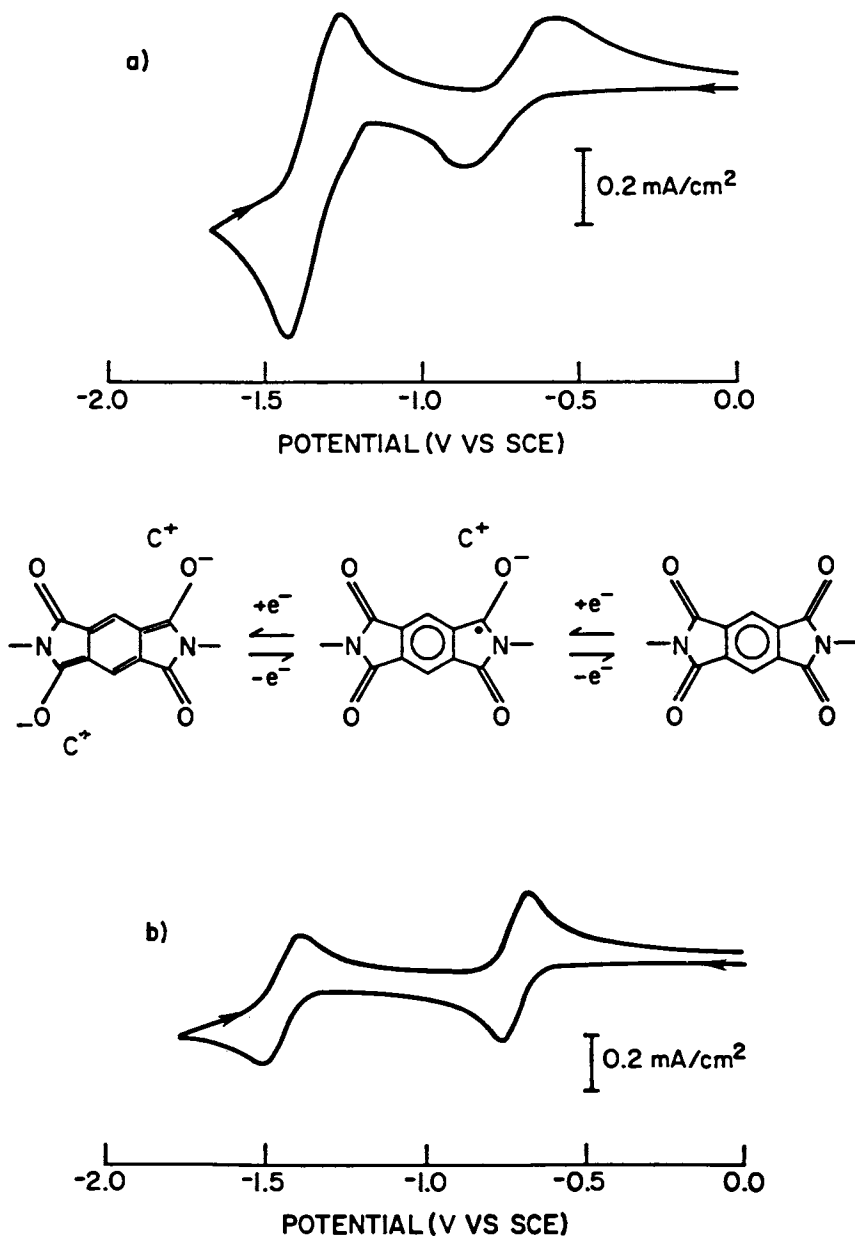
Figure 1. Cyclic voltammograms for a 12 μm thick PMDA-ODA film on an stainless steel electrode (a) and for 5 mM N,N′-di-(n-butyl)pyromellitimide model compound in 0.1 M TBAFB/ACN at a Pt electrode (b).

spin-paired dianion in order to increase charge separation on the imide. The third redox wave for BTDA-polymer films is attributed to the additional conjugation and the carbonyl group of the benzophenone structure which can be reduced. For 4,4'-(hexafluoroisopropylidene)-bis-phthalic anhydride (HFPA) system, it is likely that the second reduction leads to a diradical-dianion due to the break in conjugation by the sp^3 carbon of the hexafluoroisopropylidene group. Comparision of the redox potentials of HFPA-ODA to that for phthalimide compounds indicates that the trifluoromethyl groups have an electron withdrawing affect on the bis phthalimide groups. The effect of the imide structure on the redox potentials and spectral characterization of reduced PMDA-, BTDA-, BPDA-, and NTDA-polyimides has been reported previously *(8)*.

Chemical Surface Reduction of Polyimides. A appropriate reducing agent in solution can inject electrons into polyimide films provided that the oxidation potential for the reducing agent is negative of the reduction potential for the polyimide and provided that counter ions are available for charge balancing. Chemical reduction has been shown to occur in the presence of Zintl anions and vanadium complexes in aqueous and methanolic solutions *(5, 13)*. This work focuses mainly on the use of reducing agents which are electrochemically generated in nonaqueous electrolyte solutions. A list of redox potentials for different compounds used in various solvents is given in Table II.

Table II. Organic Reducing Agents for Polyimide Reduction

Reagent	Reaction	Solvent	E^0 (vs SCE)
Anthracene (An)	An + e- → An– •	ACN	-1.94
"		DMF	-1.88
Benzophenone (Bp)	Bp + e- → Bp– •	ACN	-1.75
"		DMF	-1.71
"		NMP	-1.68
9-Fluorenone (Fl)	Fl + e- → Fl– •	ACN	-1.28
"		DMF	-1.19
Benzil (Bz)	Bz + e- → Bz– •	ACN	-1.13
Benzoin	Benzoin + K-t-butoxide → Bz– •	ACN	-1.13
Tetrakis(dimethylamino)	TKDE+ • + e- = TKDE	MeOH	-0.76
ethylene	TKDE^{-2} + e- = TKDE+ •	MeOH	-0.64

radical-anion form represented as (– •)
radical-cation form represented as (+ •)

Cyclic voltammetry of these compounds shows that the first electron reduction (redox couple) is reversible in aprotic electrolyte solutions. A one-electron reduction of these compounds (except TKDE) results in the corresponding radical-anion form *(14)*. Under aprotic and O_2-free conditions the anion forms are sufficiently stable for use as reducing agents for the reduction of polyimide films. Reducing agents also can be generated chemically, as for example, reacting benzoin and potassium *t*-butoxide under alkaline conditions leads to the benzil radical-anion.

Tetrakis(dimethylamino)ethylene (TKDE) is a strong electron donor which oxidizes to radical-cation and dication states similar to the well-known Wurster's radicals. Cyclic

voltammetry of TKDE, $((CH_3)_2N)_2C=C((CH_3)_2N)_2$, in 0.1 M tetraethylammonium bromide in methanol exhibits reversible redox waves at -0.76 and -0.64 V vs SCE. This result is compatible with an earlier study which characterized the different oxidation states of TKDE using electrochemical and electron spin resonance techniques *(15)*. There is sufficient energy band overlap between TKDE and PMDA-ODA so that a solution of neutral TKDE can reduce Kapton films with the oxidized forms of TKDE acting as counter ions.

Spectroscopic Analysis of Chemically Reduced Polyimides. An example of a typical bath used for the reduction of Kapton films is comprised of 0.05 M benzil / 0.1 M TBAFB / ACN which is cathodically electrolyzed (using Pt gauze electrodes) to convert approximately 5 percent of of the benzil to the radical-anion form. The UV-visible spectrum shown in Figure 2 is for a 0.5 mil thick Kapton film after a 5 sec immersion in a benzil reducing solution prepared as described above. After exposure to the reducing bath, the film was rinsed in fresh ACN, prior to running the UV-visible scan. The visible absorbance peaks at 724 and 659 nm correspond to the green colored radical-anion state of PMDA-ODA. This result is in excellent agreement with previous analysis of electrochemically reduced PMDA-ODA films and PMDA-model compounds *(6, 8)*. Solutions containing benzophenone or anthracene radical-anion forms can reduce PMDA-ODA films to the dianion state (red-violet color) resulting in new absorbances at 555 and 525 nm. TKDE solutions can reduce Kapton films to the radical-anion form but do not reduce Upilex films because of the more negative reduction potential for the BPDA-group.

Reduction of Upilex-R polyimide films in a solution containing 0.05 M anthracene (15 percent radical-anion) / 0.1 M TBAFB / NMP results in a broad visible absorbance (blue colored films) with a maximum at about 625 nm as shown in Figure 3. Since the potential of the anthracene couple is quite negative, BPDA-polymers can accept two electrons per imide unit which may contribute to the broad absorbance response for the reduced films.

The rate of Kapton film reduction upon exposure to a reducing bath can be estimated by UV-Vis spectral analysis. The number of reduced imide sites is determined using the intensity of the 724 nm peak (molar extinction coefficient = 23,000) when generating the radical-anion form *(6, 7)*. The diimide (PMDA) unit concentration for Kapton is approximated at 3.2 M using a value of 1.42 g/cm^3 volume density, 382 gm/mole as the molecular weight, and taking into account a 15 % volume increase due to ACN swelling. Figure 4 shows a linear relation between the amount of film reduction and time of immersion in a 0.05 M benzil (5 percent radical-anion) / 0.1 M TBAFB / ACN solution. This result is based on a model which assumes uniform and complete conversion of the reduced surface layer to the radical-anion form with no diffuse solvent uptake. Thermally cured polyimide films reduce at a much slower rate than chemically cured films. This is attributed to slower solvent and electrolyte uptake by thermally cured films because of a more compact packing of the polymer chains during thermal curing.

Polyimide films can be reduced by appropriate organic reducing agents in solvents including N,N-dimethylformamide, N,N-dimethylacetamide, propylene carbonate, dimethylsulfoxide, methanol, and those described above. The reduced films are quite stable when maintained in a low oxygen environment such as in a nitrogen glove box. Reduced films which are thoroughly dried of solvent reoxidize quite slowly in air due to gradual uptake of moisture by the film under ambient conditions. It should be noted that under certain conditions the chemical reduction of polyimide films in aprotic solutions leads to dissolution of the reduced polyimide which will be discussed in a forthcoming paper (Viehbeck, A., et al., unpublished results).
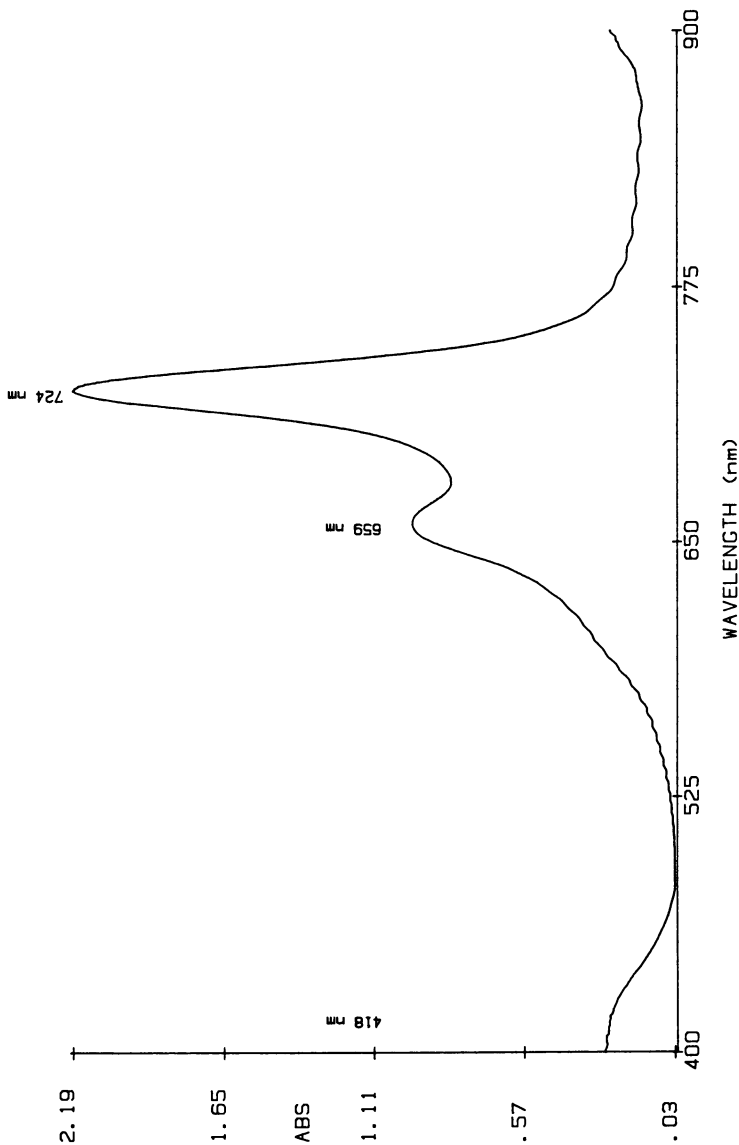
Figure 2. UV-Vis spectra for a 0.5 mil thick Kapton film after a 5 sec immersion in a solution containing 0.0475 M benzil/0.0025 M benzil radical-anion electrochemically generated in 0.1 M TBAFB/ACN solution.
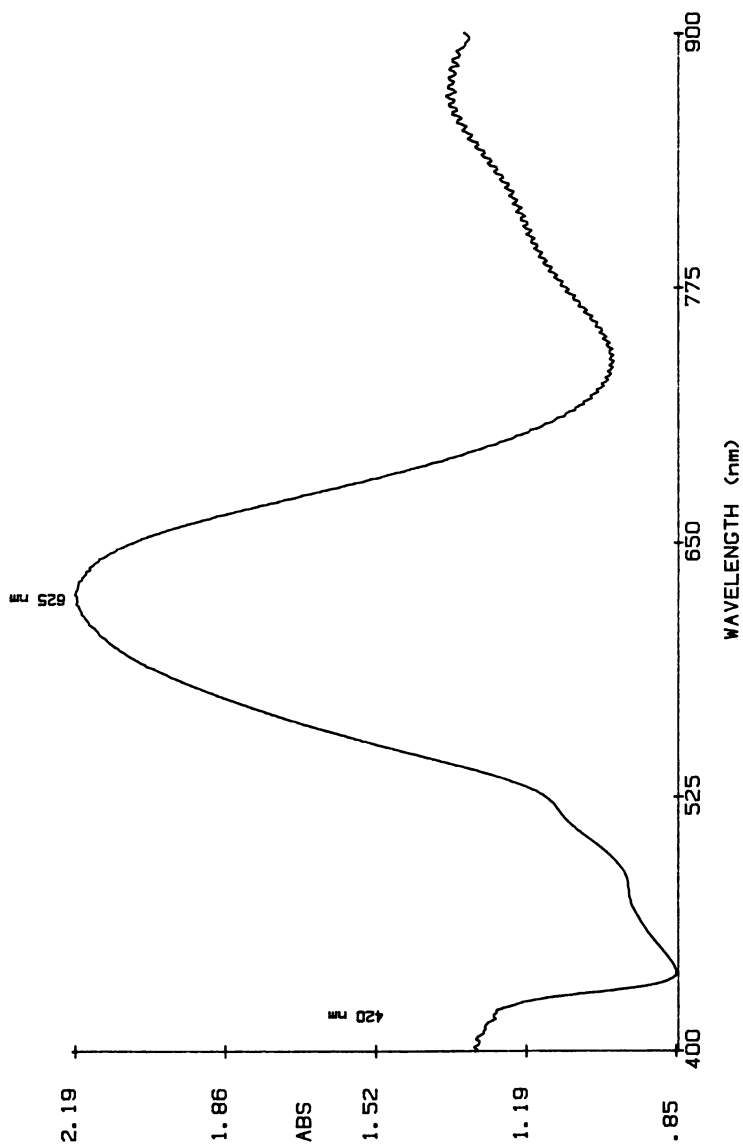
Figure 3. UV-Vis spectra for a 1 mil thick Upilex-R film after a 10 sec immersion in a solution containing 0.0425 M anthracene/0.0075 M anthracene radical-anion in 0.1 M TBAFB/NMP solution.
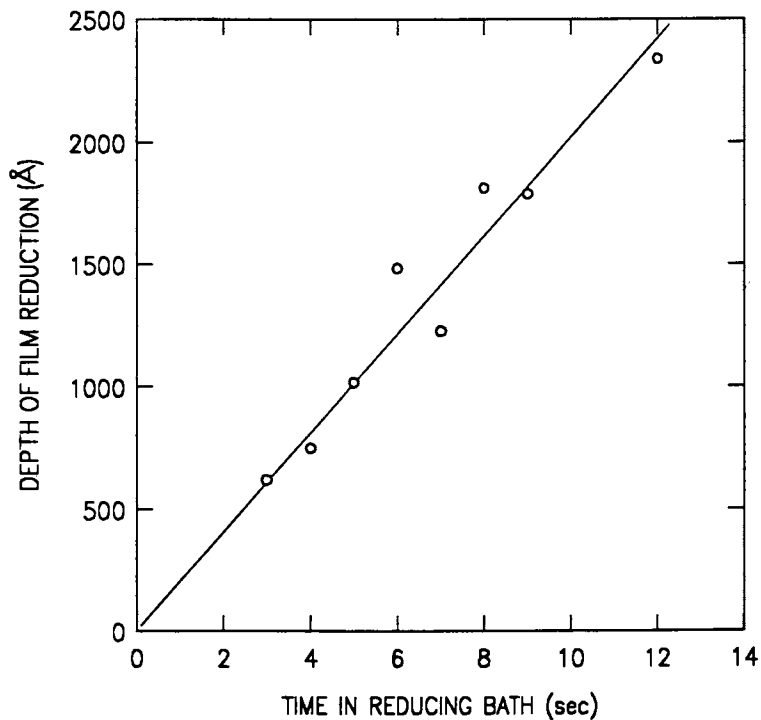
Figure 4. Estimated depth of Kapton film reduction to the radical-anion form versus exposure time in a 5 percent reduced 0.05 M benzil/ACN solution. Depth determined using value of 720 nm absorbance for PMDA-ODA radical-anion form.

Redox-Mediated Metal Deposition. A reduced polyimide surface can function as a reducing substrate for subsequent deposition of metal ions from solution. For metal reduction to occur at a polymer surface, the electron transfer reaction must be kinetically uninhibited and thermodynamically favored, i.e., the reduction potential of the dissolved metal complex must be more positive than the oxidation potential of the reduced film. Redox-mediated metal deposition results in oxidation of the polymer film back to the original neutral state. The reduction and oxidation peak potential values for different metal complexes and metal deposits in nonaqueous solvents as measured by cyclic voltammetry are listed in Table III.

Table III. Reduction and Oxidation Peak Potentials for
Catalytic Metals

Complex	Metal Valence Change	Reduction*	Oxidation*
$AgBF_4$	I→0	+ 0.22	+ 0.42
$CuIP(OCH_3)_4$	I→0	-0.44	-0.20
$PdCl_2$	II→0	-0.40, -0.75	+ 0.64
$PtBr_2$	II→0	-0.5	not meas.
$PdBr_2(NMP)$	II→0	-0.67, -1.13	+ 0.64
$NiBr_2$	II→0	-0.70, -0.80	+ 0.16

*Potentials in V vs SCE
CV's run in 0.1 M TBAFB/ACN, Pt electrode, at 50 mV/sec.

All of the solutions listed above give metal deposition onto reduced PMDA-, BTDA-, and BPDA-derived polyimides. During metal deposition, the characteristic visible absorbance of reduced films rapidly bleaches on exposure to an appropriate metal complex solution as the film reoxidizes.

Rutherford backscattering (RBS) is a powerful technique which can yield valuable information regarding elemental and depth analysis of thin metallic layers on a polymer surface. Palladium seeded Kapton films are prepared by immersing in a 0.05 M benzil (5 percent radical-anion) / 0.1 M TBAFB / ACN solution followed by rinsing with ACN and then immersing for 30 sec in a 50 mM $PdCl_2$ / DMF solution. Polyimide films reduced for 15 sec in the benzil bath and then exposed to the $PdCl_2$ solution give no visible evidence of the Pd deposit and no surface conductivity. The RBS profile for a seeded Kapton film shown in Figure 5 has a Pd signal at about 2 MeV and no detectable chloride peaks. The "tailing" of the lower energy signal of the Pd response suggests that the deposit penetrates up to 800Å into the film. The dotted curve represents the theoretical model used to calculate the depth scale as based on pure carbon, 2.62 gm/cm^2 *(16)*. The estimated area density of Pd atoms at the surface is 1.5 x 10^{16}/cm^2 which corresponds to a volume density of about 0.1 gm Pd/cm^3 (about 1 percent of bulk Pd metal density) indicative of a diffuse Pd deposit within the polyimide surface. Nickel, platinum, silver, and copper deposits can be formed in a manner similar to that described for Pd deposition.

Kapton films reduced for 15 seconds in the above benzil bath, followed by immersion in 0.05 M $PdCl_2$ / DMF solution have a 45± 10 percent charge transfer efficiency for Pd deposition based on the amount of radical-anion form available at the surface. Increasing the amount of film reduction (> 30 sec immersion in the reducing bath) results in increased metal deposition and a visibly darkened surface after exposure to the metal complex solution. Highly
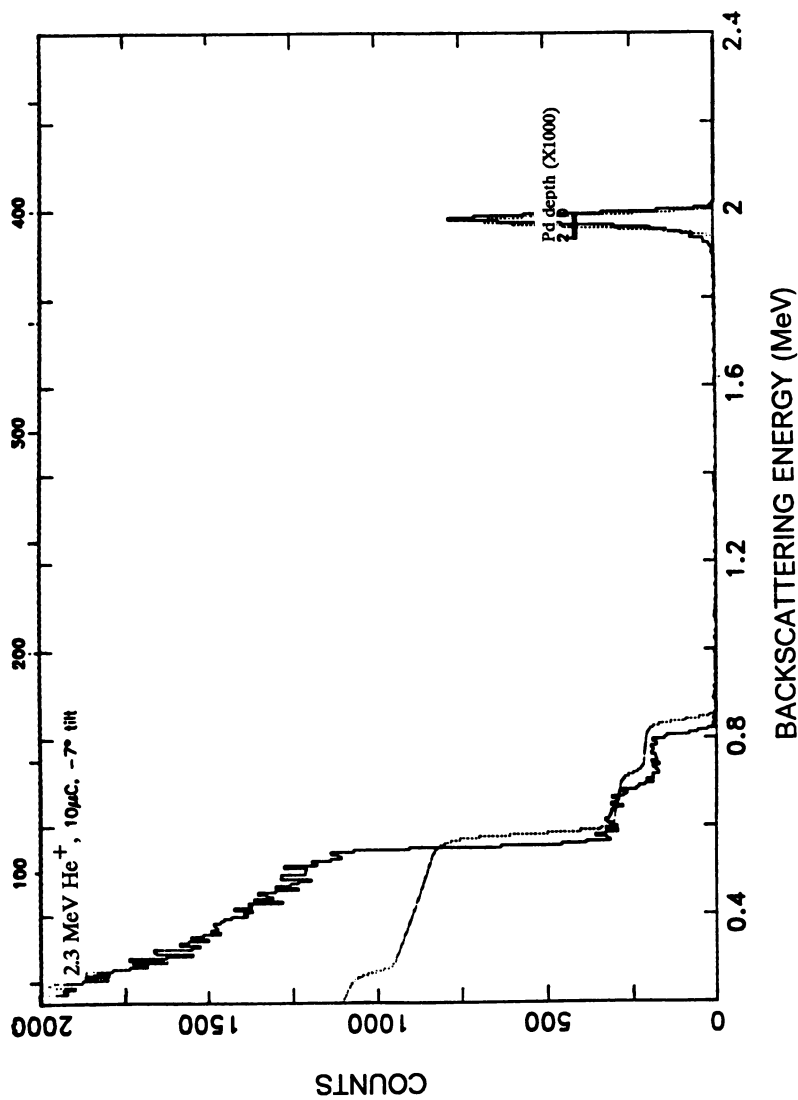
Figure 5. RBS profile for a Kapton film prepared by reducing for 15 sec in a 5 percent reduced benzil/ACN solution followed by a 30 sec immersion in a 0.05 M PdCl$_2$/DMF solution shows the presence of a Pd metal deposit at the polyimide surface.

reduced films (> 15 min immersion in the reducing bath) are able to deposit an electrically continuous metal layer onto the surface. Rutherford backscattering analysis shows that the metal deposition is limited by the amount of anionic charge available in the reduced polymer surface layer. Repeating the surface reduction and metal deposition steps also allows the build up of a continuous metal layer on the surface. It is interesting to note that for subsequent reduction/depositions the charge transfer efficiency for metal deposition is nearly 100 percent. This implies that initially deposited palladium metal might act as a catalyst or nucleation site for further Pd deposition which is kinetically favored over direct reduction of Pd ions by reduced polyimide sites. In the case of interlayer metal deposition, Mazur et al., described a scheme in which an initial homogeneous reaction between the polyimide and metal ion leads to metal reduction, followed by nucleation and heterogeneous metal growth *(12)*.

The depth at which metal is deposited is dependent on a number of parameters including the type of solvent, the degree of film reduction, and the concentration of the metal complex in solution. Increasing the $PdCl_2$ concentration results in Pd metal being deposited further into the polyimide film. Palladium metal has been detected as deep as 7000Å into Kapton films. However, for a given Pd metal complex concentration, the depth of the Pd metal deposit becomes limited due to equilibration of the diffusion fronts associated with reduced polymer sites moving toward the polymer/solution interface and metal ions moving from the solution to the polymer surface, across the polymer/solution interface, and through the polymer. The proposed redox-mediated mechanism for Pd deposition at a polyimide surface is illustrated in Scheme II which involves first, reduction of the polyimide surface to the radical-anion form followed by the reduction of Pd metal onto the film. The use of chemical reducing agents to mediate charge onto a polymer surface can be applied to other electroactive materials. For example, polyethylene terephthalate films (DuPont Mylar) have been successfully reduced and metallized in a manner similar as described for polyimides films.

Electroless Metallization. Polyimide films which are Pd seeded by the redox-mediated deposition process are active towards conventional electroless metal plating. Metal films are readily deposited onto surfaces having a diffuse Pd seed layer using standard electroless Cu (formaldehyde systems with tartrate or ethylenediaminetetraacetic acid chelating agents), electroless Ni (hypophosphite or dimethylamine borane systems), and electroless Pd (dimethylamine borane systems). Figure 6 shows the RBS response for a Pd-seeded Kapton film after a 30 sec immersion in an electroless Cu plating bath. The data is consistent with having both metals embedded in the polymer surface since the width of the Pd and Cu peaks are similar and there is no offset for the carbon signal to lower energy with respect to the theoretical model. These results clearly show that the electroless Cu is activated by the Pd metal seeds. Redox-mediated deposits of nickel or copper metal on polyimides are effective in initiating electroless Ni or Cu plating, respectively.

Typically, reflective and electrically continuous electroless metal deposits are formed in 1 to 3 minutes on Kapton surfaces having $> 1 \times 10^{16}$ Pd atoms/cm² seed concentration. Electroless metal layers adhere well to the surface and cannot be removed with adhesive tape. Electroless "strike" layers (500 to 3000Å thick) can be used as a plating base for electrolytic plating. For adhesion testing, the metallized films are patterned by subtractive metal etching ($FeCl_3$ solution) to define peel lines. Adhesion values of > 65 g/mm have been obtained for 1 mil thick plated Cu (having an electroless Cu strike) on Kapton films as measured by a 90° peel test. The scanning electron micrographs (SEM) shown in Figure 7, illustrate the rough morphology of the polyimide surface after peeling up the metal from the surface which is consistent with cohesive failure occurring within the polyimide sub-surface region. The highest metal adhesion is obtained when the Pd seed deposit penetrates only a few hundred angstroms

POLYIMIDE
FILM

SOLUTION

FILM
REDUCTION

$$C^\oplus \rightleftharpoons C^\oplus$$

$$PI^\ominus \qquad RA^\ominus \rightleftharpoons \begin{array}{l}\text{REDUCING}\\\text{AGENT}\end{array}$$

$$PI \qquad RA$$

$$C^\oplus = \begin{array}{l}COUNTER\\ION\end{array}$$

METAL
DEPOSITION

$$2\ C^\oplus$$

$$2\ PI^\ominus \qquad Pd^{\,0}$$

$$2\ PI \qquad Pd^{\oplus 2} \rightleftharpoons \text{SEED CATION}$$

RINSE

$$C^\oplus \rightleftharpoons C^\oplus$$

$$PI$$
$$Pd^{\,0}$$
$$PI$$
$$Pd^{\,0}$$
$$PI$$
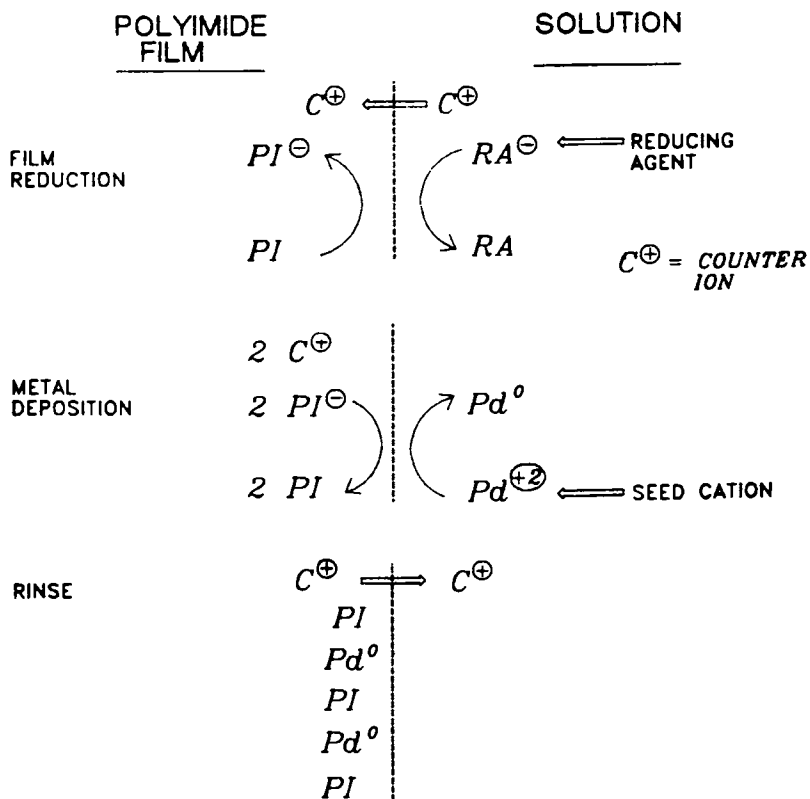
Scheme II. Proposed Charge Transfer Reactions for Redox-Mediated Pd
Metal Deposition on Polyimide.
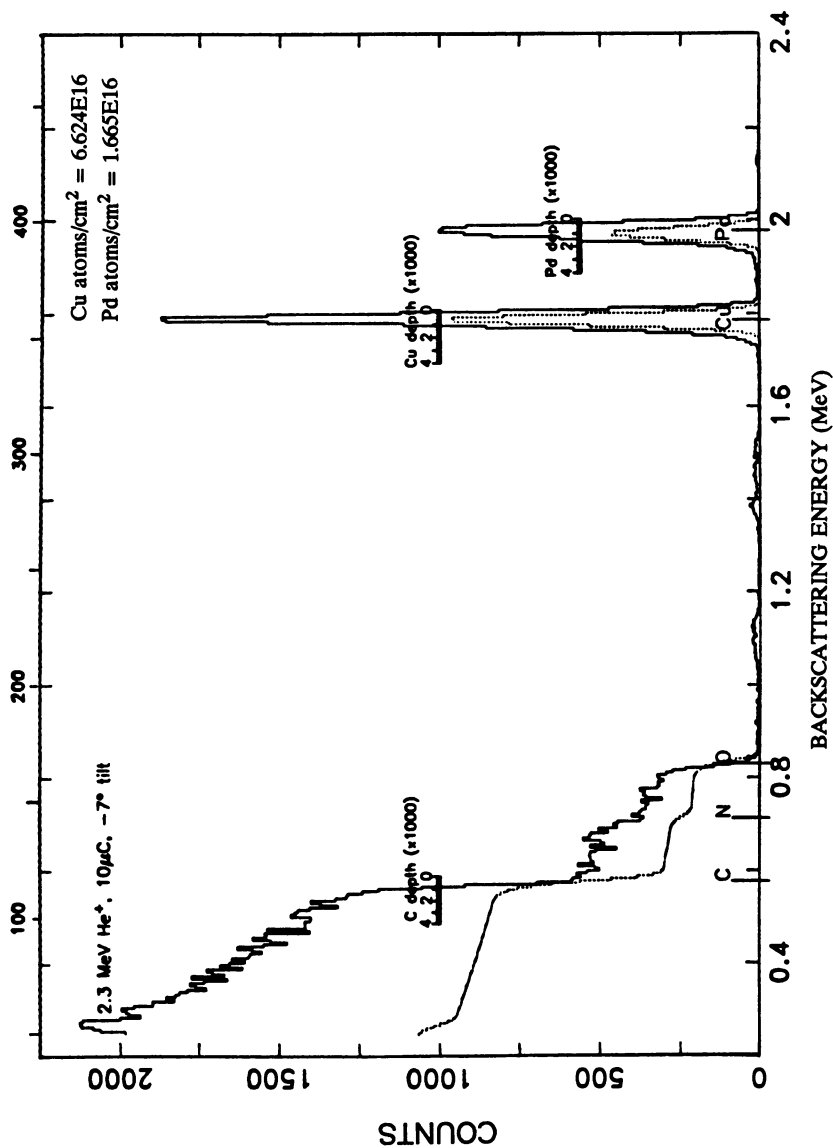
Figure 6. RBS profile of a Kapton surface after Pd seeding and brief exposure to an electroless Cu plating bath.

into the polyimide film. The proposed model for the polymer/metal interface depicted in Figure 8 shows metal seeds embedded within the polymer film and electroless metal built up through the surface. The adhesion afforded by such an interface structure is attributed primarily to a mechanical interlocking effect, since chemical interactions between the metal and polymer have not been detected.

Redox-mediated electroless seeding allows for simultaneous double-sided metallization of free standing film. The use of polar aprotic solvents during reduction and seeding eliminates the wetting problems often associated with aqueous systems for activating high-aspect ratio features. Figure 9 shows an SEM and photomicrograph of a redox Pd-seeded and Cu plated via in Kapton films. Uniform activation and copper plating is achieved on all exposed areas. Total additive or patterned metallization is realized by selective activation and electroless plating as outlined in Scheme III. This full-additive approach requires patterning the polyimide surface with a material such as a photoresist which is inert to the process solutions. In this way, the exposed areas undergo reduction, seeding, and subsequent electroless plating to generate a patterned metal deposit. The major advantages of such an approach is in eliminating a blanket plating base layer and subtractive metal etching. Figure 10 shows a patterned Cu deposit on a Kapton film formed by seeding only the exposed surface areas through a patterned resist layer. Electroless Cu then plates only on the Pd seeded regions which are seen as the light colored areas in the photograph. The uses and extendability of the redox metal deposition approach demonstrates the potential advantages of this process for fabricating catalytic surfaces and activating polyimides for electroless metallization.

Conclusions

A new method for direct metallization of electroactive polymer materials through an electroless redox-mediated deposition process has been described. This approach takes advantage of the inherent electroactive properties of polyimides in order to activate the surface with a catalytic metal seed layer. The amount of metal deposited is self-limited by the amount of polymer in the reduced form. In this way, a diffuse or continuous metal deposit can be formed on the polymer surface. The depth of metal penetration into the film is affected by the rate of ionic and electronic diffusion within the polymer and charge transport across the polymer/electrolyte interface. Most polyimides in a reduced form have an oxidation potential sufficiently negative to cause deposition of Pd, Ni, Cu, Pt, and Ag from solution. Through use of a reducing agent solution, the polyimide reduction and subsequent charge transfer reactions are confined to a very thin region near the surface of the polymer and thus, this process does not affect the bulk dielectric properties of the film. The redox-mediated deposition of catalytic metal seeds onto polymer films activates the surface towards conventional electroless plating. Advantages in the fabrication of electronic packaging devices can be realized through the use of chemical immersion techniques and plating technology.
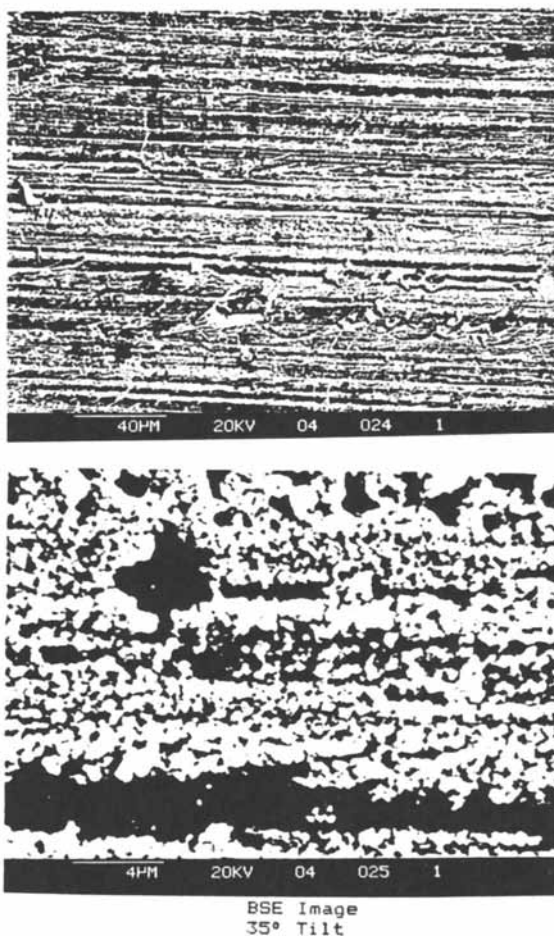
Figure 7. Scanning electron micrographs showing rough morphology remaining on a polyimide surface after the plated metal layer is peeled off. Lower photo is a higher magnification of the area shown in upper photo.
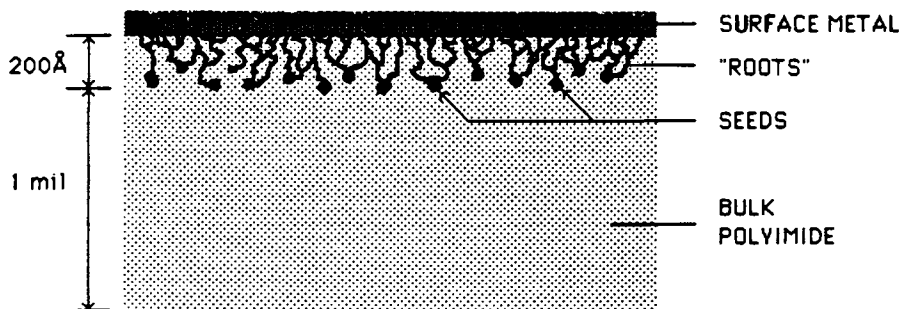
Figure 8. Proposed model for redox seeded and electroless metallized polymer/metal interface.
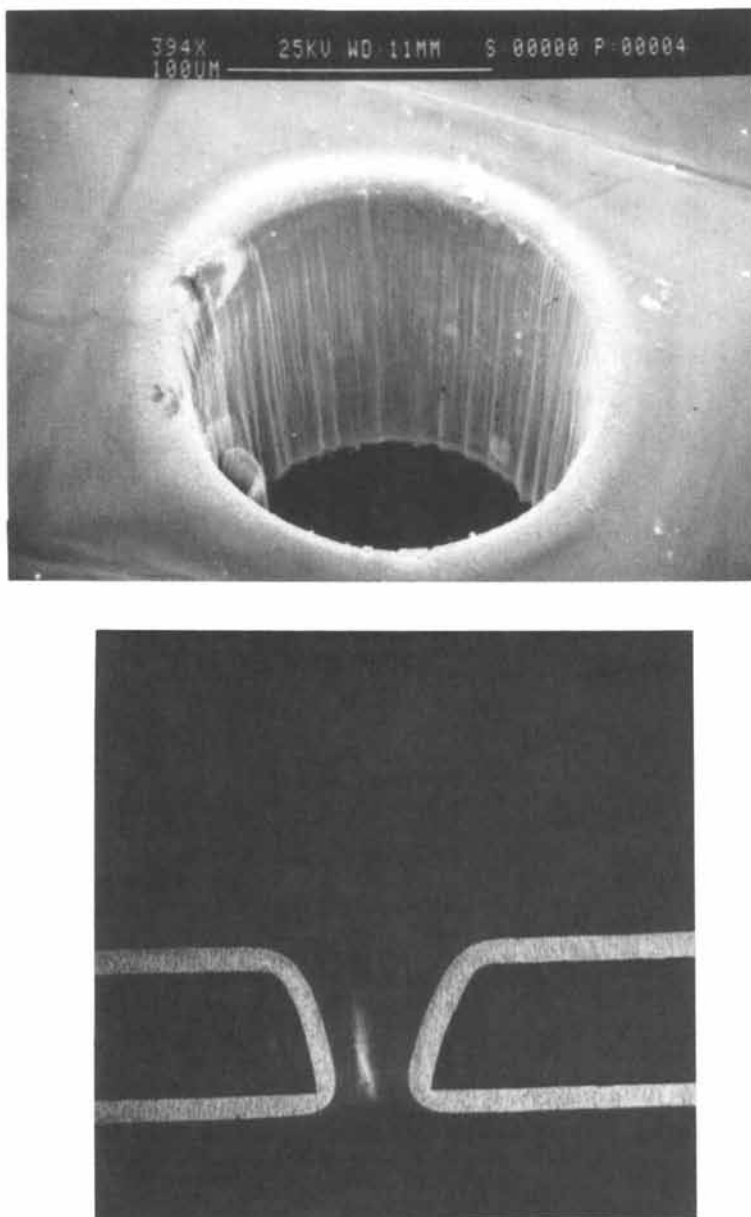
Figure 9. Scanning electron micrograph of a Pd seeded and electroless Cu plated 5 mil diameter via in Kapton film (Top). Lower photo shows the cross section of plated via in 3 mil thick Kapton film. Metallization was done by Pd seeding and electroless Cu plating, followed by electrolytic Cu plating to a thickness of 16 μm (Bottom).

POLYIMIDE FILM

1. PATTERN RESIST   RESIST LAYER

REDUCING AGENT

2. REDUCE SURFACE   REDUCED SURFACE

Pd(II)

3. DEPOSIT SEED   Pd METAL DEPOSIT

ELECTROLESS METAL
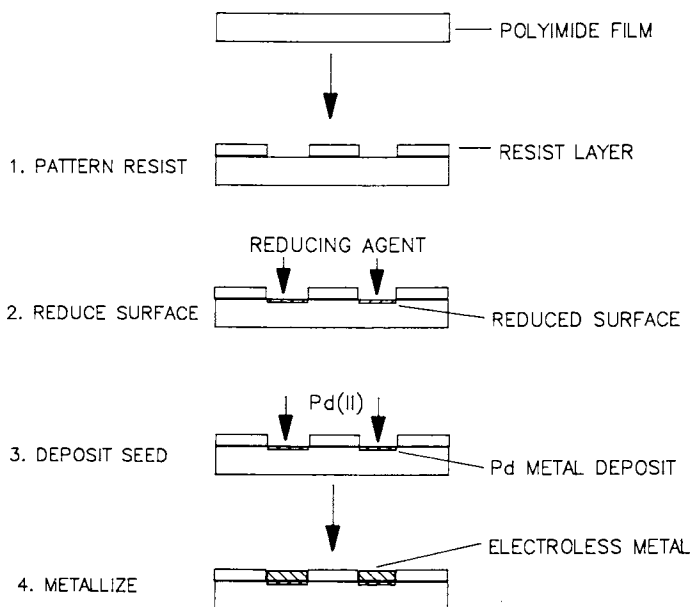
4. METALLIZE

Scheme III. Full-Additive Seeding and Electroless Metallization Approach.
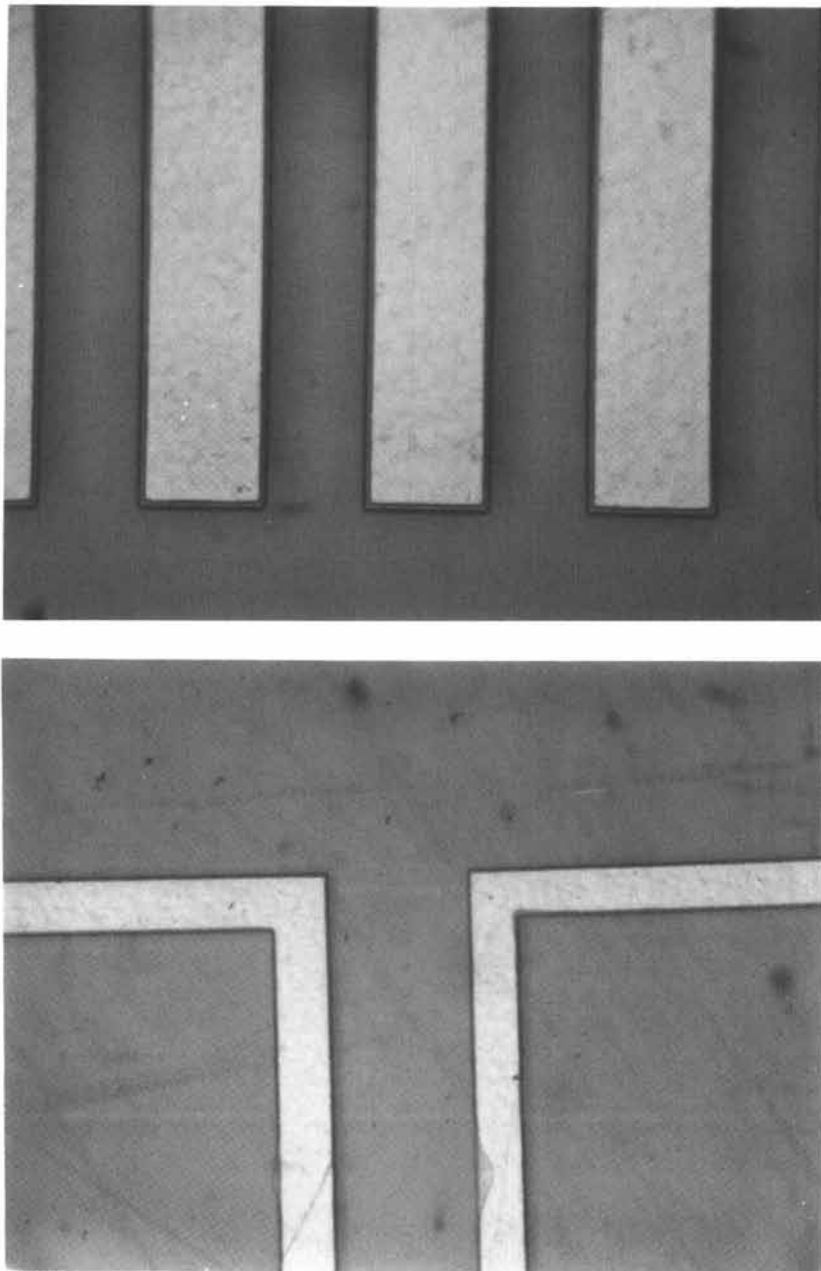
Figure 10. Photographs showing complete additive electroless Cu plated metal lines (light colored areas) on selectively seeded areas on a Kapton film patterned with a photoresist layer to define the circuit regions. Plated line width is 4 mils.

Literature Cited

1. *Polyimides, Synthesis, Characterization, and Applications;* Mittal, K. L., Ed.; Plenum Press: New York, 1984.
2. *Polymer Materials for Electronic Applications;* ACS Symposium Series No. 184; American Chemical Society: Washington, DC, 1982.
3. Kovac, C. A.; Jordan-Sweet, J. L.; Goldberg, M. J.; Clabes, J. G.; Viehbeck, A.; Pollak, R. A.; *IBM J. Res. Develop.* 1988, **32** 603.
4. Seraphim, D. P. *IBM J. Res. Develop.* 1982, **26**, 37.
5. Haushalter, R. C.; Krause, L. J. *Thin Solid Films* 1983, **102**, 161.
6. Mazur, S.; Lugg, P. S.; Yarnitzky, C. *J. Electrochem. Soc.* 1987, **134**, 346.
7. Krause, L. J.; Bales, J. L. *J. Electrochem. Soc.* 1988, **135**, 1137.
8. Viehbeck, A.; Goldberg, M. J.; Kovac, C. A. *J. Electrochem. Soc.* 1990, **137**, No. 4.
9. Bruce, J. A.; Murahashi, T.; Wrighton, M. S. *J. Phys. Chem.* 1982, **86**, 1552.
10. Pickup, P. G.; Kuo, K. M.; Murray, R. J. *J. Electrochem. Soc.* 1983 **130**, 2205.
11. Tourillon, G.; Garnier, F. *J. Phys. Chem.* 1984, **88**, 5281.
12. Mazur, S.; Reich, S. *J. Phys. Chem.* 1986, **90**, 1365.
13. Krause, L. J.; Lugg, P. S.; Speckhard, T. A. *J. Electrochem. Soc.* 1989, **136**, 1379.
14. Mann, C. K.; Barnes, K. K. *Electrochemical Reactions in Nonaqueous Systems;* Bard, A. J., Ed.; Marcel Dekker: New York, 1970.
15. Kuwata, K.; Geske, D. H. *Amer. Chem. Soc.* 1964, **86**, 2101.
16. Saunders, P.; Ziegler, J. F. *Nuc. Inst. and Meth. in Phys. Res..* 1983, **218**, 67.

Chapter 30

Adhesion of Metals to Thin-Film Fluorocarbon Polymers

Chin-An Chang, Yong-Kil Kim, and A. G. Schrott

T. J. Watson Research Center, IBM Corporation, Box 218, Yorktown Heights, NY 10598

Adhesion of metal films to several fluorocarbon polymer films is studied for Cu, Cr, Ti, Al, and Au. The polymers include polytetrafluoroethylene (PTFE), fluorinated ethylene propylene copolymer (FEP), and fluorinated ethylene perfluoroalkyl vinyl ether copolymer (PFA), all deposited on Cr/SiO_2 substrates by spin coating. Peel strengths of the metal strips on these polymers are compared, and are taken as measures of the metal-polymer adhesion. Among the polymers, FEP gives the highest peel strengths to metals, with PTFE the least. Among the metals, Ti gives the highest peel strength for each polymer, followed by Cr, with Cu being the lowest. The peel strengths for Ti on FEP, PFA, and PTFE are 85, 75, and 20 g/mm, respectively. Those for Cu to the polymers are around 5 g/mm or less. The results are correlated with the differences among the polymers and metals, and the mechanisms involved are suggested.

Metal-polymer adhesion has been of interest in recent years for the electronic packaging technology. A wide range of studies has been devoted to the understanding of interactions between metals and polymers, mostly on polyimide (1-3).

In this paper, we report the studies on the adhesion between metals and fluorocarbon polymer films. Fluorocarbon polymer has a dielectric constant of 2.1, lower than that of polyimide, 3.2-3.5, and is attractive to packaging. We have studied the adhesion of Cu to bulk Teflon, a polytetrafluoroethylene (PTFE) polymer, and found enhanced adhesion using a presputtering treatment of the Teflon prior to the deposition of Cu (4). Further analysis shows that the morphological changes of the Teflon due to the sputtering treatment could be a major contributor to the enhanced adhesion observed (5).

EXPERIMENTALS AND RESULTS

Three fluorocarbon polymers are compared here, including polytetra-
fluoroethylene (PTFE), fluoroethylenepropylene (FEP), and a copolymer
containing a perfluoroalkoxy group (PFA). Both PTFE and FEP contain
only fluorine and carbon atoms, the only difference being the pre-
sence of isopropylene for FEP. PFA contains, in addition, an oxygen
atom for each of the isopropylene unit, connecting an alkyl group to
the polymer backbone. The polymer films were made by a spin-coating
technique using polymer dispersions. Upon spinning the polymer dis-
persion on the $Cr/SiO_2/Si$ substrates, the samples were dried and
cured at different temperatures to remove the solvents, and to sin-
ter the polymer particles. The final curing temperature is 370-390°
C. Multiple coatings were made, with a final thickness around 10 um
for the polymer films. Afterwards, different metal layers of 2000A
were deposited by electron beam evaporation, followed by thick Cu
strips of 10 um with a defined geometry. Several metals were com-
pared, including Cu, Cr, Ti, Au, and Al. A 90° peel tester was used
to peel the Cu strips, and the peel strength is taken as a measure of
adhesion between the metal and the polymer. Bonding between the
metal and polymer is studied using x-ray photoelectron spectroscopy
(XPS).

Figure 1 shows the peel strengths for the different metal/poly-
mer systems. Ti gives the highest peel strength for each polymer,
followed by Cr, with Cu and Au being the lowest. For the polymers,
FEP and PFA show much higher peel strengths than those of PTFE. XPS
analysis of the metal-polymer bonding is shown in Figs. 2-4. Weak
interactions are seen between Cu and the polymers. Cr and Ti, on
the other hand, show strong interactions, as manifested by the car-
bide-like peaks shown.

DISCUSSION

We have compared the peel strengths of different metals deposited on
several fluorocarbon polymer films. Strong peel strengths exceeding
80 g/mm have been obtained for the Ti/FEP system. The difference
among the polymers is probably related to the structural differences.
Both FEP and PFA have branched structures, with some carbon atoms
being surrounded by three carbon neighbors. PTFE, on the other hand,
is linear, with all the carbon atoms, except the end ones, surrounded
by two carbon neighbors. Such a difference is consistent with the
much lower peel strength using PTFE than those of both FEP and PFA.
It is also in agreement with the observation of strong carbide-like
XPS peaks observed for FEP and PFA, but not for PTFE. The mechanism
involved, however, can be complicated. One possible mechanism is
suggested below.

For the carbon atoms with different neighbors, the consideration
of electronegativity provides a guideline of the reactivity of these
carbon atoms toward the metals. Fluorine is more electronegative
than carbon; the electronegativities are 4.0 and 2.5 for fluorine
and carbon, respectively (8). Carbon atoms with more fluorine nei-
ghbors are expected to be more electronegative than those with less
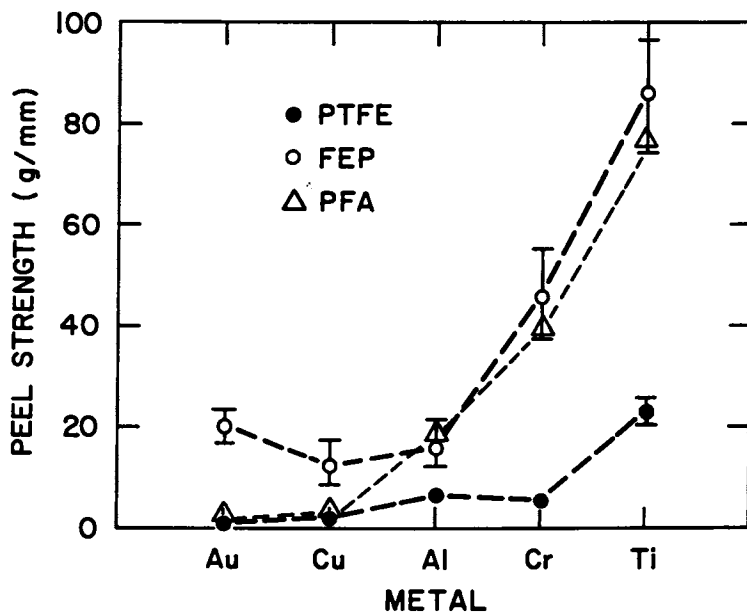
Figure 1. Peel strengths of different metals adhered to PTFE, FEP, and PFA fluorocarbon polymer films. (Reprinted with permission from Chang, C.-A. et al. *J. Vac. Sci.* 1990, *8*(4), 3306. Copyright 1990 American Institute of Physics.)
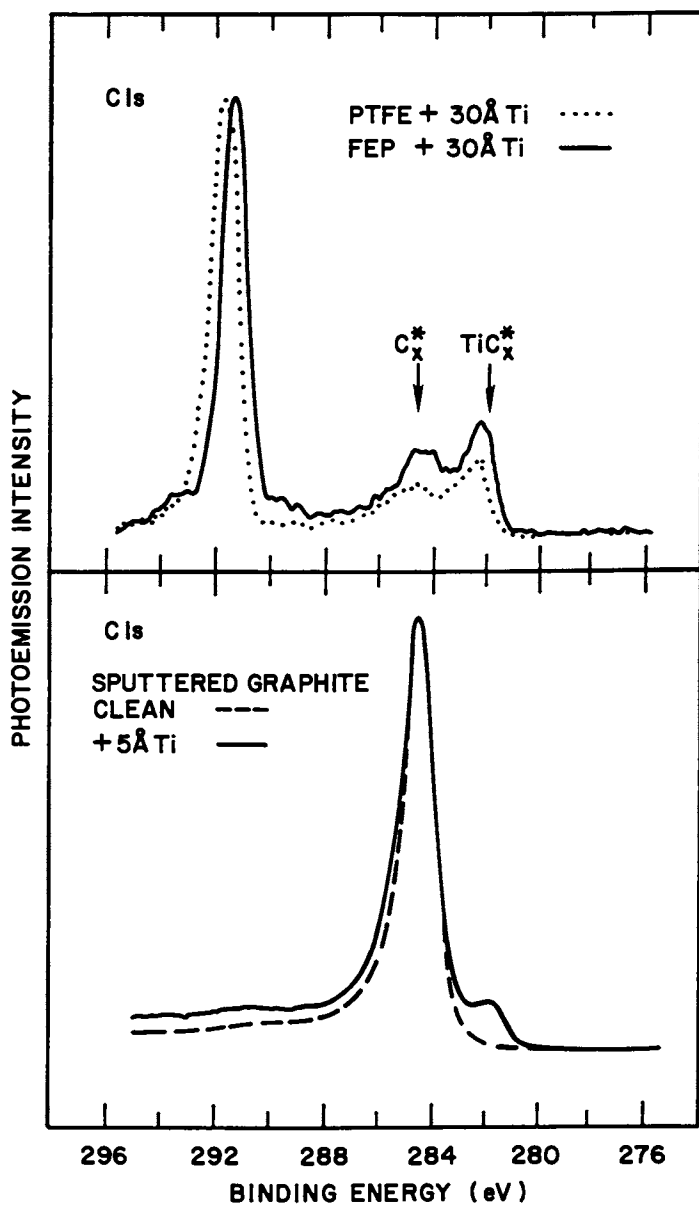
Figure 2. Upper: XPS spectra of Ti deposited on PTFE and FEP, showing carbide-like bondings. Lower: XPS spectra of TI deposited on graphite. The carbon and carbide-like peaks of the lower spectra help the assignment of peaks in the metal–polymer spectra. (Reprinted with permission from Chang, C.-A. et al. *J. Vac. Sci.* 1990, *8*(4), 3306. Copyright 1990 American Institute of Physics.)
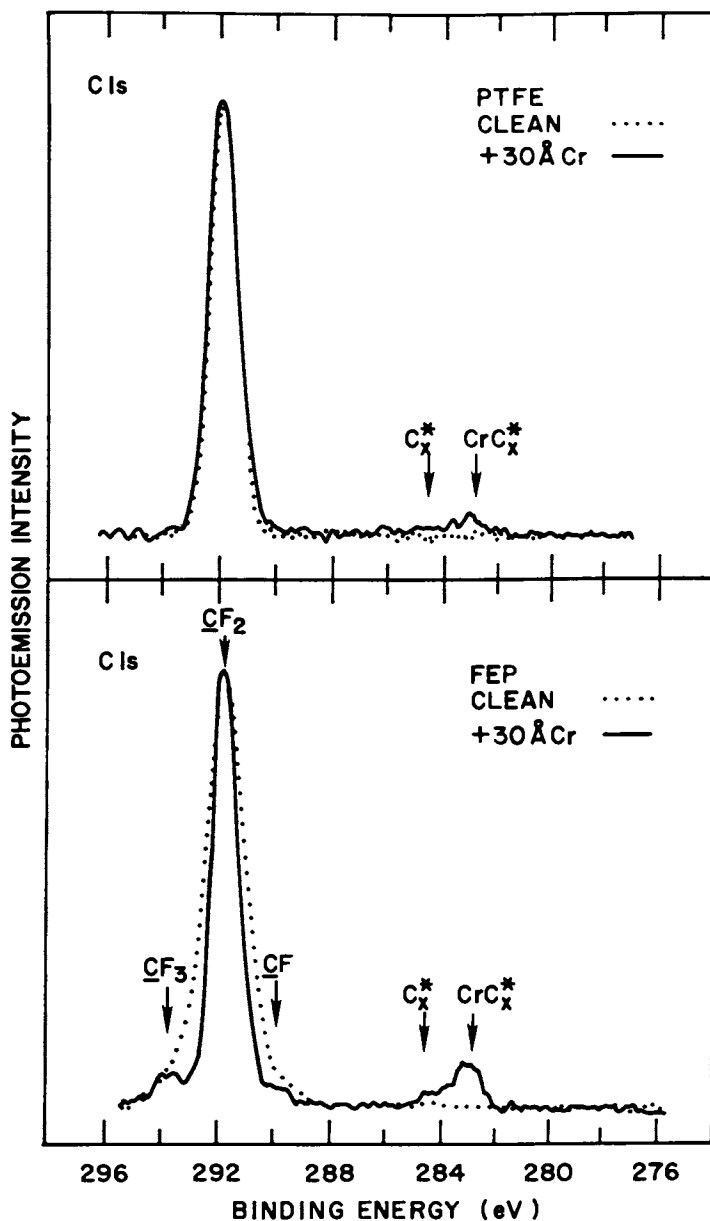
Figure 3. Upper: XPS spectra of Cr deposited on PTFE Lower: XPS spectra of Cr deposited on FEP. A strong carbide-like bonding is seen for FEP, but a very weak one for PTFE. (Reprinted with permission from Chang, C.-A. et al. *J. Vac. Sci.* 1990, *8*(4), 3306. Copyright 1990 American Institute of Physics.)
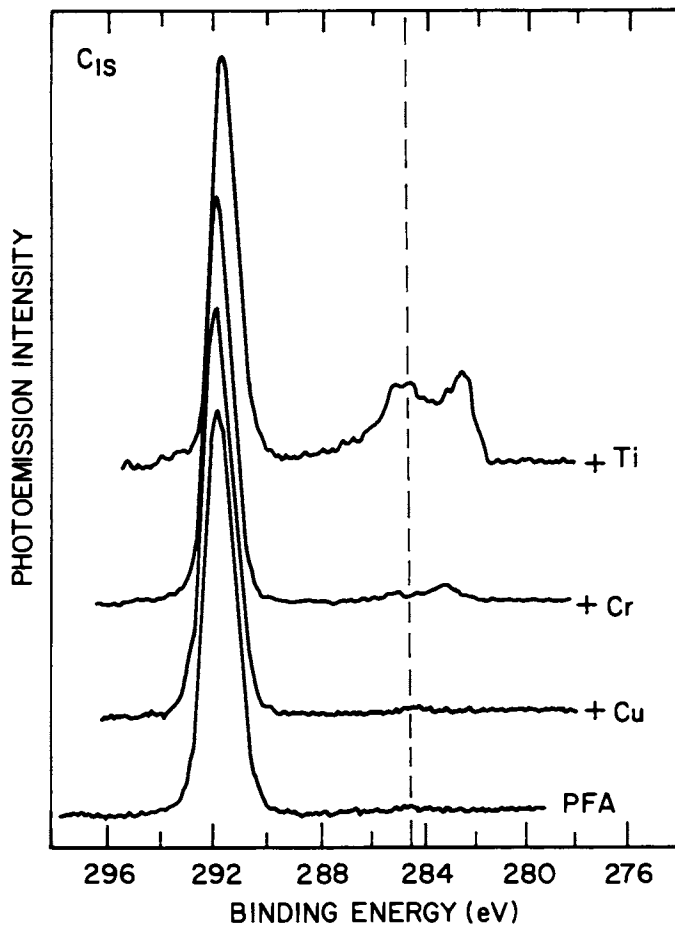
Figure 4. XPS spectra of Cu, Cr, and Ti deposited on PFA. Little reaction is seen with Cu, but strong reactions are shown with Cr and Ti, with the respective carbide-like peaks detected. The peaks around 284.5 eV are due to the surface carbon. (Reprinted with permission from Chang, C.-A. et al. *J. Vac. Sci.* 1990, *8*(4), 3307. Copyright 1990 American Institute of Physics.)

fluorine neighbors. Assuming equalized electronegativities between
carbon and fluorine for each C-F bond (9), the electronegativity of
the carbon atoms are 3.5, 3.4, 3.17, 2.8, and 2.5 for those with
four, three, two, one, and no fluorine neighbors, respectively. The
remaining neighbors are carbon. This is a first order approximation.
It shows that carbon atoms with a CF_3 configuration are more reactive
toward metals, which are less electronegative than carbon, than those
with a CF_2 configuration. This could be responsible for the higher
peel strengths observed for FEP and PFA than those for PTFE. It is
also consistent with the strong bonding from the XPS analysis for
the metals on FEP and PFA. We tentatively assign the carbide-like
peaks to the bonding involving the carbon atoms with the CF_3 configu-
ration. Detailed bonding configuration between the metal and the
polymer is not known at this moment, however.

The same consideration of electronegativity also gives some correla-
tion with the differences among the metals. The electronegativities
are 1.5, 1.5, 1.6, 1.9, and 2.4 for Ti, Al, Cr, Cu, and Au, respec-
tively (8). The peel strengths are the highest for Ti, followed by
Cr, and the lowest for Cu and Au. The two exceptions are Al and
Au/PFA. More study is needed to fully understand the differences
among the metals studied here.

SUMMARY

In summary, several fluorocarbon polymer films are compared for their
adhesion to metals. A strong adhesion, as measured by the peel
strength, is obtained for Ti and Cr bonding to the polymers with a
high concentration of carbon atoms with three fluorine neighbors.
Some correlation is observed with the electronegativities among the
different carbon sites in the polymers, and among the metals studied.

ACKNOWLEDGMENT

REFERENCES

1. Chou, N. J. and Tang, C. H., J. Vac. Sci. Technol. A2, 751 (1984)
2. Ohuchi, F. S. and Frelich, S. C., J. Vac. Sci. Technol. A4, 1039,
(1986).
3. Jordan, J. L., Sanda, P. N., Morar, J. F, Kovac, C. A.,Himpsel,
F. J., and Pollak, R. A., J. Vac. Sci. Technol. A4, 1046 (1986).
4. Chang, Chin-An, Baglin, J. E. E., Schrott, A. G., and Lin, K. C.,
Appl. Phys. Lett. 51, 103 (1987).
5. Chang, Chin-An, Appl. Phys. Lett. 51, 1236 (1987).
6. Wheeler, D. R. and Pepper, S. V., J. Vac. Sci. Technol. 20, 442
(1982).
7. Michael, R. and Stulik, D., J. Vac. Sci. Technol. A4, 1861 (1986)
8. Pauling, L., The Nature of the Chemical Bond, 3rd ed., Cornell
Press (1960), p.93.
9. Sanderson, R. T., Chemical Bonds and Bond Energy, Academic Press,
New York, (1971), p.15.

Chapter 31

Polypropylene and Aluminum Adhesion
Improvement by N_2 Low-Pressure Plasma Treatment

**V. André[1], Y. De Puydt[2], F. Arefi[1], J. Amouroux[1], P. Bertrand[2],
and J. F. Silvain[3]**

[1]Laboratoire des Réacteurs Chimiques en Phase Plasma, ENSCP, 11 rue
Pierre et Marie Curie, 75231 Paris Cedex 05, France
[2]Université Catholique de Louvain, PCPM, 1 Place Croix du Sud,
B–1348 Louvain La Neuve, Belgium
[3]Laboratoire Maurice Letort, Centre National de la Recherche Scientifique,
Villers Les Nancy, France

With the help of complementary surface analysis techniques such as XPS, Static SIMS
and AES, we have been able to show how a short (23 ms<t<7000 ms) N_2 treatment of
the PP films leads to a slight oxidation of the surface as well as to the formation of N_2
containing species. These modifications are necessary for the improvement of the
adhesion observed with a scotch-tape test. However, the presence of oxygen is not the
only factor responsible for a good adhesion, since the AES profiles of the deposited
aluminium, show the same oxidized interface in the case of the non treated metallized
polymeric film. The films are pretreated in a corona discharge configuration (hollow
electrode-grounded cylinder) and the aluminium is deposited onto the film *in situ.*

Metallized polypropylene (PP) is used today in many different fields such as:
automotive, decoration, electrical. In order to obtain a good adhesion between the
aluminium and the polymer a pretreatment of the film prior to the metallization is
necessary. Indeed, the very extreme surface of the polymer has to be modified in order
to prepare it to a good adhesion with the metal. Thus the polymer is placed in a low
pressure plasma of nitrogen with a corona discharge configuration of electrodes, and
the metallization is carried out 'in situ' after the pretreatment in nitrogen. This process,
which simulates an industrial polymer film treatment has proven a great efficiency for
very short treatment times (23 ms) (1).However, the mechanisms responsible for the
improvement of adhesion are not totally explained yet.

The aim of this work is to give a better understanding of the role of the plasma
on the surface modifications of the polypropylene. Different surface analysis
techniques such as static SIMS and XPS have helped us to point out the chemical
modifications of the plasma treated polymer. Auger depth profiles through the metallic
coatings and their interfaces with the polypropylene have been performed in the case of
both treated and non treated polypropylene. At last, Transmission Electron Microscopy
(TEM) has been carried out and has allowed us to measure precisely the thickness of
the metallic coating as well as to identify its growth process.

Experimental

The pumping unit (a turbomolecular pump and a primary chemical one) of the plasma reactor, shown on Figure 1, allows a background pressure of about 6.10^{-4} Pa. The N_2 plasma treatment is performed with a working pressure varying between 50 and 1000 Pa. A corona discharge configuration (hollow electrode-grounded cylinder) is used .The discharge is established by means of an industrial 800 Watts excitation source , with a 70 kHz frequency. Depending on the experimental conditions (applied power, gas flow and nature, interelectrode distance), the width of the discharge varies from 5 to 10 mm on the cylinder. The electrical characteristics (V, I) of the discharge are measured by a digital oscilloscope (Lecroy 9400) which shows that with the usual treatment conditions (p= 150- 800 Pa, d= 7 mm), we have a glow discharge regime for the N_2 discharge (1kV, 100 mA). The analysis of the plasma itself is possible with the help of two optical fibers placed into the discharge (one close to the electrode, the other close to the cylinder) and linked to a Jobin-Yvon U.V spectrometer.

In situ metallization described on Figure 2, is carried out by thermal evaporation right after the plasma pretreatment in N_2 . By this way, any contact of the treated polymer with air is avoided prior to the aluminium deposition.

All surface analyses (XPS, static SIMS and Auger) are performed on samples exposed to air after the plasma treatment. The static SIMS spectra are obtained with Xe-4keV ions and a total ion dose lower than $2 * 10^{13}$ ions/cm^2. The static SIMS results are interpreted as proposed by Van Ooij (3): the C_2 (27 + 29 amu) cluster intensity is used as a reference for the other C_x clusters intensities. The oxidation following the plasma treatments is assessed by the increase of the 31/27 and 45/41 fragments intensity ratios. The occurence of nitrogen containing fragments, which takes place at even atomic mass units (4), is seen from the increase of the 30/27 and 42/41 fragments intensity ratios. The experimental conditions for the Auger analyses are summarized in Table I.

Table I. Experimental conditions for the Auger analyses

Sputtering gas : krypton, gas pressure 5.10^{-5} Torr (recycled gas)	
Ion beam energy : 3 keV	Ion current density : 3 µA/cm^2
Electron energy : 9 keV	Electron current density : 90 mA/cm^2
Analyzer (semi-dispersive) energy resolution : 1.5 eV	

Results and discussion

Analysis of the Non Metallized, Pretreated Polypropylene. In a previous paper (1), we have shown that for very short treatment times (23 ms) in N_2 or NH_3 plasma, the first observed effect of the plasma was an increase of the dispersive component (γ_d) of the polypropylene surface tension. Since almost no nitrogen nor oxygen were detected by XPS for treatment times shorter than 0.7 s, it was concluded that the plasma had first a physical effect rather than a chemical one, although the efficiency of the treatment on the Al-PP adhesion was high (as proven by the use of a scotch-tape test).

For longer treatment times (> 0.7 s) it has been shown (2) with the help of complementary surface techniques such as ISS (outermost layer sensitivity), Static SIMS (0.1-1 nm of information depth) and XPS (5 nm information depth), that the topmost surface layer is highly oxidized and that further chemical modifications occur beneath. The incorporation of both nitrogen and oxygen after a N_2 plasma treatment have been evidenced by XPS whereas ISS did not reveal any trace of nitrogen (2).
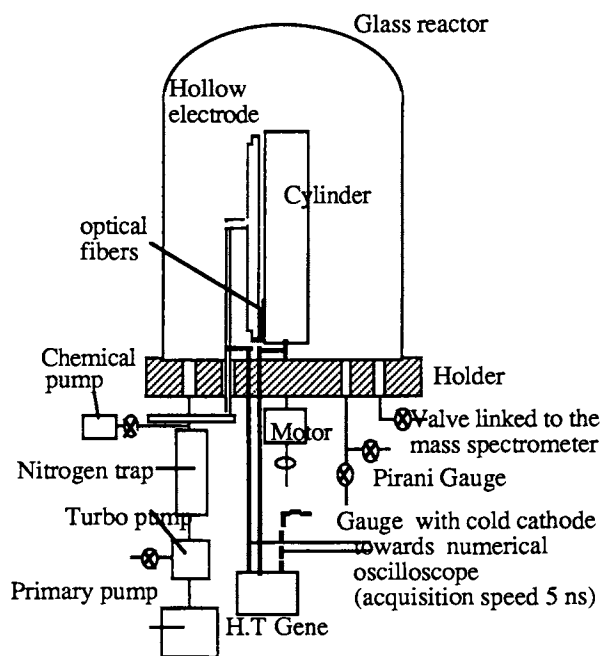
Figure 1. Apparatus used for the surface treatment

Figure 3 shows the evolution of the O_{1s}/C_{1s} and N_{1s}/C_{1s} ratios as a function of the plasma treatment time: a first increase followed by a saturation are observed for both oxygen and nitrogen after about 5 seconds. The oxidation could be induced by the oxygen present in the reactor (residual gas) or from ambient atmosphere after the treatment has been performed. Figure 4 and Figure 5 show the same features as evidenced by static SIMS: in this case, the saturation of the oxygen and nitrogen incorporation is observed for shorter times (about 1.5 s). This difference of saturation times between the XPS and SIMS observations is consistent with the difference of information depths between these two techniques. Moreover, the incorporation of oxygen and nitrogen seems to proceed simultaneously save the oxidation of the first layer (detected by ISS) . The latter mechanism is faster and may explain the slight increase of the polar component of the surface energy observed from treatment times as short as 0.23 s (5).

Previous static SIMS analyses have also shown (2) that the plasma treatment may induce fragmentation of the polymer backbone and some homogeneization of the polypropylene surface composition . Figure 6a shows static SIMS spectra obtained on a virgin polypropylene sample and Figure 6b on polypropylene which was treated in a N_2 plasma for 7 seconds.

From this last figure and from Figure 7, it is clearly seen that the relative intensity of the molecular fragments with masses greater than 100 amu, increases with the N_2 plasma treatment time. This observation may be related to the presence of low molecular weight species, which confirms the influence of the plasma treatment on the mass distribution at the surface of the treated polypropylene. From Figure 6b, it is also seen that the fragments at masses > 100 amu are essentially aromatic fragments occuring at masses 105, 115, 128, 141 ... This may be interpreted as a result of unsaturation (Typical aromatic fragments at 77 and 91 amu are also observed for the masses <100 amu). Unsaturation in the case of aliphatic polymers has also been reported from the decrease of the hydrogen content in the C_2 to C_5 clusters, seen on the SSIMS spectra as a shift of the intensity ratios towards the lower masses of these C_x clusters (3). In the present study this has not been observed because of the occurence, after the plasma treatment, of oxygen and nitrogen containing groups which induce a shift towards the higher masses in the C_x ($2<x<5$) clusters. In addition to these observations, the overall ion yield decreases with increasing plasma treatment times as seen on Figure 6: this may be caused by crosslinking induced by the N_2 plasma treatment. The SSIMS observations, unaccessible by XPS, can be helpful for the understanding of the adhesion improvement noticed on N_2 plasma treated polypropylene. All these combined mechanisms may indeed be responsible for the improvement of adhesion between the PP and the aluminium. For example, since the surface of the non treated substrate is almost free of oxygen (2), the interaction between the metal and the polymer will be too weak to lead to any adhesion. After the plasma treatment, the metallic particles can react with the modified PP surface, leading to an adhesion between the PP and the metallic layer. Since the presence of oxygen at the Al-PP interface seems to be an important factor in the adhesion, Auger depth profiles have been performed through the aluminium layers on both treated and non treated metallized PP.

Study of the Metallized Polypropylene. With the help of Auger spectrometry it has been possible to obtain the profile of the metallic coating. Figure 8 shows the profile of a virgin polypropylene and Figure 9, a N_2 pretreated one. From the TEM micrographs (picture 1), it is not possible to determine precisely either the thickness or the structure of the Al-PP interface. However, they give us a good measurement of the thickness of the metallic coating as well as the type of growth of the metal. With thicknesses above 25 nm it is possible to identify the beginning of a columnar growth, which is a very common mechanism for films deposited by thermal evaporation (6).
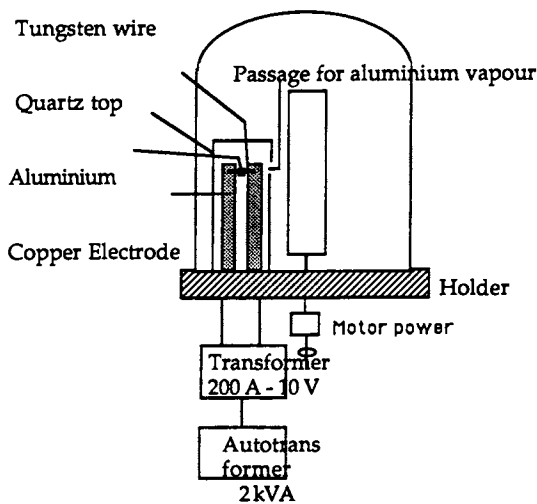
Figure 2.   Apparatus used for the metallization
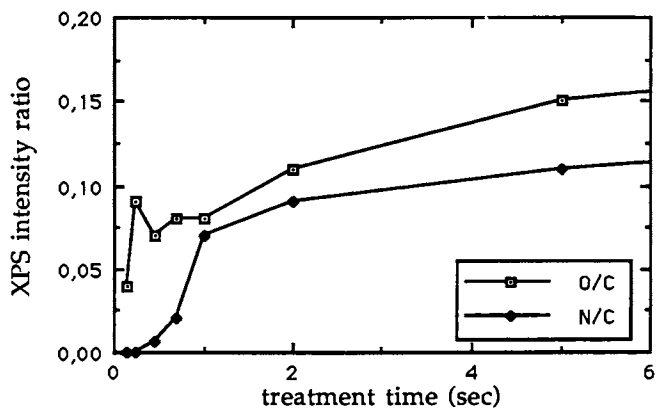
Figure 3.   O/C and N/C ratios as seen by XPS
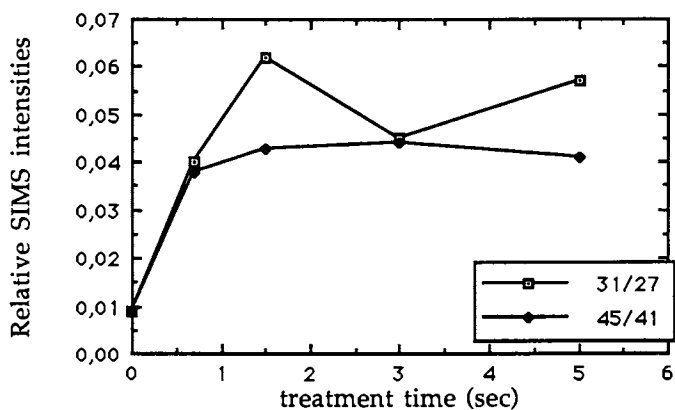
Figure 4. Oxygen incorporation as seen by Static SIMS
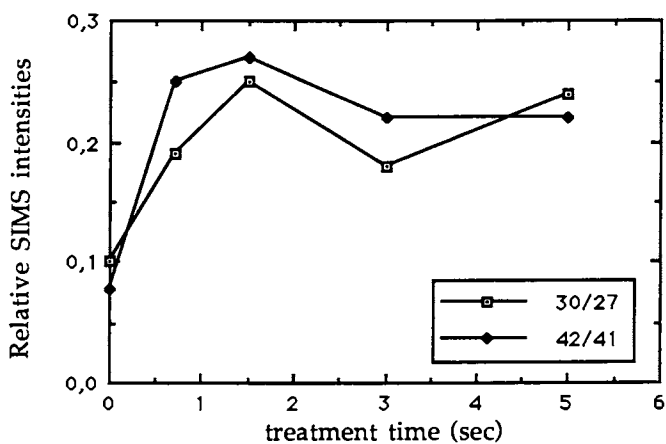
Figure 5. Nitrogen incorporation as seen by Static SIMS
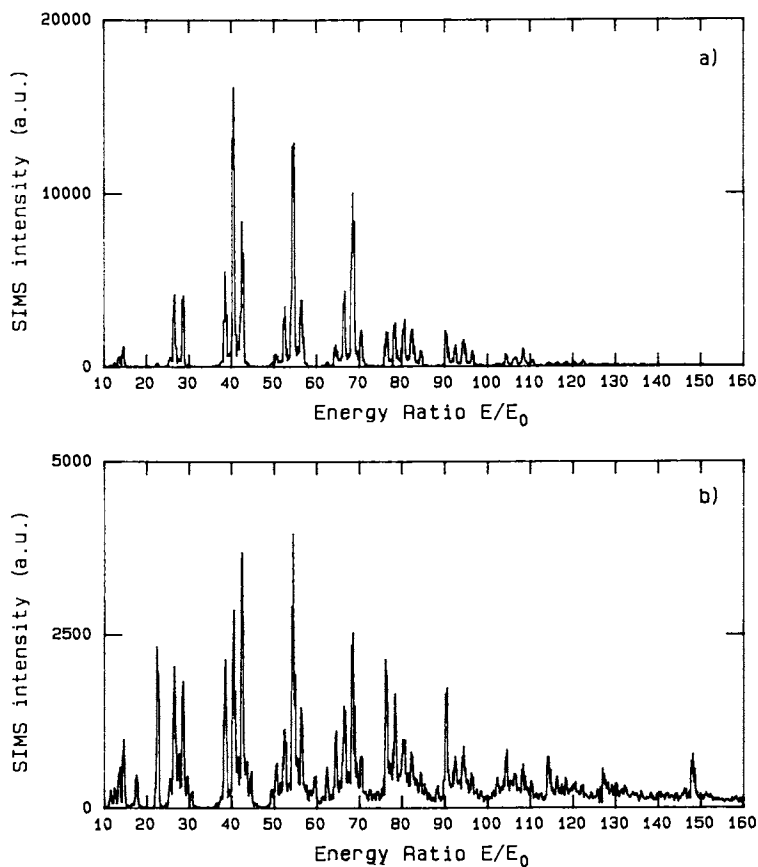
Figure 6.   a) SSIMS on a virgin polypropylene
            b) SSIMS on N_2 treated polypropylene (7 s)
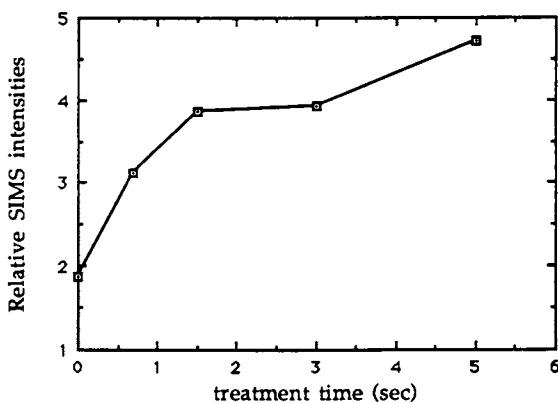
Figure 7.   High masses (>100 amu) clusters
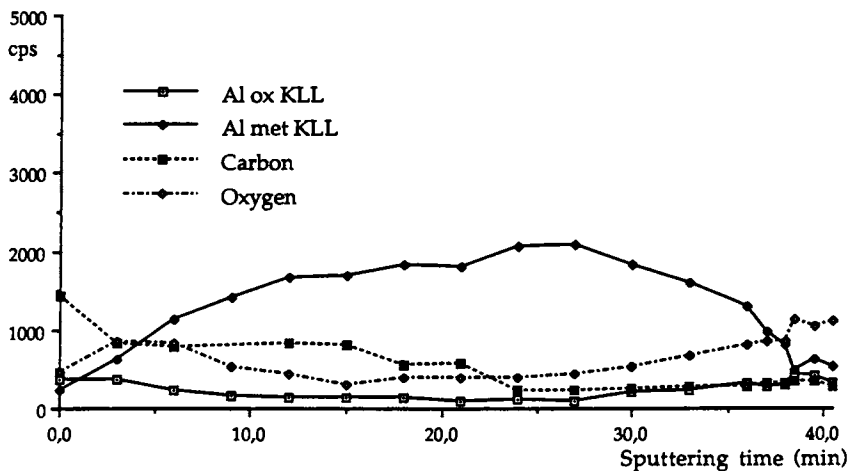
Figure 8.   Auger profile of an aluminium coating deposited on a
            non pretreated polypropylene film
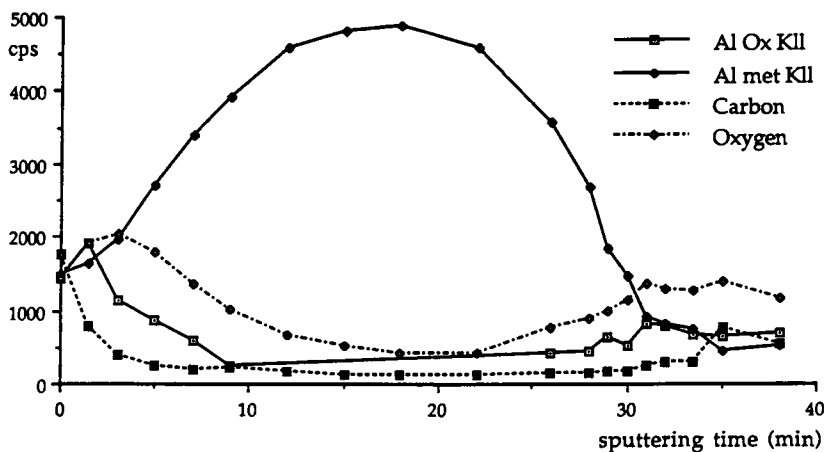
Figure 9.   Auger profile of an aluminium coating deposited on a
            N_2 pretreated polypropylene film

Since the aluminium coating is very thin (25 nm) and presents a rough surface, it is difficult to give any precise quantitative evaluation of the amount of oxygen at the interface (7). A fairly good determination can be obtained with the help of concentration profiles which require complementary calculations. This will be described elsewhere (8). However, it is possible to compare the profiles and the trends of the different elements. Figure 8 shows that the interface of the non pretreated metallized polypropylene also contains oxygen.The analyses have been carried out several times on different parts of the same sample and the profiles are all. similar. Carbon and oxygen were detected and have comparable profiles at the metal-polymer interface, both on the treated, as seen on Figure 9, and non pretreated samples. In all cases the oxygen signal increases as we get close to the polymeric substrate.

It has not been possible yet to determine the thickness of the Al-PP interface since many interferences modify the signals in the vicinity of the substrate. More experiments are being carried out in different experimental conditions in order to determine the influence of the technique itself on the observed phenomena (8).

However these results allow us to conclude that, although the oxygen is present in higher quantities on the PP after the plasma treatment, its mere presence (for example in the case of the non treated metallized polypropylene) is not enough to achieve a good interaction between the metal and the PP. It is likely that other mechanisms are responsible for the improvement of adhesion.In particular, the influence of morphology changes has been proposed by Chang et al (9). However, such changes have not been observed in our case where the treatment is not as strong as in the case of an argon beam of 500 eV (9).

Picture 1. Transmission Electron Microscopy picture of an alumi-
          -nium coating (25 nm thick) on a PP film

Conclusions

In this work, we have shown how a plasma treatment, which enables us to improve the Al-PP adhesion, leads to both chemical and physical modifications (the latter being observed for treatment time as short as 23 ms) at the polypropylene surface.

The treatment oxidizes the surface and leads to the formation of nitrogen containing species ; it also gives rise to fragmentation and unsaturation with possibly crosslinking. However the polymer is very midely destructed, especially in the range of treatment times we are using. Nevertheless, these slight modifications are indispensible to obtain adhesion between the PP and the aluminium. Since oxygen is also present at the interface between the aluminium and the non treated sample, it is possible to suggest that the nature of the bondings at the interface is different for the treated and non treated polymer. However, we have not succeeded to prove this by XPS analysis (2). In fact, it seems that the polymer has to display a particular sort of oxidation, of which the nature is not known yet, to perform the required Al-PP adhesion. These hypotheses could only be verified with the help of a quantitative test, such as, for example, a peel-test. The machine has been built but the experiments require adapted conditions which are not totally established yet. With the help of these results, we would be able to comprehend better the interactions and the respective participation of each phenomenon.

Acknowledgments

Literature cited

1. André, V ; Tchoubineh, F.; Arefi, F.; Montazer, P. ; Amouroux, J. In Proceedings of The First Plasma Surface Engineering (Garmisch-Partenkirchen.FRG, Sept.1988), Vol II, pp. 679-686
2. André, V; Arefi, F.; Amouroux, J.; De Puydt, Y.; Bertrand, P.; Lorang, G.; Delamar, M. Thin Solid Films. 1989, 181, 451-460
3. Van Ooij, W.J.; Brinkhuis, R.H.G. Surf. and Interf. Anal 1988, 11, 430-440
4. Budzikiewicz, M.; Djerassi, C.; Williams. D.H. In Mass Spectrometry of Organic Compounds, Ed.; Holden-Day : San Francisco, 1967
5. André, V; Arefi, F.; Amouroux, J.; De Puydt, Y.; Bertrand, P.; Lorang, G.; Goldman, M. In Proceedings of the ISPC 9, (IUPAC) Bari (Italy) 4-8 Sept. 1989 Vol. 3, p 1601
6. Bunshah, R.F. In Deposition Techniques for Films and Coatings; Noyes Publications 1982
7. Seah, M.P. Vacuum. 1984, 34, n 3-4, 463-478
8. André, V; Arefi, F.; Amouroux, J; Lorang, G. accepted for publication in Surface and Interface Analysis
9. Chin-An Chang, Appl. Phys.Lett. 1987, 51 (16), 1236-1238

Chapter 32

X-ray Photoelectron Spectroscopy of Modified Polymer Surfaces and Metal–Polymer Interfaces

Correlations with Adhesion

L. J. Gerenser

Research Laboratories, Eastman Kodak Company, Rochester, NY 14650

X-ray photoelectron spectroscopy (XPS) has been used to study the interfacial chemistry between evaporated Ag and polymer surfaces with and without plasma modification. The initial stages of metallization in the sub-atomic layer regime were monitored. For an oxygen-free polymer such as polyethylene (PE), which exhibits poor adhesion with evaporated Ag, the XPS results suggest no chemical interaction with the formation of very large Ag clusters. For an oxygen-containing polymer such as poly(ethylene terephthalate) (PET), where the adhesion of evaporated Ag is greater compared to PE, the XPS results suggest charge transfer between Ag and the carbonyl oxygen in PET. Plasma treatment with oxygen introduces specific reactive sites resulting in additional chemical bond formation between the evaporated Ag and the polymer surface. These results are consistent with the significant improvement in adhesion observed for plasma treatment with a reactive gas.

Surface modification of a polymer prior to metallization is widely used to improve adhesion. The most common surface modifications employed are electric discharge (corona and plasma) and, more recently, ion-beam treatments (1). Several mechanisms have been proposed for the improved adhesion after such surface modifications (2). These include mechanical interlocking, the elimination of weak boundary layers, electrostatic attractions, and chemical bonding. All of these can play a role in adhesion depending on the surface modification used, metal/polymer system, type of metal deposition, and the extent of polymer preparation employed. However, for low power, short exposure modifications, the formation of new chemical species which can provide nucleation and chemical bonding sites for subsequent overlayers is considered to be of prime importance (3-5).

Although considerable photoemission studies can be found in the literature for metallization on unmodified polymer surfaces, very few studies are reported on modified polymer surfaces. XPS has been used to investigate interactions between evaporated metals and oxygen-plasma-treated polystyrene (PS) (6,7). The XPS results suggest the formation of metal-oxygen-polymer complexes at the interface similar to that observed on oxygen-containing polymers (8). The effect of argon-ion-

bombarded polyethylene (PE) on evaporated titanium films has also been studied with XPS (9,10). The XPS results indicate the formation of Ti-C bonds at the interface of both treated and untreated films; however, the treated surface produced a higher number of nucleation sites.

Previously, the chemical effects of plasma treatment of PE were examined in detail with XPS (5). Argon-plasma treatments were found to produce no detectable chemical effects on the PE surface, whereas oxygen- and nitrogen-plasma treatments introduced various C-O and C-N functionalities into the PE surface. The effects of these plasma treatments of PE on evaporated Ag were also investigated with XPS (11). It was found that argon-plasma treatment resulted in a smaller average cluster size in the early stages of metallization but did not induce any chemical interactions between the Ag and PE. However, both oxygen- and nitrogen-plasma-treated PE surfaces exhibited definite chemical interactions with Ag through the plasma-induced oxygen and nitrogen respectively. These results are consistent with the difference in adhesion found for evaporated Ag on PE surfaces with and without plasma treatments.

This paper describes the application of XPS to investigate the interfacial chemistry of evaporated Ag on an oxygen-free polymer (PE) and an oxygen-containing polymer (PET), both before and after plasma treatment. The plasma treatment levels used in this study are well under the saturation level, unlike the previous study on PE (11). Whereas PE does not contain potential interaction sites for Ag, PET presents three possible interaction sites; the π electrons in the phenyl ring, the carbonyl oxygen, and the ester oxygen. Also, comparisons can be made on the extent of reactivity of the inherent oxygen in PET versus plasma-induced oxygen. All plasma treatments and subsequent metal depositions were done *in situ* to prevent surface contamination on exposure to atmosphere. Metal-polymer interactions were investigated by monitoring the initial stages of metallization in the sub-atomic layer regime.

Experimental

The XPS spectra were obtained on a Hewlett Packard 5950A photoelectron spectrometer with a monochromatic Al Kα x-ray source (1486.6 eV). The use of the monochromatic source minimizes sample radiation damage, which can be especially important in polymers. All materials used in this study were analyzed at ambient temperature and exhibited no evidence of x-ray damage during measurements. All measurements were made at an electron-takeoff angle of 38° which corresponds to an analysis depth of ~50 Å (12). The pressure in the spectrometer during analysis was typically 2 x 10^{-9} Torr. The full width at half maximum (FWHM) for the individual components of the C 1s peak in a clean polymer sample varied from 0.9 to 1.0 eV. All spectra were referenced to the C1s peak for neutral carbon in the polymer, which was assigned a value of 284.6 eV. Where necessary, a line-shape analysis routine utilizing a 90% Gaussian/10% Lorentzian line shape for the individual components was used.

The PET was commercial (0.18 mm) Kodak ESTAR film base. The PE was commercial (0.10 mm) high density (HD) PE. To eliminate surface contamination, the polymer samples were ultrasonically cleaned in a series of solvents (heptane, dichloromethane, ethanol and ethyl acetate) and dried in a dry nitrogen atmosphere in a glove bag attached directly around the insertion probe of the spectrometer. Immediately after drying, the polymer samples were inserted into the preparation chamber of the spectrometer where they were evacuated to ~5 x 10^{-9} Torr. The polymer samples were than annealed (PET~90° C, PE~ 60° C) for several hours to drive off any residual solvent, water, or adsorbed gases.

The plasma treatments were done in the preparation chamber of the

spectrometer (base pressure 1×10^{-9} Torr) by applying a potential to a 6 mm diameter Al rod mounted on a high-voltage feedthrough using a 5 kV, 60 Hz power supply while floating the sample rod with the chamber walls at ground potential. The sample-to-electrode distance is about 50 mm with the sample residing in the positive column of the plasma during treatment. The typical operating conditions were 10 W of primary power at 50 mTorr pressure for 15 s.

Silver evaporations were done in the same preparation chamber using an in-house-constructed evaporation assembly containing a resistively heated tungsten basket. Ag coverages were controlled by a quartz crystal thickness monitor. The deposition rates were typically 0.01 to 0.1 Å/s depending on the desired coverage. Coverages were subsequently calibrated by XPS analysis of the Ag 3d and polymer core level (C 1s and O 1s) intensities as compared to known standards, and by neutron activation analysis (11).

Samples for adhesion measurements were prepared in a separate chamber with a base pressure of 1×10^{-8} Torr under identical conditions. Typically, ~1000 Å silver coverages were used for adhesion measurements. Adhesion strength of the deposited Ag films was determined using a polyester adhesive tape and standard peel test procedures on an Instron tester.

Results and Discussion

General. The relative adhesion strength for evaporated Ag on PE and PET with and without plasma treatments is shown in Figure 1. Several observations are immediately apparent. First, the adhesion strength of Ag on untreated PET is greater compared to Ag on untreated PE. This result suggests that the inherent oxygen in PET may play a role in adhesion. Second, argon-plasma treatment provides little to no improvement in adhesion for both polymers. This result, together with the cleaning and annealing of the polymers prior to plasma treatment or metallization, suggests that boundary layers do not play a major role in the differences in adhesion observed in Figure 1. If a weak boundary layer still exists after cleaning and annealing, then plasma treatments may improve adhesion either by crosslinking or ablation of the boundary layer. However, both argon- and oxygen-plasma treatments were shown to induce a similar extent of crosslinking into PE (5). Also both argon- and oxygen-plasma treatments were found to ablate polymers at a similar rate of ~1 Å/s for the typical treatment times used in this study. Third, oxygen-plasma treatment provides a significant improvement in adhesion for both polymers. Again, suggesting the importance of a specific reactive species for improvement in adhesion.

Scanning electron microscopy (SEM) analysis of polymer surfaces treated for 60 s, which is significantly greater than the 15 s treatment times used in this study, could detect no observable morphological differences between untreated and plasma-treated polymer surfaces for magnifications up to x20,000 (5).

Based on these results, boundary layers and mechanical interlocking do not appear to play a major role in the differences in adhesion shown in Figure 1. Therefore, these differences in adhesion will be addressed from a chemical basis using XPS. Since only slight improvements were found for argon-plasma treatment and previous studies on PE (5,11) suggest no chemical effects for argon-plasma treatments, only the untreated and oxygen-plasma-treated polymers will be discussed in detail.

For all depositions, high resolution spectra of the Ag 3d and polymer (C 1s and/or O 1s) core levels and valence levels were accumulated. However, analysis of the Ag 3d core level revealed no differences for all depositions. The Ag $3d_{5/2}$ peak centroid was always 368.0 ±0.1 eV. Unfortunately, chemical bonding information is difficult to obtain from the Ag core levels since the +1 oxidation state exhibits little or
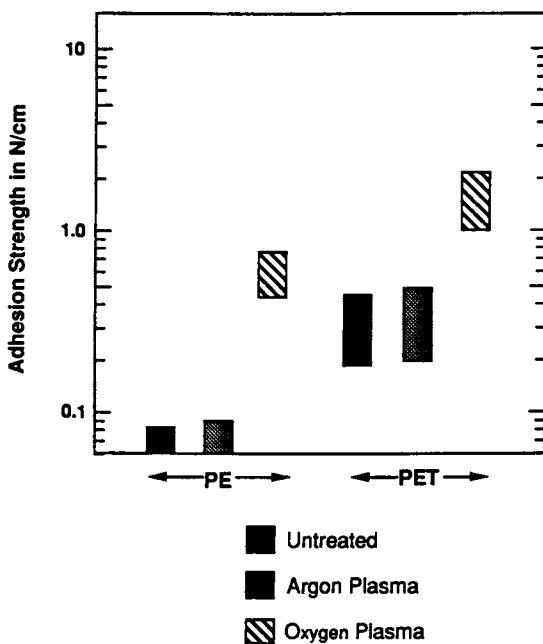
Figure 1. Relative adhesion strength for evaporated Ag on polymers.

no shift and typically the Auger Paramater is used to distinguish between the metal and +1 oxidation state of Ag. However, the Ag M_4VV Auger peak is relatively weak and broad and due to the fact that the coverages are less than a monolayer with the possibility of multiple oxidation states present, an analysis using the Auger peak proved to be uninformative. Therefore, the following discussion will focus on analysis of the polymer core levels and the Ag valence levels.

<u>Ag/untreated PE.</u> Based on the C 1s level and valence level spectra, no evidence of Ag interaction with untreated PE was found. Several depositions were done, and in all cases no changes in the shape or peak positions were found. This is consistent with the poor adhesion for Ag on untreated PE. The results for Ag depositions on argon-plasma-treated PE were similar, except for slight changes in the valence level spectra which will be discussed below.

<u>Ag/oxygen-plasma-treated PE.</u> Oxygen-plasma treatment of PE introduces a significant amount of oxygen into the PE surface (<u>5</u>). Depending on the treatment level and time between 1 to ~20 atomic percent oxygen can be incorporated. Approximately 12 atomic percent oxygen is incorporated for the 15 s treatment time used in this work. The C 1s and O 1s spectra for oxygen-plasma-treated PE are shown in Figure 2. A distribution of various C-O functionalities is observed similar to those reported previously (<u>5</u>).

An analysis of the C 1s and O 1s regions after deposition of ~ 0.6 Å Ag on the oxygen-plasma-treated PE reveals significant changes as shown in Figure 2. The C 1s spectrum indicates a depletion in the high binding energy features after deposition of Ag and some line broadening. The regions due to C-O species at 286.1 eV, and O-C=O species at 288.6 eV exhibit the largest change. This effect can be due to two sources; bond breaking induced by the thermally hot Ag atoms impinging on the polymer surface resulting in desorption of short-chain species or rearrangement of the modified surface and/or the formation of Ag-O-C species at the interface resulting in charge transfer to the carbon atoms through oxygen. Desorption of short-chain species is probably occuring to some extent, since an overall decrease in oxygen is observed after Ag deposition. The net result of the formation of Ag-O-C species is a shift to lower binding energy for the carbon atoms involved in this interaction. Ag interaction with the C-O species would result in a peak that falls within the envelope of the C-C species and might not be easily detected. However, Ag interaction with the O-C=O species should result in a peak lower in energy than the O-C=O peak but at a higher energy than expected for C=O (287.6 eV). In fact, a definite increase in intensity at 288.0 eV is observed. This peak position is identical to those observed for Ag salts of carboxylic acids (Table I).

Examination of the O 1s spectrum, Figure 2, reveals a shift in the peak centroid to lower binding energy, consistent with Ag-O bond formation (<u>13</u>). A line-shape analysis of the O 1s peak after Ag deposition is shown in Figure 3. The line-shape analysis was done by constraining the peak positions to values previously determined in this laboratory for model compounds. The best fit provides two peaks at binding energies of 531.3 eV, and 532.7 eV. The peak at 532.7 eV is identical to that observed before Ag deposition. The peak at 531.3 eV occurs at the same energy as previously determined for compounds of Ag bonded to oxygen (<u>13</u>) and is consistent with the formation of a Ag-O-C species (Table I).

The valence level spectra are shown in Figure 4. Even at coverages of less than a monolayer, the valence band spectrum is dominated by the Ag 4d band between 3-8 eV. This band directly overlaps the region of the C-H band of the untreated PE and the region where the O 2p lone pair orbitals occur for oxygen-plasma-modified PE (<u>5</u>). The two peaks comprising the C-C band (predominately C 2s character) of the PE substrate are evident in all spectra at 13.2 eV and 18.8 eV. The Ag 4d band for
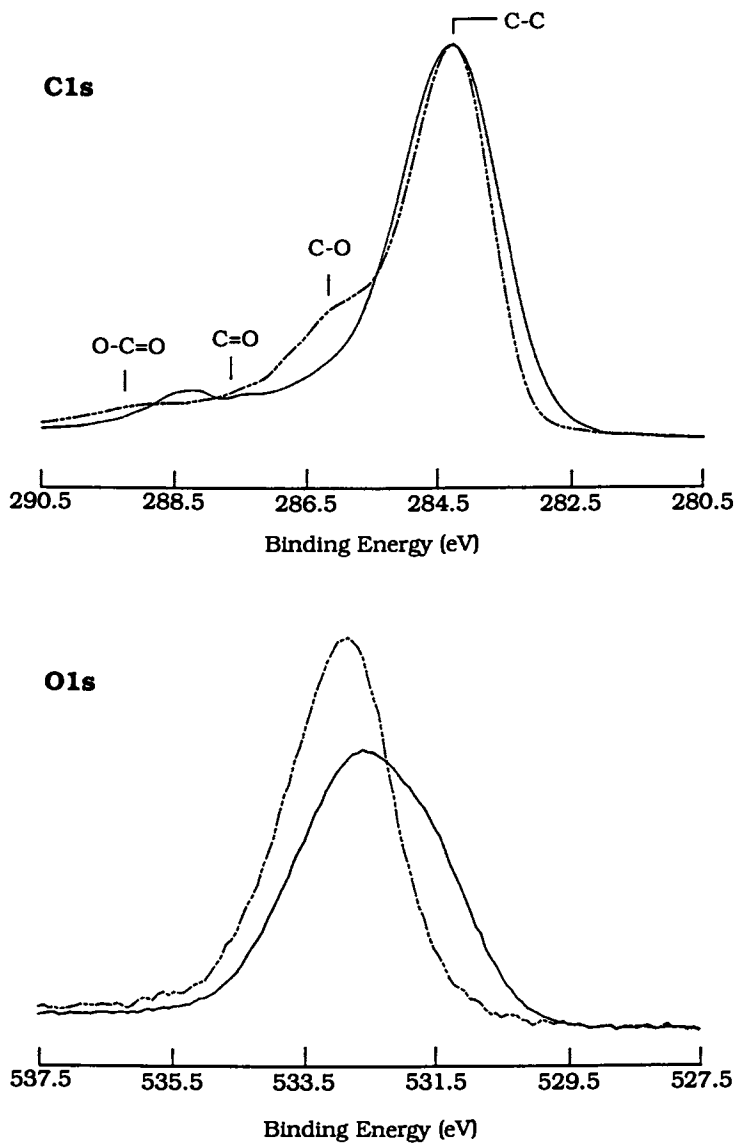
Figure 2.   Comparison of C 1s and O 1s levels before (dashed line) and after (solid line) deposition of 0.6 Å Ag on oxygen-plasma-treated PE.
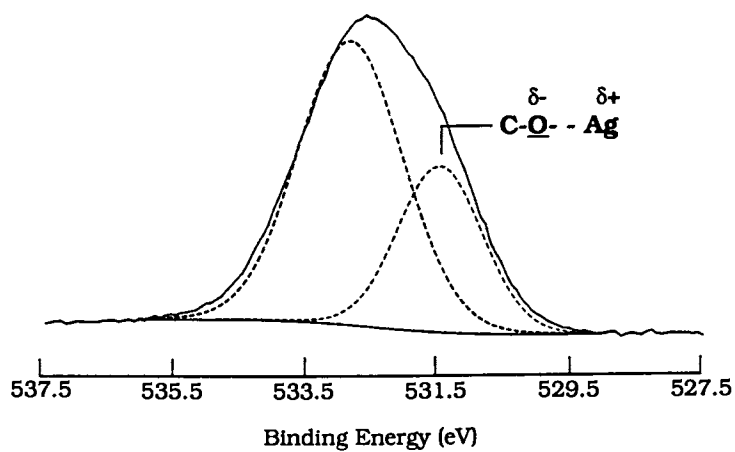
Figure 3.   O 1s line-shape analysis after deposition of 0.6 Å Ag on oxygen-plasma-treated PE.
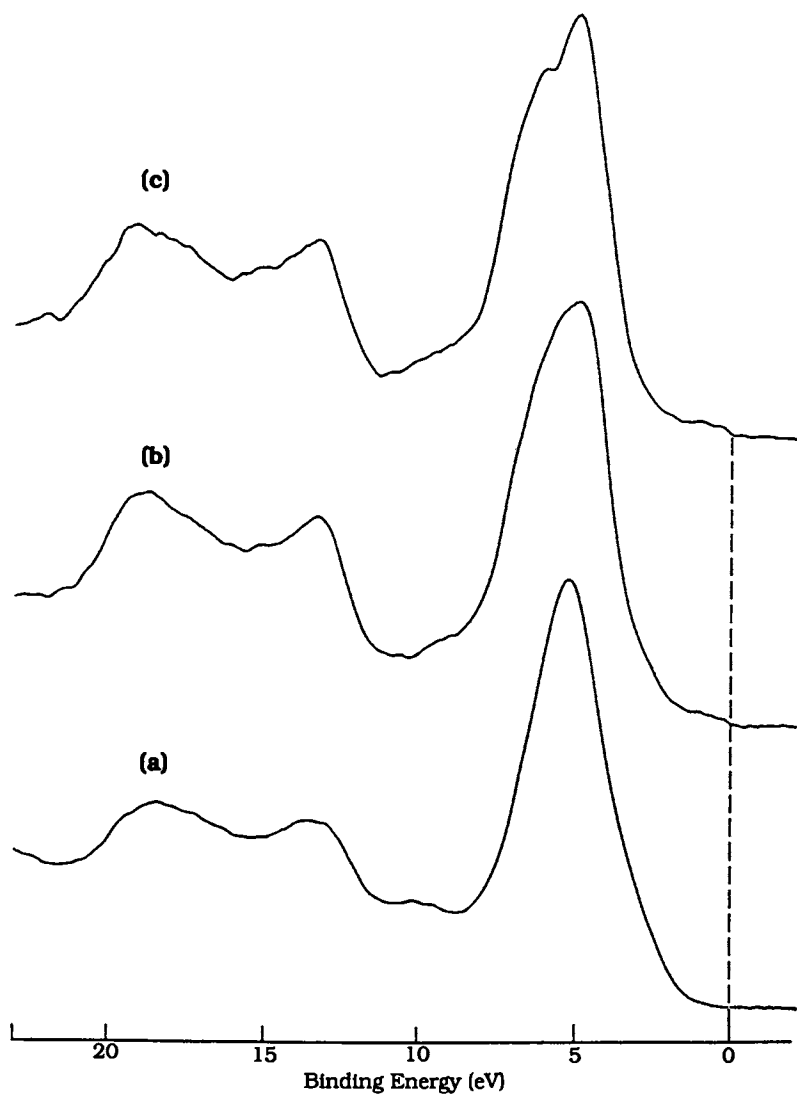
Figure 4.   Valence level region after deposition of 0.6 Å Ag on (a) oxygen-plasma-treated, (b) argon-plasma-treated, and (c) untreated PE.

the untreated PE contains two distinct features reminiscent of nearly bulk-like Ag. However, for the Ar plasma treated PE, the 4d band is somewhat narrower with a loss of the characteristic bulk-like Ag features. For the oxygen-plasma-treated PE, the 4d band is considerably narrower with a definite feature extending to low binding energy. These results can be explained due to two effects; a difference in Ag cluster size, and the formation of a Ag-O-C species at the interface. The differences between the Ag 4d band on the untreated and argon-plasma-treated PE can be attributed solely to a difference in cluster size. However, on oxygen-plasma-treated PE, the differences can be attributed to both a difference in cluster size and the formation of a Ag-O-C species at the interface.

   Based only on clustering effects, the valence band spectra suggest a very large average cluster size for the untreated PE and near the single atom limit for the oxygen-plasma-treated PE with the argon-plasma-treated PE somewhere in between. For single atom centers, the Ag 4d free-atom state is split 0.55 eV due to spin-orbit interactions (14), giving rise to one relatively narrow line. As the clusters grow, the 4d band broadens and splits due to a combination of spin-orbit and crystal field effects (15). The progression from large to small clusters does predict a narrowing of the d band and has been reported on amorphous graphite (16). However, based on clustering effects alone, the shape of the d band should be symmetrical. The asymmetric shape of the d band on the oxygen-plasma-treated PE suggests the formation of a Ag-O species. The reason for the asymmetric shape of the d band will be discussed in more detail in the section on model compounds.

Table I. Summary of XPS data for low coverage (~0.6 Å) of Ag on oxygen-plasma-treated PE and PET compared to model compounds. All data are listed in eV and are within ±0.1 eV of the stated value

	Ag $3d_{5/2}$	C 1s	O 1s $(O=C-O)^{-1}$	Ag 4d FWHM	ionization threshold
Ag/PE	368.0	------	531.2	2.6	2.0
Ag/PET	368.1	------	531.2	2.7	2.1
Ag benzoate	368.1	288.0	531.3	2.4	1.9
Ag acetate	368.0	288.0	531.3	2.7	1.8
Ag_2O	368.0	------	531.4	2.1	0.7
AgO	367.9	------	530.5	2.9	0.6

Ag/untreated PET.   The C 1s and O 1s spectra for Ag deposition on untreated PET are shown in Figure 5. The C 1s spectrum for the clean PET surface before Ag deposition consists of four distinct peaks: the carbon atoms in the phenyl ring (284.6 eV), the methylene carbon atoms singly bonded to oxygen (286.1 eV), the ester carbon atoms (288.6 eV), and the peak due to the π-π* shakeup transition (290.6 eV). The three main peaks are present in a 3/1/1 ratio as expected based on PET stoichiometry. The π-π* shakeup peak is ~4.5% of the total integrated area of the main peaks. After Ag deposition, slight line broadening occurs and the ester carbon peak decreases in intensity by ~5-10%. The attenuation of the ester carbon peak can be attributed to Ag interaction with the carbonyl oxygen. This possibility will be discussed later after examination of the O1s spectra.

   Another subtle effect that occurs after Ag deposition is loss of intensity of the π-π* shakeup peak. The π-π* shakeup intensity is plotted as a function of Ag coverage in Figure 6. There are several possible reasons for this effect. First, the
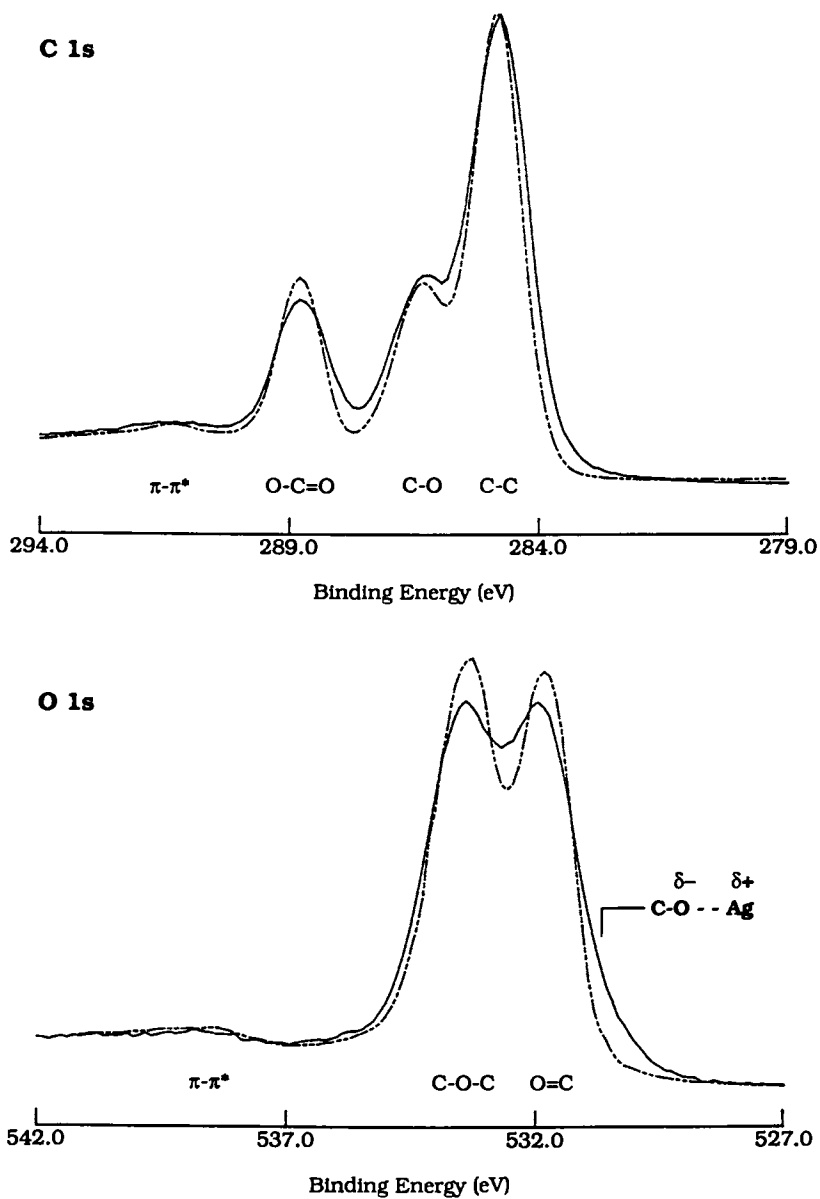
Figure 5.   Comparison of C 1s and O 1s levels before (dashed line) and after (solid line) deposition of 0.6 Å Ag on untreated PET.
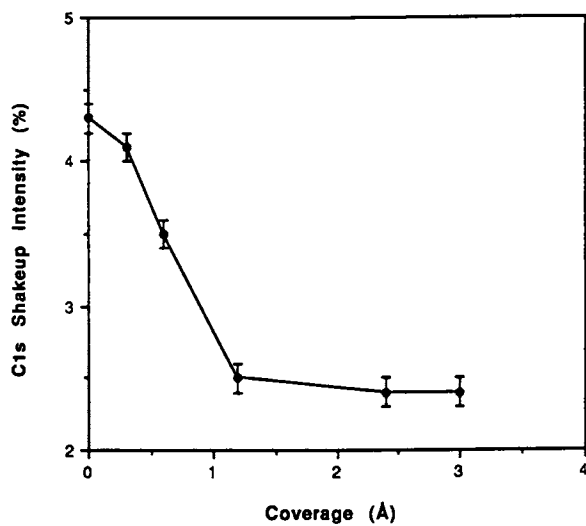
Figure 6. Intensity of C 1s shakeup peak as a function of Ag coverage.

aforementioned interaction of Ag with the carbonyl oxygen can induce a net increase in electron density in the phenyl ring through the ester carbon atom. A second possibility is charge transfer from Ag to the phenyl ring via the formation of a Ag-π complex with the phenyl ring. The formation of Ag complexes with π systems has been discussed by Cotton and Wilkinson (17). Changes in the intensity of shakeup peaks for aromatic systems has been discussed by Clark and Dilks (18) where the effect of electron donating groups on the phenyl ring was found to decrease the shakeup intensity. A third possibility is breakup of the phenyl ring due to the thermally hot Ag atoms impinging on the PET surface. The line broadening observed after Ag deposition also suggests damage to the polymer surface possibly by bond breaking. Possibilities 2 and 3 cannot be excluded with the present information.

Examination of the O 1s spectra (Figure 5) can provide further insights into the Ag/PET interactions. The O 1s spectrum for the clean PET surface contains three distinct peaks due to the carbonyl oxygen atoms at 532.2 eV, the ester oxygen atoms at 533.5 eV, and the π-π* shakeup peak at 538.5 eV. The main peaks are present in 1/1 ratio as expected for clean PET. The π-π* shakeup peak is ~ 2.5% of the total integrated area of the main peaks. After Ag deposition, the O 1s spectrum broadens slightly, similar to the C 1s spectra, and exhibits a definite skew to lower binding energy. The π-π* shakeup peak also decreases in intensity as a function of Ag coverage similar to that observed for the C 1s shakeup peak.

The skew to lower binding energy suggests the formation of a new oxygen species. A line-shape analysis of the O 1s spectrum after Ag deposition suggests the presence of a new peak at ~531.2 eV. This peak occurs at the same energy as that found on the oxygen-plasma-treated PE and is identical to the value previously determined for Ag carboxylate compounds where the Ag-oxygen bond has a significant degree of covalent character (13). Based on the line-shape analysis, this peak is estimated to be approximately 5-10% of the O 1s total integrated area. These results are consistent with the formation of a Ag-O-C species, but the formation of Ag₂O by abstraction of oxygen from the polymer cannot be excluded based on the XPS data.

Three possible reaction schemes are shown in Figure 7 to account for these observed changes. Reaction 1 involves breaking of the ester oxygen/ester carbon bond and the formation of a Ag-O-C species with the ester oxygen. This is consistent with the observed decrease in the ester carbon intensity. This reaction scheme also produces isolated carbonyls which is consistent with the observed intensity increase in the carbonyl region. However, such a scheme would result in a net shift to lower binding energy for the C-O (286.1 eV) species bonded to Ag. Experimentally this is not observed. Such a small change might be difficult to detect due to overlap of the C-O peak (286.1 eV) with the peak due to the carbon atoms in the phenyl ring (284.6 eV). Reaction 2 involves breaking of the methylene carbon/ester oxygen bond and the formation of a Ag-carboxylate structure. This structure would result in a net negative charge on the ester carbon atom causing a shift of the ester carbon peak to lower binding energy, consistent with the observed decrease in the ester carbon intensity. However, this reaction scheme would eliminate one C-O species for each Ag-carboxylate formed. Experimentally this is not observed. Reaction 3 requires no bond-breaking and is simply an interaction of Ag with the carbonyl oxygen. This interaction results in a net transfer of electron density to the ester carbon through the carbonyl oxygen and produces a net shift to lower binding energy for the ester carbon, consistent with all the XPS data.

The valence level spectra are shown in Figure 8. The valence level spectrum for clean PET consists of five main bands of which the most important are the bands between 3-10 eV. The highest occupied valence level (3-4 eV) should have significant contribution from the π electrons in the phenyl ring and are not resolvable as a separate band. The bands between 4-10 eV have significant contributions from
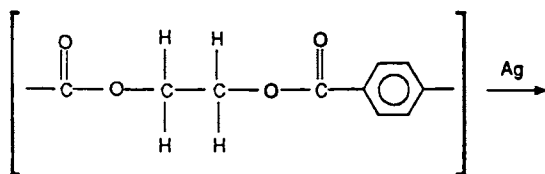
Reaction 1
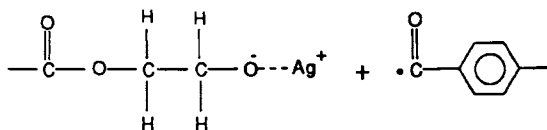
Reaction 2
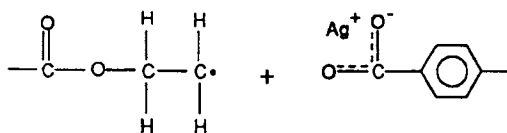
Reaction 3
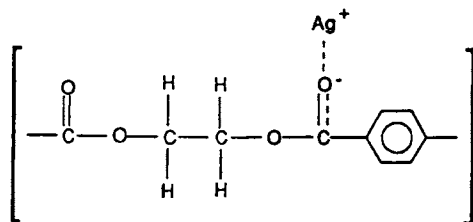
Figure 7.   Proposed reaction schemes for Ag on PET.
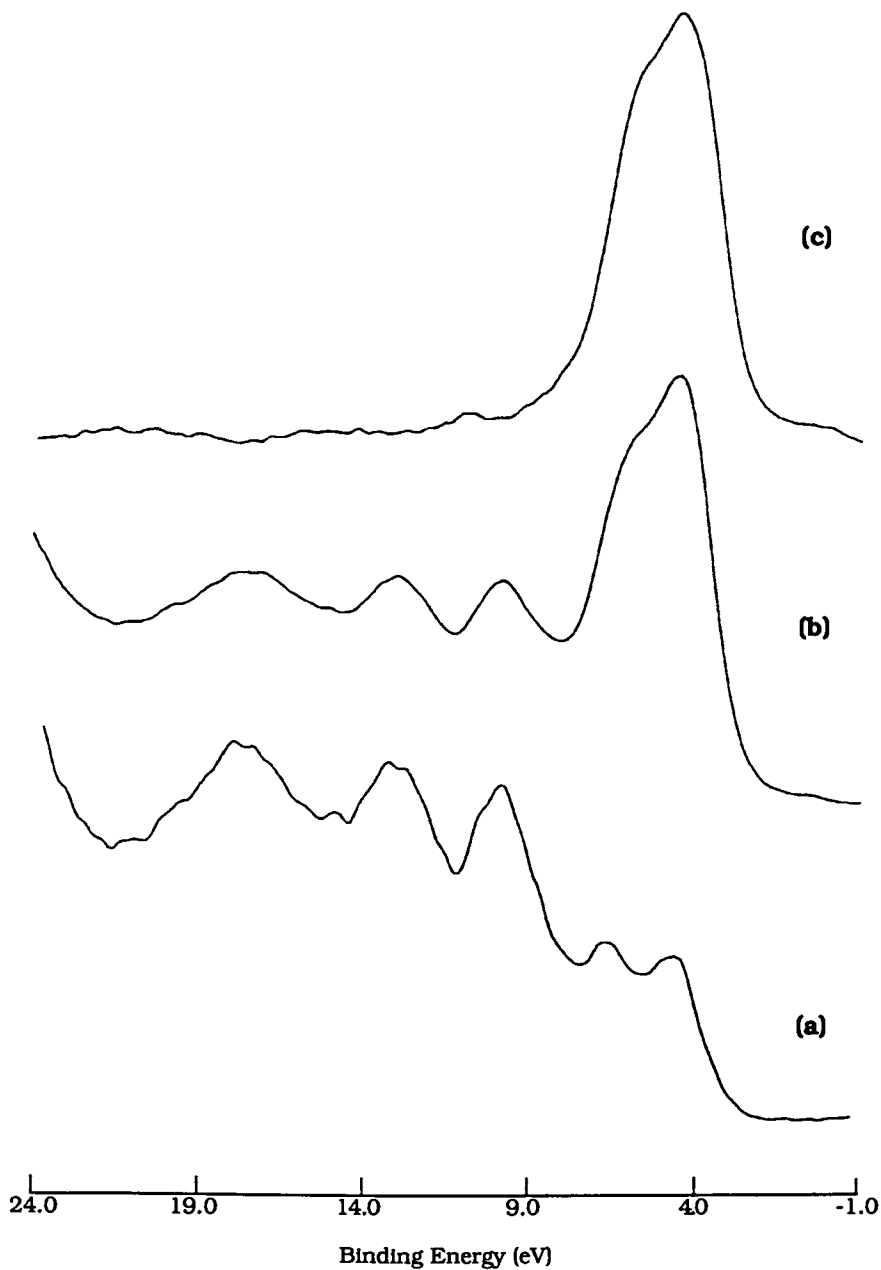
Figure 8. Valence level region (a) before and (b) after deposition of 0.6 Å Ag on untreated PET. Spectrum (c) is the difference spectrum after removal of the PET contribution.

oxygen 2p orbitals and are the most important from a chemical bonding viewpoint. After Ag deposition, the valence level region is dominated by the intense Ag 4d band between 3-8 eV. Note that the Ag 4d band overlaps the region in the PET valence level that has significant contribution from oxygen orbitals. The 5s band extending from the Fermi level to 3 eV is not as distinct as on untreated PE. The shape of the 4d band is similar to bulk-like Ag, but appears to be narrower with the two bands less resolved.

Since the valence level of PET has considerable intensity in the region of the Ag 4d band, removal of the PET contribution to the valence level provides a more realistic shape for the Ag 4d band. This has been done in Figure 8c. It is obvious that the two features of the 4d band reminescent of bulk-like Ag are not fully resolved. Also, the FWHM of the 4d band is 3.0 eV compared to 3.3 eV on untreated PE and 3.4 eV for bulk Ag. There are two possible explanations for these changes as stated previously for PE: the presence of small Ag clusters at this low coverage resulting in band narrowing due to loss of long-range periodicity (16) and the formation of a Ag-O-C species resulting in a different 4d band shape. Both of these are probably occurring to some extent. Since the core level spectra suggest only a fraction of the Ag atoms are interacting with oxygen, the resultant 4d band is probably a convolution of Ag in various cluster sizes and Ag atoms interacting with oxygen.

Based on the above observations, evidence exists for the formation of a Ag-O-C species in the early stages of Ag metallization on untreated PET. The degree of interaction is slight and, at most, only one carbonyl oxygen atom per PET repeat unit in the first molecular layer of PET is an interaction site. This corresponds to approximately 7% of the surface atoms. Although the interaction is slight, it can account for the improved adhesion compared to PE where virtually no interaction sites were observed.

Ag/oxygen-plasma-treated PET. The C 1s and O 1s spectra for Ag deposition on oxygen-plasma-treated PET are shown in Figure 9. The spectra before Ag deposition are considerably different compared to the untreated PET. It is apparent that a significant amount of oxygen is incorporated into the PET surface based on both the increase in the high binding energy region of the C 1s spectrum and the increased intensity in the O 1s peak. The ratio of the three peaks in the C 1s spectrum changes from 3/1/1 to 2/1/1 and the O 1s peak shape exhibits a significant intensity increase at ~533.0 eV. Based on previous work, the incorporated species are primarily alcohol, carbonyl, and acid groups (4).

Both the C 1s and O 1s spectra exhibit more substantial changes after Ag deposition compared to untreated PET. The C 1s spectrum exhibits some line broadening and a decrease in the intensity of the 288.8 eV peak similar to that observed for untreated PET. Also, some loss of the incorporated oxygen was found. The oxygen concentration drops from ~42% to ~38%. This loss of oxygen is similar to that observed for Ag deposition on oxygen-plasma-treated PE.

Even with this loss of incorporated oxygen, the spectral changes after Ag deposition are much greater than those observed for the untreated PET. The 288.8 eV peak decreases in intensity by ~15-20% while the other peaks remain relatively unchanged. In fact, there is an increase in intensity in the region between 286-288 eV when the initial loss of oxygen is taken into account. A significant contribution to the intensity of the 288.8 eV peak is due to acid groups formed during oxygen-plasma treatment. These results suggest Ag interaction with oxygen in the acid groups to form a Ag-O-C species, possibly a Ag salt of a carboxylic acid. Such an interaction would induce a net increase in electron density on the carbon atoms in the acid group resulting in a shift to lower binding energy. Ag interactions with the plasma-induced carbonyl and alcohol groups may also occur, however such interactions would not be obvious from the C 1s spectrum. Ag interaction with the plasma-induced carbonyl
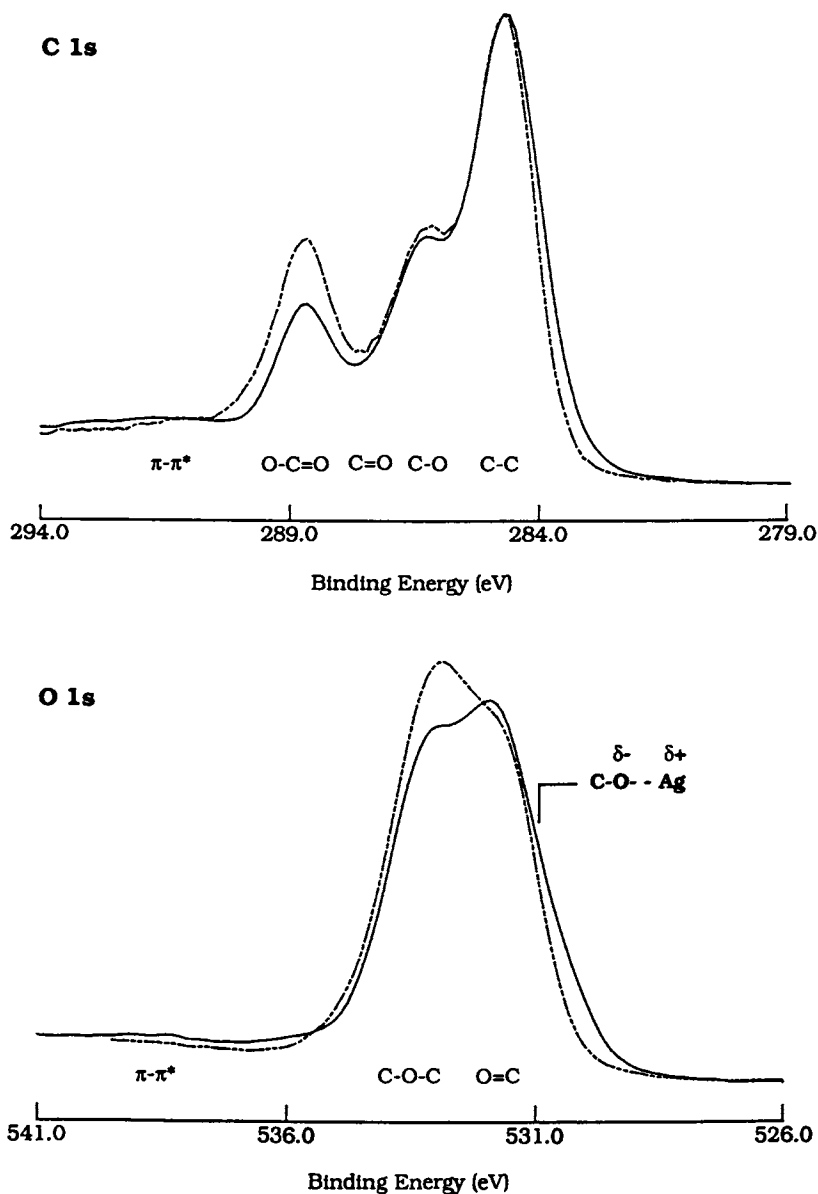
Figure 9.   Comparison of C 1s and O 1s levels before (dashed line) and after (solid line) deposition of 0.6 Å Ag on oxygen-plasma-treated PET.

would result in a shift to lower binding energy causing this species to fall within the envelope occupied by the plasma-induced alcohol peak. Similarily, Ag interaction with the plasma-induced alcohol groups would produce a species whose binding energy would fall within the envelope occupied by the peak due to the phenyl carbon atoms.

After Ag deposition, the O 1s spectrum (Figure 9), displays a large decrease in intensity of the oxygen-plasma-induced peak at ~533.0 eV and a definite skew to lower binding energy. A line-shape analysis of the O 1s spectra after Ag deposition suggests the formation of a new peak at ~531.2 eV. This peak position is identical to that found for evaporated Ag on untreated PET and oxygen-plasma-treated PE. However, unlike the untreated PET, the intensity of this peak is much greater (~15-20% of the total oxygen intensity). Since the oxygen concentration in the plasma-treated PET is ~35% greater compared to the untreated PET (taking into account the oxygen lost after the initial deposition), this change represents a three- to five-fold increase in the number of interaction sites.

Analysis of the valence level region (Figure 10) provided convincing evidence for the formation of a Ag-O-C species. The valence level region for oxygen-plasma-treated PET before Ag deposition exhibits a lower ionization threshold (~1.5 eV) and an increased intensity in the region between 4-8 eV compared to the untreated PET. These changes are due to the plasma-induced oxygen species and are similar to those previously reported for oxygen-plasma-treated PE (5). After Ag deposition, the valence region is again dominated by the Ag 4d band between 3-8 eV similar to the untreated PET. However, the shape of the 4d band is considerably different compared to the untreated PET. The band is much narrower and does not exhibit the two features reminiscent of bulk-like Ag.

These differences are more readily apparent in Figure 10c, where the contribution of PET to the valence levels has been removed. The Ag 4d band is relatively narrow (2.7 eV) and asymmetric with a definite skew toward the Fermi level. Also note the absence of the Ag 5s band. The band is very similar to that observed on oxygen-plasma-treated PE. Another feature that is present after removal of the PET contribution is a weak band centered at 10 eV. A similar feature is present on the untreated PET although not as intense. This feature may be an artifact of the spectral subtraction routine or may be due to the formation of new molecular orbitals with some Ag d character due to the interaction of Ag with oxygen in the PET. Clearly these changes could not be attributed to clustering effects alone. As stated previously for oxygen-plasma-treated PE, the asymmetric shape of the d band suggests the formation of a Ag-O species.

Model Compounds. Several model compounds of Ag were studied to provide insights into the chemical structure of evaporated Ag at the oxygen-plasma-modified polymer surface. A summary of the XPS data is listed in Table I and a comparison of the valence level spectra are shown in Figure 11. Based on the core level spectra, the formation of AgO can be eliminated because of the O 1s peak position. However the formation of Ag_2O cannot be eliminated based only on the O 1s peak position since it occurs at the same energy in the Ag salts and the newly formed oxygen peak on untreated PET and oxygen-plasma-treated PE and PET. An analysis of the valence level region suggests that the formation of Ag_2O cannot account for the spectra at the low Ag coverages on oxygen-plasma-treated PE and PET due to the fact that both the ionization threshold (0.7 eV compared to 2.1 eV) and the FWHM (2.1 eV compared to 2.7 eV) are considerably different. Both AgO and Ag_2O have a less intense band extending ~1.5 eV to lower energy compared to Ag on oxygen-plasma-treated PE and PET. However, the shape and threshold ionization for the two Ag salts are very similar to the low Ag coverages on oxygen-plasma-treated PE and PET. These results suggest that the primary species formed at the Ag/oxygen-plasma-treated polymer
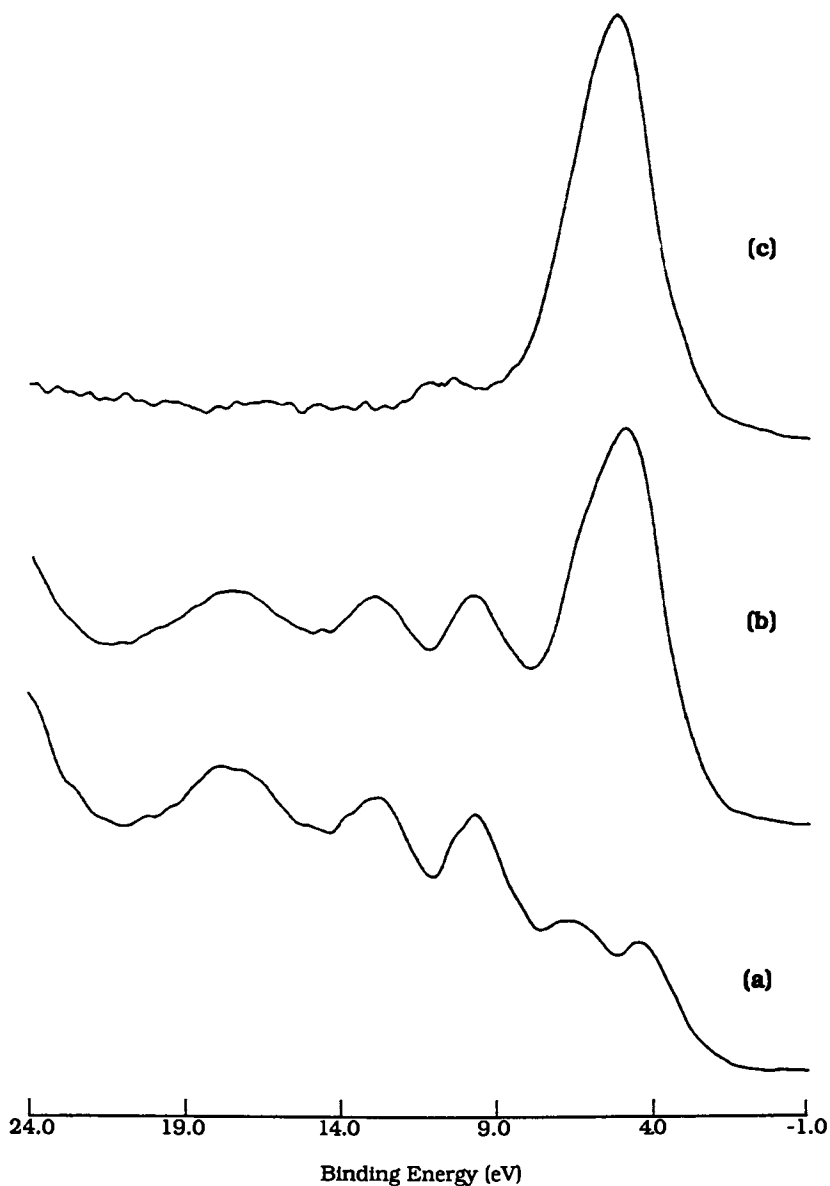
Figure 10. Valence level region (a) before and (b) after deposition of 0.6 Å Ag on oxygen-plasma-treated PET. Spectrum (c) is the difference spectrum after removal of the PET contribution.
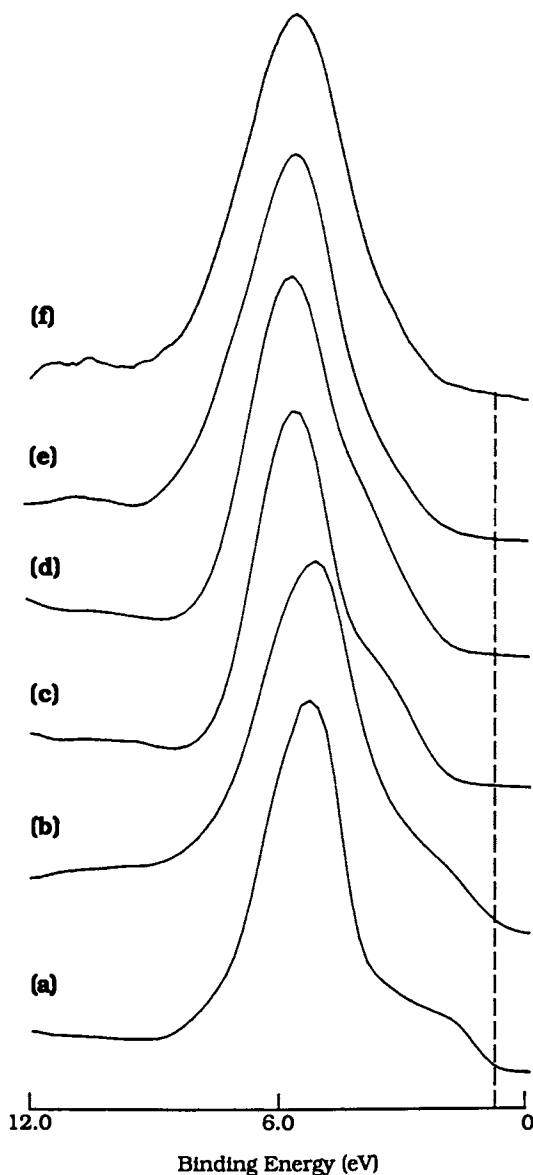
Figure 11. Comparison of valence level regions for (a) Ag(+1) oxide, (b) Ag(+2) oxide, (c) Ag benzoate, (d) Ag acetate (e) 0.6 Å Ag on oxygen-plasma-treated PE, and (f) 0.6 Å Ag on oxygen-plasma-treated PET. The dotted line indicates the ionization threshold for Ag(+1) oxide.

interface is similar to that of a Ag salt of a carboxylic acid. However the formation of other Ag-O-C species cannot be confirmed or eliminated with the present information.

Conclusions

XPS has been used to study the interfacial chemistry between evaporated Ag and polymer surfaces with and without plasma modification. The approach taken was to monitor the initial stages of metallization in the sub-atomic layer regime. Both the adhesion data and the XPS data demonstrate that the inherent oxygen in PET provides a limited number of bonding sites compared to PE but is not as reactive as plasma-induced oxygen. For the untreated PET, the XPS results suggest charge transfer between Ag and the carbonyl oxygen in PET in the early stages of metallization. The effect on the untreated PET is small with only about 7% of the PET surface atoms providing reaction sites. Plasma modification with oxygen introduces specific reaction sites resulting in additional chemical bond formation between the evaporated Ag and the polymer surfaces. The XPS results suggest the primary reaction sites are the plasma-induced acid groups. Based on both core level and valence level spectra of model compounds, the resultant structure is similar to that of a silver salt of a carboxylic acid. For both polymers, the number of oxygen-plasma-induced reaction sites is estimated at 3 to 4 times greater compared to the untreated polymer surface. These results are consistent with the significant improvement in adhesion observed for plasma treatment with oxygen.

Acknowledgments

Literature Cited

1. Boenig, H,V. Plasma Science and Technology; Cornell Press: Ithaca, NY, 1982, p 199-239.
2. Mittal, K.L. J. Vac. Sci. Technol. 1976, 13, 19.
3. Gerenser, L.J.; Elman, J.F.; Mason, M.G.; Pochan, J.M. Polymer 1985, 26, 1162.
4. Pochan, J.M.; Gerenser, L.J.; Elman, J.F. Polymer 1986, 27, 1058.
5. Gerenser, L.J. J. Adh. Sci. Technol. 1987, 4, 303.
6. Burkstrand, J.M. Appl. Phys. Lett. 1978, 5, 387.
7. Burkstrand, J.M. J. Vac. Sci. Technol. 1979, 4, 1072.
8. Burkstrand, J.M. J. Appl. Phys. 1981, 7, 4795.
9. Bodo, P.; Sundgren, J.-E. J. Vac. Sci. Technol.A 1984, 4, 1498.
10. Bodo, P.; Sundgren, J.-E. J. Appl. Phys. 1986, 3, 1161.
11. Gerenser, L.J. J. Vac. Sci. Technol. 1988, 5, 2897.
12. Seah, M.P.; Dench, W.A. Surf. Interface Anal., 1979, 1, 2.
13. Trotter, P.J.; Mason, M.G.; Gerenser, L.J. J. Phys. Chem. 1977, 81, 1325.
14. Moore, C.E. Natl. Bur. Stand (US) Circ. 1971, p 467.
15. Ley, L.; Kowalczyk, S.P.; McFeely, F.R.; Shirley, D.A. Phys. Rev. 1974, 10, 4881.
16. Wertheim, G.K.; Dicenzo, S.B.; Buchanan, D.N.E. Phys. Rev. B 1986, 33, 5384.
17. Cotton, F.A.; Wilkinson, G. Advanced Inorganic Chemistry; Interscience Publishers: NY, 1966, p 761-794.
18. Clark, D.T.; Dilks, A. J. Polym. Sci., Polym. Chem. 1977, 15, 15.

Chapter 33

Crystallographic Structure and Adhesion of Aluminum Thin Films Deposited on Mylar

J. F. Silvain[1], J. J. Ehrhardt[1], A. Picco[1], and P. Lutgen[2]

[1]Laboratoire Maurice Letort, Centre National de la Recherche Scientifique, Villers Les Nancy, France
[2]E. I. du Pont de Nemours and Company, Luxembourg

Transmission Electron Microscopy (TEM) has been used to characterize aluminum thin films thermally evaporated (vacuum around 10^{-4} Torr) on Polyethyleneterephtalate (Mylar) and to correlate the crystallographic structure of the system Al/Mylar and the adhesion of the aluminum films. The adhesion of these films has been measured by a Peel test technique. For the polymer, an amorphous layer (t=12 nm) followed by a crystalline film have been observed on a Corona treated film and the opposite configuration has been found on a bi-axially stretched film. Some spherical precipitation and interdiffusion zones have also be observed in the Mylar™ for the films which have the lower coefficient of adhesion (100 g/inch). The main conclusion is the augmentation of the adhesion of the aluminum film as the size of the grains decreases and/or as the microroughness of the Al/Mylar interface increases.

Metal thin films deposited on polymers are widely used in various industrial domains such as microelectronics (capacitors), magnetic recording, packaging, etc. Despite much attention that has been paid in the recent literature on the adhesive properties of metals films on polyimide (PI)(1 - 5) and polyethyleneterephtalate (PET)(6) it appears that a better knowledge of the metal/polymer interface is needed. In this paper we focus ourself on the relationship between the adhesion and the structural properties of the aluminum films evaporated (or sputtered) on commercial bi-axially stretched PET (Du Pont de Nemours (Luxembourg) S.A.). A variety of treatment (corona, fluorine,etc.) have been applied in order to improve the adhesion of the metallic layer to the polymer. The crystallographic

structure of these laminates has been examined by TEM using a special cross section technique(7).

The skin of the polymer, the interface of Al/PET, and the grain morphology of the aluminum film have been observed. The adhesion force has been scaled by a standard peel test.

ALUMINUM SAMPLE CHARACTERIZATIONS

The experimental procedure for the growth of the aluminum films on polymer will be described in the following paragraph for each of the three sets of samples that we have worked with.

The metallic layers were examined either by conventional or cross-section TEM in a Jeol 200 Cx microscope. For the cross section preparation a sandwich of two laminates is made, glued face to face with an epoxy, cut in small pieces, mechanically polished, and then ion milled to a final TEM observation thickness. The plane section TEM sample are prepared by dissolving the PET in trifluoroacetic acid for 5 to 10 mn. The area observed, on plane section TEM, for the grain size calculation is close to 0.2 μm^2. For the adhesion measurements, test pieces consist of aluminum support (1 mm thick) double sided tape (Permacel P-94) PET (12μm) / evaporated aluminum/ ethylene acrylic acid (EAA) copolymer film. These laminates are prepared for the peel test by compression under 1.3 10^5 N.m^2 at 120°C for 10 seconds. The peel test is performed by peeling the EAA copolymer sheet from the laminate in an INSTRON tensile tester at 180° peel angle and 5 cm min^{-1} peel rate.

EXPERIMENTAL RESULTS

In this paragraph we will examine first the adhesion properties and the structure of aluminum films evaporated i) on bi-axially oriented polymer and ii) on treated (corona and fluorine) polymer samples. Then, an analysis of the influence of some parameters of the metallization such as the thickness of the aluminum film, the evaporation angle and the aluminum deposition by sputtering, will be presented.

ALUMINUM FILM ONTO NON TREATED BI-AXIALLY STRETCHED POLYMER

Depending on the tensions and the temperatures of the heat setting during the film processing, PET with different structural properties can be produced(8). Three different PET films with low, medium, and high crystallinity have been used as substrates for the metallization by thermal evaporation. The metallic layers, with thickness ranging from 40 to 50 nm, were evaporated at a deposition rate of about 50nm/s in commercial equipment. During the deposition, the residual pressure was around 10^{-4} Torr. The studied samples are referenced as sample (1) [low crystallinity], (2) [medium crystallinity], and (3) [high crystallinity].

The adhesion coefficient, as determined by the standard peel test, and the average grain size and the microroughness, as

measured respectively on plane section and cross section TEM, are presented in table I for these three samples. The trends are :
- the polymer films with the higher crystallinity give the higher adhesion,
- the small grain size leads to a high adhesion of the metallic film deposited onto polymer. Identical results have been found by Y. de Puydt and al.(6) for the same series of films.
- the increase of the microroughness of the interface Al/Mylar™ induces the augmentation of the adhesion of the aluminum film.
   This phenomenon is described by Arslanov and al(9) as the mechanical adhesion. The aluminum should be, in this theory, linked in the pores of the PET. So, an augmentation of the specific surface of the polymer leads to an increase of the adhesion of the aluminum film evaporated onto the polymer.

   Table I :   Variation of the adhesion, the average grain size, and the microroughness for the samples (1), (2), and (3)

Properties Samples	Adhesion (g/inch)	Average grain size (nm^2)	Microroughness (nm)
(1)	100	3600	6
(2)	120	2700	6
(3)	200	1900	20

   A cross section TEM picture of sample (1) is shown in figure1. The average grain size and the thickness of the aluminum film determined from this picture are respectively 75 nm and 50 nm. Several features can be observed:
- a "Rod Like structure" (RLS) (detail A) where the grain boundaries cross the metallic layer (figure 2a),
- a micro-micro diffraction of one grain showing a {112} aluminum orientation. There are two features which enable patterns to be indexed :   1) The distance R_1 from the diffracted spot to the transmitted beam (centre spot). This parameter is characteristic of the interplanar spacing $d_{(h1,k1,l1)}$ of the reflecting plane and the magnefication due to the lens settings (the camera constant). 2) The angles between lines drawn from the centre spot to the diffracted spot.
- a rather smooth interface Al/PET,
- the presence of spherical precipitates inside the PET. No micro-micro diffraction has been made of these precipitates
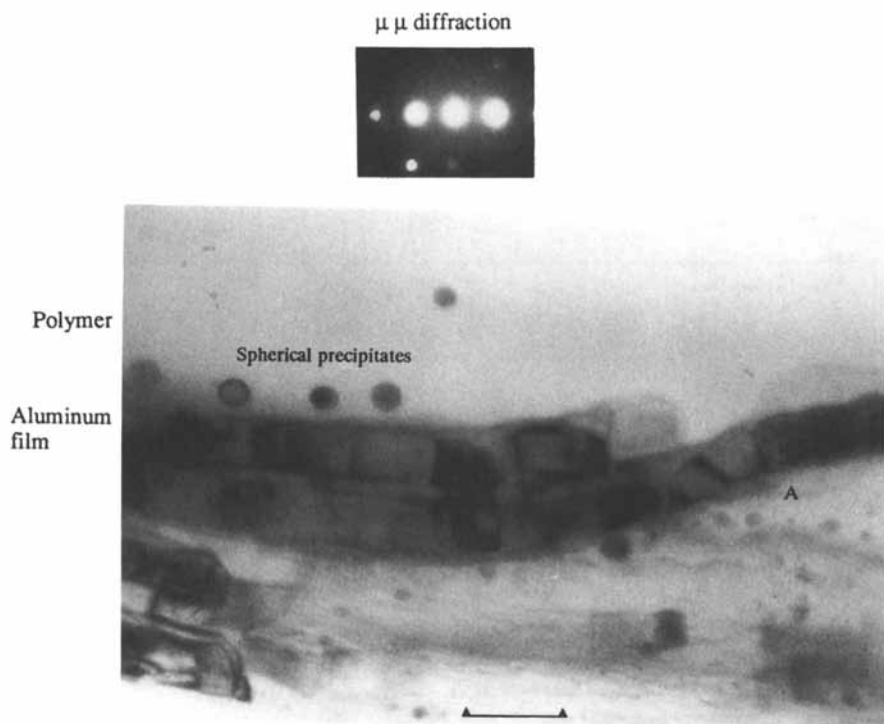
Figure1 : Morphology and structure of a low adhesion (100 g/inch) aluminum film evaporated on non treated bi-axially stretched PET.(marked is 100 nm)

because of their small size and the non stabillity of the polymer for the micro-micro diffraction spot size conditions.

Spherical precipitates in the skin of a polymer have previously been observed after the evaporation of Cu on polyimide(PI)(10). These two systems [Al/PET(sample(1)) and Cu/PI] present a low chemical interaction and a low adhesion, but the deposition rate was much lower for Cu/PI than for Al/PET (1 ML/mn compared with 50 nm/s). This behaviour has been interpreted by Le Goues and al(10) as a consequence of a poor chemical interaction between the metal and the polymer at the interface; the metal being free to diffuse in the polymer to form clusters of nearly spherical shape. However, it is difficult to compare the mechanism of formation of these precipitates because of the huge evaporation rate difference; this rate seems to be critical (Le Goues and al(10)) for the formation of these precipitates. The presence of these precipitates can only be considered as a fingerprint of a poor quality interface.

Figure 2. Schematic representation of the grain morphology of aluminum thin films deposited on PET. a) "Rod Like structure" (RLS), b) " Non Rod Like structure" (RLS).

	Film		Film
a)	Interface		Interface
	Polymer	b)	Polymer
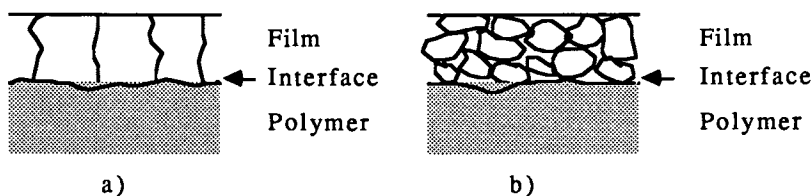
Figure 3a shows a cross section view of the sample 3. For this figure, we have focused our attention on the polymer, so the contrast of the polymer film is much better than the aluminum one. The aluminum film is located at the bottom dark part of the picture. In this high resolution polymer picture we can notice two different zones. Starting from the interface Al/PET, the first zone (thickness around 10 nm) is characterized by parallel lines separated by 1,5 nm and the second one by a usual structureless aspect of the amorphous solid. The most likely interpretation of the skin structure of the polymer could be an arrangement of the monomeric chains in the same direction giving rise to a sort of "semi-crystalline" solid. Further investigations have to be done to give more precise informations about this very interesting feature. In particular, we cannot tell with confidence if this skin structure comes from the film processing or is a consequence of the metallization, ie recrystallisation induced by the heat treatment during the deposition of aluminum (the temperature of the polymer could have risen up to 140°C during the deposition(6)).
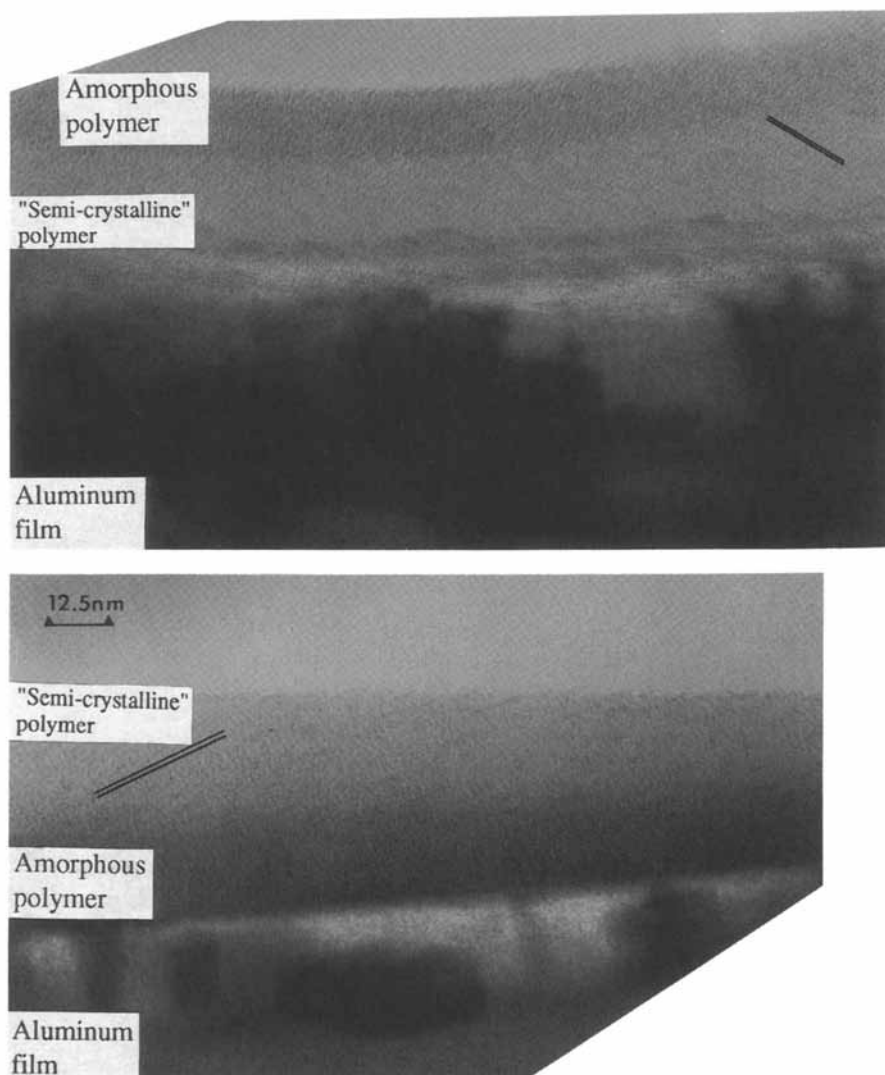
Figure 3 : "Semi crystalline" skin for the bi-axially stretched film and "Amorphous" skin for the corona treated film.(marked is 12.5 nm)

ALUMINUM FILMS ON TREATED BI-AXIALLY STRETCHED POLYMER

In this set of experiments, surface treatments have been applied to the polymer before the aluminum deposition (industrial conditions, deposition rate of about 50 nm/s, vaccum around 10^{-4} Torr). As the adhesion and the structural properties depend strongly on the PET processing (cf §A), we compare the behaviour of three laminates prepared on the same type of polymer bi-axialy stretched polymer, namely : i) an untreated film (control), ii) a film treated by corona discharge, iii) a film treated by a fluorine gas atmosphere.

These results are presented in table II. There is a moderate increase of the adhesion for the corona treated film and a huge one for the fluorine treated film. Again, a good correlation can be established for the untreated and the treated polymer between the decrease of the grain size and the increase of the adhesion.

Table II : Adhesion and structural properties of aluminum film evaporated onto corona and fluorine treated polymer

Samples / Properties	Control	Corona	Fluor treated films
Grain size (nm^2)	1230.8	872.5	472.1
Thickness of the film (nm)	30	30	30
Adhesion (g/inch)	160	220	850

Two kinds of morphology have been found in the specimens observed by cross-section TEM. The aluminum films evaporated on the control film and the corona treated film have the usual "Rod Like structure" (RLS) morphology whilst on the fluorine treated film the aluminum layer presents a " Non Rod Like structure" (NRLS) i.e. the grain boundaries are not crossing the full thickness of the metallic layer. A schematic representation of both morphologies is shown in figure 2.

Figure 3b shows a cross section view of the corona treated film. As for the figure 3a, we have focused our attention on the polymer, so the contrast of the polymer film is much better than the aluminum one. Starting from the interface Al/PET, the first

zone (thickness around 10 nm) is characterized by the usual structureless aspect of the amorphous solid and the second one by parallel line separated by 1,5 nm. The amorphization of the skin of the polymer may be due to the corona treatment of the polymer before the evaporation.

VARIATION OF DEPOSITION PARAMETERS

The metallic layers, with thickness ranging from 5 to 50 nm, were either evaporated at a deposition rate of about 50 nm/s for the industrial layers and 2 nm/s for the layers made at the Du Pont de Nemours (Luxembourg) laboratory. During the deposition, the residual pressure was around 10^{-4} Torr.

EVAPORATION TIME MODIFICATION (LABORATORY)

The conditions of evaporation are the same for all these films and we just change the thickness of the layer. Figure 4 shows typical results; in figure 4a we can see the thickness versus the adhesion and in figure 4b the average grain size versus the adhesion for the same series of films. For these two figures two domains are present: region A and B for an adhesion respectively smaller and greater than 80 g/inch. The adhesion stays constant in region A when grain size or thickness increase (figure 4a and 4b respectively) where a linear decrease of the adhesion, with the thickness, and with the grain size, is visible in region B (figure 4a and 4b).

We should mention that in the A region the aluminum film is continuous. This property is no more verified in the B region. Evidence of the discontinuity of the metallic film has been found in plane and cross section TEM micrographs. So the increase of the adhesion in region B in respect to the A region may come from the auto adhesion of the PET with the EAA which is used for the peel test. We also see that when we decrease the thickness of the film (from 10 to 3 nm), we decrease the coverage of the aluminum film on the PET and in a same way increase the auto adhesion part during the peel test.

Figure 5 shows the linear dependence between thickness and grain size. It is important to notice that this dependence can just be verified for one set of evaporation conditions and if we change just one condition (for example the flux) we will obviously modifig the linear slope dependance.

VARIATION OF THE EVAPORATION ANGLE (INDUSTRIAL)

In this series we study the influence of the angle of incidence of the metal vapour onto the PET films (table III) . Obliquely evaporated film have a much lower adhesion than the perpendicular one.

ALUMINUM SPUTTERED DEPOSITION (INDUSTRIAL)

In this experiment, we change the deposition technique of the layer, i.e. evaporation versus sputtering. Sputtered layers have a
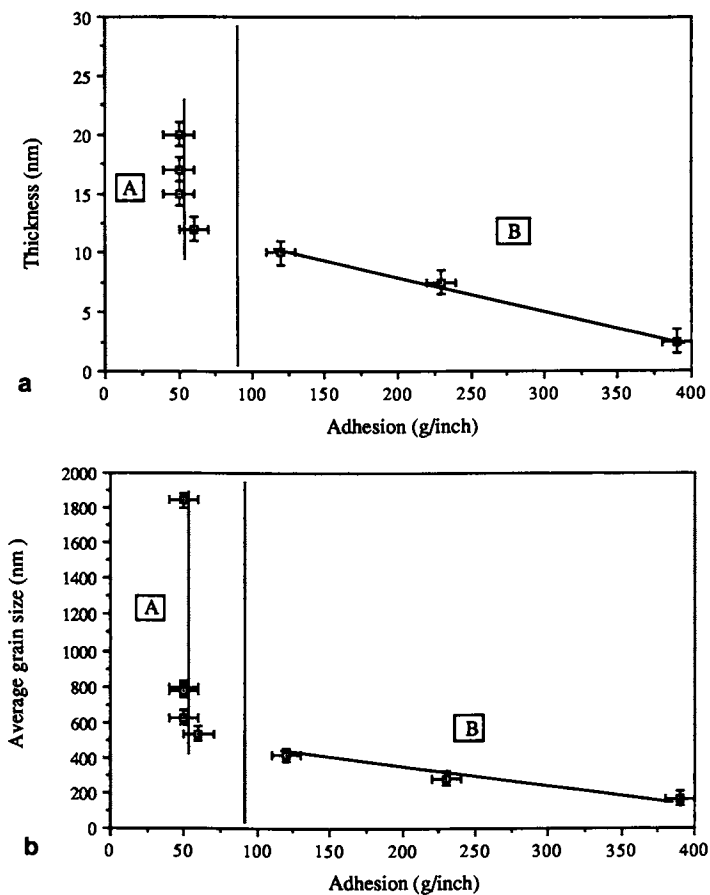
Figure 4 : a) Variation of the thickness of the aluminum thin film with the adhesion measure by peel testing. b) Variation of the average grain size of the aluminum thin film with the adhesion measure by peel testing.
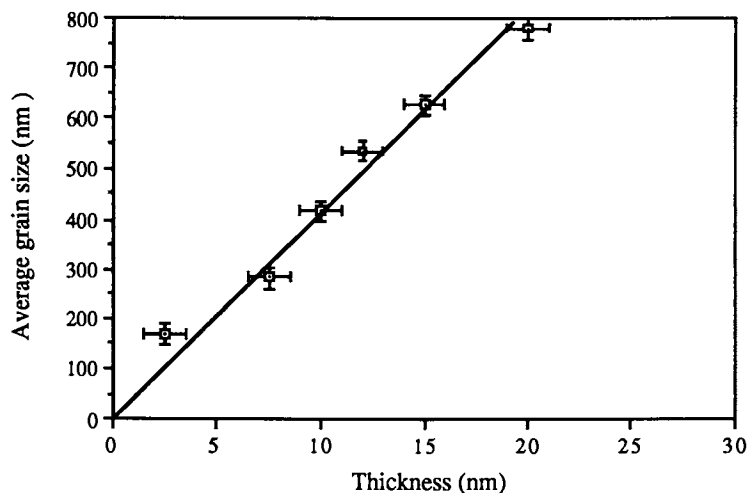
Figure 5. Linear variation between the average grain size and the thickness of the aluminum film deposited on non treated PET.

Table III : Adhesion and structural properties of perpendicular and oblique incidence evaporated aluminum onto non treated polymer

Samples Properties	Metallization	
	Perpendicular	Oblique incidence
Grain size (nm^2)	1278.0	1400.8
Thickness of the film (nm)	50	50
Adhesion (g/inch)	260	40

stronger adhesion and the small grain size again correlates with adhesion (table IV). The aluminum sputtered film and the fluorine treated film are the only two films which present a NRLS morphology.

DISCUSSION.

The main results obtained for the growth kinetics, the adhesion, and the structure and morpholy of aluminum thin films deposited on bi-axially stretched PET films are the following. (1)For a set of experimental conditions (flux, temperature, and polymer surface), the aluminum film is discontinuous up to 10 nm (island formation) and then become continue. The grain size always increases with the thickness of the aluminum film as opposeted to the adhesion which remains rather constant. (2)When the aluminum film is continuous and for one thickness of deposition, the adhesion coefficient increases when the grain size decreases. (3)We found an increase of the adhesion coefficient when the skin of the polymer is "semi-crystalline" and when the polymer is pretreated with a corona discharge. (4)The best results (for the adhesion of Al/PET) are found for a polymer treated in a fluorine atmosphere and when the deposition of the aluminum on polymer is done by sputtering.

Table IV : Adhesion and structural properties of aluminum sputtered film

Properties \ Samples	RENKER sputtered films
Grain size (nm^2)	238.3
Thickness of the film (nm)	30
Adhesion (g/inch)	700

These four points will be discussed in regard to the nucleation and growth mechanism of Al film on PET.
Even, if the growth mechanism of metallic films on metal, semi-conductor and ionic crystals, has received much attention in the recent literature(11-13) very little has been done on

amorphous films or polymer substrate. It is reasonable to think that some of the information we have on alkali halides or on MgO (i.e. weak interfacial bonding) can be applied to the polymer substrate. In all these cases the interactions, at the interface, between the metal and the substrate are always smaller than between the metal atoms and themself. This is usually what we found when we performed a peel test where the rupture usually takes place at the interface Al/PET. The fact that, for a continuous metallic layer, the adhesion coefficient is not related to the thickness tends to reinforce this last assumption.

The well known growth process of metals on substrates with weak interfacial bonding consists in the formation of nuclei, their subsequent growth, and a "liquid-like" coalescence to form successively, i) isolated 3D islands, ii) connected islands separated by channels, iii) nearly continuous film with holes and finally iv)the complete films(11). This scheme could certainly be applied to the growth of metallic layers on polymer. However we have to take into account that we have actually a "reactive" nucleation as it is usually accepted that for aluminum deposition on PET, a layer containing Al, O and C is formed at the interface(6). The consequence on the nucleation process and on the subsequent coalescence is difficult to appreciate. Earlier experiments on the influence of the gas phase during the growth of metals on metals shows that small grains are found when the evaporation is performed either in poor vacuum conditions or under a partial pressure of a reaction gas. For example, films of aluminum intentionally prepared by evaporation at a rate of about 0.5 nm/s in a partial pressure of oxygen of 5.10^{-5} torr onto an amorphous substrate at room temperature contain very small grains of mean size 3 nm(14). Likewise epitaxial growth of Co, Ni and Cu on Ag(111) has been observed when the evaporation was performed in UHV where as an "amorphous-like" deposit was obtained when performed in a conventional vacuum(15).

If we assume, for the aluminum deposited onto polymer, similar growth kinetics as we have described above, we can think that when the interaction between the metal and the polymer becomes more reactive, the adhesion which is correlated to the number of free bonds given by the polymer, will increase and the grain size will decrease. This interpretation enables us to understand the adhesion behaviour observed when the crystallinity of the skin increase or when the skin of the polymer has been changed during a corona treatment.

But the huge increase of the adhesion coefficient found after sputtering or fluorine treatment cannot be completely explained with such a model. Sputtering may be described as an ion bombardment of a metallic target which then produces atoms (neutral) and particles charged positively (ions) and negatively (ions and electrons); some of these particles, the atoms and the negative ones, are then accelerated toward the substrate (polymer). These negative particules play a very important role during the deposition of the metallic film because they may induce chemical modifications at the polymer surface (modifications of the carboxylic group) and induce charge accumulation (double layer formation). In these two cases, the

number of nucleation sites will be changed and the coalescence of the grains during the growth of the film can then be affected.

The behaviour of the fluorine treatment is much more complex. It is reasonable to think that the chemisorption of the fluorine on the carboxylic groups with formation of a strong dipole on the surface may play a very important role on the nucleation process of the aluminum film.

CONCLUSION

Aluminum was deposited onto different PET films and some of the properties (adhesion and structure) of these thin films were characterized with a Peel test and by TEM. For the deposition on a non treated polymer we find that as soon as the film is continuous, the adhesion is independant of the thickness of the film. There is also, for the same deposition conditions, a linear dependence between the thickness of the aluminum film and the mean area of the size of the grains. The number of nucleation sites should be one of the important parameters to understand the adhesion of an aluminum film evaporated onto PET. By changing the structure of the skin of the polymer with a treatment (corona, fluorine), or during the deposition (sputtering) an increase of the number of nucleation sites is induced and therefore the adhesion is increased .

ACKNOWLEDGMENTS

LITERATURE CITED

1. N. J. Chou and C. H. Tang, J. Vac. Sci. Technol. 1984, A2, 751.
2. F. S. Ohuchi and S. C, Freilich, J. Vac. Sci. Technol. 1986, A4, 1039.
3. J. W. Bartha, P. O. Hahn, F. K. Le Goues, and P. O. Ho, J. Vac. Sci. Technol. 1985, A3, 1390.
4. P. O. Ho, P. O. Hahn, J. W. Bartha,G. W. Rubloff, F. K. Le Goues, and B. D. Silverman, J. Vac. Sci. Technol. 1985, A3, 739.
5. N. J. Dinardo, J. E. Demuth, and T. C. Clark, Chem. Phys. Lett.1985, 121, 239.
6. Y. De Puydt, P. Bertrand, and P. Lutgen, Surface and Interface Analysis. 1988, VOL. 12, 486.
7. J.F. Silvain, C. L. Bauer, A. M. Guzman, and M. H. Kryder, IEEE Trans. Mag. 1986, Vol. MAG-22, No. 5, 1296.
8. C.J. Heffelinger and K.L. Knox, Science and Tech. of Polymer Films. New york, 1971; Chap.14.
9. V.V. Arslanov, and V.A. Ogarev, Kolloid Z. 1977, 89(5), 934.

10.   F.Le Goues, B. D. Silverman, and P. O. Ho <u>J. Vac. Sci.</u>
       <u>Technol.</u>1988, <u>A6(4)</u>, 2200.
11.   E. Grünbaum, <u>Vacuum</u> 1974, <u>24</u>, 153.
12.   I. Markov and S. Stoynov, <u>Contemp. Phys.</u>, 1987, <u>Vol. 28</u>, N°
       3, 267-320.
13.   B. Mutaftschiev, <u>Techniques de l'Ingénieur</u>, Paris, 1989; to
       be published.
14.   G.Deutcher, H. Feenichel, M. Gershenson, E. Grünbaum, and
       Z. Ovadyahn, <u>J. Low Temp. Phys.</u> 1973, <u>10</u>, 231.
15.   C. Gonzalez, and E. Grünbaum, <u>Proc. 5th Int. Cong. Elec.</u>
       <u>Microscopy</u> Academic : New York ,1962, Vol 1, p DD1.

Chapter 34

Chemical Bonding and Morphology of Interfaces in Aluminized Silicones from Evaporation and Sputtering

Y. Jugnet[1], J. L. Droulas[1], Tran Minh Duc[1], and A. Pouchelon[2]

[1]Institut de Physique Nucléaire de Lyon, Centre National de la Recherche Scientifique, IN₂P₃, Université Claude Bernard Lyon I, 43 Boulevard du 11 Novembre 1918, 69622 Villeurbanne Cedex, France
[2]Rhône Poulenc Recherche, Centre de Recherches des Carrières, 85 Avenue des Frères Perret, Boîte Postale 62, 69192 Saint Fons, France

Mechanism of adhesion in polymer metallization is investigated by a comparative study of in-situ Al thermal evaporation and DC sputtering under UHV conditions by XPS (X-ray Photoelectron Spectroscopy) and XAES (X-ray induced Auger Electron Spectroscopy). Core level binding energy chemical shifts, Auger parameters as well as intensity variations, are determined at different Al coverages from few Å to more than 100 Å. Direct evidence for a drastic difference in the chemical bonding and in the morphology of the interfaces between the two processes is produced. Simple deposition with abrupt interface is obtained by evaporation. On the contrary, defect creation and chemical bonding with intermixing interface take place in the sputtered films. These results are discussed as due to the higher kinetic energy of the sputtered species compared to the evaporated ones. Reactivity of polymer substrate and nature of metal deposit are also shown to play a role in metallization.

In the metallization of polymers, the characterization of the interface at atomic level is an important issue. First, the knowledge of the molecular interaction and chemical bonding between the metallic film and the substrate and that of the microscopic morphology of the interfacial region represent key routes for understanding the microscopic mechanisms of adhesion in metallized films. Second, the problem represented by the analysis of interfaces by itself is a formidable challenge for analytical chemistry, so far it has not been resolved for buried interfaces. Surface analysis techniques such as XPS (X-ray Photoelectron Spectroscopy), UPS (Ultraviolet Photoelectron Spectroscopy), AES (Auger Electron Spectroscopy) and HREELS (High Resolution Energy Electron Spectroscopy) combined with in situ metal deposition within controlled UHV conditions have been shown to be a

much valuable methodology to address the interface problem in metallizing process. Particularly XPS, in use in this work, presents many analytical capabilities for quantitative analysis and chemical state determination of prime interest for such investigations.

The bonding of metals onto polymer surfaces has received considerable attention these last few years, especially with polyimide materials. Interfacial reactions are quite dependent on the nature of the metallic deposit. For instance Ag (1), Cu (2-3) and Pd (4) do not react with polyimide while Cr (1, 3-5), Ni (1) and Ti (6) do easily react.

The specific Al-polymer interfaces have been less extensively studied and with again emphasis on polyimides (7-9). Among the two commonly used deposition processes, most studied interfaces were grown in situ by thermal evaporation (1-8) and only few by sputtering (9,10). This work, to our knowledge, presents the first comparative study of the two deposition processes. Sputtered films are in general known to exhibit better adhesion than thermal films. This can tentatively be explained by difference in the chemical interaction between the film and the substrate, together with difference in the intermixing mechanisms at the interface. These differences are ascribed as due to the energy distribution of the deposited metal atom peaking at higher energy for sputtered species. This work was prompted to investigate experimentally this issue.

The selected system is aluminum deposited onto a silicone type polymer (polyvynil trimethoxysilane) by thermal evaporation and DC sputtering with controlled coverages allowing kinetics study. The informations we look for are the chemical bonding and the morphology at the interfaces and XPS and XAES appear to be most suitable techniques for pursuing these objectives. Aluminized silicones are found in this work to present interfaces very different between the two deposition processes according to the aforementioned scheme. Preliminary results on aluminized PET (polyethylene therephtalate) show however a more complex situation where chemical interaction is observed for both evaporation and sputtering. Furthermore, Au does not react with silicone whatever the deposition technique. Thus the reactivity of both polymeric substrate and metal deposit appears to be an important factor.

The remaining of this paper is organized as follows : Section II concerns experimental details and Section III briefly reviews the theoretical frame work for interpreting the data of Section IV. In Section V we discuss the results with a conclusion indicating direction for future work.

EXPERIMENTAL

Experimental data are obtained using a Vacuum Generators ESCA III spectrometer equipped with a dual Al/Ag X-ray source. The base pressure is 10^{-10} mbar in the spectrometer. Al depositions are made in the attached preparation chamber with a residual pressure in the 10^{-9} mbar range, by thermal evaporation or sputtering as displayed in Figure 1.

For the evaporation experiment, an Al wire is placed in a V shape tungsten filament heated through Joule effect. The Al wire is first outgased for a few minutes before condensing the evaporated Al onto the polymer film which is located about 8 cm apart from the Al source.
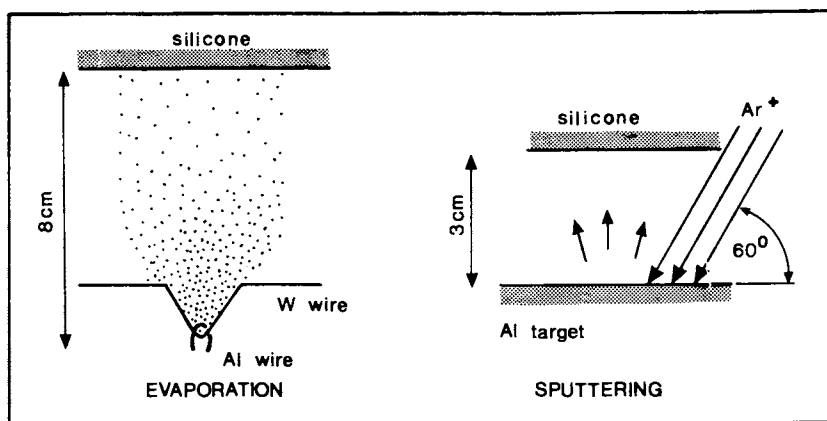
Fig. 1 Geometric experimental arrangement for evaporation and sputtering.

The sputtering technique consists in bombarding an Al target with Ar^+ ions accelerated to 5 KeV. The Ar pressure is in the 10^{-5} mbar range, and the target current measured on the Al foil is kept to 40 μA. Once the Al foil is cleaned by Ar^+ ion sputtering for 30 mn, then the polymer film is positioned in front of the Al foil to intercept the sputtered species.

The crosslinked ViSi $(OCH_3)_3$, silicone type substrates were spread with a microslide on a mechanically polished copper sample to form several tens of μm thick films. Then, they are transferred into the spectrometer chamber without passing through the atmosphere.

Measurements have been made on both photoelectron peaks and corresponding X-ray induced Auger peaks excited respectively by Al Kα (hν = 1486.6 eV) and Ag Lα (hν = 2984 eV) X-ray sources. Detection angle was 45° for all the measurements. Charging effects were found to be small in the case of these thin films and no neutralization by auxiliary flood gun was necessary. Core level energy shifts and peak areas have been determined on Si2p, Al2p, C1s and O1s. Auger parameters at the various coverage rates are determined from Si KLL and Al KLL Auger lines. Auger chemical shifts are larger than those in ESCA and yield better chemical resolution on one hand and on the other hand Auger parameter shifts are free of the experimental uncertainties encoutered with insulating polymeric materials such as charging effect and reference level shift. Auger parameter can produce additional information on the long range interaction between the deposited film and the substrate as well, as will be shown in this work.

In situ film growth allows much flexibility for investigating specifically any parameter of importance in the process. For instance coverage dependance studies are much informative for investigating the interaction mechanism.

THEORETICAL BACKGROUND

In the following, we just remind a few theoretical backgrounds we shall use to interpret our data in terms of chemical shift and deposited metal thickness.

XPS investigations of wide band gap insulating materials meet experimental difficulties arising from charging effects and reference level position. For metallized polymers, in addition, charging and Fermi level position are expected to vary with metal coverage. Happily, these shifts are found to be small. Furthermore, the extra-atomic relaxation energy released by screening the final core hole state, which actually contributes to XPS and Auger energy, is also depending on the electronic properties of those metal polymer interfaces. Thus, the photoelectron and Auger energies may here be determined with less accuracy and their shifts difficult to interpret in order to extract unambiguous chemical bonding information.

Briefly, the XPS chemical shift ΔE_b measured as the difference of core hole binding energy between two chemical states is defined by (11) :

$$\Delta E_b = \Delta \epsilon - \Delta R_{ea}$$

where $\Delta \epsilon$ is the initial state energy shift and ΔR_{ea} is the extra-atomic relaxation energy shift in the final core hole state. Auger transitions

because of their two hole final states present larger relaxation shift as shown in the expression relating the Auger chemical shift ΔE_A :

$$\Delta E_A = -\Delta\epsilon + 3 \Delta R_{ea}$$

So Auger shifts are generally larger than the corresponding ESCA shifts. The so-called Auger parameter defined as the kinetic energy difference between related Auger and XPS lines in the same sample is a very usefull quantity since experimental uncertainties due to charging and reference level problems are cancelled in the difference. The physical meaning of the shift of this parameter is obtained from the previous relations as :

$$\Delta\alpha = 2 \Delta R_{ea}$$

Rather than the afore defined α parameter, of more convenient use is the so called modified Auger parameter α', defined as the sum of α plus the photon energy. In the following, we shall use this modified Auger parameter.

The deposited Al amount is tentitatively expressed in terms of film thickness as follows. Let us consider an Al overlayer of constant thickness d on top of an infinite silicone substrate. The measured Al2p signal intensity I_{Al} can be expressed by :

$$I_{Al} = I_{Al}^\infty \left(1 - e - \left(\frac{d}{\lambda_{Al} \sin\theta}\right)\right)$$

where I_{Al}^∞ corresponds to the intensity which would be measured on an infinite thickness Al substrate, $\theta = 45°$ is the detection angle, λ_{Al} is the mean free path of the Al2p photoelectrons. Accordingly, the Si2p signal intensity I_{Si} issued from the silicone is :

$$I_{Si} = I_{Si}^\infty \; e - \left(\frac{d}{\lambda_{Al} \sin\theta}\right)$$

where I_{Si}^∞ corresponds to the intensity which would be measured on an infinitely thick clean silicone substrate. For a given Al coverage, assuming a uniform layer on a substrate with a flat surface, which is a crude approximation, we can extract the thickness d following :

$$d = \lambda_{Al} \sin\theta \; Ln \left(K \; \frac{I_{Al}}{I_{Si}} + 1\right)$$

where K is the ratio $I_{Si}^\infty / I_{Al}^\infty$ related to infinite thickness substrates of silicone and aluminum. λ_{Al} is estimated to the square root of Al2p photoelectron kinetic energy.

RESULTS

The results of this study are divided into three sections : the first section is related to the interface obtained by thermal evaporation, the second one describes the interface obtained by sputtering. Comparative results will be discussed in the third section. The corresponding spectra are reported in Figures 2, 3 and 4 for evaporation, and in Figures 5, 6
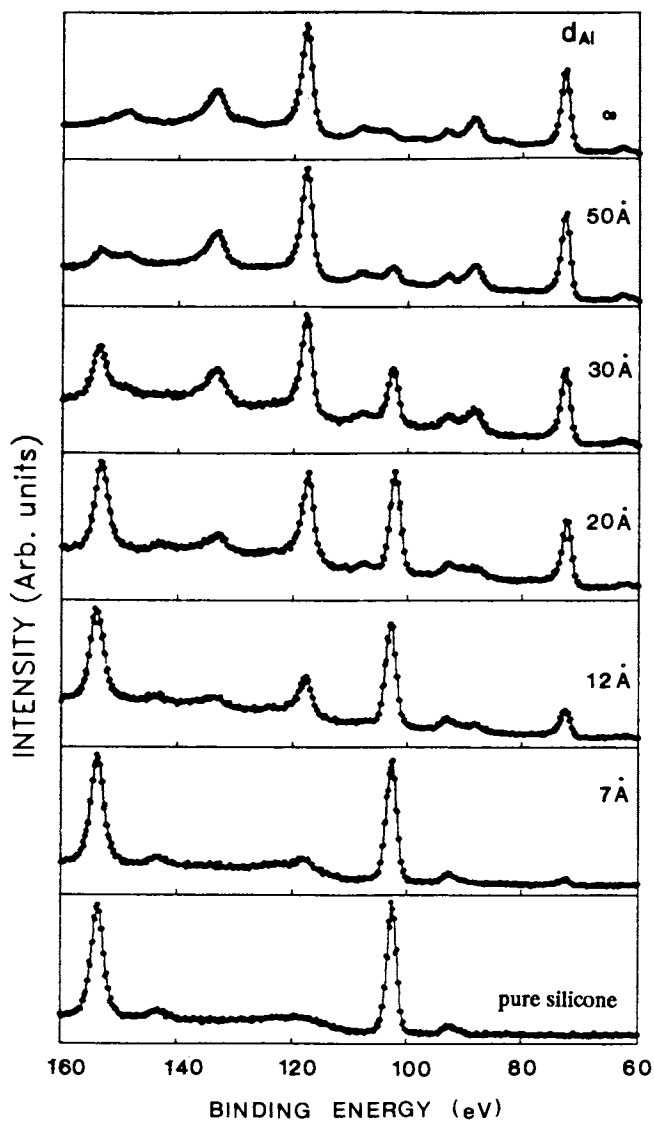
Fig. 2   Al and Si 2s and 2p core level low resolution spectra at various rates of evaporated Al on silicone.
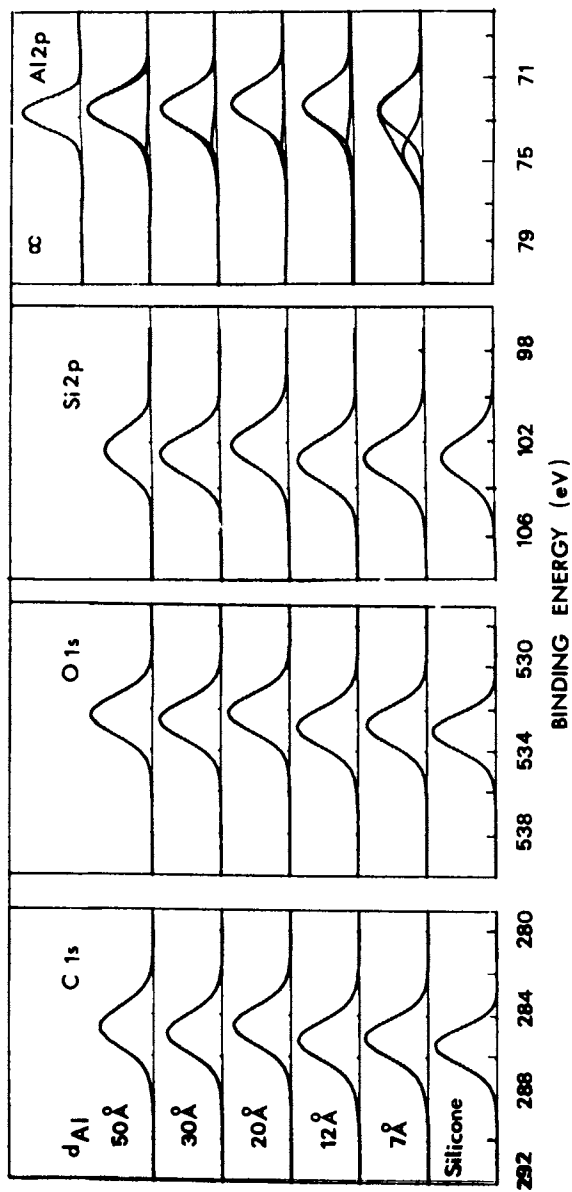
Fig. 3 C1s, Si2p and Al2p core level high resolution spectra at various rates of evaporated Al on silicone.
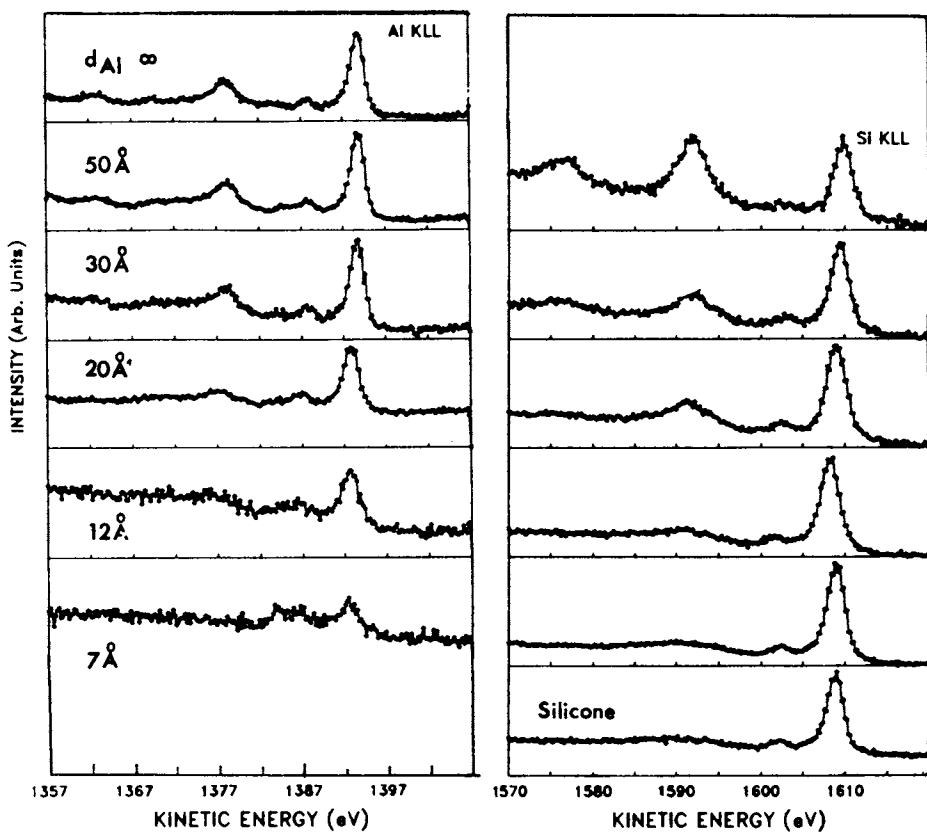
Fig. 4 Al KLL and Si KLL X-ray induced Auger peaks at various rates of evaporated Al on silicone.
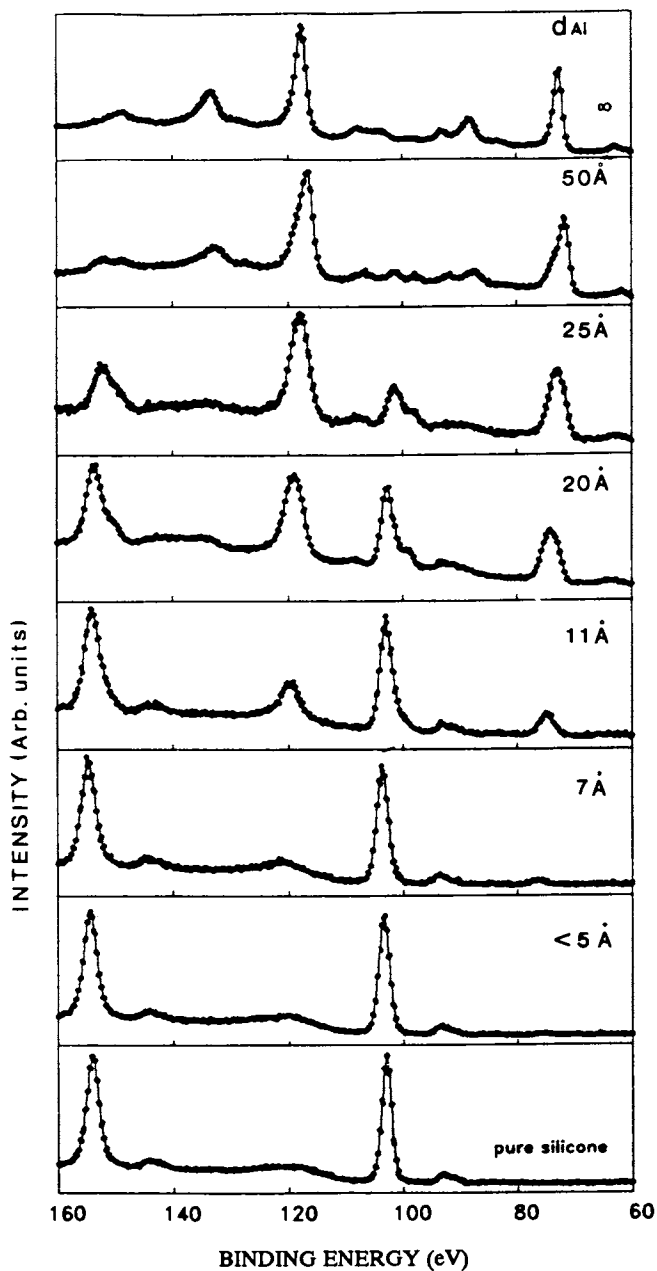
Fig. 5 Al and Si 2s and 2p core level low resolution spectra at various ratios of sputtered Al on silicone.
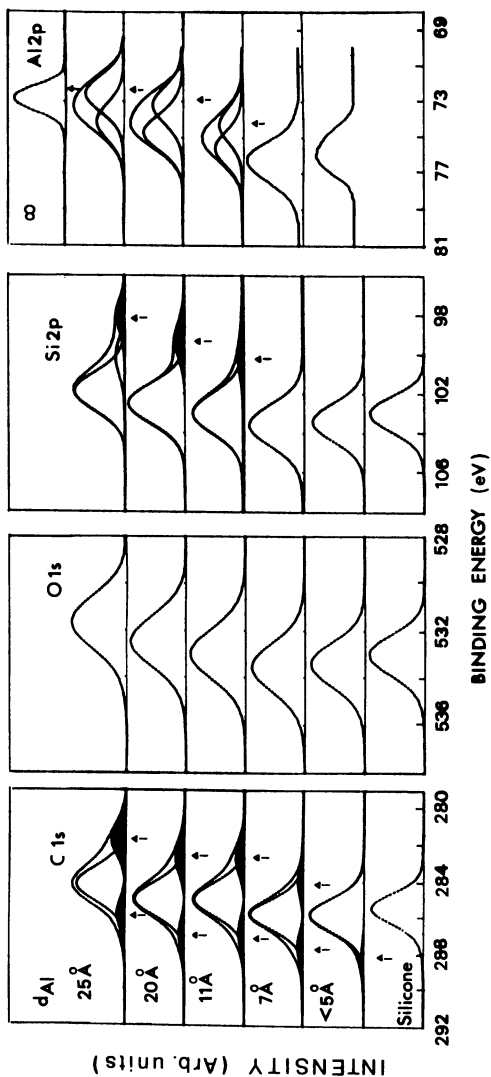
Fig. 6 C1s, Si2p and Al2p core level high resolution spectra at various rates of sputtered Al on silicone.

and 7 for sputtering respectively. Pure silicone spectra as well as those obtained from a thick (> 100 A) Al layer are reported as reference spectra. No correction for charging effect has been performed for these data.

THERMAL EVAPORATION

Figure 2 reports extended scans showing the Si2s, 2p and Al2s, 2p core levels as a function of Al thickness. The uncovered silicone spectrum displays the main structures obtained by exciting with an unmonochromatized Al Kα X-ray source the Si2s and Si2p core levels at 154.1 eV and 103.0 eV binding energy respectively. Al2s and Al2p core levels appear at 118 eV and 73 eV binding energy respectively. Their intensities increase with Al coverage. The Al chemical form will be examined with more details later on in the higher resolution spectra, but already we point out on this extended scan that even at very low thickness, are observed the Al characteristic plasmon loss structures at 15.5 eV and 31 eV higher binding energy apart from the main Al peaks. These plasmon losses are indicative of the metallic nature of the aluminum film, as stressed out on the top of Figure 2 in the case of a thick Al layer. By contrast with the results presented in Section IV-2 for sputtered films, evaporated films thus exhibit strong metallic properties at very low coverage.

The signals for C1s, O1s, Si2p and Al2p core levels are shown in Figure 3. The peak position and full width at half maximum (FWHM) for C1s, O1s and Si2p are respectively 285.3 eV (2.0 eV), 533.0 eV (2.0 eV) and 102.9 eV (2.1 eV) for pure silicone. With Al evaporation we do not observe any change on C1s, O1s or Si2p core levels, no chemical shift nor line shape modification are detected, the very small shift in peak position ($\sim$ 0.5 eV) is ascribed as due to charging effect. However at very low Al coverage (thickness < 7 A), Al2p peak is splitted into two components. The main component at 72.9 eV binding energy is characteristic of metallic aluminum. The other component occurs at 74.5 eV and may be assigned to an oxidized form of Al. This component cannot be ascribed to Al_2O_3, since the chemical shift measured here (1.6 eV) is lower than the one expected for pure Al_2O_3 (2.7 eV). Instead, it has rather to be regarded as a suboxide formed through Al-O bonds.

SiKLL and AlKLL Auger peaks measured with Ag Lα X-ray source are reported in Figure 4 as a function of Al coverage. The SiKLL spectrum remains unchanged as compared to pure silicone, the structures appearing at 1592 eV and 1577 eV kinetic energy are due to Al1s level (main peak + first associated plasmon loss) excited by the Ag Lβ_1 line. The silicon Auger parameter α'_{Si} measured on pure silicone is 1711.6 eV ; after 7 A of Al deposit, it remains unchanged at 1711.5 eV. For Al thicknesses of 12 A and 20 A, its value drops significantely to 1710.8 eV, then for larger deposits, it recovers a value of 1711.6 eV. This minimum value of α' is observed at the same time as the appearance of characteristic plasmon losses (see figure 2).

At very low Al coverage, the Al KLL Auger peaks display two components at 1392.0 eV and 1384.6 eV kinetic energies assigned respectively to metallic aluminum and interfacial aluminum suboxide. The extent of this Auger chemical shift (7.4 eV, i.e even larger than in pure Al_2O_3 ($\sim$ 5.4 eV)) can be due to extra-atomic relaxation effect

which is smaller for interfacial aluminum as compared to metallic aluminum. Differential charging is expected to be very small and can be disregarded for explaining the observed shift. The Auger parameter for the metallic component is α'_{Al} = 1464.9 eV i.e less than the one measured on the thick Al layer (1466.2 eV), and α'_{Al} = 1459.1 eV for the interfacial Al suboxide. When increasing the Al coverage, the interfacial component vanishes, since it is attenuated by the Al metallic overlayer, and the metallic component increases with appearance of plasmon losses. α'_{Al} keeps a value of 1464.9 eV up to an Al coverage of 20 A, then it goes up to a value of 1466.2 eV characteristic of metallic aluminum (12).

To summarize, evaporation leads to an abrupt interface with very limited chemical interaction, mainly through Al-O-Si or Al-O-C bonds. The so-formed suboxide is limitated to about two layers. However a long range order interaction may occur between the film and the substrate as observed from Auger spectra.

SPUTTERING

Extended spectra displaying Al2s, 2p and Si2s, 2p are reported in Figure 5 at various sputtered Al coverages including pure silicone and a thick Al layer for comparison. Al thicknesses are of the same order as those previously reported for thermal evaporation (Figure 2). Two major differences appear by comparing spectra obtained with both techniques. First, the plasmon losses observed on Al peaks appear for an Al thickness > 25 A when the interface is obtained by sputtering, while they appear at thicknesses as low as 7 A in the case of thermal evaporation. Second and more important, we notice drastic modification of the Si2s, 2p and Al2s, 2p peak line shapes. This is more clearly evidenced in Figure 6, where are reported the high resolution C1s, O1s, Si2p and Al2p spectra.

At low Al coverage (d < 5 Å), Al2p core level appears as a small and broad (FWHM = 3.4 eV) peak with at least two components characteristic of different oxidized forms. No change is observed on Si2p level whereas we notice a slight broadening of the O1s peak (FWHM = 2.2 eV instead of 2.0 eV on pure silicone) and occurence of a new component on the C1s spectrum on the high binding energy side. This C1s component at 287.3 eV binding energy is assigned to C-O bonding.

From 7 Å Al deposit and further, the C1s peak is strongly modified with appearance of a third component at 283 eV characteristic of a carbide species. Parallely, we observe the appearance of metallic aluminum superimposed to the interfacial Al component and these both components are present together even at high coverages. Meanwhile we observe the appearance of a reduced form of silicon, an increase of the carbide species observed on the C1s peak and a broadening of the O1s spectrum as well. For an Al thickness of 25 Å, Si2p level can be resolved into three components at 99.8 eV, 101.0 eV and 102.9 eV binding energy. The main component at 102.9 eV is characteristic of the silicone. The low binding energy component is due to elemental silicon issued from Si-O broken bonds and the 101.0 eV component is assigned to a suboxide specie. The O1s peak broadening presumably is due to a superposition of different oxidized species such as the Al and Si suboxides.

The SiKLL and AlKLL$_o$Auger peaks are reported in Figure 7. For Al coverages larger than 11 A, we notice a broadening of the main SiKLL Auger peak due to the occurence of a silicon suboxide kind as well as the appearance of a shoulder at 1617 eV kinetic energy characteristic of elemental silicon. The AlKLL Auger peak evolution as a function of Al coverage is the same as the one previously reported for Al2p core level : it shows the presence of oxidized aluminum at low coverage and the appearance of metallic aluminum for Al thicknesses larger than 11 A. Both Al forms are still present at a thickness of 25 A.

The silicon Auger parameter α'_{Si} is 1711.3 eV at low Al coverage. As previously noticed in the case of thermal evaporation, it drops to 1710.3 eV for Al thicknesses ranging from 11 to 20 A and then it recovers the value 1711.6 eV. The corresponding value for the elemental form of silicon observed at high coverage is 1715.5 eV, in close agreement with data reported in the litterature (12) for pure silicon.

The Al Auger parameter α'_{Al} behaves differently. At low coverage α'_{Al} = 1458.6 eV. Its value increases monotonously up to 1462.2 eV for an Al thickness of 25 A, while it kept a fixed value in the evaporation experiment. α'_{Al} measured on the metallic component is 1466.2 eV.

All of these drastic modifications observed in the sputtering experiment indicate a strong interaction between Al and silicone with complexe chemical bonding between Al, O, Si and C atoms and a diffuse interface with intermixing over several tens of A.

DISCUSSION

The results produced in the previous sections show very clearly that the interaction taking place through the aluminum//silicone interface differs between evaporated and sputtered films. By evaporation, a sharp interface corresponding to a simple metal deposition is obtained, Al plasmons are detected at very low Al coverage with thickness ~ 7 A, i.e 2-3 layers. This is a strong evidence for the metallic nature of the Al films. The same result is observed for sputtered films only after 25 A. In other words, the Al evaporated atoms do no longer chemically react with the polymer substrate when this latter is covered by 2-3 monolayer thick Al film. The chemical interaction between Al atoms and the substrate is restricted to the nearest neighbour atoms at an abrupt interface. This interaction probably takes place through Al-O-Si or Al-O-C bonds, as indicated by the Al shift observed at first stage of coverage. The substrate Si or C signals are apparently not indicative of this interaction presumably because the shift between silicone and some mixed Al-Si oxidized form is expected to be very small and also because the signal of the interfacial Si and C atoms is masked by the Si bulk substrate signal much more intense.

The interface obtained by sputtering is not abrupt but on the contrary, it is a region of strong mixing of Al with Si, O and C atoms over a depth of several tens of A, as observed from the chemical shifts. This finding is also evidenced by another type of measurements related to the intensity measurements. Figure 8 shows for instance, the comparison of the variation of Al/O and C/O atomic ratios determined for the two types of interfaces as a function of Al thickness. The Al/O ratio increases with a smaller slope for sputtered interfaces when compared to evaporated interfaces. Furthermore, the O/C ratio is constant (= 0.55) for evaporated film indicating that the attenuation of
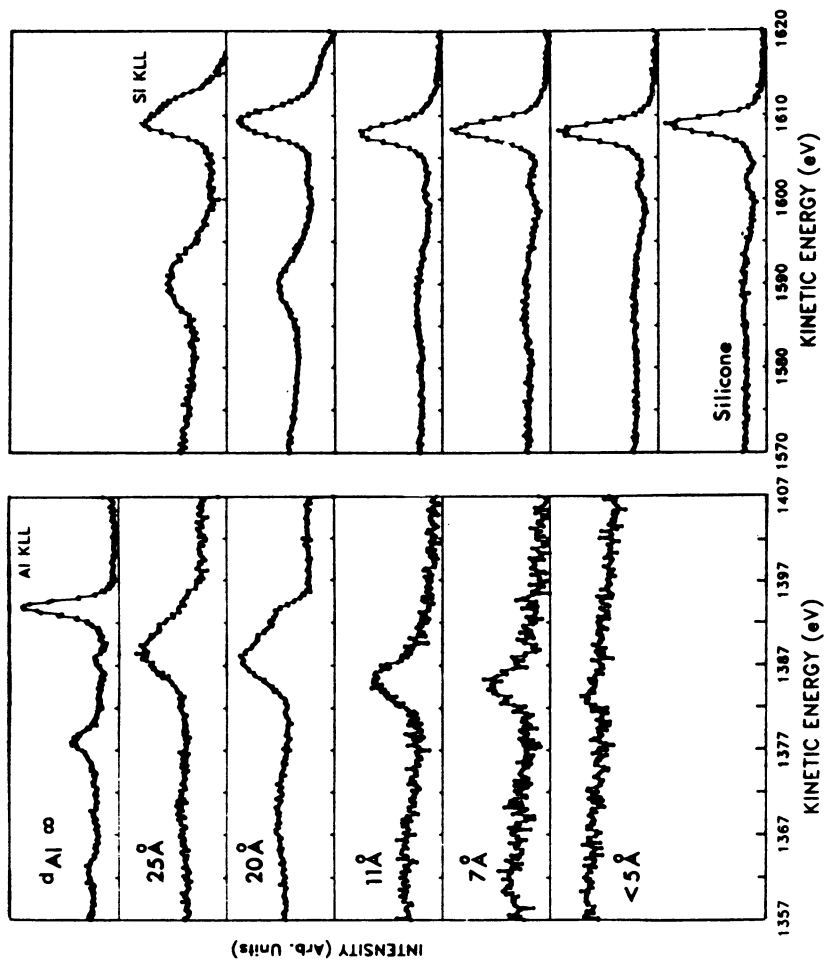
Fig. 7 Al KLL and Si KLL X-ray induced Auger peaks at various rates of sputtered Al on silicone.
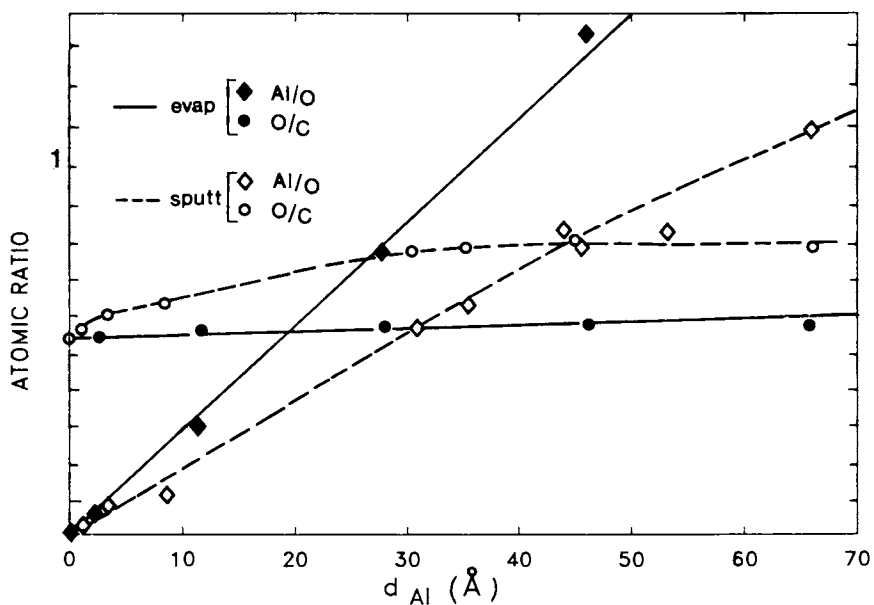
Fig. 8 Difference in the Al/O and O/C atomic ratios determined on both interfaces as a function of Al thickness.

O and C signals from the substrate by Al layer is identically constant. These results show that the silicone substrate is simply covered by evaporated Al. By contrast, this O/C ratio increases up to 0.8 for sputtered Al films, which indicates the presence of O atoms in the Al films at coverages as high as 25 A and more. These O atoms are coming obviously from the polymer substrate, any contamination from the residual gas can be safely disregarded.

At this point of the discussion, we would like just to mention the different behaviour of the modified Auger parameter between the two growth modes : the evaporated films exhibit a singularity for both Al and Si KLL transitions around Al thicknesses 10-20 A while the sputtered films show this singularity only for α'_{Si} with a monotonous increase of the α'_{Al} parameter. We have no present explanation for these observations, but we want to present them as an experimental evidence for differences in long range electronic properties of these interfaces.

The different behaviour observed on these two considered interfaces finds actually its origins in the energetics involved in the two different deposit processes. Atoms issued from thermal evaporation are deposited on the substrate with a thermal energy $\frac{3}{2}$ kT which is about 0.13 eV, T being the Al melting point. The kinetic energy distribution of atoms issued from sputtering is broad with a maximum at $U_o/2 = 1.7$ eV (U_o being the surface cohesive energy of Al in that case), with a high energy tail up to 100 eV. At this point, we can safely disregard any effect due to contingently backscattered Ar^+ ions, first since no implanted Ar has been detected and second, in the same conditions, sputtered Au atoms do not react with silicone (13).

The deposition energy involved in sputtering is thus higher than the one involved in evaporation by one order or more. This deposition energy in sputtering is also larger than the range of chemical bonding energy and can induce chemical defects and bond breaking with subsequent chemical reactions in the polymer surface. The chemical defects created by sputtered Al atoms are observed on Si with the formation of reduced Si forms going from suboxide to elemental Si and as well on C with the formation of both carbide and some oxidized species. Al atoms are found in these sputtered interfaces as a mixture of metal and oxides.

If in the case of aluminized silicone we were able to evidence a drastic difference between sputtering and evaporation, it happens not to be the case for aluminized PET (13). Our preliminary results on this latter polymer indeed show no marked differences between the two deposition processes, both giving strong chemical interaction. By contrast we have also observed that with noble metals such as Au, no chemical interaction is taking place with silicone substrate with both deposition processes. This tells us that the nature of the polymer substrate and of the metal are most important for the interfacial and adhesive properties. The fundamental parameter seems to be the reactivity of both constituents of the interface. It has been confirmed by Pireaux et al. that the carboxylic function is one of the most reactive surface entity (14) and indeed for PET, the adsorption site for the Al atoms is found to be the carboxylic function (13). During this interaction, Al is oxidized and the diffusion of O into the Al film can occur.

The Si-O and Si-C bonds are stronger than the chemical stability of

carboxylic function, so at a first level of interpretation Si-O or Si-C are expected to react with Al atoms only if the activation energy is high enough for breaking these bonds, which is the case of high kinetic energy sputtered atoms and not the evaporated atoms. However an interaction limitated at the initial stage of the evaporation deposition is observed but this reaction does not propagate further with Al deposition because the kinetic energy of evaporated atoms is not high enough to induce chemical mixing as sputtered atoms do. So evaporation forms then either a uniform metallic layer or metallic agregates. In the case of PET, the reactivity of caboxylic function is so high that it may induce a disruption of the Al overlayer. The interaction does not require high kinetic energy to propagate and intermixing interface can take place even for low energy evaporation.

CONCLUSION

We have shown in this work that the Al//silicone interfaces present very different properties according to the metallization process. By sputtering are obtained thick chemical and intermixing interfaces in contrast with the abrupt interface grown by evaporation. Oxidation of the aluminum involving oxygen atoms from the substrate plays an important role. In the present case of silicone, to break the tigth Si-O or -CH_3-O bonds and etablish Al-O-C or Al-O-Si bonds requires high energy sputtered atoms while the evaporated atoms have too low energy to induce chemical defects and intermixing. Interfaces grown by sputtering present more complex chemistry than those by evaporation where no carbide species is observed for instance.

   With more reactive polymer surfaces such as with carboxylic acid group in PET, Al deposited atoms can react with the polymer surface and produce thick chemical interface whatever their deposit energy. By contrast no chemical interaction is observed between deposited Au and silicone substrate for either sputtering or evaporation. These observations open a quite exciting investigation field where the chemical properties of the interface at an atomic level should be studied by controling the important parameters of the metallization such as deposition energy, reactivity of the substrate, reactivity of the metal atoms... and correlated with macroscopic properties such adhesion tests.

LITERATURE CITED

1.   Chou, N.J.; Tang, C.H. J. Vac. Sci. Technol. 1984, A2, 751-755
2.   Freilich, S. C.; Ohuchi, F. S. Polymer 1987, 28, 1908-1914
3.   Sanda, P. N.; Bartha, J. W.; Clabes, J. G.; Jordan, J. L.; Feger, C.; Silverman, B. D.; Ho, P. S. J. Vac. Sci. Technol. 1986, A4, 1035-1038
4.   Dinardo, N. J.; Demuth, J. E.; Clarke, T. C. Chemical Physics Letters 1985, 121, 239-244
5.   a) Jordan, J. L.; Kovac, C. A.; Morar, J. F.; Pollak, R. A. Phys. Rev. 1987, B36, 1369-1377.
     b) Jordan, J. L.; Sanda, P. N.; Morar, J. F.; Kovac, C. A.; Himpsel J. F.; Pollak, R. A. J. Vac. Sci. Technol. 1986, A4, 1046-1048
6.   Ohuchi, F. S.; Freilich, S. C. J. Vac. Sci. Technol. 1986, A4, 1039-1045

7. Ho, P. S.; Hahn, P. O.; Bartha, J. W.; Rubloff, G. W.; LeGoues, F. K.; Silverman, B. D. J. Vac. Sci. Technol. 1985, A3, 739-745
8. Pireaux, J.J.; Vermeersch, M.; Grégoire, C.; Thiry, P. A.; Caudano, R. J. Chem. Phys. 1988, 88, 3353-3362
9. Vasile, M. J.; Bachman, B. J. J. Vac. Sci. Technol. 1989, A7, 2992-2997
10. De Koven, B. M.; Hagans, P. L. Applied Surface Science 1986, 27, 199-213
11. see for exemple Wagner, C. D. in Handbook of X ray and ultraviolet Photoelectron Spectroscopy; Briggs, D.,Ed.; HEYDEN: London, 1977, Chapter 7.
12. Wagner, C. D.; Passoja, D. E.; Hillery, H.F.; Kinisky, T. G.; Six, H. A.; Jansen, W. T.; Taylor, J. A. J. Vac. Sci. Technol. 1982, 21, 933-944
13. Droulas, J. L.; Jugnet, Y.; Tran Minh Duc to be published
14. a) Pireaux, J. J.; Vermeersch, M.; Degosserie, N.; Grégoire, C.; Novis, Y.; Chtaib, M.; Caudano, R. in Adhesion and friction, Springer Series in Surface Science
    b) Grunze, M.; Kreuzer, H. J. Ed.; SPRINGER VERLAG: Berlin, Heidelberg, 1989, Vol 17.

<center>Chapter 35</center>

Polyetherimide Surfaces Chemically Treated To Improve Adhesion to Electroless Copper

<center>Donald F. Foust and William V. Dumas[1]</center>

<center>Corporate Research and Development, General Electric Company,
P.O. Box 8, Schenectady, NY 12301</center>

A method for reliably obtaining 150-250 g/mm peel strength between glass-filled ULTEM polyetherimide surfaces and electroless copper is described. Unlike existing commercial technologies for metallizing plastics which rely on the swelling of the polymer followed by the etching of mechanical anchors with strong oxidizers such as chromic acid, this new method utilizes a chemical bond between the copper and plastic surface. The bulk properties of the plastic substrate are unaffected by the new system. Through a series of chemical treatments, the outer layer of ULTEM resin (less than 10 microns) is removed, the new surface is cleaned, a chemical with the ability to improve adhesion is applied, and the sample is metallized with electroless copper. SEM/XPS analyses reveal the changes that occur during each step of the sequence. A broad class of adhesion promoting materials is also described.

The production of printed circuit boards has become a well established industry, primarily relying on sheets of copper clad glass-epoxy laminate as the base. Usage of injection moldable engineering plastics as dielectric materials offers numerous advantages [1-2]. Plastics such as General Electric's ULTEM polyetherimide have a reduced dielectric constant, increased glass transition temperature, lower Z axis expansion and a reduced coefficient of thermal expansion in comparison to glass-epoxy composites. In addition to improved properties of the substrate, the plastic can be molded into various three dimensional shapes. This design flexibility enables the plastic base to be more than just the dielectric material holding electrical circuitry; now structural ribs, component supports and mounting features can be incorporated into the circuit device, reducing assembly costs as well as parts inventory. Creation of through holes and via can be accomplished during molding thus eliminating the need for drilling and deburring. The holes can be accurately reproduced with each

[1]Current address: General Electric Armament & Electrical Systems Department, Burlington, VT 05401

molding. Tapered holes are also a design option with molded circuit boards, enabling easier assembly of through hole components.

The manufacture of a three-dimensional circuit device from a molded plastic such as the demonstration part shown in Figure 1 differs from the traditional printed circuit board. Different imaging techniques are required due to the three-dimensional features of the devices. In addition, the metal comprising the traces on the surface of the substrate are now deposited rather than formed from the laminated copper foil.

A number of novel techniques of producing conductors on plastic bases have been proposed. The use of photo-sensitive catalysts [3], recessed circuitry [4], laser decomposition of the plastic to produce electrically conductive carbon [5], laser induced deposition of metals [6], and the screen printing of conductors [7] have been examined.

Ahesion of the deposited metal to the substrate is critical to the integrity of the device. Several theories have been developed to explain the bonding of the metal to the plastic including physical and chemical interactions [8].

Early adhesion work focused on techniques developed for the plating of acrylonitrile - butadiene -styrene substrates [3] using a roughened plastic surface for physical bonding. Chromic acid solutions were used to create micropores on the surface of the plastic. The use of organic solvents to swell the plastic surface prior to etching were found to enhance the etching process [9,10]. With the development of more chemically resistant plastics, more rigorous swelling and etching treatments were required in order to produce a microporous surface suitable for metallization. Variability in molding conditions across the part brought another factor to the forefront, variable molded-in stresses. Plastic under differing stress reacts with varying degrees to the swelling solvent. This affects the amount of etching which leads to variable adhesion of the metal to the plastic.

Figure 2 is a cross section of a copper-plated sample of a glass- filled ULTEM resin pretreated with swellant and chromic acid. Cracks from the swell and etch processing extend deep into the plastic ($>300\mu$). Such a treatment affects the bulk properties of the plastic. As shown in Table I, reduction in mechanical and electrical properties occur to the plastic treated with swell and etch chemistry. Etching, extensive enough to cause sufficient adhesion, results in an irregular plastic surface. This may translate into a rough metallized surface (Figure 3). Subsequent assembly processes such as wire bonding and the surface mounting of components may be adversely affected. Still another method of etching plastics involves the use of reactive gases [11-12]; however, the production of large numbers of complex 3-D shaped plastic circuit devices makes this approach unattractive.

A number of inventions dealing with the chemical treatments of polyimides to improve adhesion to deposited copper have been described [13-16]. In these cases, a chemical modification of the plastic is believed to occur. The use of organic swellants and strong etching oxidants such as chromic acid are not required. A chemical process for obtaining high peel strengths between polyetherimide surfaces and copper without the use of swell and etch techniques is described in this work.
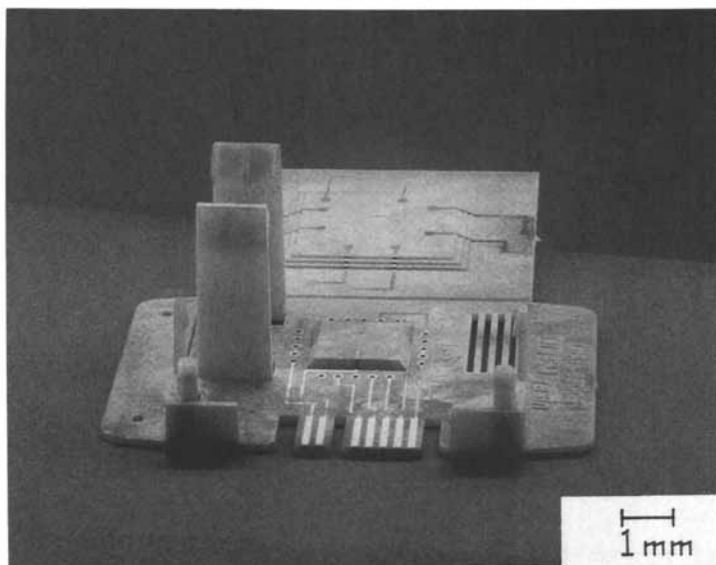
Figure 1. Example of 3-D, metallized ULTEM 2312
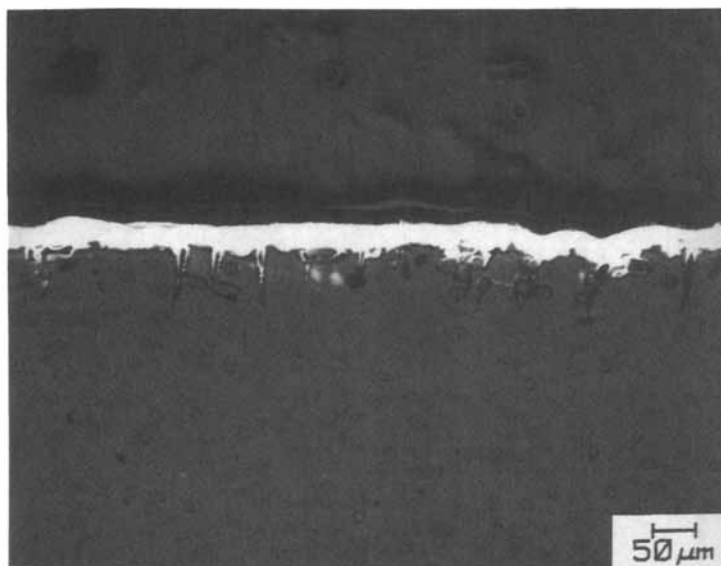
Figure 2. Example of swell and etch treated ULTEM 2312

Table I. Comparison of Polyetherimide
Properties Following Adhesion Treatment

	Traditional Swell & Etch	This Work
Flexural Strength	30% reduction	No change
Weight Loss	10-15% reduction	No change
Electrical	No change	No change
Electrical 48/50 (humidity)	25% reduction	No change
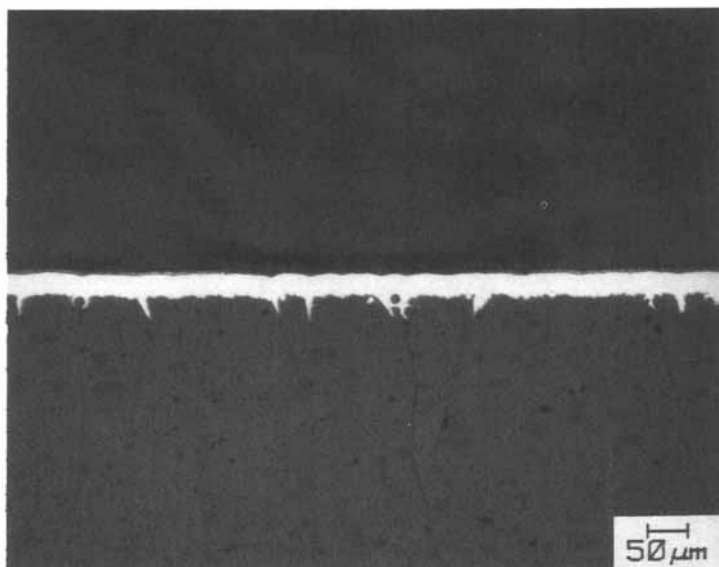
Figure 3. Example of swell and etch treated ULTEM 2312

EXPERIMENTAL

Since the molded circuit board industry requires high volumes and high throughputs of product, deposition of the initial metal onto the plastic was performed using electroless techniques. Further thicknesses of metal were obtained by electrolytic methods. The plastic substrate in this study was based on General Electric's ULTEM polyetherimide resin. In order to withstand the severe conditions required for soldering components onto the circuit board and for an improved coefficient of thermal expansion and increased rigidity, a glass-filled grade of polyetherimide was also examined (Table II).

Table II. ULTEM Polyetherimide Properties

Sample	Filler	Deflection Temperature at 1.82 MPa(°C)	Flexural Modulus (MPa)	Coefficient of Thermal Expansion (m/m/°C)
1000	None	200	3,300	5.6×10^{-5}
2312	30% Glass	210	9,000	2.0×10^{-5}

Samples of unfilled resins (ULTEM 1000) were utilized to examine the changes occurring to the plastic during the chemical treatments. Adhesion data was generated using the glass-filled resin (ULTEM 2312).

Peel strength values were obtained by peeling 32 mm (0.125 inch) copper strips from the substrate. An end of each strip was clipped to an Ametek digital force measuring gauge which was connected to a computer processor. Force values required to lift the metal strips from the substrate were converted by the computer into grams per millimeter peel values. Multiple peel values for each strip were obtained and then averaged.

RESULTS AND DISCUSSION

As an initial step in the plating sequence, (Figure 4) molded plastic samples (Figure 5) were cleaned (Figure 6). Greases and fingerprints from handling as well as silicones from molding release agents were removed prior to plating. X-Ray Photoelectron Spectroscopy (XPS) data presented in Table III show that a number of cleaners are capable of removing surface impurities from the plastic.
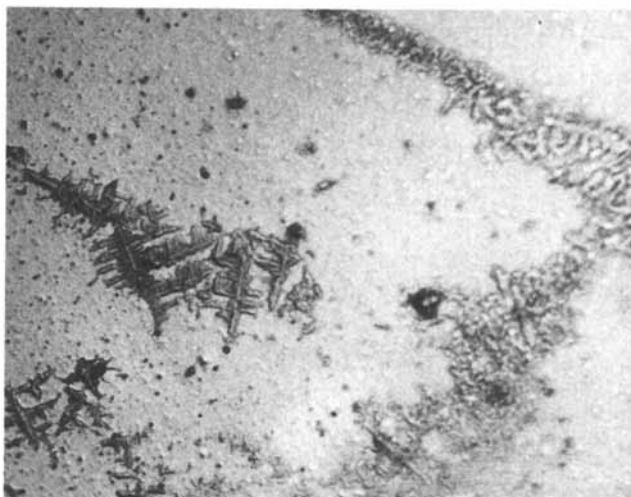
Figure 4. Metallization sequence for ULTEM resins

Table III. XPS Surface Composition, Atom & Substrate Cleaning Process

Treatment	C	N	O	Si
None	71.9	2.1	17.2	8.8
ALL detergent	81.5	3.1	13.4	2.0
SHIPLEY Acid Cleaner 1118	81.1	3.1	11.1	4.5
Freon TF	78.6	2.3	12.3	5.2
Freon TMS	84.9	3.2	10.3	1.3
Freon TA	83.2	3.9	11.5	0.4
ULTEM theoretical	82.3	4.4	13.3	--

Freon-type cleaners are preferred because of their volatility, enabling ease of drying of the sample. Drag-in problems to subsequent baths are thus eliminated.

Degreasing is insufficient to ensure consistency; the surface of the plastic must be removed. An inconsistent surface may be physical or chemical in nature. Physical differences may arise from handling or from the molding process. Chemical differences can arise from exposure to ultraviolet irradiation [17] or thermolysis during molding.

Certain reagents will attack the surface of ULTEM polyetherimide such as dimethylformamide or sulfuric acid. Concentrated sulfuric acid was chosen

AS MOLDED

XPS Atomic %

C   83.4

N   3.5

O   11.4
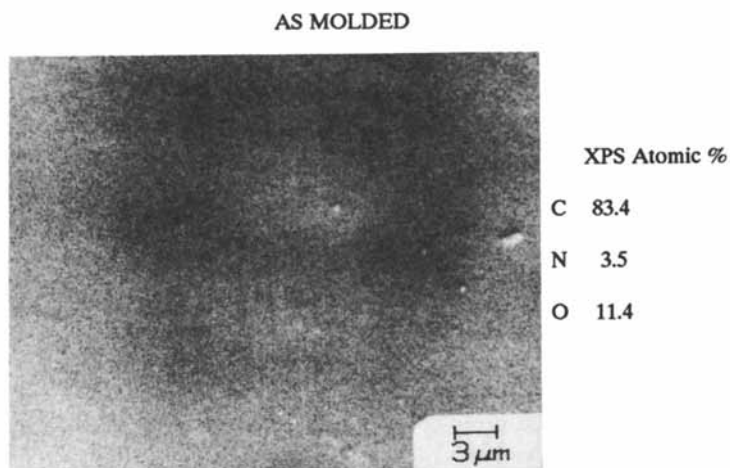
Figure 5. SEM and XPS analyses of molded ULTEM 1000 polyetherimide

AFTER FREON TF

XPS Atomic %

C   80.6

N   2.8

O   13.3
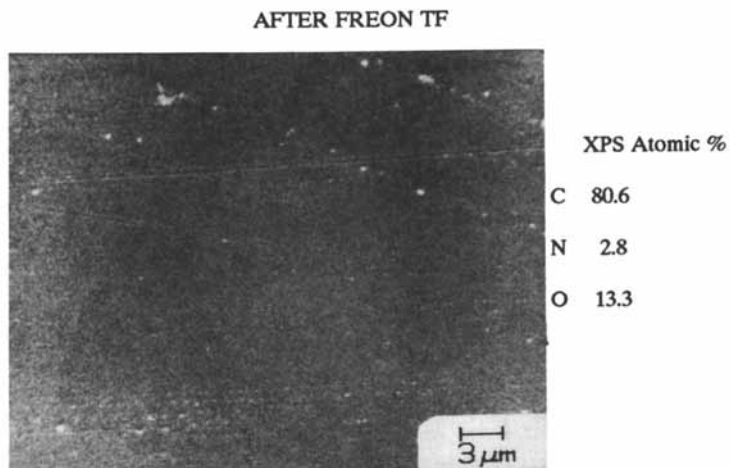
Figure 6. SEM and XPS analyses of degreased ULTEM 1000 polyetherimide

as a surface removal agent for environmental and flammability reasons. Following immersion on sulfuric acid and a water rinse, a non-adherent, white residue is present on the surface of the plastic. XPS data shows this residue to be highly oxidized and sulfur-containing (Figure 7). Figure 8 shows the amount of material removed during treatment at room temperature in 96% sulfuric acid. In general, removal of less than 5 microns of plastic is required for consistent adhesion.

The white residue is next modified by treatment with a strong base in alcohol. It is known that bases can hydrolyze the imide ring of ULTEM polyetherimide (18). Figure 9 shows that both chemical and physical changes to the residue have occurred following immersion in methanolic potassium hydroxide. XPS results are consistent with imide ring hydrolysis and formation of the potassium salt of a carboxylic acid.

Following treatment with the alcoholic base and an alcohol rinse, the modified white residues can be removed by immersion in a mixture of an alcohol and an aggressive solvent. SEM and XPS analysis of a polyetherimide sample following treatment in a 50/50 mixture of dimethylformamide/methanol is shown in Figure 10. Little physical change to the plastic surface has occurred. The plastic surface properties, however, have now been altered. The sample is now water wettable.

	XPS Atomic %
C	68.6
N	4.9
O	21.9
S	4.4
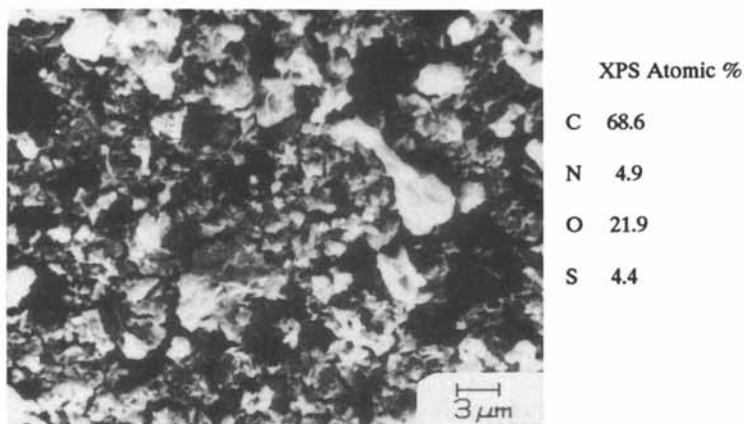
Figure 7. SEM and XPS analyses after sulfuric acid treatment of ULTEM 1000 polyetherimide
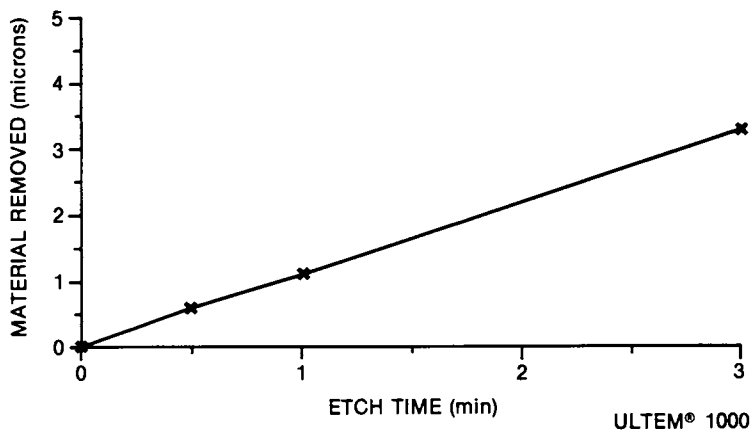
Figure 8. Effect of dwell time in sulfuric acid on surface removal

XPS Atomic %	
C	56.0
N	2.5
O	21.9
S	3.5
K	12.4
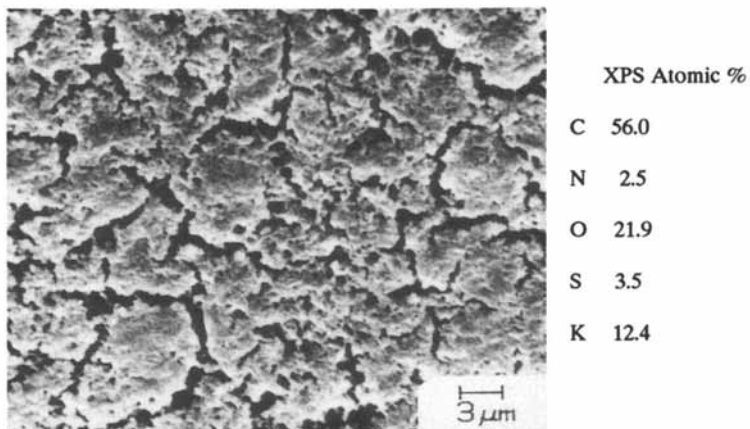
Figure 9. SEM and XPS analyses after KOH/methanol treatment of ULTEM 1000 polyetherimide

XPS Atomic %

C   74.2

N   4.1

O   16.3

S   0.9

K   —
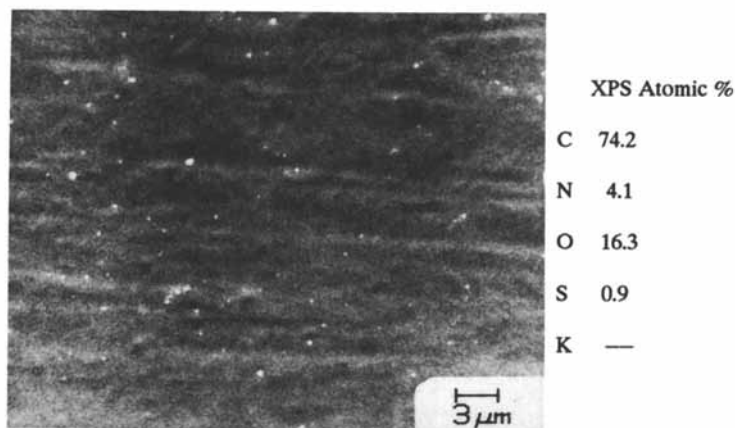
Figure 10. SEM and XPS analyses after DMF/methanol treatment of
ULTEM 1000 polyetherimide

Catalyzation with a tin/palladium colloid, acceleration by removal of
the tin coating and electroless copper deposition with commercially available
products results in an adherent copper layer to the plastic. The plated sample
is then heat treated, electroplated with copper to a thickness of 37.5μ and then
heat treated again.

It was found that an enhancement in peel strength could be affected by
immersion of the sample in a solution of hydroxylamine following residue
removal in dimethylformamide/methanol and prior to catalyzation. Peel
strength values on ULTEM 2312 increased from 125 g/mm to 150 g/mm with
this change. Through the use of model compounds, it was found that the por-
tion of hydroxylamine responsible for the adhesion increase was the -N-O- seg-
ment. Compounds containing -N-H (ethylamine), -N-CH$_3$ (trimethylamine),
-O-H (methanol) or -N=O (pyridine -N-oxide, trimethylamine -N-oxide)
bonds show no improvements in adhesion (125 g/mm or less), while reagents
containing CH$_3$-N-O- (N, N- dimethylhydroxylamine), -N-O-CH$_3$- (methoxy-
lamine), CH$_3$-N-O-CH$_3$ (O, N- dimethylhydroxylamine) or =N-O-H (acetone
oxime) show higher peel strength. As a result, a number of other adhesion
promoters could be added to the system, with peel strength values as high as
206 g/mm being obtained (Table IV).

Table IV. Adhesion Promoting Agents for Polyetherimide (ULTEM 2312)

Adhesion-Promoting Compound	Peel Strength (g/mm)
None	125
Hydroxylamine•HCl	152
N,N-dimethylhydroxylamine•HCl	155
Methoxylamine•HCl	157
N-methylhydroxylamine•HCl	172
O, N-dimethylhydroxylamine•HCl	206
Hydroxylamine-O-sulfonic acid	147
Formaldoxime trimer	175
Acetaldoxime	138
Acetone oxime	204
Cyclohexanone oxime	159
2-pyridinealdoxime	197
N-hydroxysuccinimide	152
N-hydroxyphthalimide	193
1-hydroxybenzotriazole•H_2O	191
Cycloserine	186
Hydroxyurea	129
Acetohydroxamic acid	154

Adhesion promotion could be combined with cleaning of the modified white residue without deleterious effects. Therefore a dimethylformamide/methanol solution of hydroxylamine hydrochloride could be utilized.

Peel strength was also affected by the heat treatment steps between metal deposition. The effect on adhesion of the bake time after electrolytic copper deposition is shown in Figure 11. Peel strength as high as 250 g/mm were observed on copper plated ULTEM 2312 with extended heatings at 110°C. Without a heat treatment, peel strength values were 50 g/mm.

Figure 12 represents a cross section of a plated sample of ULTEM 1000 having a peel strength of 118 g/mm. Little physical surface change of the plastic has occurred as a result of the pretreatment steps. Figure 13 is a cross section of copper plated ULTEM 2312. While a mechanical component to adhesion is present, it is much less than that found in traditional swell and etch treatment (Figure 2). Physical alteration of the plastic is confined to the outermost 25μ. The bulk properties of the plastic (flexural strength, electrical resistivity) are unaffected by this new process (Table I).

Failure during peel is occurring cohesively in the plastic. SEM analysis shows fractured plastic on both the polyetherimide and metal side of the peel for both ULTEM 1000 (Figure 14) and ULTEM 2312 (Figure 15). Glass fibers can also be found on the metal side of the peel for ULTEM 2312.
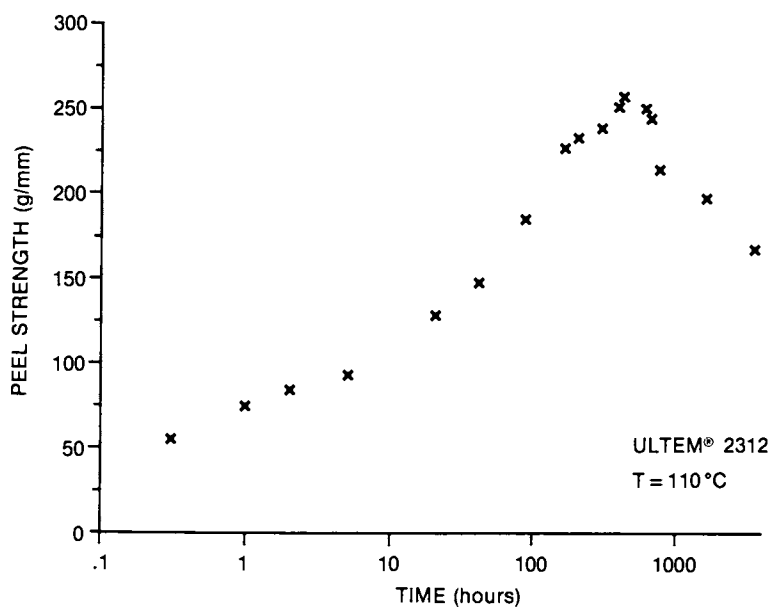
Figure 11. Effect of heat treatment on peel strength
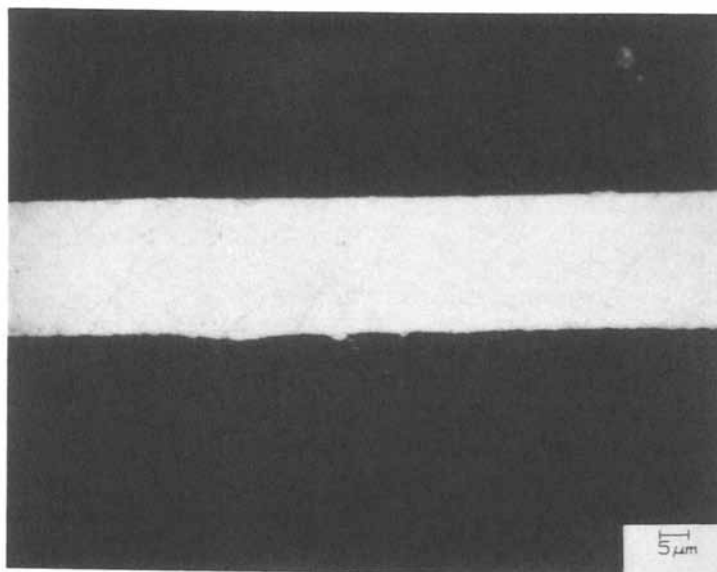
Figure 12. Cross section of plated ULTEM 1000
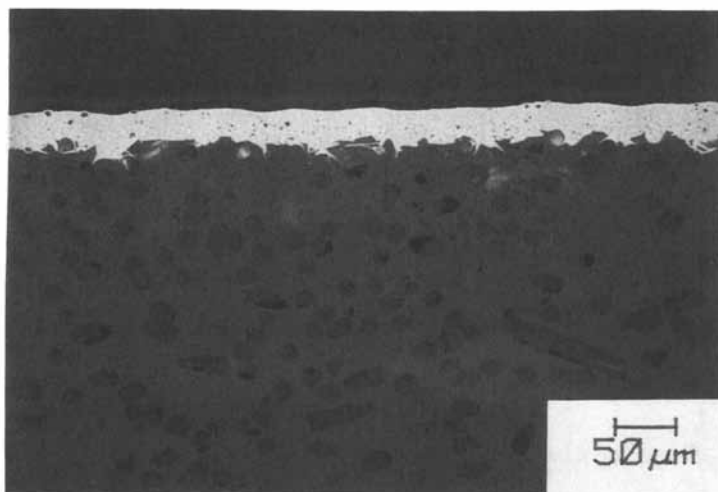
Figure 13. Cross section of plated ULTEM 2312
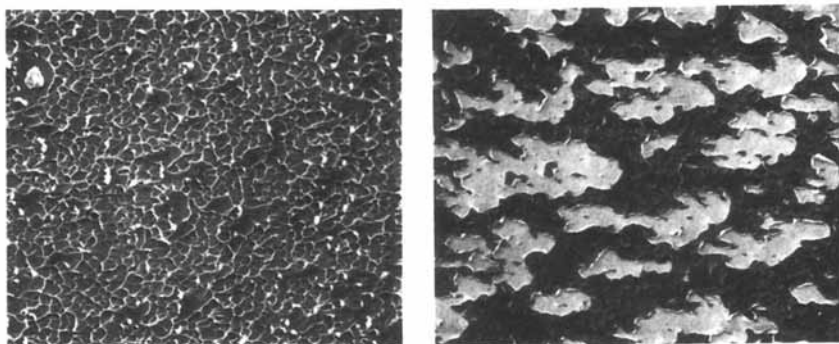
Figure 14. Peeled ULTEM 1000
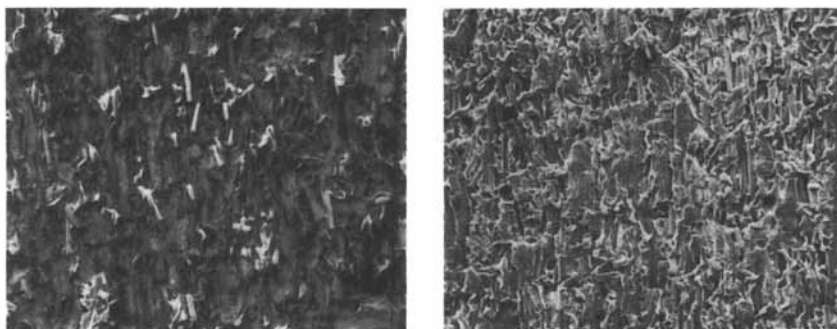
Figure 15. Peeled ULTEM 2312

SUMMARY

A method for obtaining peel strength ranging from 150 to 250 g/mm between copper and glass-filled ULTEM polyetherimide has been developed without the use of swell and etch techniques. Peel failure occurs cohesively within the plastic substrate. The bond to the glass-filled polyetherimide has both a mechanical and a chemical component. Adherence of copper to unfilled polyetherimide is basically through a chemical bond. Organic compounds containing the -N-O- moiety are found to promote the chemical bond. Such a system is of value to the manufacture of molded circuit devices.

ACKNOWLEDGMENTS

LITERATURE CITED

1. Travis, J.; Ganjei, J. *Proc. 41st Reinforced Plastics/Composites Institute*, 1986, Session 8-A, p 1.
2. Mihelcic, J. M. *Printed Circuit Design*, February 1988, p. 41.
3. Frisch, D. C., Weber, W. U.S. Patent 4 594 311, 1986.
4. Elarde, V. D. U.S. Patent 4 689 103, 1987.
5. Lyons, A. M.; Mendenhall, F. T. Jr.; Robbins, M.; Quick, N. R.; Wilkins, C. W. Jr.; U. S. Patent 4 691 091, 1987
6. Cole, H. S.; Liu, Y.S.; Rose, J. W.; Guida, R. *Applied Phys. Lett.* 1988, *53*, 2111.
7. Wolf, G. D.; Giesecke, H.; Sirinyan, K. *Galvanotecknik* 1989, *79*, 2154.
8. Townsend, W. P. In *Handbook of Adhesives*, 2nd ed.; Skiest, I., Ed.; Vos Nostrand Reinhold: New York, 1977, p 846.
9. Saubestre, E. B. In *Modern Electroplating*, 3rd ed.; Lowenheim, F. A., Ed.; Wiley-Interscience: New York, 1974; Chapter 28.
10. Yoshino, K.; Ebina, N. *Proc. Sym. Electroless Metal Deposition, Electrochem. Soc. 88-12*, 1988, p 268.
11. McCaskie, J. E. U. S. Patent 4 520 046, 1985.
12. Paik, K. W.; Ruoff, A. L. *J. Adhesion Sci. Technology* 1988, *2*, 245.
13. Mahlkow, H.; Strache, W. German Patent DE 3 612 822, 1987.
14. Mahlkow, H.; Römer, M.; Rosskamp, G.; Seidenspinner, H.-M.; Stein, L.; Strache, W. German Patent DE 3 708 214, 1988.
15. Grapentin, J.; Mahlkon, H.; Skupsch, J. U. S. Patent 4 517 254, 1985.
16. Dumas, W. V.; Foust, D. F. U. S. Patent 4 775 449, 1988.
17. Mance, A. M.; Waldo, R. A. *J. Electrochem. Soc.* 1988, *135*, 2729.
18. Burrell, M.C.; Karas, B. R.; Foust, D. F.; Dumas, W. V.; Lamby, E. J.; Grubb, W. T.; Chera, J. Electrochem. Soc. Mtg., October 1988, in press.

Chapter 36

Intrinsic Bond Strength of Metal Films on Polymer Substrates

A New Method of Measurement

Donald R. Wheeler and Hiroyuki Osaki[1]

Lewis Research Center, National Aeronautics and Space Administration, Cleveland, OH 44135

The brittle cracking and subsequent debonding of films deposited on flexible substrates subjected to uniaxial strain is described theoretically and illustrated with Ni films evaporated on ion-etched polyethylene terephthalate (PET). It is shown that, if the materials deform elastically, the shear strength of the interface, τ_o, may be evaluated from the length, ℓ_f, of the largest debonded film segment and the tensile strength, σ_o, and thickness, t, of the film:

$$\tau_o = 4\sigma_o (t/\ell_f).$$

τ_o is the intrinsic failure strength of the film-substrate system. It is shown to be independent of substrate mechanical properties and internal stress in the film and is reproducible to ±6%. For Ni on PET, ion-etching doubles the failure strength, τ_o, which reaches the strength of bulk PET.

When studying the mechanism of metal-polymer adhesion and when trying to determine the effect of surface pretreatment on this mechanism, one would like to measure the intrinsic interfacial bond strength. That is, the strength of the chemical and/or physical forces at the interface. However, adhesion of a film to a substrate is normally measured by some sort of pull-off technique which measures the practical strength of the film-substrate couple. The practical strength is affected by the presence of defects, internal stress in the film and by the particular specimen configuration. Thus it is, at best, an indirect measure of changes in the intrinsic strength.

[1]Current address: Sony Magnetic Products, Inc., 3–4–1 Sakuragi, Tagajo, Miyagi, Japan

Recently, Agrawal and Raj (1) (hereafter, AR) have described a method for the measurement of the intrinsic interfacial strength in ceramic-metal couples. Here, we apply the same technique, with some modifications, to the system of Ni films on polyethylene terephthalate (PET) substrates with varying degrees of Ar ion etching prior to film deposition. Our objective is to describe the theory behind the method, as we have adapted it, verify its applicability to the Ni-PET system by demonstrating agreement with experimental details and, finally to use the method to measure the effect of an ion-etch pretreatment of PET on the intrinsic interfacial strength of the Ni-PET couple.

Theory

The test method consists of uniaxially straining a sample of the film-substrate couple as shown schematically in Figure 1. The film thickness is t, and the specimen width is w. Under tensile strain, an interfacial shear stress, $\tau(x)$, is produced. While the film is bonded to the substrate, the shear stress, $\tau(x)$, at the interface causes a tensile stress, $\sigma(x)$, in the metal film. When the strain is sufficient, the tensile stress will reach the ultimate tensile strength of the film, σ_o. Then, if the film fails by brittle fracture, it will develop straight, parallel cracks transverse to the direction of strain. These are represented by the dotted lines in Figure 1. We now focus on one segment of the film. The x-coordinate is measured from the segment edge as shown in the figure. If the film is thin enough that $\sigma(x)$ is nearly constant throughout the thickness of the film and the peeling stress normal to the film may be ignored, the tensile and shear forces at any point, x, in the film must balance, so

$$tw\sigma(x) = w\int_0^x \tau(\xi)d\xi \qquad (1)$$

The functional form, $\tau(\xi)$, is dependent on the properties of the materials. AR assume that $\tau(\xi)$ is sinusoidal being zero at the segment edge and at a distance $\lambda/2$ from the edge. However, elastic analysis of the uniaxial strain of a bilayer (2) shows that $\tau(\xi)$ is maximum at the segment edge and decreases monotonically toward the center of the segment. Therefore, as a better approximation to the elastic shear stress distribution, we let $\tau(\xi)$ be a linear function of x with maximum, τ_m, at the segment edge decreasing to zero at some characteristic distance, ℓ_c, from the edge. Such a shear stress distribution is shown schematically as the heavy line in Figure 2 along with the corresponding tensile stress distribution, $\sigma(x)$, calculated according to Equation (1), as the dashed line.

We now consider the progress of crack formation in the film as the strain in the substrate is increased. There are three stages corresponding to the three parts of Figure 2. The first stage, random cracking, begins when the applied strain is sufficient to produce cracks in the film. The maximum shear stress at the interface, τ_m, must be less than the interfacial shear strength, τ_o, as shown in Figure 2(a), or the film would debond at the edges.
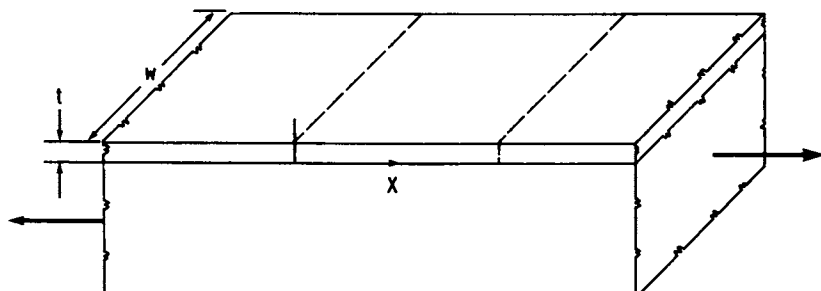
Figure 1.   Schematic diagram of test specimen: Ni film of
thickness, *t*, on PET substrate of width *w* strained in direction of
arrows.   Dotted lines represent brittle cracking.   The
x-coordinate is measured in the direction of strain from the edge
of a film segment.
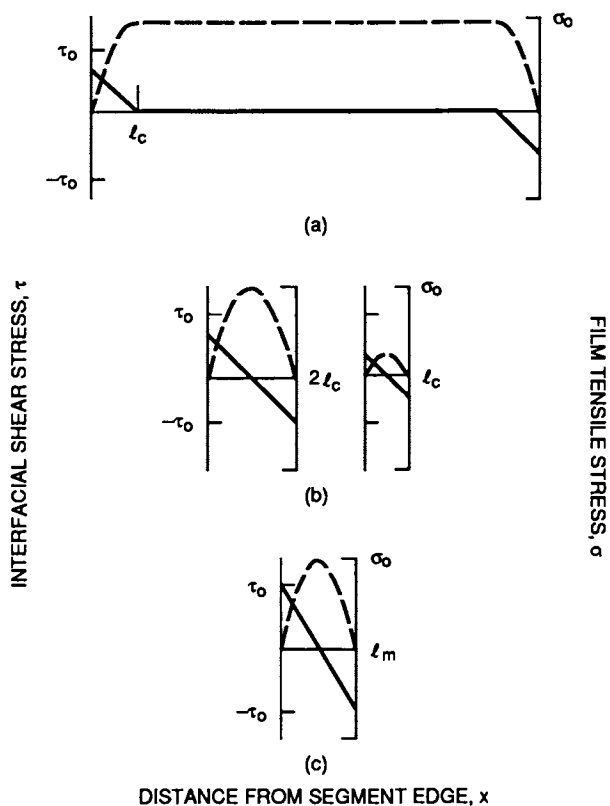
Figure 2.   Representative interfacial shear stress distribution (full line) and film tensile stress distribution (dashed line) as a function of distance, x, from a segment edge (a) during random cracking in a segment longer than $2\ell_c$, (b) at beginning of segment division in segments of length $2\ell_c$ and ℓ_c and (c) at beginning of debonding for largest segment.   Tensile strength of film, σ_o; shear strength of interface, τ_o.

Except within ℓ_c of the edges, the tensile stress in the film is nearly uniform and equal to the tensile strength of the film, σ_o. Thus, fracture of the film can occur anywhere in the segment except within a distance ℓ_c of the edges. During this stage, many cracks occur, until finally the film is divided entirely into segments with lengths between ℓ_c and $2\ell_c$, and the second stage of cracking begins.

The stress distributions in the largest (length $2\ell_c$) and smallest (length ℓ_c) segments at the beginning of this stage are shown in Figure 2b. The shear stress distribution, $\tau(x)$, is of the same form in segments of all length, since little increase in strain occurred during the formation of the segments in the random cracking stage. Thus, tensile stress is maximum in the longest segment, and it cracks first. Because the tensile stress increases within a distance ℓ_c of a segment edge, and the segments are all less than $2\ell_c$ in length, the tensile stress has a distinct maximum at the middle of the segments, which will, therefore, crack at their midpoints. To raise the maximum tensile stress, σ_m, in the smaller segments to the tensile strength, σ_o, the maximum shear stress, τ_m, must be increased by increasing the strain. As σ_m reaches σ_o in each successively smaller segment, the segment will divide, if τ_m remains less than the interfacial shear strength, τ_o.

The final stage, debonding, begins when the maximum τ_m in the largest remaining segment reaches the interfacial shear strength, τ_o. The stress distributions in the largest segment at this stage are shown in Figure 2c. Further increase of substrate strain causes debonding of successively shorter segments, but no further cracking. We designate the length of the first, longest, debonded segment as ℓ_f. The shear stress at the edge of the segment is τ_o, the shear strength of the interface. The tensile stress at the midpoint of the previous divided segment was equal to the tensile strength of the film, σ_o. If there are a large number of segments of nearly equal length, ℓ_f is approximately equal to the length of that previous segment, and the maximum tensile stress, σ_m, is nearly σ_o. Thus, using the linear shear stress distribution shown in Figure 2c and substituting $x = \ell_f/2$ in Equation 1, we get a relation between the shear strength of the interface and the measured segment length, ℓ_f.

$$\tau_o = 4\sigma_o(t/\ell_f) \tag{2}$$

This result is identical to that of AR except for the factor 4 which is a result of our assumption of a linear shear stress distribution. Had we chosen the sinusoidal distribution used by them, this would be a factor of π. Evidently, without knowledge of the exact shear stress distribution, τ_o is only determined up to a constant.

Equation 2 gives the interfacial shear strength, τ_o, in terms of the measurable quantity, ℓ_f, and film characteristics, t and σ_o, which are, at least in principle, measurable. The quantity τ_o meets the requirements for a measure of the intrinsic interfacial strength: First, while localized debonding caused by defects may occur, it is easy to distinguish it from the debonding along all of both edges of the largest segment which is due to the general failure of the interface. Second, particulars of the specimen configuration such as substrate thickness or mechanical properties do not enter into Equation 2. Finally, an important implication of the analysis is that τ_o is independent of internal stress in the film. The applied strain produces a tensile stress in the film. If the stress–strain relation of the materials is linear, the applied stress adds to any internal stress already present. The strain required to produce cracking or debonding will be affected by the internal stress, but the measured quantity, ℓ_f, is independent of the origin of the stress.

Before presenting the experimental results, we will discuss the validity of two important assumptions in the case of Ni on PET. The first is the elasticity of the materials, or more importantly, the linearity of their stress–strain relation. Unannealed, polycrystalline Ni films less than 2 μm thick work harden so severely that their stress strain curves remain approximately linear up to the breaking strain of about 1%. (3,4). Measurements in our laboratory show that the PET is linear to 7% strain. Although the overall strain in the specimen can be larger than 7%, any plastic flow must occur in the uncoated ends of the PET and between segments of the Ni film, since, under the unbroken segments of the Ni film the strain must be less than 1%. Thus, elastic analysis is appropriate for each Ni segment and the underlying PET substrate.

The second important assumption in the analysis is that interfacial failure occurs only in shear, *i.e.* that any peeling stress, normal to the interface, is negligible. Analysis of an elastic bilayer (5) shows that, for the experimental parameters employed here, the peeling stress is, in fact, an order of magnitude less than the shear stress. Furthermore, finite element analysis (6) shows that the normal stress is compressive rather than tensile for the thicknesses of PET and Ni used here. Finally, it will be shown that the experimental results are consistent with the one–dimensional analysis presented above.

Experiment

The test specimen was a PET substrate 6 μm or 12 μm thick, 2.5 mm wide and about 1.5 cm long with a 3 mm long strip of evaporated metal, 0.2 μm to 1.2 μm thick, deposited near its center. The film thickness was monitored, during evaporation, with a quartz crystal thickness monitor, and the substrate temperature was measured with a thermocouple. The substrate temperature always remained within within 10 C of room temperature. An ion gun could be used to treat the substrate surface before deposition to modify the film adhesion. After deposition, the specimen was removed from the deposition

chamber and clamped to the anvils of a blade micrometer. It was then
subjected to a slowly increasing strain applied in the lengthwise
direction. As the cracking progressed, photomicrographs were made of
portions of the films so that the segment lengths could be measured.
Finally, when debonding occurred, the largest debonded segment
length, ℓ_f, was measured.

Results and Discussion

We have observed brittle, transverse cracking of Fe, Co and Ni films.
Here, we compare the details of the cracking of Ni films with the
predictions of the theory presented above to check the applicability
of the assumptions and approximations. To confirm that τ_o, as
calculated from ℓ_f in Equation 2, does depend on interfacial
strength, the PET surface was Ar ion etched to modify the PET-Ni bond
strength. Simple, qualitative tape-pull and abrasion tests showed
that etching increased the film adhesion. In addition, both the PET
thickness and elastic modulus and the Ni thickness were varied to
confirm that τ_o was independent of these parameters. Finally,
measurements were made on specimens with differing residual stress in
the Ni film to verify that τ_o is, indeed, a measure of intrinsic
interfacial strength rather than the practical adhesion.
     The Ni films cracked in a brittle manner with straight, parallel
cracks transverse to the applied strain. With increasing strain,
cracking progressed through the three distinct stages described
above. First, the film cracked at random locations along its length.
Eventually, the film segments began to divide at their midpoints.
This process of division continued until the largest segment debonded
along both edges. Figure 3 shows both segment division and debonding
in a typical specimen. Figure 3a, was taken after the process of
segment division is nearly complete. After additional strain, Figure
3b was taken. Notice the division of the large segment at arrow A
and the debonding of the largest remaining segment at arrow B.
     According to AR, at this point, there should be a distribution
of film segment lengths from the largest, ℓ_f, to the smallest, $\frac{1}{2}\ell_f$,
and the longest segment length should decrease as the interfacial
shear strength increases. Figure 4 shows the segment length
distributions measured from photomicrographs of three different
specimens. Each specimen had been Ar ion etched to a different
degree. It is clear that the segment lengths do lie within the
required range, and that the greatest length decreases with
increasing ion etching time as would be expected, if the interfacial
strength is increased by ion etching.
     The length, ℓ_f, of the first, largest segment to debond was
used to verify several quantitative implications of Equation 2 for Ni
films on virgin and ion-etched PET. Provided the tensile strength of
the Ni film, σ_o, and the shear strength of the interface, τ_o, do not
change with film thickness, Equation 2 predicts that the length of
the first debonded segment, ℓ_f, should be proportional to the film
thickness, t. Figure 5 shows values of ℓ_f for t ranging from 0.2 μm
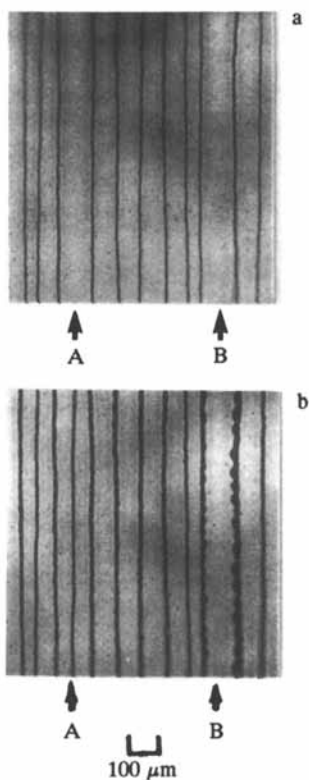
Figure 3. Photomicrographs of a portion of a 1.02 μm Ni film on
12 μm PET. (a) strained just short of debonding. (b) strained
sufficient to debond the largest remaining segment. "A" is a
segment which divides and "B" is the segment which debonds
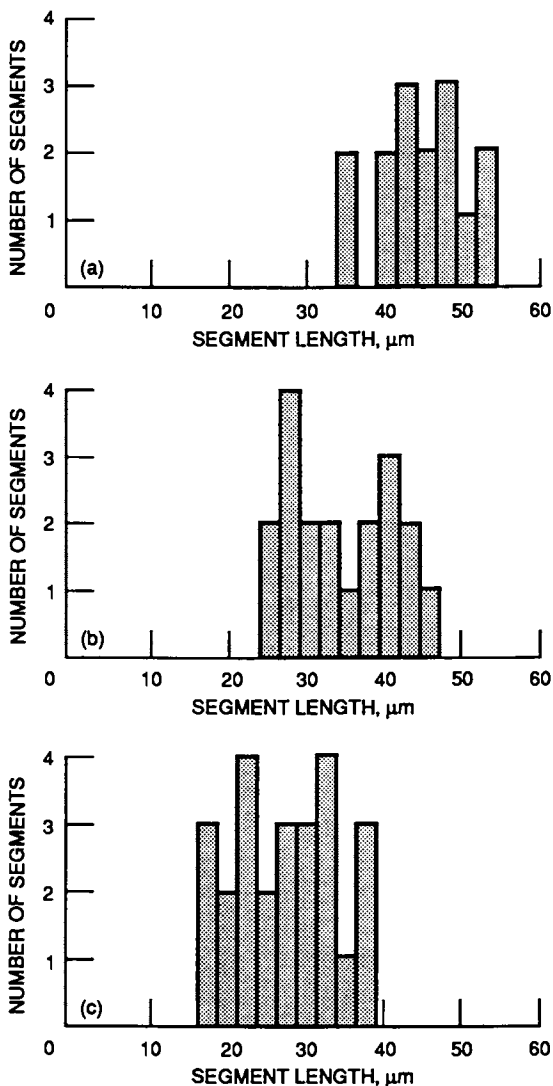
Figure 4. Distributions of film segment lengths when debonding
occurs in 0.63 μm Ni films evaporated onto 12 μm, Ar-ion etched
PET substrates. Ion energy, 2 kV; ion etch time, 10 sec. Ion gun
emission currents: (a) 5 mA, (b) 10 mA and (c) 15 mA.

to 1.3 μm. Except at the largest value of t, the proportionality is quite good. The straight line is a linear least-squares fit to the first four data points. The deviation at large t may be due to the existence of significant peel stress at the edge of the thicker film. Debonding would then be the result of the combined stress and would occur earlier in the cracking sequence, *i.e.* at larger ℓ_f.

Within the approximations used, the ratio, ℓ_f/t, should be independent of the substrate thickness and elastic properties. Measurement confirmed that there was no difference in the ratio for Ni films on 6 μm and 12 μm PET substrates. It is difficult to change the elastic properties of the substrate without also changing its surface and possibly the film adhesion. However, there was a "hard" (high modulus) and a "soft" (low modulus) direction, in the drawn PET films used for these tests. There was no difference in ℓ_f/t when the strain was applied in the two directions, indicating a degree of independence of substrate elastic properties.

An important implication of the assumption of linearity in the analysis is that τ_o is independent of internal stress in the film. By changing the mounting of the substrate during film deposition, we were able to produce Ni films with either compressive or tensile stress, as judged by the curvature of the substrate after deposition. The value of ℓ_f/t was the same in both cases. However, the strain required to cause debonding was more than twice as large for the films with compressive stress as for those with tensile stress. The strain required to produce debonding is related to the practical adhesion of the film-substrate couple (2), while the measurement of ℓ_f/t yields τ_o, the intrinsic bond strength of the interface.

The PET substrate was argon ion etched before Ni deposition to enhance film adhesion without altering the properties of the substrate. Values of ℓ_f were then measured, and τ_o was calculated from Equation 2 using σ_o = 150 kg/mm^2 (7). Figure 6 shows τ_o as a function of etch time. The four measurements at 0 sec show a reproducibility of ±6%. After 10 sec of ion etching, τ_o approximately doubled, reaching 10 kg/mm^2. It was not possible to determine the locus of failure, in these tests, but since debonding can occur in the PET as well as at the interface, the values of τ_o should not exceed the critical shear stress of PET. The tensile strength of commercial PET film is at least 17 kg/mm^2 (8), and the critical resolved shear stress is, therefore, about 10 kg/mm^2. However, the strength of the PET surface could have been changed by the ion etching. Furthermore, the values of τ_o in Figure 6 depend on the exact values chosen for σ_o and the numeric factor in Equation 2. In light of these qualifications, it can only be said that the maximum measured value of 10 kg/mm^2 seems reasonable. It also compares favorably with shear strength measurements derived from epoxy-bonded, lap-shear tests (9).
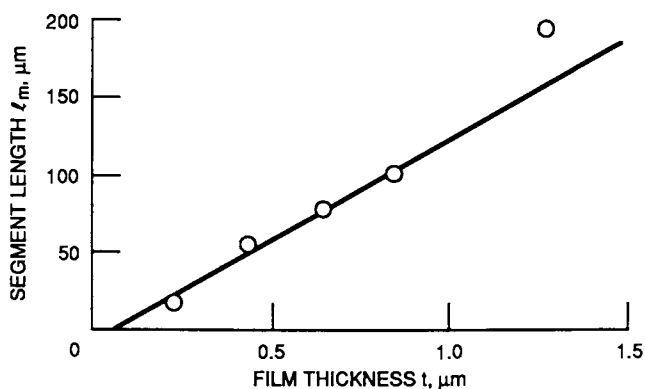
Figure 5. Length of the first debonded film segment, ℓ_f, as a function of film thickness, t, for Ni films evaporated on 12 μm PET. Solid line is a least squares fit to the first four data points.
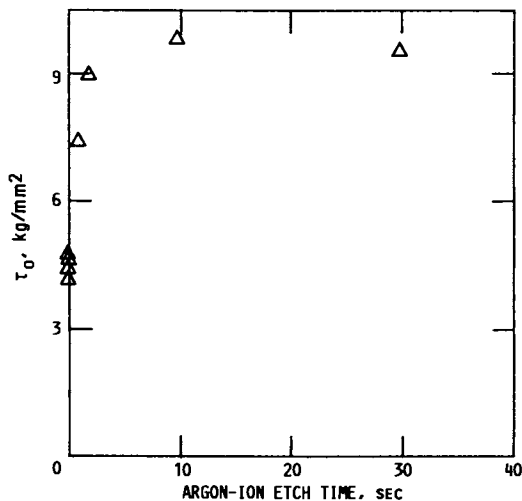
Figure 6. Experimental values of interfacial shear strength, τ_o, calculated from Equation 2 for 0.43 μm Ni films on Argon ion etched 12 μm PET as a function of ion etching time.

Conclusion

We have described a semiquantitative method for the measurement of
the intrinsic bond strength between elastic substrates and elastic
films that fail by brittle fracture. The essential features of the
analysis, adapted from AR, were verified by measurements on the
PET-Ni couple. The precision of the technique was ±6%, in this case.
The interfacial shear strength of Ni on PET doubled after ion
etching, reaching about 10 kg/mm^2.
        Quantitative bond strength measurements require knowledge of the
critical tensile stress, σ_o, of the film and the correct shear stress
distribution in Equation 1. AR calculate the film tensile strength
from the strain at which cracking first occurs and the modulus of the
film. However, such a procedure risks being affected by the internal
stress in the film. We have chosen, instead, to use independent
measurements made on free standing films. Obtaining the correct
numeric factor in Equation 2 depends on knowing the actual shear
stress distribution, which would require a detailed, three-
dimensional, analysis of the system. Lacking such analysis, AR use a
sinusoidal distribution, while we have chosen a linear one. However,
we emphasize that such considerations are only crucial for
quantitative comparisons between systems of differing metals or
substrates. Even without knowledge of the tensile strength of the
film or the correct shear stress distribution, the largest debonded
segment length is a precise measurement connecting the bulk
properties of the film, tensile strength and thickness, with the
intrinsic interfacial strength of the system. Thus it is especially
useful in evaluating the relative effect of different interface
modification procedures on the intrinsic bond strength of a
particular film on a particular substrate.
        There are some limitations to the application of this technique.
The metal films must fail in a brittle manner. We have observed
brittle cracking in Ni, Fe and Co films on PET, but Au and Cu films
failed in a ductile manner, and their adhesion could not be
evaluated. Performing the test at low temperature might cause
brittle failure in such films, or the metal under test could be
deposited as a thin interfacial layer with a thick overlayer of
nickel being deposited to determine the bulk properties of the film.
In any case, brittle fracture is easily recognized by the
characteristic straight, parallel cracks in the film. It is also
necessary that the film thickness be in a range such that the tensile
strength of the film is low enough to allow multiple cracking before
debonding occurs. Since the measurement does not depend on film
thickness or internal stress, there is no penalty in adjusting the
film thickness to the proper range. Furthermore, the film and
substrate must be elastic. Finally, the inability analyze the
interface after failure and thereby determine the locus of failure is
a serious experimental limitation.
        However, this method has several advantages compared to other
quantitative and semiquantitative adhesion measurement techniques.
It is substantially more reproducible than most other methods, and
does not require, at least for semi-quantitative results, detailed
knowledge of the properties of the film material and substrate. It
is easily applied to flexible substrates, and requires no adhesive

bond to either substrate or film. Most significantly, it measures
the intrinsic interfacial bond strength, independent of internal
stress in the film.

Literature Cited

1. Agrawal, D. C.; Raj, R. *Acta Met.*, 1989, **37**, 1265-1270
2. Ting, Bond-Yen; Winer, W.O.; Ramalingam, S. *Journal of Tribology*,
   1985, **107**, 472
3. Henning, C. A. O.; Boswell, F. W.; Corbett, J. M. *Acta Met.*,
   1975, 23, 187
4. D'Antonio, C.; Hirschhorn, J.; Tarshis, L. *Trans. Met. Soc.*,
   AIME, 1963, **227**, 1346
5. Suhir, E. *J. Appl. Mech.*, 1986, **53**, 657
6. Private Communication; Keer, L. M.; Depts. of Civil and Mechanical
   Engineering, Northwestern University
7. Grunes, R. L.; D'Antonio C.; Kies, F. K. *J. Appl. Phys.*, 1965,
   36, 2735
8. Hawthorne, J. M.; Heffelfinger, C. J. in *Encyclopedia of Polymer
   Science and Technology,* vol 11; Mark, H. F.; Gaylord, N. G.;
   Bikales, N. M.; eds. (Wiley-Interscience, NY, 1967) 53
9. Hall, J. Richard; Westerdahl, C. A. L.; Devine, A. T.; Bodnar,
   M. J. *J. Appl. Polym. Sci.*, 1969, **13**, 2085

Author Index

515

Affiliation Index

Subject Index

Affiliation Index

Subject Index